THE EFFECT OF LIPID OXIDATION ON THE ACTIVITY OF THE MEMBRANE PROTEIN ADENOSINE 2A RECEPTOR

IDOIA COMPANY MARÍN
Doctor of Philosophy

ASTON UNIVERSITY
JANUARY 2024

The effect of lipid oxidation on the activity of the membrane protein Adenosine 2A receptor

Idoia Company Marín
Doctor of Philosophy
Health and Life sciences, Aston University
2024

THESIS ABSTRACT

The Adenosine 2A receptor ($A_{2A}R$) is a prototypical G-protein coupled receptor studied as a drug target to treat inflammatory and neurodegenerative diseases involving oxidative stress. Lipids surrounding membrane proteins are important modulators of their conformation and activity; during oxidative stress these lipids can be oxidised and affect protein function. Understanding of the interaction of unoxidised and oxidised lipids with the $A_{2A}R$ and its consequences is limited, so the aim of this work was to address this knowledge gap.

Recombinant human C-terminal-truncated $A_{2A}R$ was overexpressed in *Pichia pastoris* SMD1163 and solubilized with the co-polymer styrene-maleic acid (SMA2000) into SMA lipid particles (SMALPs) or the detergent n-Dodecyl β-D-maltoside (DDM). The purified receptor was obtained in its native lipid environment ($A_{2A}R$-SMALP) or surrounded by detergent micelles ($A_{2A}R$-DDM), which were identified by LC-MS/MS. Lipids in the $A_{2A}R$-SMALP were characterised, and compared to those in bulk membranes and SMA-solubilized lipids by LC-MS/MS. The effects of oxidative treatments on protein conformation, thermostability, and ligand binding were studied using Trp fluorescence, CPM fluorescence, and radioligand-binding assays. Additionally, the $A_{2A}R$ was overexpressed in HEK293T cells to study the effect of oxidation on receptor function by measuring the cAMP levels.

$A_{2A}R$-SMALP was purified from *P. pastoris* proteins, whereas $A_{2A}R$-DDM co-eluted with alcohol dehydrogenase (mADH) contaminant. These were identified with low sequence coverage, which limited the analysis of protein lipoxidation. $A_{2A}R$-SMALP was enriched in unsaturated anionic phospholipids compared to bulk membranes, which contribute to receptor activity. $A_{2A}R$-SMALP was folded and able to undergo conformational changes under physiological and oxidising conditions, and its thermostability and ligand-binding capability were not affected by oxidation. cAMP levels were upregulated under oxidative conditions, and its production increased with an $A_{2A}R$ agonist in a dose-dependent manner, suggesting $A_{2A}R$ upregulation during oxidation. This study demonstrated the feasibility of characterizing membrane proteins in their native lipid environment using SMALPs under physiological and oxidative conditions, bringing insights into their roles in inflammatory conditions.

ACKNOWLEDGEMENTS

Firstly, I would like to express my gratitude to my supervisor, Prof. Corinne Spickett, for her guidance and support throughout my PhD. Corinne, thank you for welcoming me into the research group and for your expertise in LC-MS/MS and oxidative stress. I am grateful for your unwavering support and mentorship. I also appreciate the contributions of my co-supervisors, Dr. John Simms, and Prof. Andrew Pitt. John, your knowledge in the GPCR and lipid field, along with your help in experimental design and your insights have been invaluable. Andy, thanks for your knowledge, assistance, support, and guidance in the realm of LC-MS/MS.

I extend my thanks to Dr. Alex Cheong for your expertise and assistance with cloning, Prof. David Poyner for your guidance in radioligand binding assays, and Dr. Ivana Milic for your help with LC-MS/MS.

A special mention goes to Dr. Matthew Daly, Dr. Nyasha Munjoma, and Dr. Lee Gethings for the enriching experience during my secondment at Waters Corporation. Your insights into the Cyclic, lipid analysis strategies, and generous support, have been truly appreciated.

To my dear lab mates Bita, Sarah, and Maral. Your companionship, friendship, and technical and emotional support in the lab have made this journey more enjoyable and fulfilling. To my friends Carolina, Diana, Divya, Laura, and Luis, thank you for being an integral part of this experience and providing companionship during our time away from home. A special thanks goes to my best friends and family Júlia, Laura F, Maria, David, Laura C, Mimi, and Susi for visiting me and offering constant support despite the distance. Lastly, to my family, Mama, Papa, Nacho, and Gaia for your unconditional love, support, advice, and patience, all of which have been essential throughout this journey. I would not have reached this point without you.

This acknowledgment is a tribute to the collective efforts of those who have played a significant role in my academic and personal growth. I am truly grateful for the enriching experiences and the network of support that has shaped my doctoral journey.

TABLE OF CONTENTS

5

I. Company Marin, PhD Thesis, Aston University 2024

I. Company Marin, PhD Thesis, Aston University 2024

LIST OF ABBREVIATIONS

4-HNE	4-hydroxynonenal
$A_{2A}R$	Adenosine 2A receptor
AAPH	2,2'-azobis(2-amidinopropane) dihydrochloride
ACR	Acrolein
AD	Alzheimer's disease
ADH2/mADH	Alcohol dehydrogenase 2
AMP	Adenosine monophosphate
ANOVA	Analysis of Variance
AOX	Alcohol oxidase
APS	Ammonium persulfate
ATP	Adenosine triphosphate
ATP	Adenosine triphosphate
BCA	Bicinchoninic acid
Bmax	Maximum receptor binding capacity
BMGY	Buffered glycerol complex medium
BMMY	Buffered methanol complex medium
BPTI	Bovine pancreatic trypsin inhibitor
BSA	Albumin standard
cAMP	Cyclic adenosine monophosphate
CBP	CREB-binding protein
CCS	Collision cross section
CD	Circular dichroism
Cho	Cholesterol
cIMS	Cyclic ion mobility spectrometry
CL	Cardiolipins
CNS	Central nervous system
COX	Cyclooxygenases
CPM	7-diethylamino-3-(4'-maleimidylphenyl)-4-methylcoumarin
cpm	Counts per minute
CRE	cAMP response element
CREB	cAMP response element binding protein
CV	Column volume
CVD	Cardiovascular diseases
DAG	Diacylglycerols
DDA	Data-dependent acquisition
ddH_2O	Double-distilled water
DDM	N-Dodecyl-β-D-Maltoside
DHA	Docosahexaenoic acid
DIA	Data-independent acquisition
DIBMA	Diisobutylene maleic acid
DIBMALPs	DIBMA lipid particles
DMEM	Dulbecco's modified eagle's medium
DMSO	Dimethyl sulfoxide
DNA	Deoxyribonucleic acid
DOPC	Dioleoyl-phosphatidylcholine
DOPE	Dioleoyl-phosphatidylethanolamine
DOPG	Dioleoyl-phosphatidylglycerol

DOPI	Dioleoyl-phosphatidylinositol
DOPS	Dioleoyl-phosphatidylserine
DRY	Aspartic acid-arginine-tyrosine motif
DTT	Dithiothreitol
EC_{50}	Half maximal effective concentration
ECL	Extracellular loop
EDTA	Ethylenediamine tetraacetic acid
ELISA	Enzyme-linked immunosorbent assay
ERK	Extracellular signal-regulated kinase
ESI	Electrospray ionization
FA	Fatty acids
FBS	Fetal bovine serum
FC	Fold change
FCS	Fluorescence correlation spectroscopy
FRET	Fluorescence resonance energy transfer
FT	Flowthrough
GDP	Guanosine diphosphate
GPCR	G-protein coupled receptor
GTP	Guanosine triphosphate
HCl	Hydrochloric acid
HEK	Human embryonic kidney
HEPES	4-(2-hydroxyethyl)-1-piperazineethanesulfonic acid
$HDMS^E$	Data-Independent High-Definition MS^E
HILIC	Hydrophilic interaction liquid chromatography
His	Histidine
HPLC	High performance liquid chromatography
HRP	Horseradish peroxidase
IAA	Iodoacetamide
IBMX	3-isobutyl-1-methylxanthine
ICL	Intracellular loop
IDA	Iminodiacetic acid
IEDANS	5-({2-[(iodoacetyl)amino]ethyl}amino)naphthalene-1-sulfonic acid
IFN	Interferon
IL	Interleukin
IM	Ion mobility
IMAC	Immobilized metal affinity chromatography
IRI	Ischemia-reperfusion injury
ISs	Internal standards
Kd	Ligand-binding affinity
LB	Luria broth
LC	Liquid chromatography
LC-MS/MS	Liquid chromatography coupled to tandem mass spectrometry
$LogIC_{50}$	Half-maximal inhibitory concentration
LOX	Lipoxygenases
LPC	Lysophosphatidylcholine
LPE	Lysophosphatidylethanolamine
LPL	Lysophospholipids
λEM	Emission wavelength
m/z	Mass-to-charge ratio
MAG	Monoacylglycerols

MAPK	Mitogen-activated protein kinase
MD	Molecular dynamics
MDA	Malondialdehyde
MS	Mass spectrometry
MS/MS	Tandem mass spectrometry
MTBE	Methyl tert-butyl ether
MTT	3-(4,5-Dimethyl-2-thiazolyl)-2,5-diphenyl-2H-tetrazolium bromide
mw	Molecular weight
NADPH	Nicotinamide adenine dinucleotide phosphate
nanoDSF	Nano differential scanning fluorimetry
NECA	5'-(N-Ethylcarboxamido)adenosine
NF-kB	Nuclear factor kappa light chain enhancer of activated B cells
Ni–NTA	Nickel-nitrilotriacetic acid
NK	Natural killer
NOX	Nicotinamide adenine dinucleotide phosphate oxidase
O/N	Overnight
PA	Phosphatidic acid
PBS	Phosphate buffered saline
PC	Phosphatidylcholine
PCA	Principal component analysis
PD	Parkinson's disease
PE	Phosphatidylethanolamine
PEI	Polyethylenimine
PG	Phosphatidylglycerol
Phe	Phenylalanine
PI	Phosphatidylinositol
PIP2	Phosphatidylinositol 4,5-bisphosphate
PKA	Protein kinase A
PKC	Protein kinase C
PLs	Phospholipids
PLSDA	Partial least squares discriminant analysis
PMSF	Phenylmethylsulfonyl fluoride
PONPC	1-palmitoyl-2-(9-oxo-nonanoyl)-sn-glycero-3-phosphocholine
POPC	Palmitoyl-oleoyl phosphatidylcholine
POPS	Palmitoyl-oleoyl phosphatidylserine
POVPC	1-palmitoyl-2-(5-oxovaleroyl)-sn-glycero-3-phosphocholine
PS	Phosphatidylserine
PTEN	Phosphatase and tensin homologue
PTMs	Post-translational modifications
PUFA	Polyunsaturated fatty acids
Q	Quadrupole
QC	Quality control
RNS	Reactive nitrogen species
ROS	Reactive oxygen species
RPLC	Reverse phase liquid chromatography
RT	Room temperature
SDS	Sodium dodecyl-sulfate
SDS-PAGE	SDS polyacrylamide gel electrophoresis
Ser	Serine
SM	Sphingomyelin

SMA	Styrene-maleic acid
SMALPs	SMA lipid particles
SN	Supernatant
TAG	Triacylglycerols
TBS	Tris-buffered saline
TBS-T	Tris-buffered saline with tween20
TEMED	Tetramethylethylenediamine
TEV	Tobacco etch virus
TGF	Transforming growth factor beta
TM	Transmembrane
Tm	Melting temperature
TMB	3,3',5,5'-tetramethylbenzidine
TNF	Tumour necrosis factor
TOF	Time of Flight
Trp	Tryptophan
TW	Travelling waves
Tyr	Tyrosine
UPLC	Ultra performance liquid chromatography
VIP	Variable of importance
WT	Wild type
XAC	Xanthine amine congener
XO	Xanthine oxidase
YPD	Yeast peptone dextrose
ZM	ZM241385

LIST OF FIGURES

I. Company Marin, PhD Thesis, Aston University 2024

I. Company Marin, PhD Thesis, Aston University 2024

14
I. Company Marin, PhD Thesis, Aston University 2024

LIST OF TABLES

I. Company Marin, PhD Thesis, Aston University 2024

1. CHAPTER 1 - GENERAL INTRODUCTION

1.1. G-Protein Coupled Receptors, Adenosine Receptors, and Extracellular Adenosine

G-protein coupled receptors (GPCRs) constitute the largest family of membrane proteins. They are encoded by 5% of the human genome and over 800 different GPCRs can be found in these organisms (Vroling *et al.*, 2011). Different GPCRs have similar topology: their structure consists of seven transmembrane α-helices, three intracellular loops (ICL), three extracellular loops (ECL), an extracellular N-terminal tail, and an intracellular C-terminal tail (Lebon, Warne, *et al.*, 2011a). GPCRs act as signal transducers across cellular membranes of eukaryotic cells through undergoing conformational changes. Structural rearrangements take place once they are activated by a variety of different external stimuli or ligands, called agonists (Xu *et al.*, 2011). These extracellular inputs can be hormones and neurotransmitters, peptides or even proteins, ions, odorants, and photons of light, among others (Lundstrom, 2007). On the other hand, they can be inactivated by the binding of specific antagonists.

Ligand binding triggers conformational rearrangements that enable the receptors to bind, interact, and activate specific cytosolic proteins, such as heterotrimeric G proteins. This way they regulate several different cellular processes that include cell homeostasis, cell growth, and proliferation (Ye *et al.*, 2016). They can also be involved in a variety of pathological processes, such as inflammation and metabolic and neurological disorders (Liao *et al.*, 2019; Sushma and Mondal, 2019; Birch *et al.*, 2021). Most commonly, GPCRs interact with the alpha subunit of the heterotrimeric G proteins, which are commonly activated through the exchange of GDP with GTP. This enhances the dissociation of the alpha subunit from the beta-gamma complex, thereby initiating cytosolic signalling processes (Manglik *et al.*, 2015).

Adenosine receptors belong to the largest class of GPCRs, the Rhodopsin-like receptor family. These purinergic receptors are classified into four different subtypes: the A_1, A_{2A}, A_{2B}, and A_3. Adenosine receptors are characterised for being activated by the extracellular nucleoside adenosine as a natural agonist, and inhibited by purine base xanthines, such as caffeine and theophylline (Goulding *et al.,* 2018). Extracellular adenosine offers a distinct signalling profile depending on the receptor it activates, its expression level, tissue distribution, and binding affinity (Carpenter and Lebon, 2017). Adenosine is produced in response to bioenergetic stresses. It acts on the central nervous system and the cardiovascular system as a physiological negative regulator of stress by blocking inflammation (Ohta and Sitkovsky, 2014).

Adenosine receptors regulate a wide variety of cellular processes, including sleep, angiogenesis, vasoconstriction, vascular integrity, and neurotransmitter release (Khayat and Nayeem, 2017).

Consequently, they have been proposed as potential drug targets to treat pathophysiological conditions, including neurodegenerative diseases such as Alzheimer's disease, Parkinson's disease, and dementia, as well as other inflammatory diseases such as cancer, ischemia, type 2 diabetes mellitus, and asthma, and other conditions such as pain and sleep disorders (Effendi *et al.*, 2020). Therefore, it is crucial to study them and understand how GPCR activity can be modulated by different physiological and pathophysiological conditions.

1.2. Human Adenosine 2A Receptor Distribution, Function, and Signalling

The $A_{2A}R$ is expressed in different specific regions of the brain, such as the basal ganglia, as well as in the smooth muscle cells, blood vessels, heart, and lungs (de Lera Ruiz *et al.,* 2014). Furthermore, this protein is found in leukocytes and platelets, as well as in the central organs of the immune system, such as the spleen and thymus (Hinz *et al.*, 2018). Figure 1.1 represents a summary of the location of the $A_{2A}R$ in different tissues and organs, the protein function in those specific locations, and its possible therapeutic applications, depending on the pathological conditions in which the receptor is involved.
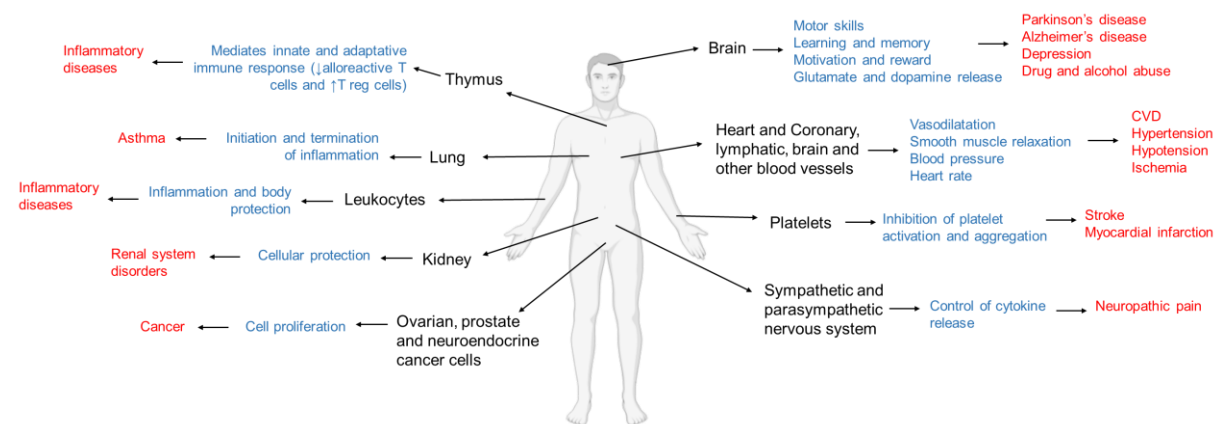
Figure 1.1. Diagram illustrating the $A_{2A}R$ distribution and location in the human body. *Tissue, organs, and cells in which the $A_{2A}R$ can be found are written in black; cellular or tissue functions of the $A_{2A}R$ are written in blue; pathological conditions in which the $A_{2A}R$ is involved, and possible therapeutic applications are written in red. Diagram produced using BioRender.*

Extracellular adenosine binds with high affinity to the $A_{2A}R$ at nanomolar concentrations to modulate inflammation, platelet aggregation, vasodilation of coronary arteries, and myocardial blood flow (causing hypotension). At the same time, it inhibits dopaminergic activity in the brain, thus affecting the central nervous system (CNS) and basal ganglia activity (Leone and Emens, 2018; Liu *et al.*, 2019; Guieu *et al.*, 2020). Nevertheless, receptor inhibition by inverse agonists activates dopaminergic activity

17

and increases inflammation, making it a potential target for treating inflammatory and neurodegenerative diseases (Bruzzese *et al.*, 2020).

To modulate these processes, the $A_{2A}R$ interacts with the α-subunit of the cytosolic heterotrimeric G_s protein. This interaction activates the G_s, which causes the dissociation of the α subunit from the βγ heterodimer to activate adenylate cyclase and the production of the secondary messenger cAMP. This activates protein kinase A (PKA), which initiates a cascade of phosphorylation as a major general pathway activated by the $A_{2A}R$. Nonetheless, the activation of specific signalling pathways may vary depending on the tissue and cell type in which the receptor is located (de Lera Ruiz *et al.*, 2014). This leads to activation of specific cellular responses (Zhao *et al.*, 2019).

The $A_{2A}R$ plays an important role in modulating the inflammatory patterns. Several studies have demonstrated the anti-inflammatory and immunosuppressive roles of different $A_{2A}R$ agonists (Wang *et al.*, 2019). The regulation of inflammation through this receptor is dependent on activation of the PKA pathway, which activates the phosphorylation of Serine Ser-133 and the translocation to the nucleus of the transcription factor CREB. This, in complex with the nuclear cofactor CBP and p300, binds to the promoter regions of cAMP responsive elements (CRE) to modulate gene expression (Morello *et al.*, 2009). Specifically, it activates the transcription of anti-inflammatory genes such as IL-10, TGF-β and FoxP3 (Jones and Kang, 2015). At the same time, it competes with one of the major mechanisms to mediate inflammation, the nuclear factor NF-kB/p65, which binds to DNA to activate the transcription of pro-inflammatory genes such as interleukin IL-1, IL-2, IL-6, IL-12, and other proinflammatory cytokines, including Tumour Necrosis Factor alpha (TNF-α) and interferon gamma (IFN-γ). Hence, the activation of the $A_{2A}R$ blocks the proinflammatory activity of NF-kB (Kermanian *et al.*, 2013; Zhao *et al.*, 2015; Ahmad *et al.*, 2017). Furthermore, the $A_{2A}R$ is expressed in a wide variety of immune cells, including macrophages, neutrophils, mast cells, natural killer (NK) cells, dendritic cells, granulocytes, and B and T lymphocytes, which also modulate inflammation (Ohta and Sitkovsky, 2014).

An important action of extracellular adenosine through $A_{2A}R$ activation is vascular smooth muscle relaxation (Sun *et al.*, 2019). This leads to vasodilation, a mechanism that regulates blood flow and heart rate (Khayat and Nayeem, 2017). Hypotension caused by low blood pressure can result in organ failure (Lehman *et al.*, 2010), whereas hypertension caused by high blood pressure is one of the main risk factors for cardiovascular diseases (CVD) (Hübner *et al.,* 2015). Thus, the smooth muscle relaxation and vasodilating action of the $A_{2A}R$, as well as its capacity to stimulate angiogenesis (Ludwig *et al.*, 2020), can help reduce the risk of suffering a stroke. The vascular endothelium accommodates all essential proteins and ion channels that regulate vascular tone (Tykocki *et al.*, 2017). Through the adenylate cyclase and PKA pathway, ATP-dependent potassium channels (K_{ATP} channels) are stimulated, which

induces hyperpolarization of smooth muscle cells, thus causing relaxation and vasodilation (Ponnoth *et al.*, 2012). It has also been demonstrated that adenosine can decrease the entry of calcium ions into the cells by blocking L-type calcium channels, which are typical cell contraction mediators (Murphy *et al.*, 2003).

Figure 1.2 represents a summary of the different signalling pathways activated by the $A_{2A}R$ when it binds adenosine to modulate inflammation, immune response, cell proliferation, platelet aggregation, and vasodilation.
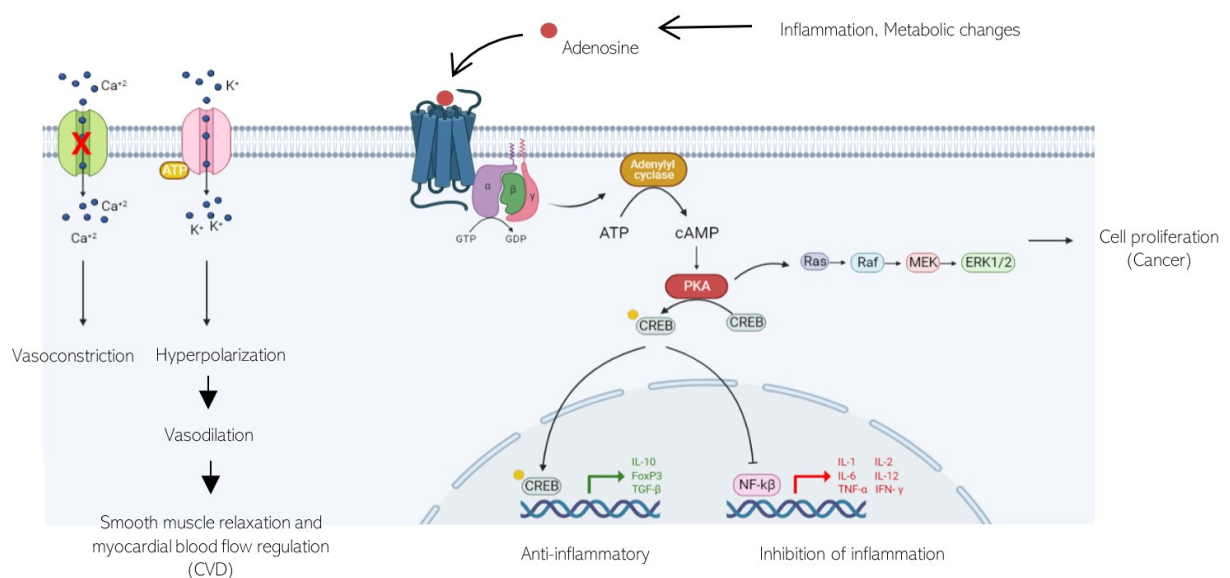
Figure 1.2. Signalling pathways activated by the $A_{2A}R$ when it binds extracellular adenosine to modulate inflammation, immune response, cell proliferation, platelet aggregation, and vasodilation. *Diagram produced using BioRender.*

1.3. Structural Characteristics of the $A_{2A}R$

GPCRs exist in a dynamic equilibrium between different activation states that are differentiated by discrete conformational changes and separated by energy barriers (Manglik *et al.*, 2015; Ye *et al.*, 2016). Although it has been found that the inactive states of diverse GPCRs are well-conserved, intermediate-active states appear to be more divergent between them (Carpenter and Tate, 2017).

In the absence of an agonist or in the presence of an antagonist, GPCRs, and specifically the $A_{2A}R$, are found in their inactive conformation (Manglik and Kruse, 2017; Weis and Kobilka, 2018). In order to be able to overcome the energy barrier for the transition from the inactive to the intermediate-active state, agonist binding to the orthosteric pocket of the receptor is required. In that event, GPCRs are able to interact with cytosolic proteins, such as the heterotrimeric G protein or β-arrestin, to reach the

I. Company Marin, PhD Thesis, Aston University 2024

fully active conformation and activate downstream signalling pathways (Prosser *et al.*, 2017). In other words, the $A_{2A}R$ exists in dynamic equilibrium between the inactive, intermediate-active, and the fully active states, which is only achieved when it binds both the agonist and cytosolic Gs protein. These findings have been possible because of the co-crystallization of the receptors in complex with binding partners, such as agonists, antagonists, and engineered cytosolic proteins and nanobodies (Steyaert and Kobilka, 2011; Carpenter and Lebon, 2017).

The $A_{2A}R$ is currently one of the most structurally characterized GPCRs, with more than 30 published structural studies. Its crystal structure has been reported in its three activation states: stabilized in its inactive conformation binding the antagonist ZM241385 (Jaakola *et al.*, 2008); stabilized in its intermediate-active conformation bound to the endogenous agonist, adenosine, and the synthetic agonists 5'-(N-Ethylcarboxamido)adenosine (NECA) (Lebon, *et al.*, 2011b) and UK-432097 (Xu *et al.*, 2011); and in its fully active conformation bound to both the agonist NECA and a mini-Gs protein, an engineered G protein (Carpenter *et al.*, 2016). A computational model representation of these structures is shown in Figure 1.3.
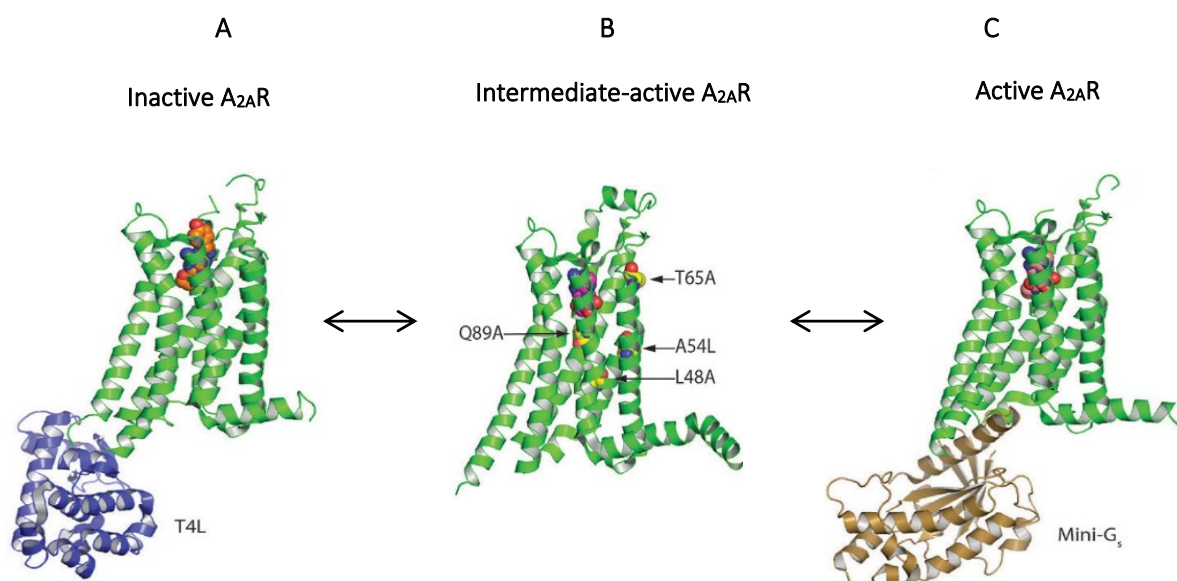
Figure 1.3. Crystallization of the $A_{2A}R$ in distinct conformations using different engineering strategies. (A) Crystal structure of the $A_{2A}R$ as a fusion protein with T4L in its inactive conformation bound to antagonist ZM241385 (Jaakola *et al.*, 2008). *(B) Crystal structure of the thermostabilized $A_{2A}R$ by point mutations in its intermediate-active conformation bound to the natural agonist adenosine* (Lebon, Warne, *et al.*, 2011b). *(C) Crystal structure of the $A_{2A}R$ complexed with a mini-Gs protein and bound to the agonist NECA in its fully active conformation* (Adapted from Carpenter et al., 2016).

The orthosteric binding pocket of the $A_{2A}R$, is highly conserved and located towards the extracellular part of the receptors (Steyaert and Kobilka, 2011). Binding of adenosine to the ligand-binding pocket triggers multiple conformational changes, mainly within the orthosteric pocket and on the intracellular

I. Company Marin, PhD Thesis, Aston University 2024

side of the receptor. Specifically, conformational changes occur in the intracellular ends of transmembrane helixes TM3, TM5, TM6, and TM7, which are essential for interaction with the cytosolic G protein (Venkatakrishnan *et al.*, 2013). This interaction is believed to stabilize the active conformation of the receptor by increasing the agonist-binding affinity in the ligand-binding pocket. However, no significant conformational rearrangements occur in the binding pocket upon G protein coupling, which suggests that the intermediate-active state of the receptor may already have a ligand-binding high-affinity conformation (Carpenter *et al.*, 2016). Even so, subtle conformational rearrangements on the extracellular side of the receptor also occur (Carpenter and Lebon, 2017; Bruzzese *et al.*, 2020).

The $A_{2A}R$ sequence contains key conserved motifs among class A GPCRs that are important for receptor activation and stability (Prosser *et al.*, 2017). The ionic lock is a salt bridge between R102 and E228 that stabilizes the inactive conformation of the receptor and is broken by the reorientation of the TM6 helix during the activation process (Carpenter *et al.*, 2016). A highly conserved hydrophobic core is formed by hydrophobic residues that cluster together in the transmembrane interior and are important for receptor stability through hydrophobic interactions. The receptor also has a conserved sodium-binding site near the ligand-binding pocket. Sodium ions (Na^+) are negative allosteric modulators of several adenosine receptors and GPCRs. This is because they can directly form polar interactions with the receptor, typically stabilizing the inactive agonist-free, or antagonist-bound conformation, which imposes a higher energy barrier for receptor activation (Katritch *et al.*, 2014). Moreover, different studies have demonstrated the importance of the interaction of water molecules with the amino acid residues of GPCRs during their activation (Liu *et al.*, 2013). Thus, a sodium-water network is formed, and its dissociation is important for receptor activation. The NPXXY motif is involved in the interaction between TM6 and TM7, and their reorientation is crucial for the activation process (Flock *et al.*, 2015). Finally, the DRY motif is located at the cytoplasmic end of the TM3 helix and is important for agonist binding and cytosolic G protein coupling (Carpenter and Tate, 2017). The amino acid sequence and structure of the $A_{2A}R$, with its conserved motifs, are shown in Figure 1.4.

Figure 1.4. Amino acid sequence and structural scheme of the A$_{2A}$R obtained from www.gpcrdb.org. The hydrophobic residues are shown in green. The ionic lock is shown in purple. The DRY motif is shown in blue. Finally, the NPXXY motif is shown in orange.

As can be seen in Figure 1.4, the A$_{2A}$R has a long extracellular Loop 2 (ECL2) which is important for ligand recognition and binding (Wheatley *et al.*, 2011; Cao *et al.*, 2018). This receptor also has an unusual long intracellular C-terminal tail, composed of a total of 122 amino acid residues, in contrast to many other adenosine receptors and GPCRs. For example, the human adenosine A1 receptor has a C-terminal tail composed of 34 residues (Bergmayr *et al.*, 2013). It has been shown that only the immediately adjacent juxtamembrane segment to the seventh transmembrane helix of the receptor is necessary for ensuring proper folding of the receptor. The other approximately 100 amino acids of the C-terminus tail are not necessary for activation of the receptor by ligand binding, G protein coupling (Klinger *et al.*, 2002), and heterodimer formation with other membrane receptors (Hinz *et al.*, 2018). Moreover, it has been suggested that this C-terminus tail is more flexible since it is not constrained by a lipid anchor, as is the case for other GPCRs. This is because in the vast majority of rhodopsin-like GPCRs a cysteine residue is found at the end of the C-terminal tail, which has been recognised as a putative palmitoylation site (Keuerleber *et al.*, 2011)

Hence, GPCRS can be directly lipidated, where lipid moieties are covalently attached to specific amino acid residues. This modification serves as a mechanism for tethering the protein to the membrane and

22

ensuring its integration and intimate association with the lipids within the lipid bilayer. Consequently, membrane proteins are profoundly influenced by their complex interplay with the surrounding lipid environment. Understanding the physicochemical characteristics of lipids in the plasma membrane is crucial to comprehend the dynamic interactions between membrane proteins and lipids, which is fundamental to their proper functioning and cellular signalling.

1.4 Biochemical Significance and Structural Diversity of Lipids in Cellular Systems

Lipids are a heterogeneous group of biomolecules that can be defined and categorized based on their chemical structure, function, solubility in organic solvents, or biosynthetic mechanisms (Fahy *et al.*, 2012). Lipids are hydrophobic biomolecules with relatively low molecular weight, commonly lower than 2000 Da, and are typically characterized by the presence of linear alkyl chains. They can be saturated or unsaturated with one or multiple double bonds in characteristic positions and can be composed of an even or odd number of carbon atoms (Sud *et al.*, 2007). Lipids can contain isoprene units in linear or cyclic structures, and can include diverse oxygenated substituents, such as hydroxyl groups and carboxylic acids, or other heteroatoms, including nitrogen in amine groups. Generally, these structures are covalently linked to glycerol, phosphate, carbohydrate, or other small polar groups, which provide amphiphilic characteristics (Liebisch *et al.*, 2020). Due to the complexity and diversity of lipids, there is a much poorer understanding of their roles and functions than that of proteins (Muro *et al.*, 2014).

Lipids have many different biological functions. They act as structural components, serve as energy storage sources in lipid droplets, and function as first and second messengers in multiple signalling pathways (Liebisch *et al.*, 2020). Lipids are key structural components of the plasma membrane and other cellular organelles. They also form trafficking vesicles such as endosomes and lysosomes (Muro *et al.*, 2014). Additionally, some lipids help in the recruitment and organization of proteins and secondary effector complexes within membranes (Van Meer *et al.*, 2008). Indeed, lipid composition can vary substantially among different cell organelles, cell types, and tissues, suggesting that lipids are function-specific (Klose *et al.,* 2013).

The complete lipid profile within a cell, tissue, or organism is defined as its "lipidome" and is a large subset of the metabolome, also comprising other biomolecules, including amino acids, carbohydrates, and nucleic acids (Tsugawa *et al.*, 2020; Wishart *et al.*, 2022). On the other hand, the term "epilipidome" is used to define a subset of the natural lipidome generated by lipid modifications through non-enzymatic and enzymatic reactions. Some examples of lipid modifications include oxidation, nitration, sulfation, and halogenation, which are essential for regulating the biological functions of lipids (Ni *et al.*, 2019).

I. Company Marin, PhD Thesis, Aston University 2024

1.4.1 Lipid Classification: From Fatty Acids to Complex Lipids

According to the LIPID MAPS classification system (Fahy *et al.*, 2005), lipids are divided into eight categories, including fatty acyls, glycerolipids, glycerophospholipids, sphingolipids, saccharolipids, and polyketides (which are derived from the condensation of ketoacyl subunits), and sterol and prenol lipids (derived from the condensation of isoprene subunits), which can be found in lipid membranes (Fahy *et al.*, 2012). Therefore, unlike proteins, which are primarily classified according to their biological function, lipids are classified based on chemical scaffolds and connectivity (Yetukuri *et al.*, 2008).

Lipids can be further subdivided into two main classes, simple and complex lipids. Simple lipids are those that give, at most, two types of primary products per mole during hydrolysis. Examples include glycerolipids and cholesterol esters. In contrast, complex lipids yield three or more primary products per mole during hydrolysis. Examples include glycerophospholipids, sphingolipids, and glycolipids. Alternatively, these two groups of lipids can be defined as "neutral" and "polar" lipids, respectively (Burdge *et al.*, 2015).

The key building blocks of most of the lipid species are fatty acids or fatty acyls (FA). The most common FA in animal and plant tissues are straight-chained with C_{16}, C_{18}, or C_{20}, and from zero to four double bonds in a *cis* configuration (Schönfeld *et al.*, 2016). These are commonly esterified forming triacylglycerols (TAG) (Ramaley *et al.*, 2021), diacylglycerols (DAG), monoacylglycerols (MAG) (Feltes *et al.*, 2013), or phospholipids (PLs) or lysophospholipids (LPL) (Sych *et al.*, 2022). PLs are the main constituents of natural cell membranes, and different phospholipid classes exist that differ in the type of polar head group linked to the phosphate moiety. They can have distinct ionic states, which influence their locations and functions within the lipid bilayers (Hishikawa *et al.*, 2014). PLs not only possess structural characteristics, but they also influence membrane protein function through direct or indirect interactions (Sych *et al.*, 2022). These include phosphatidic acid (PA), phosphatidylcholine (PC), phosphatidylethanolamine (PE), phosphatidylserine (PS), phosphatidylinositol (PI), and phosphatidylglycerol (PG) (Figure 1.5). Other lipids found in cellular membranes include cardiolipins (CL), sphingolipids, such as ceramides and sphingomyelin (SM), and cholesterol.

All the possible combinations of different hydrophobic side chains and polar head groups in esterified lipids account for much of lipid diversity. This remarkable structural diversity is reflected in the variety of lipid functions. Therefore, when investigating a specific lipid function, it is crucial to take into account its chemical structure and the contributions of the side chains and head groups (Zhang *et al.*, 2014).
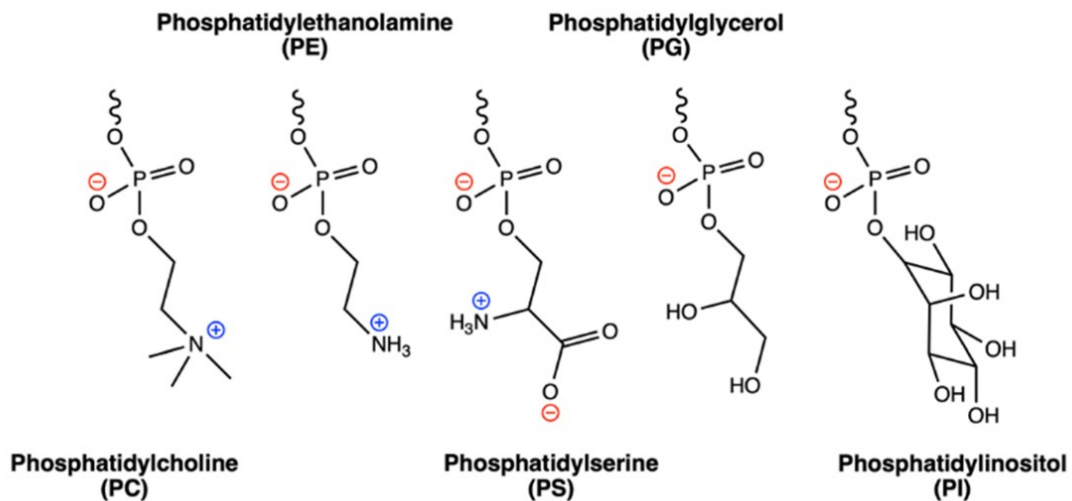
Figure 1.5. Structures of phospholipid headgroups, including phosphatidylcholine (PC), phosphatidylethanolamine (PE), phosphatidylserine (PS), phosphatidylinositol (PI), and phosphatidylglycerol (PG). Adapted from Lavington and Watts, 2020.

1.4.2 Comprehensive Insights into Plasma Membrane Structure and Functionality

Plasma membranes are complex structures composed of distinct proteins and lipids that form a lipid bilayer, which is a semipermeable barrier that isolates cells from their exterior (Casares *et al.*, 2019). These bilayers are formed owing to the amphipathic characteristics of lipids; their hydrophobic moieties tend to self-associate, whereas polar moieties interact with aqueous environments (Murate *et al.*, 2016).

There is an asymmetric distribution of lipid classes between the two bilayer leaflets, which entails functional consequences and contributes to membrane properties such as curvature or bending (Murate *et al.*, 2016). Lipid asymmetry was first proposed in 1972 by Singer and Nicolson, and is a consequence of multiple factors, including the biophysical properties of lipids, retentive mechanisms to trap lipids in a specific leaflet of the bilayer, and the existence of membrane transporters that assist lipid translocation (Singer and Nicolson, 1972; Nicolson, 2013).

The composition and organization of the plasma membrane result in an ensemble that coordinates membrane dynamics and functions. Numerous reactions for the synthesis or degradation of lipids occur in the plasma membrane, and they are involved in various signalling cascades. Hence, lipids act as signalling mediators of intracellular processes and, in numerous circumstances, they work through specific protein–lipid interactions (Grillitsch *et al.*, 2014).

1.5 Understanding Lipid-Protein Interactions and their consequences on protein activity

Lipid-protein interactions are important for membrane protein activity and play major roles in membrane function and organization. These interactions are involved in various biological processes, including cell signalling, metabolism, and transmembrane transport (Sych *et al.*, 2022).

Many membrane proteins directly interact with plasma membrane lipids through their lipid-binding motifs. Hence, specific lipids bind to membrane proteins and modulate their conformation and, consequently, their function (Yeagle, 2014). Some membrane proteins, including GPCRs and ion channels, contain conserved cholesterol-binding domains in their sequence, which have a high affinity for cholesterol-rich regions of the lipid bilayer (Laursen *et al.*, 2018; Lee, 2018; Taghon *et al.*, 2021). Another example is sphingolipids, which can bind specifically to the transmembrane domains of membrane proteins and GPCRs (Shrivastava *et al.*, 2018). Thus, the interaction of lipids with GPCRs is becoming of great interest.

Membrane protein function can also be regulated by the dynamic and collective behaviour of the plasma membrane. Lipids collectively determine the biophysical properties of membranes, hence, protein modulation by lipids goes beyond specific interactions with certain amino acids (Corin *et al.*, 2020; Fratti, 2021). Proteins can show preferences for a liquid or solid phase of the bilayer, and membrane proteins anchored by α-helix regions typically show a tendency for liquid phases (Van Meer *et al.,* 2008).

Lipids can also be divided into different subclasses according to their interaction with membrane proteins: bulk, annular, and non-annular lipids. Bulk lipids are those that do not directly interact with membrane proteins, but they contribute to a heterogeneous lipid environment that influences protein geometry and accessibility for interactors. Annular lipids are those that closely surround transmembrane domains and non-specifically interact with membrane proteins. Non-annular lipids directly interact with membrane proteins through specific lipids-protein interactions and often modulate protein conformation (Contreras *et al.*, 2011; Corradi *et al.*, 2018; Yen *et al.*, 2018). These interactions can occur on specific lipid-binding motifs or through generic electrostatic interactions between charged amino acids and lipids (Stahelin, 2009; Simcock *et al.*, 2021). These can be allosteric modulations, causing conformational changes on the protein or modifying its oligomerization state (Westerlund *et al.*, 2020). Furthermore, lipids themselves can act as protein substrates (Khelashvili *et al.*, 2020).

Different structural biology techniques can be used for the study of specific lipid-protein interactions. X-Ray crystallography has been mainly used to study the crystal structure of membrane proteins, some of which have been successfully co-crystalized with their lipid ligands (Kermani, 2021). Nevertheless,

the use of detergents is required for protein solubilization and subsequent purification and crystallization, which complicates the investigation of lipid-protein interactions, as detergents strip out the surrounding lipids (Cherezov *et al.*, 2007; Jafurulla *et al.*, 2011; Birch *et al.*, 2018). Cryogenic electron microscopy (cryo-EM) has emerged as an alternative to X-ray crystallography for studying protein structures, and it has been used to identify different protein-phospholipid interactions (Yao *et al.*, 2020; Bergh *et al.*, 2023; Biou, 2023; Sharma *et al.*, 2023). An attractive alternative for the study of lipid-protein interactions is solubilization of membrane proteins using nanodiscs or polymers forming protein-lipid particles (Unger *et al.*, 2021). Furthermore, membrane protein-lipid interactions have been probed using mass spectrometry (Bolla *et al.*, 2019).

Lipid-protein interactions can also be predicted computationally through structural prediction and simulation methods. These methods allow the recognition of lipid-binding domains from already known amino acid sequences and their characteristics such as hydrophobicity and charge. Furthermore, the affinity and orientation of lipids can be assessed by molecular docking (Tieleman *et al.*, 2021). Molecular dynamics (MD) simulations can be used for the elucidation of lipid-protein interactions. These provide information on the energetics and kinetics of lipid–protein interactions, and thus the relative probabilities of protein binding to certain lipid environments (Muller *et al.*, 2019). The influence of bulk membranes on the activity of membrane proteins can be studied by Förster resonance energy transfer (Fernandes *et al.*, 2015).

1.5.1   Insights into GPCR-Lipid Interactions

The structure, conformational dynamics, and function of GPCRs are influenced by their surrounding lipid environment. Phospholipid headgroups, acyl chain unsaturation, the presence of cholesterol or sphingolipids, and the biophysical properties of the plasma membrane, such as fluidity, thickness, and curvature, have an impact on the activity of GPCRs (Baccouch *et al.*, 2022). Lipids act as important cofactors of GPCRs as they specifically interact with a reduced number of lipids that are usually essential for their activity. The most common lipid that acts as a GPCR cofactor is cholesterol (Gimpl, 2016).

These receptors and G proteins can also be modified post-translationally by lipids. These post-translational modifications consist in the covalent binding of hydrophobic lipid molecules and comprise myristoylation, palmitoylation, and isoprenylation (Zhang *et al.*, 2022). Generally, GPCRs are palmitoylated with palmitate attached to one or multiple cysteines through thioester bonds, and usually occurs around 10-14 residues downstream of the last transmembrane domain, in the cytoplasmic C-terminal tail. Nevertheless, it can also occur in alternative regions of the protein, such as the intracellular loops. This influences membrane binding, protein trafficking, and the subsequent

I. Company Marin, PhD Thesis, Aston University 2024

activation of signalling pathways (Adams *et al.*, 2011). Therefore, these post-translational modifications are used to modulate GPCR activity. In fact, palmitoylation of the C-terminal tail affects the local conformation of the protein as it creates an additional intracellular loop, which might select for specific interactions with the G protein. In addition, it can modulate receptor phosphorylation and internalization (Goddard *et al.*, 2012). In contrast to G proteins, GPCRs do not require lipidation for membrane attachment (Vögler *et al.*, 2008).

The phospholipid headgroup charge directly influences the type of interactions established between the lipid and the receptor, such as hydrogen bonds or electrostatic interactions. Furthermore, the size and shape of the headgroups also modulate the biophysical properties of the plasma membrane, such as curvature and thickness. Some studies have suggested that the nature of the phospholipid headgroup contributes to controlling the basal activity of GPCRs affecting the equilibrium between the active and inactive states. Anionic phospholipids, including PS, PI, and PG, have been suggested to act as positive regulators of GPCRs through close interactions, whereas PE acts as a negative regulator, and PC as neutral (Dawaliby *et al.*, 2016; Jones *et al.*, 2020). Moreover, headgroups can modulate receptor interactions with G proteins and other effectors, such as β-arrestins (Baccouch *et al.*, 2022).

Polyunsaturated fatty acyl chains and cholesterol, which are located in the hydrophobic core of the membranes, have an impact on the fluidity, flexibility, packing, curvature, and ordering of the lipid bilayers, as well as the formation of microdomains or lipid rafts (Grillitsch *et al.*, 2014). Several experimental and computational studies have demonstrated the direct influence of lipid acyl chains on the activity of GPCRs and on receptor dimerization and oligomerization (Guixà-González *et al.*, 2016). Unsaturated lipids have been proposed to participate in GPCR activation by facilitating conformational changes (Yang and Lyman, 2019; Leonard and Lyman, 2021).

Due to their broad presence in the plasma membrane and their chemical properties, cholesterol molecules have a major impact on the activity of GPCRs and other membrane proteins. Specifically, cholesterol participates in regulating ligand binding affinity, the activation of downstream signalling pathways, and receptor recycling or internalization by directly or indirectly interacting with the receptors (Paila *et al.*, 2009; Geiger *et al.*, 2021; van Aalst *et al.*, 2021). Cholesterol influences GPCR activity indirectly by modulating the physicochemical properties of the plasma membrane, which is also known as indirect allosteric modulation, when it is part of the bulk lipids with respect to the receptor (Grouleff *et al.*, 2015). Additionally, cholesterol directly forms high-affinity interactions with specific amino acid residues, i.e. direct allosteric modulation (Jakubík a *et al.*, 2021), or it can modulate their activity due to its location on the annular lipids that surround the cross-sectional area of the GPCR (Paila *et al.*, 2009; Sengupta *et al.*, 2015). As cholesterol spontaneously associates with sphingolipids in the

plasma membrane, the role of cholesterol-rich lipid rafts around the GPCRs has been investigated. These allow particular physicochemical properties, increasing membrane rigidity and thickness, and enhancing lipid ordering and packing (Clarke, 2019). Consequently, membrane protein and GPCR partitioning occurs in these domains, which has an impact on receptor homo- and heterodimerization, and on the activation of downstream signalling pathways (Prasanna *et al.*, 2014).

Membrane physicochemical properties also have an impact on membrane proteins and GPCRs; the diversity in lipid structures and chemical properties influences membrane properties and dynamics, such as morphology, packing, and organization. Membrane curvature and surface tension depend closely on the shape and phospholipid headgroup volumes, as well as on the fatty acid chain region. Phospholipids with small headgroups, such as PE, tend to adopt a negative membrane curvature, whereas phospholipids with larger headgroups, such as PC, tend to adopt a more conical shape, contributing to a zero-curvature membrane. Furthermore, polyunsaturated fatty acyl chains contribute to the negative curvature of the plasma membrane (Cooke and Deserno, 2006). PE is mostly found in the inner leaflet of the bilayer, where G proteins bind to GPCRs. Hence, the presence of PE in the surrounding environment of the receptors may prevent dense packing, lower the lateral pressure, and stabilize the receptors in their favoured conformation (Brink-Van Der Laan *et al.*, 2004).

GPCRs can adapt to their lipid environment to reduce energetically unfavourable scenarios by undergoing conformational changes, resulting in the modification of their hydrophobic thickness. Consequently, lipids can reorganize around the receptor through local compression or expansion and membrane bending, which results in an optimal lipid-protein coupling (Sonntag *et al.*, 2011).

Membrane hydrophobic thickness also influences membrane protein structure and function, which is closely related to fatty acyl chain length, unsaturation, lipid heterogeneity, and the presence of cholesterol. This can result in a hydrophobic mismatch between transmembrane proteins and lipids, which occurs when the hydrophobic thickness of the transmembrane region of a GPCR does not match that of the surrounding membrane (Killian, 1998). This has energetic consequences owing to the juxtaposition of energetically unfavourable regions, so both membranes and proteins can adapt to minimize the mismatch. Membranes can deform and adjust to the length of the hydrophobic transmembrane helices, whereas proteins can undergo conformational changes or self-aggregation to prevent the exposure of specific amino acids. Moreover, proteins can also diffuse to alternative regions of the plasma membrane to satisfy the hydrophobic match (Ramadurai *et al.*, 2010; Parton *et al.*, 2011; Peruzzi *et al.*, 2022).

Membrane fluidity affects the activity of membrane proteins, GPCRs, and G-protein coupling, and it depends on the fatty acyl chain length, unsaturation, and the presence of cholesterol. Generally,

increasing the degree of fatty acyl chain unsaturation increases membrane fluidity, whereas increasing the chain length decreases it (Yoshida *et al.*, 2019; Gottesman-Katz *et al.*, 2021). Increased fluidity has been suggested to facilitate GPCR conformational changes for their activation (Yang and Lyman, 2019; Leonard and Lyman, 2021).

Understanding how lipids modulate the activity of GPCRs is crucial for their study under specific conditions, such as certain diseases that involve lipid oxidation. Examples include those characterised by oxidative stress and inflammation (Ferreira *et al.*, 2021). Moreover, the plasma membrane composition varies not only in diseases, but also with age and diet, which are closely related to oxidative stress, and makes membrane proteins behave differently in these different lipid environments (Nicolson *et al.*, 2014).

1.6 Oxidative Stress, Lipid Peroxidation, and Protein Lipoxidation

Oxidative stress is defined as an imbalance between the production of reactive species, such as reactive oxygen species (ROS), reactive nitrogen species (RNS), and other reactive species containing carbon, sulphur, and halogens, and cellular antioxidant mechanisms, such as glutathione and antioxidant enzymes (Pohl and Jovanovic, 2019). These species are highly unstable and reactive, so this imbalance may lead to pathophysiological conditions. ROS result from the partial reduction of oxygen during metabolic processes, and these can be radicals, such as hydroxyl radical (HO•) or superoxide anion radical (O_2•-), or non-radicals, such as singlet oxygen ($^1O_2$) or hydrogen peroxide (H_2O_2) (Sousa *et al.*, 2017). Nevertheless, endogenous reactive species are not only produced under pathological conditions but are also generated physiologically under normal conditions. They can be generated by the electron transport chain in the mitochondria and other metabolic enzymes localized in different cell compartments, such as the plasma membrane, peroxisomes, and endoplasmic reticulum. These enzymes include xanthine oxidase (XO), nicotinamide adenine dinucleotide phosphate (NADPH) oxidase (NOX), cyclooxygenases (COX), lipoxygenases (LOX), and the cytochrome P450 (Di Meo *et al.*, 2016; Parvez *et al.*, 2018). In addition, other environmental sources, such as xenobiotics, UV light, and ionizing radiation, can also induce ROS generation (Ray *et al.*, 2012; de Jager *et al.*, 2017). Under physiological conditions, ROS and RNS can modulate biological functions by acting as signalling molecules for energy production and cell survival, which is known as redox signalling. However, their production may increase during pathological conditions such as metabolic, immune, cardiovascular, and neurodegenerative diseases, as well as during inflammation (Griendling and FitzGerald, 2003; Ceriello, 2006; Kim *et al.*, 2015; Guzik and Touyz, 2017). Under these conditions, lipids, proteins, and DNA may be targets of oxidative modifications in all aerobic living species when their production of these reactive

species increases (Egea *et al.*, 2017). Hence, it is necessary to understand the biological effects of these oxidized biomolecules under pathological conditions (Cruciani *et al.*, 2019).

Lipids containing unsaturated fatty acyl chains, particularly polyunsaturated fatty acids (PUFAs), are vulnerable to attack by various reactive species. The process by which these reactive oxygen species attack PUFAs is known as lipid oxidation, which usually occurs under oxidative stress conditions (Zhong *et al.*, 2019). Lipid oxidation can occur enzymatically or non-enzymatically when it is mediated by carbon- and oxygen-centred radicals (Vigor *et al.*, 2014; de Bus *et al.*, 2019). Non-enzymatic mechanisms are based on adventitious oxidation that most commonly occurs on phospholipids. The attack on PUFAs by radical species is known as lipid peroxidation, in which a peroxyl radical is formed as an intermediary product (Gaschler and Stockwell, 2017). In a phospholipid bilayer environment, a single radical attack on phospholipids can entail a chain reaction based on a cascade of hydrogen abstractions and oxidations. This results in the formation of lipid peroxyl radicals and lipid hydroperoxides that are unstable and reactive. Thus, they can be readily converted into other species through subsequent reactions, including further oxidation and cleavage reactions, resulting in the formation of secondary products of lipid peroxidation (Reis & Spickett, 2012).

Multiple types of secondary products are generated, which can be classified as full-chain oxidized phospholipids, truncated fatty acyl chain phospholipids, and non-esterified breakdown products. Examples of full-chain oxidized phospholipids include 1-palmitoyl-2-(5-oxovaleroyl)-sn-glycero-3-phosphocholine (POVPC) and 1-palmitoyl-2-(9-oxo-nonanoyl)-sn-glycero-3-phosphocholine (PONPC) (Egea *et al.*, 2017). Phospholipids with a truncated fatty acyl chain include isoprostanes and isolevuglandins (Montuschi *et al.*, 2004; Salomon, 2005). Non-esterified breakdown products include small molecules that contain epoxides, hydroxides, aldehydes, ketones, and carboxylic acids as reactive carbonyl moieties (Frankel, 1987; Mol *et al*., 2019). Aldehydes, including 4-hydroxynonenal (4-HNE), malondialdehyde (MDA), and acrolein (ACR), are one of the most studied classes of lipid peroxidation products (Spickett, 2013; Ayala *et al*., 2014; Tsikas, 2017). On the other hand, some oxidized products of cholesterol, oxysterols, such as 6-cholesten-5α-hydroperoxide, 7-ketocholesterol, and 25-hydroxycholesterol, can also be generated under a redox imbalance (Iuliano, 2011).

Products of lipid peroxidation that contain aldehydes or α,β-unsaturated alkenal moieties are unstable and highly reactive, resulting in toxicity based on their ability to form covalent adducts with other molecules (Hossain *et al.*, 2019). Lipoxidation refers to the process by which covalent adducts between lipid oxidation reactive products and nucleophilic moieties on biomolecules such as proteins, DNA, and phospholipids are generated via different mechanisms (Viedma-Poyatos *et al.*, 2021). Proteins are not only modified by small and free aldehydes but also by oxidized products esterified in phospholipids

(Vistoli *et al.*, 2013). The propensity of the adduct to form depends on the reactivity of the lipid oxidation product, nucleophilicity of the amino acid in the protein that is suffering the attack, and stability of the generated product (Martyniuk *et al.*, 2011).

Lipoxidation involves the formation of Schiff Bases and Michael adducts on specific nucleophilic groups in the proteins. Typically, Schiff base formation occurs when aldehyde or ketone groups from lipid oxidation products react with the primary amines of proteins, which means that this mechanism takes place on lysine residues and the amino group of the amino-terminal extreme of the protein chain. Alternatively, Michael adducts occur between the β-carbon of an α,β-alkenal and a nucleophilic group of protein residues, usually lysine, cysteine, and histidine residues (Vazdar *et al.*, 2019; Alviz-Amador *et al.*, 2019). Figure 1.6 schematically represents the amino acid residues in a protein that are more likely to undergo lipoxidation through different mechanisms of Schiff base formation and Michael addition.
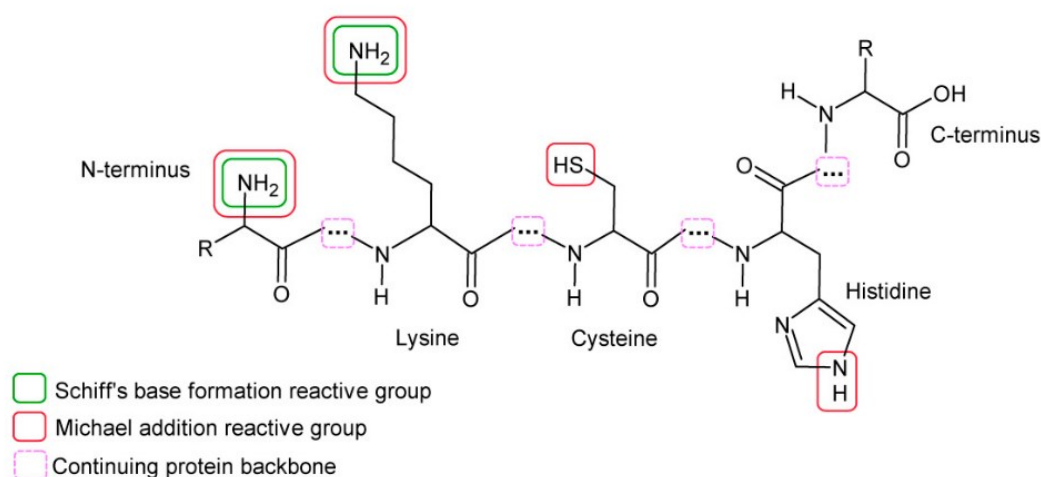
Figure 1.6. Representation of potential amino acid targets of lipoxidation in proteins by Schiff base formation or Michael addition (reproduced with permission from Viedma-Poyatos et al., 2021).

Proteins serve a large array of different functions in the cellular and extracellular contexts, and a key reason for this diversity is their capacity to undergo post-translational modifications. Protein lipoxidation is an example of a post-translational modification (Pérez-Sala, 2019). Consequently, proteins can experience alterations in their structure and function as a result of this covalent modification, which may entail different downstream cellular effects (Patinen *et al.*, 2019; Parvez *et al.*, 2018).

Modification of nucleophilic residues in the active site of enzymes or nearby tends to cause a loss of enzymatic activity by altering the active conformation or blocking substrate binding (Sousa *et al.*, 2019; Aluise *et al.*, 2015). On the other hand, lipoxidation not only produces deleterious effects, but can also

32

activate proteins and specifically receptors, thereby affecting cellular behaviour (Mol *et al.*, 2019). In addition, it can alter protein-protein interactions, which also results in changes in cell signalling (Spickett, 2020).

Reactive oxidized lipids can also alter the secondary structure of proteins causing conformational changes, which tends to give rise to protein unfolding and aggregation (Moldogazieva *et al.*, 2019). Furthermore, although lipid peroxidation products are initially likely to attack nucleophilic residues of proteins located on their surfaces, it is well known that small aldehydes can insert into their binding pockets, leading to protein instability and unfolding. Consequently, the exposure of typically hidden residues increases, so the protein becomes more vulnerable to further modifications (Takasugi *et al.*, 2019). All of these protein alterations and their physiological consequences, including the modification of catalytic residues, conformational changes, aggregation, and unfolding, are summarized in Figure 1.7.
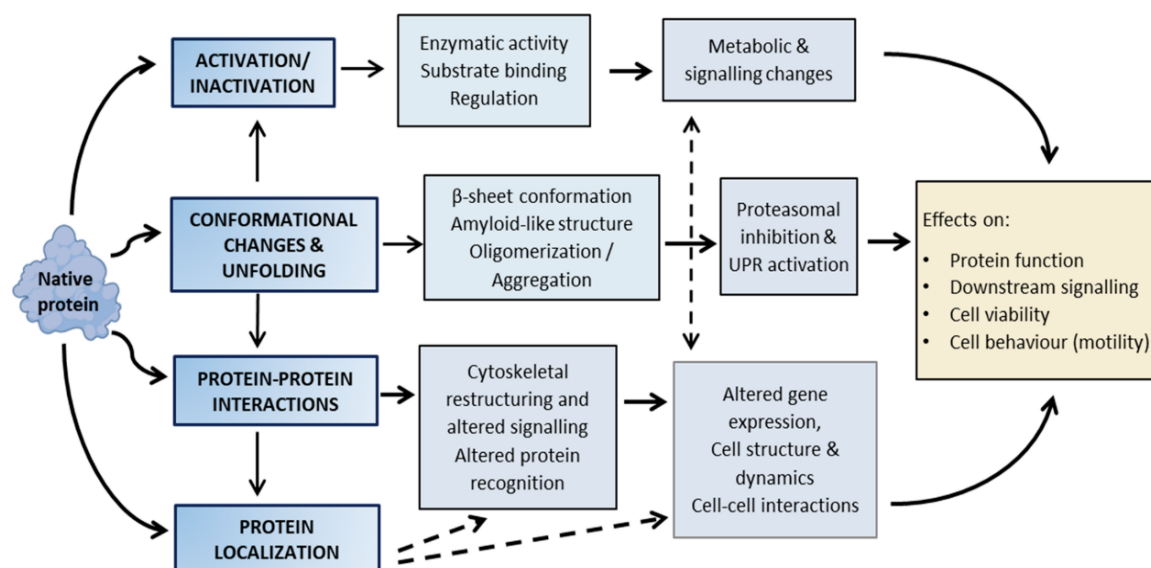
Figure 1.7. Summary scheme of protein lipoxidation consequences (reproduced with permission from Viedma-Poyatos *et al.*, 2021).

Although lipoxidation is currently a well-known process that has been thoroughly studied for many proteins, the interaction of lipid peroxidation products with mammalian membrane proteins, and how their structure, function, and activity are affected by the formation of these covalent adducts is still lacking deep research, and especially regarding the $A_{2A}R$. Multiple studies on the interaction of this mammalian receptor with lipids in the cell membrane environment and how its activity, function, and structure can be modulated by these interactions have been reported. Notwithstanding, the interaction of the receptor with oxidised lipid under oxidative stress conditions has been poorly studied thus far.

I. Company Marin, PhD Thesis, Aston University 2024

Thus, there is still a lack of knowledge about which lipid peroxidation products can bind and interact with the $A_{2A}R$ and how this covalent modification can alter the activity and function of the receptor.

1.7 The Study and Characterization of the $A_{2A}R$ and other membrane proteins

1.7.1 The Expression of Recombinant Proteins

Studies on the structure of membrane proteins, such as GPCRs, and their possible interactions with oxidized lipids require efficient overexpression of membrane proteins, so they can be extracted, purified, and analysed. Different expression systems for recombinant proteins can be used, including bacteria, yeast, and mammalian cells. The expression of recombinant proteins in mammalian cells, such as human embryonic kidney HEK293T cells, offers some advantages over other expression systems. HEK293T mammalian cells are derived from HEK293 cells, a specific cell line for Human Embryonic Kidney cells. They have a propensity for transfection and reliable growth. Consequently, they have been extensively used in biological research and the biotechnology industry for pharmaceutical and biomedical purposes. Furthermore, they can produce relatively high amounts of recombinant protein. This cell line has been employed for the heterologous expression of active GPCRs in consistent amounts for structural analysis, although these receptors are naturally expressed at low levels (Suzuki *et al.*, 2011; Chakraborty *et al.*, 2015; Jamshad *et al.*, 2015; Goulding *et al.*, 2018). Human HEK293T cells offer a native cellular and membrane environment for GPCR expression, as well as protein folding, trafficking, and post-translational modifications. Nevertheless, they are relatively expensive and difficult to scale, and possible complications from endogenous receptors and signalling components may occur (Tapaneeyakorn *et al.*, 2011).

The use of yeast as an expression system has become an attractive alternative to mammalian cells in recent years. The yeast *Pichia pastoris* has been extensively used as a recombinant protein expression system, surpassing the use of *Saccharomyces cerevisiae*. *P. pastoris* is a methylotrophic yeast that can utilize methanol as a sole carbon source through the alcohol oxidase (AOX) (Schwarzhans *et al.*, 2017). Two different genes encode the alcohol oxidase, AOX1 and AOX2, with AOX1 the most active in cells (Cregg *et al.*, 1989). *P. pastoris* cells that express intact AOX1 and AOX2 show efficient growth in presence of methanol and are phenotype Mut$^+$. In contrast, *P. pastoris* cells expressing and using AOX2, while having the AOX1 gene disrupted, are Mut^S (slow) and exhibit slower growth in the presence of methanol. Finally, strains with disrupted AOX1 and AOX2 genes are unable to grow in the presence of methanol, and their phenotype is Mut$^-$ (Krainer *et al.*, 2012). The promoter that regulates the expression of alcohol oxidase is the AOX1 promoter, which is methanol inducible. Instead, it is inhibited

in the presence of glucose or glycerol, which allows the induction of protein expression to be separated from the growth phase. (Juturu and Wu, 2018).

P. pastoris SMD1163 is a protease deficient strain (his4, pep4, and prb1) with Mut$^+$ phenotype and so it can reliably grow in presence of methanol. This strain has been extensively used for heterologous protein expression by inducing the AOX1 promoter with methanol (Chang *et al.*, 2018).

One of the aspects that must be considered when expressing heterologous proteins under the AOX1 promoter is that, once *P. pastoris* cells are transformed with the linearized plasmid, homologous recombination between the AOX1 promoter of the plasmid and the AOX1 promoter of the host genome may occur, resulting in the insertion of the gene of interest into the genome through single crossover events. Consequently, stable transformants are generated (Chen *et al.*, 2014). This may occur, for example, when using a pPICZ vector. A schematic representation of this process is shown in Figure 1.8.
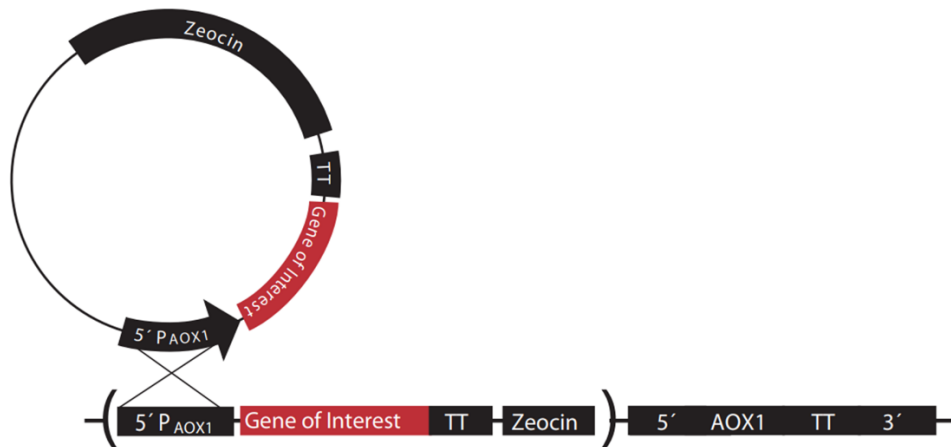
Figure 1.8. Schematic representation of homologous recombination and insertion of the gene of interest into Pichia pastoris genome in the event of transforming cells with a linearized plasmid containing the AOX1 promoter. Adapted from EasySelect™ Pichia Expression Manuals (2010).

One of the advantages of *P. pastoris* is that it can grow to high densities in short periods of time and can be adapted to large-scale fermentation, as well as being low cost, easy to manipulate*,* and non-pathogenic (Tab *et al.*, 2018). Furthermore, it can process, fold, and perform post-translational modifications on proteins, such as glycosylation, without hyperglycosylating (Karbalaei *et al.*, 2020). However, they do not provide a native cellular environment for mammalian proteins, and they have a thick cell wall that can be difficult to break.

Yeasts are eukaryotic organisms and, thus, share common cellular characteristics with higher eukaryotes. Their plasma membrane lipid composition is close to that of mammalian cells, offering a

I. Company Marin, PhD Thesis, Aston University 2024

suitable environment to produce mammalian membrane proteins (Hanson *et al.*, 2008; Baumann *et al.*, 2011). *P. pastoris* shares a typical plasma membrane structure with mammalian cells, based on asymmetrically arranged phospholipids together with sterols and sphingolipids as structural components (Malinsky *et al.*, 2010; Ziółkowska *et al.*, 2012).

In contrast to *S. cerevisiae*, which can only produce monounsaturated fatty acids, the plasma membrane of *P. pastoris* also contains polyunsaturated fatty acids (PUFA). These PUFA may contribute to a favourable environment for exocytotic and secretory processes (Ivashov *et al.*, 2013). Consequently, owing to their similarities to mammalian cells regarding the plasma membrane, *P. pastoris* have evolved as a model for the study of membrane proteins and their interaction with membrane lipids (Carlesso *et al.*, 2022).

However, one of the main differences between *P. pastoris* and mammalian cells, is that *P. pastoris* commonly produces ergosterols instead of cholesterol, which play a key role in the stability of a range of membrane proteins and GPCRs (Hanson *et al.*, 2008; Baumann *et al.*, 2011). Ergosterol structurally differs from cholesterol in that it contains an additional double bond in the steroid nucleus and alkyl side chain, together with an extra methyl group (Luchini *et al.*, 2020). These two sterols also differ in their interaction with other phospholipids in the plasma membrane, such as phosphatidylcholine (PC) (Hung *et al.*, 2016). Several studies have demonstrated that ergosterols have a stronger effect in condensing different PC phospholipids, as it has a more effective effect in ordering hydrocarbon chains (Czub *et al.*, 2006). Nevertheless, other studies have reported the opposite effect (Cournia *et al.*, 2007). Similar to cholesterol, ergosterol is a hydrophobic and rigid molecule that effectively influences the biophysical properties of membranes (Ermakova *et al.*, 2017). It is believed that the *P. pastoris* plasma membrane is characterized by relatively high fluidity since it has poor ergosterols content in combination with the presence of polyunsaturated fatty acids (Grillitsch *et al.*, 2014).

P. pastoris also has some differences in the sphingolipid content compared to mammalian cells. Substantial differences have been found in the composition of the long chain base of neutral sphingolipids and phosphosphingolipids, as well as in the length of the amide-linked acyl chains. Hence, hydroxylated or non-hydroxylated, very long chain C24:0 and C26:0 fatty acids have been found in *P. pastoris* and *S. cerevisiae* (Ternes *et al.*, 2011; Adelantado *et al.*, 2017). In contrast to mammalian cells, which contain sphingomyelin as the main sphingolipid, the *P. pastoris* plasma membrane harbours almost exclusively inositolphosphoryl-containing ceramides, together with minor amounts of hexosylceramides (Guo *et al.*, 2022). In consequence, the structural differences between these sphingolipids might influence lipid raft formation, in which sphingolipids associate with sterols and play an important role in the secretory process (Baumann *et al.*, 2011; Grillitsch *et al.*, 2014).

Despite the differences in the plasma membrane composition compared to that of mammalian cells, *P. pastoris* has been used to express multiple G-protein coupled receptors (GPCRs) for both structural and functional characterization and, specifically, for the expression of the A$_{2A}$R (Hino *et al.*, 2012; Bertheleme *et al.*, 2015). The recovery of a functional protein from host cells is dependent upon the proper functioning of the transcription, translation, and folding pathways (Hussain *et al.*, 2014). This process may be affected by many variables, such as the medium composition, temperature, pH, oxygenation of the culture, and inducer concentration. Higher protein yields are typically achieved in complex media by decreasing culture temperatures and maintaining high oxygenation of the culture in specific flasks. Furthermore, certain improvements have been reported following the addition of dimethyl sulfoxide (DMSO), histidine, and protein-specific ligands (Freigassner *et al.*, 2009).

For downstream applications, different tags can be incorporated into the construct; a frequently used tag for recombinant membrane proteins is the polyhistidine tag, which facilitates rapid purification by metal chelate chromatography using Nickel-nitrilotriacetic acid (Ni–NTA) resins (Routledge *et al.*, 2016).

1.7.2 Solubilization of Membrane Proteins – The Use of Polymers Against Traditional Detergents

The study of membrane proteins requires their solubilization and isolation from the membrane. Hence, the location of these proteins within lipid bilayers has hindered the study of their structure and function in comparison to the easier-to-isolate soluble proteins. Traditionally, membrane protein solubilization has been achieved using detergents, which substitute the protein-surrounding lipids in their hydrophobic regions by forming micelles (Pollock *et al.*, 2018). As specific lipid-protein interactions occur between membrane proteins and their close-associated lipids, their characterization should be performed in their native environment (Grime *et al.*, 2020a). This cannot be accomplished by using detergents as they strip away closely associated lipids, perturbing protein conformation and instability. This can be particularly problematic for GPCRs (Wheatley *et al.*, 2016), which need to be studied in an environment closer to their physiological context (Hauser *et al.*, 2017). In detergent solutions, many proteins have been shown to lose their activity, probably due to the loss of lateral pressure usually provided by the membrane (Brink-Van Der Laan *et al.*, 2004). In addition, finding the optimal detergent and optimizing the extraction and solubilization of a protein, while maintaining its structure and function, can be challenging as it requires a time-consuming and costly screening approach that is highly protein-specific (Hardy *et al.*, 2018).

A new alternative approach for the extraction of membrane proteins to conventional detergents has been developed using a styrene-maleic acid (SMA) copolymer, which was first reported in 2009 by Knowles *et al.* (2009). This copolymer is able to insert into the plasma membrane, forming small discs

I. Company Marin, PhD Thesis, Aston University 2024

of bilayer (~10 nm in diameter) encircled by the polymer surrounding membrane proteins, which are termed native nanodiscs, lipodiscs, or SMALPs (SMA lipid particles) (Jamshad *et al.*, 2015). The SMA polymer consists of a mixture of hydrophobic styrene and hydrophilic, charged maleic acid moieties, which provide the polymer with amphipathic properties. SMA polymers with both 2:1 and 3:1 styrene:maleic acid ratios have been successfully used to date (Vargas *et al.*, 2015). SMA has been used to effectively solubilize membrane proteins in a wide range of different expression systems, including bacteria, yeast, insect, plant, and mammalian cells (Unger *et al.*, 2021).

One of the main advantages of extracting membrane proteins using SMA2000 is that it retains the surrounding lipid bilayer. Furthermore, SMALPs are soluble, stable, and small particles that make them amenable to many downstream applications (Gulati *et al.*, 2014). For example, proteins encapsulated and solubilized with SMA containing an affinity tag can be purified by affinity chromatography, meaning that the protein of interest can be isolated in its lipid environment for subsequent studies (Rothnie, 2016). Thus, SMA provides an attractive alternative to conventional detergents for the solubilization and purification of membrane proteins, thereby enhancing their thermostability (Jamshad *et al.*, 2015). Furthermore, it provides insights into the structural, functional, and mechanistic details of protein-lipid interactions (Teo *et al.*, 2019; Routledge *et al.*, 2020).

SMALP-encapsulated proteins have been proved to be folded and active through different functional and structural techniques, such as radioligand and spectroscopic binding assays, mass spectrometry, and fluorescence correlation spectroscopy (Logez *et al.*, 2016; Unger *et al.*, 2021). However, the use of SMA also has limitations. It is sensitive to divalent cations, such as Mg^{2+}, which causes the precipitation of the polymer at 5 mM Mg^{2+} (Routledge *et al.*, 2020). SMALPs are also sensitive to pH below 7; under acidic environments, the maleic acid groups become protonated, causing the polymer to precipitate. This can be inconvenient for the study of proteins that require divalent cation binding or acidic conditions. An appropriate concentration of SMA is required for the solubilization of a target protein, as an excess of free SMA can interfere with the effective binding of SMALPs to antibodies or affinity resins for downstream applications (Gulamhussein *et al.*, 2019). In addition, the reliability of identifying co-purified lipids remains to be confirmed. This is because it is not yet clear whether SMA has a bias towards solubilising specific lipids, which can also depend on different parameters such as membrane fluidity (Dominguez Pardo *et al.*, 2017b). Moreover, lipids can diffuse between individual SMALPs (Hazell *et al.*, 2016; Cuevas Arenas *et al.*, 2017).

Owing to these limitations, multiple polymer modifications have been investigated, including diisobutylene maleic acid (DIBMA) (Stroud *et al.* 2018). DIBMA contains aliphatic diisobutylene in place of aromatic styrene moieties, offering several advantages: the diisobutylene moiety allows UV

I. Company Marin, PhD Thesis, Aston University 2024

spectroscopic studies without absorption contributions from the styrene group in the polymer belt. Furthermore, it causes less perturbation of phospholipid bilayer dynamics in the nanodiscs than SMA since the aliphatic group generates slightly larger discs. In addition, DIBMA does not precipitate in the presence of divalent cations; therefore, it is compatible with many biochemical assays that require them (Wheatley *et al.*, 2016). Similar to SMA, DIBMA is able to solubilize membrane proteins and lipids efficiently directly from the cell membrane, forming DIBMA lipid particles (DIBMALPs), which can harbour a broad range of natively folded and functionally active integral membrane proteins (Oluwole, Danielczak, *et al.*, 2017). These observations make DIBMA an attractive alternative to SMA, and suggest a new range of alternatives for the functional groups as a hydrophobic moiety of the polymer (Stroud *et al.,* 2018).

1.8 Knowledge gap, aims, and objectives

Although it is well accepted that the $A_{2A}R$, as a prototypical GPCR, is modulated by lipids in the plasma membrane, and some computational studies have demonstrated the influence of different phospholipid classes in its activity (Bruzzese *et al.*, 2020), there is still a lack of a deep experimental characterization of the lipids that closely surround the $A_{2A}R$. Furthermore, there is a need for understanding their susceptibility to oxidation or modifications, and how the modifications of these lipids or the receptor under oxidative stress can affect the activity of the $A_{2A}R$. Investigating the lipids that surround the receptor to understand their relevance in protein conformation and activity, studying their susceptibility to modification under oxidative stress, and how this affects the activity of $A_{2A}R$, is crucial for contributing to the development of new therapeutic strategies.

The overarching aim of this project was to investigate the interaction of lipids in the plasma membrane with the $A_{2A}R$ and the effects of lipid oxidation and protein lipoxidation on its activity. Consequently, the aims and objectives of the work presented in this thesis were as follows:

The first aim was to produce and isolate the $A_{2A}R$ from the plasma membrane, conserving its native lipid environment for characterization. To this end, the objective was to optimize protein expression, solubilization, and purification, as well as to confirm the $A_{2A}R$ identification as an initial step for further experiments.

The second aim was to experimentally characterize the lipid environment surrounding the $A_{2A}R$. Hence, the objective was to extract and identify the lipids that closely surround the receptor by liquid chromatography coupled to tandem mass spectrometry (LC-MS/MS), and compare them to the bulk membrane lipids to determine whether there were differences resulting from a specific receptor lipid environment.

I. Company Marin, PhD Thesis, Aston University 2024

The third aim was to study the effects of lipid oxidation and protein lipoxidation on the activity of the $A_{2A}R$ in vitro. Consequently, the objective was to investigate conformational changes of the receptor, its thermostability, and ligand-binding capability, and how these can be affected by oxidation.

The fourth aim was to investigate the effects of lipid oxidation and protein lipoxidation on the function of the $A_{2A}R$. With this purpose, the objective was to express the $A_{2A}R$ in a mammalian expression system, and characterize the activation of downstream signalling pathways under physiological and oxidative stress conditions.

2. CHAPTER 2 – EXPRESSION, SOLUBILIZATION, PURIFICATION AND IDENTIFICATION OF THE ADENOSINE 2A RECEPTOR

2.1 INTRODUCTION

2.1.1 Disruption of P. pastoris cells to obtain the membrane fraction

When coping with membrane protein expression in *P. pastoris*, preliminary preparation of the membrane fraction is the first approach. The first step is to break the protective cell wall, which is thick, robust and detergent-resistant (Bornert *et al.*, 2012). This preliminary step is crucial for downstream extraction and purification of membrane proteins, and it involves cell lysis procedures that can be more or less effective. Harsh mechanical conditions, such as those used in this study, are commonly used since they are quick and cheap. However, these mechanical methods can result in uncontrolled and undesired events, such as shear forces and heat, which may affect the integrity of membrane proteins (Wu *et al.*, 2015; Mao *et al.*, 2004; Kim *et al.*, 2013; Öztürk *et al.*, 2019). On the other hand, enzymatic treatments, using Zymolyase, Helicase or Lyticase, might avoid objectionable consequences, but they are more expensive, so they are not ideal for large-scale cultures (Wagner *et al.*, 2017). Therefore, mechanical methods were chosen for testing in this study.

2.1.2 Purification Strategies for His-Tagged Proteins

Purification of recombinant proteins is usually required for a wide variety of downstream applications, such as protein characterization, and structural and functional assays. Immobilized metal affinity chromatography (IMAC) is one of the most commonly used methods to purify recombinant proteins (Pina *et al.*, 2014), which are usually expressed with fused affinity tags to the N- or C-terminus and allow detection and purification (Spriestersbach *et al.*, 2015).

One of the most commonly used tags is His-tag, which consists of an epitope containing six or more consecutive histidine residues (Waugh, 2005). This has been extensively used for the purification of the A$_{2A}$R (Jamshad *et al.*, 2015; Routledge *et al.*, 2020). Indeed, the fusion of tags to a protein of interest can influence its expression, folding, stability, solubility, and activity, among other factors, depending on the position, sequence, length, and structure of the tag (Block *et al.*, 2009). Nevertheless, His-tag does not interfere with these parameters as it is small and uncharged at physiological pH values. Thus, it is compatible with multiple downstream applications (Carson *et al.*, 2007). Although the most common His-tag consists of six consecutive histidine residues, a different situation has been observed in the study of membrane proteins. These usually require longer tags or the use of linkers owing to their structure and because they are surrounded by membrane lipids or detergent micelles after solubilization (Mohanty and Wiener, 2004).

Purification of His-tagged proteins by IMAC is based on the affinity of histidine residues for immobilized metal ions, such as Ni^{2+} or Co^{2+}. This concept was first formulated and its feasibility was demonstrated by Porath *et al.* (1975). For this purpose, metal ions are immobilized on chromatographic matrices or resins by a chelating ligand, typically nitrilotriacetic acid (NTA) or iminodiacetic acid (IDA) (Spriestersbach *et al.*, 2015). NTA is usually preferred since it contains four metal-chelating sites, whereas IDA has only three; thus, metal ions establish more stable bonds with NTA, which results in reduced ion leaching. The NTA ligand coordinates Ni^{+2} with four valences; therefore, two valences are available for interaction with the imidazole rings belonging to histidine residues (Block *et al.*, 2009).

Considering that Ni-NTA resins can bind and retain proteins with enriched histidine domains, purification of recombinant His-tagged proteins from other proteins in a sample using NTA-based supports represents the most important application of IMAC in biological research. Ni-NTA IMAC permits the purification of proteins under native or denaturing conditions as the affinity of the His-tag toward Ni-NTA depends only on its primary structure (Hochuli *et al.*, 1988). Due to the high specificity and affinity of the His-tag, a single IMAC purification step can be sufficient to achieve reasonably efficient purification (Spriestersbach *et al.*, 2015). Furthermore, this technique allows the purification of recombinant proteins under oxidizing or reducing conditions and scalability of the purification procedure (Block *et al.*, 2009).

Despite its broad compatibility, IMAC has some limitations: the purification process may require optimization, especially if poorly expressed proteins are to be purified. Moreover, chelating agents in the sample preparation, such as ethylenediamine tetraacetic acid (EDTA), which is usually used as a strong metalloprotease inhibitor, should be avoided, or applied at low concentrations. Additionally, care should be taken with the use of other potentially chelating groups, such as Tris, ammonium salts, and certain amino acids. This is because interaction of the His-tagged proteins with the IMAC ligand can be influenced by the grade of accessibility of the tag, as well as the overall number of chelating residues on the surface of the protein (histidine, cysteine, aspartate, and glutamate). Thus, amino acids close to the His-tag, as well as the position of the tag in the N- or C-terminal tail, are of great importance (Bolanos-Garcia and Davies, 2006).

Once the His-tagged protein of interest is bound, the resin is usually washed with an appropriate buffer containing low concentrations of imidazole to remove non-captured proteins, and the elution and recovery of captured His-tagged proteins are accomplished by using a high concentration of imidazole. Imidazole is the most common elution agent, although a low pH or an excess of strong chelators can also be used (Bornhorst and Falke, 2000).

One of the main drawbacks of using Ni-NTA IMAC purification is the presence of co-purifying contaminants, which can interfere with downstream applications, such as binding assays, functional studies, and crystallography (Wagner *et al.*, 2012). This generally occurs in samples from eukaryotic expression systems due to the higher natural abundance of endogenous proteins containing consecutive histidine residues or metal-binding motifs, compared to bacterial systems (Crowe *et al.*, 1994). Thus, proteins that naturally display motifs suitable for interactions with an immobilized metal ion on their surface may bind to the resin. Nevertheless, co-eluting contaminants typically have a slightly lower binding affinity than His-tags. In many instances, these contaminants can be removed, or their adsorption can be prevented early by optimizing the procedure using more stringent binding, washing, and elution conditions. For example, the buffer, imidazole, and salt concentrations can be modified for purification optimization (Spriestersbach *et al.*, 2015). Performing additional purification steps, adjusting the protein-to-resin ratio, using an alternative support, or combining IMAC with size exclusion chromatography are also alternative approaches (Block *et al.*, 2009). Furthermore, an engineered host strain that does not express certain proteins can be used for the expression of the recombinant protein of interest. Chen et al. generated gene knock-outs *P. pastoris* strains that minimized the presence of yeast contaminating proteins and allowed rapid downstream purification of a target protein (Chen *et al.*, 2014).

2.1.3   *Protein Identification through Mass Spectrometry: Techniques, Methods, and Applications*

Proteins are essential functional entities in biological systems, and understanding their functions and roles is crucial in biochemistry. A fundamental requisite for comprehending the function of a given protein is the ability to accurately identify it with high stringency. Proteins, apart from their linear amino acid chains, fold into countless shapes, adopt multiple conformational states, and are influenced by numerous post-translational modifications, making identification particularly challenging (Khoury *et al.*, 2011).

Historically, the identification and quantification of proteins have been achieved using antibodies or associated affinity-based technologies to detect their antigens. Nevertheless, significant limitations of the use of commercial antibodies have recently been highlighted, including non-specific binding, cross-reactivity, poor characterization, and low sensitivity (Weller, 2016). In recent years, protein sequencing by mass spectrometry and its associated technologies has emerged as a new approach to validate protein identification (Huang *et al.*, 2012).

Proteomics is a branch of biochemistry that aims to identify, characterize, and quantify proteomes expressed by specific cells, tissues, or organisms under defined conditions (Anderson and Anderson,

I. Company Marin, PhD Thesis, Aston University 2024

1998). Thus, MS is an analytical technique widely used in proteomics with improved sensitivity and detailed data generation. Its principle in proteomics is based on measuring the m/z ratio of peptides in a gaseous and ionized state in a vacuum environment. Using bioinformatics tools, a complete amino acid sequence of a protein and its post-translational modifications can be defined (Noor *et al.*, 2021). Shotgun proteomics is a strategy based on digesting proteins into peptides, followed by peptide sequencing by tandem mass spectrometry (MS/MS), which allows higher data throughput and better protein detection sensitivity. MS/MS has recently become the method of choice for the identification and quantification of proteins (Washburn *et al.*, 2001).

Most biological samples consist of a highly complex mixture of biomolecules, which are required to be separated prior to their MS/MS analysis. Hence, large complex samples are usually pre-fractioned, and proteins of interest are isolated by affinity purification and electrophoresis, among other analytical techniques. The first step of the shotgun proteomics method is the digestion of proteins into peptides using proteolytic enzymes, such as trypsin or chymotrypsin, although the resulting peptide mixtures can be complex (Nesvizhskii, 2007). Therefore, peptide samples are typically separated by liquid chromatography (LC) and transferred to a mass spectrometer as they are released from the column. In standard MS for protein identification, the LC of choice is often reverse-phase liquid chromatography (RPLC), consisting of an aqueous mobile phase that is more polar than the stationary phase. The sample mixtures are then separated by a progressive transition from aqueous to organic composition of the mobile phase (Nesvizhskii, 2007). Electrospray ionization is a commonly used ionization method in proteomics (Tycova *et al.*, 2021). Subsequently, peptides are subjected to sequencing by MS or MS/MS data-acquisition processes (Nesvizhskii, 2007). In MS/MS, fragmentation is induced by providing additional energy to the precursor ions. Peptide bonds are typically fragmented at three different positions; product ions are named "a-x" when ions are formed by bond cleavage between $C\alpha$ and carbonyl carbon, "b-y" if the cleavage occurs between carbonyl carbon and nitrogen, and "c-z" between nitrogen and $C\alpha$. Hence, fragmentation forms the core of MS sequencing and peptide or protein identification (Liu and Schey, 2008). Mass analysers, including quadrupole (Q), time-of-flight (ToF), and ion traps, are commonly used in proteomics (Noor *et al.*, 2021). Thus, the acquired MS/MS spectrum is a record of the m/z values and intensities of the ions corresponding to the fragmented peptides (Noor *et al.*, 2021).

Mass spectrometric data acquisition, processing, and post-data analysis are carried out using bioinformatics tools (Deutsch *et al.*, 2008; Chen *et al.*, 2020). The sequence database search approach, spectral matching, and de novo sequencing are examples of different data analysis methods (Dančík *et al.*, 1999; Chen *et al.*, 2001; Allet *et al.*, 2004; Verheggen *et al.*, 2016). Sequence database search is based on peptide identification by searching for the fragmentation pattern encoded by the MS/MS

spectrum against protein sequence databases (UniProt and NCBI). This allows the identification of the amino acid sequences. For this purpose, all possible peptide sequences with similar m/z values are selected for investigation. The fragmentation spectra generated by MS/MS are then matched to the theoretical ion spectra of the preferred peptides. In this way, matching profiles are generated, which receive calculated scores used to examine the resemblance between the two spectra (Islam *et al.*, 2017). There is a need to statistically validate peptide-spectrum matches to determine the correct identifications with high confidence and to avoid misidentifications. There are multiple scoring schemes already incorporated in search tools, such as Mascot, and scores depict the measure of similarity between peptide sequences and spectra (Noor *et al.*, 2021). Although protein identification has become much easier in recent years, it still presents various data interpretation challenges, including high rates of false-positive identifications produced by software tools or incorrect instrument setup, incorrect conversion of data, and suboptimal search parameter setup, including the choice of search database, quality of database, and low stringency thresholds (Audain *et al.*, 2017).

2.2 AIMS AND OBJECTIVES

The objectives of this study encompass several key aspects. The first objective for this chapter was to express the $A_{2A}R$ in *P. pastoris* SMD1163. Subsequently, the focus was on isolating the *P. pastoris* membrane fraction containing the $A_{2A}R$, and comparing the effectiveness of different agents such as the detergent Dodecyl Maltoside (DDM) and the polymers SMA2000 and DIBMA for receptor solubilization. Another critical objective was to optimize the purification process of the solubilized $A_{2A}R$ through affinity chromatography. Finally, the last objective was to identify the purified $A_{2A}R$ by LC-MS/MS to confirm successful expression and purification.

2.3 METHODS

2.3.1 Plasmid for the expression of the $A_{2A}R$

The de-glycosylated C-terminal truncated $A_{2A}R$ (A316) was previously cloned into a pPICZB plasmid by Bawa *et al.* (2014).The construct was designed with multiple tags, including deca-histidine, FLAG, and biotin tags, and included a Kozak consensus sequence, bovine pancreatic trypsin inhibitor (BPTI) sequence, thrombin, and TEV cleavage sites, and two Gly-Ser linkers (Figure 2.1).

2.3.2 Expression of the A$_{2A}$R in Pichia pastoris SMD1163 - Growing P. pastoris

Yeast peptone dextrose (YPD) plates containing 2% bacto-peptone, 1% yeast extract, 2% glucose, 1.5% bacto-agar, and zeocin at 100 μg/ml, were streaked with *P. pastoris* SMD1163 cells transformed with the pPICZB-hA$_{2A}$R(A316) plasmid from a glycerol stock. The plates were incubated for 48h at 30°C and stored at 4°C for a period of two weeks.

Selected colonies were cultured in 50 mL of buffered glycerol complex medium (BMGY) (1% yeast extract, 2% peptone, 100 mM potassium phosphate at pH 6.0, 1,34% yeast nitrogen base without amino acids, 0.00004% biotin, 1% glycerol) also containing zeocin (100 μg/ml) at 30°C and 220 rpm for an overnight period, until the OD$_{600}$ was around 2.0. For the secondary culture, 200 mL of BMGY were inoculated with 5 mL of the primary culture and incubated for 24h at 30°C and 220 rpm. Baffled flasks containing a culture volume of 1/10 of the total capacity were used to ensure proper aeration.

2.3.3 Inducing the expression of the A$_{2A}$R

To induce the expression of the A$_{2A}$R, secondary cultures were harvested by centrifugation at 3000 g for 5 min at room temperature and washed twice with deionized water to remove the glycerol present in the medium. The cells were resuspended in 500 mL of buffered methanol complex medium (BMMY) medium consisting of BMGY medium where glycerol was replaced with methanol. The cultures were incubated at 22°C and 220 rpm for 48h by adding methanol at a final concentration of 1% at 24h. Finally, cultures were harvested, and pellets were either immediately used for cell membrane preparation and analysis of protein expression, or frozen at -80°C for subsequent experiments.

2.3.4 P. pastoris membrane preparation

P. pastoris cells expressing the A$_{2A}$R were thawed on ice and resuspended in breaking buffer (50 mM sodium phosphate pH 7.4, 100 mM NaCl, 2 mM EDTA, 5% glycerol and 1 mM PMSF) to a final concentration of 0.3 g/mL.

For small-scale membrane preparation, the cell walls were lysed using an equal volume of acid-washed glass beads (425-600 μm). The tubes were subjected to 10 cycles of vortexing for 30 s followed by 1 min on ice. For large-scale membrane preparation, cells were broken either by using glass beads (following the same protocol as for the small-scale preparation), the French press (by 3-5 passes) or the Avestin Emulsiflex C3 cell-disrupter (by 10 passes). Unbroken cells and large debris were removed by centrifugation at 4000 g for 5 min at 4°C and 10.000 g (SS-34 Fixed-angle rotor, Sorval MX120

centrifuge, Thermo Scientific) for 10 min at 4°C. The A$_{2A}$R-expressing membrane fraction was obtained by ultra-centrifugation at 100.000 g for 1 hour at 4°C in a Type 70 Ti Fixed-angle rotor (Optima XPN ultracentrifuge, Beckman Coulter Life Sciences).

Aliquots of the non-membrane fraction were stored at -80 °C for monitoring purposes, and the pellet corresponding to the membrane fraction was weighed and re-suspended to 80 mg/mL wet weight in membrane buffer (50 mM Tris/HCl pH 8, 500 mM NaCl, 10% glycerol). Alternatively, 300 mM NaCl, 20 mM HEPES, pH 7.5 was used as membrane buffer. Finally, the membranes were homogenized and either used directly for the solubilization of the A$_{2A}$R or stored at -80°C.

2.3.5   A$_{2A}$R solubilization using SMA2000 and DIBMA polymers, or the detergent DDM

The styrene maleic acid co-polymer Poly(styrene-co-maleic anhydride) was prepared in a ratio of 2:1 styrene to maleic anhydride. For this, a 10% solution of SMA co-polymer in 1 M NaOH (1 M) was prepared and solubilized overnight at room temperature in a round-bottomed flask and agitation. The solution was heated, boiled, and refluxed for 2h. The solution was allowed to cool to room temperature, and the polymer was precipitated by the gradual addition of concentrated HCl under agitation. The polymer solution was mixed with distilled water and centrifuged at 10,000 ×g for 10 min at room temperature. The supernatant was carefully poured off, and the polymer was mixed with distilled water by shaking and centrifuged again at 10,000 ×g for 10 min at room temperature five times. The polymer was dissolved in 0.6 M NaOH by shaking and the pH was adjusted to 8. The SMA co-polymer was freeze-dried and stored at room temperature until further use. DIBMA free acid, DIBMA monosodium salt and Glyco-DIBMA were purchased from GLYCON Biochemicals GmbH (Im Biotechnologie Park, Luckenwalde, Germany). Alternatively, the detergent n-Dodecyl-B-D-maltoside (DDM) was purchased from Melford Laboratories Ltd (Suffolk, United Kingdom).

The A$_{2A}$R was solubilized from the membrane fraction using the polymers SMA2000, DIBMA free acid, DIBMA monosodium salt, and Glyco-DIBMA or, alternatively, with the detergent DDM. A$_{2A}$R-expressing membranes were thawed on ice and re-dissolved to 40 mg/mL in solubilization buffer (50 mM Tris/HCl pH 8, 500 mM NaCl, 10% glycerol; or 300 mM NaCl, 20 mM HEPES, pH 7.5) containing SMA2000, DIBMA free acid, DIBMA monosodium salt, and Glyco-DIBMA at a final concentration of 2.5% (w/v), or DDM at 2% (w/v). Alternatively, a final concentration of 5% (w/v) of the DIBMA polymers was used. The membrane fraction was incubated for 1h at room temperature with gentle agitation, and for 3h at 4°C for solubilization with the detergent. The non-solubilized material was removed by ultra-centrifugation at 100.000 xg, for 1h at 4°C to yield supernatants containing the A$_{2A}$R-SMALP, A$_{2A}$R-DIBMALP or A$_{2A}$R-

I. Company Marin, PhD Thesis, Aston University 2024

DDM. The non-solubilized pellet was resuspended in membrane buffer and stored at -20°C for monitoring purposes.

2.3.6 Purification of the A$_{2A}$R-SMALP by immobilized metal affinity chromatography

A$_{2A}$R-SMALP and A$_{2A}$R-DIBMALP were purified away from other solubilized proteins using the 10-His tag and Ni^{2+}-NTA resins. For small-scale purification, 1 mL of the sample was recirculated overnight at 4°C on an end-over-end rotator with 100 µL of His-select nickel resin affinity gel (Sigma), which was previously equilibrated with equilibration buffer (50 mM Tris/HCl pH 8, 500 mM NaCl, 10% glycerol) containing 10 mM imidazole or without imidazole. Alternatively, HisPur™ Ni-NTA Resin (ThermoFisher), Ni-NTA Agarose (Invitrogen), and Super Ni-NTA affinity resin (Generon) were tested. The resin was washed with 20 column volumes (CV) of wash buffer (50 mM Tris/HCl pH 8, 500 mM NaCl, 10% glycerol) containing 1 mM, 5 mM, 10 mM, 20 mM, or 40 mM imidazole using 1 mL Pierce™ Spin Columns by centrifugation. The A$_{2A}$R was eluted from the resin with 1 CV at a time using elution buffer (50 mM Tris/HCl pH 8, 500 mM NaCl, 10% glycerol) containing 60 mM or 250 mM imidazole. For large-scale purification, 10 mL of the solubilized fraction were recirculated overnight at 4°C on an end-over-end rotator with 1 mL of HisPur™ Ni-NTA Resin (Thermo Scientific™) which was previously equilibrated with equilibration buffer (50 mM Tris/HCl pH 8, 500 mM NaCl, 10% glycerol) without imidazole. The resin was washed with 20 CV of wash buffer (50 mM Tris/HCl pH 8, 500 mM NaCl, 10% glycerol) containing 10 mM or 20 mM imidazole by gravity flow purification. The A$_{2A}$R was eluted from the resin with 1 CV at a time using elution buffer (50 mM Tris/HCl pH 8, 500 mM NaCl, 10% glycerol) containing 60 mM imidazole.

A$_{2A}$R-DDM was purified following the same protocol as for small- and large-scale purification. The resin was equilibrated with equilibration buffer (50 mM Tris/HCl pH 8, 500 mM NaCl, 10% glycerol) containing 0.1% DDM, and was recirculated with the sample O/N at 4°C on an end-over-end rotator. Alternatively, the resin was equilibrated with equilibration buffer containing 0.1% DDM and 10 mM imidazole, and recirculated with the sample for 2h or O/N at 4°C on an end-over-end rotator. The resin was washed with 20 CV of washing buffer containing 20 mM or 60 mM imidazole and 0.1% DDM, and the A$_{2A}$R-DDM was eluted with 1 CV at a time with elution buffer containing 60 mM, 100 mM, 150 mM, 200 mM, or 250 mM imidazole and 0.1% DDM.

Elution fractions were pooled and buffer-exchanged into assay buffer (50 mM Tris/HCl pH 8, 500 mM NaCl; or 300 mM NaCl, 20 mM HEPES, pH 7.5) to remove imidazole. Samples were concentrated using

30 kDa cut-off spin-concentrators, and protein concentration was assessed by bicinchoninic acid (BCA) assay and densitometry analysis using Image J.

2.3.7   Protein quantification

The total protein in the membrane preparation, non-membrane fraction, solubilized fraction, non-solubilized material, and $A_{2A}R$-SMALP in the elution fraction from the purification were quantified using the PierceTM BCA Protein Assay Kit, following the manufacturer's instructions. In short, 2 mg/mL Albumin Standard (BSA) was diluted with phosphate buffer (100 mM, pH 7.4) to prepare the standards for the assay within a working range of 20–2,000 µg/mL. The working reagent was prepared by mixing 50 parts of BCA Reagent A with one part of BCA Reagent B. 25 µL of each standard or unknown sample were pipetted per triplicate onto a microplate well (Thermo Scientific™ Pierce 96-well plate, 15041), and 200 µL of the working reagent were added to each well. The microplate was shaken for 30 s and then incubated at 37°C for 30 min. Finally, the absorbance was measured at 562 nm using a Multiskan™ GO Microplate Spectrophotometer (N10588, Thermo Scientific™).

2.3.8   Analysis of $A_{2A}R$ expression, solubilization and purification by SDS-PAGE, Coomassie staining and Western blotting

The samples were prepared with Laemmli Buffer 5X and incubated at room temperature for 10 min. Samples were loaded on polyacrylamide gels prepared at 4% acrylamide with 126 mM Tris (pH 6.8), 0.1% SDS, 0.1% TEMED and 10% APS for the stacking gel, and 12% acrylamide, 375 mM Tris (pH 8.8), 0.1% SDS, 0.1% TEMED and 0.1% APS, for the resolving gel. SDS-PAGE was performed for 30 min at 50 V, followed by 90 min at 120 V and room temperature. Duplicates of each gel were performed before alternative staining. Gels for total protein analysis were stained overnight at room temperature and shaken at 50 rpm with PageBlue protein staining solution. For western blotting, proteins were transferred from the acrylamide gel to a PVDF membrane for 1h at 100 V, and membranes were dyed with Ponceau staining for 5 min and washed three times for 5 minutes with Tris Buffered Saline (TBS-T) (20 mM Tris, 150 mM NaCl, and 1 mL Tween-20 per litre). Membranes were blocked for 1 hour at room temperature with 5% milk in TBS-T and rinsed for 5 minutes with TBS-T. Membranes were incubated with the monoclonal primary antibody anti-Adenosine Receptor A_{2A} (ab79714, Abcam), which recognises amino acids 213-220 (SQPLPGER) within the third intracellular loop, at 1 µg/mL in 5% milk in TBS-T O/N at 4°C. The secondary antibody anti-mouse IgG HRP was diluted 1:3000, and the membranes were incubated for 1h at room temperature. To image the membranes, SuperSignal west

pico chemiluminescent substrate was used following the manufacturer's instructions. The Working Solution was prepared by mixing equal parts of the Stable Peroxide Solution and the Luminol/Enhancer Solution and was added to the membrane, which was incubated for 5 min at room temperature. Excess of working solution was removed, and the image was obtained using the G Box Gene System.

2.3.9 Analysis of the A$_{2A}$R by LC-MS/MS - In-gel trypsin and chymotrypsin digestion of Coomassie-stained proteins

After Coomassie staining of the gels obtained by SDS-PAGE, bands of interest corresponding to the A$_{2A}$R monomer, A$_{2A}$R dimer, and *P. pastoris* main contaminants were excised and cut into 2-3 mm pieces. Gel pieces were placed in Eppendorf tubes and washed with 500 µL of 100 mM ammonium bicarbonate for 1h on a shaker. To remove the excess of stain and SDS, the supernatant was discarded, and the gel pieces were washed in 500 µL of 50% acetonitrile and 50% ammonium bicarbonate for 1h of shaking. To reduce the protein and break the disulphide bonds to produce a completely unfolded protein for digestion, 150 µL of 100 mM ammonium bicarbonate and 10 µL of 45 mM dithiothreitol (DTT) were added to the bands, which were incubated for 30 min at 60°C. To prevent the re-formation of disulphide bonds, proteins were cooled to room temperature, alkylated with 10 µL of 100 mM iodoacetamide (IAA), and incubated for 30 min in the dark. To remove any excess of DTT and IAA, the solvent was discarded, and the gel pieces were washed with 500 µL of 50% acetonitrile/50% 100 mM ammonium bicarbonate for 1h on the shaker. The wash was discarded and 50 µL of acetonitrile were added to shrink the gel pieces. After 10 min of incubation, the solvent was removed, and the gel pieces were dried completely in a vacuum centrifuge for 10 min at 30°C and V-AQ mode. Gel pieces were rehydrated with a sufficient amount of trypsin (25 ng/µL), or chymotrypsin (20 ng/µL), and 25 mM ammonium bicarbonate to cover just over the gel pieces (~20 µL). Proteins were digested overnight at 37°C. The tubes were briefly centrifuged to pellet the gel pieces and the solvent was transferred to clean Eppendorf tubes. To extract any peptides remining in the gel pieces, 20 µL of 5% formic acid were added and incubated for 20 min at 37°C. The tubes were briefly centrifuged to pellet the gel pieces and the liquid was transferred to the tubes used for the first extract. Finally, the combined extracts were dried down completely in the centrifugal evaporator for 1 h at 30°C and V-AQ mode, and stored at -20°C until further analysis by LC-MS/MS. Prior to MS analysis, the samples were resuspended in 25 µL of HPLC solvent A (98% H$_2$O, 2% acetonitrile, 0.1% formic acid) and loaded into MS grade screw-top glass autosampler vials with 0.3 mL inserts (Chromacol, Speck and Burke analytical, Clackmannanshire, UK).

I. Company Marin, PhD Thesis, Aston University 2024

2.3.10 Liquid chromatography-tandem mass spectrometry (LC-MS/MS) analysis

Peptides were separated and analysed using an ACQUITY UPLC M-Class LC System (Waters, US) coupled to a 5600 TripleTOF (ABSciex, Warrington, UK) controlled by Chrome-leon Xpress and Analyst software (TF1.5.1, ABSciex, Warrington,UK). The peptide solution (5 μL) was loaded onto a nanoEase MZ Symmetry C18 Trap (180 μm x 20 mm) (Waters, UK), and washed at 20 μl/min for 4 minutes, before separation on a nanoEase MZ Peptide C18 column (15 cm x 75 μm) (Waters, UK) at 35°C. The samples were eluted at 500 nL/min using a gradient elution running from 2% to 45% HPLC Solvent B (99% acetonitrile, and 0.1% formic acid) over 45 min. The peptides were subjected to tandem mass spectrometry. The peptides ionized through electrospray ionization (ESI) with a spray voltage of 2.4 kV, source temperature of 150°C, declustering potential of 50 V, and curtain gas setting of 15. Survey scans were collected in the positive mode from 350 to 2000 Da using a high-resolution TOF-MS mode (MS/MS IDA settings) with 10 ions selected, +2 to +5 charges, dynamic exclusion times of 12s, and rolling collision energy.

2.3.11 Database searches

The Mascot® probability-based search engine (Matrix Science, London, version 2.4.0) was used to interrogate SwissProt 2021_03 (565,254 sequences; 203,850,821 residues) - Homo sapiens (human) (20,387 sequences) and Other fungi (22,282 sequences). LC-MS .wiff files of each sample were searched for protein identification using fixed modification of cysteine carbamidomethylation and variable modification of methionine oxidation. Searches were performed for the enzyme trypsin and chymotrypsin, and the MS/MS and peptide tolerance was set at ± 0.5 Da and maximum missed cleavages at 1 for ions with 2+, 3+, and 4+ charge states, #13C: 0, and experimental mass values: Monoisotopic.

2.4 RESULTS

2.4.1 Expression of the $A_{2A}R$ in P. pastoris SMD1163

The multi-tagged de-glycosylated C-terminal truncated $A_{2A}R$ (A316) cloned into the pPICZB plasmid (Figure 2.1A) was expressed in *Pichia pastoris* SMD1163 under the AOX1 promoter, and the expression of the $A_{2A}R$ (52 kDa) was assessed by western blotting (Figure 2.1B). Full western blot images of this chapter are shown in the appendix section (Supplementary Figure 8.1-Figure 8.6).
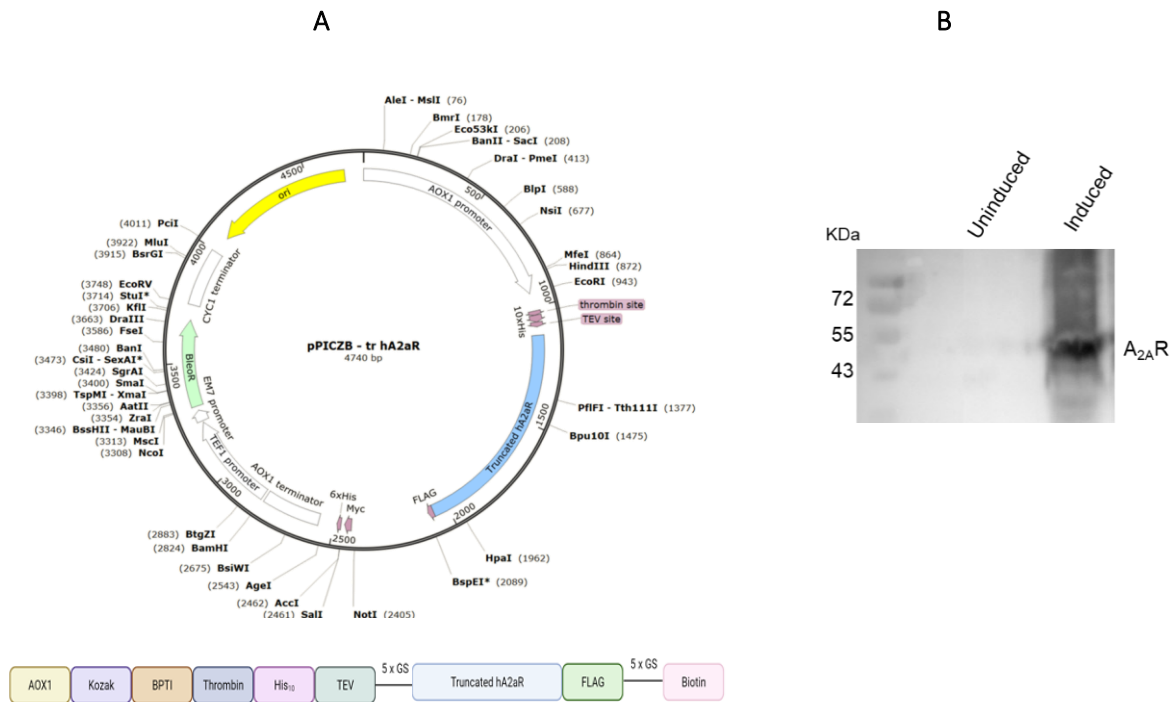
Figure 2.1 Expression of the A₂ₐR in *Pichia pastoris*. (A) *Multi-tagged de-glycosylated C-terminal truncated A₂ₐR (A316) cloned into a pPICZB plasmid.* **(B)** *The A₂ₐR was expressed in stably transformed P. pastoris SMD1163 cells with the pPICZB-A₂ₐR plasmid, and the expression was assessed by SDS-PAGE and Western blotting using a specific primary antibody against the A₂ₐR and a horseradish peroxidase (HRP)-conjugated secondary antibody.*

2.4.2   *P. pastoris SMD1163 cell breaking and membrane fraction preparation*

The membrane preparation was obtained by serial centrifugation steps, and the presence of the A₂ₐR in each fraction was analysed by western blotting (Figure 2.2A). The intensity of the bands corresponding to the A₂ₐR was analysed by densitometry, and the percentage of the band signal in each sample was calculated. Therefore, 100% of the signal corresponding to the A₂ₐR was considered the sum of the supernatant (SN) and the pellet for each centrifugation step (Figure 2.2B). The A₂ₐR was absent in the non-induced sample, as no bands were observed in the Western blot, whereas a band around 52 KDa was obtained in the induced sample prepared as a whole lysate, which indicated that the A₂ₐR is not a natively expressed protein in *P. pastoris,* and its expression was achieved by the induction of the AOX1 promoter. In the first centrifugation step, 30% of the A₂ₐR was lost in the non-broken cell fraction, whereas 70% was recovered in the broken cells. In the second centrifugation step, 64% of the A₂ₐR was lost in the large debris fraction, whereas the remaining 36% was recovered in the supernatant corresponding to the fraction containing the membranes and solubilized materials. Thus, after this centrifugation step, most of the protein was discarded. Nevertheless, this is a crucial step in obtaining a purified protein after solubilization and purification. Finally, the membrane fraction was

I. Company Marin, PhD Thesis, Aston University 2024

pelleted together with 91% of the A$_{2A}$R, while the remaining 9% was lost in the non-membrane fraction, indicating efficient protein recovery and the presence of the A$_{2A}$R in the cell membrane.
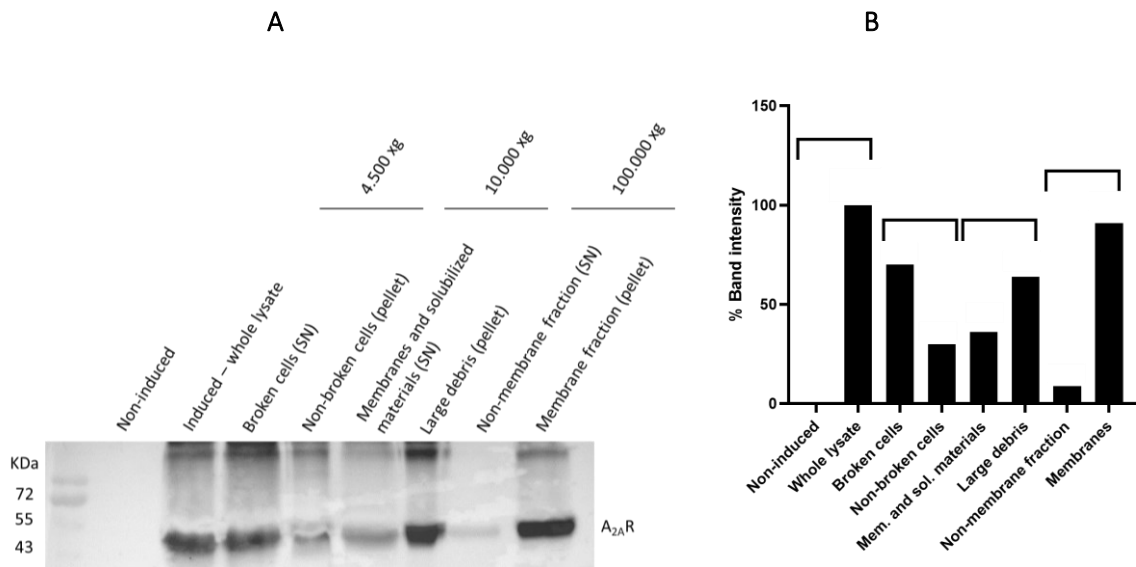
Figure 2.2. Presence of the A$_{2A}$R in different centrifugation fractions during membrane preparation. (A) P. pastoris SMD1163 cells expressing the A$_{2A}$R were broken using acid-washed glass beads, and the non-broken cells were discarded by centrifugation at 4.500 xg. The membranes and solubilized materials were separated from the large and non-soluble debris by centrifugation at 10.000 xg. The membrane fraction was isolated by ultracentrifugation at 100.000 xg. Aliquots of the supernatant (SN) and pellet at each centrifugation step were analysed by Western blotting using an anti-A$_{2A}$R primary antibody and HRP-conjugated secondary antibody after normalizing the total protein concentration of the samples. (B) Bands corresponding to the A$_{2A}$R on the western blot were analysed by densitometry using ImageJ software, and the results were expressed as the percentage of the band signal (n=1).

2.4.3   Solubilization of the A$_{2A}$R with SMA2000 and DIBMA

The solubilization of the A$_{2A}$R is a critical stage in its characterization. Two solubilization agents, SMA2000 and DIBMA, were utilized and compared to determine the most effective solubilization method. The solubilization efficiency of the A$_{2A}$R with SMA2000 (Figure 2.3A) and DIBMA (Figure 2.3B) was analysed by western blotting. Regarding solubilization with SMA2000, the results showed the presence of the A$_{2A}$R as a monomer and dimer in the membrane preparation, although 8.5% of this protein was lost in the non-membrane fraction. The A$_{2A}$R was successfully solubilized with SMA2000 with an average efficiency of 64%. For solubilization with DIBMA free acid, 15% of the A$_{2A}$R was lost in the non-membrane fraction and it was not efficiently solubilized with DIBMA, as no bands could be detected in the solubilized fraction.
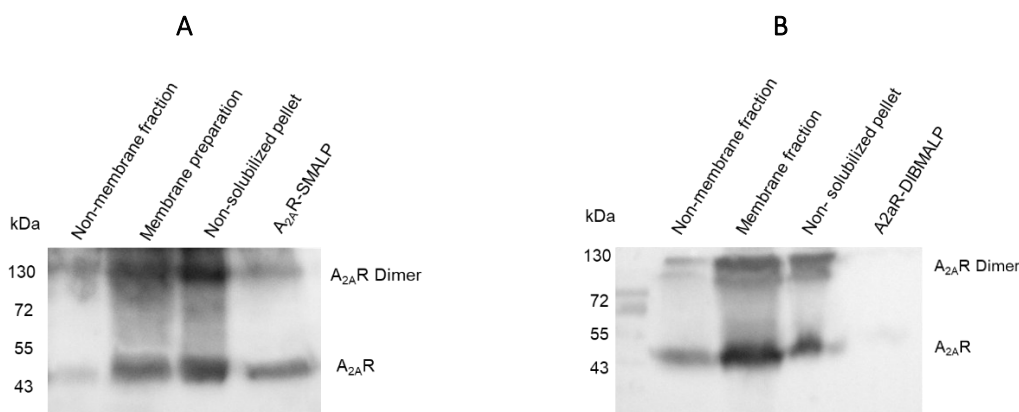
*Figure 2.3. Solubilization of the A₂ₐR with SMA2000 and DIBMA free acid at 2.5% (w/v). The A₂ₐR was solubilized from the membrane preparation using (**A**) SMA2000 at 2.5% (w/v) and (**B**) DIBMA free acid at 2.5% (w/v). Aliquots of the non-membrane fraction, membrane preparation, non-solubilized material and solubilized protein were taken. Preparation of the solubilized A₂ₐR-SMALP and A₂ₐR-DIBMALP was monitored by SDS-PAGE and Western blotting using an anti-A₂ₐR primary antibody and HRP-conjugated secondary antibody.*

To investigate DIBMA agents further, the solubilization of the A₂ₐR from the membrane fraction was attempted with DIBMA free acid, DIBMA monosodium salt, and Glyco-DIBMA, and aliquots at each preparation step were analysed by western blotting to monitor the solubilization efficiency (Figure 2.4). The A₂ₐR was not efficiently solubilized with DIBMA free acid or DIBMA monosodium salt as no bands corresponding to the monomer or dimer of the A₂ₐR could be detected on the blot. Nevertheless, a less intense signal of the target protein was obtained for the non-solubilized fraction after DIBMA monosodium salt solubilization when compared to the non-solubilized fraction after using DIBMA free acid, which is potentially related to the sample preparation process for SDS-PAGE. On the other hand, bands corresponding to the solubilized A₂ₐR-Glyco-DIBMALP could be detected, and densitometry analysis revealed that the protein was solubilized with 20% efficiency.
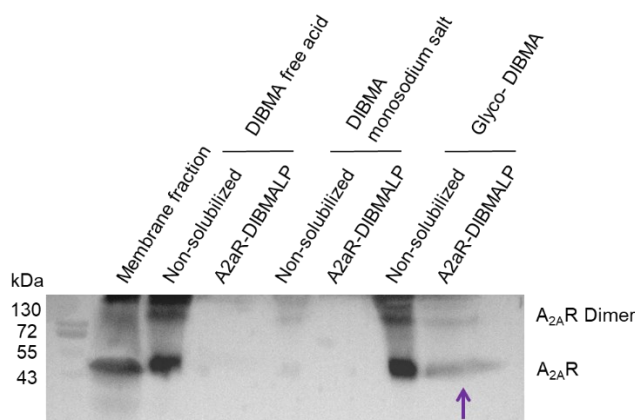
Figure 2.4. Solubilization of the A₂ₐR with DIBMA free acid, DIBMA monosodium salt, and Glyco-DIBMA at 5% (w/v). The A₂ₐR was solubilized from the membrane preparation using DIBMA free acid, DIBMA

I. Company Marin, PhD Thesis, Aston University 2024

monosodium salt, and Glyco-DIBMA at a final concentration of 5%, and aliquots of the membrane fraction, non-solubilized material, and solubilized fractions were taken. A_{2A}R-DIBMALP solubilization was monitored by SDS-PAGE and Western blot using an anti-A_{2A}R primary antibody and HRP-conjugated secondary antibody.

2.4.4 Purification of the A_{2A}R-SMALP through affinity chromatography

After solubilization of the A_{2A}R with SMA2000, the encapsulated A_{2A}R-SMALP was purified from other proteins by affinity chromatography using nickel-NTA resins through the 10-His tag included in the construct. Imidazole concentrations to equilibrate and wash the resin, and to elute the protein of interest were optimized, and different Ni^{+2}-NTA resins were tested to obtain the purest and most concentrated protein. For this purpose, small-scale procedures were carried out after breaking the *P. pastoris* cells expressing the A_{2A}R with acid-washed glass beads, and the results were analysed by SDS-PAGE and Western blotting.

The elution of the A_{2A}R from the resin was monitored by increasing the imidazole concentrations. Western blot results allowed the detection of an intense band corresponding to the A_{2A}R in the recirculated flow-through and its presence in the washes with 1, 5 and 10 mM imidazole (Figure 2.5A). However, the intensity of the A_{2A}R bands increased as the imidazole concentration increased to 20, 40, 60, and 250 mM (Figure 2.5B). Densitometry analysis demonstrated that 1, 5, and 10 mM imidazole caused lower elution of the A_{2A}R compared to the first 1 mM imidazole wash. Imidazole at 20 mM caused a slight increase in the intensity of the bands, and the elution increased as the imidazole concentration was incremented from 40 to 250 mM (Figure 2.5C).

C
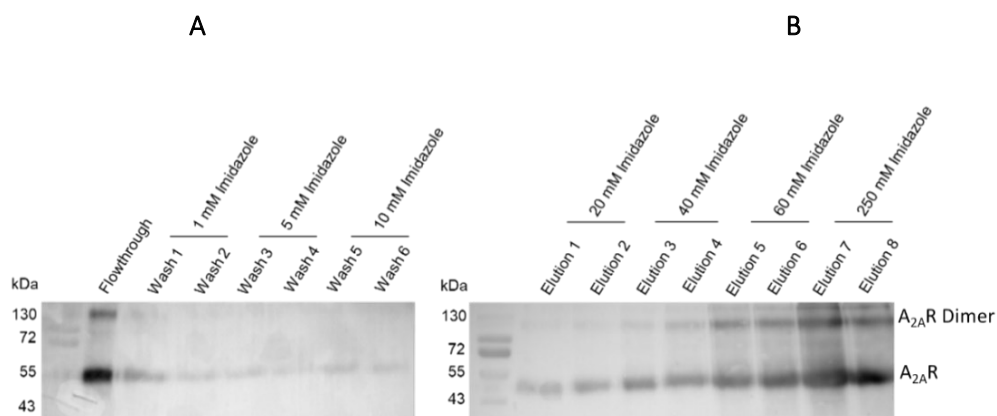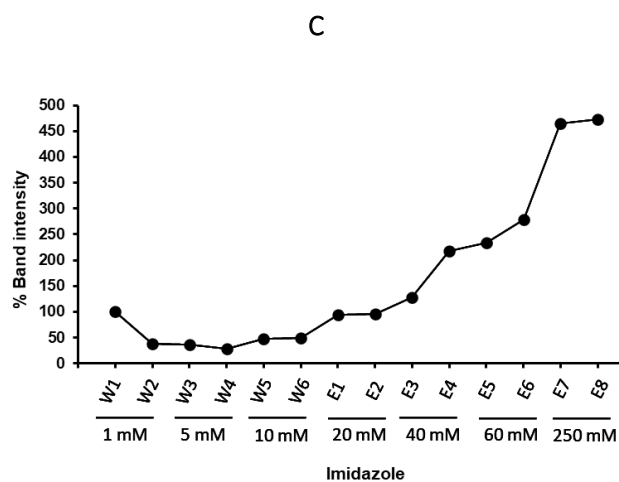
Figure 2.5. Optimal imidazole concentrations for the purification of the $A_{2A}R$-SMALP by affinity chromatography using Ni-NTA His-select affinity gel. *The solubilized fraction containing the $A_{2A}R$-SMALP was recirculated with a previously equilibrated resin without imidazole. The column was washed with 1, 5, and 10 mM imidazole, and the $A_{2A}R$-SMALP was eluted from the resin using 20, 40, 60, and 250 mM imidazole. The results were analysed by SDS-PAGE, Coomassie staining, and Western blotting using an anti-$A_{2A}R$ primary antibody and HRP-conjugated secondary antibody. (**A**) Western blot analysis of the flow-through and wash fractions. (**B**) Western blot analysis of the elution fractions. (**C**) Densitometry analysis of bands corresponding to the $A_{2A}R$ detected by western blotting in the different wash and elution fractions using ImageJ software (n=1).*

SDS-PAGE and Coomassie staining were performed to analyse the purity of the $A_{2A}R$-SMALP (Figure 2.6A and Figure 2.6B). Imidazole at 1mM caused the elution of multiple *P. pastoris* proteins and, thus, served to clean the resin from them. After washing the resin with 1, 5, and 10 mM imidazole, the elution of contaminants was less evident. Imidazole at 20 mM caused the elution of contaminants, and no bands corresponding to the $A_{2A}R$ could be observed. Imidazole at 40, 60, and 250 mM also provoked the elution of contaminants, but more intense $A_{2A}R$ bands were obtained as the imidazole concentration increased. These imidazole concentrations caused the co-elution of the main *P. pastoris* contaminant, and its elution intensified as imidazole concentrations increased. Using densitometry analysis (Figure 2.6C), the ratio between the elution of the $A_{2A}R$, the main contaminant, and other contaminants was determined. The results showed that, although the most intense band for the $A_{2A}R$ was obtained with 250 mM imidazole, it was highly contaminated by other proteins and the *P. pastoris* main contaminant. Notably, the band corresponding to the $A_{2A}R$ was the most intense compared to that of the contaminants. On the other hand, 60 mM imidazole allowed the most intense and enriched elution of the $A_{2A}R$ since the ratio $A_{2A}R$/contamination was higher. Hence, this imidazole concentration was used in further experiments as it was optimal for the purification of the $A_{2A}R$.

I. Company Marin, PhD Thesis, Aston University 2024
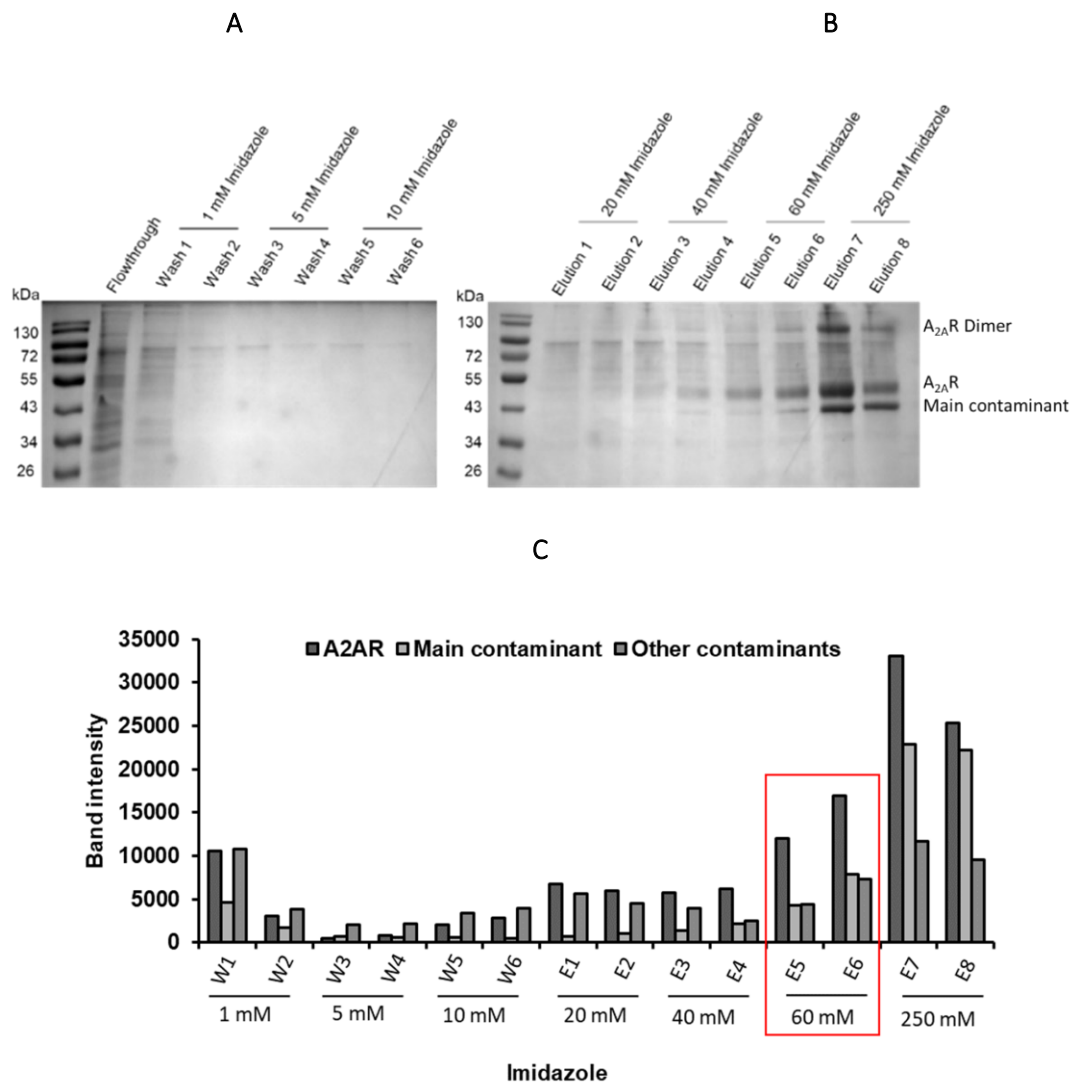
Figure 2.6. Optimal imidazole concentrations for the purification of the $A_{2A}R$-SMALP through affinity chromatography using Ni-NTA His-select affinity gel. The solubilized fraction containing the $A_{2A}R$-SMALP was recirculated with a previously equilibrated resin without imidazole. The column was washed with 1, 5, and 10 mM imidazole and the $A_{2A}R$-SMALP was eluted from the resin with 20, 40, 60, and 250 mM imidazole. The results were analysed by SDS-PAGE and Coomassie staining. (**A**) SDS-PAGE and Coomassie staining of the flow-through and wash fractions. (**B**) SDS-PAGE and Coomassie staining of the elution fractions. (**C**) Densitometric analysis of bands corresponding to the $A_{2A}R$, P. pastoris main contaminant, and other contaminants detected by SDS-PAGE and Coomassie staining in the different wash and elution fractions using ImageJ software (n=1).

Different Ni^{+2}-NTA resins were tested to optimize the purity and yield of the $A_{2A}R$-SMALP, including His-pur Ni-NTA resin (Figure 2.7), His-select affinity gel (Supplementary Figure 8.7-Figure 8.8), Ni-NTA agarose (Supplementary Figure 8.9), and Super Ni-NTA affinity resin (Supplementary Figure 8.10). The results were analysed by SDS-PAGE and Coomassie staining, and densitometry of the bands corresponding to the $A_{2A}R$-SMALP, the main *P. pastoris* contaminant and other contaminants of higher and lower molecular weight than the $A_{2A}R$ was measured. Among the tested resins for $A_{2A}R$ purification,

I. Company Marin, PhD Thesis, Aston University 2024

His-pur Ni-NTA Resin was optimal as it facilitated the highest recovery of the target protein with minimal contamination.

The A_{2A}R-SMALP eluted from the His-pur Ni-NTA Resin with 60 and 250 mM imidazole, and no bands for the protein were observed in the lanes corresponding to the washing steps. This suggests that the protein was not lost with 1, 5, or 10 mM imidazole (Figure 2.7A). Low-intensity bands corresponding to the main contaminant of *P. pastoris* were obtained with 60 mM imidazole, and they could be clearly observed when 250 mM imidazole was used. Densitometry analysis revealed a high intensity of bands corresponding to the A_{2A}R after elution with 60 mM imidazole compared to the main contaminant (Figure 2.7B). The elution of the main contaminant increased with 250 mM imidazole, being predominant against the A_{2A}R-SMALP in the last elution step but not for Elution 3, in which the A_{2A}R was still the predominant protein. The intensity of the bands corresponding to other contaminants was low in all the elution steps in comparison to the main contaminant and the A_{2A}R-SMALP.
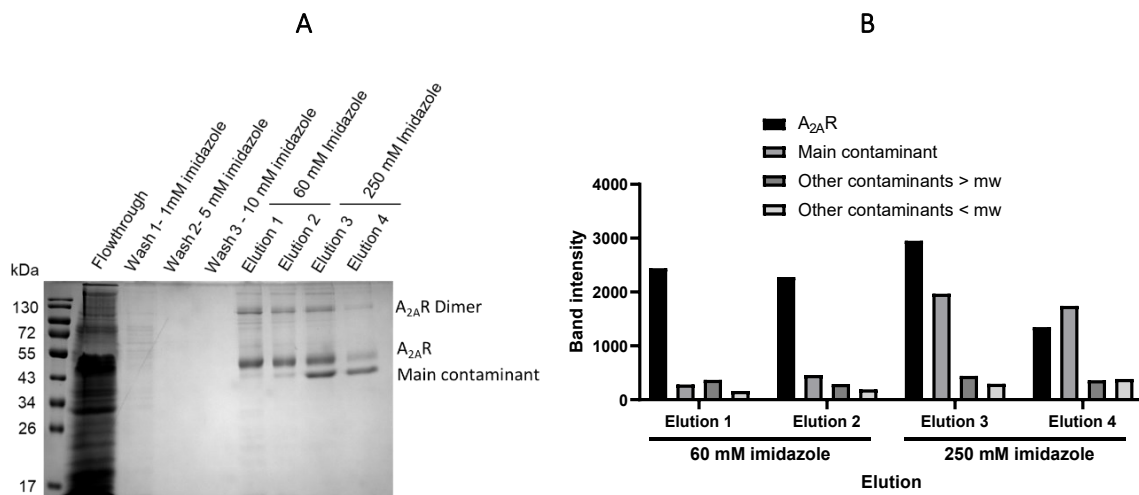
Figure 2.7. A_{2A}R-SMALP purification by affinity chromatography using His-pur Ni-NTA resin. The solubilized fraction containing the A_{2A}R-SMALP was recirculated with His-pur Ni-NTA resin previously equilibrated without imidazole. The resin was washed with 1, 5, and 10 mM imidazole and the A_{2A}R-SMALP was eluted with 60 and 250 mM imidazole. (A) Flow-through, wash, and elution fractions were analysed by SDS-PAGE and Coomassie staining, and (B) bands corresponding to the A_{2A}R, P. pastoris main contaminant, and other contaminants were analysed by densitometry using ImageJ (n=1).

Once it was determined that the optimum imidazole concentration for washing the resin was between 10 and 20 mM, and the optimum concentration to elute the A_{2A}R was 60 mM, the number of elution steps was extended to assess at which step the elution of the target protein started to decrease, as well as to study if the elution of the *P. pastoris* main contaminant increases with the elution steps. The elution fractions were analysed by SDS-PAGE and Coomassie staining (Supplementary Figure 8.11), and the band intensity of the A_{2A}R and *P. pastoris* main contaminant was analysed by densitometry (Figure 2.8).

I. Company Marin, PhD Thesis, Aston University 2024

Densitometry analysis showed that the A_{2A}R-SMALP eluted from E1, its elution reached a maximum point in E3 and started progressively decreasing from E4 until it reached basal levels in E8-E10. Conversely, the *P. pastoris* main contaminant had low elution in E1-E4, although a slight increase in the band intensities was observed, and it started eluting more intensely from E5, reaching a maximum point in E7. Finally, its elution started decreasing from E8, reaching basal levels in E9-E10. Hence, the elution of the A_{2A}R and the main contaminant could be separated using 60 mM imidazole in the elution steps E1 to E4, they coeluted at E5, and the elution of the main contaminant was predominant from E6 to E10, suggesting that a maximum of five elution steps should be performed to obtain the purified A_{2A}R from the main contaminant under these experimental conditions.
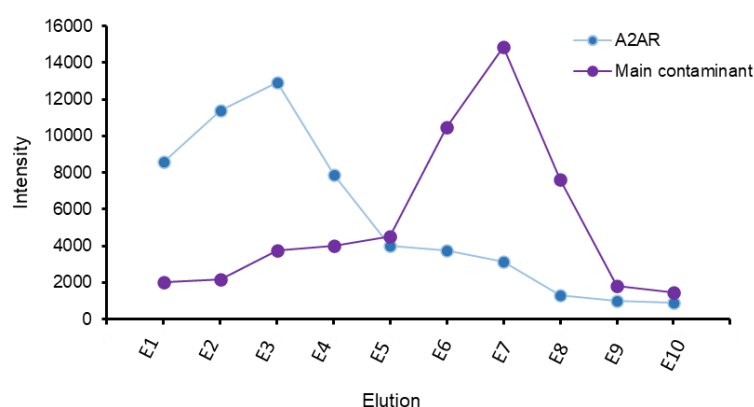
Figure 2.8. A_{2A}R-SMALP and P. pastoris main contaminant elution from His-pur Ni-NTA resin with 60 mM imidazole. The solubilized fraction containing the A_{2A}R-SMALP was recirculated with previously equilibrated His-pur Ni-NTA resin without imidazole. The resin was washed with 1, 5, and 10 mM imidazole and the A_{2A}R-SMALP eluted with 60 mM and 1 CV at a time for a total of 10 elution steps. Results were analysed by SDS-PAGE and Coomassie staining and bands corresponding to the A_{2A}R-SMALP and P. pastoris main contaminant were analysed by densitometry using ImageJ (n=1).

The A_{2A}R-SMALP purification under these optimized conditions was tested on a large-scale level. SDS-PAGE and Coomassie staining revealed optimized purification of the A_{2A}R-SMALP (Figure 2.9A), as clear and intense protein bands corresponding to the A_{2A}R-SMALP were obtained in the elution fractions but not in the washes, which indicated that the protein of interest was not lost during the procedure. Western blot analysis revealed that little amounts of protein were lost in the flow-through and wash fractions, and eluted from the column in the elution fractions, although its intensity was low in E1, and increased from E2 to E6 (Figure 2.9B).

A_{2A}R-SMALP purification on a large-scale level was also tested using different cell-breaking methods, including the Avestin Emulsiflex C3 cell disrupter and French press with samples prepared in HEPES pH 7.5 buffer (Supplementary Figure 8.12-Figure 8.17). However, the use of glass beads and Tris-HCl buffer were found optimal for A_{2A}R-SMALP purification.
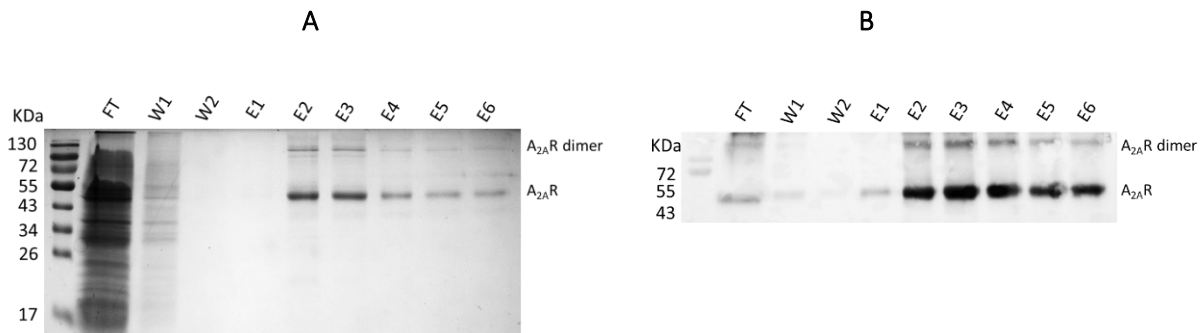
Figure 2.9. Large-scale purification of the A₂ₐR-SMALP prepared with glass beads in Tris-HCl buffer. P. pastoris cells expressing the A₂ₐR were broken using acid-washed glass beads to obtain the membrane preparation in Tris-HCl buffer, from which the A₂ₐR was solubilized using SMA2000 at 2.5%. The solubilized fraction containing the A₂ₐR-SMALP was recirculated with a previously equilibrated His-pur Ni-NTA resin without imidazole. The column was washed with 20 mM imidazole, and A₂ₐR-SMALP eluted with 60 mM imidazole. (A) SDS-PAGE and Coomassie staining and (B) Western blot analysis of the flow-through, wash, and elution fractions.

For subsequent experiments and optimal storage conditions, the purified A₂ₐR-SMALP was buffer-exchanged and concentrated. Aliquots of each fraction during the buffer exchange and concentration process were analysed by SDS-PAGE and Coomassie staining (Figure 2.10). Bands corresponding to the A₂ₐR-SMALP monomer and dimer were obtained in the pooled elution fractions, and their intensities increased with their concentration. A₂ₐR-SMALP was not lost in the spin concentrator and PD-10 flow-through (FT), as no bands were observed on the gel, whereas it eluted from the PD-10 column in the A₂ₐR elution fraction. Similarly, it was not lost in the PD-10 wash fraction. Finally, a more intense band of the A₂ₐR-SMALP was obtained after concentration and no protein of interest was lost in the flow-through of the spin concentrator.
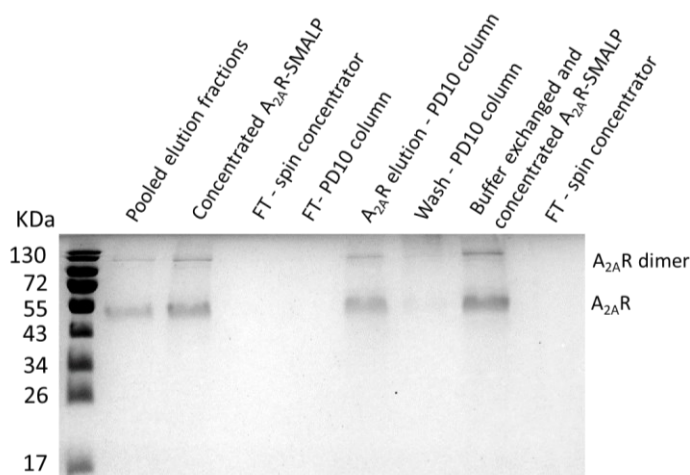
Figure 2.10. Buffer exchange and concentration of the A₂ₐR-SMALP. The A₂ₐR-SMALP was buffer-exchanged and concentrated 5X in Tris-HCl buffer using PD-10 desalting columns to remove imidazole for subsequent experiments and optimal storage conditions. Aliquots of each fraction were analysed by SDS-PAGE and Coomassie staining.

I. Company Marin, PhD Thesis, Aston University 2024

After optimizing the solubilization and purification protocol using SMA2000, the A$_{2A}$R was solubilized using Glyco-DIBMA. The optimized protocol for the purification of the A$_{2A}$R-SMALP was followed. No intense bands corresponding to the A$_{2A}$R-DIBMALP were observed in the SDS-PAGE gel after Coomassie staining (Figure 2.11). Nevertheless, light, and low-intensity bands were detected at the expected molecular weight for the A$_{2A}$R-Glyco-DIBMALP, which indicated poor solubilization efficiency and low protein binding to the Ni-NTA resin. No protein bands corresponding to other *P. pastoris* contaminants were observed either in the elution fractions.
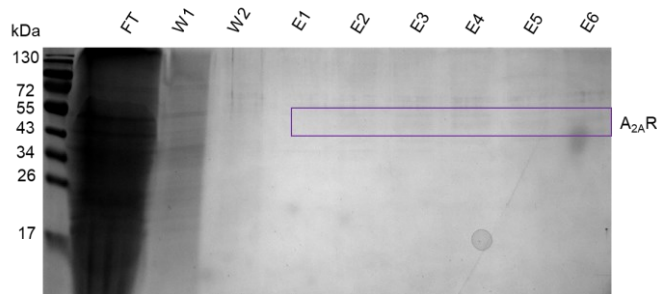
Figure 2.11. Large-scale purification of the A$_{2A}$R-Glyco-DIBMALP prepared with Glass beads in Tris-HCl buffer. P. pastoris cells expressing the A$_{2A}$R were broken using acid-washed Glass beads to obtain the membrane preparation in Tris-HCl buffer, from which the A$_{2A}$R was solubilized using Glyco-DIBMA at 5% (w/v). The solubilized fraction containing the A$_{2A}$R-Glyco-DIBMALP was recirculated with a previously equilibrated His-pur Ni-NTA resin without imidazole. The column was washed with 20 mM imidazole and A$_{2A}$R-Glyco-DIBMALP eluted with 60 mM imidazole. The results were analysed by SDS-PAGE and Coomassie staining.

2.4.5 A$_{2A}$R solubilization with DDM and its purification by affinity chromatography

As an alternative to membrane protein solubilization using polymers, the A$_{2A}$R was solubilized from the membrane fraction with the non-ionic detergent DDM, and its solubilization efficiency was analysed by western blotting (Figure 2.12). Bands corresponding to the A$_{2A}$R monomer were analysed by densitometry, and the results showed that the protein of interest was solubilized with 60% efficiency.
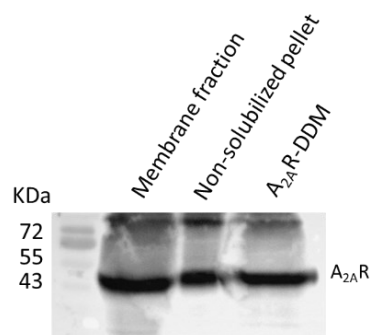
Figure 2.12. Solubilization of the A$_{2A}$R with DDM at 2% (w/v). The A$_{2A}$R was solubilized from the membrane fraction with DDM, and its solubilization was monitored by analysing aliquots of the

membrane fraction, non-solubilized pellet, and solubilized supernatant by western Blotting with an anti-A$_{2A}$R primary antibody and HRP-conjugated secondary antibody.

The purification of the A$_{2A}$R-DDM was attempted by affinity chromatography following the same protocol optimized for the purification of the A$_{2A}$R-SMALP. Aliquots of all fractions were analysed by SDS-PAGE and Coomassie staining (Figure 2.13). Numerous protein bands were observed in all fractions in the gel corresponding to protein contaminants, although a more intense band corresponding to the A$_{2A}$R-DDM could still be observed in the elution fractions. These results suggest that the optimized protocol for the purification of the A$_{2A}$R-SMALP was not optimal for the purification of the A$_{2A}$R-DDM, as the resin could not be properly washed and the protein of interest co-eluted with many other protein contaminants.
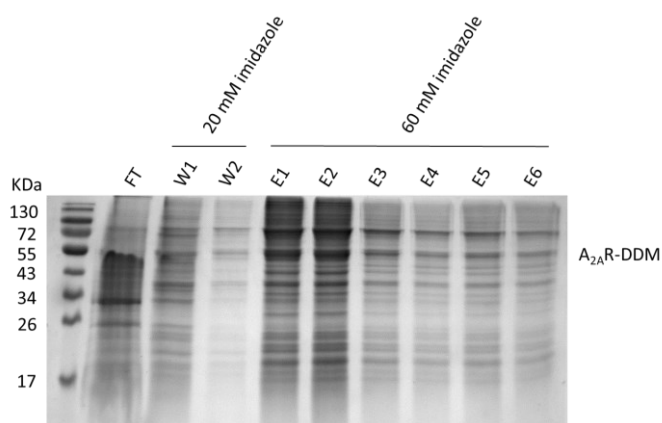
Figure 2.13. Purification of the A$_{2A}$R-DDM by affinity chromatography using low concentrations of imidazole. *The purification of the A$_{2A}$R-DDM away from other proteins in the sample was attempted following the optimized protocol for the purification of the A$_{2A}$R-SMALP. The resin was pre-equilibrated without imidazole, washed with wash buffer containing 20 mM imidazole, and the A$_{2A}$R was eluted with elution buffer containing 60 mM imidazole. Aliquots of the flow-through, washes, and elution fractions were analysed by SDS-PAGE and Coomassie staining.*

The A$_{2A}$R-DDM was purified by minimising the incubation time with the resin and increasing the imidazole concentrations to wash the resin and elute the protein of interest (Figure 2.14). Imidazole at 60 mM served to wash the columns since many protein bands were observed in the Wash 1 (W1) fraction, whereas less intense bands were obtained in the Wash 2 and 3 (W2 and W3). The separation of the A$_{2A}$R-DDM monomer and dimer from the main contaminant was not possible using 200 mM or 150 mM imidazole, although bands corresponding to the A$_{2A}$R showed higher intensity compared to those for the main contaminant when 150 mM imidazole was used. In contrast, both proteins showed similar intensities when 200 mM imidazole was used. Imidazole at 100 mM was not sufficient to elute the A$_{2A}$R at concentrations comparable to those obtained with higher imidazole concentrations. Thus,

low-intensity bands for the A$_{2A}$R monomer and dimer were obtained in the elution fractions and lower-intensity bands for the main contaminant, indicating that their separation was not accomplished with 100 mM imidazole.
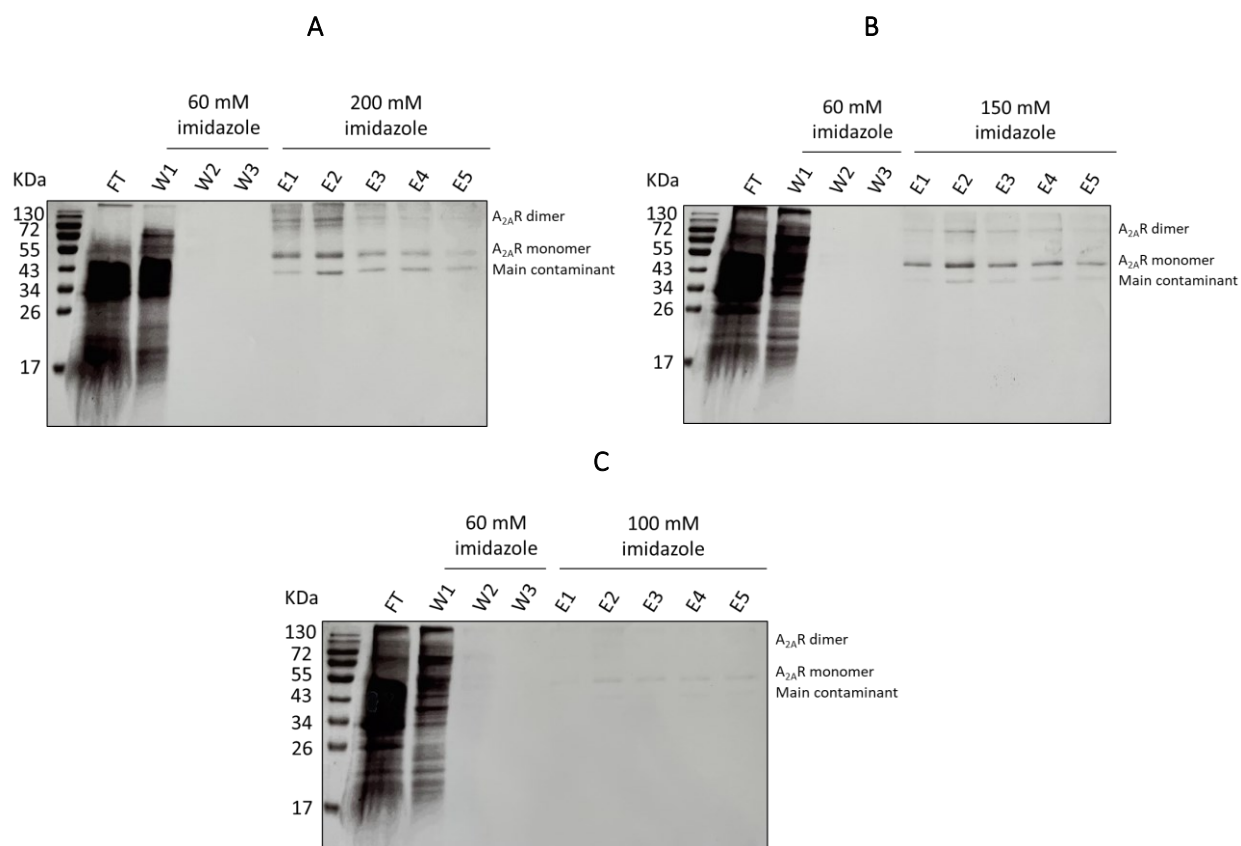
*Figure 2.14. Purification of the A$_{2A}$R-DDM by affinity chromatography by decreasing the imidazole concentration in the elution fractions. The A$_{2A}$R-DDM was purified away from other proteins in the sample by recirculating the solubilized fraction with the resin for 2h, washing the resin with wash buffer containing 60 mM imidazole, and eluting the A$_{2A}$R-DDM with elution buffer with (**A**) 200 mM, (**B**) 150 mM, and (**C**) 100 mM imidazole. Aliquots of the flow-through, washes, and elution fractions were analysed by SDS-PAGE and Coomassie staining.*

The A$_{2A}$R-DDM was buffer exchanged with Tris-HCl buffer without imidazole and concentrated for subsequent experiments and optimal storage conditions. The buffer exchanged and concentrated A$_{2A}$R-DDM was compared to the buffer exchanged and concentrated A$_{2A}$R-SMALP by SDS-PAGE and Coomassie staining, and the results showed the presence of the *P. pastoris* main contaminant in the A$_{2A}$R-DDM sample, whereas it was absent in the A$_{2A}$R-SMALP sample (Figure 2.15).

I. Company Marin, PhD Thesis, Aston University 2024
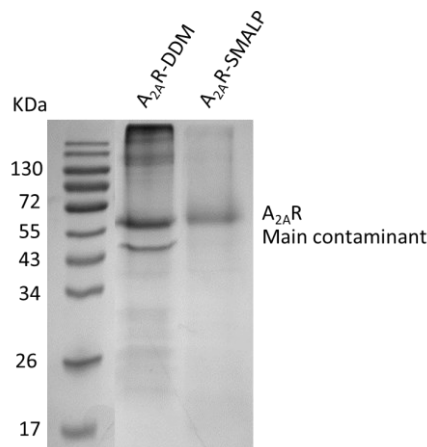
Figure 2.15. Buffer exchange and concentration of the A$_{2A}$R-DDM and A$_{2A}$R-SMALP. The A$_{2A}$R-DDM was buffer exchanged and concentrated with Tris-HCl buffer to remove imidazole for subsequent experiments and optimal storage conditions. It was compared to the A$_{2A}$R-SMALP preparation under the same conditions by SDS-PAGE and Coomassie staining.

2.4.6   Identification of the A$_{2A}$R monomer and dimer and the P. pastoris main contaminant by in-gel digestion and LC-MS/MS

Bands corresponding to the A$_{2A}$R monomer and dimer, and the *P. pastoris* main contaminant, were digested in-gel with trypsin or chymotrypsin, and the resulting peptides were analysed by LC-MS/MS. For protein identification, searches were performed for both proteases against SwissProt Homo sapiens and Other Fungi databases using the Mascot® probability-based search engine. Therefore, the most probable human and fungal proteins were identified for each band in the gel (Table 2.1).

The A$_{2A}$R monomer digested with chymotrypsin was identified in the first position among all possible human identifications with a score of 242. Its score was higher than the *cut-off* criteria for protein identification acceptance, which was set at 50, and it was also used to compare identifications found in the Other Fungi database. In this case, the most probable fungal protein was identified as the Reducing polyketide synthase DEP5 from *Fusarium langsethiae*, with a score of 41, which was lower than the score for the A$_{2A}$R monomer. This allowed the identification of the A$_{2A}$R monomer digested with chymotrypsin. The A$_{2A}$R dimer after chymotrypsin digestion was identified in the first position among all possible human identifications, with a score of 56. Nevertheless, the most probable fungal protein for this gel band was identified as Peroxisomal catalase from *Candida albicans* with a score of 77, which is higher than the score received by the A$_{2A}$R dimer.

The A$_{2A}$R monomer digested with trypsin was identified in the third position with a score of 120, which was above the acceptance criteria, following Keratin type II cytoskeletal 1 and Keratin type I cytoskeletal

64

10, which received scores of 266 and 126, respectively. The most probable fungal protein for this gel band was the Phosphoglycerate kinase from *Komagataella pastoris (*also known as *Pichia pastoris)*, with a lower score of 52. The $A_{2A}R$ dimer digested with trypsin was not detected.

The *P. pastoris* main contaminant was identified as the Alcohol dehydrogenase 2 (ADH2) from *Kluyveromyces marxianus* in the first place with a score of 158, and the most probable human protein identified for this band was Albumin from *Homo sapiens*, with a score of 97, which was lower than the score for the ADH2. This allowed the acceptance of its identification. In all cases, the $A_{2A}R$ was identified with a mass of 45534 Da.

Table 2.1. Identification of the $A_{2A}R$ and P. pastoris main contaminants by in-gel digestion and LC-MS/MS. *The resulting peptides from the in-gel digestion with trypsin or chymotrypsin of the $A_{2A}R$ monomer and dimer, and in-gel digestion with trypsin of the P. pastoris main contaminant, were detected by LC-MS/MS. Data were analysed using Mascot Daemon against the SwissProt Homo sapiens and Other Fungi databases. Both the $A_{2A}R$ monomer and dimer, and the main contaminant, were identified with acceptable score values (>50), with two or more unique peptides detected.*

		Taxonomy	Position	Protein	Description	Score
Chymotrypsin	A2AR monomer	Homo sapiens	1	AA2AR_HUMAN	Adenosine receptor A2a OS=Homo sapiens OX=9606 GN=ADORA2A PE=1 SV=2	242
		Fungi	1	DEP5_FUSLA	Reducing polyketide synthase DEP5 OS=Fusarium langsethiae OX=179993 GN=DEP5 PE=2 SV=1	41
	A2AR dimer	Homo sapiens	1	AA2AR_HUMAN	Adenosine receptor A2a OS=Homo sapiens OX=9606 GN=ADORA2A PE=1 SV=2	56
		Fungi	1	CATA_CANAL	Peroxisomal catalase OS=Candida albicans OX=237561 GN=CAT1 PE=2 SV=5	77
Trypsin	A2AR monomer	Homo Sapiens	1	K2C1_HUMAN	Keratin, type II cytoskeletal 1 OS=Homo sapiens OX=9606 GN=KRT1 PE=1 SV=6	266
			2	K1C10_HUMAN	Keratin, type I cytoskeletal 10 OS=Homo sapiens OX=9606 GN=KRT10 PE=1 SV=3	126
			3	AA2AR_HUMAN	Adenosine receptor A2a OS=Homo sapiens OX=9606 GN=ADORA2A PE=1 SV=2	120
		Fungi	1	PGK_PICPA	Phosphoglycerate kinase OS=Komagataella pastoris OX=4922 GN=PGK1 PE=3 SV=1	52
	Main contaminant	Homo sapiens	1	ALBU_HUMAN	Albumin OS=Homo sapiens OX=9606 GN=ALB PE=1 SV=2	97
		Fungi	1	ADH2_KLUMA	Alcohol dehydrogenase 2 OS=Kluyveromyces marxianus OX=4911 GN=ADH2 PE=3 SV=3	158

The $A_{2A}R$ monomer digested with trypsin was identified with a total sequence coverage of 4% and two unique peptides were detected (Figure 2.16A). The YNGLVTGTR peptide corresponded to part of the intracellular loop 2 (ICL2) and the intracellular side of the transmembrane helix 4 (TM4), whereas the QMESQPLPGER peptide corresponded to the intracellular loop 3 (ICL3) and the cytoplasmic ends of the transmembrane helixes 5 (TM5) and 6 (TM6) (Figure 2.16B). The YNGLVTGTR peptide obtained a score of 54 (Table 2.2), which was above the *cut-off* criteria for peptide identification acceptance. The QMESQPLPGER peptide obtained a score of 43 (Table 2.2); therefore, it did not meet the minimum criteria to be accepted. Peptide fragmentation spectra are shown in the appendix section (Supplementary Figure 8.18-Figure 8.20).

I. Company Marin, PhD Thesis, Aston University 2024

Protein sequence coverage: 4%

Matched peptides shown in **bold red**.

```
  1  MPIMGSSVYI  TVELAIAVLA  ILGNVLVCWA  VWLNSNLQNV  TNYFVVSLAA
 51  ADIAVGVLAI  PFAITISTGF  CAACHGCLFI  ACFVLVLTQS  SIFSLLAIAI
101  DRYIAIRIPL  RYNGLVTGTR  AKGIIAICWV  LSFAIGLTPM  LGWNNCGQPK
151  EGKNHSQGCG  EGQVACLFED  VVPMNYMVYF  NFFACVLVPL  LLMLGVYLRI
201  FLAARRQLKQ  MESQPLPGER  ARSTLQKEVH  AAKSLAIIVG  LFALCWLPLH
251  IINCFTFFCP  DCSHAPLWLM  YLAIVLSHTN  SVVNPFIYAY  RIREFRQTFR
301  KIIRSHVLRQ  QEPFKAAGTS  ARVLAAHGSD  GEQVSLRLNG  HPPGVWANGS
351  APHPERRPNG  YALGLVSGGS  AQESQGNTGL  PDVELLSHEL  KGVCPEPPGL
401  DDPLAQDGAG  VS
```

Figure 2.16. A$_{2A}$R monomer identification by LC-MS/MS after trypsin in-gel digestion. *Bands corresponding to the A$_{2A}$R monomer were in-gel digested with trypsin and analysed by LC-MS/MS. (**A**) Sequence coverage of the A$_{2A}$R with the identified unique peptides highlighted in red. (**B**) Sequence coverage on the secondary structure of the A$_{2A}$R with the identified unique peptides highlighted in purple.*

The A$_{2A}$R dimer digested with chymotrypsin was identified with a sequence coverage of 6%, and three unique peptides were detected (Figure 2.17). The peptide AIAIDRY corresponded to the transmembrane helix TM3, and it obtained a score of 40 (Table 2.2). The peptide EDVVPMNY corresponded to the end of the extracellular loop 2 (ECL2) and the extracellular side of the transmembrane helix TM5, and its score was 40 (Table 2.2). The SHTNSVVNPF peptide corresponded to the transmembrane helix TM7, with a score of 40 (Table 2.2).

Protein sequence coverage: 6%

Matched peptides shown in **bold red**.

```
  1  MPIMGSSVYI  TVELAIAVLA  ILGNVLVCWA  VWLNSNLQNV  TNYFVVSLAA
 51  ADIAVGVLAI  PFAITISTGF  CAACHGCLFI  ACFVLVLTQS  SIFSLLAIAI
101  DRYIAIRIPL  RYNGLVTGTR  AKGIIAICWV  LSFAIGLTPM  LGWNNCGQPK
151  EGKNHSQGCG  EGQVACLFED  VVPMNYMVYF  NFFACVLVPL  LLMLGVYLRI
201  FLAARRQLKQ  MESQPLPGER  ARSTLQKEVH  AAKSLAIIVG  LFALCWLPLH
251  IINCFTFFCP  DCSHAPLWLM  YLAIVLSHTN  SVVNPFIYAY  RIREFRQTFR
301  KIIRSHVLRQ  QEPFKAAGTS  ARVLAAHGSD  GEQVSLRLNG  HPPGVWANGS
351  APHPERRPNG  YALGLVSGGS  AQESQGNTGL  PDVELLSHEL  KGVCPEPPGL
401  DDPLAQDGAG  VS
```

Figure 2.17. A$_{2A}$R dimer identification by LC-MS/MS after chymotrypsin in-gel digestion. *Bands corresponding to the A$_{2A}$R dimer were in-gel digested with chymotrypsin and analysed by LC-MS/MS. (**A**) Sequence coverage of the A$_{2A}$R dimer, with the identified unique peptides highlighted in red. (**B**) Sequence coverage on the secondary structure of the A$_{2A}$R with the identified unique peptides highlighted in green.*

The A$_{2A}$R monomer digested with chymotrypsin was identified with a sequence coverage of 16%, and 7 unique peptides were detected (Figure 2.18). The LNSNLQNVTNY peptide corresponded to the cytoplasmic end of the transmembrane helixes TM1 and TM2, and the intracellular loop 1 (IL1). It obtained a score of 61, which was above the acceptance criterion (Table 2.2). The AAADIAVGVL peptide corresponded to the transmembrane helix 2 (TM2), with a score of 58 (Table 2.2). The AITISTGF peptide corresponded to the extracellular side of the transmembrane helix TM2 and part of the extracellular loop 1 (EL1), with a score of 43 (Table 2.2). The SLLAIAIDRY peptide corresponded to the transmembrane helix TM3, with a score of 61 (Table 2.2). The AIGLTPMLGW peptide corresponded to the extracellular end of the transmembrane helix TM4, with a score of 43 (Table 2.2). The FEDVVPMNY peptide corresponded to the end of the extracellular loop 2 (EL2) and the extracellular side of the transmembrane helix TM5, with a score of 60 (Table 2.2). Finally, the SHTNSVVNPFIY peptide corresponded to the transmembrane helix TM7, and it obtained the highest score of 72 (Table 2.2).

A   B

Protein sequence coverage: 16%

Matched peptides shown in **bold red**.

```
  1 MPIMGSSVYI TVELAIAVLA ILGNVLVCWA VWLNSNLQNV TNYFVVSLAA
 51 ADIAVGVLAI PFAITISTGF CAACHGCLFI ACFVLVLTQS SIFSLLAIAI
101 DRYIAIRIPL RYNGLVTGTR AKGIIAICWV LSFAIGLTPM LGWNNCGQPK
151 EGKNHSQGCG EGQVACLFED VVPMNYMVYF NFFACVLVPL LLMLGVYLRI
201 FLAARRQLKQ MESQPLPGER ARSTLQKEVH AAKSLAIIVG LFALCWLPLH
251 IINCFTFFCP DCSHAPLWLM YLAIVLSHTN SVVNPFIYAY RIREFRQTFR
301 KIIRSHVLRQ QEPFKAAGTS ARVLAAHGSD GEQVSLRLNG HPPGVWANGS
351 APHPERRPNG YALGLVSGGS AQESQGNTGL PDVELLSHEL KGVCPEPPGL
401 DDPLAQDGAG VS
```

Figure 2.18. A$_{2A}$R monomer identification by LC-MS/MS after chymotrypsin in-gel digestion. Bands corresponding to the A$_{2A}$R were in-gel digested with chymotrypsin and analysed by LC-MS/MS. (A) Sequence coverage of the A$_{2A}$R monomer with the identified unique peptides is highlighted in red. (B) Sequence coverage on the secondary structure of the A$_{2A}$R with the identified unique peptides highlighted in blue.

Table 2.2. Identification of A$_{2A}$R unique peptides after in-gel digestion by LC-MS/MS. *The resulting peptides from in-gel digestion with trypsin or chymotrypsin of the A$_{2A}$R monomer and dimer were detected by LC-MS/MS. Data were analysed using Mascot Daemon against the SwissProt database.*

Identified protein	Form	Digestion	Matches	Unique peptides	Peptide score
AA2AR_HUMAN	Monomer	Trypsin	2	KQMESQPLPGER	54
				RYNGLVTGTR	43
AA2AR_HUMAN	Dimer	Chymotrypsin	3	LAIAIDRYI	40
				FEDVVPMNY	40
				LSHTNSVVNPF	40
AA2AR_HUMAN	Monomer	Chymotrypsin	7	LNSNLQNVTNY	61
				AAADIAVGVL	58
				AITISTGF	43
				SLLAIAIDRY	61
				AIGLTPMLGW	43
				FEDVVPMNY	60
				SHTNSVVNPFIY	72

2.5 DISCUSSION

The main aims of this chapter were to express, solubilize, purify, and identify the A$_{2A}$R. For this, the C-terminal truncated A$_{2A}$R was expressed in *Pichia pastoris* SMD1163, and the membrane fraction was prepared by breaking the yeast's cell wall. The use of glass beads proved to be optimal. The A$_{2A}$R was successfully solubilized from the membrane fraction using SMA2000 or DDM, but it could not be solubilized effectively using DIBMA polymers. However, solubilization efficiency improved when Glyco-DIBMA was used at higher concentrations. After an optimization procedure, the A$_{2A}$R-SMALP was successfully purified using His-pur Ni-NTA resin in Tris-HCl buffer. In contrast, the A$_{2A}$R-Glyco-DIBMALP could not be purified using this method. Similarly, it was not possible to purify the A$_{2A}$R-DDM away from the main *P. pastoris* contaminant. Identification of the A$_{2A}$R-SMALP monomer and dimer was confirmed by in-gel digestion and LC-MS/MS after trypsin and chymotrypsin digestion. Higher sequence coverage was obtained after chymotrypsin digestion, and the dimer was identified only after chymotrypsin digestion. The main *P. pastoris* contaminant was identified as the alcohol dehydrogenase 2 (ADH2) from *Kluyveromyces marxianus*.

Similar to this project, the expression of the A$_{2A}$R in *Pichia pastoris* has been achieved successfully by many researchers (Fraser, 2006; Asada *et al.*, 2011; Bertheleme *et al.*, 2015; Jamshad *et al.*, 2015), and a wide range of publications have reported heterologous protein expression of mammalian membrane proteins and GPCRs in *Pichia pastoris* (Jamshad *et al.*, 2008; Bertheleme *et al.*, 2015; Byrne, 2015; Routledge *et al.*, 2016). Furthermore, on many occasions, the AOX1 promoter has been used and enhanced for the production of recombinant proteins in this expression system (Vogl and Glieder, 2013;

Yang and Zhang, 2018). Proper expression of the $A_{2A}R$ was achieved at low temperatures according to previous optimization procedures for the expression of this receptor in *P. pastoris* (Jamshad *et al.*, 2015). In the present study, no additives were incorporated in the culture medium, although it has been demonstrated that its supplementation with specific receptor ligands, DMSO, and histidine can benefit GPCR expression (André *et al.*, 2006).

In this study, the C-terminal truncated sequence was used for the expression of the $A_{2A}R$, as it has been shown to code for a stable, functional, and degradation-resistant protein (Jaakola *et al.*, 2008; Doré *et al.*, 2011; Hino *et al.*, 2012; Cheng *et al.*, 2017; Prosser *et al.*, 2017; Hinz *et al.*, 2018).

To isolate the membrane fraction, where the $A_{2A}R$ was located, the thick cell wall of *P. pastoris* was disrupted by different mechanical methods, including the use of acid-wash glass beads, the French press, and the Avestin Emulsiflex C3 cell-disrupter. All of them were effective in breaking the cell wall. Nevertheless, the use of glass beads proved to be the fastest, easiest, and most effective method, as substantial amounts of membrane pellets could be recovered, and the beads could be used for small- and large-scale preparations. Furthermore, they are inexpensive, require small amounts of beads, can be reused, are not heavy, and can disrupt the cells by simply vortexing the tubes. Similarly, glass beads have been extensively used to disrupt *Pichia pastoris* cells (Kielkopf *et al.*, 2021; Al-Jubair *et al.*, 2022), as well as other yeast cells such as *Saccharomyces cerevisiae* (Stowers and Boczko, 2007) and *Candida spp.* (Lim *et al.*, 2008). In addition to cell disruption, glass beads are used for genetic transformation of yeast (Rivera *et al.*, 2014).

Alternatively, the use of the Avestin Emulsiflex C3 cell-disrupter was also an effective method to break the yeast cell wall, as it is a benchtop high-pressure homogeniser ideal for cell disruption and particle size reduction, and has already been used to effectively disrupt *P. pastoris* cell walls to solubilize the $A_{2A}R$ from the membrane fraction (Routledge *et al.*, 2020). However, it can only be used for large-scale cultures, as a minimum of 50 mL of cell suspension is required; therefore, it is not suitable for small-scale preparations. In addition, the breaking process can take longer and can complicate possible downstream processes such as protein purification, as observed in the present study. In this project, many protein bands corresponding to *P. pastoris* contaminants were obtained after IMAC purification in comparison to the results obtained when glass beads or the French press were used following the same protocol. This can be explained by the fact that C3 disrupted the cells more efficiently than the other methods, but simultaneously caused solubilization of proteins that interacted with the Ni-NTA resin and co-eluted with the protein of interest. On the other hand, the French press was also effective in breaking the yeast cell wall, although it showed lower disruption efficiency than glass beads. Similarly, *Goldberg et al*. observed that using the French press to break untreated bacterial cells or yeast, fungus,

and spores with tough cell walls was not effective (Goldberg, 2021). In contrast, it has been successfully used to disrupt mammalian cells and fragile bacteria (Sheng *et al.*, 2012).

The $A_{2A}R$ was successfully extracted and solubilized from the membrane fraction encapsulated in SMALPs and Glyco-DIBMALPs, or solubilized with DDM, for downstream experiments. Similarly, Jamshad et al. successfully solubilized the $A_{2A}R$ from *Pichia pastoris* membranes using SMA2000 at 2.5% and compared its solubilization and thermostability after solubilization with DDM (Jamshad *et al.*, 2015). Likewise, different GPCRs, including melatonin and ghrelin receptors and CD81, have been solubilized from *P. pastoris* membranes with SMA2000 (Logez *et al.*, 2016; Ayub *et al.*, 2020). Moreover, SMA2000 has been used to solubilize membrane proteins from other expression systems, including *E. coli* (Gulamhussein *et al.*, 2019), insect cells (Hardy *et al.*, 2019), and mammalian cells (Horsey *et al.*, 2020). Thus, SMA2000 has been broadly used to effectively solubilize membrane proteins, and its solubilization efficiency is comparable to that of detergents.

Gulamhussein et al. compared the solubilization of membrane proteins BmrA and ZipA from *E. coli* and the $A_{2A}R$ from *P. pastoris* using SMA2000 and DIBMA polymers, and reported that both polymers were able to solubilize the three membrane proteins. The solubilization efficiency of ZipA was significantly lower with DIBMA than with SMA2000, as was observed in the present study for the $A_{2A}R$. Nevertheless, the authors observed that SMA2000 did not offer any improvements over DIBMA in the solubilization of $A_{2A}R$, in contrast to the results obtained in this study. Moreover, elongating the incubation times with the polymers to 18h and 24h did not improve the solubilization efficiency (Gulamhussein *et al.*, 2020). They also reported that the method used for preparing DIBMA determines the solubilization efficiency, as small variations in the protocol can lead to large variations in results. Despite these previous findings, the solubilization of the $A_{2A}R$ with DIBMA polymers was intended for this study because it contains an aliphatic side chain instead of an aromatic styrene group. This makes it larger than SMA polymers that have been successfully used to date, which can lead to the formation of larger nanodiscs surrounding membrane proteins and allow their complete movement to undergo conformational changes upon ligand binding by applying less lateral pressure (Oluwole *et al.*, 2017).

The $A_{2A}R$ was purified by IMAC after optimization. The results demonstrated that no imidazole should be used during the recirculation process to allow the $A_{2A}R$-SMALP to bind to the resin strongly enough to avoid its loss in the flow-through and wash fractions. Nevertheless, 10 mM imidazole has been used in previous studies for the equilibration of Ni-NTA resins for the purification of GPCRs (Logez *et al.*, 2016) and the $A_{2A}R$ (Carpenter and Tate, 2017).

In the present study, 60 mM imidazole was optimal for the elution of the $A_{2A}R$, as it allowed the attainment of the highest $A_{2A}R$-SMALP concentration while minimizing the co-eluting contaminants. In

contrast, Gulamhussein *et al*. did not observe elution of the $A_{2A}R$-SMALP with 60 mM imidazole, but they used 200 mM imidazole for elution (Gulamhussein *et al.*, 2020). Moreover, no contaminants co-eluted with the protein of interest, in contrast to the results observed in this study (Gulamhussein *et al.*, 2020). Similar results were obtained under identical conditions for purification of the $A_{2A}R$-SMALP (Jamshad *et al.*, 2015) and the $A_{2A}R$-DDM (Singh *et al.*, 2012). This could be explained by the fact that the presence of high concentrations of mADH can be dependent on the strain, construct, and transformation method used. Chen *et al*. identified the mitochondrial alcohol dehydrogenase isozyme III (mADH) as one of the major contaminants in native *P. pastoris* proteins that co-elute when 100 mM imidazole is used for IMAC purification (Chen *et al.*, 2014). Hence, they engineered an mADH gene-knockout *P. pastoris* strain by gene disruption, which allowed the downstream purification of target proteins (Chen *et al.*, 2014). Although ADH plays a key role in yeast fermentation, it is not directly involved in basic metabolic pathways; therefore, disruption of the mADH gene did not affect cell growth, and represents an attractive approach to eliminate the presence of the co-eluting contaminant, which can interfere in downstream experiments after protein purification (De Schutter *et al.*, 2009). This could be an alternative approach for purifying the $A_{2A}R$-DDM away from this contaminant.

His-pur Ni-NTA offered the highest recovery and purity of the $A_{2A}R$-SMALP, and it has been used for the purification of the $A_{2A}R$ in previous studies (Gulamhussein *et al.*, 2020). Alternative resins have been successfully used for this purpose (Jamshad *et al.*, 2015). Singh *et al*. compared the purification of the detergent-solubilised $A_{2A}R$ using Ni^{+2} and Co^{+2} resins, and used higher imidazole concentrations to elute the target protein from the Ni^{+2} resin. This is because Co^{+2} resins have higher specificity and at the same time lower affinity for His-tagged proteins than Ni^{+2} resins do. Consequently, cleaner protein preparations are usually obtained using Co^{+2} resins (Singh *et al.*, 2012). Hence, the use of Co^{+2} resins is an attractive approach for optimizing $A_{2A}R$-DDM purification.

Although it was possible to confirm the solubilization of the $A_{2A}R$ from the membrane fraction using Glyco-DIBMA, purification was not possible. This can be explained by the low solubilization efficiency, which causes low protein concentration to be detected after purification. Although Gulamhussein *et al*. reported the successful purification of $A_{2A}R$-DIBMALP expressed in *P. pastoris*, lower protein yields were obtained with DIBMA than with SMA, similar to the results obtained in this study (Gulamhussein *et al.*, 2020). Moreover, it has been shown that the contamination grade obtained using DIBMA was higher that that obtained using SMA2000 (Oluwole *et al.*, 2017). A challenge associated with the use of DIBMA is that it can cause substantial streaking on SDS-PAGE gels, and obscure visualisation of the sample (Oluwole *et al.*, 2017). Hence, DIBMA polymers can affect the migration and detection of solubilised proteins by Coomassie staining and western blotting. Therefore, an alternative to determine solubilisation efficiency is to compare the intensity of the bands corresponding to the non-solubilized

fraction (which does not contain the polymer) with that of a negative control (Gulamhussein *et al.*, 2020).

After purification, the $A_{2A}R$ monomer and dimer were identified by in-gel digestion and LC-MS/MS with low sequence coverage. Many membrane proteins have a limited number of tryptic cleavage sites, indicating that this protease does not provide adequate proteolysis for identification. In other cases, proteins can show a suboptimal distribution of tryptic cleavage sites, resulting in the formation of peptides that are too long or too short to be detectable by MS. In addition, post-translational modifications (PTMs) can limit trypsin access to cleavage sites or render Lys and Arg residues resistant to trypsin digestion. As a membrane protein, the $A_{2A}R$ can be challenging to digest into detectable peptides by mass spectrometry due to the limited access of proteases to tightly folded regions, such as transmembrane helices, and its suboptimal distribution of cleavage sites, which results in the formation of peptides with a certain length that can be difficult to detect by MS. To overcome these challenges, alternative proteases can be used alone or in combination to achieve optimal protein digestion. To test their applicability in proteomics, Giansanti *et. al.* optimized protocols for six alternative proteases: chymotrypsin, Lys-C, Lys-N, Asp-N, Glu-C, and Arg-C (Giansanti *et al.*, 2016). Although the use of chymotrypsin improved the $A_{2A}R$ digestion and sequence coverage, optimization is needed for further downstream applications of peptide detection by MS.

In conclusion, the $A_{2A}R$ was successfully expressed, solubilized, and purified from the membrane using SMA2000 after extensive optimization. In contrast, it could not be successfully solubilized and purified using DIBMA polymers. Similarly, it was not possible to purify the $A_{2A}R$-DDM away from the mADH contaminant in *P. pastoris*. Purified $A_{2A}R$ monomer and dimer were identified by LC-MS/MS with low sequence coverage, which was improved by using chymotrypsin instead of trypsin. The identification of the purified $A_{2A}R$-SMALP by in-gel digestion and LC-MS/MS has been shown for the first time, which is a pioneering work for the identification of other membrane proteins and GPCRs.

3. CHAPTER 3 – ANALYSIS OF THE LIPID ENVIRONMENT OF THE A$_{2A}$R EXPRESSED IN P. PASTORIS SMD1165 BY LC-MS/MS

3.1 INTRODUCTION

Membrane proteins perform multiple biochemical functions, including transport, signalling, and energy production (Kharche *et al.*, 2020). These membrane proteins directly and indirectly interact with lipids and are susceptible to changes in their lipid environment (Pan *et al.*, 2022; Levental *et al.*, 2023). Hence, lipids in the plasma membrane play a crucial role in membrane protein activity and function. The influence of the most abundant phospholipids and cholesterol on membrane properties and function of GPCRs is summarised in Table 3.1.

Table 3.1. Presence of phospholipids, sphingomyelin, and cholesterol in mammalian membranes and their influence on membrane properties and GPCR activity.

	Charge	% in mammalian membranes	Membrane leaflet	Membrane curvature	Functions	References
PC	Zwitterionic	45-50% of PL	Outer	No influence (cylindrical)	Membrane building block Can influence membrane protein activity Neutral on GPCRs	(Joardar *et al.*, 2022) (Murate *et al.*, 2016) (Zhukovsky *et al.*, 2019) (Różalska *et al.*, 2018)
PE	Zwitterionic	15-25% of PL	Inner>outer	Negative (cone-shape)	Membrane building block Forms H-bonds with Arg residues Lateral pressure and membrane curvature Negative regulator of GPCRs	(Chakrabarti, 2021) (Dawaliby *et al.*, 2016) (Pohl *et al.*, 2019)
PS	Anionic	5-10% of PL	Inner	No influence (cylindrical)	Organization of the cell membrane Modulates the local membrane potential Influences membrane protein activity Positive regulator of GPCRs	(Leventis *et al.*, 2010) (Vance, 2018) (Kashikuma *et al.*, 2023)
PI	Anionic	10-15% of PL	Inner	No influence (cylindrical)	Signalling (phosphorylation) Interacts with membrane proteins Attracts signalling components to the plasma membrane Positive regulator of GPCRs	(Arumugam *et al.*, 2015) (Blunsom *et al.*, 2020) (Barneda *et al.*, 2019)
PG	Anionic	1-2% of PL	Inner	No influence (cylindrical)	Interacts with membrane proteins Positive regulator of GPCRs	(Furse, 2017) (Numata *et al.*, 2023) (Dawaliby *et al.*, 2016)
SM	Zwitterionic	up to 20% of total lipids	Outer	No influence (cylindrical)	Membrane building block Interacts with cholesterol Interacts with membrane proteins Forms lipid rafts	(Adada *et al.*, 2016) (Gault *et al.*, 2010) (Scassellati *et al.*, 2010).
Cho	Hydrophobic	20-40% of total lipids	Outer	Negative (cone-shape)	Structural component of membranes Modulates membrane fluidity increases the membrane thickness Interacts with GPCRs Required for GPCR activity	(Risselada, 2019) (Subczynski *et al.*, 2017) (Jakubík *et al.*, 2021)

The A$_{2A}$R has a high propensity to bind lipids as allosteric modulators. Hence, its conformation dynamics are dependent on its lipid environment, and studying the A$_{2A}$R in its native environment is essential for its accurate characterization (Bruzzese *et al.*, 2020). Several methods have been developed to study the role of the lipid environment in protein function. The use of detergents as the most common approach for integral membrane protein extraction and solubilisation but is arguable if this is the best method because of the inherent removal of native lipids and the disruption of lipid-protein interactions (Cecchetti *et al.*, 2021). The development of membrane mimetics, including nanodiscs and SMALPs, has enabled the identification of lipids surrounding membrane proteins (Schuler *et al.*, 2013; Teo *et al.*, 2019). Alternatively, associated lipids from purified plasma membrane proteins have been studied through native MS experiments (Bolla *et al.*, 2019). Various studies demonstrate the applicability of SMALPs and nanodiscs in characterizing the lipid environment surrounding membrane proteins. Nonetheless, these membrane mimetic systems have typically been used as controlled membrane surfaces to mechanistically examine lipid-protein interactions (Cuevas Arenas *et al.*, 2016; Routledge *et al.*, 2020; Swainsbury *et al.*, 2014). Nanodiscs and SMALPs of defined phospholipid compositions have also been used for the reconstitution and characterization of GPCRs (Guo *et al.*, 2023). At the same time, it has been demonstrated that phospholipids in SMALPs can also be exchanged, offering an alternative approach for studying the activity of isolated membrane proteins surrounded by specific lipid environments (Hazell *et al.*, 2016). In addition to lipid-protein interactions, GPCRs have been shown to preserve protein-protein interactions in SMALPs (Damian *et al.*, 2018). However, GPCRs are not only modulated by direct interactions with lipids. Their behaviour also depends on the lipid composition of their surrounding environment as bilayer thickness, curvature, ordering, geometry and lateral pressure can modulate the GPCR activity (Gutierrez *et al.*, 2019).

P. pastoris has been used as an expression system for the study of membrane proteins and their interaction with the lipid environment (Routledge *et al.*, 2020). The lipid profile of *P. pastoris* cells exhibits significant variability and diversity in terms of lipid abundance, fatty acid chain lengths, and the degree of unsaturation (Yu *et al.*, 2022). In contrast to *S. cerevisiae*, *P. pastoris* can produce polyunsaturated fatty acids (PUFAs), and it has been demonstrated that the relative amount of PUFAs is much higher in *P. pastoris* than in other yeasts (Wriessnegger *et al.*, 2009). It has been shown that the most abundant PC, PE, PS, PI, PG, and CL species in *P. pastoris* contain mono- and polyunsaturated fatty acyl chains of 34 and 36 carbon atoms, with 1 to 5 double bonds. In some cases, phospholipid species with 6 double bonds have been identified (Adelantado *et al.*, 2017).

Therefore, membranes are heterogeneous in composition, and it has been extensively demonstrated that lipids in the plasma membrane influence the membrane protein activity. For example, it has been proposed that anionic lipids, including PS, PG, and PI, together with cholesterol, act as positive

I. Company Marin, PhD Thesis, Aston University 2024

regulators of GPCR activity, whereas PE can act as a negative regulator and PC as neutral (Dawaliby *et al.*, 2016; Jakubík and El-Fakahany, 2021). Consequently, great interest has emerged over the recent years for characterizing the relevant lipids for protein structure and function (Tzortzini and Kolocouris, 2023).

Although there is currently an extensive understanding of lipids, a full definition of the function of the eukaryotic lipidome remains elusive. Compared to protein analysis, this can be explained by the high structural diversity that exist among all lipids, as well as their nature, solubility, how they assemble, and the complexity of the techniques needed for their study and manipulation (Orešič *et al.,* 2008). Nonetheless, advances in the analysis of lipid characteristics and their roles in the context of genomics and proteomics are being made that are leading to an understanding of their role in cellular physiology and pathology. This emphasizes the need for an integrated study of cellular lipids using lipidomic methods (Hu *et al.*, 2018). Lipidomics is a branch of metabolomics based on the large-scale study of lipids. It aims to address the identification and quantification of lipid species in a given sample, as well as their cellular and tissue distribution, together with their related signalling pathways and networks in a biological system (Postle, 2012). Eventually, the aim is to integrate all the branches of metabolomics to understand cellular metabolism, shed light on human disease states, and understand lipid changes under pathological conditions (Fonteh *et al.*, 2006; Suvitaival *et al.*, 2018). Advances in chromatography and mass spectrometry (MS) technologies, together with NMR spectroscopy, have enabled more comprehensive lipid profiling of biological samples (Jurowski *et al.*, 2017). MS is an excellent qualitative and quantitative technique that has been the most relevant approach in lipidomics in recent years. Routine procedures in MS-based lipidomics consist of sample collection, lipid extraction, lipid separation, MS data acquisition, post-acquisition data processing, and physiological significance clarification (Hu *et al.*, 2018).

Various lipid extraction methods can be used for sample preparation for MS-based lipid analysis. Liquid phase lipid extraction has been the predominant extraction method owing to its applicability to a wide range of biological samples (Folch *et al.*, 1957; Bligh and Dyer, 1959). An alternative lipid extraction method, methyl tert-butyl ether (MTBE), was developed by Matyash *et al*. (2008) using MTBE, methanol, and water. This offers some practical advantages compared to the Folch method, as the lipid-containing organic phase forms the upper layer during phase separation due to the low density of MTBE, which simplifies sample collection and minimizes contamination (Matyash *et al.*, 2008). Moreover, it improved the recovery of most of the lipid classes (Qu *et al.*, 2014).

Lipid samples can be analysed by direct infusion shotgun MS (Wang *et al.*, 2016). Nevertheless, MS is typically coupled to chromatographic separation techniques. Chromatographic methods allow the

I. Company Marin, PhD Thesis, Aston University 2024

separation of isomeric species with identical m/z values. Hence, they are used for the analysis of complex biological samples (Fabritius *et al.*, 2021). In the present study, lipid samples were analysed by reverse-phase (RP) liquid chromatography (LC). LC is commonly used for the separation and analysis of phospholipids, sphingolipids, and neutral lipids as it integrates excellent lipid separation efficiency (Harvey *et al.* 2023). High-performance liquid chromatography (HPLC) is the most widely used separation method in lipidomics since it offers a high separation efficiency (Bielawski *et al.*, 2010). RP chromatography is the most commonly used LC technique in lipidomics. It consists of a polar mobile phase and a non-polar stationary phase; therefore, it relies on the interaction of the non-polar functional groups of the analytes with the hydrophobic surface of the stationary phase (Moldoveanu *et al.*, 2013; Žuvela *et al.*, 2019). Highly aqueous initial conditions are used for analyte elution in RP columns, moving progressively to higher organic solutions. Consequently, lipids are separated according to the hydrophobicity of their fatty acyl chains in RP chromatography, and their elution order is associated with the carbon chain length and number of double bonds. In contrast, lipids are separated according to their head groups in normal-phase chromatography; lipids with identical polar head groups elute together (Bang *et al.*, 2012).

Once the analytes are separated, they are analysed in the mass spectrometer. The analysis of lipids and other molecules by mass spectrometry consists of three crucial steps: sample ionization, ion separation, and ion detection. In the ionization step, ions are formed from molecules in the sample by an ion source. In the separation step, lipids and other metabolites are separated under an electric or magnetic field, based on their m/z ratios. Finally, the separated ions reach the detector, which detects the mass and relative amount of the analytes (Züllig *et al.*, 2021).

ESI is a soft-ionization technique in which the samples are dissolved in a volatile solvent and pushed through a fine charged capillary held at a high voltage. This results in the spraying of the analyte-containing solution into tiny droplets, in which ions are transferred from the solution into a gaseous phase (Isaac, 2011). In ESI, the transition of ions from the solution into a gas phase involves the dispersal of a fine spray of charged droplets followed by solvent evaporation, also termed desolvation, and ion ejection from the droplets. A constant stream of the sample in solution is directed through a capillary tube. This generates a mist of highly charged droplets with the same polarity as the capillary voltage (Wilm, 2011). With the assistance of an increased ESI source temperature and an additional stream of nitrogen drying gas, the charged droplets undergo continuous size reduction as the solvent evaporates. The decrease in the droplet size leads to an increase in the surface charge density, which causes an electric field strength within the charged droplets. At this point, droplets deform owing to the electrostatic repulsion of like charges, which becomes more powerful than the surface tension for holding the droplet together (Tycova *et al.*, 2021). Eventually, an unstable kinetic and energetic critical

I. Company Marin, PhD Thesis, Aston University 2024

point is reached, known as the Rayleigh limit, where the ions located on the surface of the droplets are expelled into the gaseous phase. The emitted ions are collected by a sampling skimmer cone and subsequently accelerated into the mass analyser (Ho *et al.*, 2003).

Most lipids are ionized as single-charged molecules, with the exception of CL under certain conditions. The ionization efficiency and type of adduct formation depend on the chemical properties and the propensity of an individual analyte to gain or lose a charge in a given environment (Gonzalez-Riano *et al.*, 2021). Furthermore, it also depends on the additives in the solvents or LC mobile phase to enhance adduct ion formation (Kostiainen *et al.*, 2009). Anionic lipids such as FA, PA, PS, PG, PI, and CL, carry a net negative charge at physiological pH, which makes them easily detectable in the negative ion mode as $[M-H]^-$ adducts. Weakly anionic lipids such as PE, Ceramides, and eicosanoids carry a net negative charge at alkaline pH, which facilitates their detection in the negative ion mode as $[M-H]^-$ adducts, although they can also be detected in positive ion mode as $[M+H]^+$ adducts (Buyukpamukcu *et al.*, 2007). In positive ion mode, lipid species that contain nitrogen atoms, such as PC, PE, PS, SM, and Cer, are predominantly detected as protonated molecules. In contrast, lipid species that do not contain nitrogen, such as PI, PG, CL, TAG, and DAG, are commonly detected as $[M+NH_4]^+$ when ammonium acetate or formate are used as mobile phase additives (Rush and van Breemen, 2017; Warren, 2018). Lipids that are usually detected in the positive ion mode can also be detected in the negative ion mode as $[M-H]^-$, $[M+COO]^-$, or $[M+CH_3COO]^-$ adducts, depending on the phospholipid classes and on the LC-MS buffer used, although at relatively low intensity (Godzien *et al.*, 2015; Gonzalez-Riano *et al.*, 2021).

ESI, which was employed in the present study, is commonly used in lipidomics as it overcomes the propensity of labile macromolecules to fragment when they ionize, including lipids. Therefore, this soft-ionization offers the advantage of conserving molecular ions (Hu and Zhang, 2018). Nevertheless, very limited structural information is obtained from the MS spectra, which contain information on the elemental composition of each analyte, and peaks correspond to molecular ions without fragmentation. Hence, each peak may correspond to a specific lipid in a sample. However, a lipid cannot be identified only by its elemental composition, as many different isomeric or isobaric lipid species can correspond to one peak with a specific m/z ratio (Vinaixa *et al.*, 2016; Chen *et al.*, 2022). The main challenge in lipidomics is caused by the high number and variability of lipid molecular species, which occupy a relatively narrow m/z window. Moreover, lipid analysis by MS is further complicated by the high number of isomeric and isobaric species. Isomeric lipids are those that have identical molecular formulas, but differ in atom arrangement and molecular properties; therefore, they have identical m/z ratios and cannot be resolved by MS. In contrast, isobaric species have a very similar nominal mass but a slightly different exact mass, which means they have highly similar m/z ratios and complicates their differentiation by MS, depending on the mass accuracy and resolution of the mass spectrometers. This

reflects the high diversity in natural lipidomes, high dynamic range of lipid concentrations, and different chemical properties (Batarseh *et al.*, 2018; Züllig *et al.*, 2021). To obtain structural information on the detected ions, chromatographic systems are commonly coupled to tandem mass spectrometry (MS/MS) (Seger *et al.*, 2020). In MS/MS, ions of interest or precursor ions, are selected in a first mass analyser and subsequently fragmented in a collision cell. Fragmented ions are separated in a second mass analyser and detected by the detector to obtain the fragmentation spectrum, which corresponds to the product ion spectrum for the specifically selected precursor ions (Mittal, 2015).

Different mass spectrometers can be used for MS/MS analysis. Here, lipid samples were analysed using the Select Series Cyclic ion mobility (IMS) system with an instrument geometry consisting of a quadrupole mass filter coupled to a trap cell, a circular path of ion mobility (cIM), a transfer region, and an extended time-of-flight (TOF) mass analyser (Figure 3.1).
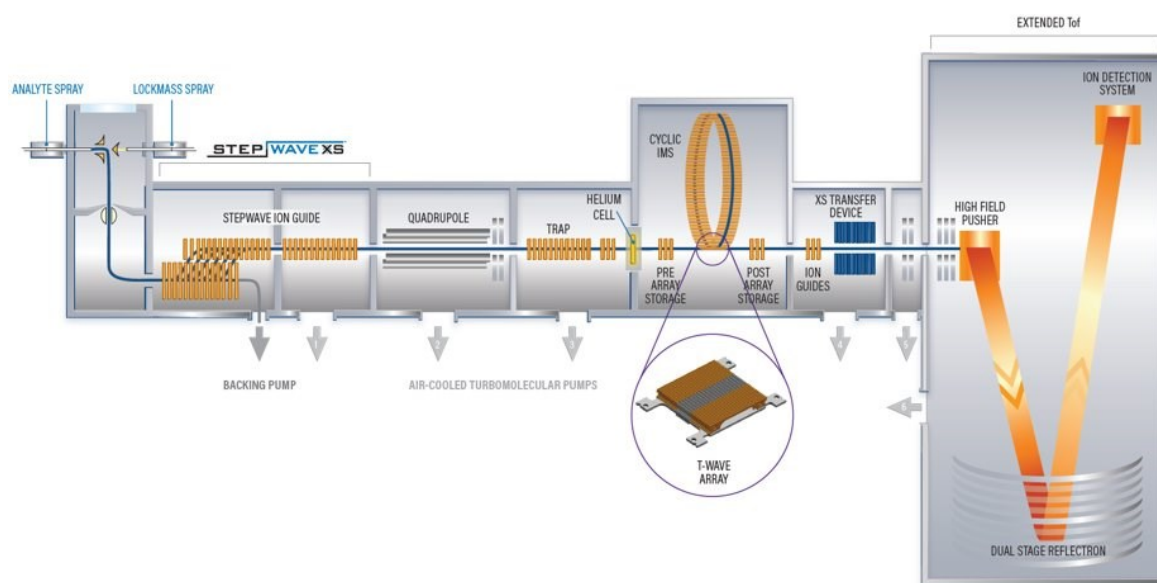
Figure 3.1. Instrument schematic of the Select Series Cyclic ion mobility (IMS) system showing the Q-cIM-ToF geometry (adapted from Giles et al., 2019).

Quadrupole mass analysers (Q) are low mass resolution mass spectrometers usually used as scanning instruments (Li *et al.*, 2021). Triple quadrupoles (QQQ) are the most routinely employed instruments for targeted qualitative and quantitative applications, although quadrupoles are often coupled to TOF or ion trap instruments, in which their elemental function is to isolate a given set of m/z ranges (Saleem *et al.*, 2023). Ion trap mass analysers function as mass spectrometers for ion storage, in which volatile positive and negative ions of a variable range of m/z values can be confined under appropriate electrode potential conditions (Patil *et al.*, 2017). By changing the voltages, the trajectories of the trapped ions become sequentially unstable according to their m/z ratio, and the ions leave the trapping field in order of m/z (Raffaelli and Saba, 2023). However, ion traps offer a lower mass resolution than

I. Company Marin, PhD Thesis, Aston University 2024

TOF instruments (Nolting *et al.*, 2019). TOF analysers are high-resolution mass spectrometers based on flight tubes that are employed to separate ions according to their mass and detect their relative abundance in a given sample. In the flight tube, the beam of ions is located in a plane at a fixed distance from the detector, and the ions are accelerated by an electric field after receiving the same kinetic energy (Volný, 2020). The traveling velocity of the ions is dependent on their mass, allowing the separation of analytes according to their m/z ratios. Ions of lower mass and the same charge travel down the flight tube faster, whereas ions of higher mass travel slower (Boesl, 2017) . Improvements in TOF technology have included the use of ion mirrors, which increase the travel distance within the tube and significantly improve TOF resolution (Scherer *et al.*, 2006). The separated ions hit a detector located at the end of the flight tube, which consists of a charged plate. The impact of ions on the plate generates an electric current of electrons, which can be computationally monitored and converted to a mass spectrum. This contains information regarding the m/z values of the ions and their relative abundances (Tamura *et al.*, 2021).

To contribute to a more comprehensive characterization of complex molecular mixtures, ion mobility instruments have been designed to provide additional ion separation and structural information. IMS involves the study of how ions move and interact with an inert gas under the influence of an electric field. In IMS, an electric field forces the ions to migrate through the gas in a drift section at a certain velocity. This velocity correlates with the friction of a specific analyte with the gas, which is dependent on its physicochemical characteristics, such as mass, charge, spatial atom arrangement, electronic distribution, and three-dimensional structure (Dodds and Baker, 2019). Hence, different ions are separated by their mobility (K). More mobile ions have higher velocities, so they travel faster under a specific electric field strength, whereas less mobile ions travel more slowly (May and McLean, 2015). Furthermore, the mobility of an analyte can be affected by the ionization source, solvents, voltage and pressure, polarity, type of adduct, and site of adduction, which in turn affect the molecular structure, conformation, and internal energy of the ion. Routinely, the measured mobility is converted into collision cross section values for each analyte (CCS) and provides information about the ion conformation according to their collision with the inert gas (Jurneczko and Barran, 2011; Mairinger *et al.*, 2018; Leaptrot *et al.*, 2019). Over the past few years, advances in instrumental design have further enhanced the sensitivity and selectivity of IMS; for example, with cyclic ion mobility instruments. Cyclic ion mobility (cIMS) consists of a unique circular path that enables the extension of the path length in which ions can be passed around the drift region multiple times (IMS[n]), allowing excellent analyte separation (Giles *et al.*, 2019).

In metabolomics, various experiments can be performed using MS/MS. Targeted metabolomics involves the analysis of a defined group of chemically characterized analytes and may be more

applicable to solving particular biological questions (Roberts *et al.*, 2012). Alternatively, untargeted metabolomics is based on the comprehensive analysis of all measurable analytes in each sample. Hence, it aims to identify or quantify all lipids in a sample, and is commonly used to obtain an overview of the lipid profile of a system (Hu and Zhang, 2018). Two main untargeted approaches are commonly used in lipidomics: data dependent acquisition (DDA) and data independent acquisition (DIA) (Rudt *et al.*, 2023). In DDA, a fixed number of precursor ions within a certain m/z range are selected and analysed by MS/MS. Generally, the mass spectrometer selects the most intense ions in the first analyser, which are subsequently fragmented and analysed. It offers a large coverage of identified lipids in a sample without previous knowledge, as well as high-quality MS/MS spectra for highly abundant precursors (Schwudke *et al.*, 2007). However, this method offers poor detection for low-abundance precursors. Alternatively, DIA is an untargeted MS/MS method in which all ions within a selected m/z range in a given sample are fragmented and analysed. In this case, the instrument focuses on a narrow m/z window of precursor ions in each cycle. This mass window is stepped across the entire m/z range, so that all the detected precursor ions are fragmented, and their corresponding MS/MS data is collected. Hence, DIA offers high-quality MS/MS spectra for all high- and low-abundance precursor ions (Alcoriza-Balaguer *et al.*, 2019).

Here, high definition MS^E (HDMS^E), a DIA method, was used to investigate the lipids that closely surround the A$_{2A}$R and could potentially be crucial for the conformation and activity of the receptor. Despite recognizing the importance of lipids in these processes, there exists a knowledge gap corresponding to a thorough empirical characterization of the lipids that surround this receptor and could have relevant roles in modulating its activity, emphasizing the need for further research and investigation in this area.

3.2 AIMS AND OBJECTIVES

The work reported in this chapter aimed to characterize the lipid environment of the A$_{2A}$R by identifying the phospholipids that closely surround the receptor in the plasma membrane. Therefore, this study aimed to test a lipid extraction and LC-MS/MS method to analyse the lipid composition of a purified protein encapsulated in SMALPs. The first aim was to identify the lipids that closely surround the A$_{2A}$R and co-purify with the receptor in the SMALP (A$_{2A}$R-SMALP). The second aim was to determine whether the lipids in the A$_{2A}$R-SMALP are different from those found in *P. pastoris* bulk membranes or from those solubilized from the membrane using SMA2000 in SMALPs (SMA-solubilized fraction). The last aim was to investigate whether SMA2000 has some preference for solubilizing certain lipids, and thus, to investigate whether lipids in the SMA-solubilized fraction are substantially different from those found in bulk membranes. Consequently, the objective was to extract lipids from *P. pastoris* bulk membranes,

SMA-solubilized fraction, and those co-purified in the A$_{2A}$R-SMALP, and to analyse and compare the lipids extracted from the three experimental groups by LC-MS/MS.

3.3 METHODS

3.3.1 Lipid extraction following the methyl tertiary-butyl ether (MTBE) method

Lipids from *P. pastoris* bulk membranes, SMA-solubilized lipids from the *P. pastoris* membrane fraction, and lipids contained in the purified A$_{2A}$R-SMALP were extracted following the MTBE method (Matyash *et al.*, 2008) (Figure 3.2). Prior to lipid extraction, total protein in the samples was quantified by the BCA assay and normalized to 250 µg protein/mL. For lipid extraction, 200 µL of the normalized sample was mixed with 300 µL of methanol and 1 mL of methyl tertiary-butyl ether (MTBE) using DNA low-binding Eppendorf tubes and Hamilton syringes. The mixture was sonicated for 30 s, vortexed for 1 min, and incubated on ice for 1 min a total of three times. LC-MS-grade water (200 µL) was added to obtain a final mixture of 2:3:10:2 (sample:methanol:MTBE:water). The mixture was vortexed for 1 min at maximum speed and centrifuged for 10 min at 1000 x g. The lipid-containing supernatant was collected into glass vials and the sample dried with nitrogen gas. The dried lipids were stored at -20°C until further analysis.

The Avanti EquiSPLASH reference sample was prepared by diluting 10 µL of Avanti EquiSPLASH in 990 µL isopropanol, and the mixture was vortexed for 15 s to ensure homogeneity of the solution. For LC-MS/MS lipid analysis, samples were resuspended in 50 µL isopropanol, and Avanti EquiSPLASH mix was added to the samples to obtain a final mixture of 20:5 sample:EquiSPLASH. A pooled mix composed of an aliquot (5 µL) from every sample (*P. pastoris* bulk membranes, SMA-solubilised fraction and A$_{2A}$R-SMALP lipids in triplicate) containing the Avanti EquiSPLASH internal standards was prepared for quality control (QC), and all samples were transferred to total recovery LC glass vials.

I. Company Marin, PhD Thesis, Aston University 2024
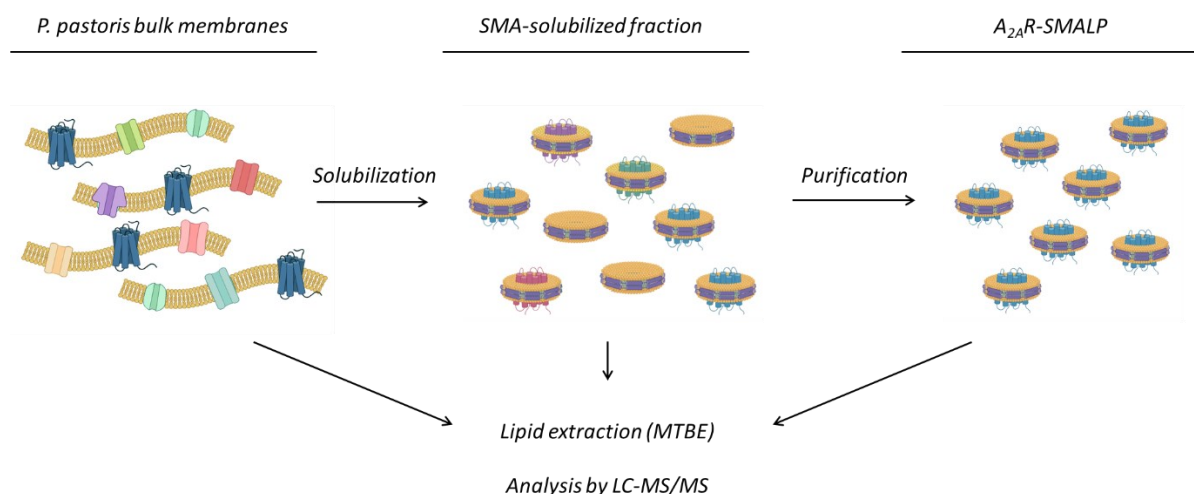
Figure 3.2. Schematic representation of the lipid samples under study. *P. pastoris bulk membranes were isolated and solubilized using SMA2000 to obtain the SMA-solubilized fraction. The A$_{2A}$R-SMALP was purified, and lipids from the three experimental samples were extracted following the MTBE method. The extracted lipids were analysed by LC-MS/MS.*

3.3.2 Lipid analysis by LC-MS/MS

Samples were analysed at Waters Corporation (Wilmslow, UK) using an ACQUITY UPLC I-Class PLUS System (Waters) coupled to a SELECT SERIES Cyclic ion mobility separation (IMS) mass spectrometry system (Waters) by reverse phase (RPLC) liquid chromatography.

For lipid analysis by RPLC, 2 and 4 µL of sample in the positive and negative ion modes, respectively, were injected onto an ACQUITY Premier CSH C18 Column 1.7 µm, 2.1 x 100 mm thermostated at 55°C. The sample temperature was set at 8°C to prevent solvent evaporation. A 10% isopropanol solution was used for the seal wash, and a 45:35:20 mixture of isopropanol:acetonitrile:water was used for the weak wash. The strong wash, needle wash, and purge were performed using 100% isopropanol. The analytes were eluted at 0.4 mL/min with solvent A (a 60:39:1 mixture of acetonitrile:water:1M ammonium formate with 0.1% formic acid) and solvent B (a 90:9:1 mixture of isopropanol:acetonitrile:1M ammonium formate with 0.1% formic acid). The gradient started from 50% solvent A and 50% solvent B, and was modified to 47% solvent A and 53% solvent B by 0.5 min, to 45% solvent A and 55% solvent B by 4 min, to 35% solvent A and 65% solvent B by 7 min, to 20% solvent A and 80% solvent B by 7.5 min, to 1% solvent A and 99% solvent B by 10 min, and returned to the starting conditions by 12 min, for a total run time of 12 min per sample. Leucine enkephalin (Leu-Enk) prepared at 200 pg/µL in a 50:50 mixture of acetonitrile:water was infused as a Lockspray.

Data were collected in ESI positive (+) ionization mode in separate runs. The capillary voltage was set to 2.8 kV. The cone voltage was set to 40 V and the source offset was set to 30 V. The source

82

temperature was set to 120°C and the desolvation gas temperature to 500°C. The cone gas flow was 150 L/h and the desolvation gas flow was 750 L/h. The nebulizer gas pressure was set to 6 bar and the reference capillary was set to 3 kV. The Lockspray flow rate was set to 20 μL/min. The MS was operated in full scan V-mode with an acquisition mass range from 100 to 2000 m/z. The scan time of 0.1 s was used on the MS and MS/MS levels. An identical scan time was used to acquire the lockspray and apply corrections, with an interval of 30 seconds, scans to average 4, and a mass window of ±0.5.

The cIM was operated with a single pass and data collected at 5 pushes per bin. Travelling wave (TW) static and start height were set to 15 V, and the TW limit height to 35 V, with a TW ramping rate set to 2.5 V/ms, and sideways and FWD/REV TW velocity to 375 m/s. The ADC Start Delay was set to 18 ms for an IMS cycle time of 78 ms. The cyclic sequence was as follows: injection for 10 ms, separation for 8 ms, and ejection and acquisition for 24 ms.

The samples were analysed using data independent acquisition (DIA - HDMS^E). The HDMS^E experiment was based on full scan precursor and fragment ion scanning. For tandem MS/MS, a collision energy of 20 eV ramping to 45 eV was used.

The detector, lockmass, calibration, resolution, and sensitivity checks were performed prior to sample processing. Briefly, Leucine enkephalin was infused at 20 μL/min with the attenuation set to 5%, and once the beam was stable, MS at 1 scan/s was acquired and 20 scans were combined. A peak corresponding to the lockmass leucine enkephalin ion was expected at m/z 556.2771 in the positive ion mode. The resolution (FWHM) was expected to be ≥30,000 and the sensitivity ≥8,000 cps.

For LC-MS and LC-MS/MS acquisition, a suitable number of conditioning injections were incorporated to ensure the stability and reproducibility of the test injections. A minimum of 3 solvent blanks and 4 Avanti EquiSPLASH standards were injected for column conditioning. Once the column was conditioned, Avanti EquiSPLASH standard mixture was injected six times, and biological replicates of the experimental samples were randomized and injected once. Quality control (QC) samples were injected once every 5 runs.

3.3.3 Data treatment and lipid identification

Lipid identification was performed by manual MS and MS/MS spectral interpretation using the MassLynx mass spectrometry software (Waters) and LIPID MAPS® Lipidomics Gateway to search for possible lipid identifications on a computationally generated database of phospholipid classes (https://www.lipidmaps.org/tools/ms/gp_ox_form.php). Lipid identification was also performed by comparing the acquired MS/MS data with a Waters proprietary database using the Progenesis QI

Software (Waters). MassLynx was used to generate the total ion chromatogram and extracted ion chromatograms, as well as the combined spectra, while Progenesis QI was used to obtain the experimental m/z of the identified compounds, their retention times, mass errors, abundances, and scores.

Progenesis QI was used to calibrate the data using the standard Leucine enkephalin lock mass, considering its m/z 556.2771 in the positive ion mode. Sample ions were automatically aligned to compensate for drifts in the retention time between runs, and the compounds in the sample were located by performing an automatic peak picking. The adduct forms $[M+H]^+$, $[M+Na]^+$, $[M+K]^+$, and $[M+NH_4]^+$ were included for lipid identification. To allow comparisons across different sample runs, total ion abundance was used as a normalization method. Alternatively, data were normalized to a set of housekeeping compounds obtained from the added internal standard EquiSPLASH mix to the samples. Compounds were identified by employing the Progenesis MetaScope method using Waters database with a precursor tolerance of 6 ppm and performing a theoretical fragmentation with a fragment tolerance of 6 ppm.

To filter the data for lipid identification, features with no possible identifications were discarded. The data were sorted by maximum abundance, and the fragmentation spectra of all the compounds were checked to accept their identification. The areas of the ion map showing the different adduct forms, and the mass spectrum and retention time profiles in the deconvolution window were checked to confirm the validity of the compounds with accepted identifications. The 3D-montage was checked for all compounds with accepted identifications to determine whether it was possible to observe clear peaks corresponding to each compound.

From these data, lists of identified lipids with high and low confidence were generated. Compounds were included in the high-confidence list if the fragmentation data had clearly matched fragments, the 3D-montage displayed clear peaks, and the deconvolution ion profiles had clearly separated isotopic peaks and a chromatographic peak shape, whereas they were included in the low-confidence list if those characteristics were ambiguous.

For data interpretation, the identified lipids were classified into phospholipid classes, including phosphatidylcholine (PC), phosphatidylethanolamine (PE), phosphatidylserine (PS), phosphatidylglycerol (PG), phosphatidylinositol (PI), and lysophospholipids (LPL). The peak intensities of the identified lipids given as "normalized abundance" by Progenesis QI were combined to obtain the total signal intensity. The relative percentage abundance of each lipid was calculated to obtain the signal abundance using Microsoft Excel and plotted using GraphPad Prism 8. Statistical differences between analyte signal abundances were determined using GraphPad Prism 8 according to One-way

ANOVA followed by Tukey's multiple comparison test. Their calculated percentage of signal abundance in each sample were plotted as bar graphs. Alternatively, differences between samples were interpreted by generating Principal Components Analysis (PCA), ANOVA plots, and Volcano plots using Metaboanalyst Software after data Pareto scaling. Pareto scaling was employed as a data normalization method using the square root of the standard deviation as the scaling factor to emphasize the influence of the most important variables in the dataset, while reducing the impact of less critical ones. Volcano plots are visualization tools commonly used to simultaneously assess the statistical significance and magnitude of changes in a dataset. These combine the results obtained from the Fold Change (FC) Analysis and T-tests into a single graph to highlight the significant features based on biological and statistical significance.

3.4 RESULTS

To investigate whether the $A_{2A}R$ lipid environment showed distinctive phospholipids with relative abundance variations compared to their presence in *P. pastoris* bulk membranes or the SMA-solubilized fraction, and to assess whether substantial differences between the lipids identified in the SMA-solubilized fraction and bulk membranes resulted from SMA2000 preferences for solubilizing certain lipids, the lipids in bulk membranes, SMA-solubilized fraction, and co-purified in the $A_{2A}R$-SMALP were compared using LC-MS/MS (Figure 3.2).

To validate the data quality and reproducibility, base peak intensity (BPI) chromatograms were obtained in low-energy mode without precursor ion fragmentation (Figure 3.3). These correspond to one biological replicate for each experimental sample as a representative example. BPI chromatograms showed intense peaks between 0.5 to 10 min, indicating analyte elution during this time interval. Similar elution patterns were observed for the *P. pastoris* bulk membranes (Figure 3.3A) and SMA-solubilized fraction (Figure 3.3B), whereas the $A_{2A}R$-SMALP BPI chromatogram showed subtle differences in analyte elution patterns compared to the other lipid fractions at 0.5-1, 1.7, 4.97, 6, and 7.87 min. Nevertheless, it is unclear from the BPI chromatograms whether the observed peaks correspond to the lipids of interest in the samples. Consequently, high-energy extracted ion chromatograms (XIC) of m/z 184.1 were generated from the BPI chromatograms to investigate the elution of PCs from the chromatography (Figure 3.4).
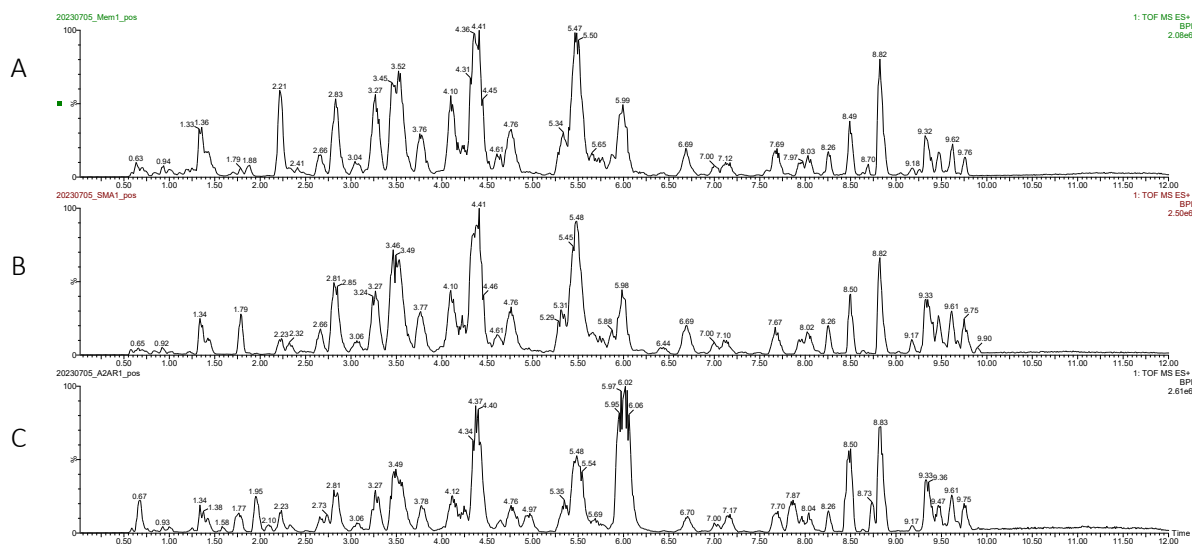
Figure 3.3. Low-energy base peak intensity (BPI) chromatogram for comparative lipid profiling of P. pastoris bulk membranes, SMA-solubilized fraction, and purified A$_{2A}$R-SMALP. *Lipids were extracted from (**A**) P. pastoris bulk membranes, (**B**) SMA-solubilized fraction, and (**C**) purified A$_{2A}$R-SMALP, and analysed by LC-MS/MS in ESI positive ion mode using MassLynx software.*

An m/z of 184.1 corresponds to the mass observed for the phosphatidylcholine (PC) headgroup fragment; therefore, the peaks observed on these XIC correspond to analytes that were fragmented under high-energy conditions, giving place to the detection of the PC headgroup in the positive ion mode. Hence, PCs were used as a representative phospholipid class to determine the estimated elution times for all the phospholipids. Comparable analyte elution patterns were observed for the three samples; the most intense peaks were obtained from 2 to 7 min, indicating PCs elution at this time interval. Low-intensity peaks were also obtained at 0.5–1.5 min, potentially corresponding to lysophosphatidylcholine (LPC) species. Similarly, low-intensity peaks were obtained at 8.5–9 min in *P. pastoris* bulk membranes, potentially corresponding to long fatty acyl chained PCs. These XIC served to visualise that it was possible to extract the lipids that were co-purified with the A$_{2A}$R, which was obtained at low protein concentrations (250 µg/mL), and to detect and compare them to those extracted from bulk membranes and SMA-solubilized fraction following this LC-MS/MS method.
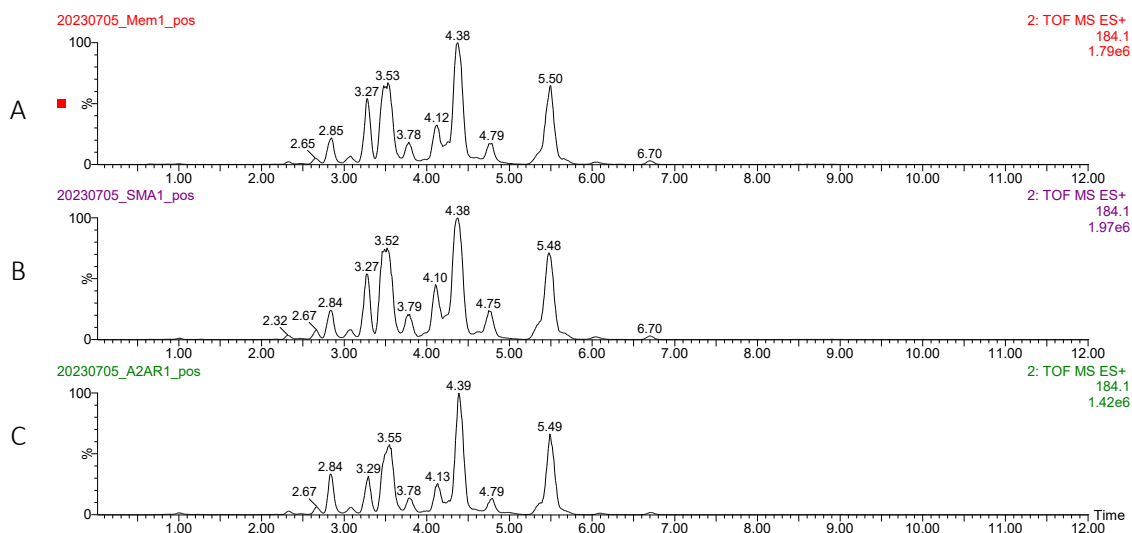
Figure 3.4. High-energy extracted ion chromatogram (XIC) of m/z 184.1 for comparative phosphatidylcoline profiling in P. pastoris bulk membranes, SMA-solubilized fraction, and purified A$_{2A}$R-SMALP. Lipids were extracted from (*A*) P. pastoris bulk membranes, (*B*) SMA-solubilized fraction, and (*C*) purified A$_{2A}$R-SMALP, and analysed by LC-MS/MS using MassLynx software.

To obtain the m/z values and peak intensities of the analytes and correlate them with possible lipid identifications, low-energy combined spectra (MS) were generated from the BPI chromatograms in the positive ion mode. *P. pastoris* bulk membranes (Figure 3.5A), SMA solubilized fraction (Figure 3.5B), and A$_{2A}$R-SMALP (Figure 3.5C) showed similar peak patterns with m/z values between 100 and 1200 Da. The most intense peaks were obtained between 700 and 850 Da, potentially corresponding to phospholipids in the samples. The most intense peaks were observed at m/z 784.59, 786.60, and 782.57, as well as their isotopic peaks. Other notable peaks were detected at m/z 758.57, 756.55, and 780.55, potentially corresponding to the most abundant phospholipids in the samples. Intense peaks at m/z 338.34 and 663.46 appeared in the three samples, with a noticeable intensity of the second analyte in the A$_{2A}$R-SMALP, which might correspond to contaminant features. However, it remains ambiguous from the low-energy MS combined spectra whether the observed peaks correspond to specific phospholipids of interest in the samples or not. Moreover, the analysis of low-intensity peaks from these spectra using MassLynx can be challenging. Therefore, Progenesis QI was used to process the data and identify the most abundant phospholipid species in the three experimental groups.

I. Company Marin, PhD Thesis, Aston University 2024
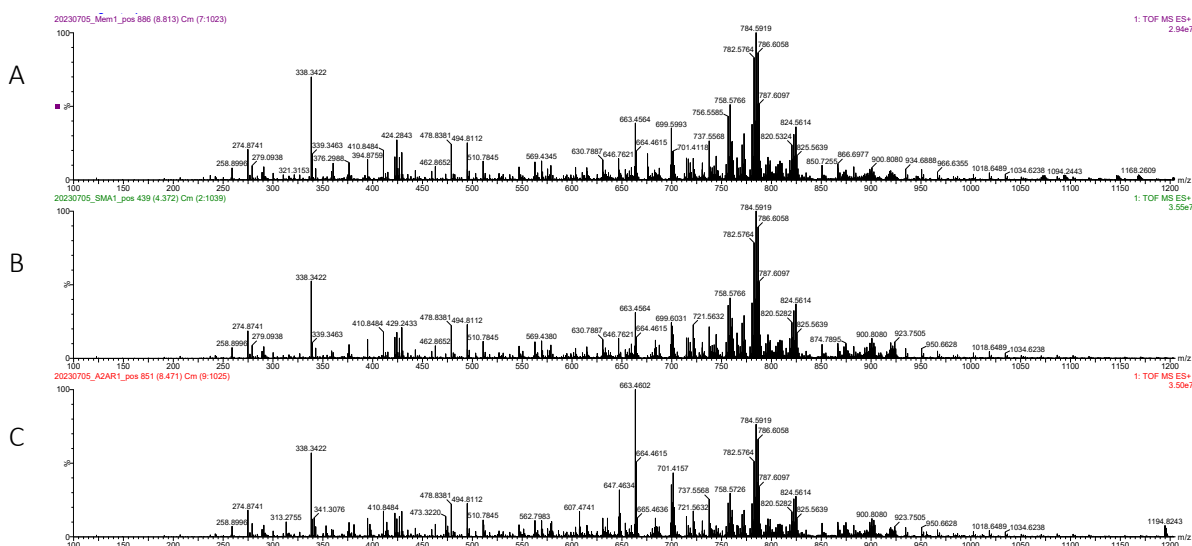
Figure 3.5. Low-energy (MS) combined spectrum in the 100-1200 m/z range for comparative lipid profiling of P. pastoris bulk membranes, SMA-solubilized fraction, and purified A₂R-SMALP. Lipids were extracted following the MTBE method from (A) P. pastoris bulk membranes, (B) SMA-solubilized fraction, and (C) purified A₂R-SMALP. Lipids were analysed by LC-MS/MS using MassLynx software.

3.4.1 Analysis of the phospholipid composition across the experimental groups

To study the lipid composition and possible differences between the experimental groups, phospholipid species were identified using Progenesis QI from the HDMS^E data in positive ion mode (Table 3.2). Multiple phospholipid species were identified with high confidence, with the highest number of molecular ions corresponding to PCs and PEs. The most abundant adduct considered for the identification of PC, PE, PS, and lysophospholipid species was $[M+H]^+$, whereas it was $[M+NH_4]^+$ for PGs and PIs.

Table 3.2. Phospholipid and lysophospholipid classes identified in P. pastoris bulk membranes, SMA-solubilized fraction, and A₂R-SMALP by LC-MS/MS using Progenesis QI software.

Phospholipid classes	Number of molecular ions identified	Formula	Most abundant adducts in positive ion mode
PC	38	$C_nH_mNO_8P$	$[M+H]^+$
PE	30	$C_nH_mNO_8P$	$[M+H]^+$
PS	13	$C_nH_mNO_{10}P$	$[M+H]^+$
PG	6	$C_nH_mNO_{10}P$	$[M+NH_4]^+$
PI	15	$C_nH_mNO_{13}P$	$[M+NH_4]^+$
LPC	10	$C_nH_mNO_7P$	$[M+H]^+$
LPE	10	$C_nH_mNO_7P$	$[M+H]^+$

For a general comparison of the phospholipid contents of the three experimental groups, a principal component analysis (PCA) plot was generated. This consists of a dimensionality reduction technique to explore patterns in multivariate data. Hence, PCA is effective in reducing the dimensionality of data while preserving meaningful information. Quality control (QC) samples consisting of a mixture of *P. pastoris* bulk membranes, SMA-solubilized fraction, and $A_{2A}R$-SMALP extracted lipid aliquots were included in the experiment. This provides reference points for assessing the reliability, reproducibility, and consistency of the results obtained. Different clusters in the PCA plot corresponded to different experimental groups, and each data point corresponded to a biological replicate (Figure 3.6A). A clear separation of the experimental groups was observed, which provided an insight into the dissimilarities of the groups regarding their phospholipid content. QC samples were positioned at an intermediate point between the three experimental groups. This indicated that the QC samples correctly represented the experimental conditions and confirmed the reproducibility and consistency of the results. Tight clustering was observed for QC, bulk membranes, and SMA-solubilized samples, indicating similarities between sample replicates. In contrast, the sample replicates within the $A_{2A}R$-SMALP group were less tight, suggesting certain differences between replicates. However, no clear outliers that appeared to be distant from the main cluster were identified.

For a general overview of the compounds that showed significant differences between the experimental groups, a One-way ANOVA plot with Tukey's post-hoc analysis and raw p-value 0.05 cutoff was generated (Figure 3.6B). Each data point corresponding to an identified phospholipid was plotted according to its $-\log_{10}$(p-value). The results indicated that the majority of the identified phospholipid species showed significant differences between the groups (Supplementary

Table **8.1**-Table 8.7).

A

B

I. Company Marin, PhD Thesis, Aston University 2024
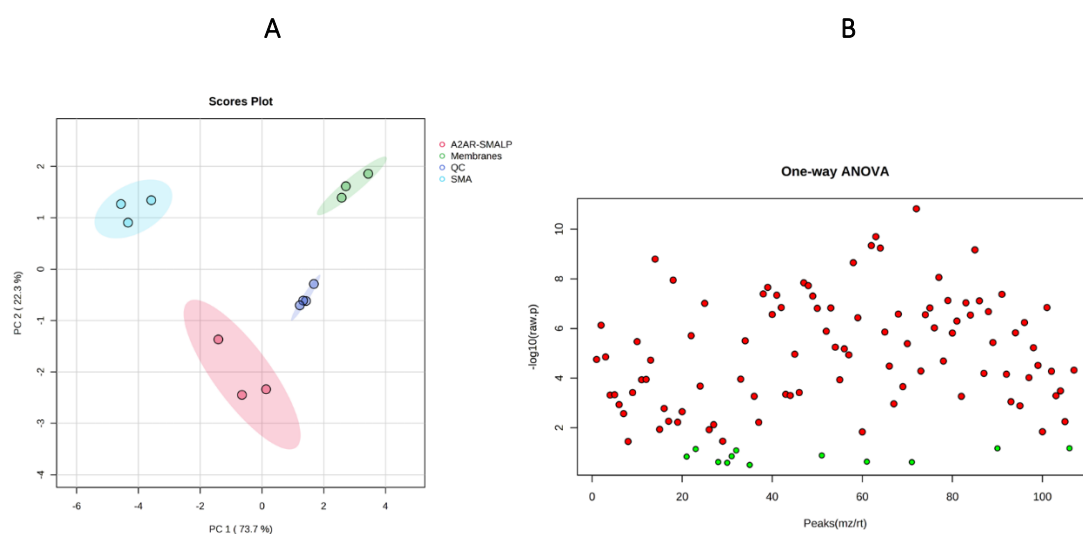
Figure 3.6. Statistical comparison of phospholipid profiles of P. pastoris bulk membranes, SMA-solubilized fraction, and purified A_{2A}R-SMALP. (A) Principal Component Analysis (PCA) of the phospholipid profiles of P. pastoris bulk membranes, SMA-solubilized fraction, and purified A_{2A}R-SMALP was conducted using MetaboAnalyst software after data Pareto scaling. The 95% confidence region is displayed. Each data point represents a sample replicate; n=3 for experimental samples, and n=4 for quality control (QC) samples. (B) One-way ANOVA for the comparison of the identified phospholipids in the experimental samples was conducted using MetaboAnalyst software with a p-value cut-off of 0.05, and Tukey's post-hoc analysis. Features that were significantly different between the samples are shown in red, whereas non-significantly different species are shown in green.

To investigate whether the three experimental groups showed differences in the relative abundance of the different phospholipid classes, the percentage (%) signal abundance of all identified species was calculated, and the species were classified into their corresponding phospholipid class groups (Figure 3.7). The phospholipid class with the highest signal abundance in the three samples was PC, representing 50–60% of the total signal, followed by PE and PS, which represented 20–30% and 1–2% of the total signal, respectively. PG and PI were less abundant, representing less than 1% of the total signal, similar to the identified lysophospholipids. Significant differences in the percentage abundance of different phospholipid species were detected between the experimental groups. The A_{2A}R-SMALP showed a significantly lower percentage of PC and LPL species than bulk membranes, whereas it showed a significant increase in the percentage of PS, PG, and PI species. In contrast, no significant differences were detected in terms of the PE content, compared to that of bulk membranes. The SMA-solubilized fraction had a significantly lower percentage of PC and LPL and a significantly higher percentage of PE, PS, and PG than the bulk membranes, whereas there were no significant differences in their PI content. Finally, PE, PS, and PG, were significantly decreased in the A_{2A}R-SMALP compared to the SMA-solubilized fraction, whereas there were no significant differences in their PC, PI, and LPL content.

Figure 3.7. Phospholipid class composition in P. pastoris bulk membranes, SMA-solubilized fraction, and purified A₂ₐR-SMALP. *Lipid samples were analysed by LC-MS/MS in ESI positive ion mode. Phosphatidylcholine (PC), phosphatidylethanolamine (PE), phosphatidylserine (PS), phosphatidylglycerol (PG), phosphatidylinositol (PI), and lysophospholipids (LPL) were identified, and their relative abundance was calculated as a percentage (%) of total phospholipids. Data are presented as the mean of all replicates (n=3) ± SD. Statistical differences were determined by One-way ANOVA followed by Tukey's multiple comparison test (*p-value<0.05 and **p-value<0.01).*

Considering that the three experimental groups showed significant differences in the relative signals of the phospholipid classes, the most differentially detected phospholipids among the experimental groups were identified generating volcano plots. First, phospholipid species that were differentially detected in the A₂ₐR-SMALP compared with bulk membranes were investigated (Figure 3.8A). Consistently with the results corresponding to the relative signal abundance of the phospholipid classes (Figure 3.7), certain PS and PI species were upregulated in the in A₂ₐR-SMALP, including PS(36:2), PS(36:5), PS(38:7), PS(40:7), and PI(24:0), PI(40:0), PI(40:3). Interestingly, PI species showed higher fold change values than PS species, indicating a higher upregulation in the A₂ₐR-SMALP. Nevertheless, certain PS and PI species were downregulated in the A₂ₐR-SMALP, including PS(38:2) and PI(44:0). Similarly, certain PC, PE, and the majority of the identified LPE were downregulated in the A₂ₐR-SMALP, whereas no LPC species were differentially downregulated in this experimental group. PE(32:0) showed the lowest fold change value, indicating a major downregulation of this lipid in the A₂ₐR-SMALP. Although the relative signal abundance of PG species was significantly higher in the A₂ₐR-SMALP than

in bulk membranes (Figure 3.7), some PG species were downregulated in the A_{2A}R-SMALP, including PG(38:5) and PG(38:6).
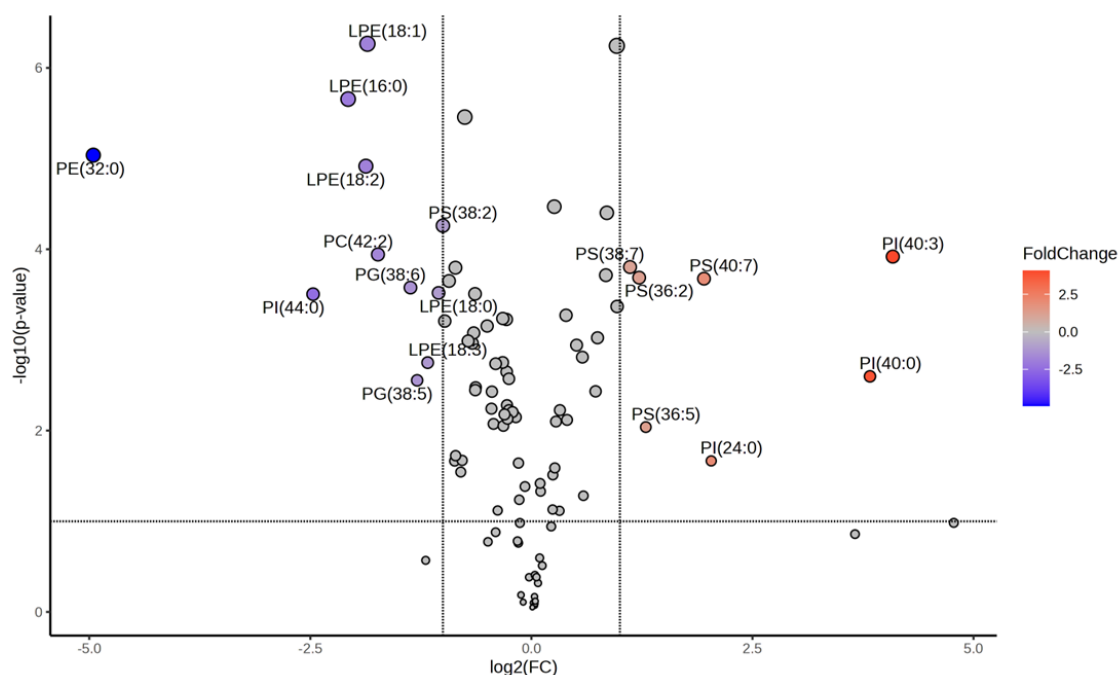
Figure 3.8. Volcano plot for statistical comparison of the phospholipid profiles of the A_{2A}R-SMALP and P. pastoris bulk membranes. *Each data point represents an identified lipid species, including phosphatidylcholine (PC), phosphatidylethanolamine (PE), phosphatidylserine (PS), phosphatidylglycerol (PG), phosphatidylinositol (PI), lysophosphatidylcholine (LPC), and lysophosphatidylethanolamine (LPE). Analytes with foldchange values (FC) ≥ 2 and p-value <0.05 (T-test) were upregulated (red), whereas analytes with foldchange values (FC) ≤ -2 and p-value <0.05 were downregulated (blue) in A_{2A}R-SMALP vs. bulk membranes.*

To investigate whether the differences between the A_{2A}R-SMALP and bulk membrane lipids were also observed in the SMA-solubilized fraction, phospholipid species that exhibited differential detection in the SMA-solubilized fraction compared to bulk membranes were examined (Figure 3.9). The same PS and PI species that were upregulated in the A_{2A}R-SMALP, together with other PS species containing shorter acyl chains, including PS(32:1), PS(33:1), PS(34:1), PS(34:3), and PI(36:1), were upregulated in the SMA-solubilized fraction, compared to bulk membranes. However, PG(36:4) was also upregulated in the SMA-solubilised fraction, which was not observed in the A_{2A}R-SMALP (Figure 3.8). The same PC, PE, and LPE species that were downregulated in the A_{2A}R-SMALP were downregulated in the SMA-solubilized fraction, with the exception of LPE(18:0). Similarly, PG(38:6) and PI(44:0), were also downregulated in the SMA-solubilized fraction, together with other PG and PI species, including PG(34:2) and PI(33:0).

I. Company Marin, PhD Thesis, Aston University 2024
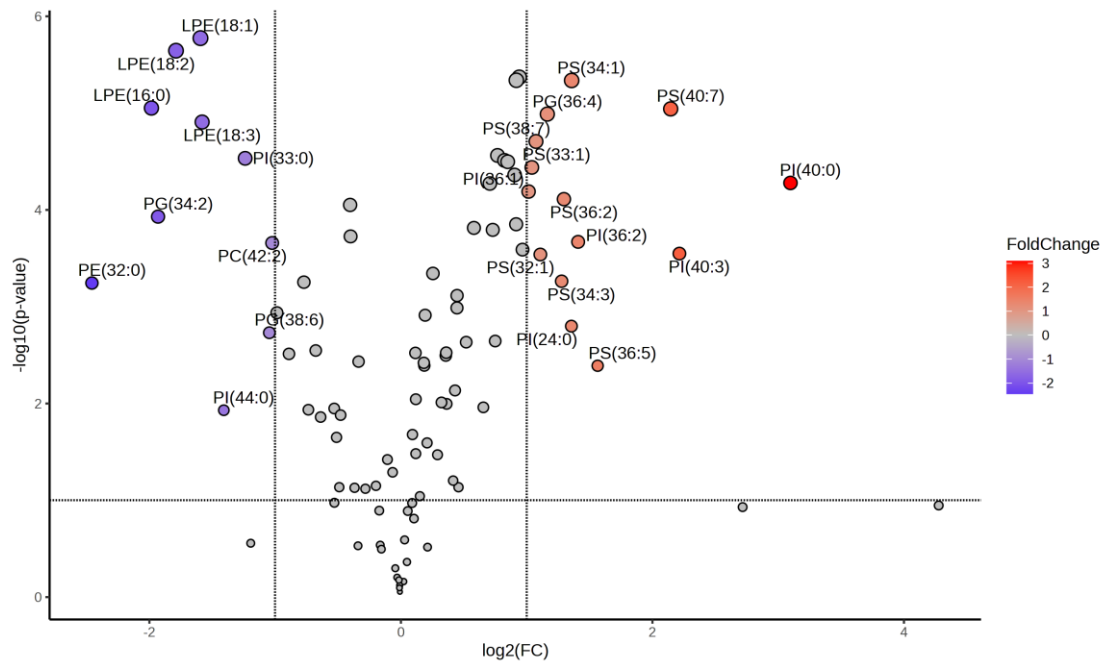
Figure 3.9. Volcano plot for statistical comparison of the phospholipid profiles of the SMA-solubilized fraction and P. pastoris bulk membranes. Analytes were upregulated (FC ≥ 2 and p-value < 0.05, red), or downregulated (FC ≤ -2 and p-value <0.05, blue) in the SMA-solubilized fraction vs. bulk membranes.

Considering that similar patterns in the upregulation and downregulation of certain phospholipid species were detected in the A_{2A}R-SMALP and SMA-solubilized fraction compared to bulk membranes, phospholipid species differentially detected in the A_{2A}R-SMALP compared to the SMA-solubilized fraction were investigated (Figure 3.10). The A_{2A}R-SMALP was upregulated in PI(40:3), which was also upregulated in the SMA-solubilized fraction compared to bulk membranes (Figure 3.9). Similarly, PG(34:2) was upregulated in the A_{2A}R-SMALP compared to the SMA-solubilized fraction, while no PG species were upregulated in the A_{2A}R-SMALP and SMA-solubilized fraction compared with bulk membranes. In contrast, the A_{2A}R-SMALP was mainly downregulated in PE species, which was not observed in the previous comparisons. Notably, PE(32:0), which was the most downregulated PE in the A_{2A}R-SMALP and SMA-solubilized fraction compared to bulk membranes, was not significantly lower in the A_{2A}R-SMALP vs. SMA-solubilized fraction.
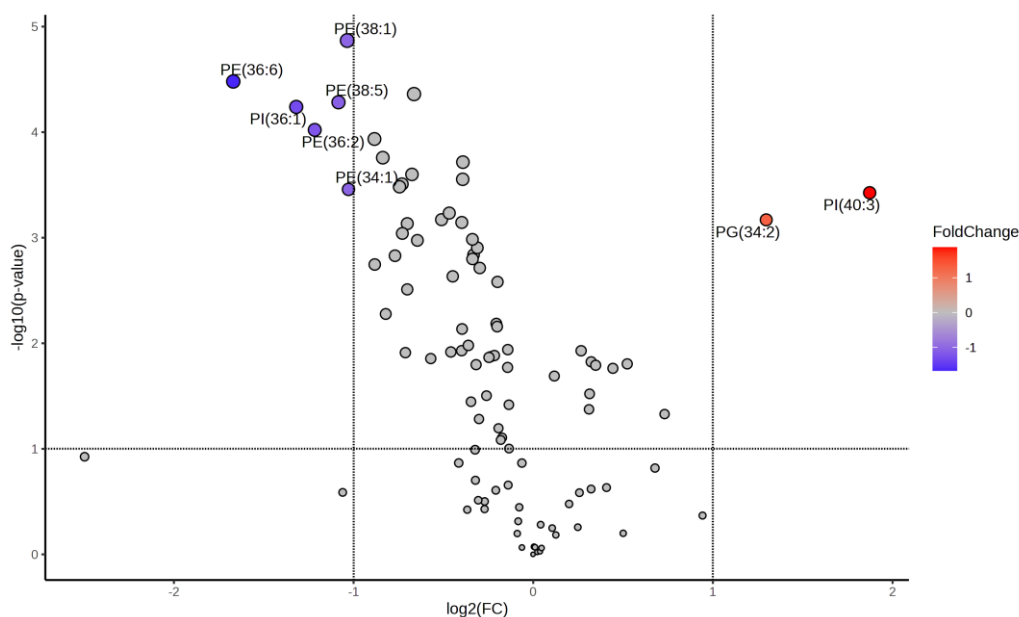
Figure 3.10. Volcano plot for statistical comparison of the phospholipid profiles of the A_{2A}R-SMALP and SMA-solubilized fraction. Analytes were upregulated (FC ≥ 2 and p-value < 0.05, red), or downregulated (FC ≤ -2 and p-value <0.05, blue) in the A_{2A}R-SMALP vs. SMA-solubilized fraction.

Following a broad comparison of phospholipid content across the three experimental groups, it was observed that certain phospholipid species were upregulated or downregulated in the A_{2A}R-SMALP compared to bulk membranes and SMA-solubilised fraction, as well as in the SMA-solubilised fraction, compared to bulk membranes. Subsequently, a more detailed examination of the identified phospholipid species was conducted to investigate their relative abundance within their respective phospholipid classes, and to discern their relevance. Hence, variations within each lipid class concerning fatty acyl chain composition and degree of unsaturation were explored.

3.4.2 Analysis of the PC composition across the experimental groups

PCs are the most abundant phospholipid class in eukaryotic plasma membranes, and act as building blocks (Joardar *et al.*, 2022). It has been proposed they can influence membrane protein activity, although they can have a neutral role on GPCR function (Zhukovsky *et al.*, 2019). Taking into account their relevance to eukaryotic plasma membranes, the relative signal abundance of the most abundant PC species identified in the three experimental groups was investigated (Figure 3.11). The ten most abundant PC species contained unsaturated fatty acyl chains, and significant differences were detected in their relative signals between the experimental groups. However, the order of relative abundances of the PC species remained consistent within each experimental group. The most abundant PC species

were PC(36:2) and PC(36:3), representing 25–30% of the signal, followed by PC(34:2) and PC(34:3), with abundances of 10–15%. PC species containing fatty acyl chains of 32 and 34 carbon atoms, together with PC(36:1), were decreased in the A_{2A}R-SMALP compared to the SMA-solubilised fraction, whereas these increased in the SMA-solubilised fraction compared to bulk membranes. In contrast, PC(36:2) and PC(36:3) were increased in the A_{2A}R-SMALP compared to the SMA-solubilised fraction, whereas they were decreased in the SMA-solubilised fraction compared to bulk membranes. Despite these variations, no major differences were observed between the experimental groups. This was consistent with the results from the volcano plots (Figure 3.8, Figure 3.9, Figure 3.10), indicating that none of the most abundant PC species was significantly upregulated or downregulated in the experimental groups.
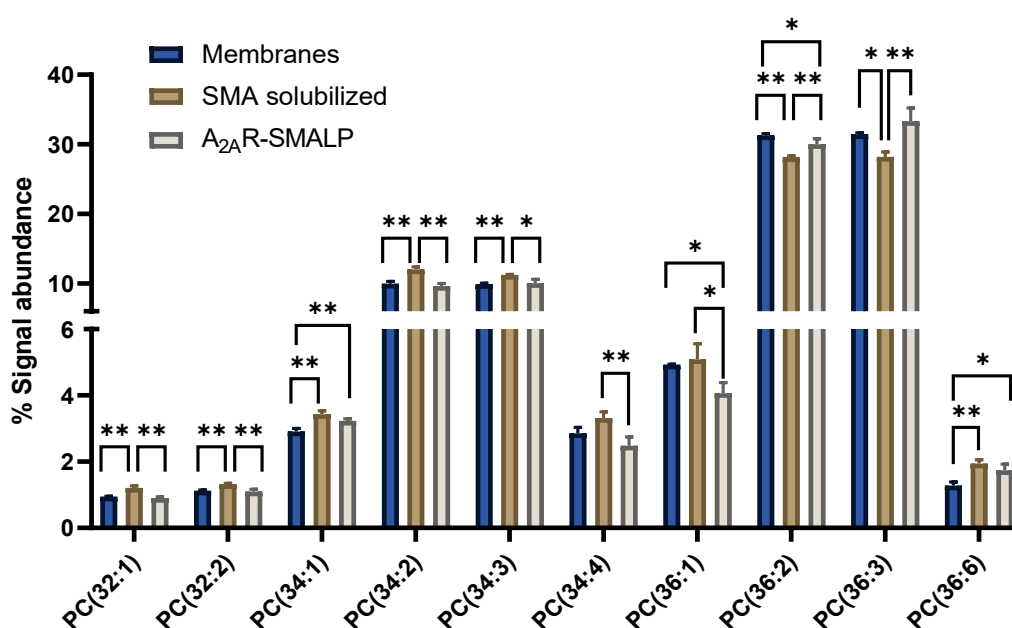
Figure 3.11. Phosphatidylcholine (PC) composition in P. pastoris *bulk membranes, SMA-solubilized fraction, and purified A_{2A}R-SMALP. Lipid samples were analysed by LC-MS/MS in ESI positive ion mode. The ten most abundant PCs were identified as [M+H]$^+$ adducts, and their relative abundance was calculated as a percentage (%) of the total PCs. Data are presented as the mean of all replicates (n=3) ± SD. Statistical differences were determined by One-way ANOVA followed by Tukey's multiple comparison test (*p-value<0.05 and **p-value<0.01).*

3.4.3   Analysis of the PE composition across the experimental groups

PEs are the second most abundant phospholipids in eukaryotic membranes and can modulate membrane properties, inducing negative curvature (Chakrabarti, 2021). Hence, they can modulate membrane protein activity by direct interactions and exercising lateral pressure (Pohl *et al.*, 2019), and have been proposed to act as negative regulators of GPCRs (Dawaliby *et al.*, 2016). Considering their relevance in modulating membrane properties and protein activity, the most abundant PE species

I. Company Marin, PhD Thesis, Aston University 2024

detected in the three experimental groups were investigated (Figure 3.12), all of which contained unsaturated acyl chains. Similar to what was observed for the PC species (Figure 3.11), the order of relative abundances of the PE species was consistent within each experimental group, although significant differences were observed in the relative signal of each PE between the groups. The most abundant PE species were PE(38:2) and PE(38:3), which contained longer fatty acyl chains than the most abundant PCs, although they had the same number of double bonds. Interestingly, PEs with shorter acyl chains, containing 34 or 36 carbon atoms, were increased in the SMA-solubilized fraction compared to bulk membranes, whereas those with longer acyl chains, containing 38 carbon atoms, were significantly decreased. In contrast, these were significantly increased in the A_{2A}R-SMALP compared to those in the SMA-solubilised fraction or bulk membranes. As indicated by the volcano plot (Figure 3.10), certain PE species with shorter acyl chains containing 34 and 36 carbon atoms were downregulated in the A_{2A}R-SMALP. Hence, the A_{2A}R-SMALP was increased in PEs containing longer acyl chains and decreased in those with shorter acyl chains.
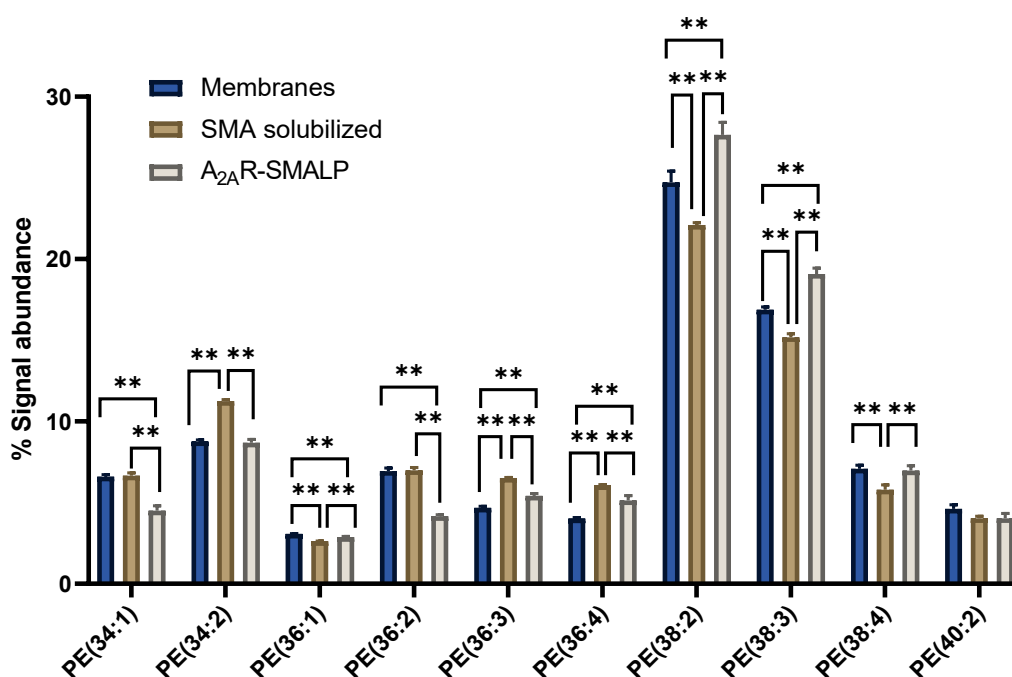
*Figure 3.12. Phosphatidylethanolamine (PE) composition in P. pastoris bulk membranes, SMA-solubilized fraction, and purified A_{2A}R-SMALP. Lipid samples were analysed by LC-MS/MS in ESI positive ion mode. The ten most abundant PEs were identified as $[M+H]^+$ adducts, and their relative abundance was calculated as a percentage (%) of the total PEs. Data are presented as the mean of all replicates (n=3) ± SD. Statistical differences were determined by One-way ANOVA followed by Tukey's multiple comparison test (*p-value<0.05 and **p-value<0.01).*

I. Company Marin, PhD Thesis, Aston University 2024

3.4.4 Analysis of the PS composition across the experimental groups

PSs are relatively abundant phospholipids in plasma membranes and are mainly found in the inner leaflet (Leventis *et al.*, 2010). Consequently, they modulate membrane potential and influence membrane protein activity (Vance, 2018). Indeed, it has been observed that PS can act as positive regulator of GPCRs (Dawaliby *et al.*, 2016). Considering their relevance in the activity of these receptors, the most abundant PS species detected in the three experimental groups were examined (Figure 3.13). Similar to the results obtained for PC and PE species, the ten most abundant PSs contained unsaturated fatty acyl chains, and the order of relative signal abundance of each PS was consistent within the experimental groups. The most abundant PS species were PS(34:1), PS(34:2), and PS(36:3). Therefore, they contained shorter fatty acyl chains than the most abundant PC and PE species. Significant differences were observed between the experimental groups and, as indicated by the volcano plots (Figure 3.8 and Figure 3.9), certain PS species were upregulated in the A_{2A}R-SMALP and SMA-solubilized fraction compared to bulk membranes, which were found among the ten most abundant identified PS species (Figure 3.13). The most abundant PS, PS(34:1), was significantly increased in the SMA-solubilized fraction and A_{2A}R-SMALP, compared to bulk membranes. PS(36:2) followed the same trend. Instead, the second and third most abundant PS species, PS(34:2) and PS(36:3) respectively, were decreased. Interestingly, the most abundant PS species were not significantly different between the A_{2A}R-SMALP and SMA-solubilized fraction, whereas PS(36:2) and PS(36:3) were significantly increased in the A_{2A}R-SMALP. In contrast, PS(36:4) was significantly decreased. On the other hand, PS(38:2) containing longer acyl chains was decreased the A_{2A}R-SMALP and SMA-solubilized fraction compared to bulk membranes (Figure 3.8, Figure 3.9, Figure 3.13).
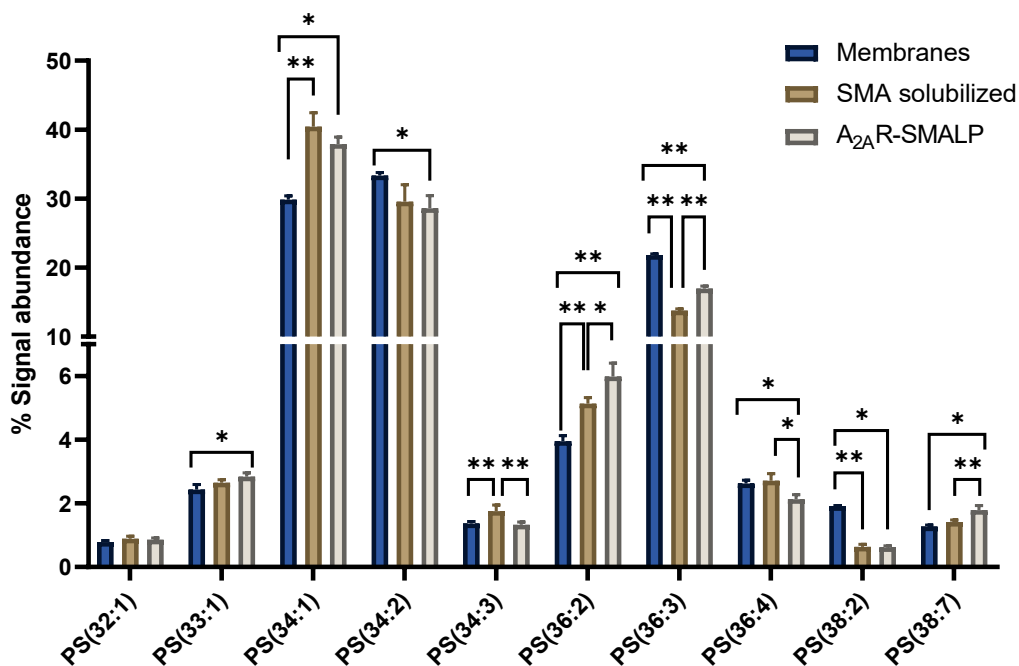
Figure 3.13. Phosphatidylserine (PS) composition in P. pastoris bulk membranes, SMA-solubilized fraction, and purified A$_{2A}$R-SMALP. Lipid samples were analysed by LC-MS/MS in ESI positive ion mode. The ten most abundant PSs were identified as [M+H]$^+$ adducts, and their relative abundance was calculated as a percentage (%) of the total PSs. Data are presented as the mean of all replicates (n=3) ± SD. Statistical differences were determined by One-way ANOVA followed by Tukey's multiple comparison test (*p-value<0.05 and **p-value<0.01).

3.4.5   Analysis of the PG composition across the experimental groups

Although PGs are minor components of eukaryotic plasma membranes, it has been demonstrated that they interact with membrane proteins and play positive roles in activating GPCRs (Dawaliby *et al.*, 2016). Consequently, the relative signal abundance of the identified PG species in the experimental groups was investigated (Figure 3.14). Similar to the results for the other phospholipid classes, the most abundant PG species were unsaturated. PG(36:4) was the most abundant, representing more than 40% of the total identified PG species in the three experimental groups. As corroborated by the volcano plots (Figure 3.8 and Figure 3.9), this was significantly upregulated in the A$_{2A}$R-SMALP and SMA-solubilized fraction compared to bulk membranes, whereas it was not different between the A$_{2A}$R-SMALP and SMA-solubilized fraction (Figure 3.10). In contrast, the other identified PG species were decreased in the A$_{2A}$R-SMALP and SMA-solubilized fraction compared to bulk membranes, although their relative signal abundance was lower. These were not significantly different between the A$_{2A}$R-SMALP and SMA-solubilized fraction, with the exception of PG(34:2) (Figure 3.14), which was significantly upregulated in the A$_{2A}$R-SMALP (Figure 3.10). However, its relative abundance was low in both experimental groups, compared to that in bulk membranes (Figure 3.14).
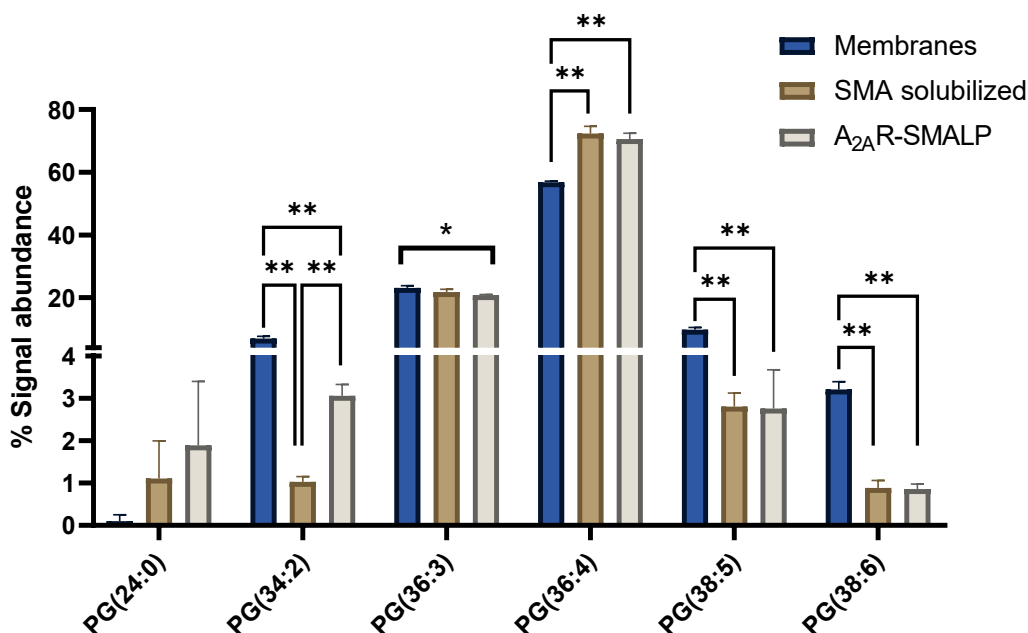
Figure 3.14. Phosphatidylglycerol (PG) composition in P. pastoris bulk membranes, SMA-solubilized fraction, and purified A$_{2A}$R-SMALP. Lipid samples were analysed by LC-MS/MS in ESI positive ion mode. The six most abundant PGs were identified as [M+NH$_4$]$^+$ adducts, and their relative abundance was calculated as a percentage (%) of the total PGs. Data are presented as the mean of all replicates (n=3) ± SD. Statistical differences were determined by One-way ANOVA followed by Tukey's multiple comparison test (*p-value<0.05 and **p-value<0.01).

3.4.6 Analysis of the PI composition across the experimental groups

Similar to other anionic phospholipids, PIs are located in the inner leaflet of the plasma membrane and interact with membrane proteins to modulate their activities (Numata *et al.*, 2023). Specifically, comparable to PGs, PIs act as positive regulators of GPCRs (Dawaliby *et al.*, 2016). Considering their relevance in regulating GPCR function, and the results obtained from the volcano plots indicating upregulation of certain PI species in the A$_{2A}$R-SMALP and SMA-solubilised fraction (Figure 3.8 and Figure 3.9), the relative signal abundance of the identified PIs was investigated (Figure 3.15). In contrast to the results obtained for the other phospholipid classes, the ten most abundant PI species mainly contained saturated or monounsaturated fatty acyl chains, with the exception of PI(36:2) and PI(40:3). The most abundant PI species contained saturated or monounsaturated acyl chains of 34 and 36 carbon atoms, and the order of relative signal abundance of each identified PI was mainly maintained within the experimental groups. Exceptionally, notable differences in the relative abundance of PI(40:3) were observed, representing 49% in the A$_{2A}$R-SMALP, 19% in the SMA-solubilized fraction, and 5.85% in the bulk membranes of the PI signal. This, together with PI(40:0), was increased in the A$_{2A}$R-SMALP and

SMA-solubilised fraction, compared to bulk membranes, as corroborated by the volcano plots (Figure 3.8 and Figure 3.9). Moreover, PI(40:3) was significantly increased in the A_{2A}R-SMALP compared to that in the SMA-solubilised fraction (Figure 3.10 and Figure 3.15). In contrast, PI species containing saturated or monounsaturated fatty acyl chains of 36 carbon atoms or shorter were decreased in the A_{2A}R-SMALP and SMA-solubilised fraction, compared to bulk membranes (Figure 3.15).
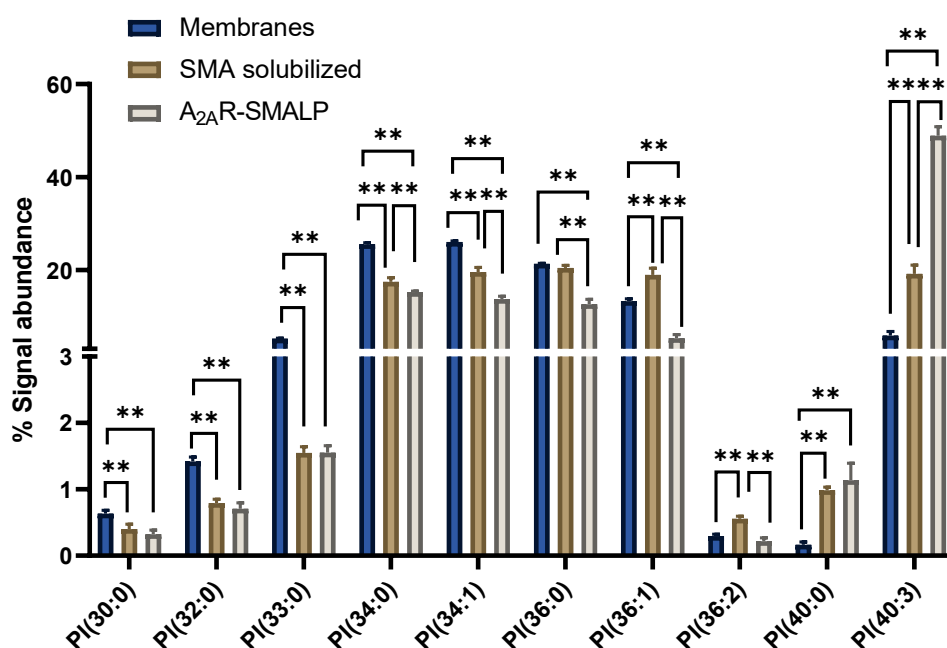
Figure 3.15. Phosphatidylinositol (PI) composition in P. pastoris bulk membranes, SMA-solubilized fraction, and purified A_{2A}R-SMALP. Lipid samples were analysed by LC-MS/MS in ESI positive ion mode. The ten most abundant PIs were identified as [M+NH₄]⁺ adducts, and their relative abundance was calculated as a percentage (%) of the total PIs. Data are presented as the mean of all replicates (n=3) ± SD. Statistical differences were determined by One-way ANOVA followed by Tukey's multiple comparison test (*p-value<0.05 and **p-value<0.01).

3.4.7 Analysis of the lysophospholipid composition across the experimental groups

Lysophospholipids are found in biological membranes at about 0.5–6% of the total lipid weight (Ailte *et al.*, 2016), and can modulate membrane properties, consequently influencing membrane protein activity (Kano *et al.*, 2021). LPC and LPE species were identified in the three experimental groups, which provided insights into the most abundant esterified fatty acids on phospholipids in the samples. The most abundant LPCs contained a fatty acyl chain of 18 carbon atoms (Figure 3.16). LPC(18:1) and LPC(18:2) represented 20-50% of the total LPC signal, followed by LPC(18:0) and LPC(18:3), representing 6-15%. LPCs with shorter and longer acyl chains were less abundant. Interestingly, the

I. Company Marin, PhD Thesis, Aston University 2024

SMA-solubilised fraction and A$_{2A}$R-SMALP were increased in the saturated LPC(18:0), whereas no significant differences were detected between groups for the monounsaturated LPC(18:1). In contrast, the SMA-solubilised fraction and A$_{2A}$R-SMALP were decreased in LPC(18:2) and LPC(18:3), indicating a decrease in polyunsaturated fatty acyl chains in these experimental groups, compared with bulk membranes.

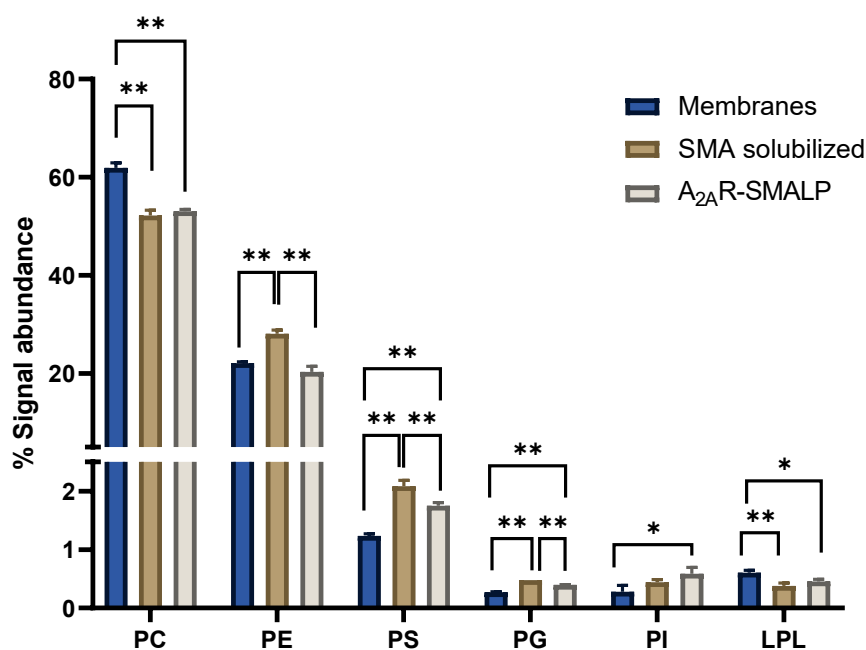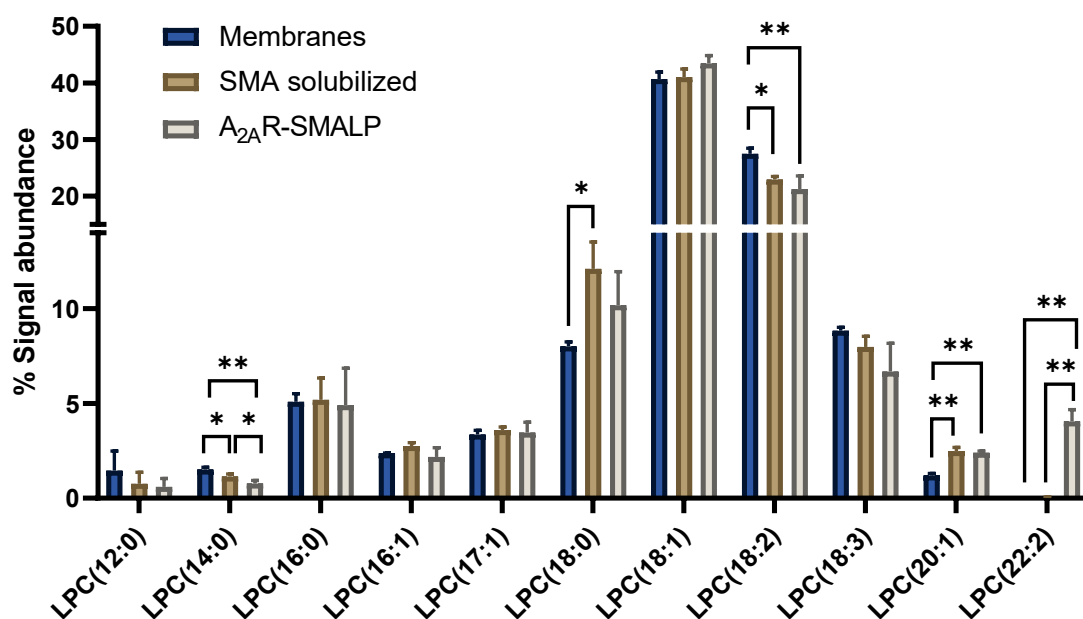*Figure 3.16. Lysophosphatidylcholine (LPC) composition in P. pastoris bulk membranes, SMA-solubilized fraction, and purified A$_{2A}$R-SMALP. Lipid samples were analysed by LC-MS/MS in ESI positive ion mode. The eleven most abundant LPCs were identified as [M+H]$^+$ adducts, and their relative abundance was calculated as a percentage (%) of the total LPCs. Data are presented as the mean of all replicates (n=3) ± SD. Statistical differences were determined by One-way ANOVA followed by Tukey's multiple comparison test (*p-value<0.05 and **p-value<0.01).*

Similarly, the most abundant LPE species contained saturated or unsaturated fatty acyl chains of 16 or 18 carbon atoms (Figure 3.17). Comparable to LPC, LPE(18:1) was the most abundant, representing 30% of the total LPE signal, followed by LPE(18:2), representing 10-20%. In this case, the abundance of LPE(16:0) was comparable to that of LPE(18:2), which was not observed for LPC. LPE(18:0) was increased in the A$_{2A}$R-SMALP and SMA-solubilised fraction, compared to bulk membranes, whereas LPEs with a higher number of double bonds were decreased in these experimental groups. Similarly, LPE(16:0) and LPE(16:1) were decreased in these experimental groups, which was corroborated by the volcano plots (Figure 3.8 and Figure 3.9). In contrast, LPE(18:4), together with LPE species containing

I. Company Marin, PhD Thesis, Aston University 2024

acyl chains of 20 carbon atoms or longer, was increased in the A_{2A}R-SMALP and SMA-solubilised fraction.
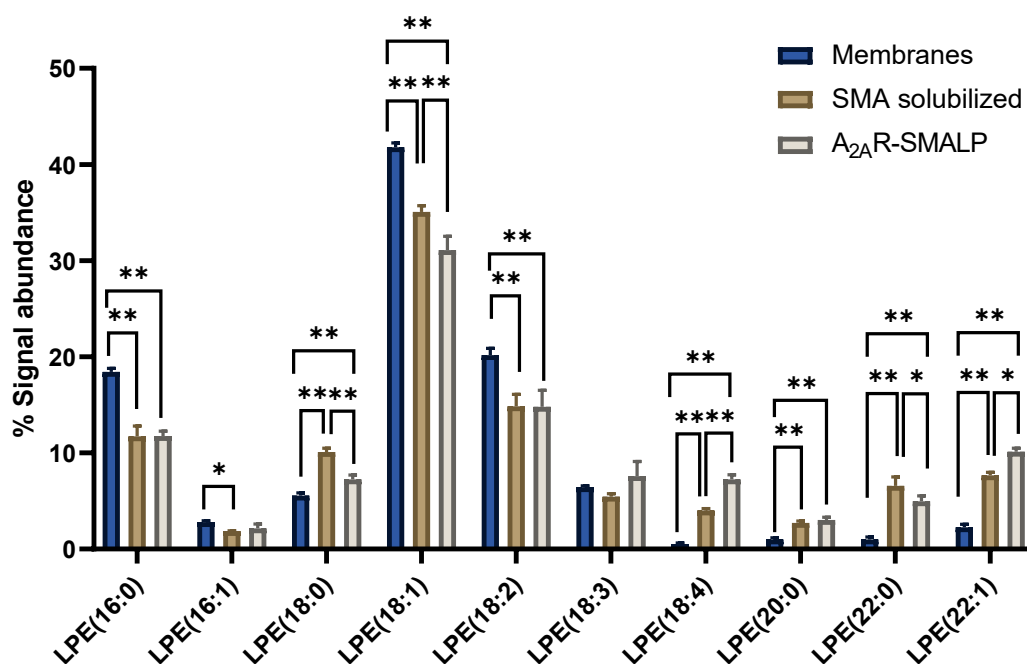
Figure 3.17. Lysophosphatidylethanolamine (LPE) composition in P. pastoris bulk membranes, SMA-solubilized fraction, and purified A_{2A}R-SMALP. *Lipid samples were analysed by LC-MS/MS in ESI positive ion mode. The ten most abundant LPEs were identified as [M+H]$^+$ adducts, and their relative abundance was calculated as a percentage (%) of the total LPEs. Data are presented as the mean of all replicates (n=3) ± SD. Statistical differences were determined by One-way ANOVA followed by Tukey's multiple comparison test (*p-value<0.05 and **p-value<0.01).*

3.5 DISCUSSION

This study aimed to characterize the lipid environment of the A_{2A}R in the SMALP and compare it to that of *P. pastoris* bulk membranes and the SMA-solubilized fraction using advanced mass spectrometry equipment and methodologies. To this end, the work reported in this chapter aimed to gain insights into the lipids that closely surround the receptor and may be crucial for its stability, conformation, and activity. Additionally, the aim was to investigate whether the bulk membrane and SMA-solubilized lipids were comparable, or whether SMA2000 showed some preference for solubilizing certain lipids from yeast membranes, potentially causing an effect on the lipids observed in the A_{2A}R-SMALP.

The key findings of this chapter were that, although the A_{2A}R-SMALP was obtained at low protein concentrations, it was possible to extract and detect the lipids that co-purified in the A_{2A}R-SMALP, and compare them to those in *P. pastoris* bulk membranes and the SMA-solubilized fraction following this methodology. The three experimental groups showed differences in their phospholipid content. PCs

I. Company Marin, PhD Thesis, Aston University 2024

had the highest signal abundance in the three experimental groups, followed by PE, and PS, whereas PG, PI, and LPL were identified in lower signal abundance. Bulk membranes were enriched in PC and LPE, whereas the A_{2A}R-SMALP was enriched in PS, PG, and PI. In contrast, the SMA-solubilised fraction was enriched in PE, PS, and PG. The A_{2A}R-SMALP and SMA-solubilized fraction were similarly upregulated in certain PS and PI species and downregulated in LPE species, compared to bulk membranes. Instead, the A_{2A}R-SMALP was upregulated in PG and PI species, and downregulated in PE species, compared to the SMA-solubilised fraction. The most abundant phospholipid species in the three groups contained mono- or polyunsaturated fatty acyl chains of 34, 36, or 38 carbon atoms. These generally contained 1, 2, or 3 double bonds. However, the most abundant PIs contained a higher degree of fatty acyl chain saturation than other phospholipid classes.

The findings in the present study are in good agreement with previous publications on the *P. pastoris* lipidome, which have determined the variability and diversity of lipids in its membrane fraction (Yu *et al.*, 2022). The observed relative signal abundances of the different phospholipid classes were consistent with those expected in *P. pastoris* membranes (Yu *et al.*, 2022). However, the percentage signal abundance calculated in this study does not necessarily directly correspond to the absolute abundance of such species in the samples, representing a limitation of this approach. Different phospholipid classes can ionise differently; PC species are easily detected in the positive ion mode, whereas anionic phospholipids are better detected in the negative ion mode (Reis *et al.*, 2015). This makes the relative comparison between phospholipid classes challenging. Nevertheless, the analysis of the relative signal abundance allowed the comparison of the experimental groups within the phospholipid classes.

The detection of polyunsaturated fatty acids of different chain lengths was expected, as it has been demonstrated that *P. pastoris* can synthetise fatty acids with multiple double bonds, in contrast to *S. cerevisiae* (Wriessnegger *et al.*, 2009). It has been previously reported that specific phospholipid classes do not have specific selectivity for mono- or poly-unsaturation of the acyl chains (Ivashov *et al.*, 2013). However, it was observed that the most abundant PI species detected in the present study mainly contained saturated or monounsaturated fatty acyl chains, which was not observed for the other phospholipid classes, which were mainly unsaturated. The fatty acyl chai length and number of double bonds of the phospholipids detected in this study align well with previous publications (Adelantado *et al.*, 2017b). Klug *et al*. investigated the lipidome of *P. pastoris* and found that almost all phospholipids contained at least one double bond and that the most abundant fatty acids were 18:1, 18:2, 18:3, and 16:0. Moreover, the authors observed that the most abundant phospholipid classes were PC and PE, followed by PI and PS, consistently with the results observed in this study. PA, CL, and LPL species were also identified in lower abundance, but in the present study, PA and CL were not identified, possibly

because they were below the detection limit (Klug *et al.*, 2014). Ghellink *et al.* also detected PG species in an abundance similar to that of CL, but lower than that of PI and PS (De Ghellinck *et al.*, 2014), similar to the results obtained in this study.

Specific patterns in the fatty acid content of phospholipid species have been reported previously (De Ghellinck *et al.*, 2014), with the authors suggesting that PS and PI species tend to contain larger proportions of 34:1 and 34:2 acyl chains. This was less clear for other phospholipids, with almost randomized patterns, which is also what was observed in this study. Differences could be explained by the biosynthetic origin of phospholipid species. PS, PG, PI, and CL are synthesized through *de novo* pathways, and PS and PI are derived from the same precursor, Cytidine diphosphate diacylglycerol (Jani and Lopes, 2009). In contrast, PC and PE synthesis results from a combination of *de novo* and Kennedy pathways (Fagone and Jackowski, 2013). It is also important to note that C16 and C18 fatty acids, which are the most abundant in *P. pastoris*, are usually synthesised *de novo*, even though they can be assimilated from the growth medium (De Ghellinck *et al.*, 2014). It has also been shown that the phospholipid composition of the *P. pastoris* plasma membrane, as well as the degree of fatty acyl chain unsaturation, is dependent on the time of growth in the cultivation process. Yu *et al*. found that PG content increased during growth; it was low in the log phase and high in the stationary phase. Fatty acyl chains of 32, 34, and 36 carbon atoms were the most abundant fatty acyl chains. However, the abundance of C32 lipids increased with the time of growth, whereas that of C34 and C36 remained high. The authors also observed that the abundance of saturated species increased with incubation time and were high in the stationary phase, whereas these were low in the log phase (Yu *et al.*, 2022). These findings are consistent with the results obtained in the present study as the cells were harvested during the log phase, and unsaturated C34 and C36 were the most abundant fatty acyl chains.

Nanodiscs and SMALPs have been used to investigate the influence of lipids on the activity of membrane proteins in other studies (Cecchetti *et al.*, 2021), and extensive research has been conducted to characterise nanodiscs and SMALPs (Schuler *et al.*, 2013; Hazell *et al.*, 2016; Dominguez Pardo *et al.*, 2017). Dominguez Pardo *et al*. investigated whether SMA had a preference for solubilization of specific types of lipids or specific bilayer phases (Dominguez Pardo *et al.*, 2017). The authors found that SMA had no significant lipid preferences in homogenous binary lipid mixtures, indicating that SMALPs offer a good representation of the lipid composition in biological membranes. Nevertheless, binary lipid mixtures do not faithfully replicate real membranes, which consist of a diverse combination of lipids (Dominguez Pardo *et al.*, 2017). Teo *et al*. analysed the SMALP co-extracted phospholipids from bacterial membranes and suggested that SMA did not preferentially extract specific phospholipids from the membrane, while they demonstrated enrichment of certain phospholipid

classes surrounding purified membrane proteins in the SMALPs, compared to bulk membranes (Teo *et al.*, 2019).

Although it has been proposed that SMA does not preferentially solubilise specific phospholipid classes, more extensive research is still lacking in the field to accurately determine whether SMA has a preference for interacting with certain lipids from different host membranes. Differences between the *P. pastoris* bulk membranes and SMA-solubilized fraction were detected in this study. Therefore, the lipid composition of yeast membranes, which differs from that of bacterial hosts, may contribute to some variations in the lipid fractions resulting from different membrane solubilities.

On the other hand, although SMA can selectively interact with specific lipids in the plasma membrane, this interaction would not alter those lipids situated in the core of the SMALP, which are not in direct contact with the polymer. These core lipids would be replaced by membrane proteins in protein-containing SMALPs, as in the case of the $A_{2A}R$-SMALP, resulting in the modification of the lipid composition within the particles. The overexpression of the $A_{2A}R$ in *P. pastoris* membranes could lead to a significant portion of SMALPs containing this receptor, together with its lipid environment, affecting the lipids observed in the SMA-solubilized fraction. This could explain the similar variances detected between the $A_{2A}R$-SMALP or SMA-solubilised lipids and those of the bulk membranes. Based on this data, it is suggested that differences in lipid composition between the SMA-solubilized fraction and bulk membrane can be attributed to the specific lipids incorporated into the discs and those surrounding the $A_{2A}R$.

It has been proposed that short-chained phospholipids, such as PC(32:1), could be preferentially incorporated into SMALPs due to their chain length and degree of unsaturation (Dominguez Pardo *et al.*, 2017). Similarly, it was observed in here that PE species with acyl chains of 36 carbon atoms or shorter tended to be higher in the SMA-solubilised fraction, compared to bulk membranes, whereas those of 38 carbon atoms or longer tended to be decreased in the SMA-solubilised fraction. However, this was less clear for the other phospholipid classes, and it was observed that PIs and LPEs followed the opposite trend. Despite the differences, it was observed in this study that within each phospholipid class, the detected species were maintained in the same order of relative abundance in the three experimental groups. Hence, the most abundant phospholipid species in bulk membranes were, in general, the most abundant ones in the SMA-solubilised fraction and $A_{2A}R$-SMALP within the different phospholipid classes.

In other studies, SMA has shown a preference for solubilizing lipids in the fluid phase, in which lipids are more loosely packed and have greater mobility, as compared to those in the gel phase with tightly packed lipids resulting in a more rigid structure (Swainsbury *et al.*, 2014). These findings validated the

use of SMALPs to study the interplay of lipids and proteins in biological membranes, provided that these proteins reside in a fluid lipid environment. Tight phospholipid packing influenced by long fatty acyl chains with a low degree of unsaturation can decrease lipid solubilization efficiency (Cuevas Arenas *et al.*, 2016). A high degree of fatty acyl chain unsaturation was not observed in the present study, which suggests that $A_{2A}R$ solubilization from *P. pastoris* membranes provides relevant information on the lipid composition of the domains in which the receptor resides.

The use of SMALPs to study the local lipid environment of the solubilized and purified $A_{2A}R$ from *P. pastoris* membranes has been reported by Routledge *et al* (Routledge *et al.*, 2020). As in the present study, lipids in the $A_{2A}R$-SMALP were analysed by LC-MS/MS and compared to those in *P. pastoris* bulk membranes. In contrast to the present study, lipids were separated on a HILIC column. PC and PE species were identified, whereas PS and PI levels were below the detection limit, in contrast to the present study, potentially due to the increased instrument sensitivity and advanced methodology. The authors concluded that $A_{2A}R$-SMALP and bulk membrane lipid profiles were generally similar. In contrast, some dissimilarities between the lipid profiles of similarly prepared samples were observed in the present study.

Nanodiscs and SMALPs have not only been used to analyse the lipids that closely surround membrane proteins, but also to demonstrate how phospholipids participate in the activity of GPCRs. It has been shown using nanodiscs that phospholipids can modulate GPCR activity by direct interaction of their polar head groups with the $\beta_{1A}R$ (Rues *et al.*, 2016; Lavington and Watts, 2020), $\beta_{2A}R$ (Dawaliby *et al.*, 2016), and $A_{2A}R$ (Mizumura *et al.*, 2020) subunits. This was shown by testing receptor activation by ligand binding and conformational changes, and demonstrated the power of nanodiscs and SMALPs as tools to assess the role of specific lipids in GPCR activity. The modulatory effect of specific lipids on the activity of the $A_{2A}R$ has also been studied using alternative methodologies. Previous studies by MD simulations have suggested that the $A_{2A}R$ interacts with DOPG through H-bonding and electrostatic interactions between positively charged amino acid side chains and negatively charged lipid phosphate groups (Bruzzese *et al.*, 2020). In the present study, the $A_{2A}R$-SMALP lipid environment was enriched in anionic lipids, including PS, PG, and PI, compared to bulk membranes. It has been suggested that PG promotes $A_{2A}R$ activation through allosteric modulation by stabilising its intermediate-active conformation and enhancing agonist and G-protein binding. In contrast, this was not observed for DOPC, probably because of the bulky PC headgroup (Bruzzese *et al.*, 2020). PC is seemingly unable to penetrate between TM6 and TM7 to the same extent as PG, which has a smaller hydrophilic headgroup (Neale *et al.*, 2015). Consequently, PC is less suited for forming H-bonds or electrostatic protein-lipid interactions (Bruzzese *et al.*, 2018). Hence, the results observed in the present study may indicate that the receptor was in an environment favourable for its activation.

There is a consensus that anionic phospholipids are important for class A GPCR function, as they enhance the constitutive activity of these receptors (Díaz *et al.*, 2019). Although PG is a minor component of mammalian cell membranes, representing only 2% of all phospholipids, the results obtained in the present study and others indicate that its abundance in the local lipid environment of membrane proteins is increased (Dawaliby *et al.*, 2016).

Similarly, an experimental study showed that DOPG acts as a positive allosteric regulator of the β_{2A}R through H-bonding and electrostatic protein-lipid interactions. In contrast, DOPE acts as a negative modulator and DOPC has a neutral effect (Dawaliby *et al.*, 2016). DOPG facilitated agonist binding, whereas DOPE provided a better environment for antagonist binding. Moreover, DOPG maintained the cytoplasmic side of the β_{2A}R in an open conformation. This indicates that anionic lipids favour TM6 opening through specific phospholipid headgroup interactions; this was not observed for DOPE or DOPC. DOPS and DOPI were also identified as positive modulators of the receptor, although these did not stabilize the active conformation as DOPG did. This suggests that the negative charge in the headgroup is not sufficient for positive allosteric modulation. In contrast, DOPE provided the least supportive environment for receptor activation (Dawaliby *et al.*, 2016). In the present study, PC was decreased in the A_{2A}R-SMALP with respect to that in the bulk membranes. In addition, a decrease in PE content was observed compared to that of the SMA-solubilized fraction. This corroborates the suggestion that the A_{2A}R was surrounded by a lipid environment conducive to its activation. In contrast to these previous findings, Song *et al*. did not observe a close contact between the A_{2A}R and PC, PE, PS, or SM by molecular dynamic simulations. These were referred to as bulk lipids, with no specific binding site to any activation state. Instead, the authors reported that GM3, cholesterol, and Phosphatidylinositol 4,5-bisphosphate (PIP2) modulate the conformational dynamics of the A_{2A}R through specific interactions (Song *et al.*, 2019), and favour receptor stabilization, activation, and oligomerization (Song *et al.*, 2021).

Not only anionic phospholipids, but also cholesterol, is known to be an important modulator of GPCR function, favouring receptor activation. It was not possible to explore the role of cholesterol in this study, as *P. pastoris* produces ergosterol instead. Cholesterol has been shown to interact with the A_{2A}R at hydrophobic transmembrane helices and facilitate receptor activation and dimerization kinetics (Song *et al.*, 2019). Nevertheless, ergosterol has been proposed to have a stabilizing effect on membrane proteins, similar to cholesterol (Taghon *et al.*, 2021).

Similarly, some studies have suggested that the local lipid environment of the A_{2A}R is significantly enriched in unsaturated lipids, and it is believed that this might facilitate A_{2A}R activation by aiding TM6 rotation (Yang and Lyman, 2019). It was observed consistently in the present study that the A_{2A}R-SMALP

I. Company Marin, PhD Thesis, Aston University 2024

was mainly surrounded by mono- and polyunsaturated phospholipids. Mizumura *et al*. observed that DHA enhanced G-protein activation by the $A_{2A}R$ (Mizumura *et al.*, 2020). This can be explained by the fact that unsaturated and flexible lipids can more easily adapt to the structured surface of receptor TMs with lower energy costs (Gahbauer and Böckmann, 2016). The entropic penalty for lipid-protein interactions is significantly smaller for unsaturated chains than for saturated chains due to the higher conformational flexibility of the polyunsaturated chains. This allows protein conformational adaptation by modulating lateral pressure and equilibrium between different receptor states (Gahbauer and Böckmann, 2016). Moreover, an inhibitory effect of saturated phospholipids has been observed for rhodopsin (Mitchell *et al.*, 2003). Polyunsaturated fatty acids, together with cholesterol, have been proposed to modulate $A_{2A}R$ oligomerization, and hence activity, by similarly altering the receptor surface (Guixà-González *et al.*, 2016). Nevertheless, although the most abundant phospholipids surrounding the $A_{2A}R$ in the present study were unsaturated, the relative abundance and structure of these were not significantly different from those identified in the bulk membranes, so an increased chain unsaturation surrounding the $A_{2A}R$ cannot be confirmed.

In this study, the $A_{2A}R$ was purified in the absence of ligands. Hence, the results obtained must be regarded as the lipidome surrounding the apo receptor, which can potentially be modified by ligand binding. Lipids can influence membrane protein behaviour by altering the localization of proteins. Hence, the differential partitioning of GPCRs in lipid regions with different bulk properties can modulate their activity (Goddard *et al.*, 2013). It has been demonstrated that lipid ordering supports the ligand-bound configurations of $A_{2A}R$, whereas apo $A_{2A}R$ partitions into liquid disordered phases (Gutierrez *et al.*, 2019). Therefore, it has been proposed that the presence of membrane proteins induces the formation of a lipid annulus around them, and due to interactions, lipids within the annulus exhibit decreased motional freedom (Marsh and Páli, 2004).

Overall, accumulating evidence suggests that GPCR conformation and activity are modulated by its interaction with lipids, the physical properties of the lipid bilayer, and receptor locations in membrane domains. Anionic lipids and polyunsaturated chains reportedly influence GPCR activity (Mizumura *et al.*, 2020), which have been demonstrated to be close to the $A_{2A}R$ in the SMALP in the present study.

It is worth noting, however, that characterization of the lipid environment of the $A_{2A}R$ using SMALPs has some limitations. This methodology does not allow the identification of lipids that directly interact with the receptor. Instead, annular lipids are characterized, which might be in close contact or not with the receptor in the SMALP. Indeed, 50-100 lipids are expected to be copurified in a receptor-containing SMALP, in which the $A_{2A}R$ monomer occupies approximately 30% of the surface (Serebryany *et al.*, 2012). However, lipids surrounding the receptor, even without direct contact, can influence receptor

I. Company Marin, PhD Thesis, Aston University 2024

activity by modulating the membrane properties and lateral pressure. This can still exert a significant impact on membrane protein activity. Additionally, lipid extraction and analysis methods have some limitations. Although LC-MS/MS allows accurate lipid measurements and identification of low-abundance species, as a highly specific and sensitive technique, variability introduced in sample preparation and lipid extraction can affect the accuracy and reproducibility of the results (Piehowski *et al.*, 2013). In addition, it generates a complex dataset that can be challenging to analyse. Consequently, misidentification of isomeric and isobaric species with similar fragmentation patterns can arise (Batarseh *et al.*, 2018; Züllig *et al.*, 2021). Moreover, different adduct forms, as well as in-source lipid fragmentation, can lead to the generation of a number of different ions from a single analyte, potentially causing the misidentification of lipid species (Hu *et al.*, 2022). This can be aggravated for low-abundance species near the detection limit (Hu *et al.*, 2020). Complex samples containing a diverse range of lipid species, such as *P. pastoris* membranes, increase this likelihood of misidentification. Moreover, lipid databases used for identification may not encompass all possible lipid species, leading to a failure to accurately identify them. In contrast, the use of complex databases can lead to false-positive identifications (Hu *et al.*, 2020). Manual curation of lipid identification can be performed, and may be necessary, but this is time-consuming and may still result in misidentifications even for experienced researchers. To overcome this, rigorous quality control and internal standards should be employed and accurately analysed prior to sample processing (Drotleff and Lämmerhofer, 2019), which was conducted in the present study using the EquiSPLASH mix and investigating the elution and fragmentation of the lipid standards. Additionally, cross-referencing and collaboration with lipidomics experts can help improve the accuracy of lipid identification by LC-MS/MS.

The identification of the lipids surrounding the $A_{2A}R$ in SMALPs, along with the identification of lipids in the *P. pastoris* plasma membrane, has contributed to characterising the lipid environment of a membrane protein. The findings can be used to improve the understanding of how these lipids might affect the protein function, which has implications for cell signalling, and biological processes (Pan *et al.*, 2022; Levental *et al.*, 2023). This is valuable knowledge for structural biology, as well as for developing bioengineering of membrane proteins and drug-delivery systems (Van Der Westhuizen *et al.*, 2015). The composition of biological membranes is affected by various pathological conditions, including inflammation, aging, cancer, and neurodegenerative diseases, for which multiple GPCRs are implicated as drug targets. Underlying the influence of lipids on the activity of these receptors is crucial for understanding GPCR function under normal and pathological conditions (Marzoog *et al.*, 2021). On the other hand, *P. pastoris* lipid profiling has enhanced the understanding of the lipid composition of this host organism, which is broadly used for heterologous expression of recombinant proteins for functional and structural studies. Moreover, this study contributed to characterizing the applicability of

I. Company Marin, PhD Thesis, Aston University 2024

SMALPs for the study of membrane proteins. This methodology can be applied to the characterization of other membrane proteins or expression hosts, broadening its applicability to different biological contexts.

In addition to identifying the annular lipids surrounding the $A_{2A}R$, detecting those that directly interact with the receptor would provide a more comprehensive understanding of the role of the lipid environment surrounding the $A_{2A}R$ in SMALPs. This would help identify unique lipids that may play specific roles in protein stability or function and contribute to a broader understanding of lipid-protein interactions. Based on these findings, the lipid environment of the receptor in the SMALP could be modified to characterize the role of specific lipids in the activity of the $A_{2A}R$. SMALPs could be enriched in certain phospholipid classes such as PE, PS, PG, or PI, and the activity of the receptor could be tested to investigate how different lipid environments affect the receptor conformation, stability, and ligand binding (Hazell *et al.*, 2016). On the other hand, lipid oxidation could be induced in the samples using radical initiators to analyse the oxidised lipids that closely interact with the $A_{2A}R$. This would provide specific information on lipid-protein interactions under oxidative conditions. Moreover, it would provide an enhanced understanding of how oxidative stress influences membrane protein environments, which has implications for various biological processes. In addition, it may have potential relevance in diseases involving oxidative stress. These directions align with the current trends in membrane protein research, which increasingly emphasizes the complex interplay between proteins and lipids in the plasma membrane. Moreover, to understand the relevance of the $A_{2A}R$ lipid environment, it is crucial to confirm the folding state and functionality of the purified receptor in the SMALP, which was conducted in the following thesis chapter.

In conclusion, an in-depth analysis of the co-purified $A_{2A}R$ lipid environment in SMALPs was reported for the first time using novel mass spectrometry equipment and advanced methodology, employing the high-sensitivity Select Series Cyclic ion mobility (IMS) system, and analysing the data using HDMS^E methods. Saturated and unsaturated phospholipid species were identified in *P. pastoris* bulk membranes, SMALPs, and closely surrounding the $A_{2A}R$. Differences were detected in the phospholipid content between the bulk membranes and the SMA-solubilized fraction, potentially due to the overexpression of the A2AR and its solubilization with the polymer. The vast majority of the most abundant phospholipids contained unsaturated fatty acids, and the $A_{2A}R$-SMALP showed an increase in anionic phospholipids, which potentially contribute to the activation of the receptor. These analytical data are important knowledge on the *P. pastoris* lipidome and GPCR-lipid environment characterization, which is crucial for receptor folding, conformation, and activity.

4. CHAPTER 4 – STUDY OF THE CONFORMATION, THERMOSTABILITY, AND PHARMACOLOGY OF THE A$_{2A}$R

4.1 INTRODUCTION

4.1.1 Tryptophan fluorescence spectroscopy

Once the A$_{2A}$R has been expressed, solubilized, purified, and properly identified, its folding state and functionality can be characterised. Characterisation of its folding state and its ability to undergo conformational changes can be achieved using fluorescence spectroscopy (Gorbenko, 2011). Ligand binding to GPCRs and A$_{2A}$R can result in conformational, structural, and functional changes, which can be monitored by measuring their intrinsic fluorescence (Monici, 2005) (Royer, 2006).

Proteins exhibit intrinsic fluorescence originating from aromatic amino acids. This property has been extensively explored to study protein dynamics without any protein modifications (Hellmann and Schneider, 2019). Intrinsic fluorescence is predominantly derived from tryptophan residues (Trp), owing to their aromatic rings in the side chain: pyrrole and benzene rings. Among the three fluorescent amino acid constituents of proteins, including tryptophan (Trp), tyrosine (Tyr), and phenylalanine (Phe), Trp is the most abundant, with concentrations of ~1% in soluble proteins and up to 3% in membrane proteins (Du *et al.*, 2018). Although Tyr has a quantum yield similar to Trp, the indole group of Trp is considered to be the dominant source of absorbance at ~280 nm and emission at ~350 nm in proteins. Moreover, Tyr emission is often quenched in native proteins, presumably by energy transfer to Trp or by its interaction with the peptide chain. On the other hand, the contribution of phenylalanine (Phe) to the intrinsic fluorescence of protein is negligible due to its absorptivity and very low quantum yield (Liu *et al.*, 2020).

Tryptophan fluorescence wavelength and intensity are strongly influenced by the residue local environment. This high dependency of Trp fluorescence on its surroundings has been used to elucidate conformational changes in membrane proteins (Ghisaidoobe and Chung, 2014). Specifically, Trp fluorescence is influenced by the polarity of its microenvironment and non-covalent interactions such as hydrogen bonding. Trp emits at shorter wavelengths (λEM) (330-340 nm) when buried in the hydrophobic core of a protein in its ground state, whereas it emits at longer wavelengths (340-355 nm) when exposed to water in its excited state (Burstein *et al.*, 1973). Thus, a red shift in λEM is observed as the polarity increases. In contrast, a blue shift in Trp fluorescence is observed in increasing non-polar or hydrophobic environments. Indeed, water molecules are prone to form bonds with the excited and polar state of Trp, whereas the hydrophobic side chains of amino acid residues in the protein are prone to form bonds with the less polar ground state of Trp. Thus, Trp fluorescence may vary depending on the surface accessibility of Trp residues and their interaction with other amino acids or water molecules

in their excited or ground states (Hellmann and Schneider, 2019). In contrast, although Tyr and Phe are also fluorescent residues, their emission characteristics do not depend so extensively on their local environment (Vladislav *et al.*, 2021).

The wild-type $A_{2A}R$ contains seven Trp residues, but the construct used for this study consisted of the C-terminal truncated sequence of the protein, so it only contained six Trp residues. The localization of these six residues in the active and inactive conformations of the $A_{2A}R$ is shown in Figure 4.1. The tryptophan residues W29 and W32 are located at the bottom of TM1, close to the junction with the first intracellular loop (ICL1). The residue W129 is found in the TM4, W143 in the junction between TM4 and extracellular loop 2 (ECL2), W246 in the TM6. Finally, W268 is found at the extracellular face of TM7, in the junction with the extracellular loop 3 (ECL3) (Routledge *et al.*, 2020).
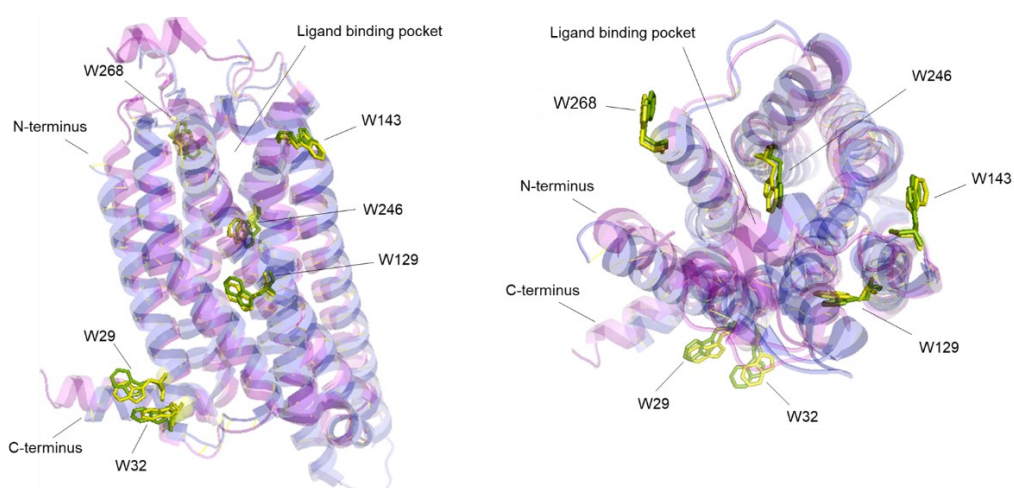
Figure 4.1. Location of tryptophan residues in the C-terminal truncated $A_{2A}R$. *The structure of the $A_{2A}R$ in the inactive conformation bound to the antagonist ZM241385 (blue; PDB ID:3EML) was aligned to the structure of the $A_{2A}R$ in the active conformation bound to the agonist 5'-N-Ethylcarboxamidoadenosine (NECA) (purple; PDB ID:2YDV) and presented through (**A**) the plane of the receptor and (**B**) from above. Tryptophan residues in the inactive and active conformations are indicated in yellow and green, respectively. The diagram was created using PyMOL software.*

The $A_{2A}R$ exists in dynamic equilibrium between different conformational states (Prosser *et al.*, 2017), which are achieved through conformational changes upon ligand binding (Venkatakrishnan *et al.*, 2016). The most discernible changes relate to rearrangements of the transmembrane (TM) helices TM3, TM5, and particularly TM6 and TM7 (Jaakola *et al.*, 2008; Lebon *et al.*, 2011b; Xu *et al.*, 2011). The secondary structure of these membrane proteins remains intact during the conformational changes (Lebon *et al.*, 2011). The addition of ligands causes remodelling of the equilibrium to preferentially stabilise specific conformers (Prosser *et al.*, 2017), and the balance of conformers is not only modified

I. Company Marin, PhD Thesis, Aston University 2024

by the presence of a ligand, but also by allosteric modulators such as salt concentration and cholesterol (Guixà-González *et al.*, 2017). Despite the activation barriers, basal activity of the $A_{2A}R$ occurs owing to the presence of receptors in the active conformation in the absence of agonists (Prosser *et al.*, 2017). Hence, the apo $A_{2A}R$ exhibits constitutive activity, accounting for over 50% of its activity stimulated by the agonist (Bertheleme *et al.*, 2013). Interestingly, Ye *et al.* noted that 70% of apo receptors adopt active S3 and S3' states (Ye *et al.*, 2016).

Routledge *et al.* studied the conformational changes of the encapsulated $A_{2A}R$-SMALP upon ligand binding by measuring Trp fluorescence and reported that the antagonist ZM241385 binding caused changes in the local environments of the intrinsic Trp residues. Specifically, they observed an increase in fluorescence emission upon ZM241385 binding and suggested that Trp246[6.48] and Trp268[7.33] were responsible for the observed increase (Routledge *et al.*, 2020). Nevertheless, changes in Trp fluorescence emission upon ligand binding could also be explained by the fact that ZM241385 could alter the solvent accessibility of Trp246[6.48], as it is located in the ligand-binding cavity (Jaakola *et al.*, 2010). Notwithstanding, NECA also binds close to Trp246[6.48], and thus, the same effect on Trp fluorescence emission would be expected if it was dependent on the presence of the ligand. However, Routledge *et al.* did not observe any changes in Trp fluorescence upon NECA binding. This suggests that the detected changes in Trp fluorescence are a consequence of conformational changes in the receptor, and are not caused by the presence of ligands in the binding pocket (Routledge *et al.*, 2020). Additionally, the fluorescent moiety IEDANS was introduced into the cytoplasmic face of TM6 and reported dynamic changes in the intracellular face of the receptor during its activation process, which was also previously used to monitor the activation of the $\beta_{2A}R$ receptor (Yao *et al.*, 2006). $A_{2A}R$ TM6 was found to be in an open conformation in a more polar environment, which is characteristic of the active conformation of the receptor that accommodates G-protein binding (Routledge *et al.*, 2020).

4.1.2   *Profiling the thermal unfolding of the $A_{2A}R$*

The stability of the $A_{2A}R$, can be investigated by profiling its thermal unfolding characteristics. This can be achieved using the 7-Diethylamino-3-(4'-Maleimidylphenyl)-4-Methylcoumarin (CPM) fluorescent probe (Marino *et al.*, 2010). CPM is a highly sensitive probe for changes in protein conformation, making it highly useful for detecting unfolding events (Alexandrov *et al.*, 2008).

CPM binds specifically to cysteine amino acids as the protein unfolds, consequently emitting fluorescence at 470 nm. Therefore, adducts are formed as CPM gains access to the transmembrane-embedded thiols during thermal denaturation (Park *et al.*, 2020). Nevertheless, the fluorescence signal is reduced by protein aggregation, which occurs as the protein denatures. Secondary processes,

I. Company Marin, PhD Thesis, Aston University 2024

including amino acid modification and thiol-CPM adduct hydrolysis, can also modify the unfolding curves (Naranjo *et al.*, 2016). CPM binding to exposed cysteines can be monitored in real time using qPCR, allowing dynamic observation of the protein unfolding process. This technique is based on non-invasive probe binding to protein residues, which does not significantly alter the native structure of proteins (Alexandrov *et al.*, 2008).

The $A_{2A}R$ contains 14 Cysteine residues that are susceptible to CPM binding during protein thermal unfolding. The localization of these residues in the active conformation of the $A_{2A}R$ is shown in Figure 4.2.
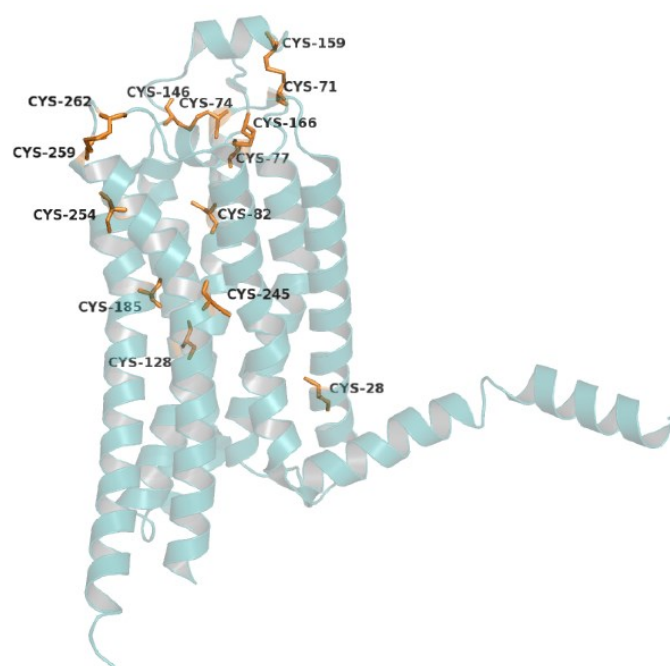
Figure 4.2. Location of cysteine residues in the C-terminal truncated $A_{2A}R$. *The structure of the $A_{2A}R$ in the active conformation bound to the agonist NECA (PDB ID:2YDV) was presented from the plane of the receptor, and cysteine residues are indicated in orange. The diagram was created using PyMOL software.*

The flexible regions of membrane proteins are prone to unfolding. GPCRs are α-helices organized into two blocks. TM1-TM5 form a rigid core that does not vary substantially during the activation process, whereas TM6-TM7 are highly dynamic (Schwartz *et al.*, 2006). ICL3 is highly flexible and known to be a hotspot of instability in GPCRs (Hubbell *et al.*, 2003). Consequently, thermal unfolding assays using a CPM probe allow the separation of flexible regions, potentially mimicking the functional activation of the receptor. Simulations of the thermal unfolding process of rhodopsin suggested that protein denaturation begins with the loss of hydrogen and disulphide bonds within the extracellular loops. This is closely related to the orientation of transmembrane helices, which do not fully unfold (Rader *et al.*,

I. Company Marin, PhD Thesis, Aston University 2024

2004). Popot and Engelman established that α-helices act as stable and independent folding domains that do not denature to the same extent as the flexible regions (Popot and Engelman, 1990). Their interactions define the tertiary structure of the protein, which undergoes a separate folding transition (Vogel and Siebert, 2002; Booth and Curnow, 2006). Similarly, Jamshad *et al*. indicated that the thermal denaturation of the $A_{2A}R$ is a two-state process, correlating with a folded to unfolded transition, and indicated that the secondary structure of the $A_{2A}R$-SMALP was resistant to thermal denaturation (Jamshad *et al.*, 2015).

CPM fluorescence assays have been used to study the effects of ligand binding and the surrounding lipid environment on the thermostability of membrane proteins. Alexandrov *et al*. observed that FAAH inhibitor binding increased the thermal stability of the detergent-solubilized protein, as it increased the melting temperature (Tm), whereas no differences were detected for the purified APJ receptor upon ligand binding (Alexandrov *et al.*, 2008). Naranjo *et al*. examined the effects of different lipid environments on thermal unfolding of the $A_{2A}R$-DDM by CPM fluorescence (Naranjo *et al.*, 2016). Their results indicated that protein purification using different detergents and lipid conditions did not affect the secondary and tertiary structures of the receptor (Naranjo *et al.*, 2016).

Alternative techniques have been used to study $A_{2A}R$ thermostability. Haffke *et al.* explored the use of NanoTemper Technologies Prometheus NT.48 (nanoDSF), which uses low-volume differential intrinsic Trp scanning fluorimetry to study the stabilizing effects of ligand binding to the detergent-solubilized $A_{2A}R$ (Haffke *et al.*, 2016). The Tm values obtained by nanoDSF correlated well with those obtained from traditional thermal unfolding experiments. It was also demonstrated that this methodology can be used to determine the thermal stability of other GPCRs, for which the CPM-DSF method is challenging. Moreover, ligand binding stabilized the $A_{2A}R$, which was found in its active conformation in a lipid-free environment (Haffke *et al.*, 2016).

Alternatively, protein thermostability can be studied using circular dichroism (CD) or radioligand binding assays. O'Malley *et al.* observed a single transition between the folded and unfolded states of the $A_{2A}R$-DDM by CD, and agonist and antagonist binding shifted the unfolding transition to a higher Tm (O'Malley *et al.*, 2010).

The thermostability of SMALP-encapsulated proteins has also been studied, and it has been observed that SMA-solubilised proteins exhibit higher thermostability than DDM-solubilised proteins (Pollock *et al.*, 2018). Gulati *et al.* demonstrated by CMP fluorescence that Pgp-SMALP showed significantly higher stability than detergent-solubilized Pgp (Gulati *et al.*, 2014). Jamshad *et al*. studied the thermostability of the $A_{2A}R$-SMALP and $A_{2A}R$-DDM by CD, and observed that the $A_{2A}R$-SMALP showed increased thermostability compared to $A_{2A}R$-DDM (Jamshad *et al.*, 2015). Similarly, Dörr *et al*. demonstrated by

115

CD that the ion channel KcsA-SMALP was more stable than KcsA-DDM (Dörr *et al.*, 2014). Comparably, hENT1 thermostability was studied using radioligand binding assays, and hENT1-SMALP showed a higher Tm than the detergent-solubilized protein (Rehan *et al.*, 2017).

4.1.3   The study of $A_{2A}R$-ligand interactions by radioligand binding assays

Studying the ligand-binding capacity of $A_{2A}R$ using radioligand binding assays is essential not only for characterizing the proper folding and stability of the protein but also for its application in drug discovery, development, and screening. This highly specific and sensitive methodology allows the detection of low-affinity ligand binding at low receptor concentrations. It can also be used for quantitative analysis of ligand-binding affinity (Kd) and maximum receptor binding capacity (Bmax). Hence, these assays are useful for receptor characterization (Bylund and Murrin, 2000).

These assays offer high versatility because they can be applied to multiple biological systems, including intact cells, tissue homogenates, and isolated cell membranes. Moreover, the pharmacology of GPCRs can be studied on membrane-bound receptors, which facilitates and shortens sample preparation and avoids membrane protein solubilization. This allows receptor studies to be conducted in their natural environment (Maguire *et al.*, 2012; Dong *et al.*, 2015).

Radioligand binding assays have been widely used to study $A_{2A}R$ ligand binding. Fraser *et al*. conducted radioligand binding assays on the purified and membrane-bound $A_{2A}R$ expressed in *P. pastoris* SMD1163 (Fraser, 2006). Displacement binding assays were performed on the membrane-bound receptor using ZM241385, xanthine amine congener (XAC), NECA, and theophylline, to displace [^{3}H]-ZM241385. The IC_{50} values were calculated, which represent the concentration of the unlabelled drug required to displace 50% of the radioligand, and showed that ZM241385 had the highest affinity as an antagonist, with a Log IC_{50} of -8.5. These findings provide valuable information regarding the pharmacological properties of the membrane-bound $A_{2A}R$ expressed in *P. pastoris*. Moreover, the results indicated that this receptor showed native-like pharmacological properties and could specifically bind to ZM241385 with a high affinity, comparable to that of the receptor expressed in mammalian cells. This suggested that the membrane-bound receptor had a native-like structure, and demonstrated the validity of *P. pastoris* as an expression system (Fraser, 2006).

Similarly, Yang *et al*. conducted competition radioligand binding assays on the membrane-bound $A_{2A}R$ expressed in mammalian HEK293 cells using unlabelled ZM241385 to displace [^{3}H]-ZM241385. A displacement curve was obtained, with a pKi value of 8.9 (Yang *et al.*, 2017). Comparable experiments were performed on the $A_{2A}R$, A_1R, and A_3R expressed in mammalian cells using ZM241385 (Guo *et al.*,

116
I. Company Marin, PhD Thesis, Aston University 2024

2016; Arruda *et al.*, 2017) and on the $A_{2A}R$ displacing [^{3}H]-ZM241385 with other ligands such as caffeine and CGS21680 (Bonaventura *et al.*, 2015) .

Despite their advantages, radioligand binding assays are subjected to multiple sources of bias that may affect data accuracy and reliability. If different receptor isoforms exist, they may have different affinities for radioligands, which can lead to skewed observations. Variations in assay conditions, such as buffer composition, temperature, and incubation time, can lead to changes in radioligand binding characteristics and kinetics. Moreover, endogenous ligands in sample preparation can compete with the radioligand for receptor binding, thus biasing the results observed. Finally, the use of nonhuman expression systems for the expression of human receptors may have an impact on binding characteristics. (Magnani *et al.*, 2008; Singh *et al.*, 2012; García-Nafría *et al.*, 2018).

Alternative techniques have been developed to study receptor-ligand interactions. Massink and colleagues developed and validated an LC-MS binding assay for the $A_{2A}R$ using ZM241385. A deuterated isotope of ZM241385 served as an internal standard, and the unbound ligand was separated from the receptor-bound ligand in the cell membrane preparation and detected in the pM range. Saturation and displacement binding assays were conducted, and the results were in good agreement with those obtained using radioligand binding assays. Hence, their study validated the use of MS for studying receptor-ligand binding, and provided a potential alternative to conventional radioligand binding assays (Massink *et al.*, 2015).

Grime *et al.* used fluorescence correlation spectroscopy (FCS) to characterize the binding capability of the $A_{2A}R$-SMALP expressed in *P. pastoris*. The specific binding of CA200645 to the $A_{2A}R$-SMALP was investigated, and the authors demonstrated that fluorescent ligand binding resulted in a biphasic autocorrelation curve. Moreover, a displacement binding assay of the fluorescent ligand was conducted using FCS with ZM241385. These results indicated that ZM241385 competed for the ligand binding site of the $A_{2A}R$-SMALP, and prevented CA200645 binding. The calculated Log Ki for ZM241385 was -8.2 ± 0.5, which was not significantly different from the previously reported affinity of ZM241385 binding to $A_{2A}R$ in the original membranes. Furthermore, this was comparable to the results obtained by radioligand binding assays in the previous studies. Hence, fluorescent ligands could be used to study the pharmacology of GPCRs and replace radiolabelled ligands (Grime *et al.*, 2020).

4.2 AIMS AND OBJECTIVES

The work reported in this chapter aimed to explore how oxidative stress induced by acrolein or AAPH could impact the structure, folding, and conformational dynamics of the $A_{2A}R$. The first objective was

to determine whether the purified A$_{2A}$R was properly folded and active after purification assessing the conformational changes that the receptor can undergo by tryptophan fluorescence. The second objective was to determine whether the oxidative treatments affected its conformational changes. The third objective was to determine whether ligand binding and the oxidative treatments affected protein stability as assessed by thermal unfolding. The forth objective was to study whether oxidation affected ligand binding using radioligand binding assays.

4.3 MATERIALS AND METHODS

4.3.1 Tryptophan fluorescence measurements

Fluorescence measurements were made using a PTI QuantaMaster 300 fluorimeter with continuous Xe arc excitation. Emission spectra were obtained by exciting the protein at 280 nm, and emission spectra were measured between 290 and 500 nm. Excitation slit widths of 10 nm (±0.8 nm) and emission slit widths of 20 nm (±3.2 nm) were used for all measurements with a scan speed of 1000 nm/min for 3 accumulation scans.

Samples of A$_{2A}$R-SMALP, A$_{2A}$R-DIBMALP, A$_{2A}$R-DDM, and L-Tryptophan control (Sigma-Aldrich) at 50 μg/mL in membrane buffer (50 mM Tris/HCl pH 8, 500 mM NaCl, 10% glycerol) containing SMA at 2.5% (w/v) or DDM at 2% (w/v) were placed individually in a 0.3 cm quartz fluorescence cuvette (Starna Scientific). Trp fluorescence was also measured for the membrane buffers (50 mM Tris/HCl pH 8, 500 mM NaCl, 10% glycerol, or 300 mM NaCl, 20 mM HEPES, pH 7.5), dimethyl sulfoxide (DMSO), the A$_{2A}$R antagonist ZM241385, and the A$_{2A}$2 agonist NECA as negative controls. Alternatively, the A$_{2A}$R-SMALP was treated with acrolein (ACR) or 2,2'-azobis(2-amidinopropane) dihydrochloride (AAPH) at final concentrations of 20 μM, 40 μM, and 100 μM for 24 hours, and Trp fluorescence was measured.

To determine the effect of ligand binding on the A$_{2A}$R, ZM241385 and NECA were titrated into the cuvette at concentrations from 1 pM and 100 pM, up to final concentrations of 10 μM and 1 mM, respectively. To study the effect of sample dilution on the fluorescence signal after titration, the protein preparation was titrated with membrane buffer. The emission intensity of tryptophan was measured at each titration point. The resulting intensity data were adjusted to take into account the effect A$_{2A}$R-SMALP dilution.

For data analysis, fluorescence results were analysed using SpectraGryph 1.2 - spectroscopy software and the percentage of tryptophan signal was calculated taking into account the dilution effect by titration and apo A$_{2A}$R-SMALP, A$_{2A}$R-DDM, or Trp control as 100% of the signal. GraphPad Prism 8 was used to plot the % of Trp signal results, and the data were expressed as the mean ± standard deviation

I. Company Marin, PhD Thesis, Aston University 2024

(SD), for n=3. For statistical data analysis, the percentage of Trp fluorescence at each ligand concentration was compared between the A_{2A}R-SMALP samples treated with different ACR and AAPH concentrations through an ordinary One-way ANOVA and Tukey's multiple comparisons test. Statistical significance was set at p-value <0.05.

4.3.2 Thermal unfolding by CPM fluorescence

7-Diethylamino-3-(4'-Maleimidylphenyl)-4-Methylcoumarin (CPM) probe stock was prepared at 5 mg/mL, and aliquots were stored at -80°C and protected from light. CPM was diluted to 200 µg/mL in SMA buffer (50 mM Tris/HCl pH 8, 500 mM NaCl, 10% glycerol, 2% w/v SMA2000) or DDM buffer (50 mM Tris/HCl pH 8, 500 mM NaCl, 10% glycerol, 2% DDM w/v), vortexed, and allowed to equilibrate for 1 h at room temperature protected from light. A_{2A}R-SMALP and A_{2A}R-DDM samples were prepared at final concentrations of 150, 100, 50, 25, or 12.5 µg/mL in SMA or DDM buffer, respectively, and 45 µL of the sample was mixed with 5 µL of CPM.

To study the effect of ligand binding on the thermal stability of the A_{2A}R-SMALP and A_{2A}R-DDM, 1 µM ZM241385 and 10 µM NECA were added to the mixture. To study the effect of incubating the protein preparations at higher temperatures, A_{2A}R-SMALP and A_{2A}R-DDM were incubated at 37°C or room temperature for 1 h. To study the effect of the oxidative treatments acrolein and AAPH on the protein thermal unfolding, A_{2A}R-SMALP and A_{2A}R-DDM were pre-incubated for 20 min at room temperature with CPM. Acrolein or AAPH were added to final concentration of 100 µM and incubated for 1 h at room temperature. The sample preparation was mixed by pipetting up and down and allowed to equilibrate on ice for 10 min protected from light.

The samples were transferred to PCR white-opaque 96-well plates, which were sealed and transferred to the LightCycler® 480 System (Roche Diagnostics). The PCR machine was pre-set to allow the temperature to equilibrate at 20°C and fluorescence was measured at an excitation wavelength of 465 nm and an emission wavelength of 510 nm using SYBR Green filter from 20 to 99°C with a ramp rate of 3.6°C/min. For data analysis and calculation of the melting temperatures (Tm), fluorescence results were plotted against the temperature range, and the first derivative of the blank-subtracted fluorescence results was calculated using GraphPad Prism 8.

4.3.3 Radioligand binding assays on the membrane-bound A_{2A}R

Saturation and displacement binding assays were performed on the membrane-bound A_{2A}R. Membrane preparations (10 mg protein/mL) in membrane buffer (50 mM Tris/HCl pH 8, 500 mM NaCl, 10% glycerol) were diluted to 0.5 mg/mL of protein in binding buffer (50 mM Tris/HCl pH 8, 500 mM

NaCl). Additionally, 0.5 U/mL of adenosine deaminase were added to the membrane preparations to degrade any adenosine released from *P. pastoris* membranes. To study the effect of the oxidative treatments on the pharmacology of the $A_{2A}R$, membranes at 10 mg/mL were treated with acrolein and AAPH at final concentrations of 20 mM and 1 mM, respectively, and incubated overnight at 37°C. Alternatively, the membranes were treated with vehicle (membrane buffer) and incubated overnight at 37°C.

All radioligand-binding assays were performed using the $A_{2A}R$ antagonist [3H]ZM241385 diluted in Binding Buffer. For displacement binding assays, [3H]ZM241385 was diluted to a final concentration of 1 nM (40.000 cpm/5 µL), and 500 µL of membranes was incubated with 5 µL of radioligand and 5 µL of unlabelled ZM241385, which was previously diluted to reach final concentrations of 10 pM, 100 pM, 1 nM, 10 nM, 100 nM, and 1 µM. For the saturation binding assays, [3H]ZM241385 dilutions were prepared to reach final concentrations of 0.1, 0.5, 1, 5, 10, and 20 nM, and 5 µL of each radioligand dilution was added to 500 µL of the membrane sample. To determine total binding, 5 µL of DMSO was added to each membrane sample together with the radioligand dilution, whereas to determine non-specific binding, 5 µL of unlabelled ZM241385 at a final concentration of 1 µM was added to each sample tube. All samples were tested in duplicate. The membrane samples were incubated with the ligands at room temperature for 30 min and centrifuged at 14.000 rpm and 4°C for 5 min. The membrane pellets were washed twice with ddH$_2$O to discard the unbound ligand and resuspended in 100 µL of Solvable^{TM} solution overnight at room temperature. Optiphase 'Hisafe' scintillation cocktail (1 mL) was added to each sample tube and mixed well by vortexing. Counts per minute (cpm) were counted. The results were analysed using GraphPad Prism 8, and statistical differences between the non-treated and oxidized membranes were determined by Multiple T-test. Statistical significance set at a p-value<0.05.

4.4 RESULTS

4.4.1 The effect of $A_{2A}R$ ligand binding on tryptophan fluorescence

Tryptophan fluorescence measurements were performed to study the effect of ligand binding on the conformational changes in the $A_{2A}R$-SMALP. The fluorescence of the $A_{2A}R$-SMALP in the absence of any ligand was measured, and the spectrum exhibited a broad peak with maximum intensity at ~340 nm (Supplementary Figure 8.23). These results indicated that the fluorescence of tryptophan residues of the $A_{2A}R$ could be measured in low-concentration protein preparations (~50 µg/mL); therefore, changes in its conformation could be monitored.

A$_{2A}$R-SMALP tryptophan fluorescence after antagonist ZM241385 and agonist NECA addition was measured to study whether any changes were observed upon ligand binding. A$_{2A}$R-SMALP showed a broad peak in the emission spectrum at ~340 nm (Figure 4.3A), and an increase in its intensity, accompanied by a red shift, was observed upon the addition of ZM241385 at 1 µM. This indicated that the A$_{2A}$R was folded in the SMALP, and its conformation could be modified upon antagonist binding. In contrast, NECA addition at 10 µM caused a decrease in the fluorescence intensity (Figure 4.3B). A greater decrease in the fluorescence peak was observed when the concentration of NECA was increased to 100 µM. Thus, NECA induced the opposite effect on the Trp fluorescence of the A$_{2A}$R-SMALP compared to the antagonist ZM241385. Furthermore, the red shift observed after the addition of ZM241385 was not obtained after NECA binding.
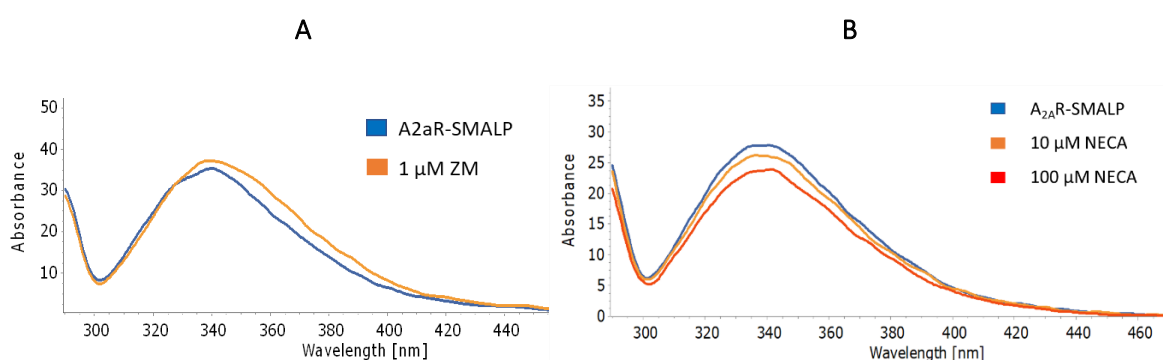
*Figure 4.3. Fluorescence of the A$_{2A}$R-SMALP in the absence and presence of ligands . The fluorescence emission of A$_{2A}$R-SMALP was measured between 290 and 500 nm after excitation at 280 nm before (apo) and after the addition of (**A**) the antagonist ZM241385 and (**B**) the agonist NECA. The results are presented as raw data (n=1).*

The decrease in Trp fluorescence intensity after ligand addition due to dilution of the sample must be considered. The effect of diluting the sample on the intensity of Trp fluorescence was assessed by the addition of 2 µL of Tris-HCl buffer 10 times, simulating titration experiments. A broad peak was observed in the emission spectrum corresponding to the tryptophan fluorescence of the A$_{2A}$R-SMALP (Figure 4.4A), and the intensity of fluorescence decreased at each dilution step. This indicated that the fluorescence intensity is affected by the concentration of the protein in the sample, and must be considered when analysing the effect of ligand binding. The percentage decrease in the Trp fluorescence signal at each dilution step was calculated considering the fluorescence of apo A$_{2A}$R-SMALP as 100% (Figure 4.4B). The results showed that the dilution of the sample by the addition of 2 µL of buffer decreased the Trp signal by an average of 3.5% per step, and after ten dilution steps, the Trp signal decreased by 40%. These results were used to normalise the Trp fluorescence signal after the addition of ligands by titration.

I. Company Marin, PhD Thesis, Aston University 2024

A

B
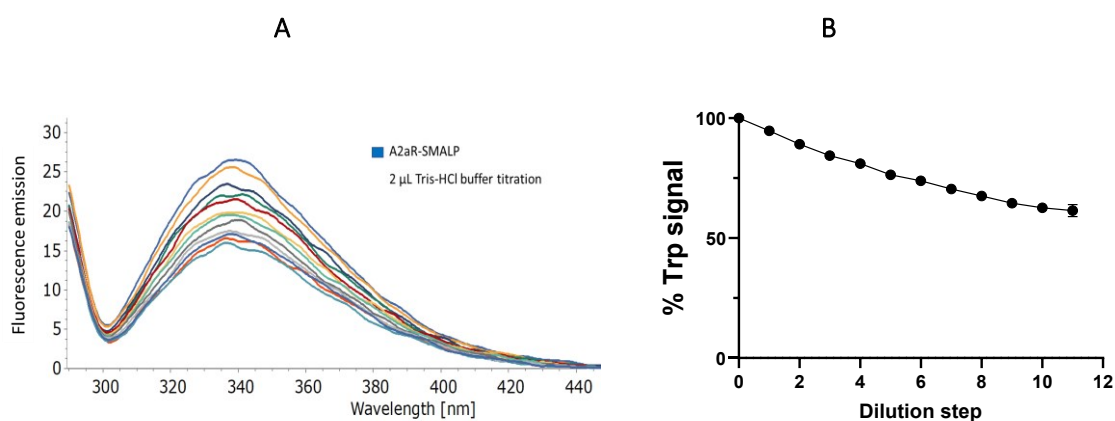
***Figure 4.4. Dilution effect on A₂ₐR-SMALP fluorescence emission**. The fluorescence emission of apo A₂ₐR-SMALP (blue) and after the addition of 2 μL of Tris-HCl buffer for 10 dilution steps was measured between 290 and 500 nm after excitation at 280 nm. The results are presented as (**A**) raw data and (**B**) percentage Trp signal of the dilution effect on the overall fluorescence, considering apo A₂ₐR-SMALP as 100%. Data are presented as the mean of all replicates (n=3) ± SD.*

The effect of antagonist ZM241385 binding to the A₂ₐR-SMALP on the Trp fluorescence signal was studied by the addition of increasing concentrations of the ligand from 1 pM to 10 μM by titration (Supplementary Figure 8.25). The percentage Trp fluorescence signal was calculated by normalizing the fluorescence intensity to the decrease in the signal due to the dilution effect (Figure 4.5A). The data demonstrated an increase in the Trp fluorescence signal after the addition of the antagonist, with a greater increase above 100 nM, provoking a final 40% increase in Trp fluorescence. In contrast, ZM241385 addition to the Trp control did not increase the fluorescent signal. Similarly, the effect of the agonist NECA binding to the A₂ₐR-SMALP on the Trp fluorescence signal was studied by titration of increasing concentrations of the ligand (Supplementary Figure 8.26). NECA progressively decreased the Trp signal with a greater decrease above 10 μM, reducing it to 60%. Hence, the addition of the agonist to the A₂ₐR-SMALP preparation induced an opposite effect on the emission of the Trp fluorescence compared to the addition of the antagonist ZM241385. Conversely, NECA addition to the Trp control did not decrease the fluorescent signal (Figure 4.5B).
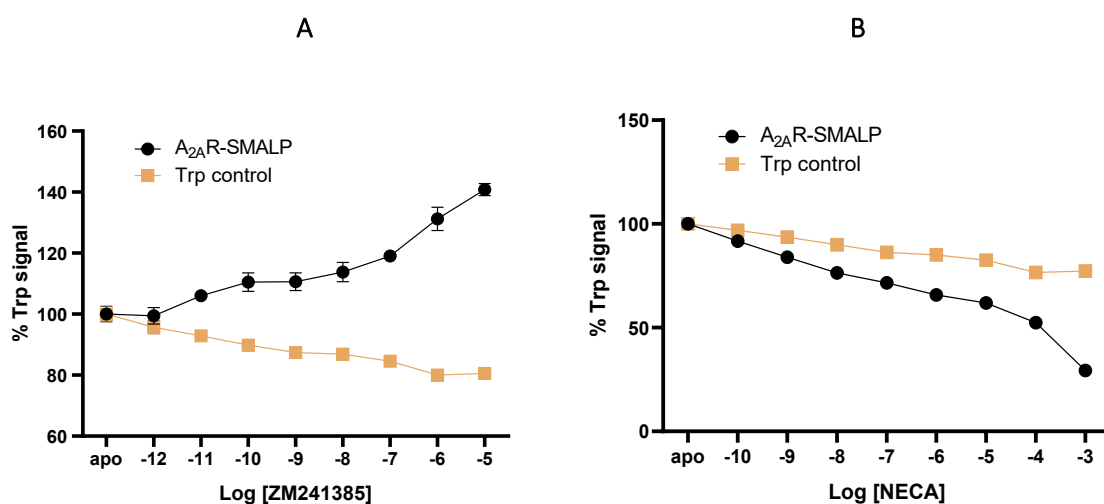
*Figure 4.5. Ligand-induced changes in overall A$_{2A}$R-SMALP fluorescence. The fluorescence emission of apo A$_{2A}$R-SMALP and Trp control after the addition of increasing concentrations of the (**A**) antagonist ZM241385 and (**B**) agonist NECA by titration were measured between 290 and 500 nm after excitation at 280 nm. Results are presented as percentage Trp signal of dose-dependent effect of ligand binding on the overall fluorescence, considering apo A$_{2A}$R-SMALP and apo Trp control to be 100% and normalized by the dilution effect. Data are presented as the mean of all replicates (n=3) ± SD.*

To assess whether the A$_{2A}$R-SMALP was able to undergo conformational changes upon ligand binding from the active to the inactive conformation, 10 µM NECA was added to the A$_{2A}$R-SMALP preparation, and increasing concentrations of the antagonist ZM241385 were added by titration (Figure 4.6A). An initial 3% increase in Trp signal was observed with NECA addition, and ZM241385 caused a biphasic increase in the signal, with a greater increase above 100 nM, provoking a final 44% increase. Thus, a similar increase in the Trp fluorescence signal was observed when the antagonist was bound to the A$_{2A}$R-SMALP in the absence or presence of NECA at saturating concentrations.

To determine whether the A$_{2A}$R-SMALP was able to undergo conformational changes upon ligand binding from the inactive to the active conformation, 1 µM ZM241385 was added to the A$_{2A}$R-SMALP preparation and increasing concentrations of the agonist NECA were added by titration (Figure 4.6B). Antagonist binding induced a 20% increase in fluorescence, and although NECA slightly increased Trp fluorescence, the signal decreased at 10 µM NECA, with a greater decrease at 1 mM NECA. This resulted in an 85% decrease in the signal. Thus, 1 mM NECA caused a 15% decrease in Trp fluorescence compared to apo A$_{2A}$R-SMALP. This was consistent with the results obtained when the agonist was added to the protein preparation in the absence of the antagonist.

A

A$_{2A}$R + NECA 10 µM + ZM titration

B

A$_{2A}$R + ZM 1 µM + NECA titration
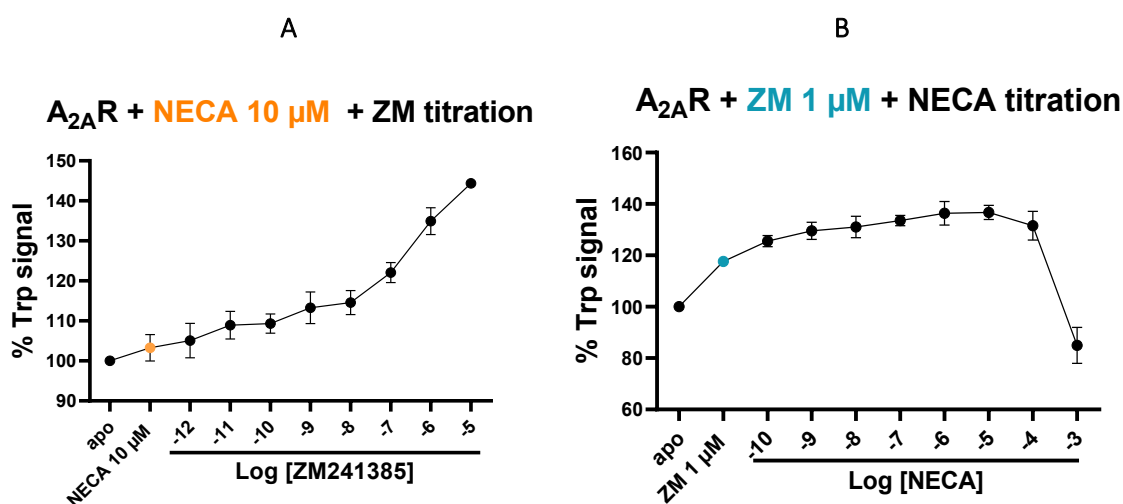
Figure 4.6. Conformational transition of A$_{2A}$R-SMALP upon agonist and antagonist binding. *The fluorescence emission of apo A$_{2A}$R-SMALP after the addition of (**A**) NECA at 10 µM and increasing concentrations of the ZM241385, and (**B**) ZM241385 at 1 µM and increasing concentrations of the NECA by titration were measured between 290 and 500 nm after excitation at 280 nm. The results are presented as percentage of Trp signal of dose-dependent effect of NECA and ZM241385 binding on overall fluorescence. The apo A$_{2A}$R-SMALP was considered to be 100%, and the data were normalized to the dilution effect. Data are presented as the mean of all replicates (n=3) ± SD.*

The effect of agonist and antagonist binding on the conformational changes of the A$_{2A}$R was studied for the protein solubilized with detergent DDM. A Trp control was prepared in DDM buffer and included in the experiment. The effect of diluting the sample on the intensity of the Trp signal was assessed by titration of the protein sample with 2 µL of DDM buffer 8 times. Sample dilution decreased the Trp signal by an average of 4% per step, and a total decrease in the Trp signal of 30% after 8 dilution steps (Supplementary Figure 8.29). These results were used to normalise the Trp fluorescence signal after the addition of increasing ligand concentrations by titration.

The effect of adding ZM241385 to the A$_{2A}$R-DDM and Trp control on the Trp fluorescence signal was studied by ligand titration. ZM241385 binding to the A$_{2A}$R-DDM caused an initial decrease in the signal, and a noteworthy increase and a red shift at 10 µM (Figure 4.7A). Similarly, ligand addition from 1 pM to 100 nM decreased the fluorescent signal of the Trp control, whereas ZM241385 at 10 µM caused an increase in fluorescence emission, although a red shift did not occur in this case (Figure 4.7B).

A

B
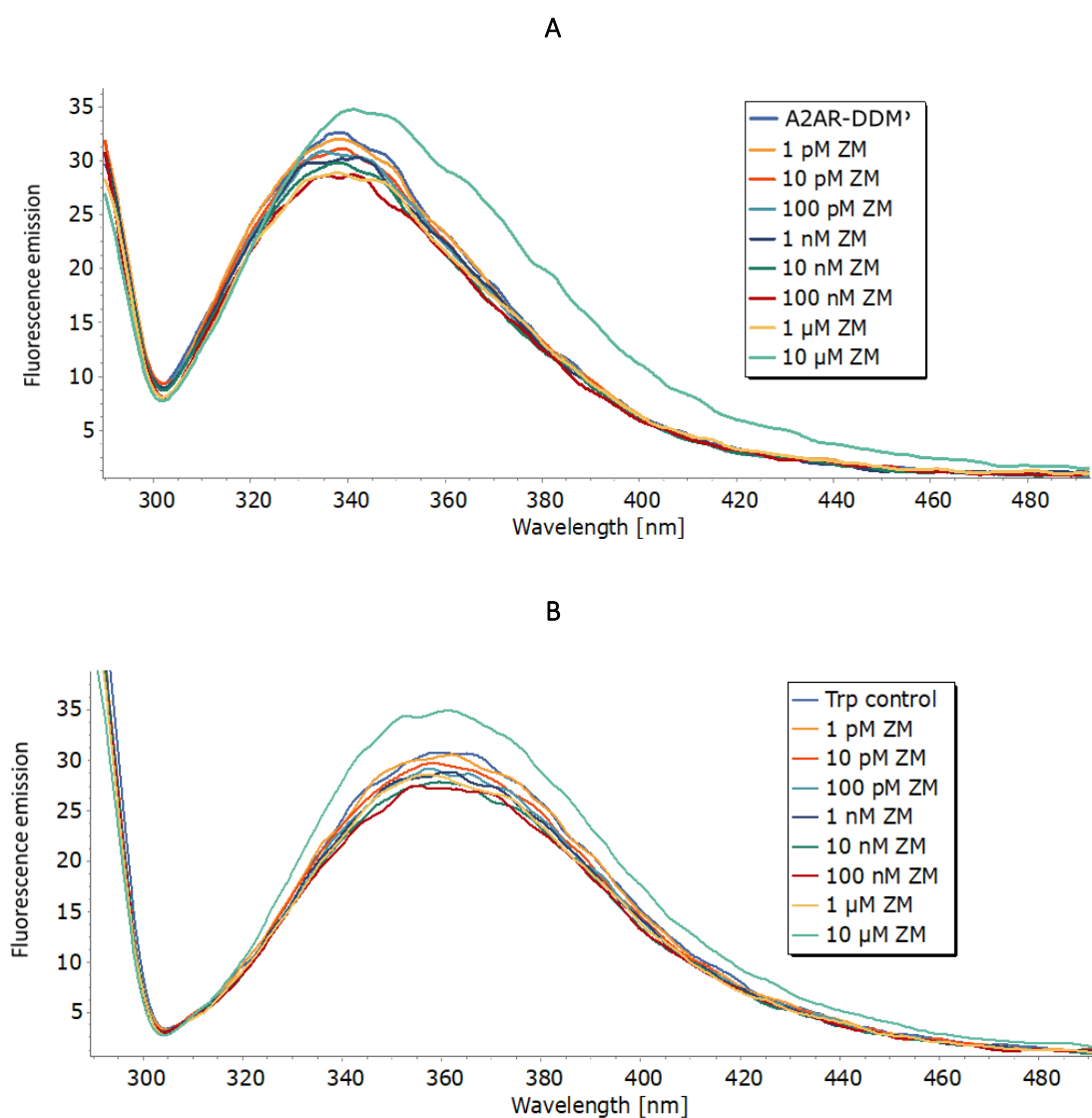
*Figure 4.7. ZM241385-induced changes in the overall fluorescence of $A_{2A}R$-DDM and Trp control. The fluorescence emission of apo $A_{2A}R$-DDM and Trp control after the addition of increasing concentrations of ZM241385 by titration was measured between 290 and 500 nm after excitation at 280 nm. The results are presented as (**A**) raw data for the $A_{2A}R$-DDM, (**B**) raw data for the Trp control (n=1).*

Calculating the percentage of Trp signal corroborated that $A_{2A}R$-DDM and Trp control in DDM buffer had similar fluorescence emission patterns caused by ZM241385 titration (Figure 4.8A), and did not show the same progressive increase in the fluorescence emission observed for the $A_{2A}R$-SMALP. The effect of NECA addition to the $A_{2A}R$-DDM and Trp control fluorescence was studied by ligand titration (Supplementary Figure 8.29). NECA caused a progressive decrease in fluorescence intensity in both the $A_{2A}R$-DDM and Trp control in DDM buffer (Figure 4.8B). In contrast to the results obtained for $A_{2A}R$-SMALP, NECA binding did not notably decrease the Trp signal compared to the Trp control.
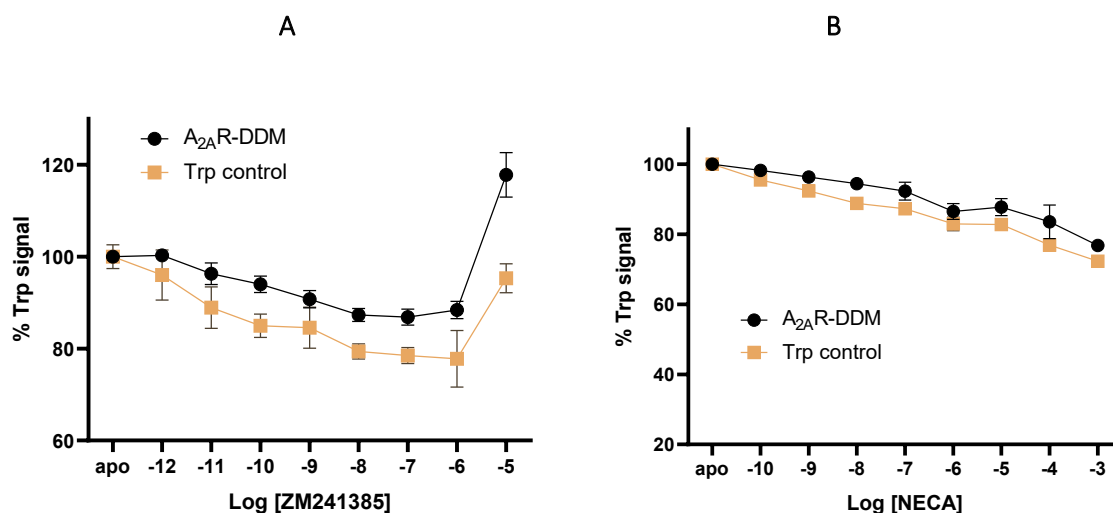
Figure 4.8. Ligand-induced changes in the overall fluorescence of A₂AR-DDM and Trp control. *The fluorescence emission of apo A₂AR-DDM and Trp control after the addition of increasing concentrations of (**A**) ZM241385 and (**B**) NECA by titration was measured between 290 and 500 nm after excitation at 280 nm. The results are presented percentage Trp signal of the dose-dependent effect of ligand binding on the overall fluorescence. Apo A₂AR-DDM and apo Trp control were considered to be 100%. The data were normalized to the dilution effect and presented as the mean of all replicates (n=3) ± SD.*

4.4.2   The effect of acrolein and AAPH treatments on A₂AR on tryptophan fluorescence upon ligand binding

After validating the method for assessing Trp fluorescence in the A₂AR-SMALP by studying receptor conformational changes upon ligand binding, the effect of the oxidative treatments on the folding status and the capability of the A₂AR to undergo conformational changes was investigated. To induce oxidtion, the A₂AR-SMALP was treated with AAPH and acrolein, and the Trp fluorescence was measured upon antagonist and agonist binding.

The A₂AR-SMALP was treated with different concentrations of acrolein and titrated with increasing concentrations of ZM241385 or NECA. An increase in the percentage of Trp signal was obtained after titrating the untreated A₂AR-SMALP with the antagonist, and a similar increase was observed for the acrolein-treated protein (Figure 4.9A). No significant differences were observed between the untreated A₂AR-SMALP and treated protein at different acrolein concentrations. NECA caused a decrease in Trp fluorescence at concentrations above 10 µM in the untreated and acrolein-treated samples, with similar patterns (Figure 4.9B). No significant differences between the untreated and treated A₂AR-SMALP with different acrolein concentrations were detected.
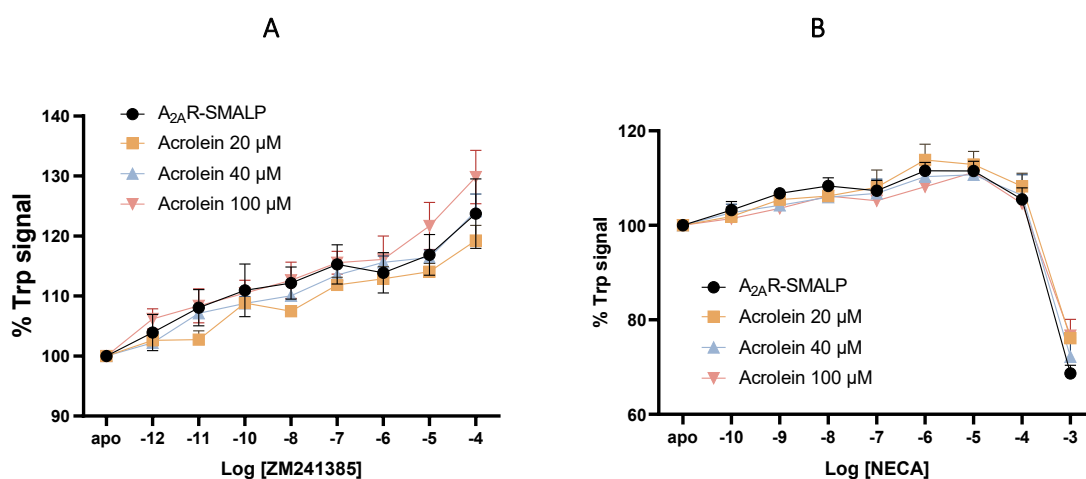
Figure 4.9. ZM241385- and NECA-induced changes in the overall fluorescence of the $A_{2A}R$-SMALP treated with acrolein. *The fluorescence emission of the untreated and treated $A_{2A}R$-SMALP with increasing concentrations of acrolein, was measured between 290 and 500 nm after excitation at 280 nm before (apo) and after the addition of increasing concentrations of (**A**) the antagonist ZM241385 and (**B**) the agonist NECA by titration. The results are presented as the percentage of Trp signal of the dose-dependent effect of ZM241385 and NECA binding on overall fluorescence. The apo $A_{2A}R$-SMALP was considered 100% of the signal. The data were normalized to the dilution effect and presented as the mean of all replicates (n=3) ± SD. Statistical differences were investigated by One-way ANOVA followed by Tukey's multiple comparison test, considering p-value<0.05 significant.*

The effect of lipid oxidation on the conformational changes of the $A_{2A}R$ was studied by treating the $A_{2A}R$-SMALP with AAPH at different concentrations, and measuring the Trp fluorescence upon antagonist and agonist titration. An increase in the percentage of Trp signal was obtained after titrating the untreated $A_{2A}R$-SMALP with the antagonist, and a similar increase in the fluorescence was observed for the protein treated with AAPH at different concentrations (Figure 4.10A). No significant differences were observed between the non-treated and treated $A_{2A}R$-SMALP with AAPH at different concentrations. On the other hand, the $A_{2A}R$-SMALP was titrated with the agonist NECA, which caused a decrease at concentrations above 10 µM. A similar Trp signal profile was observed when the AAPH-treated $A_{2A}R$-SMALP was titrated with NECA. Hence, no significant differences between the untreated and the treated $A_{2A}R$-SMALP with increasing concentrations of APPH were detected.
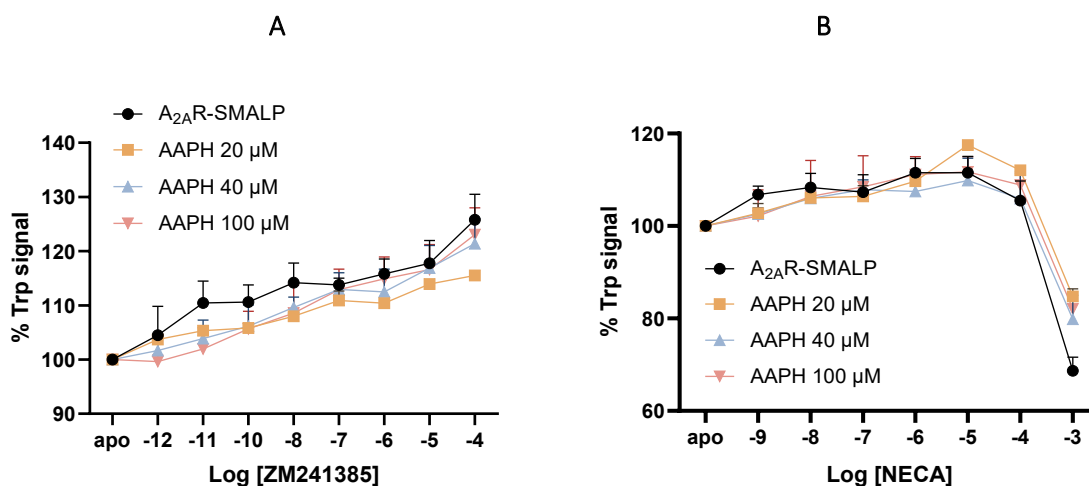
Figure 4.10. ZM241385- and NECA-induced changes in the overall fluorescence of the A₂AR-SMALP treated with AAPH. *The fluorescence emission of the untreated and treated A₂AR-SMALP with increasing concentrations of AAPH was measured between 290 and 500 nm after excitation at 280 nm before (apo) and after titration with increasing concentrations of (A) the antagonist ZM241385 and (B) the agonist NECA. The results are presented as the percentage of Trp signal of the dose-dependent effect of ZM241385 and NECA binding on overall fluorescence. The apo A₂AR-SMALP was considered as 100% of the signal. The data were normalized to the dilution effect and presented as the mean of all replicates (n=3) ± SD. Statistical differences were investigated by One-way ANOVA followed by Tukey's multiple comparison test, considering p-value<0.05 significant.*

4.4.3   The effect of ligand binding and lipid oxidation by acrolein and AAPH on the A₂AR thermal unfolding

After observing that the conformational changes of the A₂AR remained unaffected by oxidation under the experimental conditions, the goal shifted to studying whether the thermostability of the receptor was affected by oxidation. This investigation aimed to elucidate how oxidation could either disrupt or maintain the stability of the A₂AR.

The effect oxidative treatments with acrolein or APPH on the thermal stability of the A₂AR was studied by measuring the fluorescence of CPM. CPM is a high-affinity probe that binds to cysteine residues. Upon interacting with reactive cysteines, the CPM dye transitions from a non-fluorescent to a fluorescent state, allowing easy detection of protein unfolding.

SMA and DDM buffers in the presence of CPM and absence of A₂AR did not show intrinsic fluorescence as the temperature increased (Supplementary Figure 8.30). Similarly, ZM241385, NECA, acrolein, AAPH, or encapsulated lipids in SMALPs did not show intrinsic fluorescence in the presence of CPM and absence of A₂AR. These measurements were conducted as negative controls and ensured that fluorescence detected during the assay originated specifically from CPM binding to the A₂AR.

In order to determine the optimal protein concentration to conduct the assay with the maximum sensitivity, the fluorescence caused by CPM binding to the $A_{2A}R$-SMALP at different concentrations was measured and compared to the fluorescence of the SMA buffer containing the CPM dye (Figure 4.11). An increase in fluorescence was observed as the temperature increased from ~50°C when the $A_{2A}R$-SMALP was at 100 and 150 μg/mL. This signified the initiation of the unfolding process of the $A_{2A}R$-SMALP. Instead, an increase in the fluorescence was detected at ~60°C when the $A_{2A}R$-SMALP was at 50 μg/mL, and this could not be observed for lower protein concentrations, compared to the fluorescence of the SMA buffer. This suggested that the protein concentration was too low to detect changes in fluorescence. In addition, there was a dose-dependent effect from 50 μg/mL up on the fluorescence intensity. The optimal protein concentration was determined to be 150 μg/mL since its fluorescence from 20 to 50°C was comparable to the fluorescence of the buffer, whereas the samples prepared at lower concentrations exhibited weaker fluorescence than the buffer, which resulted in negative values when the first derivative was calculated (Haffke *et al.*, 2016). Thus, the $A_{2A}R$ was prepared at a concentration of 150 μg/mL protein for subsequent experiments.
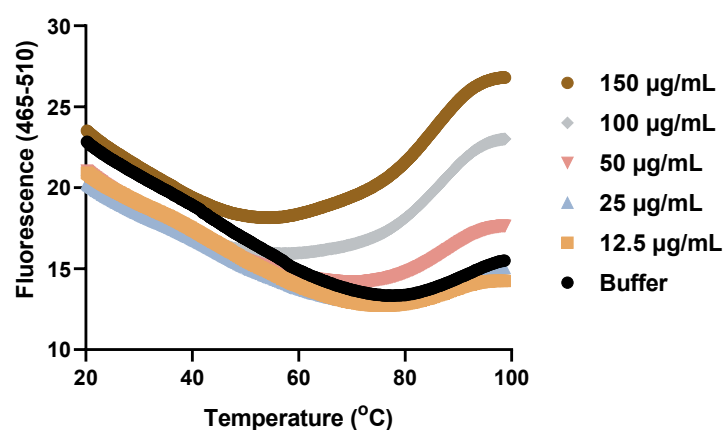
Figure 4.11. Thermal unfolding of the $A_{2A}R$-SMALP at different concentrations monitored by CPM fluorescence. Fluorescence caused by CPM binding to the $A_{2A}R$-SMALP at different concentrations was measured by increasing the temperature from 20 to 100°C to determine the optimal protein concentration for the assay.

The effect of ligand binding on the thermal stability of the $A_{2A}R$ was tested as a methodological control, as ligand binding is expected to stabilise the receptor. The fluorescence of the apo $A_{2A}R$-SMALP in the presence of the vehicle DMSO, $A_{2A}R$-SMALP bound to the ZM241385, and receptor bound to NECA was measured. The apo- and ligand-bound $A_{2A}R$-SMALP showed an increase in fluorescence when the temperature increased from 35 to 100°C, compared to SMA buffer, and the three protein-containing samples exhibited a similar increase pattern as the temperature ramped (Figure 4.12A). To compare

I. Company Marin, PhD Thesis, Aston University 2024

the thermal unfolding profile of the apo- and ligand-bound A$_{2A}$R-SMALP, and to determine their melting temperatures (Tm), the data were normalized by subtracting the fluorescence of the blank (SMA buffer with CPM) from the fluorescence of the protein-containing samples (Figure 4.12B). The results indicated that unfolding of the protein started at ~35°C and finished at ~60°C. This indicated that the A$_{2A}$R-SMALP was completely unfolded at this temperature. An analogous profile for the increase in fluorescence was obtained for the three protein samples. To visualise changes in the fluorescence caused by protein unfolding with increasing the temperature, the first derivative of the blank-subtracted results was calculated and plotted against temperature (Haffke *et al.*, 2016) (Figure 4.12C). To calculate the sample Tm, a Gaussian nonlinear regression was performed on the first derivative results (Figure 4.12D). A progressive increase in the first derivative from 30 to 60°C was observed for the apo- and ligand-bound A$_{2A}$R-SMALP, reaching a maximum point at 45 and 46°C, respectively. Therefore, no differences were detected in protein thermal unfolding caused by ligand binding using this methodology.
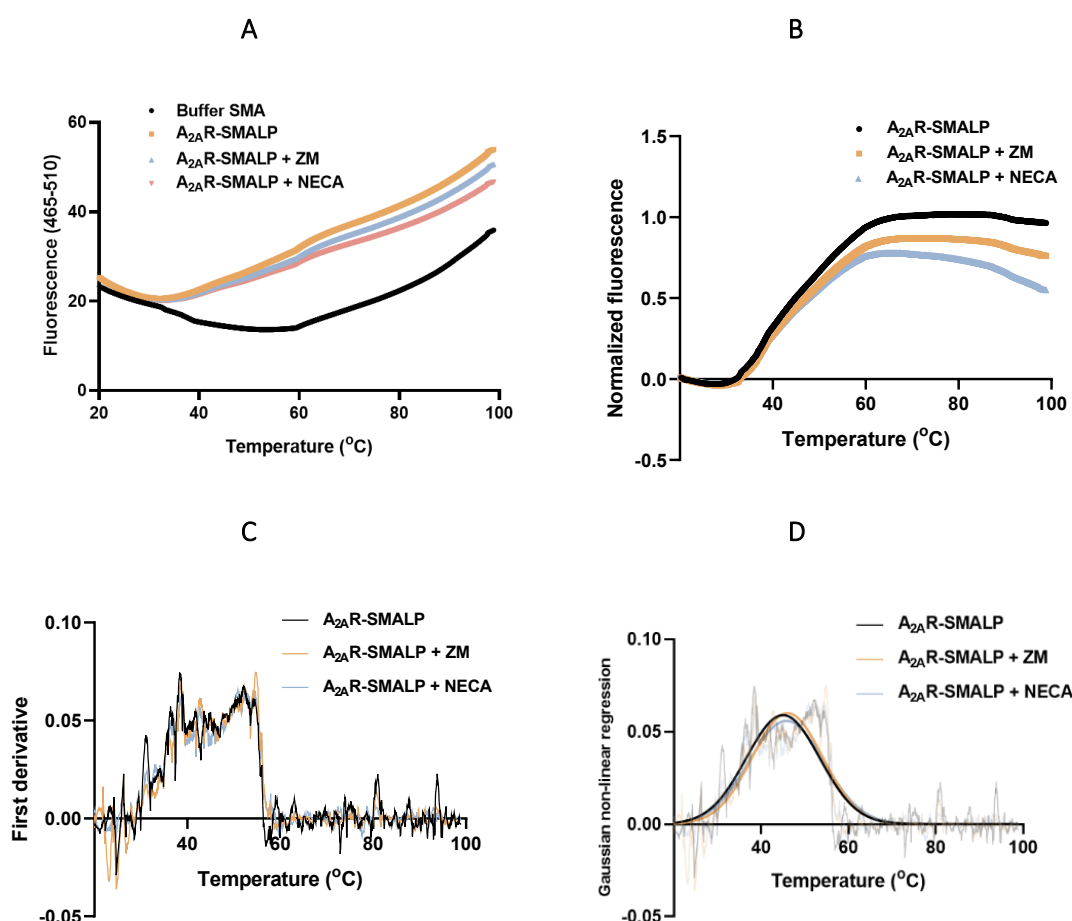
Figure 4.12. Impact of ligand binding on thermal unfolding of the A$_{2A}$R-SMALP monitored by CPM fluorescence. *(**A**) Fluorescence caused by CPM binding to apo- (with the vehicle DMSO), ZM241385-bound, and NECA-bound A$_{2A}$R-SMALP, and the fluorescence of the SMA buffer was measured as the temperature increased from 20 to 100°C. (**B**) Fluorescence of the SMA buffer (blank) was subtracted*

I. Company Marin, PhD Thesis, Aston University 2024

*from the fluorescence of the apo-, ZM241385-bound, and NECA-bound A$_{2A}$R-SMALP. (**C**) The first derivative of the blank-subtracted fluorescence data of apo-, ZM241385-bound, and NECA-bound A$_{2A}$R-SMALP were calculated and plotted against temperature. (**D**) Gaussian nonlinear regression was performed on the first-derivative data to calculate the Tm.*

The effect of ligand binding on the thermostability of the A$_{2A}$R-DDM was also tested. Fluorescence caused by CPM binding to the apo-, ZM241385-, and NECA-bound A$_{2A}$R-DDM was compared to the fluorescence of the DDM buffer (Figure 4.13A). Apo- and ligand-bound A$_{2A}$R-DDM had higher fluorescence than the DDM buffer across the range of different temperatures, and the three protein-containing samples showed a comparable fluorescence profile, with a subtle change at ~60°C. To compare the effects of ligand binding on A$_{2A}$R-DDM thermal stability, the data were normalized (Figure 4.13B). Subsequently, the first derivative was calculated, and a Lorentzian nonlinear regression was performed on the first-derivative data to calculate the Tm for optimal curve fitting (Figure 4.13C). The results displayed similar protein unfolding patterns for the apo-, ZM241385-, and NECA-bound A$_{2A}$R-DDM, as the three samples had a change in the fluorescence at approximately 60°C. In this case, a single peak was obtained when the first derivative was calculated, in contrast to the unfolding profile obtained for apo- and ligand-bound A$_{2A}$R-SMALP, which showed a progressive increase in fluorescence (Figure 4.12). Nonlinear regression data confirmed that the Tm of apo- and ligand-bound A$_{2A}$R-DDM was 62°C, indicating protein unfolding at this temperature.

A

B

I. Company Marin, PhD Thesis, Aston University 2024
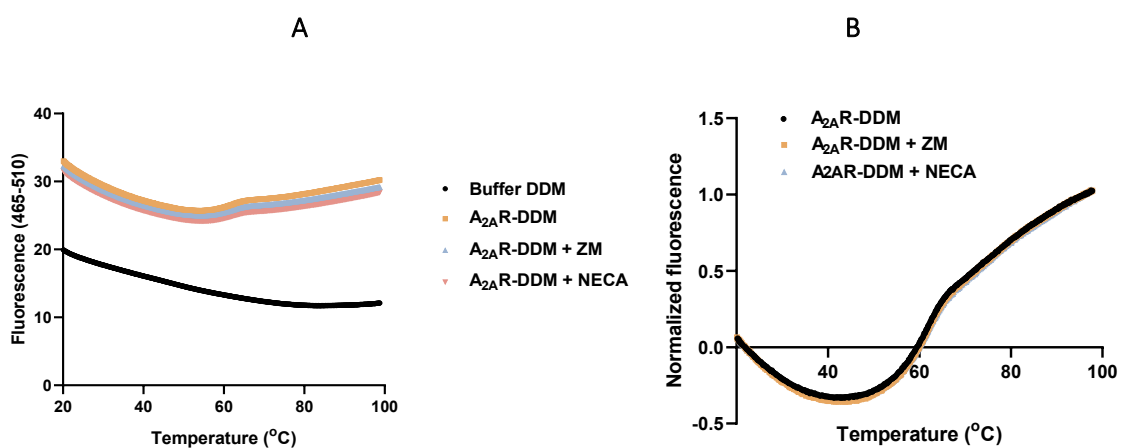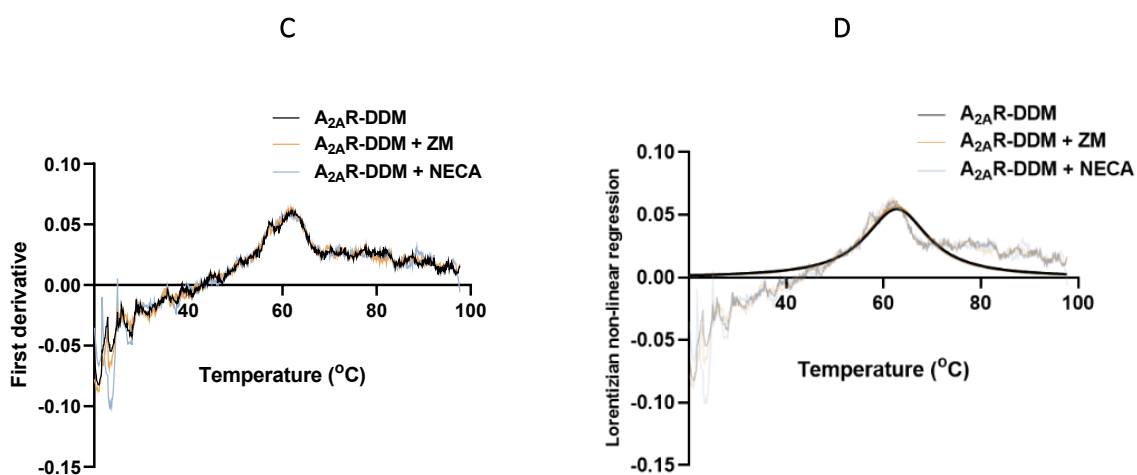
Figure 4.13. Impact of ligand binding on thermal unfolding of the A$_{2A}$R-DDM monitored by CPM fluorescence. *(A) Fluorescence caused by CPM binding to apo- (with the vehicle DMSO), ZM241385-bound, and NECA-bound A$_{2A}$R-DDM, and the fluorescence of the DDM buffer was measured as the temperature increased from 20 to 100°C. (B) The DDM buffer (blank) fluorescence was subtracted from the fluorescence of apo-, ZM241385-bound, and NECA-bound A$_{2A}$R-DDM. (C) The first derivatives of the blank-subtracted fluorescence data for the apo-, ZM241385-bound, and NECA-bound A$_{2A}$R-DDM were calculated and plotted against temperature. (D) Lorentzian nonlinear regression was performed on the first-derivative data to calculate sample Tm.*

Once it was determined that the thermal unfolding of the A$_{2A}$R-SMALP and A$_{2A}$R-DDM could be characterised using this methodology, the effect of treating the receptor with acrolein (ACR) and AAPH on its thermostability was tested. The fluorescence caused by CPM binding to ACR- and AAPH-treated A$_{2A}$R was compared to the fluorescence of untreated A$_{2A}$R. The results for A$_{2A}$R-SMALP showed that the treated and untreated samples exhibited comparable fluorescence as the temperature increased (Figure 4.14A). As expected, untreated A$_{2A}$R-SMALP and A$_{2A}$R-SMALP treated with ACR or AAPH showed similar patterns when the first derivative was calculated, all of which showed a progressive increase from 40 to 60°C (Figure 4.14B). Nonlinear regression data showed a maximum peak at 54°C, indicating the unfolding of the protein in this temperature (Figure 4.14C).

I. Company Marin, PhD Thesis, Aston University 2024
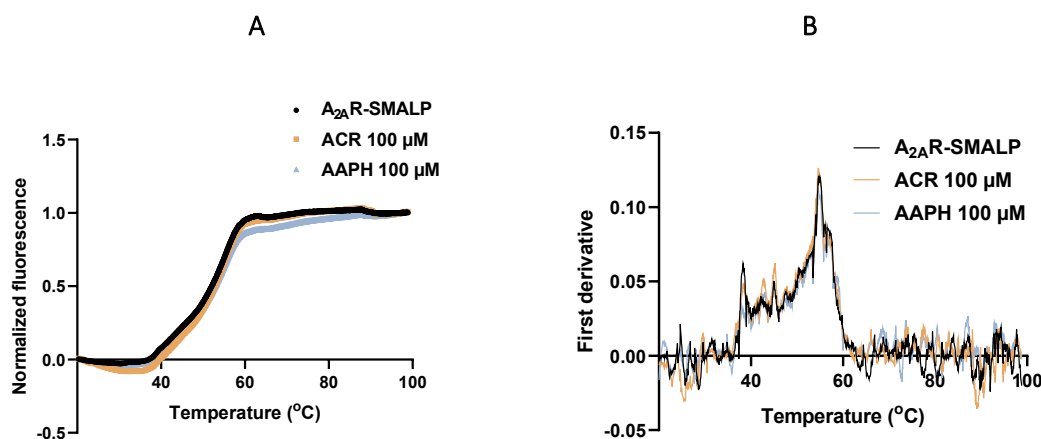
C
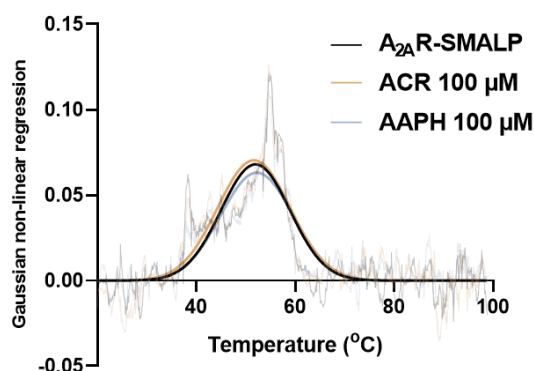
Figure 4.14. Impact of oxidative treatment with acrolein (ACR) and AAPH at 100µM on the thermal unfolding of the A$_{2A}$R-SMALP monitored by CPM fluorescence. (A) Blank-subtracted fluorescence caused by CPM binding to untreated, ACR-, and AAPH-treated A$_{2A}$R-SMALP with temperatures increasing from 20 to 100°C. (B) The first derivative of the blank-subtracted fluorescence data of the untreated, ACR-, and AAPH-treated A$_{2A}$R-SMALP was calculated and plotted against temperature. (C) Gaussian nonlinear regression was performed on the first-derivative data to calculate the Tm.

Similarly, untreated and treated A$_{2A}$R-DDM showed comparable fluorescence patterns as the temperature increased, all of which exhibited a change in fluorescence at ~60°C (Figure 4.15A). The three samples showed a single broad peak at ~60°C when the first derivative was calculated (Figure 4.15B), and nonlinear regression results confirmed that the three sample preparations had a maximum peak at 62°C, indicating that the treated and non-treated A$_{2A}$R-DDM had similar Tm (Figure 4.15C).

A   B

I. Company Marin, PhD Thesis, Aston University 2024

C
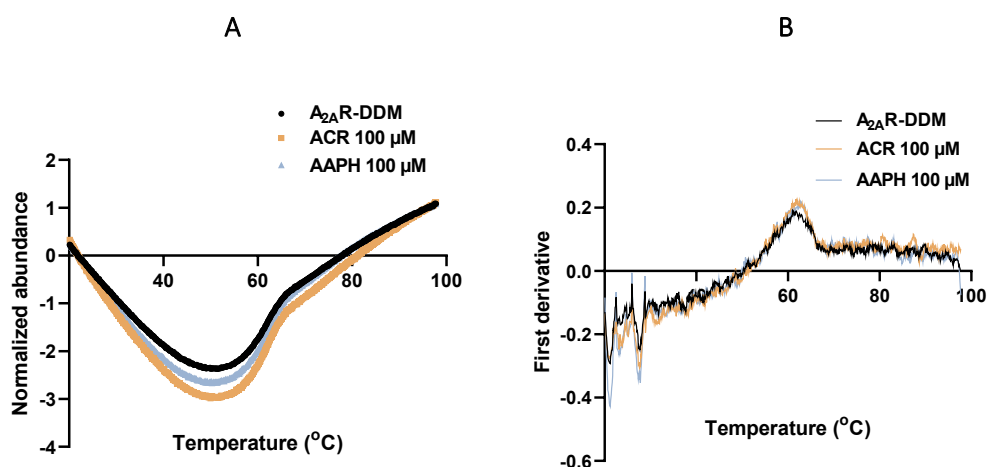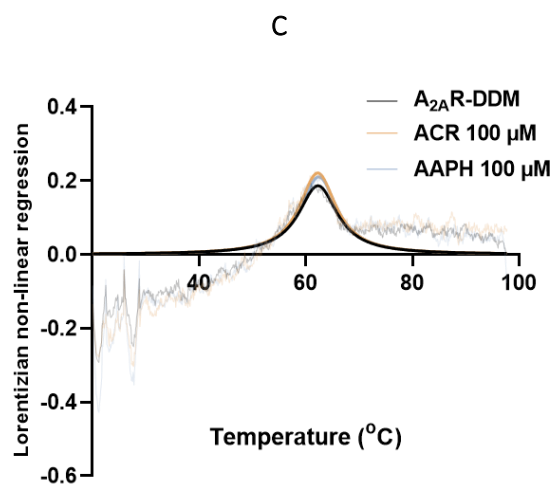
Figure 4.15. Impact of oxidative treatment with acrolein (ACR) and AAPH at 100µM on the thermal unfolding of the $A_{2A}R$-DDM monitored by CPM fluorescence. (A) Blank-subtracted fluorescence caused by CPM binding to untreated, ACR-, and AAPH-treated $A_{2A}R$-DDM with increasing temperature 20 to 100ºC. (B) The first derivative of the blank-subtracted fluorescence results for the untreated, ACR-, and AAPH-treated $A_{2A}R$-DDM was calculated and plotted against temperature. (C) Lorentzian nonlinear regression was performed on the first-derivative data to calculate the Tm.

4.4.4 The effect of acrolein and AAPH on the pharmacology of the P. pastoris membrane-bound $A_{2A}R$

To study the effect of the oxidative treatments on the membrane-bound $A_{2A}R$, *P. pastoris* membranes were treated with acrolein or AAPH, and $A_{2A}R$ pharmacology was determined by displacement and saturation radioligand binding assays. The first approach was to characterize the ligand binding capability of the $A_{2A}R$. Displacement binding assays of the radioligand [3H]ZM241385 with increasing concentrations of the unlabelled ZM241385 were performed. The results showed ligand competition at high concentrations of the $A_{2A}R$-bound radioligand with a $LogIC_{50}$ value of -6.36 and, thus, higher than the expected and previously published $LogIC_{50}$ of -9 (Fraser, 2006) (Figure 4.16A).

In case the higher values were due to adenosine released from the *P. pastoris* membranes and that could be competing with ZM241385, adenosine deaminase was added to the membrane samples to degrade adenosine (Figure 4.16B), and the effect of acrolein and AAPH on the binding capability of the $A_{2A}R$ were tested. The results for the untreated membranes were comparable to the previous results in the absence of adenosine deaminase, with $LogIC_{50}$ of -5.663. This suggested that the competition at high concentrations of the radiolabelled ligand was not caused by the presence of adenosine released from the *P. pastoris* membranes and could be explained by the degradation and expiry of the unlabelled ZM241385. The results for treated samples showed lower binding of the [3H]ZM241385 on the $A_{2A}R$ after ACR and AAPH treatment, as the cpm signal was lower compared to the untreated membranes. Nonetheless, both membrane samples subjected to the treatments showed earlier displacement of the

radioligand, with $LogIC_{50}$ of -8.568 and -8.473, respectively. These were comparable to the published $LogIC_{50}$.

Consequently, a new unlabelled ZM241385 was used to perform the displacement binding assay on the untreated and treated $A_{2A}R$-membranes (Figure 4.16C). Membranes treated with ACR showed a prototypical radioligand displacement curve with a $LogIC_{50}$ of -9.17, similar to the expected published $LogIC_{50}$. However, untreated membranes and membranes treated with AAPH had low [^{3}H]ZM241385 binding, which complicated the data analysis.
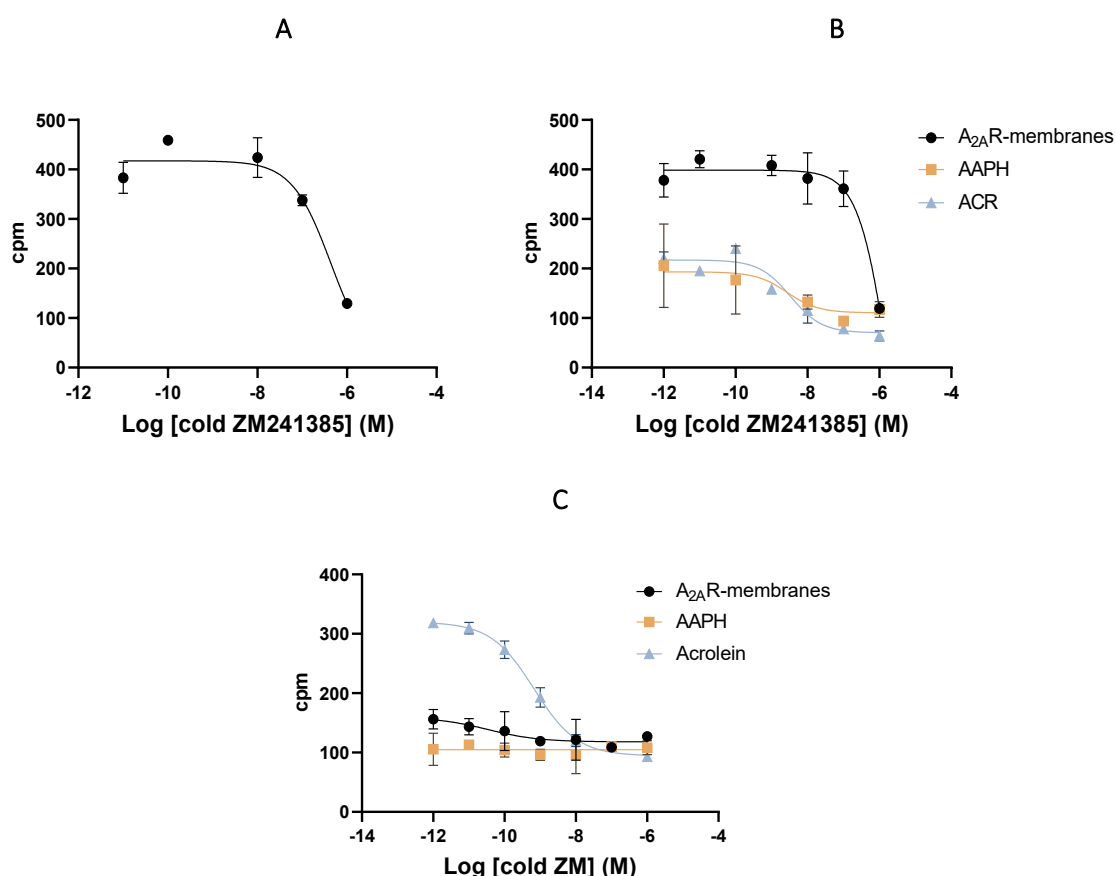
Figure 4.16. Displacement radioligand binding assays on the untreated and acrolein- or AAPH-treated P. pastoris membrane-bound $A_{2A}R$ using [^{3}H]ZM241385. Displacement binding assays on the untreated, or treated membrane-bound $A_{2A}R$ with acrolein or AAPH were performed using 1nM [^{3}H]ZM241385 and increasing concentrations of the (A) old unlabelled antagonist ZM241385 in the absence of adenosine deaminase, (B) old unlabelled ZM241385 in the presence of adenosine deaminase at 0.5U/mL, and (C) new unlabelled ZM241385 in the presence of adenosine deaminase at 0.5U/mL. The results are presented as the mean of counts per minute (cpm) of the replicates (n=4) ± SD.

Due to the inconsistency of the results obtained from the displacement binding assays, saturation radioligand binding assays were performed. Untreated and treated membranes were incubated with increasing concentrations of [^{3}H]ZM241385, and to determine the non-specific binding, the assay was

conducted in the presence of 1 µM unlabelled ZM241385 (Figure 4.17A). Increasing concentrations of the radioligand increased the cpm signal, which suggested radioligand binding to the A_{2A}R-membrane. The radioligand also increased the cpm signal in a dose-dependent manner of the three samples in the presence of unlabelled ZM241385, which demonstrated the non-specific radioligand binding. The unlabelled ligand caused a decrease in the cpm signal due to its binding to the A_{2A}R. To determine the [^{3}H]ZM241385 specific binding on the A_{2A}R, the non-specific binding was subtracted from the total binding (Figure 4.17B). The data showed that no significant differences were detected among the untreated and treated membranes.
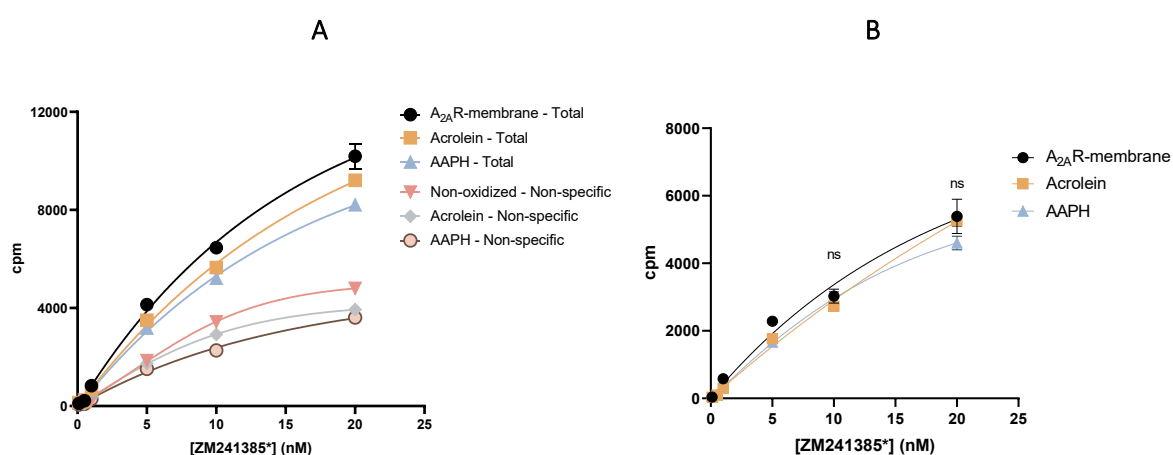
Figure 4.17. Saturation radioligand binding assays on the untreated and acrolein- or AAPH-treated P. pastoris membrane-bound A_{2A}R using [^{3}H]ZM241385. Saturation binding assays on the untreated, or treated membrane-bound A_{2A}R with AAPH or acrolein, were performed using increasing concentrations of the radiolabelled [^{3}H]ZM241385. (A) Total [^{3}H]ZM241385 binding to the membrane-bound A_{2A}R and radioligand non-specific binding was determined in the presence of unlabelled ZM241385 at 1 µM. (B) Specific [^{3}H]ZM241385 binding was determined by subtracting the non-specific to total binding results. Data are presented as the mean of counts per minute (cpm) of the replicates (n=4) ± SD. Statistical differences were determined by One-way ANOVA followed by Tukey's multiple comparison test, considering p-value<0.05 significant.

4.5 DISCUSSION

The aim of this chapter was to address key questions regarding the conformational dynamics, folding state, stability, and ligand binding capability of the A_{2A}R. The first objective was to study the conformational changes of the A_{2A}R-SMALP and A_{2A}R-DDM by tryptophan fluorescence upon ligand binding, and to investigate whether these conformational changes were affected by the oxidative treatments. The second objective was to investigate the thermal unfolding profile of the A_{2A}R-SMALP and A_{2A}R-DDM by CPM binding, and to determine whether their thermostability was affected by oxidation. The third objective was to assess the binding capability of the membrane-bound A_{2A}R using radioligand binding assays and to determine whether this was affected by the oxidative treatments.

The key findings of this chapter were that Trp fluorescence, CPM fluorescence, and radioligand binding assays permitted the evaluation of the conformational changes, thermostability, and ligand binding capability of the $A_{2A}R$, respectively. Moreover, these methodologies served to observe that these parameters were not perturbed by the oxidative treatments, indicating that the receptor was folded and responded to ligand binding under the oxidative conditions.

The $A_{2A}R$ showed intrinsic fluorescence at 340 nm, originating from the six Trp residues in the construct. This allowed the investigation of conformational changes upon ligand binding using Trp fluorescence at low protein concentrations and small volumes of protein preparation. In contrast, the Trp control exhibited a fluorescence peak at 360 nm. ZM241385 binding to the $A_{2A}R$-SMALP caused an increase and red-shift in fluorescence, whereas NECA caused a decrease, compared to the Trp control. The same Trp fluorescence characteristics were observed when $A_{2A}R$-SMALP was initially saturated with NECA and titrated with ZM241385, and vice versa. An increase in Trp fluorescence of $A_{2A}R$-DDM and Trp control in DDM buffer was observed with 1 µM ZM241385, although a red shift was observed in the $A_{2A}R$-DDM, and no red shift was observed in the Trp control in DDM buffer. In both cases, a subtle decrease in the fluorescence was observed after titration with NECA. Finally, no significant differences were observed in the Trp fluorescence of acrolein- and AAPH-treated $A_{2A}R$-SMALP compared to that of the untreated controls, suggesting that the $A_{2A}R$ was able to undergo conformational changes upon ligand binding under oxidising conditions.

The fact that the $A_{2A}R$-SMALP showed a fluorescence peak at 340 nm, whereas the Trp control at 360 nm, suggests that Trp residues in the $A_{2A}R$ were surrounded by a more hydrophobic environment, according to Hellmann and Schneider (Hellmann and Schneider, 2019).

Comparable to the present study, Routledge *et al*. studied the conformational changes of the $A_{2A}R$-SMALP upon ligand binding using Trp fluorescence (Routledge *et al.*, 2020). Similar to the results obtained in this study, antagonist binding increased Trp fluorescence and caused Trp residues to move to a more polar environment, triggering conformational changes in the $A_{2A}R$-SMALP. However, the authors did not observe changes in Trp fluorescence upon NECA binding, whereas a decrease in Trp fluorescence was observed in the current study, in contrast to the effect of antagonist binding. This suggested that changes in Trp fluorescence were a consequence of conformational changes in the receptor upon ligand binding. Moreover, the authors reported that apo $A_{2A}R$-SMALP retained substantial characteristics of the active state, characterised by an open conformation of TM6 in a more polar environment (Routledge *et al.*, 2020). These results are comparable to those obtained in the present study, as the antagonist induced changes in the Trp fluorescence. This indicated that the receptor underwent conformational changes from the apo state to the inactive state. Additionally, the

agonist and antagonist caused opposite changes in the fluorescence emission, suggesting that the receptor could transit to both active and inactive conformations from its apo state within the SMALP.

On the other hand, O'Malley and colleagues investigated the conformational changes of the $A_{2A}R$ upon ligand binding by circular dichroism and measuring Trp fluorescence. Binding of agonist (N6-cyclohexyladenosine) and antagonist (theophylline) did not alter the secondary structure of the protein (O'Malley et al., 2010). Instead, it induced conformational changes in its tertiary structure. In contrast to the results obtained in this study, the $A_{2A}R$ had a maximum peak at 328 nm, suggesting a nonpolar environment surrounding these residues, and antagonist binding did not alter the Trp fluorescence. In contrast, agonist binding caused a blue shift to 326 nm. Similar results were observed for the GPCR BLT1 receptor (Baneres et al., 2003). In opposition to the results obtained in this study, a decrease in the fluorescence signal was observed upon agonist and antagonist binding, indicating that the ligands might bury the tryptophan residues of the receptor. Furthermore, the authors noted that Trp 246 in the solvent-exposed region of the receptor plays a critical role in ligand binding in the orthosteric pocket (O'Malley et al., 2010).

The fact that ZM241385 binding caused an increase in the fluorescence emission, whereas NECA binding caused a decrease could be explained by the existence of mixed populations of apo-encapsulated $A_{2A}R$-SMALP in different conformational states, which could be biased upon ligand binding through conformational changes. $A_{2A}R$ activation is a dynamic cooperative process in which key intermediates are frequently sampled, and apo $A_{2A}R$ can be found in different active and inactive states in the absence of a ligand (Ye et al., 2016). $A_{2A}R$ activation is dependent on the populations of functional states (Ye et al., 2016), and the addition of ligands alters the distribution of these conformational states (Prosser et al., 2017). Apo $A_{2A}R$ shows basal activity due to the presence of receptors in the active or intermediate active conformation, which can account for over 50% (Bertheleme et al., 2013). The present study confirmed the presence of active $A_{2A}R$ by observing the changes in Trp fluorescence upon exposure to an antagonist. These changes indicated the induction of an inactive conformation in the receptor, leading to a shift in the equilibrium distribution toward the inactive state. Moreover, the findings indicated that the $A_{2A}R$ was able to transition from the active to the inactive conformation and vice versa in the SMALP.

ZM241385 caused a red shift in the Trp fluorescence of the $A_{2A}R$, indicating that ligand binding modified the local environment of the residues, transitioning to a more excited state. However, a red shift was not observed in the Trp control, suggesting that the state of the Trp residues did not change. Some ligands can interact with Trp residues through hydrogen bonds and other interactions, which can lead to changes in fluorescence properties. In this case, DDM might facilitate the interaction of ZM241385

I. Company Marin, PhD Thesis, Aston University 2024

with the free Trp control in the sample, inducing an increase in the fluorescence intensity. This interaction and modification of the fluorescence properties did not occur in the absence of DDM and presence of SMA. Alternatively, the presence of DDM in the sample preparation together with the antagonist might influence the photophysics of Trp fluorescence, potentially leading to changes in signal intensity (Vivian and Callis, 2001; Akbar *et al.*, 2016; Sindrewicz *et al.*, 2019).

Oxidative treatments did not affect the agonist or antagonist titration profiles, suggesting that the $A_{2A}R$ was still able to undergo conformational changes upon ligand binding after oxidative treatment. This might indicate that protein lipoxidation caused by ACR adduct formation on the receptor, or lipid and protein oxidation caused by AAPH did not affect the secondary and tertiary structure of the protein, allowing it to be properly folded and active. Alternatively, the experimental conditions of the oxidative treatments might not have been sufficient to affect the $A_{2A}R$. Nevertheless, acrolein concentrations comparable to those used in this study, ranging from 20 to 100 µM, were sufficient to cause Protein Kinase A (PKA) lipoxidation, resulting in a significant reduction in protein activity (Sousa *et al.*, 2019b). Other studies have demonstrated Phosphatase and tensin homolog (PTEN) lipoxidation and inactivation with 10 µM acrolein, and thus lower treatment concentrations than those used in the present study (Covey *et al.*, 2010). Identical AAPH concentrations were used in the present study for comparison, considering that previous cell-based studies have substantiated the lipid peroxidation induced by these AAPH concentrations (Duan *et al.*, 2016; Parathodi Illam *et al.*, 2019). Considering that no effects on $A_{2A}R$ conformation were observed in this study, protein lipoxidation and lipid oxidation should be confirmed using alternative techniques, such as mass spectrometry (Maciel *et al.*, 2014; Sousa *et al.*, 2019).

Studying protein conformational changes using Trp fluorescence has some limitations. Trp fluorescence can be highly influenced by pH, ionic strength, buffer composition, and the presence of molecules other than the protein of interest in the sample, as observed in the present study for the $A_{2A}R$ and Trp control in DDM buffer.

Trp residues in the transmembrane core of the $A_{2A}R$, such as Trp129, might be buried in the protein structure. This makes their fluorescence less informative regarding conformational changes around their location as they are less accessible. Indeed, Routledge *et al.* suggested that Trp246 and Trp268 are the responsible residues for the increase in fluorescence emission upon ZM241385 binding (Routledge *et al.*, 2020). Additionally, Trp fluorescence may not be suitable for distinguishing between the different conformational states of the $A_{2A}R$, as it does not fully capture the complexity of its conformational changes (Royer, 2006; Moon and Fleming, 2011).

I. Company Marin, PhD Thesis, Aston University 2024

Trp fluorescence measurements are highly specific as the $A_{2A}R$ ligands are used. However, these can be biased by protein contaminants in the sample, such as mADH in the $A_{2A}R$-DDM preparation, which contribute to the overall fluorescence and attenuate signal changes after ligand binding.

Buffer characteristics, environmental perturbations, temperature, sample dilution, and bubbles, can lead to variations in fluorescence intensity, thereby influencing the assessment of conformational changes. Moreover, ligand binding can also influence the fluorescence properties of the protein under study, which may not directly correspond to protein conformational changes. On the other hand, quenching effects can lead to underestimation of conformational changes. Finally, variations in sample preparation, handling, and storage, as well as instrument sensitivity, settings, and calibration, can introduce bias in the fluorescence records (Ghisaidoobe and Chung, 2014; Talukder *et al.*, 2014).

After determining that the conformational changes in the $A_{2A}R$ were not affected by oxidation under the experimental conditions, the effect of oxidation on the thermostability of the receptor was tested by CPM binding. $A_{2A}R$-SMALP at 150 µg/mL was optimal for the assay, which was consistent with previous studies on the thermostability of the $A_{2A}R$ (Alexandrov *et al.*, 2008).

$A_{2A}R$-SMALP and $A_{2A}R$-DDM experienced unfolding with increasing temperatures, suggesting that the protein was in a folded state before undergoing the unfolding process. This aligns with the findings of the Trp fluorescence assays.

Agonist and antagonist binding did not affect the unfolding profile of the $A_{2A}R$-SMALP and $A_{2A}R$-DDM, which had Tm values of 45°C and 60°C, respectively. Different studies have demonstrated a lower Tm of ~30°C for the $A_{2A}R$-DDM than that detected in the present study (Haffke *et al.*, 2016; Nehmé *et al.*, 2017; Tippett *et al.*, 2020), suggesting lower protein stability. Lebon *et al.* showed that the Tm for the NECA-bound $A_{2A}R$ was 28.5^{o}C, whereas the Tm for the ZM241385-bound receptor was 32°C (Lebon *et al.*, 2011). O'Malley *et al.* detected lower $A_{2A}R$-DDM Tm values than those observed in the present study; however, these values were similar to those observed for $A_{2A}R$-SMALP (O'Malley *et al.*, 2010). In contrast, Haffke *et al.* showed that the ligand-bound $A_{2A}R$ had Tm values of 60°C, comparable to those observed in the present study (Haffke *et al.*, 2016).

In contrast to the results observed in the present study, Haffke *et al.* observed that ligand binding stabilized detergent-solubilized $A_{2A}R$ (Haffke *et al.*, 2016). Comparably, O'Malley and colleagues observed that agonist and antagonist binding increased $A_{2A}R$-DDM thermostability by ~5°C (O'Malley *et al.*, 2010), and Jun *et al.* observed that ZM241385 binding increased the thermostability of $A_{2A}R$-nanodisc and $A_{2A}R$-DDM (Jun Ma, 2017). Similarly, Alexandrov *et al.* observed that FAAH antagonist binding increased the thermal stability of the detergent-solubilized membrane protein (Alexandrov *et*

I. Company Marin, PhD Thesis, Aston University 2024

al., 2008). In addition to ligand binding, $A_{2A}R$ thermostability is increased by G-protein binding (Nehmé *et al.*, 2017). Nevertheless, the stabilizing effect of ligand binding may be compound-dependent. Park *et al.* observed that only caffeine and SCH442416 shifted the $A_{2A}R$-DDM stability to a higher Tm, whereas the other tested compounds did not affect its thermostability, comparable to the results obtained in this study (Park *et al.*, 2020). Similarly, Jaakola *et al.* reported an increase in the thermostability of the $A_{2A}R$ in the presence of specific antagonists, while they did not observe any changes upon agonist binding (Jaakola *et al.*, 2008). Comparable to the results observed in the present study, ligand binding did not modify APJ receptor thermostability (Alexandrov *et al.*, 2008).

Therefore, the stabilizing effect of ligand binding to GPCRs is controversial. The absence of changes in Tm values upon ligand binding can be explained by the principle of entropy, which states that spontaneous transformations in isolated systems proceed in the direction of increasing entropy. Considering that ligand binding stabilizes the orthosteric pocket of the receptor, a decrease in entropy in the protein region occurs, which can be compensated by an increase in entropy in other regions of the protein, including the transmembrane and cytosolic regions. This may be reflected in the CMP assay, in which no significant changes were observed in the thermostability of the protein by ligand binding (Dagan *et al.*, 2013; Bigman and Levy, 2020).

In contrast to the results observed in the present study, several studies demonstrated a higher stability of SMALP-encapsulated proteins than DDM-solubilized proteins (Dörr *et al.*, 2014; Gulati *et al.*, 2014; Rehan *et al.*, 2017; Pollock *et al.*, 2018). Jamshad *et al.* indicated that the $A_{2A}R$-SMALP had a marked increase in thermostability compared to $A_{2A}R$-DDM (Jamshad *et al.*, 2015). The results obtained for the $A_{2A}R$-SMALP were comparable to those observed in the present study using CPM fluorescence, whereas $A_{2A}R$-DDM showed a lower Tm. However, the authors observed that thermal denaturation of the $A_{2A}R$-SMALP was a two-state process, in contrast to the results observed in the present study.

In the present study, $A_{2A}R$-DDM followed a two-state unfolding process, with folded and denatured states, whereas $A_{2A}R$-SMALP unfolding was gradual. Alexandrov and colleagues observed that the GPCR APJ, followed a two-state unfolding model, which is comparable to the results obtained for the $A_{2A}R$-DDM in the present study (Alexandrov *et al.*, 2008). Similarly, O'Malley *et al.* observed a single transition between folded and unfolded states of the $A_{2A}R$-DDM (O'Malley *et al.*, 2010). This is a general observation for α-helical membrane proteins, in which the unfolding processes proceed with only limited changes in their secondary structure (Grinberg *et al.*, 2001). Hence, the unfolded state is typically achieved by the loss of tertiary structures, which displays an almost complete preservation of the α-helices (Vogel and Siebert, 2002). In contrast, Duy and Fitter suggested the loss of α-helical structures of the $A_{2A}R$ during the thermal unfolding process (Duy and Fitter, 2006). On the other hand,

I. Company Marin, PhD Thesis, Aston University 2024

Naranjo *et al*. observed a gradual transition of the $A_{2A}R$-DDM from the folded to the unfolded state as the temperature increased, so the data did not fit a single-transition unfolding model (Naranjo *et al.*, 2016). This is consistent with the results observed for the $A_{2A}R$-SMALP in the present study, but not for the $A_{2A}R$-DDM. Similarly, Hesketh *et al.* demonstrated that TRPM2-SMA showed a more gradual increase in the fluorescence signal as the temperature increased, compared to TRPM2-DDM. Comparable to the results obtained in the present study, the first derivative of TRPM2-SMA showed a higher area under the curve than that of TRPM2-DDM (Hesketh, 2020).

Hence, most published studies have observed that the $A_{2A}R$ and other membrane proteins follow a two-state unfolding model. However, in some studies, a progressive unfolding process was observed. SMALPs encapsulating the $A_{2A}R$ exert lateral pressure on the receptor, potentially hindering the unfolding process of the protein. As a result, the receptor may undergo a gradual unfolding process, leading to progressive dissociation of the transmembrane helices, which protrude from the SMALP gradually, thereby exposing the Cys residues to CPM. Instead, $A_{2A}R$-DDM is not subjected to such lateral pressure and unfolding hindrance, allowing a more natural unfolding process of the protein.

This phenomenon presumably influenced the Tm obtained for the $A_{2A}R$-SMALP, which was lower than that obtained for the $A_{2A}R$-DDM. This can be explained by the progressive thermal unfolding process of the $A_{2A}R$-SMALP, which modified the fluorescence curve shape. Nevertheless, these results indicated that the unfolding of the $A_{2A}R$-SMALP started at lower temperatures than that of the $A_{2A}R$-DDM. However, it is worth noting that the $A_{2A}R$-DDM preparation contained a higher percentage of the main contaminant, mADH, which contains six Cys residues. As a result, the presence of mADH in the sample preparation may influence in the overall fluorescence observed, thus contributing to the shifts in Tm.

Moreover, Tm was not affected by lipid oxidation or protein lipoxidation on the $A_{2A}R$-SMALP or $A_{2A}R$-DDM, although an early $A_{2A}R$ thermal unfolding and lower Tm were expected after oxidation. This was comparable to the results obtained by Trp fluorescence, which might indicate that the oxidative treatments did not destabilize the $A_{2A}R$-SMALP or $A_{2A}R$-DDM. Alternatively, this might suggest that the experimental conditions may not be sufficient to alter protein stability and adduct formation, and lipid oxidation should be confirmed using alternative techniques. An earlier oxidised $A_{2A}R$ thermal unfolding was expected, as thiol groups of cysteine residues are susceptible to oxidation, resulting in the formation of disulphide bonds when oxidised. This can be intramolecular when they occur within the same protein, or intermolecular when they occur between different proteins. The formation of disulphide bonds can alter the conformation and stability of proteins, leading to changes in their folding and structure. Eventually, this can result in protein denaturation and aggregation, leading to the disruption of the native protein structure and function. However, this might affect CPM binding, which

might challenge the interpretation of results, as alterations in the fluorescence signal could have been due to lower CPM binding (O'Malley *et al.*, 2010). Nevertheless, as various publications have suggested, intramolecular S-S bonds in the $A_{2A}R$ are important for protein stability, which are preserved under oxidative stress conditions (O'Malley *et al.*, 2010).

Moreover, the Tm values observed in different experiments on the $A_{2A}R$-SMALP were inconsistent. Instead, they were consistent for the $A_{2A}R$-DDM in both experiments. The encapsulation of the $A_{2A}R$ in SMALPs can influence the unfolding process of proteins, which may alter the fluorescence results. Moreover, these discrepancies might be explained by the stability of the sample preparation, storage period, and conditions, which might differ in every sample preparation prior to the CPM assay. This is because multiple sample preparations were required to perform the assay due to the low yield of purified protein obtained after SMA solubilization. Instead, DDM offers a higher protein solubilization efficiency, and multiple sample preparations can be performed simultaneously.

Studying $A_{2A}R$ unfolding by CPM binding has some limitations. Non-accessible cysteines and those forming disulphide bonds might not be suitable for studying protein thermal unfolding using this technique. This might be the case for non-accessible cysteines in the $A_{2A}R$-SMALP due to the presence of surrounding lipids, or the disulphide bond formation under oxidative conditions. Moreover, the temperature ramp rate may affect the unfolding profile, and the choice of curve-fitting model introduces bias in the determination of the unfolding parameters.

The presence of mADH in the $A_{2A}R$-DDM sample might have influenced the unfolding results, as mADH has Cys residues to which CPM binds. This can have a different thermal unfolding profile than that of $A_{2A}R$, which might bias the results obtained.

$A_{2A}R$-SMALP and $A_{2A}R$-DDM had different fluorescence profiles, indicating that the solubilization method influenced the receptor thermal unfolding. In addition to protein solubilization, salt concentration, glycerol, detergent, buffer composition, sample storage, and handling can interfere with the stability of GPCRs (Alexandrov *et al.*, 2008; Nehmé *et al.*, 2017). Nevertheless, it has been suggested that different solubilization conditions do not significantly affect the thermal unfolding of the $A_{2A}R$ (Naranjo *et al.*, 2016).

Alternative methods for measuring protein thermal unfolding include circular dichroism (CD) (Jamshad *et al.*, 2015), nanodifferential scanning fluorimetry (nanoDSF) (Haffke *et al.*, 2016), Fluorescence Resonance Energy Transfer (FRET) (Jin *et al.*, 2021), and intrinsic protein fluorescence (Naranjo *et al.*, 2016). These techniques provide information on protein secondary structures and can detect conformational changes, aggregation, and protein unfolding.

Once it was observed that the oxidative treatments did not affect $A_{2A}R$ conformational changes and unfolding, the binding capability of the $A_{2A}R$ under oxidation was confirmed by radioligand binding assays. Competition assays on the membrane-bound $A_{2A}R$ showed inconsistent results. A sigmoidal radioligand displacement curve with the expected IC_{50} value was obtained for acrolein-treated membranes. However, such displacement curves were not observed for the unoxidised or AAPH-treated $A_{2A}R$-membranes. On the other hand, saturation curves were obtained for the untreated or oxidised $A_{2A}R$-membranes with Kd values in the range of 25-30 nM, and no significant differences were observed in the specific radioligand binding between samples. This indicated that the oxidative treatments did not affect the ligand-binding capability of the $A_{2A}R$.

The pharmacology of the $A_{2A}R$ using ZM241385 by radioligand binding assays has been extensively characterized in the literature. Fraser *et al*. conducted radioligand displacement assays on the $A_{2A}R$-membrane and observed a Log ZM241385 IC_{50} of -8.5, which is comparable to the results obtained for ACR-treated membranes in the present study (Fraser, 2006). This suggested that the membrane-bound receptor had a native-like structure under oxidative conditions, which aligned well with the results obtained from the Trp fluorescence and thermal unfolding experiments. In contrast, the authors observed a lower Kd (0.34 nM) for the $A_{2A}R$-DDM (Fraser, 2006) in the saturation assays, suggesting higher receptor affinity for ligand binding compared to that of the $A_{2A}R$-membranes in the present study.

Similarly, lower ZM241385 Kd values than those observed in the present study have been obtained in previous publications, including 12 nM (Magnani *et al.*, 2008), 9 nM (Singh *et al.*, 2012), and 0.5 nM (García-Nafría *et al.*, 2018). Moreover, displacement radioligand binding assays have been validated for the detergent-solubilized (McNeely *et al.*, 2017; García-Nafría *et al.*, 2018a) and membrane-bound $A_{2A}R$ (Singh *et al.*, 2012) with ZM241385 Log IC_{50} values comparable to those observed for ACR-treated membranes in this study.

In this study, the saturation of the receptor was not reached. This could be explained by the expiry of the radioligand or defects in protein folding and conformation, which might have affected the ligand binding to the orthosteric pocket. Nevertheless, this was less probable considering the results obtained from the displacement radioligand binding experiments, which indicated that it was possible to observe a sigmoidal displacement curve with the expected ZM241385 IC_{50} value following oxidation. Additionally, Trp fluorescence and unfolding assays suggested that the protein was folded and able to respond to ligand binding. Consequently, unexpected results from the radioligand binding assays may be attributed to inaccuracies during the experiment performance and sample preparation.

Studying the ligand binding capability of the membrane-bound A$_{2A}$R using radioligand binding assays has some limitations. Nonspecific binding of radioligands to sample and tube components other than the target receptor may occur, leading to inaccurate measurements. Hence, nonspecific binding must be considered when interpreting the results. As an in vitro assay conducted on a membrane-bound receptor from *P. pastoris* membranes, this might not fully capture the complexity of ligand-receptor interactions in cells or living organisms. Radioligands have a limited shelf life owing to the decay of radioactive isotopes, which can affect the results over time (Bylund and Toews, 1993; De Jong *et al.*, 2005; McKinney and Raddatz, 2006). Buffer composition, temperature, and incubation time can lead to variations in radioligand binding characteristics and kinetics. Indeed, different buffer compositions can alter electrostatic interactions between the receptor and ligand. HEPES buffer has been previously used for radioligand binding assays on the A$_{2A}$R, whereas Tris-HCl buffer was used in the present study (Fraser, 2006). In addition, fitting curves and algorithms can introduce bias in the determination of the binding parameters.

Alternative techniques for studying receptor-ligand binding exist, including Fluorescence-Based Binding Assays such as FRET, Chemiluminescence-Based Assays, AlphaScreen/AlphaLISA Assays, Enzyme-Linked Immunosorbent Assay (ELISA), and Mass Spectrometry-Based Assays (Massink *et al.*, 2015; Grime *et al.*, 2020).

The study of the effect of oxidative treatments on conformational changes, thermostability, and ligand binding in the A$_{2A}$R was developed for the first time. This was a pioneering study on the characterization of other membrane proteins and GPCRs for disease treatment through drug development. Furthermore, the resistance of A$_{2A}$R to oxidative treatments holds potential significance in drug discovery and development to address inflammatory diseases in which lipid oxidation and oxidative stress occur. These methodologies can be alternatively applied to the study and characterization of other GPCRs subjected to different treatments or ligand binding.

Various areas for future research can be proposed, based on the gaps identified in this study. Considering that it was possible to detect conformational changes in A$_{2A}$R-SMALP, a methodology to study the conformational changes of DDM-solubilized A$_{2A}$R by modifying the buffer conditions is needed. Importantly, to properly understand the effect of lipid or protein oxidation on the A$_{2A}$R activity, lipid oxidation and protein lipoxidation after acrolein and AAPH treatment should be confirmed using alternative methodologies, such as LC-MS/MS.

In conclusion, Trp fluorescence, thermal unfolding, and radioligand binding assays confirmed that the A$_{2A}$R was properly folded, capable of binding the antagonist and agonist, and able to respond to ligand binding through conformational changes. Moreover, these assays showed that protein conformation,

I. Company Marin, PhD Thesis, Aston University 2024

thermostability, and ligand binding were not affected by oxidation under the experimental conditions. Nevertheless, lipid oxidation and protein lipoxidation should be confirmed using alternative techniques, such as mass spectrometry. These results offer insights into $A_{2A}R$ conformational changes, thermal unfolding profiles, and ligand binding in its native lipid environment under physiological and oxidative conditions, which are relevant for protein characterization, novel drug discovery, and drug development for treating diseases involving inflammation and oxidative stress.

5. CHAPTER 5 – A$_{2A}$R EXPRESSION IN MAMMALIAN HEK293T CELLS AND THE EFFECT OF LIPID OXIDATION ON ITS FUNCTION

5.1 INTRODUCTION

5.1.1 The study of the function of the A$_{2A}$R in its cellular context

After observing that oxidation did not impact the conformation, stability, and ligand binding of the isolated A$_{2A}$R under the experimental conditions, the goal was to explore the influence of lipid oxidation and protein lipoxidation on the functionality of the A$_{2A}$R in a cellular context. The A$_{2A}$R is a prototypical GPCR that plays a crucial role in modulating multiple physiological processes through the activation of the Gs protein and adenylate cyclase to produce the second messenger cAMP (de Lera Ruiz *et al.*, 2014). Studying the activity of the A$_{2A}$R in the context of oxidative stress in the cellular environment could offer relevant perspectives on its function and potential implications in pathological conditions characterized by inflammation and oxidative stress.

Mammalian cells provide a natural environment for protein expression, allowing proper protein production and folding machinery. At the same time, they provide post-translational modifications, which are particularly important for proteins that require them to function. Moreover, mammalian cell cultures can be scaled up to produce large quantities of protein for biopharmaceutical applications. Choosing an appropriate cell line for the expression of a specific mammalian protein is crucial because of their unique characteristics. However, these systems are complex and expensive compared to bacteria or yeasts, and heterogeneity in post-translational modifications may occur. Culturing mammalian cells requires controlled and sterile conditions, specialized media, and serum supplements. Moreover, they typically produce lower protein yields than microbial systems, and grow more slowly, especially in the case of adherent cells. This leads to longer experiments and higher cost. Additionally, they are susceptible to microbial contamination, which requires precautionary measures while performing experiments (Khan, 2013; Hunter *et al.*, 2019).

5.1.2 Adenosine and A$_{2A}$R in inflammation and oxidative stress in the cellular context

Adenosine is an endogenous modulator that helps to maintain cellular and tissue homeostasis under pathological and stress conditions involving inflammation, including rheumatic diseases, neurological disorders, and cancer (Antonioli *et al.*, 2019). Under physiological conditions, extracellular adenosine is maintained at low levels owing to its rapid metabolism and uptake. Nevertheless, adenosine levels in the extracellular compartment increase considerably during oxidative stress, inflammation, tissue injury, hypoxia, or high metabolic demand (Pasquini *et al.*, 2021). Hence, adenosine is considered a

protective mediator against stress and tissue damage, as it plays a key role in regulating inflammation and immune responses (Borea *et al.*, 2017).

The increase in extracellular adenosine during oxidative stress and inflammation results from the release of Adenosine triphosphate (ATP) and other adenine nucleotides from the affected cells. Moreover, cellular metabolic changes during inflammation favour the release of adenosine into the extracellular compartments. Thus, the release of adenosine is used as a mechanism to downregulate inflammation and immune responses through the activation of adenosine receptors, such as the $A_{2A}R$ (Ohta and Sitkovsky, 2014) .

In addition to activating GPCRs, extracellular adenosine can also be taken up by adenosine transporters in the plasma membrane and rapidly converted to Adenosine monophosphate (AMP) by adenosine kinase, contributing to the inhibition of inflammation (Howie *et al.*, 2014). Alternatively, adenosine can be deaminated to form inosine, or phosphorylated to form ATP (Pasquini *et al.*, 2021).

Thus the $A_{2A}R$ has a strong anti-inflammatory function and participates in immune response control (Leone and Emens, 2018), preventing excessive inflammation. Furthermore, local adenosine levels can be high enough to activate both the $A_{2A}R$ and $A_{2B}R$, and it has been observed that $A_{2B}R$ stimulation inhibits inflammation and is immunosuppressive (Koeppen *et al.*, 2011).

The relationship between $A_{2A}R$ activation or inactivation and oxidative stress in the treatment of inflammatory diseases has been extensively studied. El-Shamarka *et al.* suggested a close relationship between oxidative stress and the $A_{2A}R$ in the context of Parkinson's disease (PD), in which oxidative stress-induced neurodegeneration occurs. Moreover, the accumulation of oxidatively damaged cytoplasmic organelles induces endoplasmic reticulum stress and dopaminergic cell death in PD. The authors reported that $A_{2A}R$ plays a key role in PD neuropathogenesis. They observed that the blockade of $A_{2A}R$ has anti-parkinsonian properties (El-Shamarka *et al.*, 2020). Li *et al*. observed that $A_{2A}R$ inhibition with caffeine helped eliminate ROS and protected skin cells against oxidative stress-induced senescence, by activating cell autophagy. Hence, $A_{2A}R$ inhibition protected the cells against oxidative stress-induced damage (Li *et al.*, 2018). Similarly, Wang *et al.* suggested that the $A_{2A}R$ is involved in the regulation of oxidative stress in various cell types, and stated that inhibition of the $A_{2A}R$ with caffeine helps protect cells against oxidative stress (Wang *et al.*, 2022). Ribe *et al*. stated that the $A_{2A}R$ plays a functional role in regulating cardiac ROS production through Mitogen-activated protein kinase (MAPK) signalling and NADPH oxidase regulation. The authors observed that receptor blockade decreased ROS production in the heart. Similarly, it has been observed that $A_{2A}R$ blockade is a promising therapeutic strategy to enhance immune-mediated control in cancer, as it enhances T cell-mediated tumour regression, improves effector function, and increases anti-tumour responses (Leone and Emens, 2018).

In contrast, Castro *et al*. reported that A$_{2A}$R stimulation enhanced mitochondrial metabolism and mitigated oxidative stress by reducing ROS-mediated injury while it improved mitochondrial function. Consequently, a lack of A$_{2A}$R signalling would lead to an increase in the ROS burden and mitochondrial dysfunction. Mitochondrial dysfunction and oxidative stress are associated with multiple diseases, such as osteoarthritis (Castro *et al.*, 2020). Morello *et al*. investigated the role of the A$_{2A}$R in regulating inflammation and the immune response, and observed that receptor activation led to a downregulation of inflammatory networks and tissue injury, while it reduced ROS production in neutrophils (Morello *et al.*, 2009). In addition, Milne *et al*. suggested that A$_{2A}$R activation protected tissues against inflammatory damage caused by ischemia-reperfusion injury (IRI), including the liver, kidney, lung, and heart. This suggests a potential role of the A$_{2A}$R in mitigating oxidative stress (Milne and Palmer, 2011).

Ikram *et al*. studied the role of the A$_{2A}$R in the pathology of Alzheimer's disease (AD) and Parkinson's disease (PD), and stated that oxidative stress can upregulate the expression of the A$_{2A}$R. This can trigger dopaminergic neurodegeneration and neuroinflammation, contributing to the progression of neurodegenerative diseases (Ikram *et al.*, 2020). Nevertheless, the mechanism by which oxidative stress upregulates A$_{2A}$R production needs to be elucidated.

5.1.3 *A$_{2A}$R internalization beyond its signalling dynamics in the cellular context*

GPCR desensitization refers to the process by which these receptors become less responsive to agonists, while they undergo internalization within the cell. This is a relatively rapid and extensive process that typically occurs within minutes to an hour (Calebiro *et al.*, 2010). GPCR activation not only results in G-protein binding but also interact with other intracellular proteins such as β-arrestins (βarrs). These mediate agonist-induced receptor internalization through the clathrin-dependent endocytosis machinery. Nonetheless, the GPCR internalization process is complex and involves various mechanisms (Kang *et al.*, 2014; Peterson and Luttrell, 2017; Ranjan *et al.*, 2017). Indeed, receptor internalization is mediated by GPCR kinases (GRKs), which interact with the receptors and phosphorylate them at the serine, threonine, and tyrosine residues. The phosphorylated protein interacts with β-arrestins, along with the protein kinases PKA and PKC, which promote receptor desensitization and internalization. Once internalised, GPCRs can be recycled back to the plasma membrane or targeted for degradation (Calebiro *et al.*, 2010).

The C-terminal tail of the A$_{2A}$R plays a critical role in its regulation; it contains specific amino acids that are potential phosphorylation sites and are important for β-arrestin interactions. In addition to phosphorylation, GPCRs undergo various post-translational modifications that play critical roles in regulating their function and internalization. These include ubiquitination, glycosylation, and

I. Company Marin, PhD Thesis, Aston University 2024

palmitoylation (Patwardhan *et al.*, 2021). Understanding the role and regulation of GPCR internalization is crucial for unravelling the complexities of these proteins and developing targeted therapies for diseases associated with receptor dysfunction. Ubiquitination of lysine residues is required to control receptor signalling, trafficking, and degradation. Glycosylation, apart from being important for receptor formation and regulatory processes, including folding, transport, ligand binding, and dimerization, is also important for receptor internalization. Palmitoylation occurs by the addition of palmitic acid to cysteine residues, and is essential for protein conformation, stability, plasma membrane localization, signalling, and trafficking (Patwardhan *et al.*, 2021; Tang *et al.*, 2022).

Whole-cell enzyme-linked immunosorbent assay (ELISA) is a highly sensitive technique that provides a semiquantitative measure of GPCR cell surface expression levels, allowing precise comparisons between different experimental conditions in intact cells. It uses specific antibodies against the receptor of interest, ensuring high specificity. Hence, it permits preservation of the cellular environment and receptor interactions with extracellular ligands and intracellular interactors. It is a versatile methodology that can be adapted for high-throughput screening of multiple cell types, including adherent and suspension cells, in a microplate format (Wang *et al.*, 2007; Pandey *et al.*, 2019).

5.1.4   *Characterizing A$_{2A}$R function by measuring cAMP levels in the cellular context*

Characterization of the activation of downstream signalling pathways and receptor internalization provides insights into the function of the A$_{2A}$R in the context of oxidative stress. Analysing the function of the A$_{2A}$R by measuring cAMP levels in a cellular context provides specific advantages compared to measuring other signalling molecules. cAMP is a direct downstream secondary messenger of the A$_{2A}$R, which provides a direct assessment of receptor activity. Alternative downstream signalling molecules can be influenced by other signalling pathways that are modified under the experimental conditions. Hence, measuring cAMP levels reduces potential bias in the results due to interference from unrelated pathways (Wang and Zhou, 2019). Nevertheless, its production is dependent on Gs-protein activation and adenylate cyclase activity in the A$_{2A}$R signalling pathway. In contrast to the study of other adenosine receptors that bind Gi proteins and inhibit cAMP production, this methodology is easily applicable to the study of the A$_{2A}$R; it couples the Gs protein and activates cAMP production (Prosser *et al.*, 2017). Multiple validated and well-established techniques exist for measuring cAMP levels, including radioligand binding assays (Brown *et al.*, 2009), ELISA (Luo *et al.*, 2022), and assay kits, such as the AlphaScreen kit (Gao *et al.*, 2023). These have been widely used in GPCR research, and offer sensitive and quantitative measurements, enabling the accurate assessment of intracellular cAMP levels in response to GPCR activation. Additionally, measuring cAMP levels has translational relevance, as its

signalling pathway is broadly conserved across multiple cell types and organisms, and its downstream signalling pathways have been extensively characterised (Pavlos and Friedman, 2017). Finally, it is a well-established pharmacological assay, as it allows direct evaluation of ligand and pharmacological compound binding targeting the $A_{2A}R$.

Measurement of intracellular cAMP levels for studying GPCR function has been commonly performed using the AlphaScreen cAMP Assay Kit. This has high sensitivity and allows the detection of low levels of cAMP, at the same time it does not imply radioactivity, unlike traditional assays. This offers a simplified workflow that reduces experimental variability and is suitable for high-throughput screening. This assay kit offers a wide dynamic range for measuring cAMP levels at various concentrations, which provides flexibility for studying different experimental conditions, and has been reported to yield robust and reproducible results if proper assay optimization and controls are carried out (Thakur *et al.*, 2023).

The AlphaScreen cAMP detection kit allows the quantitative detection of cAMP molecules based on the interaction and light emission between the Streptavidin-coated Donor and anti-cAMP-conjugated Acceptor beads. Streptavidin-coated Donor beads bind to biotinylated cAMP tracer, resulting in interaction with the anti-cAMP antibody conjugated to AlphaScreen Acceptor beads. This causes the beads to come into close proximity in the absence of endogenous cAMP. The excitation of the Donor beads at 680 nm triggers the release of singlet oxygen molecules, which diffuse towards the Acceptor beads, causing light emission at 520-620 nm. Competition by endogenous cAMP for interaction with the anti-cAMP antibody on the Acceptor beads results in a decreased signal owing to the separation of the Donor and Acceptor beads. Hence, the higher the endogenous cAMP production by the cells, the lower the AlphaScreen signal.

5.2 AIMS AND OBJECTIVES

The work reported in this chapter aimed to study the effect of lipid oxidation on the function of the $A_{2A}R$ in a mammalian expression system. Therefore, the first objective was to design a construct for the expression of the $A_{2A}R$ in mammalian cells and subclone it into the pcDNA3 expression vector. The second objective was to transfect mammalian HEK293T cells and optimize the transfection process to investigate the expression of $A_{2A}R$ in the cells. The third objective was to explore the impact of acrolein- and AAPH-induced oxidation on cell viability, with the aim of determining the optimal concentrations for inducing oxidation without compromising cell viability. The fourth objective was to study the effect of acrolein- and AAPH-induced oxidation on the activity of the $A_{2A}R$ by measuring cAMP production. The final objective was to study the effect of these oxidative treatments on $A_{2A}R$ cell surface expression, further expanding the understanding of receptor behaviour under oxidative stress conditions.

5.3   METHODS

5.3.1   Design of the hA$_{2A}$R sequence cloned in a pcDNA3 vector

All the available sequences of the hA$_{2A}$R in the membrane protein database "Membrane proteins of Known 3D structure" (mpstruc, Stephen White laboratory at UC Irvine and the Bridge Institute at USC) that had been employed to study the crystal structure of the A$_{2A}$R were utilized (Supplementary Table 8.8). The FASTA sequences of all relevant structures were obtained from the Protein Data Bank (PDB, 177910 Biological Macromolecular Structures). The endogenous sequence of the human A$_{2A}$ Receptor published in UniprotKB - P29274 (AA2AR_HUMAN) (2002 – 2021 UniProt Consortium) was obtained as a FASTA file and included in the comparison. FASTA sequences were clustered using the multiple sequence alignment tool "Clustal Omega" from EMBL-EBI (EMBL-EBI, Genome Campus, Hinxton, Cambridgeshire, CB10 1SD, UK) (Supplementary Figure 8.32) to obtain the amino acid sequence. The reverse translation server "Sequence Manipulation Suite: Reverse translate" (2000, 2004 Paul Stothard) was used to obtain the nucleotide sequence. FLAG tag (DYKDDDDAMGQPVGAPPI), deca-histidine tag (HHHHHHHHHH) (Supplementary Table 8.9), Kozak consensus sequence (GCCACC), unstructured flexible linker (GGSGSG) (Supplementary Table 8.10) and *EcoR*I and *Not*I restriction sites were added to the sequence. The designed sequence was purchased from Eurofins Scientific cloned into a pEX-K248 standard vector.

5.3.2   DH5α E. coli cell transformation

DH5α *E. coli* competent cells were transformed with the pcDNA3 empty vector and the pEX-K248-hA$_{2A}$R plasmid. Aliquots of DH5α competent cells (50 µL) were thawed on ice for 30 min, and 100 ng of vector and plasmid were gently added to the cells. In each case, a positive control using 2.5 µL of the pUC plasmid and a negative control for the transformation were included in the experiment. All the tubes were mixed by flicking and incubated on ice for 30 min. The cells were subjected to heat shock at 42°C for 60 s, and the tubes were incubated on ice for 5 min. The cells were suspended in pre-heated S. O. C medium and incubated for 45 min at 37°C and 220 rpm. Finally, the cells were spread on LB agar plates containing the appropriate antibiotic (100 µg/mL ampicillin for cells transformed with the pcDNA3 vector and 50 µg/mL kanamycin for cells transformed with the pEX-K248-hA$_{2A}$R plasmid) and incubated at 37°C overnight.

5.3.3 Growing transformed DH5α E. coli cells in LB medium

Single colonies of transformed DH5α *E. coli* were used to inoculate 5 mL of Luria Broth (LB) medium containing the appropriate antibiotic. The inoculated cultures were incubated overnight at 37°C and 180 rpm until they reached an OD_{600} of approximately 2.0. Alternatively, 5 mL of LB medium containing the appropriate antibiotic was inoculated with colonies from the transformation experiments and incubated overnight at 25°C and 180 rpm to generate glycerol stocks. For this, the cultures were diluted by ½ with sterile 50% glycerol and stored at -80°C.

5.3.4 Plasmid extraction through Miniprep

The pcDNA3 empty vector and pEX-K248-hA$_{2A}$R plasmid were extracted from DH5α *E. coli* cells using the PureYieldTM Plasmid Miniprep System following the alternative protocol for larger culture volumes. Briefly, 1.5 mL of the bacterial culture was centrifuged for 30 s at maximum speed, and an additional 1.5 mL of bacterial culture was added to the cell pellet. The centrifugation step was repeated, and the cell pellets were resuspended in 600 µL of water and mixed by inverting the tubes with 100 µL of Cell Lysis buffer. Cold neutralization solution (350 µL) was added to the tubes and mixed thoroughly by inversion. The tubes were centrifuged at 10000 g for 3 min and the supernatant was transferred to the columns without disturbing the cell pellet. The columns were then placed in collection tubes and centrifuged for 15 s. The flow-through was discarded, and 200 µL of Endotoxin Removal Wash solution were added to the columns and centrifuged at 10000 g for 15 s. Column wash solution (400 µL) was added to the column and centrifuged at 10000 g for 30 s. The columns were transferred to clean microcentrifuge tubes and 30 µL of Elution buffer were added directly to the column matrix and incubated at room temperature for 1 min. Finally, the columns were centrifuged at 10000 g or 15 s, and the flow-through containing the DNA of interest was stored at -20°C. The quality and plasmid concentrations were verified using a NanoDrop™ 2000/2000c Spectrophotometer (ND-2000, Thermo Scientific™) by measuring the absorbance at 230, 260, and 280 nm.

5.3.5 Plasmid and vector digestions

The extracted pcDNA3 vector and pEX-K248-hA$_{2A}$R plasmid were digested with *Eco*RI and *Not*I restriction enzymes. The digestion reactions were prepared for 1 µg of plasmid with 12 units of *Eco*RI and 10 units of *Not*I, using H and D buffers, respectively, to a final volume of 20 µL. The digestion mixtures were incubated for 30 min at 37°C, and the enzymes were heat-inactivated at 65°C for 20 min. Vector and plasmid double digestion was performed under the same conditions with both enzymes using Multicore® Buffer.

153

5.3.6 Agarose gel electrophoresis

DNA samples were analysed by electrophoresis on 0.9% agarose gels. All samples and the 1 KB DNA Ladder were prepared with 10X BlueJuice™ Gel Loading Buffer, and each well was loaded with 100 ng of sample. Electrophoresis was performed for 70-90 minutes at 75 V, and the gels were stained with SYBR™ Safe DNA Gel Stain for 30 min at 50 rpm. Finally, images were obtained using the G Box Gene System.

5.3.7 Subcloning the hA$_{2A}$R into the pcDNA3 vector

The pcDNA3 empty vector and pEX-K248-hA$_{2A}$R plasmid were double-digested with *EcoR*I and *Not*I, and 200 ng of the digested products were loaded on a 0.9% agarose gel and subjected to electrophoresis. The agarose gel was visualized using a transilluminator, and bands corresponding to the double-digested pcDNA3 and the hA$_{2A}$R insert were excised to trim excess agarose.

DNA was extracted from the gel using the Monoarch^R DNA Gel Extraction kit (#T10205, New England Biolabs), following the manufacturer's instructions. Briefly, excised DNA bands were transferred to microfuge tubes and weighed. Gel dissolving buffer was added to the gel slices at four volumes (in µL) per milligram of agarose gel, and the samples were incubated at 50°C by inverting the tubes periodically until the gel slices were completely dissolved. The samples were added to the columns placed in collection tubes and centrifuged for 1 min at 10000 g. The flow-through was discarded, and 200 µL of DNA Wash buffer was added to the column and centrifuged for 1 min. The columns were transferred to clean microfuge tubes and 10 µL of DNA Elution buffer was added directly to the centre of the matrix. The columns were incubated for 1 min at room temperature and centrifuged for 1 min at 10000 g to elute the DNA. DNA quality and concentration were assessed using a NanoDrop™ 2000/2000c spectrophotometer (ND-2000, Thermo Scientific™).

The double-digested pcDNA3 and the hA$_{2A}$R insert were ligated using T4 DNA ligase (Promega) following the manufacturer's recommendations. The ligation reaction was prepared for 100 ng of vector at a 3:1 ratio of insert:vector for a final volume of 20 µL. The ligation reaction was incubated overnight at 4°C and DH5α *E. coli* competent cells were transformed with the ligation product. LB agar plates containing ampicillin at 100 µg/mL were spread with the transformation product and incubated overnight at 37°C. The resulting colonies were used to inoculate 5 mL of LB medium containing ampicillin, and cell cultures were incubated overnight at 37°C and 180 rpm. The plasmids were extracted by Miniprep, double digested with *EcoR*I and *Not*I, and the digestion products were analysed by agarose gel electrophoresis. Finally, the clones obtained were sent to Eurofins Scientific for sequencing.

5.3.8 Mammalian cell culture

Human Embryonic Kidney 293T (HEK293T) cells were cultured in high-glucose Dulbecco's Modified Eagle's Medium (DMEM) containing 4 mM L-glutamine, 4500 mg/L glucose, 1 mM sodium pyruvate, 1500 mg/L sodium bicarbonate, and phenol red. The medium was supplemented with 10% fetal bovine serum (FBS), penicillin (100 U/ml), and streptomycin (100 µg/ml). Cells were grown in T-25 or T-75 cm^2 flasks in a humidified incubator at 37°C and 5% CO_2 until they reached 70-80% confluency. For subculturing, the cells were washed twice with sterile PBS 1X (10 mM Na_2HPO_4, 1.8 mM KH_2PO_4, 137 mM NaCl, 2.7 mM KCl) before addition of 2 mL of 1X trypsin-EDTA (0.25 % w/v) solution prepared from a 10X solution (5 g porcine trypsin and 2 g EDTA 4Na per litre of 0.9% sodium chloride). The cells were incubated with 1X trypsin-EDTA for 5 min in a humidified incubator at 37°C and 5% CO_2, and diluted 1/10 with DMEM complete medium.

5.3.9 Mammalian Cell Counting and cell viability

Cell suspensions were diluted 1:1 with filter-sterilised Trypan Blue stain (0.4%), and 10 µL of the mixture was loaded onto a chamber of a Neubauer haemocytometer. The number of living and dead cells in each section was recorded and the average was multiplied by the dilution factor to obtain the final number of X10^4 cells/mL. Cell viability was calculated as the number of viable cells divided by the total number of cells and expressed as a percentage.

5.3.10 Mammalian cell transfection with the pcDNA3-hA$_{2A}$R

For the analysis of mammalian cell transfection by Western Blotting, 9x10^5 HEK293T cells per well were seeded onto 6-well plates in 1 mL of high-glucose DMEM. The cells were incubated for 24 h at 37°C and 5% CO_2 until they reached 80-90% confluency. Alternatively, for the analysis of cell transfection by Whole Cell ELISA, 2.5x10^5 cells per well were seeded onto 24-well plates in 500 µL of DMEM.

The cells were transfected with the cationic polymer polyethylenimine (PEI) or Lipofectamine 2000 (Invitrogen). For cell transfection with PEI in 6-well plates, 100 µL of Gibco™ Opti-MEM™ medium was mixed with 2 µg of plasmid, and 4, 8, or 12 µL of PEI (1mg/ml, pH 7.5 in 1X PBS) was added to the mix. The mixture was vortexed for 15 s, incubated at room temperature for 10 min, and 600 µL of DMEM was added. The cell medium was aspirated, the cells were washed once with 1X (Phosphate buffered saline) PBS, and the transfection mix was added to each well to reach a final volume of 1 mL of complete medium per well. Alternatively, for cell transfection in a 24-well plate, 25 µL of Gibco™ Opti-MEM™ medium was mixed with 0.5 µg of plasmid, and 2 µL of PEI was added. After the incubation time, 150

155

µL of complete DMEM was added to the mix, and the cells were incubated with the transfection mix in a final volume of 500 µL per well. For cell transfection with Lipofectamine in 6-well plates, 150 µL of Gibco™ Opti-MEM™ medium was mixed with 3 µg of plasmid in a microcentrifuge tube, and 6, 9, 10, or 12 µL was added to 150 µL of Gibco™ Opti-MEM™ medium in a different microcentrifuge tube. DNA and Lipofectamine preparations were combined and incubated for 20 min at room temperature. The medium in each well was aspirated, and 250 µL of the transfection mix was added. The wells were topped up to 1 mL with complete DMEM medium, and the plates were incubated for 48 h at 37°C and 5% CO_2. The cell medium was changed after 24 h of incubation.

For transfection analysis by Western blotting, the cells were washed twice with ice-cold 1X PBS (137 mM NaCl, 2.7 mM KCl, 10 mM Na_2HPO_4, 1.8 mM KH_2PO_4) and lysed with 250 µL RIPA buffer (150 mM NaCl, 1% Triton X-100 w/v, 0.5% sodium deoxycholate w/v, 0.1% SDS w/v, 50 mM Tris, pH 8 containing 1X cOmplete™, EDTA-free Protease Inhibitor Cocktail (Roche) per well. Cells were detached by pipetting up and down, and the cell suspensions were transferred to microcentrifuge tubes and incubated for 45 min and 4°C on an end-over-end rotor. Cell lysates were centrifuged at 3000 x g and 4°C for 10 min, and the protein-containing supernatant was collected and stored at -20°C until further analysis.

For transfection analysis by whole cell ELISA, the cell medium was aspirated, and the cells were washed three times with 1X PBS. Paraformaldehyde at 3.7% (250 µL) was added to each well and the plates were incubated for 15 min at 4°C and 30 rpm. Paraformaldehyde was discarded, and the cells were washed three times with 1X PBS. The cells were blocked for 45 min at room temperature and 30 rpm with 250 µL of 1X PBS containing 2% BSA (w/v) and 0.05% Tween20 (v/v). The blocking solution was removed, and 125 µL of the primary antibody (monoclonal anti-polyhistidine produced in mouse, H1029 Sigma-Aldrich) diluted 1:2000 in 1X PBS and 2% BSA (w/v) was added to each well. The plates were incubated for 1 h at room temperature and 30 rpm, and the primary antibody solution was discarded. The cells were washed three times with 1X PBS and 0.05% Tween20 (v/v) and re-blocked with blocking solution for 15 min at room temperature. The blocking solution was removed, and 125 µL of the secondary antibody (anti-mouse HRP-conjugated) diluted 1:2000 in 1X PBS and 2% BSA (w/v) was added to each well. The plates were incubated for 1 h at room temperature and 30 rpm. The cells were washed three times with 1X PBS and 0.05% Tween20 (v/v), and 300 µL of Tetramethylbenzidine (TMB) substrate solution (Thermo Scientific™) was added to each well. The plates were incubated for 30 min at room temperature and 30 rpm, and 100 µL of the reaction solution was mixed with an equal volume of 3M HCl in a 96-well plate. Finally, the absorbance was measured at 492 nm at room temperature using a Multiskan™ GO Microplate reader.

5.3.11   A$_{2A}$R mini-prep purification by IMAC

For A$_{2A}$R mini-prep purification, HEK293T cell were lysed with RIPA buffer (150 mM NaCl, 1% Triton X-100 w/v, 0.5% sodium deoxycholate w/v, 0.1% SDS w/v, 50 mM Tris, pH 8 containing protease inhibitor cocktail). A$_{2A}$R was purified by mini-prep purification using 1 mL Pierce™ Spin Columns following the manufacturer's instructions. Briefly, 100 µL of His-pur Ni-NTA resin bed was equilibrated with 10 CV of equilibration buffer (50 mM sodium phosphate, 0.3 M sodium chloride, pH 8) without imidazole, and the flow-through was discarded by centrifugation at 5000 x g for 30 s. The resin was recirculated with the cell lysates for 2 h at 4°C and the flow-through was discarded by centrifugation. The resin was washed with 20 CV of equilibration buffer and the wash fractions were discarded by centrifugation. The A$_{2A}$R was eluted from the resin with 1 CV at a time of elution buffer (50 mM sodium phosphate, 0.3 M sodium chloride, 250 mM imidazole, pH 8). All centrifugation steps were performed at 4°C.

5.3.12   Cell viability assays - MTT assay

MTT assay was first described by Mosmann *et al*. (1983). For the standard curve, HEK293T cell dilutions were prepared from the original culture to seed $1x10^5$, $8x10^4$, $7x10^4$, $6x10^4$, $5x10^4$, $4x10^4$, $3x10^4$, $2x10^4$ and $1x10^4$ of cells/well in a 96-well plate. For this, 10X cell dilutions with complete DMEM were prepared, and 100 µL was loaded onto the plates in quadruplicate. For the cell treatments, $3x10^4$, $4x10^4$, and $5x10^4$ of cells/well were seeded to be treated with acrolein or 2,2'-Azobis(2-methylpropionamidine) dihydrochloride (AAPH), and the plates were incubated for 24 h at 37°C and 5% CO_2. The cells were treated with final concentrations of 5, 10, 20, 50, 100, 200, and 400 µM acrolein or 0.25, 0.5, 1, 2, 5, 10, and 15 mM AAPH. For this, 10X dilutions were prepared with PBS 1X for each desired final concentration, and 10 µL of the oxidative treatment was added to the wells, in a final volume of 100 µL. The cells were then incubated for 2 or 24 h at 37°C and 5% CO_2. For both the standard curve and treatments, the medium was removed, and the wells were washed once with PBS 1X. The cells were incubated with 3-(4,5-Dimethyl-2-thiazolyl)-2,5-diphenyl-2H-tetrazolium bromide (MTT) solution at 0.5 mg/mL final concentration. For this, 10 µL of a 10X MTT solution in 1X PBS was added to each well containing 90 µL of high-glucose DMEM supplemented with 10% fetal bovine serum (FBS), penicillin (100 U/ml) and streptomycin (100 µg/ml) without phenol red. All plates were incubated for 3 h at 37°C and 5% CO_2, and 100 µL of solubilization solution (10% SDS w/v in 10 mM HCl) was added to each well. To allow formazan crystals to solubilize, two different conditions were studied: plates were incubated for 30 min under agitation at room temperature, or overnight at 37°C and 5% CO_2. Finally, absorbance was measured at 570 nm with a reference wavelength of 670 nm using a Multiskan™ GO Microplate reader.

5.3.13 Cyclic AMP (cAMP) measurements

Cyclic AMP (cAMP) measurements were performed using the AlphaScreen cAMP Detection Kit (PerkinElmer). For this, 30000 HEK293T cells/well were seeded onto 96-well plates and incubated overnight at 37°C and 5% CO_2 in 100 µL/well of complete DMEM, until 70-80% cell confluency was reached. The cells were transiently transfected with the pcDNA3-hA$_{2A}$R plasmid and PEI following the previously optimized protocol and incubated at 37°C and 5% CO_2 for 24 h. The cells were either treated with vehicle (1X PBS), AAPH at 250 µM, or acrolein at 20 µM. AAPH (2.5 mM) and acrolein (200 µM) were prepared in 1X PBS and filter-sterilized. For cell treatment, the cells were washed once with 1X PBS, 10 µL of each 10X treatment was added to 90 µL of complete DMEM, and plates were incubated for either 2 or 24 h at 37°C and 5% CO_2. After the oxidative treatments, the cells were washed once with 1X PBS and starved in 90 µL/well of pre-warmed and sterile Stimulation Buffer (0.1% w/v BSA, 1 mM 3-isobutyl-1-methylxanthine (IBMX) in phenol-free DMEM) for 1 h at 37°C and 5% CO_2. When studying the effect of the two A$_{2A}$R ligands simultaneously, the cells were starved in 80 µL/well of Stimulation Buffer. The cells were stimulated with 10 µL of 10X ligand serial dilutions for 30 min at 37°C and 5% CO_2. Ligand serial solutions were prepared by making half-log dilutions in Stimulation Buffer, so the final ligand concentration in the assay ranged from 100 µM to 1 nM for Forskolin and NECA, or from 1 µM to 10 pM for ZM241385. The effect of the antagonist ZM241385 was studied in the presence of 316 nM NECA (calculated NECA EC$_{75}$). A "no ligand" blank control was included on each occasion. The ligand-containing medium was aspirated, and 50 µL of ice-cold 98% ethanol was added to each well to lyse and dehydrate the cells. Ethanol was allowed to evaporate overnight at room temperature, and the plates were stored at -20°C until further analysis. Lysis Buffer (0.1% w/v BSA, 0.3% v/v Tween-20, 5 mM HEPES buffer, pH 7.5) was added to each well (75 µL) and the cell lysates were incubated at room temperature on an orbital shaker for 10 min. For accurate cAMP measurements, the samples were further diluted ten times in Lysis Buffer. The Acceptor and Donor bead mixes were prepared following the manufacturer's instructions under subdued lighting and kept away from light once diluted. Briefly, anti-cAMP AlphaScreen Acceptor beads were diluted to 100 µg/mL in Stimulation Buffer by making a 1:50 dilution of the Acceptor bead stock solution. Biotin-cAMP (41.7 nM) and Streptavidin Donor bead (33.3 µg/mL) were mixed to obtain a 1.67X preparation in 1X Immunoassay Buffer by diluting the 1 µM biotin-cAMP stock 1:24 and the Donor bead stock 1:150. Prior to this, biotinylated cAMP tracer was dissolved in 1X PBS to make a 10 µM stock solution and further diluted in 1X PBS to obtain a 1 µM working solution. A 1X Immunoassay buffer (PerkinElmer AL000) was prepared by diluting the 10X stock. Biotin-cAMP and Streptavidin Donor bead mixture was prepared fresh every time and incubated for 30 min at room temperature in the dark before being added to the assay plate. To determine the sensitivity (IC$_{50}$ value) and dynamic range (IC$_{10}$ – IC$_{90}$) of the cAMP assay, and to extrapolate the amount

I. Company Marin, PhD Thesis, Aston University 2024

of cAMP produced by the cells in the assay, a cAMP standard curve was prepared fresh prior to each assay. For this, 5X cAMP standard serial solutions were prepared from the 50 µM cAMP standard supplied with the kit by making half-log dilutions in Stimulation Buffer, so final cAMP concentration in the assay ranged from 1 µM to 10 pM. A "no cAMP" blank control was included on each occasion. cAMP standards or samples (5 µL) were transferred to a 384-well white opaque Optiplate and, under reduced light conditions, 5 µL of the Acceptor bead and 15 µL of the Streptavidin Donor bead mixtures were added to each well. The plates were sealed, briefly centrifuged to collect the contents at the bottom of the plate, and incubated in the dark at room temperature for 1 h. Prior to fluorescence measurements, the plates were centrifuged again. For cAMP measurement, samples were excited with an excitation wavelength of 680 nm, and emission was measured between 520-620 nm using a Mithras LB 940 Multimode Microplate Reader (Berthold Technologies).

5.3.14   Receptor internalization by whole cell ELISA

$A_{2A}R$ internalization in mammalian HEK293T cells was measured by whole cell ELISA, consistent with the experimental design for cAMP measurements. Briefly, 30000 cells/well were seeded in 96-well plates and incubated overnight at $37^{\circ}C$ until 70-80% cell confluency was reached. The cells were transiently transfected with the pcDNA3-$A_{2A}R$ plasmid using PEI and incubated at $37^{\circ}C$ for 24 h. The cells were either treated with 10 µL of 1X PBS (vehicle), AAPH (250 µM), or acrolein (20 µM), and incubated for 2 or 24 h at $37^{\circ}C$. The cells were starved in 90 µL/well of pre-warmed and sterile Stimulation Buffer (0.1% w/v BSA, 1 mM IBMX in phenol-free DMEM) for 1 h at $37^{\circ}C$ and stimulated with 10 µL of 10X NECA to reach a final concentration of 1 µM in the well. The cells underwent NECA stimulation for various durations, ranging from 5 to 60 min at intervals of 5 min. After each desired incubation time, NECA-containing medium was aspirated, and cells were washed three times with 1X PBS and fixed with 3.7% paraformaldehyde for 15 min at room temperature. The cells were washed three times in 1X PBS and blocked with 50 µL of blocking solution (2% w/v BSA, 0.05% v/v Tween-20 in 1X PBS) overnight at $4^{\circ}C$ on an orbital shaker. The blocking solution was removed, and the cells were incubated with 20 µL of anti-$A_{2A}R$ primary antibody solution (5 µg/mL anti-A2AR primary antibody, 2% w/v BSA in 1X PBS) for 1 h at room temperature on an orbital shaker. The cells were washed thrice with washing solution (0.05% v/v Tween-20 in 1X PBS) and blocked in blocking solution for 15 min at room temperature on an orbital shaker. The blocking solution was removed, and the cells were incubated with 20 µL of the secondary antibody solution (1:3000 dilution of the HRP-conjugated anti-mouse secondary antibody, 2% w/v BSA in 1X PBS) for 1 h at room temperature with shaking. The cells were washed three times with washing solution, 100 µL of 3,3',5,5'-Tetramethylbenzidine (TMB) substrate

solution was added to each well, and the plates were incubated at room temperature on an orbital shaker for 30 min in the dark. To stop the reaction, 50 µL of TMB substrate solution was transferred to a new plate and mixed with an equal volume of 3 M HCl. Finally, absorbance was measured at 492 nm using a Multiskan™ GO Microplate reader.

5.4 RESULTS

5.4.1 Final design of the hA2AR sequence to be cloned into the pcDNA3 vector

To investigate the effect of lipid oxidation on the function of the $A_{2A}R$, the expression of this receptor in mammalian cells was required. Hence, a DNA construct was created to induce $A_{2A}R$ overexpression in mammalian cells. This construct involved the incorporation of the optimal receptor sequence for protein expression and stability into a pcDNA3 plasmid. The receptor sequence consisted of the C-terminal-truncated and de-glycosylated $A_{2A}R$, which was obtained by clustering the published sequences in *mpstruc* database. These sequences had previously been used for structural studies of the $A_{2A}R$. Two different tags, a FLAG tag and a deca-His tag, were added at the N-terminus and C-terminus of the $A_{2A}R$ sequence, respectively, for protein detection and purification. To ensure proper protein expression in mammalian cells, a Kozak consensus sequence was added upstream of the FLAG tag and initiating methionine. The GGSGSG unstructured flexible linker was also included at the C-terminus of the receptor. The *EcoR*I and *Not*I restriction sites were added upstream and downstream of the sequence, respectively. This sequence was designed to be inserted into the pcDNA3 vector, resulting in the generation of the pcDNA3-hA$_{2A}$R plasmid (Figure 5.1). The nucleotide and amino acid sequences are shown in Supplementary Figure 8.33.
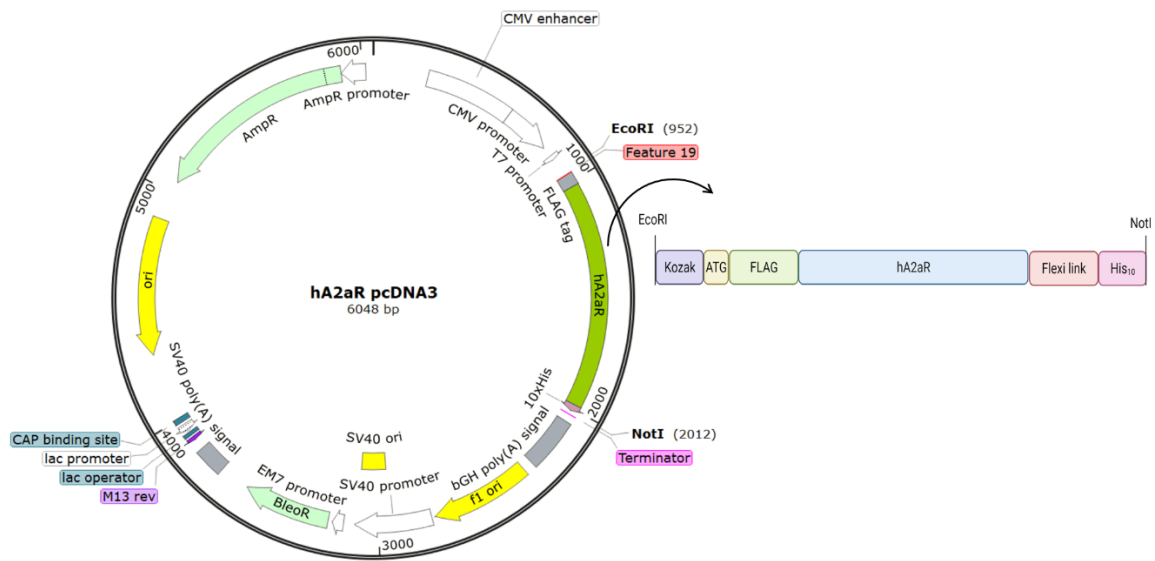
Figure 5.1. Design A₂ₐR-pcDNA3 plasmid. *The schematic representation of the A$_{2A}$R insert and final construct of the A$_{2A}$R cloned into the pcDNA3 vector obtained using SnapGene Software are shown.*

5.4.2 Transformation of DH5α competent cells with the pcDNA3 empty vector, extraction, and digestion.

To obtain sufficient amounts of pcDNA3 empty vector (Figure 5.2A) for cloning purposes, *E. coli* DH5α competent cells were transformed with the empty vector and grown in ampicillin-containing medium to select for cells containing the vector. The pcDNA3 vector was extracted from the transformed cells and digested using *EcoR*I and *Not*I restriction enzymes. Plasmid digestion was analysed on an agarose gel (Figure 5.2B). A prominent band was observed on the gel aligning with the undigested pcDNA3 empty vector at approximately 4 Kp. This suggested that most of the undigested vector was supercoiled, as its apparent length appeared shorter than its real size (5446 bp). On the other hand, a light band was observed at the top of the lane with an apparent length of 10 Kb, which corresponded to the nicked form of the vector. After vector digestion with *EcoR*I, a band was observed at 5446 bp, corresponding to the linearized vector. A light band was also obtained in the same lane, corresponding to the undigested and supercoiled vector. The vector was partially digested with *Not*I, as three bands were obtained in the lane, which coincided with the nicked, linearized (5446 bp), and supercoiled vector. Although vector digestion with *Not*I was less efficient than with *EcoR*I, both restriction enzymes were able to digest the vector, generating the corresponding ends with the restriction sites for cloning purposes.
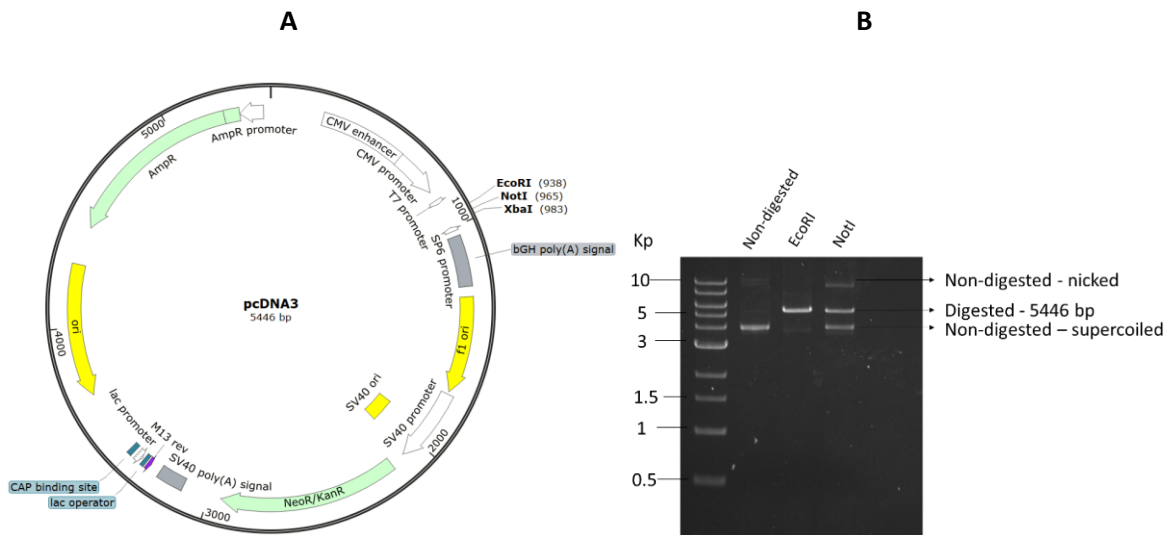
Figure 5.2. Amplification of the pcDNA3 empty vector by DH5α competent cell transformation, vector extraction, and digestion. (A) The pcDNA3 vector map was generated using SnapGene software. (B) The vector was subjected to digestion with the restriction enzymes EcoRI and NotI individually, and to double digestion with both restriction enzymes simultaneously. The resulting fragments were separated by electrophoresis on a 0.9% agarose gel to visualize the different bands and analyse the digestion pattern of the vector.

5.4.3 Transformation of DH5α competent cells with the pEX-K248-hA$_{2A}$R plasmid, extraction, and digestion.

The A$_{2A}$R sequence designed was obtained in a commercial pEX-K248 vector. To amplify the pEX-K248-hA$_{2A}$R plasmid for cloning the A$_{2A}$R insert (Figure 5.3A), *E. coli* DH5α competent cells were transformed and grown in kanamycin-containing medium. Consequently, the plasmid was extracted, digested with *EcoR*I and *Not*I restriction enzymes, and analysed on an agarose gel (Figure 5.3B). A band was obtained on the gel corresponding to the undigested pEX-K248-hA$_{2A}$R plasmid with an apparent length of 2.5 Kb. This suggested that most of the undigested plasmid was supercoiled, as its apparent length appeared shorter than its real size (3574 bp). After plasmid digestion with *Not*I, a unique band was obtained corresponding to the linearized vector with a length of 3574 bp. After plasmid digestion with *EcoR*I, two different bands were obtained. This was due to the presence of a second *EcoR*I restriction site at the position 1092 bp, downstream of the insert of interest. A band matching with pEX-K248 (2483 bp) and a band matching with the hA$_{2A}$R insert plus 24 bp (1091 bp) were obtained. After plasmid double digestion with *EcoR*I and *Not*I, a band corresponding to the pEX-K248 (2507 bp) and a second band corresponding to the hA$_{2A}$R insert (1067 bp) were obtained. Hence, both restriction enzymes served to digest the pEX-K248-hA$_{2A}$R plasmid, generating the corresponding ends with *EcoR*I and *Not*I restriction sites to obtain the insert of interest for cloning purposes.
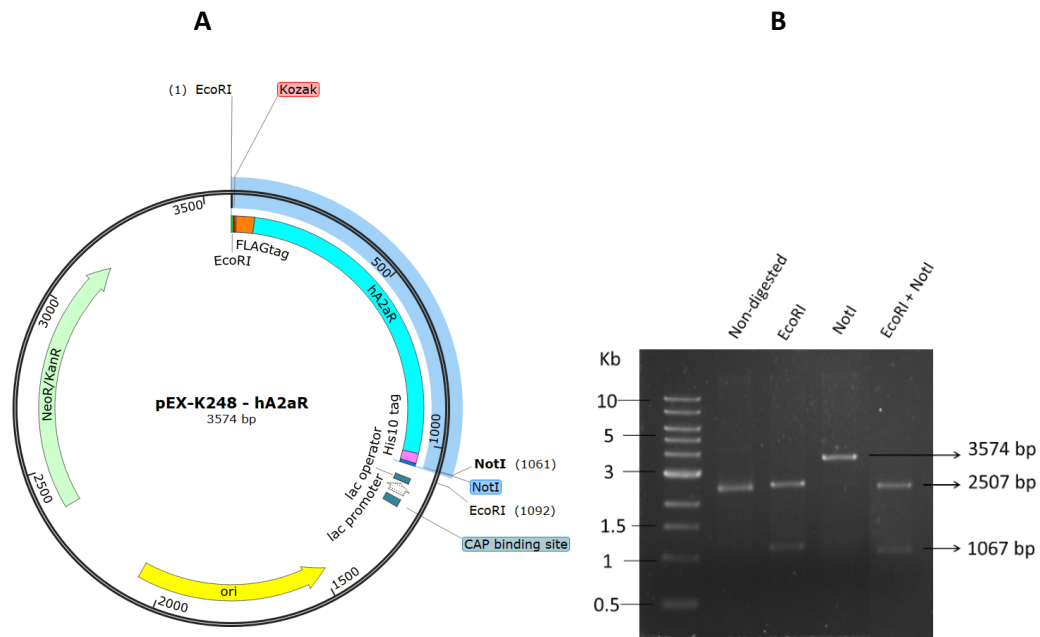
Figure 5.3. Amplification of the pEX-K248-hA$_{2A}$R plasmid by DH5α competent cell transformation, vector extraction, and digestion. (A) The pEX-K248-hA$_{2A}$R plasmid map was generated using SnapGene software. (B) The plasmid was subjected to digestion with the restriction enzymes EcoRI and NotI individually, and to double digestion with both restriction enzymes simultaneously. The resulting fragments were separated by electrophoresis on a 0.9% agarose gel to visualize the different bands and analyse the digestion pattern of the plasmid.

To clone the A$_{2A}$R insert into the pcDNA3 empty vector, both the pEX-K248-hA$_{2A}$R plasmid and the pcDNA3 vector were subjected to double digestion with *EcoR*I and *Not*I restriction enzymes. The digestion products were subsequently analysed by agarose gel electrophoresis to confirm the presence of the desired fragments. The bands corresponding to the A$_{2A}$R insert and double-digested pcDNA3 were excised, and the DNA was extracted from the gel (Figure 5.4A). Both DNA fragments were ligated, and the resulting ligation product was used to transform competent *E. coli* DH5α cells. Antibiotic-resistant colonies were grown on LB agar plates containing ampicillin. Three colonies were obtained on the plates, indicating that the cells incorporated the pcDNA3-hA$_{2A}$R plasmid and had ampicillin resistance. The three colonies were used to inoculate ampicillin-containing medium to amplify the plasmid of interest. The pcDNA3-hA$_{2A}$R plasmid was extracted, digested with the restriction enzymes *EcoR*I and *Not*I, and analysed on an agarose gel (Figure 5.4B). The three colonies were transformed with the plasmid that incorporated the A$_{2A}$R insert, as bands at 1067 bp were obtained in all lanes. In addition, bands corresponding to the double-digested pcDNA3 backbone were obtained in all lanes at 4519 bp, together with less intense bands corresponding to the supercoiled and undigested plasmid, with an apparent length of 3500 bp. These results indicated that *E. coli* DH5α transformation was

successful, and the A$_{2A}$R insert was correctly integrated into the pcDNA3-hA$_{2A}$R plasmid in all three clones.
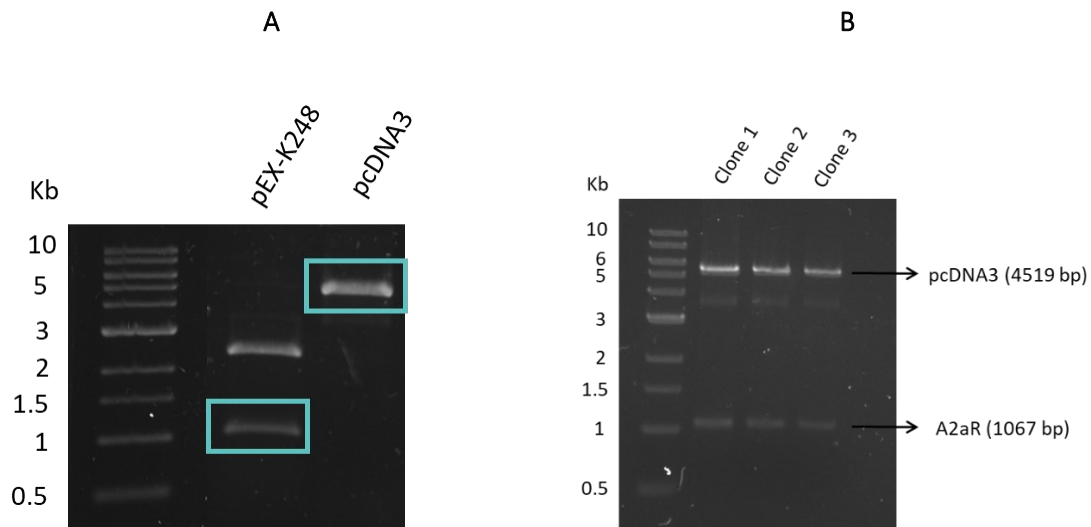
Figure 5.4. Subcloning the hA$_{2A}$R insert from the pEX-K248 plasmid into the pcDNA3 vector. (A) The pEX-K248-hA$_{2A}$R plasmid and pcDNA3 empty vector were subjected to double digestion with the restriction enzymes EcoRI and NotI, and the resulting fragments were separated by electrophoresis on a 0.9% agarose gel. Bands corresponding to the hA$_{2A}$R insert and double-digested empty vector were extracted from the gel and ligated with T4 DNA ligase. (B) pcDNA3-hA$_{2A}$R was extracted from transformed DH5α cells and subjected to double digestion with EcoRI and NotI. The resulting fragments were separated by electrophoresis on a 0.9% agarose gel to visualize the different bands and analyse the digestion pattern of the plasmid.

To confirm the integrity of the A$_{2A}$R insert in the pcDNA3 plasmid, the clones were subjected to Sanger sequencing (Supplementary Table 8.11). Clone 3 had the highest insert integrity, so it was used to transfect mammalian cells for the expression of the A$_{2A}$R.

5.4.4 *Mammalian HEK293T cell transfection with the pcDNA3-hA$_{2A}$R plasmid and analysis of A$_{2A}$R production*

To express the A$_{2A}$R in a mammalian expression system, HEK293T cells were transfected with the pcDNA3-hA$_{2A}$R plasmid, and cell transfection was optimized using different volumes of PEI or Lipofectamine. The expression of the A$_{2A}$R in transfected cells was analysed by SDS-PAGE and western blotting using a specific primary antibody against the A$_{2A}$R (Figure 5.5A), and the band intensity corresponding to the A$_{2A}$R monomer was analysed by densitometry (Figure 5.5B). No bands were observed in the lane corresponding to non-transfected cells, indicating that it was not possible to detect endogenous A$_{2A}$R expressed by the cells. This served as a negative control for transfection. In contrast, bands of ~42 KDa corresponding to the A$_{2A}$R were observed in the lanes of transfected cells. This

164

suggested that transfection using both reagents led to the successful expression of the $A_{2A}R$. The intensity of the $A_{2A}R$ bands increased as the volume of Lipofectamine was also increased, indicating a higher protein expression. A similar band intensity was detected in cells transfected with 4 and 8 µL of PEI per well, and a decrease was observed when 12 µL of PEI per well was used for a 6-well plate. Densitometric analysis indicated the $A_{2A}R$ bands in PEI-transfected cells were slightly less intense than those obtained in lipofectamine-transfected cells. Although maximum protein production was achieved with 12 µL of Lipofectamine, it was possible to detect the protein of interest when cells were transfected with lower amounts of Lipofectamine or with PEI.
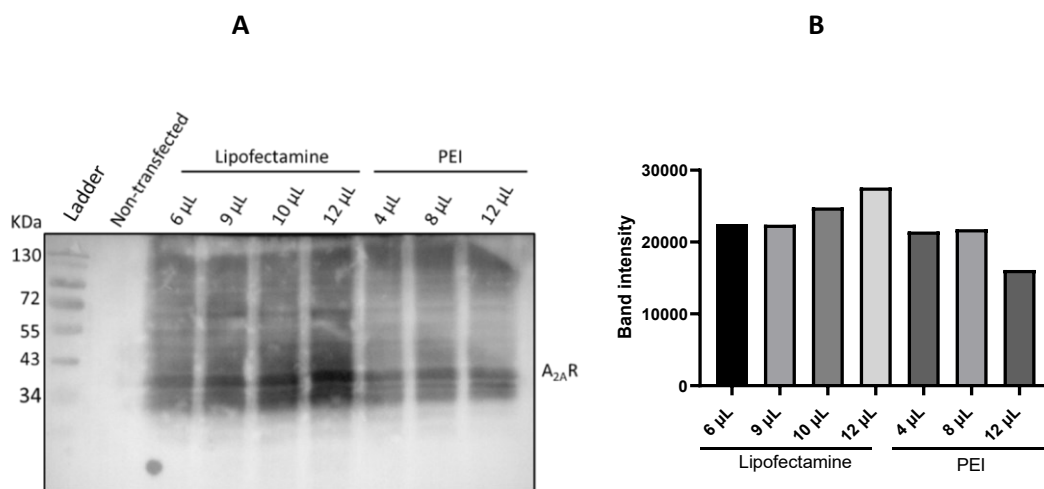
Figure 5.5. Optimization of HEK293T cell transfection with the pcDNA3-hA$_{2A}$R clone 3 using different volumes of Lipofectamine and PEI. HEK293T cells seeded onto 6-well plates were transiently transfected with 2 or 3 µg of pcDNA3-hA$_{2A}$R clone 3 using different amounts of Lipofectamine or polyethylenimine (PEI), respectively. A non-transfected control using 1X PBS as the vehicle was included in this experiment. (A) For protein expression analysis, the cells were lysed and analysed by western blotting using a specific anti-A$_{2A}$R primary antibody and HRP-conjugated secondary antibody. (B) Bands corresponding to the A$_{2A}$R were analysed by densitometry using ImageJ software (n=1).

Considering the results obtained and the transfection agent cost, HEK293T cells were transfected using 8 µL of PEI per well for further experiments. $A_{2A}R$ expression on the cell surface was analysed by western blotting and whole cell ELISA using an anti-His tag primary antibody. Western blotting confirmed the absence of bands corresponding to the $A_{2A}R$ in non-transfected cells, or in cells treated with PEI in the absence of the plasmid (Figure 5.6A). In contrast, a strong band corresponding to the $A_{2A}R$ was observed in cells transfected with PEI and the plasmid, indicating correct transfection and protein production. Furthermore, smeared bands were observed in the lane corresponding to the transfected sample. Whole cell ELISA indicated that transfected cells showed a significant increase in absorbance at 492 nm compared to the non-transfected or vehicle-transfected cells (Figure 5.6B). This could be explained by higher antibody binding to the His-tagged protein, and thus, higher $A_{2A}R$ expression.
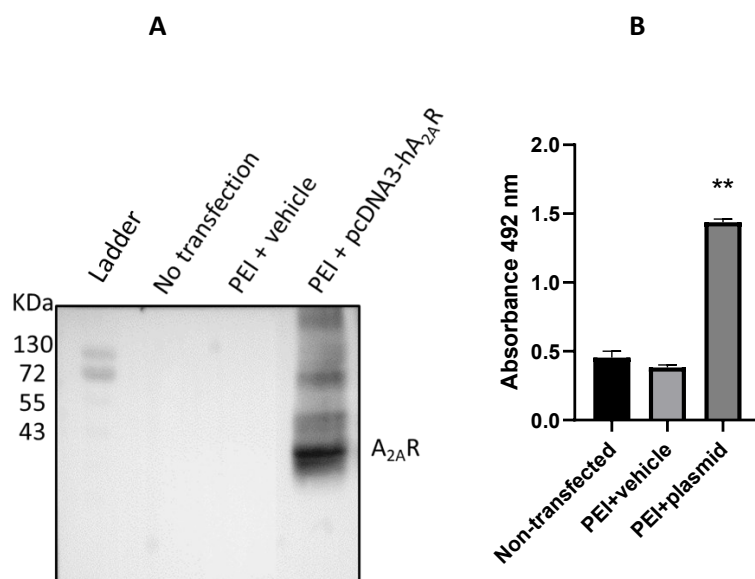
Figure 5.6. HEK293T cell transient transfection with pcDNA3-hA$_{2A}$R clone 3 using 8 µL of PEI. *HEK293T cells seeded onto 6-well plates were transiently transfected with 2 µg of pcDNA3-hA$_{2A}$R clone 3 and 8 µL polyethylenimine (PEI). A non-transfected and a vehicle-transfected control with 1X PBS were included in this experiment. For the analysis of protein expression, the cells were either (**A**) lysed and analysed by western blotting using a specific anti-A$_{2A}$R primary antibody and HRP-conjugated secondary antibody or (**B**) analysed by whole cell ELISA using an anti-His tag primary and HRP-conjugated secondary antibody. The His-tagged A$_{2A}$R levels on the cell surface were detected by measuring the absorbance at 492 nm after the addition of the TMB substrate. Data are presented as the mean of all replicates (n=3) ± SD. Statistical differences were determined by One-way ANOVA followed by Tukey's multiple comparison test (*p-value<0.05, **p-value<0.005 vs. non-transfected).*

To confirm the identification of the A$_{2A}$R, the receptor was purified by small-scale IMAC and analysed LC-MS/MS. SDS-PAGE results showed that most of the A$_{2A}$R did not bind to the resin as it eluted in the flow-through (FT) fraction, which had multiple protein bands comparable to the whole lysates (Figure 5.7A). No bands were observed in the lanes corresponding to washes 1 and 2 (W1 and W2), and the A$_{2A}$R eluted from the resin in the elution fractions, being more abundant in E1. Multiple protein bands were observed on the gel in E1, indicating the low purification efficiency of the A$_{2A}$R. Western blotting confirmed the loss of some of the A$_{2A}$R in the flow-through (Figure 5.7B). The A$_{2A}$R was not lost during the washes, and it eluted mainly in E1, in which a strong band for the A$_{2A}$R monomer was obtained, together with a smear on the lane. Thus, it was not possible to remove smears by IMAC purification. Interestingly, a strong signal was obtained on the top of the lanes of whole lysates, FT, and elution fractions, which could correspond to A$_{2A}$R aggregates. Consequently, multiple protein bands indicated by the yellow arrows on the SDS-PAGE gel were analysed by in-gel digestion and LC-MS/MS to identify possible protein contaminants and confirm the presence of the A$_{2A}$R in the samples.
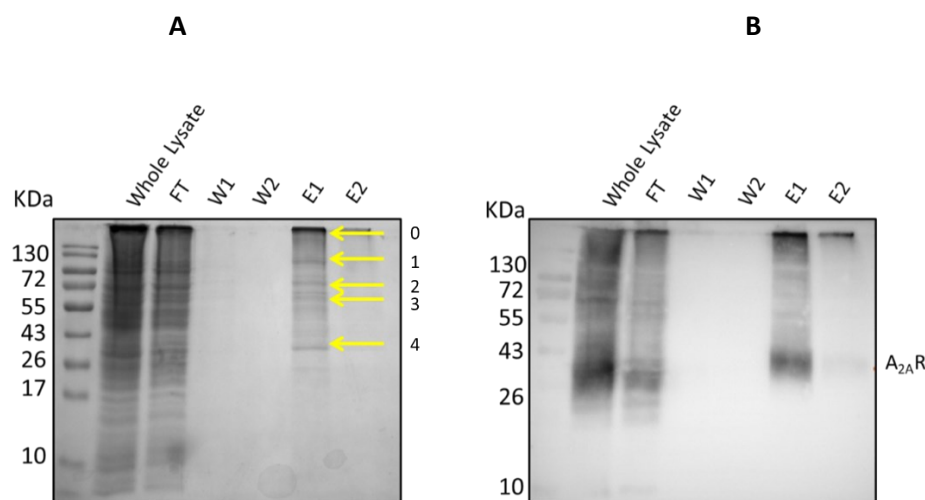
Figure 5.7. A$_{2A}$R mini-prep IMAC purification from HEK293T whole cell lysates. *HEK293T cells seeded onto 6-well plates were transiently transfected with the pcDNA3-hA$_{2A}$R plasmid. The cells were lysed, and the A$_{2A}$R was purified by mini-prep IMAC purification. Whole lysates were recirculated with His-pur Ni-NTA resin equilibrated without imidazole. The resin was washed twice with wash buffer without imidazole, and the A$_{2A}$R was eluted with elution buffer containing 250 mM imidazole. The results were analysed by (A) SDS-PAGE and Coomassie staining, and (B) western blotting using a specific primary antibody against the A$_{2A}$R. Certain bands potentially corresponding to the A$_{2A}$R (yellow arrows) were selected for identification by LC-MS/MS.*

The selected bands were digested in-gel with trypsin or chymotrypsin, and the resulting peptides were analysed by LC-MS/MS. The A$_{2A}$R identifications with the highest position and score after trypsin and chymotrypsin digestion are shown in Table 5.1. The A$_{2A}$R digested with trypsin was identified in the 29th position among all possible human identifications with a score of 104, and thus above the *cut-off* criteria for protein identification acceptance, which was set at 50. The A$_{2A}$R digested with chymotrypsin was identified in the 93rd position with a score of 49, and thus below the *cut-off* criteria for protein identification. In both cases, the most probable identification of the A$_{2A}$R corresponded to band 4 on the gel. Hence, the identification of the A$_{2A}$R expressed in HEK293T cells was confirmed by western blotting, and LC-MS/MS data supported the identification, although low protein sequence coverage was obtained.

Table 5.1. Identification of the A₂ₐR expressed in mammalian HEK293T cells by in-gel digestion and LC-MS/MS.

	Taxonomy	Position	Protein	Score	Sequence coverage
Trypsin	*Homo sapiens*	29	A2AR_HUMAN	104	4%
Chymotrypsin	*Homo sapiens*	93	A2AR_HUMAN	49	2%

The A₂ₐR digested with trypsin was identified with a total sequence coverage of 4%, and two unique peptides were detected (Figure 5.8A). The YNGLVTGTR peptide corresponded to part of the intracellular loop 2 (ICL2) and the intracellular side of the transmembrane helix 4 (TM4), whereas the QMESQPLPGER peptide corresponded to the intracellular loop 3 (ICL3) and the cytoplasmic ends of the transmembrane helices 5 (TM5) and 6 (TM6). The A₂ₐR digested with chymotrypsin was identified with a total sequence coverage of 2%, and one unique peptide was detected (Figure 5.8B). The identified SHTNSVVNPF peptide corresponded to the central region of the transmembrane helix 7 (TM7). Hence, the identification of the A₂ₐR in HEK293T cells using chymotrypsin digestion was below the acceptance criteria, which requires the detection of 2 unique peptides.
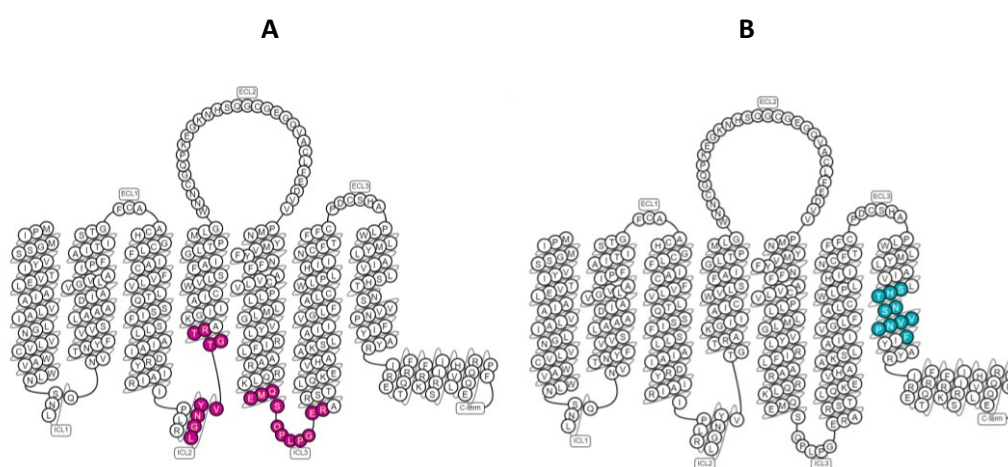
*Figure 5.8. A₂ₐR identification by LC-MS/MS after in-gel digestion with trypsin or chymotrypsin. Bands corresponding to the A₂ₐR were in-gel digested with trypsin or chymotrypsin and analysed by LC-MS/MS. (**A**) Sequence coverage of the A₂ₐR digested with trypsin, with the identified unique peptides highlighted in pink. (**B**) Sequence coverage of the A₂ₐR digested with chymotrypsin, with the identified unique peptides highlighted in blue.*

5.4.5   The effect of acrolein and AAPH treatments on HEK293T cell viability measured by MTT assays

To study the effect of lipid oxidation on the A₂ₐR in mammalian cells, it was essential to establish the optimal concentrations of oxidants (AAPH and acrolein) for cell treatment, considering their impact on

cell viability. This essential step ensured that subsequent experiments accurately reflected the influence of lipid oxidation on the $A_{2A}R$ without significantly perturbing cell viability.

To this end, MTT assays were performed, which are based on measuring cell mitochondrial activity by converting MTT reagent into formazan crystals, which has light absorbance at 450 nm (Mosmann, 1983). To determine the optimal cell density to conduct the assay, a standard curve was generated (Figure 5.9). To optimize formazan solubilization, two different methods were tested: cells were incubated for 30 minutes at room temperature (RT) with the solubilization solution or, alternatively, at $37^{\circ}C$ overnight. In both cases, higher cell seeding density led to increased absorbance at 450 nm, indicating elevated formazan production and, therefore, mitochondrial activity. Samples incubated overnight at $37^{\circ}C$ had higher absorbance values for a given number of cells per well, suggesting higher formazan solubilization. Furthermore, samples solubilized for 30 minutes at RT had higher standard deviation, indicating increased variability between replicates. Linearity of the standard curve was observed between 0 and 1 $x10^5$ cells/well in both cases, with R^2 values of 0.9667 for O/N incubation at $37^{\circ}C$, and 0.9838 for 30 minutes incubation at RT. Consequently, 40000 cells/well were seeded for subsequent experiments, as the absorbance values for this cell density fell within the linear range of the standard curve.
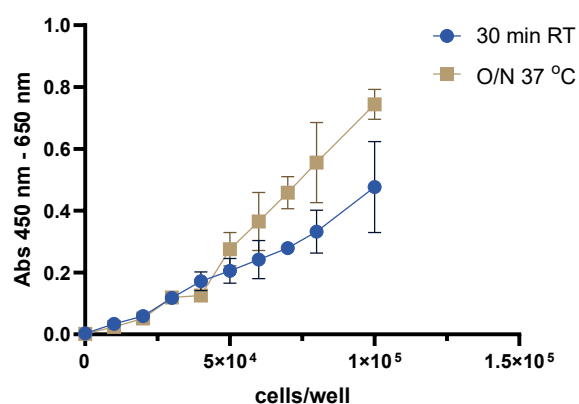
Figure 5.9. MTT assay standard curve to determine the optimal number of HEK293T cells seeded per well. Different numbers of HEK293T cells were seeded per well to determine the optimal cell density for MTT assays. Cell viability was determined by measuring the absorbance after incubating the plates for 30 minutes at RT shaking, or overnight at $37^{\circ}C$. Results are expressed as the mean OD $570 - 670$ nm of all replicates (n=4) ± SEM.

To determine the optimal acrolein and AAPH concentrations to induce oxidative stress in cells without substantially reducing cell viability, HEK293T cells were treated with increasing concentrations of both oxidative treatments for 2 and 24 hours. Cell viability was determined by MTT assay, and the percentage of cell viability at each oxidant concentration was calculated.

Acrolein decreased cell viability in a concentration-dependent manner after 2 and 24 hours of treatment (Figure 5.10A). Acrolein at 100 µM significantly decreased cell viability in cells treated for 24 hours, and acrolein at 200 and 400 µM significantly decreased cell viability in cells treated for 2 and 24 hours. Therefore, viability percentages were comparable in cells subjected to acrolein treatment for 2 or 24 hours at concentrations of 50 µM or lower, whereas cells exposed to higher concentrations showed a significant decrease in cell viability, according to One-way ANOVA.

On the other hand, AAPH decreased cell viability in a concentration-dependent manner in cells subjected to a 24h treatment, whereas it had little effect on cells treated for 2h (Figure 5.10B). Cell treatment with AAPH up to 15 mM for 2h was not sufficient to significantly decrease cell viability, while cells treated with AAPH at 5 mM or higher concentrations for 24h showed a significant decrease in cell viability compared to the control, according to One-way ANOVA.

To ensure appropriate cell viability, HEK293T cells were treated with 20 µM acrolein and 250 µM AAPH for further experiments, which maintained a cell viability higher than 85% in all cases.
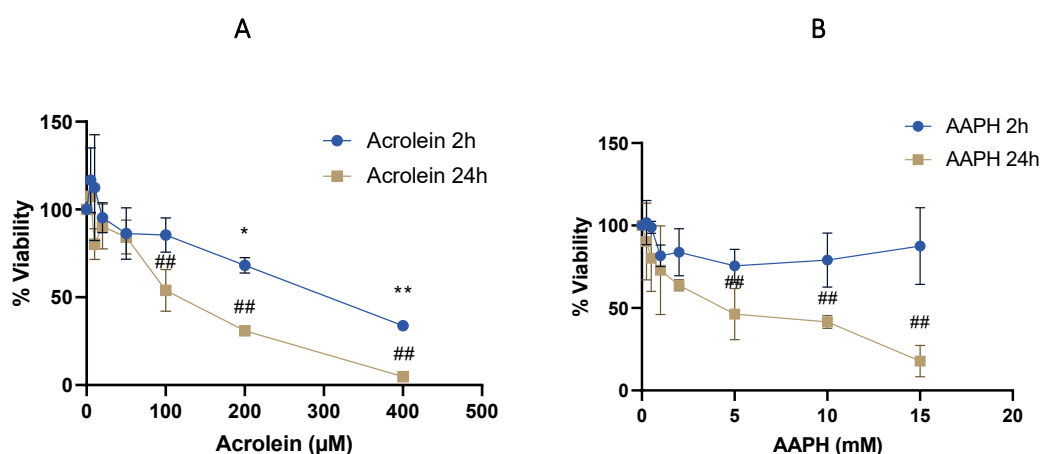
*Figure 5.10. The effect of acrolein and AAPH treatment on HEK293T cell viability. HEK293T cells were seeded at 40000 cells/well onto 96-well plates and treated with increasing concentrations of (**A**) acrolein or (**B**) AAPH for 2 and 24 hours. Cell viability was determined by MTT assay after formazan solubilization for 30 minutes at room temperature shaking. Data are presented as mean viability percentage of all replicates (n=3) ± SD. Statistical differences were determined by One-way ANOVA followed by Tukey's multiple comparison test (*p-value<0.05, **p-value<0.01 2h vs control; #p-value<0.05, ##p-value<0.01 24h vs control).*

5.4.6 The effect of acrolein and AAPH on the function of the $A_{2A}R$ by measuring cAMP production

The effect of a reactive aldehyde (acrolein) or radical generator (AAPH) on the function of the $A_{2A}R$ was studied by measuring the cAMP production using the AlphaScreen cAMP detection kit in cells subjected to treatments with acrolein and AAPH.

First, the cAMP assay was tested on untreated cells to determine its sensitivity (EC$_{50}$ value) and dynamic range (EC$_{10}$ – EC$_{90}$). To extrapolate the amount of cAMP produced by the cells, a cAMP standard curve was prepared on each occasion. To accurately determine the cAMP levels, cell confluency and sample dilution were optimized to fit the sample measurements into the dynamic range of the cAMP standard curve. Cell confluency at 70-80% by the time of transfection was optimal, as higher cell densities saturated the assay and gave cAMP values outside the dynamic range of the standard curve.

To determine the optimal cell lysate dilution, transfected HEK293T cells were stimulated with forskolin to induce cAMP production by adenylate cyclase activation (Figure 5.11A). The maximum capacity of cAMP production by the cells was determined by bypassing the activation of the A$_{2A}$R. As cAMP concentrations in the standard curve increased, the AlphaScreen signal decreased, indicating that the free standard cAMP was competing for the anti-cAMP antibody on the acceptor bead and, thus, decreased the interaction with the Donor beads. Similarly, increasing concentrations of forskolin induced cAMP production in the cells, which could be translated into a decrease in the AlphaScreen signal.

The dynamic range of the cAMP standard curve was between 85401 AlphaScreen cps (EC$_{10}$), and 10802 AlphaScreen cps (EC$_{90}$). Results from HEK293T cell activation by forskolin without diluting the samples were between 14847 and 5459 AlphaScreen cps; hence, most of the data points of the curve were within the dynamic range of the standard. Cell lysates were subsequently diluted ten-fold, and cAMP values then ranged from 77957 to 14231 AlphaScreen cps, thus, fitting the dynamic range. This allowed the accurate quantification of the cAMP levels.

Similarly, cAMP production stimulated by NECA in transfected and non-transfected HEK293T cells was measured. Transfected cells were stimulated with increasing concentrations of NECA, and cell lysates were either undiluted or diluted ten-fold (Figure 5.11B). NECA stimulated cAMP production by activating the A$_{2A}$R, as a decrease in the AlphaScreen signal was observed in an agonist-concentration-dependent manner. The dynamic range of the cAMP standard curve was compressed between 117009 AlphaScreen cps (EC$_{10}$), and 13639 AlphaScreen cps (EC$_{90}$). Undiluted samples ranged from 42613 to 15776 AlphaScreen cps, whereas diluted samples ranged from 66494 to 15775 AlphaScreen cps. These results suggested that diluted and undiluted samples were in the dynamic range, although diluted samples were more centred. On the other hand, non-transfected cells had higher values of AlphaScreen cps, ranging from 157452 to 26513 AlphaScreen cps, which suggested lower endogenous cAMP production compared to the transfected cells. Furthermore, cAMP production by non-transfected cells had a NECA LogEC$_{50}$ of -4.792, whereas it was -7.213 for the undiluted and transfected cells, and -7.173 for the diluted and transfected cells. This suggested that lower concentrations of NECA were required

I. Company Marin, PhD Thesis, Aston University 2024

to induce 50% of the maximum cAMP production when cells were overexpressing the $A_{2A}R$, compared to non-transfected cells.

cAMP production was quantified by data interpolation with the cAMP standard curve. Forskolin induced an increase in cAMP levels in a concentration-dependent manner in both diluted and undiluted transfected samples (Figure 5.11C). Although higher cAMP values were obtained for the undiluted samples, it was not possible to calculate them for data points outside the dynamic range. Furthermore, these had high SD values, indicating a wide dispersion of the data when the samples were not diluted. In contrast, cAMP could be quantified for all the data points of the diluted samples. In this case, cAMP ranged from 0.04 fmol in the absence of forskolin, to 1.3 fmol with 100 µM forskolin.

cAMP levels were quantified after NECA stimulation (Figure 5.11D). NECA increased cAMP production in a concentration-dependent manner in both non-transfected and transfected cells that were either diluted or undiluted. The highest cAMP production was detected in the undiluted transfected samples, in which cAMP ranged from 0.14 fmol in the absence of NECA to 0.86 fmol at 100 µM NECA with high SD values, whereas it ranged from 0.07 to 0.78 fmol in the diluted transfected samples. Therefore, NECA stimulation of transfected cells caused comparable cAMP production to forskolin stimulation after sample dilution (Figure 5.11C). Nevertheless, it is worth noting that the cAMP standard curve had higher AlphaScreen signal values compared to the standard curve for forskolin stimulation, indicating slightly lower cAMP concentrations. Finally, NECA stimulation also increased cAMP production in non-transfected cells, although only a few data points could be calculated as most of them were not within the dynamic range. In this case, 100 µM NECA induced total production of 0.3 fmol of cAMP.

I. Company Marin, PhD Thesis, Aston University 2024
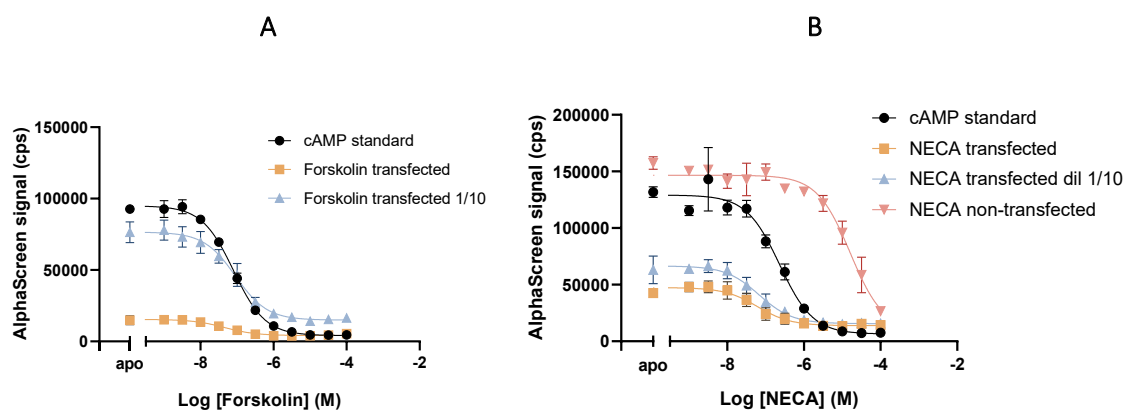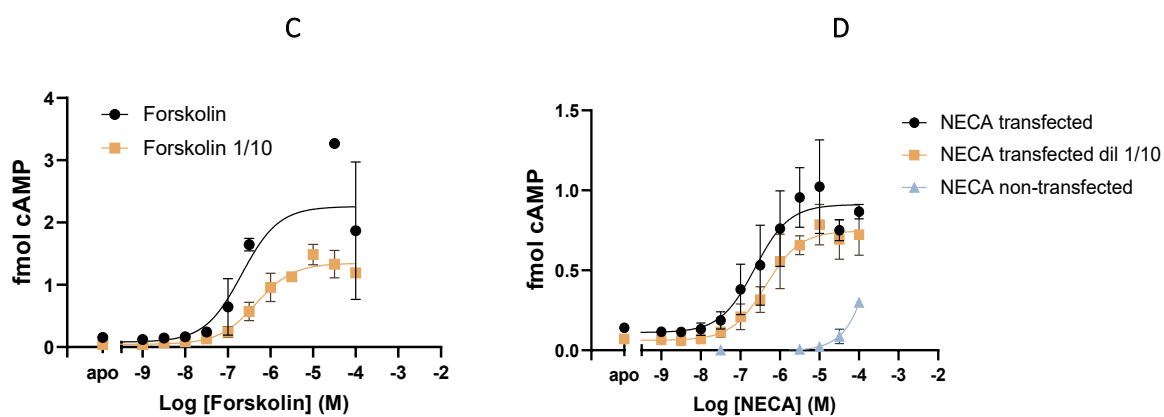
*Figure 5.11. cAMP production measured as AlphaScreen signal and fmoles of cAMP in HEK293T cells stimulated by Forskolin and NECA. Transiently transfected HEK293T cells expressing the $A_{2A}R$, or non-transfected cells, were stimulated with (**A**) Forskolin or (**B**) NECA, and cAMP production was measured as AlphaScreen signal and plotted against the logarithm of the agonist concentration before and after sample dilution. cAMP production was quantified by interpolation with the cAMP standard curve after cell stimulation with (**C**) Forskolin or (**D**) NECA, and plotted against the logarithm of the agonist concentration. Data are presented as the mean of all replicates (n=3) ± SD.*

To study the effect of acrolein and AAPH on the function of the $A_{2A}R$, transfected HEK293T were either treated with vehicle (1X PBS) as a negative control, or with acrolein and AAPH as oxidative treatments. cAMP production stimulated with NECA was measured after cell treatment for 2 and 24 hours (Figure 5.12 A and B).

All data points fell within the dynamic range of the standard curve. In both cases, the untreated controls had higher AlphaScreen signal values than the treated samples. Therefore, a major production of cAMP in treated cells was observed after $A_{2A}R$ activation with NECA.

NECA $LogEC_{50}$ values were calculated (Table 5.2), and the results indicated that treated samples after 2 and 24 hours had lower NECA EC_{50} values, suggesting that lower concentrations of agonists were required to induce 50% of the maximum cAMP production, compared to the untreated samples.

cAMP levels were quantified by interpolation with the standard curves. In all cases, NECA increased the cAMP levels in a concentration-dependent manner (Figure 5.12C), and treated samples showed higher cAMP production than the untreated controls. Statistical analysis by One-way ANOVA indicated that acrolein and AAPH-treated samples had significantly higher values than the untreated control for all data points, including the apo control in the absence of NECA (Figure 5.12C). In contrast, the acrolein- and AAPH-treated samples were not significantly different. This suggested that the oxidative treatments induced cAMP production in cells in the absence of $A_{2A}R$ agonist, and NECA increased its production through $A_{2A}R$ activation.

Cells subjected to the treatments for 24h exhibited higher cAMP production than the untreated control (Figure 5.12D), consistent with the findings from the 2h treatment. Noticeably, cAMP levels with 100 µM NECA in samples treated for 24h were 20-fold lower of those in samples treated for 2h. Statistical analysis indicated that acrolein and AAPH-treated samples had significantly higher cAMP values than the untreated control for all data points, including the apo control in the absence of NECA (Figure 5.12D).
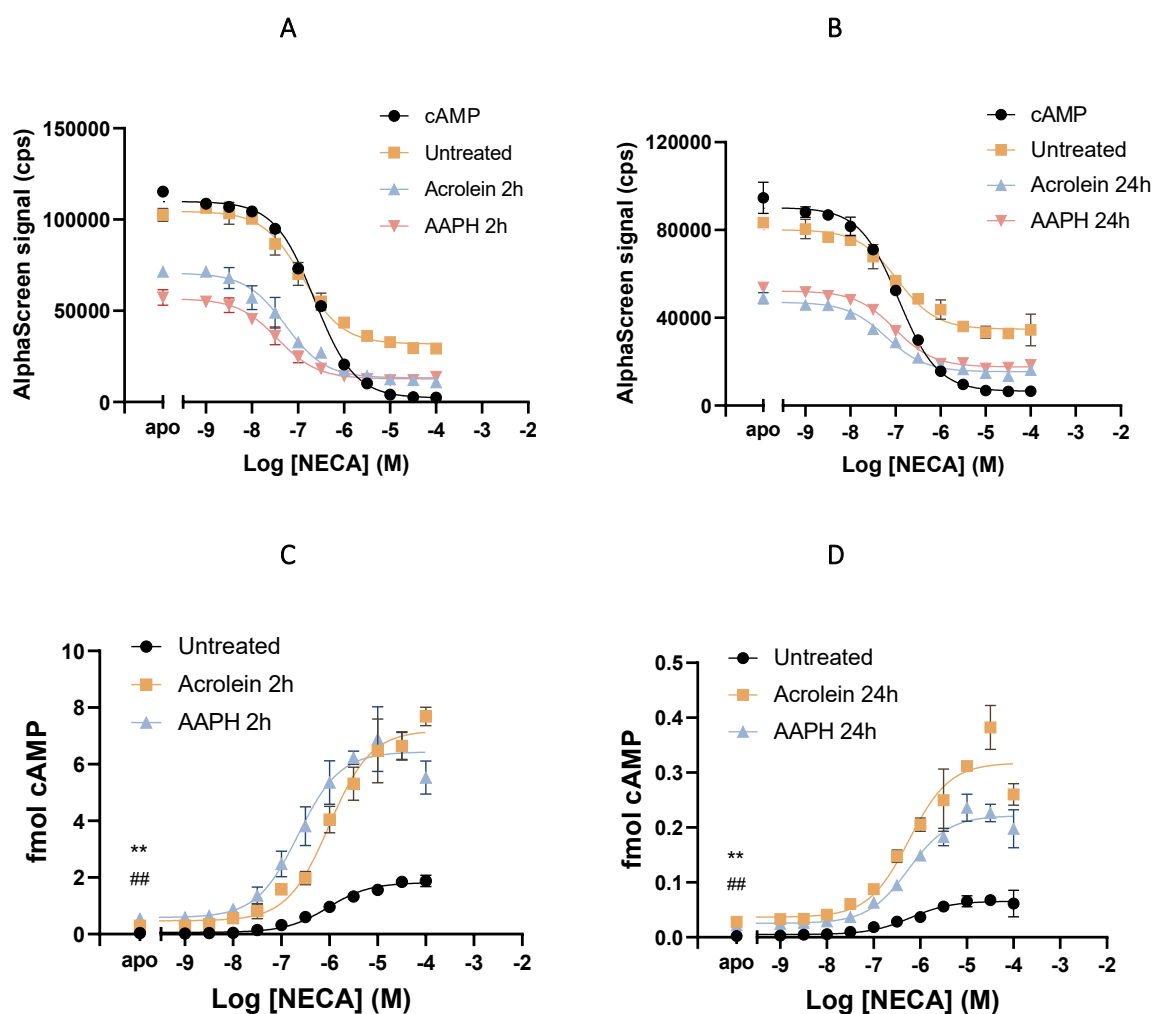
Figure 5.12. Effect of acrolein and AAPH on cAMP production in HEK293T cells stimulated with NECA. *Transiently transfected HEK293T cells expressing the $A_{2A}R$ were either untreated or treated with acrolein and AAPH for (**A**) 2 or (**B**) 24 hours. cAMP production was measured as AlphaScreen signal and plotted against the logarithm of NECA (M). cAMP production was quantified by interpolation with a cAMP standard curve and plotted against the logarithm of NECA (M) after cell treatment for (**C**) 2 h or (**D**) 24 h. Data are presented as the mean of all replicates (n=3) ± SD. Statistical differences were determined by One-way ANOVA followed by Tukey's multiple comparisons test (**p-value<0.01 acrolein vs untreated; ##p-value<0.01 AAPH vs untreated).*

Table 5.2. NECA Log EC$_{50}$ for cAMP production measured as AlphaScreen signal in untreated and treated HEK293T cells with acrolein and AAPH.

	Untreated	Acrolein	AAPH
2 hours	-6.9	-7.27	-7.45
24 hours	-6.97	-7.21	-7.02

To assess whether the increased cAMP production in treated cells was primarily due to A$_{2A}$R activation, or whether it was influenced by downstream signalling pathways, non-transfected HEK293T cells were subjected to acrolein and AAPH treatments and cAMP production was stimulated using forskolin. All data points corresponding to the untreated, and acrolein- or AAPH-treated samples fell within the dynamic range of the standard curve. In both cases, the samples corresponding to the untreated controls had AlphaScreen signal values comparable to those of the treated samples, suggesting similar cAMP production, in contrast to the results obtained after NECA stimulation in transfected cells (Figure 5.13A and B).

Forskolin LogEC$_{50}$ values were calculated (Table 5.3). In contrast to the results obtained after NECA stimulation (Figure 5.12), acrolein and AAPH-treated samples showed slightly higher forskolin LogEC$_{50}$ values compared to the untreated controls. These findings suggested that slightly higher concentrations of forskolin were needed to induce 50% of the total cAMP production in the treated cells, compared to untreaded cells.

cAMP production induced by forskolin was quantified after the 2h treatments (Figure 5.13C). The results indicated that forskolin increased cAMP levels in a concentration-dependent manner and treated samples had slightly higher cAMP levels than the untreated control with 100 µM forskolin. Nevertheless, statistical analysis by One-way ANOVA indicated that no significant differences were detected between groups. This suggested that the oxidative treatments did not induce higher cAMP production by activating adenylate cyclase in cells and, thus, downstream the A$_{2A}$R. Additionally, cAMP production induced by forskolin in non-transfected cells was substantially lower than that induced by NECA in transfected cells after the treatments (Figure 5.12).

The results obtained after 24h of treatment indicated that forskolin increased cAMP production in a concentration-dependent manner, and cells subjected to the treatments had slightly higher cAMP production than the untreated control (Figure 5.13D). This is consistent with the results obtained for the 2h treatment. Indeed, cAMP levels in cells treated with acrolein were significantly higher than those in untreated cells stimulated with 100 µM forskolin, according to One-way ANOVA. However, AAPH-treated samples did not show a significant increase in cAMP production compared to the untreated control, indicating that acrolein treatment could contribute to cAMP production stimulated with

175

forskolin at high concentration. Interestingly, the maximum cAMP values with 100 µM forskolin after 24h of treatment were higher than those reached after 2h, in contrast to the results obtained after $A_{2A}R$ activation with NECA (Figure 5.12).
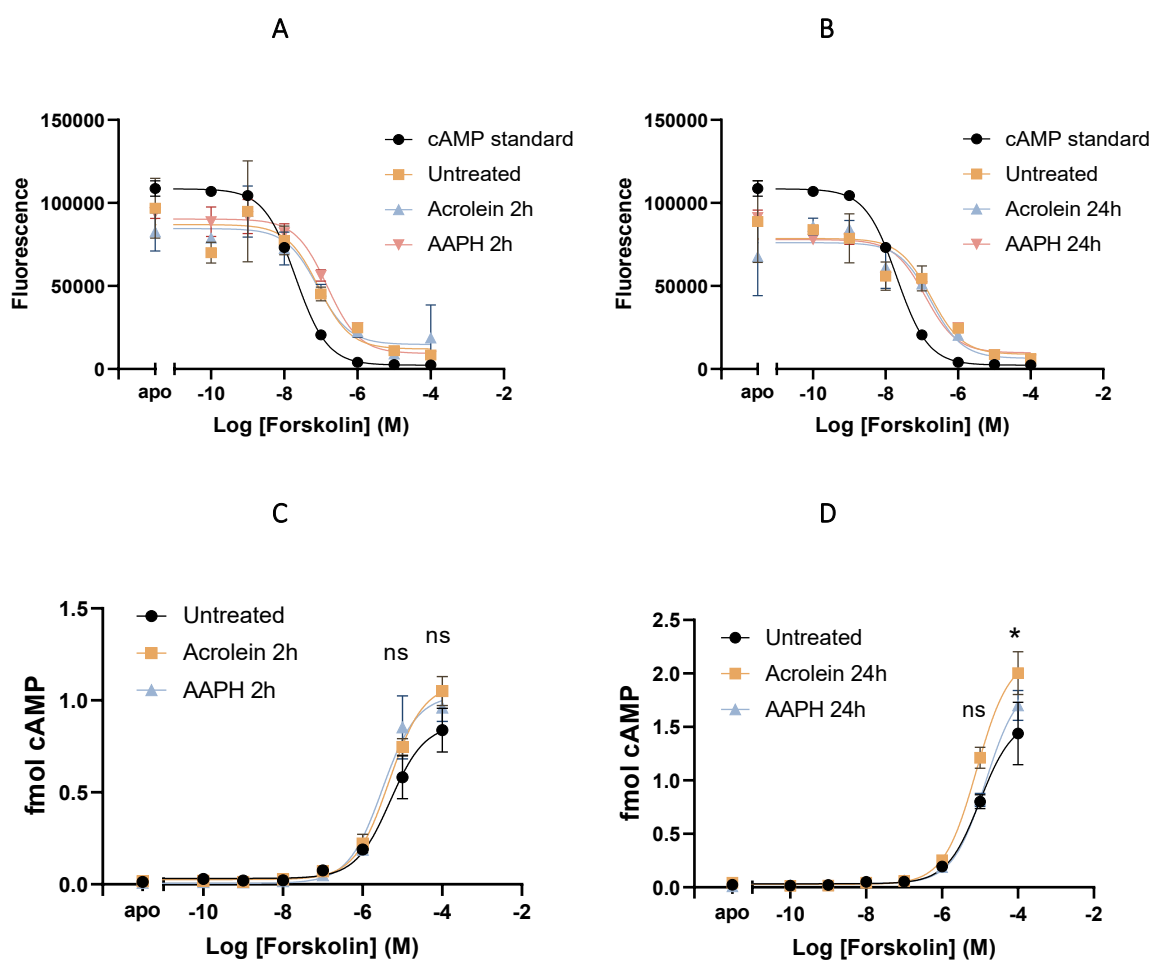
*Figure 5.13. Effect of acrolein and AAPH on cAMP levels produced in HEK293T cells stimulated with Forskolin. HEK293T cells were either untreated or treated with acrolein and AAPH for (**A**) 2h or (**B**) 24h. cAMP production was measured as AlphaScreen signal and plotted against the logarithm of Forskolin (M). cAMP production was quantified by interpolation with a cAMP standard curve, and plotted against the logarithm of Forskolin concentration after cell treatment for (**C**) 2h or (**D**) 24h. Data are presented as the mean of all replicates (n=3) ± SD. Statistical differences were determined by One-way ANOVA followed by Tukey's multiple comparisons test (*p-value<0.05 acrolein vs untreated).*

Table 5.3. Forskolin Log EC_{50} for cAMP production measured as AlphaScreen signal in untreated and treated HEK293T cells with acrolein and AAPH.

	Untreated	Acrolein	AAPH
2 hours	-7.06	-7.09	-6.82
24 hours	-6.76	-6.76	-6.9

5.4.7 Cell surface expression of the $A_{2A}R$ in transiently transfected HEK293T cells

To determine whether the increase in cAMP production stimulated by NECA was due to a higher expression of the $A_{2A}R$, receptor expression over time was tested by whole cell ELISA. Treated and untreated transfected cells were stimulated with NECA EC_{90} for a duration of one hour, with the interruption of receptor activation occurring at five-minute intervals. A decrease in the absorbance at 492 nm was observed for the untreated and treated samples from 5 to 40 minutes, whereas a subtle increase in the signal at 60 min was obtained (Figure 5.14A). Although the initial signal of the acrolein-treated samples was lower than that of the untreated and AAPH-treated cells, statistical analysis of the data by One-way ANOVA indicated that there were no significant differences between the three groups at 5, 20, and 40 minutes of stimulation. Nevertheless, acrolein and AAPH caused a significant increase in the signal at 60 minutes compared to the untreated control, but the treatments were not significantly different. This suggested an increase in the exposure of the $A_{2A}R$ on the cell surface of treated cells after receptor activation with NECA.

Data corresponding to cells subjected to a 24h treatment suggested that there was an increase in the absorbance at 492 nm from 5 to 60 minutes of incubation for the untreated and AAPH-treated samples (Figure 5.14B). Acrolein-treated cells showed a similar pattern, with an increase in the signal from 5 to 40 minutes of activation, whereas the signal decreased at 60 minutes. Nonetheless, the absorbance remained higher than the initial signal. Statistical analysis of the data indicated that there were no significant differences among the three experimental groups at different activation times. These results suggested that $A_{2A}R$ cell surface exposure did not differ between the groups over time upon activation with NECA.
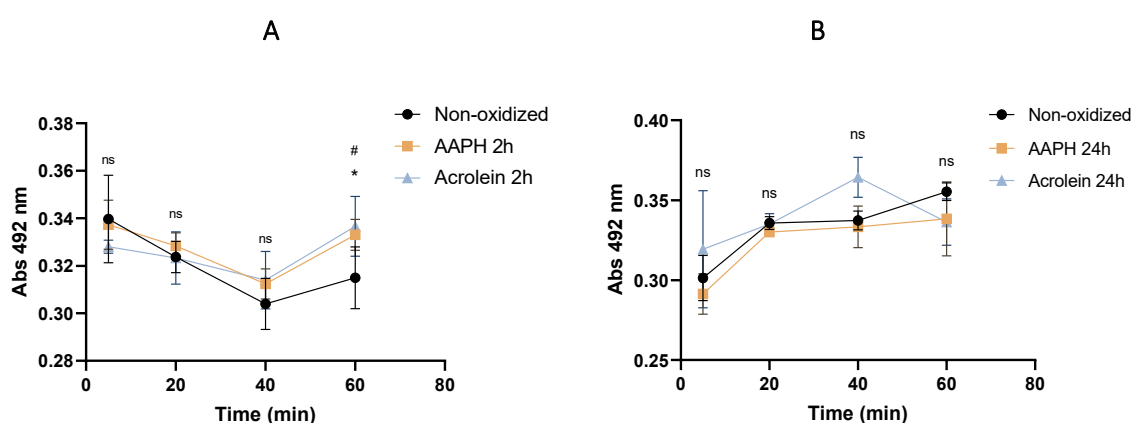
Figure 5.14. Cell surface expression of the $A_{2A}R$ in HEK293T cells measured by whole cell ELISA. Transiently transfected HEK293T cells expressing the $A_{2A}R$ were either untreated or treated with acrolein and AAPH for (A) 2h or (B) 24h. After cell stimulation with the $A_{2A}R$-agonist NECA at 1 µM, receptor expression on the cell surface over time was measured by whole cell ELISA. A specific primary antibody against $A_{2A}R$ and HRP-conjugated secondary antibody were used. The results were expressed as the

absorbance at 492 nm, corresponding to the TMB substrate signal. Data are presented as the mean of all replicates (n=3) ± SD. Statistical differences were determined by One-way ANOVA followed by Tukey's multiple comparison test (*p-value<0.05 acrolein vs untreated; #p-value<0.05 AAPH vs untreated).

5.5 DISCUSSION

This study aimed to examine the effect of oxidative stress and lipid oxidation products on $A_{2A}R$ function in mammalian cells. The first step was to create a construct to express the $A_{2A}R$ and clone it into an expression vector. HEK293T cells were transfected, and the transfection process was optimized. Next, the effect of acrolein and AAPH as oxidative treatments on cell viability was measured to determine the optimal treatment concentrations without harming cells. Lastly, the effect of the oxidative treatments on $A_{2A}R$ activity was investigated by measuring cAMP production and its effect on $A_{2A}R$ cell surface expression.

The key findings of this chapter were that the sequence that was designed and subcloned for the expression of the $A_{2A}R$ in mammalian cells served to express the functional protein, as verified by measuring the production of cAMP. Moreover, the oxidative treatments were found to upregulate the production of cAMP through the activation of the $A_{2A}R$, indicating that the function of the receptor was not impaired by the oxidative treatments.

The FLAG- and His-tagged C-terminal truncated $A_{2A}R$ sequence was successfully designed and subcloned into the pcDNA3 vector and transfected into HEK293T cells using PEI. $A_{2A}R$ overexpression was confirmed by western blotting, although the quality of the blots was not ideal. The $A_{2A}R$ was identified by LC-MS/MS, albeit with low scores and sequence coverage. It was found that acrolein and AAPH treatments decreased cell viability in a concentration-dependent manner, with the optimal concentrations being 20 µM for acrolein and 250 µM for AAPH without perturbing cell viability. Forskolin and NECA induced cAMP production in HEK293T cells in a dose-dependent manner, with a higher NECA EC_{50} value in non-transfected cells. In cells subjected to the oxidative treatments, increased cAMP production was observed with NECA stimulation compared to that in untreated controls, which was not observed with forskolin. No differential $A_{2A}R$ cell surface expression was detected between untreated and treated cells.

The C-terminal truncated sequence of the $A_{2A}R$ used in the present study encodes a stable, functional, and degradation-resistant protein (Prosser *et al.*, 2017). Moreover, it is well known that the long C-terminal tail is dispensable for receptor folding and dimerization (Hinz *et al.*, 2018). Most structural studies of the $A_{2A}R$ have considered the use of C-terminal truncated sequences appropriate for their

investigations, similar to this study (Jaakola *et al.*, 2008; Doré *et al.*, 2011; Hino *et al.*, 2012; Cheng *et al.*, 2017; García-Nafría *et al.*, 2018b; Lee *et al.*, 2020). Notwithstanding, the cDNA sequence encoding the $A_{2A}R$ has been used for protein expression in mammalian cells for functional and pharmacological studies (Arnault Massink *et al.*, 2015; Jamshad *et al.*, 2015; Franco *et al.*, 2019; McGraw *et al.*, 2019).

In the present study, the C-terminal truncated $A_{2A}R$ was expressed in transiently transfected HEK293T cells using lipofectamine and PEI as transfection agents. Different transient transfection methods have been validated to characterize the $A_{2A}R$ in mammalian cells. Similar to the methodology employed in the present study, transient transfection of mammalian cells using PEI has been used on several occasions to contribute to the characterization of the $A_{2A}R$ (Suzuki *et al.*, 2011; Jamshad *et al.*, 2015; Lanznaster *et al.*, 2019). However, alternative transfection methods, including lipofectamine (Hinz *et al.*, 2018), TransFectin^{TM} Lipid Reagent (Fernández-Dueñas *et al.*, 2012, 2013), and calcium phosphate precipitation (Ferré *et al.*, 2002) have been used. On the other hand, stable cell lines expressing the $A_{2A}R$ have been used on several occasions (Mediavilla-Varela *et al.*, 2017; Masih *et al.*, 2020; Skopál *et al.*, 2023). Mammalian cell transient transfection has certain limitations. This commonly results in lower protein yields than those achieved in stable cell lines, thus limiting experiments in which substantial amounts of protein are required. Moreover, protein expression has a limited duration, as the plasmid is diluted during cell division. Hence, it is unsuitable for studying protein activity for longer than 72 h, which limits the characterization of the $A_{2A}R$ under oxidative conditions. Consequently, to ensure efficient protein expression, the effect of the oxidative treatments on the function and expression of the $A_{2A}R$ in the present study was studied for a maximum duration of 24h. Moreover, each transfection may result in different protein yields, leading to batch-to-batch variability, which can affect the cAMP production after $A_{2A}R$ stimulation with NECA. Finally, transfection reagents can be cytotoxic, affect cell viability, and induce cell stress, altering the activity of the $A_{2A}R$ (Savage *et al.*, 2013; Stepanenko and Heng, 2017; Fus-Kujawa *et al.*, 2021).

Several strategies were attempted to demonstrate the $A_{2A}R$ expression, including western blotting, whole cell ELISA, and protein identification by LC-MS/MS. Western blotting and *whole-cell ELISA* were used as qualitative techniques to detect the $A_{2A}R$. However, the limitation of these techniques is that they do not allow the transfection efficiency to be determined. In the present study, a smear on the western blot was observed when detecting the $A_{2A}R$. This could be attributed to the cell lysate preparation using a detergent, resulting in a thick solution. This could influence the migration of proteins through SDS-PAGE gel, preventing protein packing into single bands. Alternatively, incomplete $A_{2A}R$ denaturation during sample preparation can result in the formation of protein complexes, leading to smearing (Mahmood and Yang, 2012).

Incomplete protein denaturation can also result in an ineffective $A_{2A}R$ in gel digestion by trypsin and chymotrypsin, leading to the low sequence coverage observed by LC-MS/MS. The $A_{2A}R$ structure can hinder protease accessibility to potential cleavage sites if the secondary structure of the protein is not fully denatured in the gel (Min *et al.*, 2015). Moreover, insufficient sample amounts containing low protein concentrations and other impurities can reduce the digestion efficiency. This may be the case in the present study, where a low protein concentration was obtained from cell transfection in whole lysates, without prior protein purification. Alternative proteases, and digestion strategies, as well as protocol optimization and protein purification, can be employed.

Once the $A_{2A}R$ was properly expressed in mammalian cells, the effect of acrolein and AAPH on the function of the $A_{2A}R$ was studied, and cell viability assays were performed on HEK293T cells subjected to oxidative treatments. MTT assays have been used previously to assess the effect of oxidative stress on mammalian cell viability (Guan *et al.*, 2012; Chang and Pumera, 2013; Bala *et al.*, 2022). The findings of the current work align with previous publications regarding the decrease in cell viability induced by AAPH at the specific concentrations and incubation times (Duan *et al.*, 2016; Hu *et al.*, 2017; Ariza *et al.*, 2018; Parathodi Illam *et al.*, 2019). In contrast, higher concentrations of AAPH, in the range of 30-60 mM, were required to induce a reduction in HaCaT cell viability comparable to that in HEK293T cells in the present study (Maciel *et al.*, 2014; Chou *et al.*, 2019). This could be due to the higher sensitivity of HEK293T cells to AAPH than that of other cell lines, or to the development of antioxidant resistance in cells after treatment with high concentrations of oxidants (Cui *et al.*, 2004). Similarly, the findings of this study align with prior publications regarding the decrease in cell viability induced by acrolein at the specific concentrations and incubation times (Wang *et al.*, 2016; Sousa *et al.*, 2019; Gupta *et al.*, 2021). The acrolein concentrations used in these studies, which were comparable to those used in the present study (20 µM), were lower than those found under physiological conditions in human serum (50 µM) (Satoh *et al.*, 1999; Lovell *et al.*, 2001; Hamann *et al.*, 2008). Nevertheless, other studies on HEK293T cells demonstrated a higher cell sensitivity to acrolein than that observed in the present study (Jaganjac *et al.*, 2010). Comparably, studies on HT22 cells demonstrated that treatment with 25 µM acrolein for 24h significantly decreased cell viability (below 80%) (Huang *et al.*, 2013). However, the 2h treatment did not decrease cell viability, which is comparable to the results of this study. Similar results were reported in other studies (Zhang *et al.*, 2011; Yin *et al.*, 2020). Comparably, 1 µM acrolein significantly decreased PC12 cell viability compared to that of the untreated control (Luo *et al.*, 2005).

Although lipid oxidation and oxidative stress could not be confirmed in the present study, these previous studies demonstrated that AAPH and acrolein at the concentrations used induced oxidative stress and an inflammatory response in cells in a dose- and time-dependent manner by activating COX-2 (Chou *et al.*, 2019), and increasing ROS levels (Hu *et al.*, 2017; Ariza *et al.*, 2018, Yin *et al.*, 2020) and

TBARs levels (MDA) (Duan *et al.*, 2016; Huang *et al.*, 2013; Parathodi *et al.*, 2019). On the other hand, AAPH and acrolein decreased cellular antioxidant activity, inhibiting Nrf2 (Chou *et al.*, 2019), GPx activity (Hu *et al.*, 2017), GHS, and catalase levels (Zhang *et al.*, 2011; Parathodi *et al.*, 2019; Gupta *et al.*, 2021), compared to the unoxidised control. Hence, different studies have evaluated the effect of APPH and acrolein on cell viability, and it has been demonstrated that both induce oxidative stress and lipid peroxidation in cells. Consequently, it is hypothesised that lipid oxidation should be occurring under the treatment conditions used in the current study.

Once appropriate oxidative treatment conditions had been established, the effect on $A_{2A}R$ function in its native environment was explored by measuring cAMP levels. Similar to the present study, cAMP production in HEK293T cells overexpressing the $A_{2A}R$ has been reported in numerous studies (Arnault Massink *et al.*, 2015; Igonet *et al.*, 2018; Franco *et al.*, 2019; Lanznaster *et al.*, 2019). These demonstrated an increase in cAMP levels stimulated by $A_{2A}R$ agonists in a dose-dependent manner, as observed in here. Other articles have demonstrated inhibition of cAMP production by $A_{2A}R$ antagonists (Brandon *et al.*, 2006; Yang *et al.*, 2017; Sorrentino *et al.*, 2019). Thus, the measurement of cAMP to investigate $A_{2A}R$ function has been thoroughly validated, including its application in assessing the folding and functional state of the receptor in cells.

Forskolin, which directly activates the adenylate cyclase, is typically used as a control for cAMP assays. Some authors have reported higher cAMP production after adenylate cyclase stimulation than after $A_{2A}R$ stimulation (Franco *et al.*, 2019), while other studies suggested greater cAMP production with NECA than forskolin, which is more similar to the results obtained in this study, and with comparable EC_{50} values (Goulding *et al.*, 2018).

The NECA EC_{50} values observed in the present study are in good agreement with pharmacologically proven data (Yan *et al.*, 2003; Gao *et al.*, 2004; Welihinda *et al.*, 2016; Muller and Stein, 2022), although lower values have been obtained in other studies (Brandon *et al.*, 2006), indicating higher affinity and receptor response to agonist binding. Interestingly, Klinger and colleagues investigated the role of the C-terminal tail of the $A_{2A}R$ expressed in HEK293 cells in regulating cAMP production. They compared the $A_{2A}R$ stimulation with CGS21680 in cells expressing the full-length receptor to that in cells expressing the C-terminal truncated receptor. The results suggested that the truncated receptor showed reduced constitutive activity, resulting in lower basal cAMP levels, compared to the full-length $A_{2A}R$ (Klinger *et al.*, 2002). These findings suggested that the C-terminal tail of the $A_{2A}R$ plays a key role in regulating receptor activity and cAMP levels.

A similar NECA EC_{50} value but lower cAMP concentrations would be expected in non-transfected cells compared to transfected cells, caused by agonist binding to the $A_{2A}R$. However, the results showed that

I. Company Marin, PhD Thesis, Aston University 2024

the NECA EC_{50} value for cAMP production in non-transfected cells was higher than that in transfected cells. Comparable results were obtained by Igonet *et al.* (2018). Higher NECA EC_{50} values could be explained by the activation of other adenosine receptors in HEK293T cells. NECA is a potent agonist of adenosine receptors, with Ki values of 6.2, 14, 20, and 330 nM for A_3R, A_1R, $A_{2A}R$, and $A_{2B}R$, respectively. Hence, it activates with higher affinity A_1R and A_3R, and with lower affinity the $A_{2B}R$, compared to the $A_{2A}R$ (Gao *et al.*, 1999; Matharu *et al.*, 2001). A_1R and A_3R couple to the Gi protein, which inhibits adenylate cyclase and decreases cAMP production. Instead, $A_{2B}R$, similarly to $A_{2A}R$, couples to the Gs protein; therefore, it activates cAMP production through adenylate cyclase. Considering that HEK293T cells express the $A_{2B}R$ natively (Gessi *et al.*, 2005), the higher EC_{50} value in non-transfected cells could correspond to the activation of this adenosine receptor by NECA (Kalhan *et al.*, 2012; Gao *et al.*, 2018; Goulding *et al.*, 2018). Gao *et al.* demonstrated that NECA and forskolin significantly increased cAMP levels in HEK293T cells that endogenously express the $A_{2B}R$. However, NECA had a pEC_{50} value of 6.5, which was lower than that detected in non-transfected cells in the present study (Gao *et al.*, 2023). In contrast, other studies did not observe cAMP production in non-transfected HEK293T cells stimulated with $A_{2A}R$ agonists (Massink *et al.*, 2015). Hence, it has been demonstrated that the $A_{2A}R$ and $A_{2B}R$ are natively expressed in HEK293T cells, and both can be stimulated with NECA, although some controversy exists regarding the observed EC_{50} values, depending on the cell lines and experimental conditions.

Once the functionality of the $A_{2A}R$ was confirmed, the effect of stress induced by acrolein and AAPH was investigated. The observed increase in cAMP levels in the absence of ligands in cells overexpressing the $A_{2A}R$ could be explained by an increase in extracellular adenosine during oxidative stress, which activates the receptor to modulate inflammation and stress (Pasquini *et al.*, 2021). Moreover, an increase in cAMP levels through specifically stimulating the $A_{2A}R$ with NECA was observed, suggesting upregulation of the receptor under these conditions, potentially to modulate oxidative stress and inflammation (Castro *et al.*, 2020). Additionally, an increase in basal cAMP levels in cells under oxidative stress could be attributed to the activation of adenylate cyclase and a decrease in the activity of phosphodiesterases to counteract ROS production (Tanzarella *et al.*, 2019). Hussain *et al.* suggested that disruption of the redox balance can influence cAMP production by activating adenylate cyclase (Hussain *et al.*, 2023). Nevertheless, in contrast to the statements by Tanzarella *et al.* and Hussain *et al.*, Shim and colleagues observed that oxidative stress can decrease cAMP levels and PKA activity in astrocytes, which was associated with a protective mechanism against oxidation (Shim *et al.*, 2018). Hence, it has been suggested that an increase in cAMP levels might accelerate cell dysfunction during oxidative stress.

Despite these observations, an increase in the basal levels of cAMP in treated non-transfected cells with acrolein and AAPH was not observed in the present study, in comparison to the untreated controls. This suggests that differences in cAMP levels are probably related to $A_{2A}R$ expression and activity.

Investigating the effect of oxidation on the activity of the $A_{2A}R$ in a cellular context using oxidants, such as AAPH and acrolein, reflects a more physiologically relevant environment than isolated proteins or in vitro systems. This can provide insights into how oxidative stress may modulate GPCR function, and its implications in diseases involving $A_{2A}R$ signalling, including inflammation, neurodegenerative disorders, and cardiovascular diseases (Leone and Emens, 2018; Li *et al.*, 2018; Castro *et al.*, 2020; El-Shamarka *et al.*, 2020; Ikram *et al.*, 2020; Wang *et al.*, 2022). However, this methodology has some limitations. Cellular environments are highly complex, making it challenging to isolate the specific effects of lipid oxidation on the activity of the $A_{2A}R$ from alternative cellular responses. This is because oxidants, such as AAPH, can induce oxidative stress that affects various cellular components beyond this receptor (Zhao *et al.*, 2018). This leads to non-specific side effects and makes it challenging to attribute the observed changes solely to the activity of the $A_{2A}R$. Moreover, the results observed under oxidative conditions may be induced by changes in the membrane properties or downstream cell signalling (Itri *et al.*, 2014). Oxidative stress dynamics are influenced by the intensity and duration of cell exposure to oxidants; therefore, understanding how these dynamics affect the $A_{2A}R$ in a cellular context can be complicated. Additionally, different cell types may respond differently to oxidant treatments, and GPCR activity may be influenced by specific cellular environments (Baccouch *et al.*, 2022).

It is well established that GPCRs typically undergo internalization and trafficking from the plasma membrane into endosomes upon activation by an agonist (Pandey *et al.*, 2019). Measuring receptor internalization is a key readout for investigating ligand-binding GPCR function, and whole-cell ELISA has recently emerged as an attractive approach (Pandey *et al.*, 2019).

Pandey *et al*. demonstrated agonist-induced $A_{2A}R$ internalization in HEK293T cells measured using whole-cell ELISA (Pandey *et al.*, 2019), which could not be observed in here. A 20% decrease in $A_{2A}R$ surface expression was detected 5 and 10 min after activation, and a 30% decrease was observed from 20 to 60 min after activation. Agonist-induced $A_{2A}R$ internalization has been demonstrated in other studies (Burgueño *et al.*, 2003; Genedani *et al.*, 2005; Brand *et al.*, 2008). In contrast, other studies have suggested that the $A_{2A}R$ is resistant to agonist-induced internalization (Charalambous *et al.*, 2008; Zezula and Freissmuth, 2008). This resistance could be explained, in part, by the constitutive activity of the $A_{2A}R$, which might lead to receptor internalization, independent of agonist activation (Klinger *et al.*, 2002).

Mundell *et al*. suggested that the C-terminal truncated receptor was resistant to NECA-induced internalization, as measured by whole-cell ELISA (Mundell and Kelly, 2011). Instead, internalization of the wild type $A_{2A}R$ was demonstrated. Similar experiments were performed on the $A_{2B}R$ (Mundell *et al.*, 2010) and a subtle decrease in the C-terminal truncated $A_{2A}R$ cell surface expression was also observed, although it was maintained at >90% 30 min after ligand addition, and its expression increased after 60 min of activation (Mundell and Kelly, 2011). This was comparable to the results obtained in the present study after cell oxidation for 2h. Hence, the absence of receptor internalization and degradation upon agonist activation could be due to the use of the C-terminal truncated $A_{2A}R$. Mundell *et al*. reported that the rat $A_{2A}R$ contains five serine residues in the distal C-terminus that are crucial for receptor desensitization and internalization, whereas the human $A_{2A}R$ contains a single serine residue (Mundell and Kelly, 2011). Therefore, the regulation of the $A_{2A}R$ may be species dependent.

These results may also be attributed to inherent limitations in the methodology and potential inconsistencies in experimental results. For example, this methodology may not always distinguish between intracellular and membrane-localized receptors, and it can also detect receptors that are not fully functional or unproperly folded (Pandey *et al.*, 2019). Hence, it may overestimate receptor cell surface expression depending on the experimental conditions. Further optimization is required for a more accurate interpretation of the effects of these oxidative treatments on $A_{2A}R$ cell surface expression over time upon activation (Pandey *et al.*, 2019). Additional work is required to gain a more comprehensive understanding of the $A_{2A}R$ turnover dynamics under oxidative stress conditions.

Despite receptor endocytosis, it has been observed that these proteins have persistent signalling function to cAMP and MAPK pathways into endosomes. This intracellular signalling function is believed to have specific outcomes that differ from those of the plasma membrane (Calebiro *et al.*, 2010). Hence, although receptor internalization had been confirmed in the present study, it could be still functional and activate adenylate cyclase to produce cAMP. This challenges the traditional understanding of GPCR signalling and highlights the relevance of considering the subcellular localization and function of the $A_{2A}R$ in determining its function and signalling properties. Consequently, further analysis of the effects of oxidative stress on $A_{2A}R$ function is required.

The methodology employed in this chapter could be applied to study other GPCRs and membrane proteins in mammalian cells. Moreover, studying the effects of AAPH and acrolein on the function of the $A_{2A}R$ can be extrapolated to the study of other oxidised lipids or radical generators on the activity of this receptor, as well as their effect on cell viability.

To further validate the results obtained, the effects of oxidative treatments on other downstream signalling pathways, including PKA expression, CREB phosphorylation, and anti-inflammatory

interleukin expression, should be tested. Moreover, analysing ERK phosphorylation, NF-kB, and proinflammatory interleukin expression, or alternative pathways, such as intracellular calcium levels, would be of great interest. On the other hand, the effect of the oxidative treatments on other adenosine receptors natively expressed in HEK293T cells, which contribute to the regulation of cAMP levels in the cells, should be considered. Alternatively, the study of the effect of oxidative stress on the function of the $A_{2A}R$ in an isolated system, rather than in a cellular context, could provide a more accurate understanding of the close relationship between the receptor and oxidation. In addition, an optimization of the study of receptor expression on the cell surface is proposed to further comprehend the increase in cAMP production in the cellular context under the experimental conditions. Finally, the oxidative stress induced by AAPH and acrolein should be assessed, and lipid oxidation could be confirmed by LC-MS/MS.

In conclusion, the C-terminal truncated $A_{2A}R$ sequence served to overexpress the functional receptor in transfected HEK293T cells, whose viability was affected by acrolein and AAPH as oxidative treatments. The effect of treating HEK293T cells with increasing concentrations of AAPH on cell viability was shown for the first time. Similarly, determination of the influence of oxidative stress on the function of the $A_{2A}R$ in a cellular context, measured by cAMP production, has been pioneered. The function of this receptor was not impaired under oxidative stress conditions. Instead, the downstream receptor signalling pathways were upregulated, which could not be attributed to the reduced receptor internalization upon activation. This provides insights into the effects of oxidative stress on adenosine receptors and other GPCRs, which have been investigated as drug targets to treat inflammatory diseases involving oxidative stress.

6. CHAPTER 6 - CONCLUSION AND FUTURE PERSPECTIVES

The overall aim of this study was to investigate the effects of oxidative stress, lipid oxidation, and protein lipoxidation on the activity of the $A_{2A}R$. In order to achieve this, it was necessary to express the $A_{2A}R$ in two validated expression systems, *P. pastoris* SMD1163 and HEK293T mammalian cells, to study the receptor properties under physiological and oxidative stress conditions.

P. pastoris was used for the expression and solubilization of the $A_{2A}R$ using polymers and detergents. SMA2000 was the most efficient polymer for the solubilization of the receptor, compared to different DIBMA polymers. This allowed $A_{2A}R$ solubilization and purification, together with its native membrane environment, permitting protein characterization in the presence of lipids, which are crucial for GPCR structure and function (Pan *et al.*, 2022; Levental *et al.*, 2023). In contrast, detergents, such as DDM, which are typically used for membrane protein characterization, strip out the surrounding lipids (Singh *et al.*, 2012). This makes the use of polymers advantageous for membrane protein characterization (Jamshad *et al.*, 2015). Moreover, $A_{2A}R$ solubilized with DDM could not be purified away from the mADH contaminant, which limited protein characterization in subsequent experiments. Instead, $A_{2A}R$-SMALP could be isolated from other *P. pastoris* proteins after extensive optimization.

Liquid chromatography coupled to tandem mass spectrometry (LC-MS/MS) was used to identify the in-gel digested $A_{2A}R$-SMALP using trypsin and chymotrypsin. Although the $A_{2A}R$ monomer and dimer could be identified after protein digestion optimization, the sequence coverage obtained was 4% for the monomer digested with trypsin, and 16% for the monomer digested with chymotrypsin. This low sequence coverage limited the identification of $A_{2A}R$-oxidised lipid adducts under oxidative stress conditions. The sequence coverage was comparable to that obtained for the $A_{2A}R$ expressed in HEK293T cells. Despite this limitation, purified $A_{2A}R$-SMLAP was identified by in-gel digestion and LC-MS/MS for the first time. This study pioneered the identification of the $A_{2A}R$ using LC-MS/MS with the aim of characterising protein-lipid adducts that may occur under oxidative stress conditions, and this approach could in the future be applied more broadly to study other membrane proteins.

Additionally, $A_{2A}R$ solubilization with SMA2000 allowed the identification of annular lipids that surround the receptor and co-purify into the $A_{2A}R$-SMALP. These lipids were compared to those in *P. pastoris* bulk membranes and those solubilized with SMA2000 prior to receptor purification. PC and PE were the predominant phospholipid classes across all three experimental groups, followed by PS. In contrast, PG, PI, and LPL signals were less abundant. The most abundant phospholipids contained mono- and polyunsaturated fatty acyl chains of 34, 36, or 38 carbon atoms. These findings are in good agreement with previous studies on the *P. pastoris* lipidome, which has been extensively characterized (Yu *et al.*, 2022), and fatty acid unsaturation has been suggested to contribute to GPCR activity (Yang and Lyman,

I. Company Marin, PhD Thesis, Aston University 2024

2019). The A_{2A}R-SMALP showed some differences in its phospholipid content compared to that of *P. pastoris* bulk membranes. The A_{2A}R-SMALP was enriched in anionic lipids, including PS, PG, and PI, which have been suggested to stabilize the active conformation of the receptor (Dawaliby *et al.*, 2016; Bruzzese *et al.*, 2018), whereas the bulk membranes were rich in zwitterionic lipids, including PC and LPE.

There has been limited characterization in the literature of the lipids that co-purify with membrane proteins solubilized in lipid particles (Routledge *et al.*, 2020); this study is the first to report an in-depth analysis of the co-purified A_{2A}R lipid environment in SMALPs using novel mass spectrometry equipment and methodologies. Overall, this investigation contributes to the understanding of the importance of lipids in the functioning of membrane proteins, which have implications for receptor activity and the consequent cell signalling to modulate biological processes (Pan *et al.*, 2022; Levental *et al.*, 2023). A limitation of this methodology is that the lipids that form direct interactions with the A_{2A}R cannot be identified. Instead, annular lipids were characterised, which can be closer to or further from the protein within the SMALP, and therefore can be more or less relevant to protein activity (Serebryany *et al.*, 2012).

This methodology can be used to identify oxidised lipids that closely surround the A_{2A}R and other membrane proteins under oxidative stress conditions. Alternatively, oxidised and unoxidised lipids that can be covalently attached to the A_{2A}R could be identified by protein analysis using LC-MS/MS after protein digestion with a high sequence coverage (Sousa *et al.*, 2019). Lipid oxidation can occur in inflammatory diseases, including cardiovascular and neurodegenerative diseases, and it may influence protein function (Zhong *et al.*, 2019).

Within the SMALP, the A_{2A}R appeared to be folded and able to undergo conformational changes upon ligand binding according to the analysis of Trp fluorescence and radioligand binding assays. Notably, addition of the antagonist to the apo A_{2A}R-SMALP increased Trp fluorescence, which suggests that protein conformational changes were occurring (Ghisaidoobe and Chung, 2014). This suggested that a considerable number of apo receptors were sampled in the active or intermediate active conformations. This could be explained by the constitutive activity of the apo A_{2A}R in a favourable lipid environment enriched in anionic lipids, such as PG (Ye *et al.*, 2016; Bruzzese *et al.*, 2018), as corroborated by LC-MS/MS in the present study. Moreover, the A_{2A}R-SMALP was able to transition from the active to the inactive conformation and vice versa upon the addition of ligands, whereas this could not be detected for the A_{2A}R-DDM. The work reported in this study demonstrated that ligand binding and membrane protein conformational changes can be studied using Trp fluorescence in its native environment without protein modification in agreement with previous studies (Routledge *et al.*, 2020).

I. Company Marin, PhD Thesis, Aston University 2024

Treatment with AAPH and acrolein did not prevent the $A_{2A}R$-SMALP from radioligand binding or undergoing conformational changes. This suggested that the oxidative treatments did not cause major modifications to the secondary and tertiary structures of the protein, allowing it to remain properly folded and responsive to ligand binding (Fraser, 2006). However, lipid oxidation and protein lipoxidation induced by the oxidative treatments could not confirmed, representing a limitation of this study. This could be addressed in the future through the analysis of oxidised lipids using LC-MS/MS and improving the $A_{2A}R$ sequence coverage observed by in-gel digestion and LC-MS/MS to detect the formation lipid-protein covalent adducts.

These results are in good agreement with the thermal unfolding profile of the untreated and treated $A_{2A}R$-SMALP and $A_{2A}R$-DDM, which showed similar melting temperatures using CPM fluorescence and suggested that the oxidative treatments did not modify the thermostability of the solubilized protein. Nevertheless, these results should be considered in terms of methodological limitations, as Trp fluorescence, CPM fluorescence, and radioligand binding assays can be highly influenced by the sample solubilization method, buffer composition, and the presence of other protein contaminants, such as mADH in the $A_{2A}R$-DDM sample (Alexandrov *et al.*, 2008; Nehmé *et al.*, 2017). It is possible that the lack of effect of the oxidative treatments on $A_{2A}R$ activity was due to a lack of oxidative modification on the lipids and the receptor, which could not be detected in this study. However, previous studies have demonstrated using LC-MS/MS that AAPH and acrolein, with equal concentrations to the ones used in this study, have resulted in lipid oxidation and protein lipoxidation, consequently reducing protein activity (Covey *et al.*, 2010; Duan *et al.*, 2016; Parathodi Illam *et al.*, 2019; Sousa *et al.*, 2019). The novelty of this study was the investigation into the effects of oxidative treatments on conformational changes, thermostability, and ligand binding on the $A_{2A}R$. This contributed to the understanding of the behaviour of membrane proteins under oxidative stress conditions.

It was demonstrated that the function of the $A_{2A}R$ expressed in mammalian HEK293T cells was not impaired by the oxidative treatments when measuring cAMP levels. Instead, cAMP production was upregulated in the transfected cells treated with AAPH and acrolein. The oxidant concentrations used in this study did not significantly reduce cell viability; however, they previously have been shown to induce oxidative stress and lipid peroxidation in cells (Luo *et al.*, 2005; Huang *et al.*, 2013; Yin *et al.*, 2020). Indeed, under these conditions, cAMP production increased with the $A_{2A}R$ agonist in a dose-dependent manner. In contrast, this was not observed after adenylate cyclase activation with forskolin in the non-transfected cells, showing that adenylate cyclase was not responsible for the effect. Instead, this suggested an upregulation of the $A_{2A}R$ resulting in an increase in cAMP in response to oxidative stress as a negative feedback loop to control inflammation (Tavares *et al.*, 2020). As no change in $A_{2A}R$ cell surface expression was detected, this suggested that the activity of the $A_{2A}R$ was upregulated under

I. Company Marin, PhD Thesis, Aston University 2024

oxidative stress conditions. Investigating receptor internalization upon ligand binding under oxidative stress conditions would be of great interest for understanding the upregulation of downstream signalling pathways. These results were consistent with those from the characterization of the solubilized A$_{2A}$R-SMALP under oxidative conditions; the in vitro analysis of the A$_{2A}$R conformation, stability, and ligand binding under oxidative treatments, and the study of the protein function in the cellular environment revealed no impairment.

The effect of activating or inhibiting the A$_{2A}$R on the treatment of inflammatory conditions has been extensively explored (Leone and Emens, 2018; Li *et al.*, 2018; Castro *et al.*, 2020; El-Shamarka *et al.*, 2020; Ikram *et al.*, 2020; Wang *et al.*, 2022) but, this is the first report of the impact of oxidative stress on the function, structure, and conformation of the A$_{2A}$R. Investigating the effect of oxidation on the activity of the A$_{2A}$R in a cellular context reflects a more physiologically relevant environment than isolated proteins or in vitro systems. Nonetheless, cellular environments are highly complex, making it challenging to isolate the specific effects on the A$_{2A}$R from alternative cellular responses (Zhao *et al.*, 2018). To overcome this, more extensive characterization of A$_{2A}$R downstream signalling pathways could be explored, including the analysis of PKA expression and ERK phosphorylation. Additionally, lipid peroxidation and A$_{2A}$R lipoxidation on HEK293T cell should be confirmed to make this study robust. Demonstrating the presence of oxidised lipids around the protein or protein lipoxidation would help determine the mechanism by which this membrane protein can be modulated under oxidative stress conditions (Duan *et al.*, 2016; Illam *et al.*, 2019).

Overall, this study demonstrated the feasibility of characterizing the ligand binding capability, conformational changes, and thermostability of the A$_{2A}$R expressed in *P. pastoris* in its native lipid environment using SMA2000. Moreover, this approach allowed characterization of the lipid environment that was co-purified with the receptor by LC-MS/MS. The methodology enabled investigation of the effect of lipid oxidation and protein oxidation on the A$_{2A}$R properties, revealing no significant alterations compared to unoxidised controls. This aligns with the observations of oxidation effects on the function of the A$_{2A}$R expressed in mammalian cells, where cAMP was upregulated under oxidative conditions. However, it remains essential to confirm lipid oxidation and protein lipoxidation using LC-MS/MS to comprehensively understand the impact of oxidative treatments on this membrane protein.

In the realm of biochemistry, this study contributed to the characterization of a membrane protein in its lipid environment under oxidative conditions, and the results challenge conventional assumptions regarding membrane protein susceptibility to oxidative stress. The results point to the importance of investigating lipid peroxidation in the receptor-lipid environment, as well as the analysis of protein

lipoxidation on the $A_{2A}R$ and other membrane proteins to expand the understanding of oxidative impact on protein structures. In terms of cell signalling, in a cellular context with intricate regulatory responses to oxidative stress, an upregulation of the $A_{2A}R$ and its capacity to increase cAMP production under oxidative conditions highlights its potential in modulating inflammatory processes. In the broader context of pathophysiology, these findings have implications for understanding diseases where oxidative stress plays a significant role, and contribute to understanding the role of the $A_{2A}R$ in the cellular anti-inflammatory response under oxidative conditions, representing a natural mechanism against oxidative damage in vivo.

7. REFERENCES

Aalst, Evan van, and Benjamin J. Wylie. "Cholesterol Is a Dose-Dependent Positive Allosteric Modulator of CCR3 Ligand Affinity and G Protein Coupling." Frontiers in Molecular Biosciences, Sec. Biophysics, Volume 8, 2021. https://doi.org/10.3389/fmolb.2021.724603.

Adada, Mohamad, Chiara Luberto, and Daniel Canals. "Inhibitors of the Sphingomyelin Cycle: Sphingomyelin Synthases and Sphingomyelinases." Chemistry and Physics of Lipids, Volume 197, May 2016, Pages 45-59, 2016. https://doi.org/10.1016/j.chemphyslip.2015.07.008.

Adams, Mark N., Melinda E. Christensen, Yaowu He, Nigel J. Waterhouse, and John D. Hooper. "The Role of Palmitoylation in Signalling, Cellular Trafficking and Plasma Membrane Localization of Protease-Activated Receptor-2." Edited by Jean Kanellopoulos. PLoS ONE 6, no. 11, 2011. e28018. https://doi.org/10.1371/journal.pone.0028018.

Adelantado, Núria, Pablo Tarazona, Karlheinz Grillitsch, Xavier García-Ortega, Sergi Monforte, Francisco Valero, Ivo Feussner, Günther Daum, and Pau Ferrer. "The Effect of Hypoxia on the Lipidome of Recombinant Pichia Pastoris." Microbial Cell Factories, 2017. https://doi.org/10.1186/s12934-017-0699-4.

Ahmad, Sheikh F., Mushtaq A. Ansari, Ahmed Nadeem, Saleh A. Bakheet, Laila Yousef AL-Ayadhi, and Sabry M. Attia. "Toll-like Receptors, NF-KB, and IL-27 Mediate Adenosine A2A Receptor Signaling in BTBR T+ Itpr3tf/J Mice." Progress in Neuro-Psychopharmacology and Biological Psychiatry 79, no. June, 2017. 184–91. https://doi.org/10.1016/j.pnpbp.2017.06.034.

Ailte, Ieva, Anne Berit Dyve Lingelem, Simona Kavaliauskiene, Jonas Bergan, Audun Sverre Kvalvaag, Anne Grethe Myrann, Tore Skotland, and Kirsten Sandvig. "Addition of Lysophospholipids with Large Head Groups to Cells Inhibits Shiga Toxin Binding." Scientific Reports, 6, 30336, 2016. https://doi.org/10.1038/srep30336.

Akbar, S. M.D., K. Sreeramulu, and Hari C. Sharma. "Tryptophan Fluorescence Quenching as a Binding Assay to Monitor Protein Conformation Changes in the Membrane of Intact Mitochondria." Journal of Bioenergetics and Biomembranes, Volume 48, pages 241–247, 2016. https://doi.org/10.1007/s10863-016-9653-0.

Al-Jubair, Tamim, Jonas Hyld Steffen, Julie Winkel Missel, Philip Kitchen, Mootaz M. Salman, Roslyn M. Bill, Pontus Gourdon, and Susanna Törnroth-Horsefield. "High-Yield Overproduction and Purification of Human Aquaporins from Pichia Pastoris." STAR Protocols 3, no. 2, 2022. https://doi.org/10.1016/j.xpro.2022.101298.

Alcoriza-Balaguer, María Isabel, Juan Carlos García-Cañaveras, Adrián López, Isabel Conde, Oscar Juan, Julián Carretero, and Agustín Lahoz. "LipidMS: An R Package for Lipid Annotation in Untargeted Liquid Chromatography-Data Independent Acquisition-Mass Spectrometry Lipidomics." Analytical Chemistry, 91, 1, 836–845, 2019. https://doi.org/10.1021/acs.analchem.8b03409.

Alexandrov, Alexander I., Mauro Mileni, Ellen Y.T. Chien, Michael A. Hanson, and Raymond C. Stevens. "Microscale Fluorescent Thermal Stability Assay for Membrane Proteins." Structure 16, no. 3, 2008. 351–59. https://doi.org/10.1016/j.str.2008.02.004.

Allet, Nadia, Nicolas Barrillat, Thierry Baussant, Celia Boiteau, Paolo Botti, Lydie Bougueleret, Nicolas Budin, et al. "In Vitro and in Silico Processes to Identify Differentially Expressed Proteins." In Proteomics, 2004. https://doi.org/10.1002/pmic.200300840.

Anderson, N. Leigh, and Norman G. Anderson. "Proteome and Proteomics: New Technologies, New Concepts, and New Words." In Electrophoresis, Volume19, Issue11, Pages 1853-1861, 1998. https://doi.org/10.1002/elps.1150191103.

André, Nicolas, Nadia Cherouati, Cécile Prual, Tania Steffan, Gabrielle Zeder-Lutz, Thierry Magnin, Franc Pattus, Hartmut Michel, Renaud Wagner, and Christoph Reinhart. " Enhancing Functional Production of G Protein-Coupled Receptors in Pichia Pastoris to Levels Required for Structural Studies via a Single Expression Screen ." Protein Science 15, no. 5, 2006. 1115–26. https://doi.org/10.1110/ps.062098206.

Antonioli, Luca, Matteo Fornai, Corrado Blandizzi, Pál Pacher, and György Haskó. "Adenosine Signaling and the Immune System: When a Lot Could Be Too Much." Immunology Letters, Volume 205, Pages 9-15, 2019. https://doi.org/10.1016/j.imlet.2018.04.006.

Ariza, María Teresa, Tamara Y. Forbes-Hernández, Patricia Reboredo-Rodríguez, Sadia Afrin, Massimiliano Gasparrini, Lucía Cervantes, Carmen Soria, Elsa Martínez-Ferri, Maurizio Battino, and Francesca Giampieri. "Strawberry and Achenes

I. Company Marin, PhD Thesis, Aston University 2024

Hydroalcoholic Extracts and Their Digested Fractions Efficiently Counteract the AAPH-Induced Oxidative Damage in HEPG2 Cells." International Journal of Molecular Sciences 19, no. 8, 2018. https://doi.org/10.3390/ijms19082180.

Arruda, Maria Augusta, Leigh A. Stoddart, Karolina Gherbi, Stephen J. Briddon, Barrie Kellam, and Stephen J. Hill. "A Non-Imaging High Throughput Approach to Chemical Library Screening at the Unmodified Adenosine-A3 Receptor in Living Cells." Frontiers in Pharmacology 8, no. DEC, 2017. 1–13. https://doi.org/10.3389/fphar.2017.00908.

Arumugam, Senthil, and Patricia Bassereau. "Membrane Nanodomains: Contribution of Curvature and Interaction with Proteins and Cytoskeleton." Essays in Biochemistry, 57, 2015. 109–119. https://doi.org/10.1042/BSE0570109.

Asada, Hidetsugu, Tomoko Uemura, Takami Yurugi-Kobayashi, Mitsunori Shiroishi, Tatsuro Shimamura, Hirokazu Tsujimoto, Keisuke Ito, et al. "Evaluation of the Pichia Pastoris Expression System for the Production of GPCRs for Structural Analysis." Microbial Cell Factories 10, 2011. 1–13. https://doi.org/10.1186/1475-2859-10-24.

Audain, Enrique, Julian Uszkoreit, Timo Sachsenberg, Julianus Pfeuffer, Xiao Liang, Henning Hermjakob, Aniel Sanchez, et al. "In-Depth Analysis of Protein Inference Algorithms Using Multiple Search Engines and Well-Defined Metrics." Journal of Proteomics, 2017. https://doi.org/10.1016/j.jprot.2016.08.002.

Ayala, Antonio, Mario F. Muñoz, and Sandro Argüelles. "Lipid Peroxidation: Production, Metabolism, and Signaling Mechanisms of Malondialdehyde and 4-Hydroxy-2-Nonenal." Oxidative Medicine and Cellular Longevity, Volume 150, 2017, Pages 170-182. https://doi.org/10.1155/2014/360438.

Ayub, Hoor, Michelle Clare, Ivana Milic, Nikola P. Chmel, Heike Böning, Andrew Devitt, Thomas Krey, Roslyn M. Bill, and Alice J. Rothnie. "CD81 Extracted in SMALP Nanodiscs Comprises Two Distinct Protein Populations within a Lipid Environment Enriched with Negatively Charged Headgroups." Biochimica et Biophysica Acta - Biomembranes 1862, no. 11, 2020. 183419. https://doi.org/10.1016/j.bbamem.2020.183419.

Baccouch, Rim, Estelle Rascol, Kaja Stoklosa, and Isabel D. Alves. "The Role of the Lipid Environment in the Activity of G Protein Coupled Receptors." Biophysical Chemistry 285, June 2022. 106794. https://doi.org/10.1016/j.bpc.2022.106794.

Bala, Renu, Bhawna Pareek, Ahmad Umar, Saroj Arora, Davinder Singh, Ashun Chaudhary, Abdulrab Ahmed M. Alkhanjaf, et al. "In-Vitro Cytotoxicity of Nickel Oxide Nanoparticles against L-6 Cell-Lines: MMP, MTT and ROS Studies." Environmental Research 215, no. P1, 2022. 114257. https://doi.org/10.1016/j.envres.2022.114257.

Baneres, Jean Louis, Aimée Martin, Pierre Hullot, Jean Pierre Girard, Jean Claude Rossi, and Joseph Parello. "Structure-Based Analysis of GPCR Function: Conformational Adaptation of Both Agonist and Receptor upon Leukotriene B4 Binding to Recombinant BLT1." Journal of Molecular Biology, 2003. 329(4):801-14. https://doi.org/10.1016/S0022-2836(03.00438-8.

Bang, Dae Young, Sangsoo Lim, and Myeong Hee Moon. "Effect of Ionization Modifiers on the Simultaneous Analysis of All Classes of Phospholipids by Nanoflow Liquid Chromatography/Tandem Mass Spectrometry in Negative Ion Mode." Journal of Chromatography A, Volume 1240, 2012, Pages 69-76. https://doi.org/10.1016/j.chroma.2012.03.073.

Barneda, David, Sabina Cosulich, Len Stephens, and Phillip Hawkins. "How Is the Acyl Chain Composition of Phosphoinositides Created and Does It Matter?" Biochemical Society Transactions, 2019, 47 (5): 1291–1305. https://doi.org/10.1042/BST20190205.

Batarseh, Amani M., Sarah K. Abbott, Eva Duchoslav, Ayedh Alqarni, Stephen J. Blanksby, and Todd W. Mitchell. "Discrimination of Isobaric and Isomeric Lipids in Complex Mixtures by Combining Ultra-High Pressure Liquid Chromatography with Collision and Ozone-Induced Dissociation." International Journal of Mass Spectrometry, Volume 431, 2018, Pages 27-36. https://doi.org/10.1016/j.ijms.2018.05.016.

Baumann, Kristin, Núria Adelantado, Christine Lang, Diethard Mattanovich, and Pau Ferrer. "Protein Trafficking, Ergosterol Biosynthesis and Membrane Physics Impact Recombinant Protein Secretion in Pichia Pastoris." Microbial Cell Factories, 2011, 10:93. https://doi.org/10.1186/1475-2859-10-93.

Bawa, Zharain. "Improving Recombinant Human Adenosine A2A Receptor Production in Yeast." Aston PhD Reviews 1, no. 1, 2014. 1–272.

Bergh, Cathrine C., Urska Rovsnik, Rebecca J. Howard, and Erik R. Lindahl. "Discovery of Lipid Binding Sites in the Ligand-Gated Ion Channel GLIC through Simulations and Cryo-EM." Biophysical Journal 122, no. 3S1, 2023. 374a-375a. https://doi.org/10.1016/j.bpj.2022.11.2062.

I. Company Marin, PhD Thesis, Aston University 2024

Bergmayr, Christian, Patrick Thurner, Simon Keuerleber, Oliver Kudlacek, Christian Nanoff, Michael Freissmuth, and Christian W. Gruber. "Recruitment of a Cytoplasmic Chaperone Relay by the A2A Adenosine Receptor." Journal of Biological Chemistry 288, no. 40, 2013. 28831–44. https://doi.org/10.1074/jbc.M113.464776.

Bertheleme, Nicolas, Shweta Singh, Simon Dowell, and Bernadette Byrne. Heterologous Expression of G-Protein-Coupled Receptors in Yeast. Methods in Enzymology. 1st ed. Vol. 556. Elsevier Inc., 2015. https://doi.org/10.1016/bs.mie.2014.11.046.

Bertheleme, Nicolas, Shweta Singh, Simon J. Dowell, Julia Hubbard, and Bernadette Byrne. "Loss of Constitutive Activity Is Correlated with Increased Thermostability of the Human Adenosine A2A Receptor." British Journal of Pharmacology, Volume169, Issue5, 2013, Pages 988-998. https://doi.org/10.1111/bph.12165.

Bielawski, Jacek, Jason S. Pierce, Justin Snider, Barbara Rembiesa, Zdzislaw M. Szulc, and Alicja Bielawska. "Sphingolipid Analysis by High Performance Liquid Chromatography-Tandem Mass Spectrometry, HPLC-MS/MS." Advances in Experimental Medicine and Biology, 2010, pp 46–59. https://doi.org/10.1007/978-1-4419-6741-1_3.

Bigman, Lavi S., and Yaakov Levy. "Entropic Contributions to Protein Stability." Israel Journal of Chemistry, Volume 60, Issue7, 2020, Pages 705-712. https://doi.org/10.1002/ijch.202000032.

Biou, Valérie. "Lipid-Membrane Protein Interaction Visualised by Cryo-EM: A Review." Biochimica et Biophysica Acta - Biomembranes, Volume 1865, Issue 1, 2023, 184068. https://doi.org/10.1016/j.bbamem.2022.184068.

Birch, Cierra A, Olivia Molinar-Inglis, and Joann Trejo. "Subcellular Hot Spots of GPCR Signaling Promote Vascular Inflammation." Current Opinion in Endocrine and Metabolic Research 16, no. January, February 2021. 37–42. https://doi.org/10.1016/j.coemr.2020.07.011.

Birch, James, Danny Axford, James Foadi, Arne Meyer, Annette Eckhardt, Yvonne Thielmann, and Isabel Moraes. "The Fine Art of Integral Membrane Protein Crystallisation." Methods, Volume 147, 1 September 2018, Pages 150-162. https://doi.org/10.1016/j.ymeth.2018.05.014.

Block, Helena, Barbara Maertens, Anne Spriestersbach, Nicole Brinker, Jan Kubicek, Roland Fabis, Jörg Labahn, and Frank Schäfer. "Chapter 27 Immobilized-Metal Affinity Chromatography, IMAC. A Review." Methods in Enzymology 463, no. C, 2009. 439–73. https://doi.org/10.1016/S0076-6879(09.63027-5.

Blunsom, Nicholas J., and Shamshad Cockcroft. "Phosphatidylinositol Synthesis at the Endoplasmic Reticulum." Biochimica et Biophysica Acta - Molecular and Cell Biology of Lipids, 2020. https://doi.org/10.1016/j.bbalip.2019.05.015.

Boesl, Ulrich. "Time-of-Flight Mass Spectrometry: Introduction to the Basics." Mass Spectrometry Reviews, Volume36, Issue1, 2017, Pages 86-109. https://doi.org/10.1002/mas.21520.

Bolanos-Garcia, Victor Martin, and Owen Richard Davies. "Structural Analysis and Classification of Native Proteins from E. Coli Commonly Co-Purified by Immobilised Metal Affinity Chromatography." Biochimica et Biophysica Acta - General Subjects, Volume 1760, Issue 9, September 2006, Pages 1304-1313. https://doi.org/10.1016/j.bbagen.2006.03.027.

Bolla, Jani Reddy, Mark T. Agasid, Shahid Mehmood, and Carol V. Robinson. "Membrane Protein-Lipid Interactions Probed Using Mass Spectrometry." Annual Review of Biochemistry 88, 2019. 85–111. https://doi.org/10.1146/annurev-biochem-013118-111508.

Bonaventura, Jordi, Gemma Navarro, Verònica Casadó-Anguera, Karima Azdad, William Rea, Estefanía Moreno, Marc Brugarolas, et al. "Allosteric Interactions between Agonists and Antagonists within the Adenosine A2A Receptordopamine D2 Receptor Heterotetramer." Proceedings of the National Academy of Sciences of the United States of America 112, no. 27, 2015. E3609–18. https://doi.org/10.1073/pnas.1507704112.

Booth, Paula J., and Paul Curnow. "Membrane Proteins Shape up: Understanding in Vitro Folding." Current Opinion in Structural Biology, Volume 16, Issue 4, August 2006, Pages 480-488. https://doi.org/10.1016/j.sbi.2006.06.004.

Borea, Pier Andrea, Stefania Gessi, Stefania Merighi, Fabrizio Vincenzi, and Katia Varani. "Pathological Overproduction: The Bad Side of Adenosine." British Journal of Pharmacology, Volume174, Issue13, 2017, Pages 1945-1960. https://doi.org/10.1111/bph.13763.

Bornert, Olivier, Fatima Alkhalfioui, Christel Logez, and Renaud Wagner. "Overexpression of Membrane Proteins Using Pichia Pastoris." Current Protocols in Protein Science 1, no. SUPPL.67, 2012. 1–24. https://doi.org/10.1002/0471140864.ps2902s67.

I. Company Marin, PhD Thesis, Aston University 2024

Bornhorst, Joshua A., and Joseph J. Falke. "[16] Purification of Proteins Using Polyhistidine Affinity Tags." In BiotechnologyProteins to PCR, 245–54, 2000. https://doi.org/10.1016/S0076-6879(00.26058-8.

Brand, Frank, Athena M. Klutz, Kenneth A. Jacobson, Bertil B. Fredholm, and Gunnar Schulte. "Adenosine A2A Receptor Dynamics Studied with the Novel Fluorescent Agonist Alexa488-APEC." European Journal of Pharmacology, Volume 590, Issues 1–3, 2008, Pages 36-42. https://doi.org/10.1016/j.ejphar.2008.05.036.

Brandon, C. I., M. Vandenplas, H. Dookwah, J. Linden, and T. F. Murray. "Cloning and Pharmacological Characterization of the Equine Adenosine A 2A Receptor: A Potential Therapeutic Target for the Treatment of Equine Endotoxemia." Journal of Veterinary Pharmacology and Therapeutics 29, no. 4, 2006. 243–53. https://doi.org/10.1111/j.1365-2885.2006.00746.x.

Brink-Van Der Laan, Els Van Den, J. Antoinette Killian, and Ben De Kruijff. "Nonbilayer Lipids Affect Peripheral and Integral Membrane Proteins via Changes in the Lateral Pressure Profile." Biochimica et Biophysica Acta - Biomembranes, Volume 1666, Issues 1–2, 2004, Pages 275-288. https://doi.org/10.1016/j.bbamem.2004.06.010.

Brink-Van Der Laan, Els Van Den, Vladimir Chupin, J. Antoinette Killian, and Ben De Kruijff. "Stability of KcsA Tetramer Depends on Membrane Lateral Pressure." Biochemistry, 2004, 43, 14, 4240–4250. https://doi.org/10.1021/bi036129d.

Brown, Justin T., Andrew Kant, and Richard B. Mailman. "Rapid, Semi-Automated, and Inexpensive Radioimmunoassay of CAMP: Application in GPCR-Mediated Adenylate Cyclase Assays." Journal of Neuroscience Methods, Volume 177, Issue 2, 2009, Pages 261-266. https://doi.org/10.1016/j.jneumeth.2008.10.016.

Bruzzese, Agustín, James A. R. Dalton, and Jesús Giraldo. "Insights into Adenosine A2A Receptor Activation through Cooperative Modulation of Agonist and Allosteric Lipid Interactions." Edited by Bert L. de Groot. PLOS Computational Biology 16, no. 4, April 16, 2020. e1007818. https://doi.org/10.1371/journal.pcbi.1007818.

Bruzzese, Agustín, Carles Gil, James A.R. Dalton, and Jesús Giraldo. "Structural Insights into Positive and Negative Allosteric Regulation of a G Protein-Coupled Receptor through Protein-Lipid Interactions." Scientific Reports 8, no. 1, 2018. 1–14. https://doi.org/10.1038/s41598-018-22735-6.

Burdge, Graham C., and Philip C. Calder. "Introduction to Fatty Acids and Lipids." World Review of Nutrition and Dietetics 112, 2015. 1–16. https://doi.org/10.1159/000365423.

Burgueño, Javier, Derek J. Blake, Matthew A. Benson, Caroline L. Tinsley, Christopher T. Esapa, Enric I. Canela, Petronila Penela, et al. "The Adenosine A2A Receptor Interacts with the Actin-Binding Protein α-Actinin." Journal of Biological Chemistry, Volume 278, Issue 39, 2003, Pages 37545-37552. https://doi.org/10.1074/jbc.M302809200.

Burstein, E. A., N. S. Vedenkina, and M. N. Ivkova. "Fluorescence And The Location Of Tryptophan Residues In Protein Molecules." Photochemistry and Photobiology, 1973, 18(4):263-79. https://doi.org/10.1111/j.1751-1097.1973.tb06422.x.

Bus, Ian de, Renger Witkamp, Han Zuilhof, Bauke Albada, and Michiel Balvers. "The Role of N-3 PUFA-Derived Fatty Acid Derivatives and Their Oxygenated Metabolites in the Modulation of Inflammation." Prostaglandins and Other Lipid Mediators 144, no. June, 2019. 106351. https://doi.org/10.1016/j.prostaglandins.2019.106351.

Buyukpamukcu, Elif, Jöerg Hau, Laurent-Bernard Fay, and Fabiola Dionisi. "Analysis of Phospholipids Using Electrospray Ionisation Tandem Mass Spectrometry." Lipid Technology, Volume 19, Issue 6, 2007, Pages 136-138. https://doi.org/10.1002/lite.200700046.

Bylund, D. B., and M. L. Toews. "Radioligand Binding Methods Practical Guide and Tips." American Journal of Physiology - Lung Cellular and Molecular Physiology, Volume 265, Issue 5, 1993. Pages L421-L429. https://doi.org/10.1152/ajplung.1993.265.5.l421.

Bylund, David B., and L. Charles Murrin. "Radioligand Saturation Binding Experiments over Large Concentration Ranges." Life Sciences, 67, 2000. 2897–2911. https://doi.org/10.1016/S0024-3205(00.00877-8.

Byrne, Bernadette. "Pichia Pastoris as an Expression Host for Membrane Protein Structural Biology." Current Opinion in Structural Biology, Volume 32, June 2015, Pages 9-17. https://doi.org/10.1016/j.sbi.2015.01.005.

Calebiro, Davide, Viacheslav O. Nikolaev, Luca Persani, and Martin J. Lohse. "Signaling by Internalized G-Protein-Coupled Receptors." Trends in Pharmacological Sciences 31, no. 5, 2010. 221–28. https://doi.org/10.1016/j.tips.2010.02.002.

I. Company Marin, PhD Thesis, Aston University 2024

Cao, Ruyin, Alejandro Giorgetti, Andreas Bauer, Bernd Neumaier, Giulia Rossetti, and Paolo Carloni. "Role of Extracellular Loops and Membrane Lipids for Ligand Recognition in the Neuronal Adenosine Receptor Type 2A: An Enhanced Sampling Simulation Study." Molecules 23, no. 10, 2018. 1–17. https://doi.org/10.3390/molecules23102616.

Carlesso, Antonio, Raquel Delgado, Oriol Ruiz Isant, Owens Uwangue, Dylan Valli, Roslyn M. Bill, and Kristina Hedfalk. "Yeast as a Tool for Membrane Protein Production and Structure Determination." FEMS Yeast Research, Volume 22, Issue 1, 2022. https://doi.org/10.1093/femsyr/foac047.

Carpenter, Byron, and Guillaume Lebon. "Human Adenosine A 2A Receptor : Molecular Mechanism of Ligand Binding and Activation" 8, no. December, 2017. 1–15. https://doi.org/10.3389/fphar.2017.00898.

Carpenter, Byron, Rony Nehmé, Tony Warne, Andrew G.W. Leslie, and Christopher G. Tate. "Structure of the Adenosine A2A Receptor Bound to an Engineered G Protein." Nature 536, no. 7614, 2016. 104–7. https://doi.org/10.1038/nature18966.

Carpenter, Byron, and Christopher Tate. "Expression, Purification and Crystallisation of the Adenosine A2A Receptor Bound to an Engineered Mini G Protein." Bio-Protocol 7, no. 8, 2017. https://doi.org/10.21769/bioprotoc.2234.

Carpenter, Byron, and Christopher G. Tate. "Active State Structures of G Protein-Coupled Receptors Highlight the Similarities and Differences in the G Protein and Arrestin Coupling Interfaces." Current Opinion in Structural Biology 45, no. Figure 1, 2017. 124–32. https://doi.org/10.1016/j.sbi.2017.04.010.

Carson, Mike, David H. Johnson, Heather McDonald, Christie Brouillette, and Lawrence J. DeLucas. "His-Tag Impact on Structure." Acta Crystallographica Section D: Biological Crystallography, D63, 2007, 295-301. https://doi.org/10.1107/S0907444906052024.

Casares, Doralicia, Pablo V. Escribá, and Catalina Ana Rosselló. "Membrane Lipid Composition: Effect on Membrane and Organelle Structure, Function and Compartmentalization and Therapeutic Avenues." International Journal of Molecular Sciences, 2019, 20(9), 2167. https://doi.org/10.3390/ijms20092167.

Castro, Cristina M., Carmen Corciulo, Maria E. Solesio, Fengxia Liang, Evgeny V. Pavlov, and Bruce N. Cronstein. "Adenosine A2A Receptor, A2AR. Stimulation Enhances Mitochondrial Metabolism and Mitigates Reactive Oxygen Species-mediated Mitochondrial Injury." The FASEB Journal 34, no. 4, April 13, 2020. 5027–45. https://doi.org/10.1096/fj.201902459R.

Cecchetti, Cristina, Jannik Strauss, Claudia Stohrer, Claire Naylor, Edward Pryor, Jeanette Hobbs, Simon Tanley, Adrian Goldman, and Bernadette Byrne. "A Novel High-Throughput Screen for Identifying Lipids That Stabilise Membrane Proteins in Detergent Based Solution." PLoS ONE 16, no. 7 July, 2021. https://doi.org/10.1371/journal.pone.0254118.

Ceriello, Antonio. "Oxidative Stress and Diabetes-Associated Complications." In Endocrine Practice, Volume 12, Supplement 1, 2006, Pages 60-62. https://doi.org/10.4158/ep.12.s1.60.

Chakrabarti, Abhijit. "Phospholipid Asymmetry in Biological Membranes: Is the Role of Phosphatidylethanolamine Underappreciated?" Journal of Membrane Biology, Volume 254, pages 127–132, 2021. https://doi.org/10.1007/s00232-020-00163-w.

Chakraborty, Raja, Bing Xu, Rajinder P. Bhullar, and Prashen Chelikani. Expression of G Protein-Coupled Receptors in Mammalian Cells. Methods in Enzymology. 1st ed. Vol. 556. Elsevier Inc., Volume 556, 2015, Pages 267-281. https://doi.org/10.1016/bs.mie.2014.12.013.

Chang, Ching Hsiang, Hao An Hsiung, Kai Lin Hong, and Ching Tsan Huang. "Enhancing the Efficiency of the Pichia Pastoris AOX1 Promoter via the Synthetic Positive Feedback Circuit of Transcription Factor Mxr1." BMC Biotechnology 18, no. 1, 2018. 1–10. https://doi.org/10.1186/s12896-018-0492-4.

Charalambous, Christoforos, Ingrid Gsandtner, Simon Keuerleber, Laura Milan-Lobo, Oliver Kudlacek, Michael Freissmuth, and Jürgen Zezula. "Restricted Collision Coupling of the A2A Receptor Revisited: Evidence for Physical Separation of Two Signaling Cascades." Journal of Biological Chemistry, Volume 283, Issue 14, 2008, Pages 9276-9288. https://doi.org/10.1074/jbc.M706275200.

Chen, Chao Jung, Der Yen Lee, Jiaxin Yu, Yu Ning Lin, and Tsung Min Lin. "Recent Advances in LC-MS-Based Metabolomics for Clinical Biomarker Discovery." Mass Spectrometry Reviews, Volume 42, Issu 6, Taiwan Regional Special Issue, 2023, Pages 2349-2378. https://doi.org/10.1002/mas.21785.

I. Company Marin, PhD Thesis, Aston University 2024

Chen, Chen, Jie Hou, John J. Tanner, and Jianlin Cheng. "Bioinformatics Methods for Mass Spectrometry-Based Proteomics Data Analysis." International Journal of Molecular Sciences, 21(8), 2873,2020. https://doi.org/10.3390/ijms21082873.

Chen, Ting, Matthew Tepel, John Rush, George M. Church, and Ming Yang Kao. "A Dynamic Programming Approach to de Novo Peptide Sequencing via Tandem Mass Spectrometry." Journal of Computational Biology, Vol. 8, No. 3, 2001. https://doi.org/10.1089/10665270152530872.

Chen, Yong, Yang Li, Peng Liu, and Qun Sun. "Optimized Expression in Pichia Pastoris Eliminates Common Protein Contaminants from Subsequent His-Tag Purification," 2014, 711–18. https://doi.org/10.1007/s10529-013-1411-3.

Chen, Yong, Yang Li, Peng Liu, Qun Sun, and Zhu Liu. "Optimized Expression in Pichia Pastoris Eliminates Common Protein Contaminants from Subsequent His-Tag Purification." Biotechnology Letters, Volume 36, pages 711–718, 2014. https://doi.org/10.1007/s10529-013-1411-3.

Cheng, Robert K.Y., Elena Segala, Nathan Robertson, Francesca Deflorian, Andrew S. Doré, James C. Errey, Cédric Fiez-Vandal, Fiona H. Marshall, and Robert M. Cooke. "Structures of Human A1 and A2A Adenosine Receptors with Xanthines Reveal Determinants of Selectivity." Structure 25, no. 8, 2017. 1275-1285.e4. https://doi.org/10.1016/j.str.2017.06.012.

Cherezov, Vadim, Daniel M. Rosenbaum, Michael A. Hanson, Søren G.F. Rasmussen, Sun Thian Foon, Tong Sun Kobilka, Hee Jung Choi, et al. "High-Resolution Crystal Structure of an Engineered Human B2-Adrenergic G Protein-Coupled Receptor." Science, Vol 318, Issue 5854, 2007. https://doi.org/10.1126/science.1150577.

Chng, Elaine Lay Khim, and Martin Pumera. "The Toxicity of Graphene Oxides: Dependence on the Oxidative Methods Used." Chemistry - A European Journal 19, no. 25, 2013. 8227–35. https://doi.org/10.1002/chem.201300824.

Chou, Chun Hsu, Ming Shiun Tsai, Hsin Yu Lu, Chao Kai Chang, Kuan Chen Cheng, Mei Hsin Jhan, and Chang Wei Hsieh. "Enzymatic Hydrolysates Obtained from Trametes Versicolor Polysaccharopeptides Protect Human Skin Keratinocyte against AAPH-induced Oxidative Stress and Inflammatory." Journal of Cosmetic Dermatology 18, no. 6, 2019. 2011–18. https://doi.org/10.1111/jocd.12959.

Clarke, Ronald J. "Effect of Cholesterol on the Dipole Potential of Lipid Membranes." In Advances in Experimental Medicine and Biology, 2019, pp 135–154. https://doi.org/10.1007/978-3-030-04278-3_6.

Contreras, Francesc Xabier, Andreas Max Ernst, Felix Wieland, and Britta Brügger. "Specificity of Intramembrane Protein-Lipid Interactions." Cold Spring Harbor Perspectives in Biology, 2011. https://doi.org/10.1101/cshperspect.a004705.

Cooke, Ira R., and Markus Deserno. "Coupling between Lipid Shape and Membrane Curvature." Biophysical Journal, Volume 91, Issue 2, 15 July 2006, Pages 487-495, 2006. https://doi.org/10.1529/biophysj.105.078683.

Corin, Karolina, and James U. Bowie. "How Bilayer Properties Influence Membrane Protein Folding." Protein Science, Volume29, Issue12, 2020, Pages 2348-2362. https://doi.org/10.1002/pro.3973.

Corradi, Valentina, Eduardo Mendez-Villuendas, Helgi I. Ingólfsson, Ruo Xu Gu, Iwona Siuda, Manuel N. Melo, Anastassiia Moussatova, et al. "Lipid-Protein Interactions Are Unique Fingerprints for Membrane Proteins." ACS Central Science, 2018, 4, 6, 709–717. https://doi.org/10.1021/acscentsci.8b00143.

Cournia, Zoe, G. Matthias Ullmann, and Jeremy C. Smith. "Differential Effects of Cholesterol, Ergosterol and Lanosterol on a Dipalmitoyl Phosphatidylcholine Membrane: A Molecular Dynamics Simulation Study." Journal of Physical Chemistry B, 2007, 111, 7, 1786–1801. https://doi.org/10.1021/jp065172i.

Covey, Tracy M., Kornelia Edes, Gary S. Coombs, David M. Virshup, and Frank A. Fitzpatrick. "Alkylation of the Tumor Suppressor PTEN Activates Akt and β-Catenin Signaling: A Mechanism Linking Inflammation and Oxidative Stress with Cancer." PLoS ONE, 2010. https://doi.org/10.1371/journal.pone.0013545.

Cregg, J M, K R Madden, K J Barringer, G P Thill, and C A Stillman. "Functional Characterization of the Two Alcohol Oxidase Genes from the Yeast Pichia Pastoris." Molecular and Cellular Biology, 1989. https://doi.org/10.1128/mcb.9.3.1316.

Crowe, J., H. Döbeli, R. Gentz, E. Hochuli, D. Stüber, and K. Henco. "6xHis-Ni-NTA Chromatography as a Superior Technique in Recombinant Protein Expression/Purification." Methods in Molecular Biology, Clifton, N.J., 1994, pp 371–387. https://doi.org/10.1385/0-89603-258-2:371.

Cruciani, Gabriele, Pedro Domingues, Maria Fedorova, Francesco Galli, and Corinne M. Spickett. "Redox Lipidomics and Adductomics - Advanced Analytical Strategies to Study Oxidized Lipids and Lipid-Protein Adducts." Free Radical Biology and Medicine 144, no. July, 2019. 1–5. https://doi.org/10.1016/j.freeradbiomed.2019.07.027.

I. Company Marin, PhD Thesis, Aston University 2024

Cuevas Arenas, Rodrigo, Bartholomäus Danielczak, Anne Martel, Lionel Porcar, Cécile Breyton, Christine Ebel, and Sandro Keller. "Fast Collisional Lipid Transfer among Polymer-Bounded Nanodiscs." Scientific Reports 7, no. February, 2017. 1–8. https://doi.org/10.1038/srep45875.

Cuevas Arenas, Rodrigo, Johannes Klingler, Carolyn Vargas, and Sandro Keller. "Influence of Lipid Bilayer Properties on Nanodisc Formation Mediated by Styrene/Maleic Acid Copolymers." Nanoscale, Article number: 45875, 2016. https://doi.org/10.1039/c6nr02089e.

Cui, Yong, Dong Seok Kim, Seo Hyoung Park, Jin A. Yoon, Soon Kyum Kim, Sun Bang Kwon, and Kyoung Chan Park. "Involvement of ERK and P38 MAP Kinase in AAPH-Induced COX-2 Expression in HaCaT Cells." Chemistry and Physics of Lipids 129, no. 1, 2004. 43–52. https://doi.org/10.1016/j.chemphyslip.2003.11.004.

Czub, Jacek, and Maciej Baginski. "Comparative Molecular Dynamics Study of Lipid Membranes Containing Cholesterol and Ergosterol." Biophysical Journal, Volume 90, Issue 7, 1 April 2006, Pages 2368-2382. https://doi.org/10.1529/biophysj.105.072801.

Dagan, Shlomi, Tzachi Hagai, Yulian Gavrilov, Ruti Kapon, Yaakov Levy, and Ziv Reich. "Stabilization of a Protein Conferred by an Increase in Folded State Entropy." Proceedings of the National Academy of Sciences of the United States of America, 2013, 110 (26) 10628-10633. https://doi.org/10.1073/pnas.1302284110.

Damian, Marjorie, Véronique Pons, Pedro Renault, Céline M'Kadmi, Bartholomé Delort, Lucie Hartmann, Ali I. Kaya, et al. "GHSR-D2R Heteromerization Modulates Dopamine Signaling through an Effect on G Protein Conformation." Proceedings of the National Academy of Sciences of the United States of America 115, no. 17, 2018. 4501–6. https://doi.org/10.1073/pnas.1712725115.

Dančík, Vlado, Theresa A. Addona, Karl R. Clauser, James E. Vath, and Pavel A. Pevzner. "De Novo Peptide Sequencing via Tandem Mass Spectrometry." In Journal of Computational Biology, Vol. 6, No. 3-4, 1999. https://doi.org/10.1089/106652799318300.

Dawaliby, R, C Trubbia, C Delporte, M Masureel, P van Antwerpen, B Kobilka, and C Govaerts. "Allosteric Regulation of GPCR Activity by Phospholipids." Nat Chem Biol. 12, no. 1, 2016. 35–39. https://doi.org/10.1038/nchembio.1960.ALLOSTERIC.

Dawaliby, Rosie, Cataldo Trubbia, Cédric Delporte, Matthieu Masureel, Pierre Van Antwerpen, Brian K. Kobilka, and Cédric Govaerts. "Allosteric Regulation of G Protein-Coupled Receptor Activity by Phospholipids." Nature Chemical Biology, 12, 35–39, 2016. https://doi.org/10.1038/nchembio.1960.

Dawaliby, Rosie, Cataldo Trubbia, Cédric Delporte, Caroline Noyon, Jean Marie Ruysschaert, Pierre Van Antwerpen, and Cédric Govaerts. "Phosphatidylethanolamine Is a Key Regulator of Membrane Fluidity in Eukaryotic Cells." Journal of Biological Chemistry, Volume 291, Issue 7, 2016, Pages 3658-3667. https://doi.org/10.1074/jbc.M115.706523.

Deutsch, Eric W., Henry Lam, and Ruedi Aebersold. "Data Analysis and Bioinformatics Tools for Tandem Mass Spectrometry in Proteomics." Physiological Genomics, Volume 33, Issue 1, 2008, Pages 18-25. https://doi.org/10.1152/physiolgenomics.00298.2007.

Díaz, Óscar, James A.R. Dalton, and Jesús Giraldo. "Revealing the Mechanism of Agonist-Mediated Cannabinoid Receptor 1, CB1. Activation and Phospholipid-Mediated Allosteric Modulation." Journal of Medicinal Chemistry, 2019, 62, 11, 5638–5654. https://doi.org/10.1021/acs.jmedchem.9b00612.

Dodds, James N., and Erin S. Baker. "Ion Mobility Spectrometry: Fundamental Concepts, Instrumentation, Applications, and the Road Ahead." Journal of the American Society for Mass Spectrometry 30, no. 11, 2019. 2185–95. https://doi.org/10.1007/s13361-019-02288-2.

Dominguez Pardo, Juan J., Jonas M. Dörr, Aditya Iyer, Ruud C. Cox, Stefan Scheidelaar, Martijn C. Koorengevel, Vinod Subramaniam, and J. Antoinette Killian. "Solubilization of Lipids and Lipid Phases by the Styrene–Maleic Acid Copolymer." European Biophysics Journal, 2017. https://doi.org/10.1007/s00249-016-1181-7.

Dong, Chengyan, Zhaofei Liu, and Fan Wang. "Radioligand Saturation Binding for Quantitative Analysis of Ligand-Receptor Interactions." Biophysics Reports, Volume 46, pages 91–101, 2015. https://doi.org/10.1007/s41048-016-0016-5.

Doré, Andrew S., Nathan Robertson, James C. Errey, Irene Ng, Kaspar Hollenstein, Ben Tehan, Edward Hurrell, et al. "Structure of the Adenosine A 2A Receptor in Complex with ZM241385 and the Xanthines XAC and Caffeine." Structure 19, no. 9, 2011. 1283–93. https://doi.org/10.1016/j.str.2011.06.014.

I. Company Marin, PhD Thesis, Aston University 2024

Dörr, Jonas M., Martijn C. Koorengevel, Marre Schäfer, Alexander V. Prokofyev, Stefan Scheidelaar, Elwin A.W. Van Der Cruijsen, Timothy R. Dafforn, Marc Baldus, and J. Antoinette Killian. "Detergent-Free Isolation, Characterization, and Functional Reconstitution of a Tetrameric K+ Channel: The Power of Native Nanodiscs." Proceedings of the National Academy of Sciences of the United States of America, 111 (52) 18607-18612, 2014. https://doi.org/10.1073/pnas.1416205112.

Drotleff, Bernhard, and Michael Lämmerhofer. "Guidelines for Selection of Internal Standard-Based Normalization Strategies in Untargeted Lipidomic Profiling by LC-HR-MS/MS." Analytical Chemistry, 91, 15, 9836–9843, 2019. https://doi.org/10.1021/acs.analchem.9b01505.

Du, Meng Ze, Shuo Liu, Zhi Zeng, Labena Abraham Alemayehu, Wen Wei, and Feng Biao Guo. "Amino Acid Compositions Contribute to the Proteins' Evolution under the Influence of Their Abundances and Genomic GC Content." Scientific Reports, 8, Article number: 7382, 2018. https://doi.org/10.1038/s41598-018-25364-1.

Duan, Wen Jun, Yi Fang Li, Fang Lan Liu, Jie Deng, Yan Ping Wu, Wei Lin Yuan, Bun Tsoi, et al. "A SIRT3/AMPK/Autophagy Network Orchestrates the Protective Effects of Trans-Resveratrol in Stressed Peritoneal Macrophages and RAW 264.7 Macrophages." Free Radical Biology and Medicine 95, 2016. 230–42. https://doi.org/10.1016/j.freeradbiomed.2016.03.022.

Duy, C., and J. Fitter. "How Aggregation and Conformational Scrambling of Unfolded States Govern Fluorescence Emission Spectra." Biophysical Journal, Volume 90, Issue 10, 15 May 2006, Pages 3704-3711. https://doi.org/10.1529/biophysj.105.078980.

Effendi, Wiwin Is, Tatsuya Nagano, Kazuyuki Kobayashi, and Yoshihiro Nishimura. "Focusing on Adenosine Receptors as a Potential Targeted Therapy in Human Diseases." Cells 9, no. 3, 2020. 1–36. https://doi.org/10.3390/cells9030785.

Egea, Javier, Isabel Fabregat, Yves M Frapart, Pietro Ghezzi, Agnes Görlach, Thomas Kietzmann, Kateryna Kubaichuk, et al. "Redox Biology European Contribution to the Study of ROS : A Summary of the Fi Ndings and Prospects for the Future from the COST Action BM1203, EU-ROS ." 13, no. May, 2017. 94–162. https://doi.org/10.1016/j.redox.2017.05.007.

El-Shamarka, Marwa E.A., Magy R. Kozman, and Basim A.S. Messiha. "The Protective Effect of Inosine against Rotenone-Induced Parkinson's Disease in Mice; Role of Oxido-Nitrosative Stress, ERK Phosphorylation, and A2AR Expression." Naunyn-Schmiedeberg's Archives of Pharmacology 393, no. 6, 2020. 1041–53. https://doi.org/10.1007/s00210-019-01804-1.

Elguero, Belén, David Gonilski Pacin, Carolina Cárdenas Figueroa, Mariana Fuertes, and Eduardo Arzt. Modifications in the cellular proteome and their clinical application. Modificaciones en el proteoma celular y su aplicación en la clínica. Medicina (B Aires). 2019;79(Spec 6/1):570-575.

Ermakova, Elena, and Yuriy Zuev. "Effect of Ergosterol on the Fungal Membrane Properties. All-Atom and Coarse-Grained Molecular Dynamics Study." Chemistry and Physics of Lipids, Volume 209, December 2017, Pages 45-53. https://doi.org/10.1016/j.chemphyslip.2017.11.006.

Fabritius, Mikael, and Baoru Yang. "Direct Infusion and Ultra-High-Performance Liquid Chromatography/Electrospray Ionization Tandem Mass Spectrometry Analysis of Phospholipid Regioisomers." Rapid Communications in Mass Spectrometry, Volume35, Issue18, 2021, e9151. https://doi.org/10.1002/rcm.9151.

Fagone, Paolo, and Suzanne Jackowski. "Phosphatidylcholine and the CDP-Choline Cycle." Biochimica et Biophysica Acta - Molecular and Cell Biology of Lipids, Volume 1831, Issue 3, 2013, Pages 523-532. https://doi.org/10.1016/j.bbalip.2012.09.009.

Fahy, E, D Cotter, M Sud, and S Subramaniam. "Lipidomics NIH Public Access." Biochim Biophys Acta. 1811, no. 11, 2012. 637–47. https://doi.org/10.1016/j.bbalip.2011.06.009.Lipid.

Fahy, Eoin, Shankar Subramaniam, H. Alex Brown, Christopher K. Glass, Alfred H. Merrill, Robert C. Murphy, Christian R.H. Raetz, et al. "A Comprehensive Classification System for Lipids." Journal of Lipid Research, Volume 46, Issue 5, May 2005, Pages 839-861. https://doi.org/10.1194/jlr.E400004-JLR200.

Fahy, Eoin, Shankar Subramaniam, Robert C. Murphy, Masahiro Nishijima, Christian R.H. Raetz, Takao Shimizu, Friedrich Spener, Gerrit Van Meer, Michael J.O. Wakelam, and Edward A. Dennis. "Update of the LIPID MAPS Comprehensive Classification System for Lipids." Journal of Lipid Research 50, no. SUPPL., 2009. 9–14. https://doi.org/10.1194/jlr.R800095-JLR200.

I. Company Marin, PhD Thesis, Aston University 2024

Feltes, Maria Manuela Camino, Débora de Oliveira, Jane Mara Block, and Jorge Luiz Ninow. "The Production, Benefits, and Applications of Monoacylglycerols and Diacylglycerols of Nutritional Interest." Food and Bioprocess Technology, Volume 6, pages 17–35, (2013). https://doi.org/10.1007/s11947-012-0836-3.

Fernandes, Fábio, Ana Coutinho, Manuel Prieto, and Luís M.S. Loura. "Electrostatically Driven Lipid-Protein Interaction: Answers from FRET." Biochimica et Biophysica Acta - Biomembranes, Volume 1848, Issue 9, September 2015, Pages 1837-1848. https://doi.org/10.1016/j.bbamem.2015.02.023.

Fernández-Dueñas, Víctor, Maricel Gõmez-Soler, Kenneth A. Jacobson, Santhosh T. Kumar, Kjell Fuxe, Dasiel O. Borroto-Escuela, and Francisco Ciruela. "Molecular Determinants of A 2AR-D 2R Allosterism: Role of the Intracellular Loop 3 of the D 2R." Journal of Neurochemistry 123, no. 3, 2012. 373–84. https://doi.org/10.1111/j.1471-4159.2012.07956.x.

Fernández-Dueñas, Víctor, Maricel Gómez-Soler, Xavier Morató, Fabiana Núñez, Arijit Das, T. Santhosh Kumar, Serge Jaumà, Kenneth A. Jacobson, and Francisco Ciruela. "Dopamine D2 Receptor-Mediated Modulation of Adenosine A 2A Receptor Agonist Binding within the A2AR/D2R Oligomer Framework." Neurochemistry International 63, no. 1, 2013. 42–46. https://doi.org/10.1016/j.neuint.2013.04.006.

Ferré, Sergi, Marzena Karcz-Kubicha, Bruce T. Hope, Patrizia Popoli, Javier Burgueño, M. Angeles Gutiérrez, Vicent Casadó, et al. "Synergistic Interaction between Adenosine A2A and Glutamate MGlu5 Receptors: Implications for Striatal Neuronal Function." Proceedings of the National Academy of Sciences of the United States of America 99, no. 18, 2002. 11940–45. https://doi.org/10.1073/pnas.172393799.

Ferreira, Helena Beatriz, Tânia Melo, Artur Paiva, and Maria Do Rosário Domingues. "Insights in the Role of Lipids, Oxidative Stress and Inflammation in Rheumatoid Arthritis Unveiled by New Trends in Lipidomic Investigations." Antioxidants, 2021, 10(1), 45. https://doi.org/10.3390/antiox10010045.

Flock, Tilman, Charles N.J. Ravarani, Dawei Sun, A. J. Venkatakrishnan, Melis Kayikci, Christopher G. Tate, Dmitry B. Veprintsev, and M. Madan Babu. "Universal Allosteric Mechanism for Gα Activation by GPCRs." Nature 524, no. 7564, 2015. 173–79. https://doi.org/10.1038/nature14663.

Folch, Jordi, M Lees, and G H Sloane. A simple method for the isolation and purification of total lipides from animal tissues. J Biol Chem. 1957;226(1):497-509.

Fonteh, Alfred N., Robert J. Harrington, Andreas F. Huhmer, Roger G. Biringer, James N. Riggins, and Michael G. Harrington. "Identification of Disease Markers in Human Cerebrospinal Fluid Using Lipidomic and Proteomic Methods." Disease Markers, Volume 22 | Article ID 202938, 2006. https://doi.org/10.1155/2006/202938.

Franco, Rafael, Irene Reyes-Resina, David Aguinaga, Alejandro Lillo, Jasmina Jiménez, Iu Raïch, Dasiel O. Borroto-Escuela, et al. "Potentiation of Cannabinoid Signaling in Microglia by Adenosine A2A Receptor Antagonists." Glia 67, no. 12, 2019. 2410–23. https://doi.org/10.1002/glia.23694.

Frankel, Edwin N. "Secondary Products of Lipid Oxidation." Chemistry and Physics of Lipids, Volume 44, Issues 2–4, July–September 1987, Pages 73-85. https://doi.org/10.1016/0009-3084(87.90045-4.

Fraser, Niall J. "Expression and Functional Purification of a Glycosylation Deficient Version of the Human Adenosine 2a Receptor for Structural Studies." Protein Expression and Purification 49, no. 1, 2006. 129–37. https://doi.org/10.1016/j.pep.2006.03.006.

Fraser, Niall J. "Expression and Functional Puri W Cation of a Glycosylation de W Cient Version of the Human Adenosine 2a Receptor for Structural Studies" 49, 2006. 129–37. https://doi.org/10.1016/j.pep.2006.03.006.

Fratti, Rutilio A. "Editorial: Effects of Membrane Lipids on Protein Function." Frontiers in Cell and Developmental Biology, Volume 9, 2021. https://doi.org/10.3389/fcell.2021.675264.

Freigassner, Maria, Harald Pichler, and Anton Glieder. "Tuning Microbial Hosts for Membrane Protein Production." Microbial Cell Factories 8, 2009. 1–22. https://doi.org/10.1186/1475-2859-8-69.

Fus-Kujawa, Agnieszka, Pawel Prus, Karolina Bajdak-Rusinek, Paulina Teper, Katarzyna Gawron, Agnieszka Kowalczuk, and Aleksander L. Sieron. "An Overview of Methods and Tools for Transfection of Eukaryotic Cells in Vitro." Frontiers in Bioengineering and Biotechnology, Volume 9, 2021. https://doi.org/10.3389/fbioe.2021.701031.

Gahbauer, Stefan, and Rainer A. Böckmann. "Membrane-Mediated Oligomerization of G Protein Coupled Receptors and Its Implications for GPCR Function." Frontiers in Physiology 7, no. 2016. 1–17. https://doi.org/10.3389/fphys.2016.00494.

I. Company Marin, PhD Thesis, Aston University 2024

Gao, Zhan Guo, Asuka Inoue, and Kenneth A. Jacobson. "On the G Protein-Coupling Selectivity of the Native A2B Adenosine Receptor." Biochemical Pharmacology, Volume 151, May 2018, Pages 201-213. https://doi.org/10.1016/j.bcp.2017.12.003.

Gao, Zhan Guo, Ian M. Levitan, Asuka Inoue, Qiang Wei, and Kenneth A. Jacobson. "A2B Adenosine Receptor Activation and Modulation by Protein Kinase C." IScience 26, no. 7, 2023. 107178. https://doi.org/10.1016/j.isci.2023.107178.

Gao, Zhan Guo, Liaman K. Mamedova, Peiran Chen, and Kenneth A. Jacobson. "2-Substituted Adenosine Derivatives: Affinity and Efficacy at Four Subtypes of Human Adenosine Receptors." Biochemical Pharmacology, Volume 68, Issue 10, 15 November 2004, Pages 1985-1993. https://doi.org/10.1016/j.bcp.2004.06.011.

Gao, Zhenhai, Taosheng Chen, Michael J. Weber, and Joel Linden. "A(2B. Adenosine and P2Y2 Receptors Stimulate Mitogen-Activated Protein Kinase in Human Embryonic Kidney-293 Cells: Cross-Talk between Cyclic AMP and Protein Kinase C Pathways." Journal of Biological Chemistry 274, no. 9, 1999. 5972–80. https://doi.org/10.1074/jbc.274.9.5972.

García-Nafría, Javier, Yang Lee, Xiaochen Bai, Byron Carpenter, and Christopher G. Tate. "Cryo-EM Structure of the Adenosine A2A Receptor Coupled to an Engineered Heterotrimeric G Protein." ELife 7, no. e35946, April 2020. https://doi.org/10.7554/eLife.35946.001.

Gaschler, Michael M., and Brent R. Stockwell. "Lipid Peroxidation in Cell Death." Biochemical and Biophysical Research Communications 482, no. 3, January 2017. 419–25. https://doi.org/10.1016/j.bbrc.2016.10.086.

Gault, Christopher R., Lina M. Obeid, and Yusuf A. Hannun. "An Overview of Sphingolipid Metabolism: From Synthesis to Breakdown." Advances in Experimental Medicine and Biology, 2010, pp 1–23. https://doi.org/10.1007/978-1-4419-6741-1_1.

Geiger, James, Rick Sexton, Zina Al-Sahouri, Ming Yue Lee, Eugene Chun, Kaleeckal G. Harikumar, Laurence J. Miller, Oliver Beckstein, and Wei Liu. "Evidence That Specific Interactions Play a Role in the Cholesterol Sensitivity of G Protein-Coupled Receptors." Biochimica et Biophysica Acta - Biomembranes, Volume 1863, Issue 9, 1 September 2021, 183557. https://doi.org/10.1016/j.bbamem.2021.183557.

Genedani, Susanna, Diego Guidolin, Giuseppina Leo, Monica Filaferro, Maria Torvinen, Amina S. Woods, Kjell Fuxe, Sergi Ferré, and Luigi F. Agnati. "Computer-Assisted Image Analysis of Caveolin-1 Involvement in the Internalization Process of Adenosine A2A-Dopamine D2 Receptor Heterodimers." In Journal of Molecular Neuroscience, Volume 26, pages 177–184, 2005. https://doi.org/10.1385/JMN:26:2-3:177.

Gessi, Stefania, Katia Varani, Stefania Merighi, Elena Cattabriga, Cecilia Pancaldi, Youri Szabadkai, Rosario Rizzuto, et al. "Expression, Pharmacological Profile, and Functional Coupling of A 2b Receptors in a Recombinant System and in Peripheral Blood Cells Using a Novel Selective Antagonist Radioligand, [3H]MRE 2029-F20." Molecular Pharmacology 67, no. 6, 2005. 2137–47. https://doi.org/10.1124/mol.104.009225.

Ghellinck, Alexis De, Hubert Schaller, Valérie Laux, Michael Haertlein, Michele Sferrazza, Eric Maréchal, Hanna Wacklin, Juliette Jouhet, and Giovanna Fragneto. "Production and Analysis of Perdeuterated Lipids from Pichia Pastoris Cells." PLoS ONE 9, no. 4, 2014. 1–9. https://doi.org/10.1371/journal.pone.0092999.

Ghisaidoobe, Amar B.T., and Sang J. Chung. "Intrinsic Tryptophan Fluorescence in the Detection and Analysis of Proteins: A Focus on Förster Resonance Energy Transfer Techniques." International Journal of Molecular Sciences 15, no. 12, 2014. 22518–38. https://doi.org/10.3390/ijms151222518.

Giansanti, Piero, Liana Tsiatsiani, Teck Yew Low, and Albert J.R. Heck. "Six Alternative Proteases for Mass Spectrometry-Based Proteomics beyond Trypsin." Nature Protocols, 11, pages993–1006, 2016. https://doi.org/10.1038/nprot.2016.057.

Giles, Kevin, Jakub Ujma, Jason Wildgoose, Steven Pringle, Keith Richardson, David Langridge, and Martin Green. "A Cyclic Ion Mobility-Mass Spectrometry System." Analytical Chemistry 91, no. 13, 2019. 8564–73. https://doi.org/10.1021/acs.analchem.9b01838.

Gimpl, Gerald. "Interaction of G Protein Coupled Receptors and Cholesterol." Chemistry and Physics of Lipids, Volume 199, September 2016, Pages 61-73. https://doi.org/10.1016/j.chemphyslip.2016.04.006.

Goddard, Alan D., Patricia M. Dijkman, Roslin J. Adamson, and Anthony Watts. Lipid-Dependent GPCR Dimerization. Methods in Cell Biology. 1st ed. Vol. 117. Elsevier Inc., Volume 117, 2013, Pages 341-357,2013. https://doi.org/10.1016/B978-0-12-408143-7.00018-9.

I. Company Marin, PhD Thesis, Aston University 2024

Goddard, Alan D., and Anthony Watts. "Regulation of G Protein-Coupled Receptors by Palmitoylation and Cholesterol." BMC Biology, 10, Article number: 27, 2012. https://doi.org/10.1186/1741-7007-10-27.

Godzien, Joanna, Michal Ciborowski, María Paz Martínez-Alcázar, Paulina Samczuk, Adam Kretowski, and Coral Barbas. "Rapid and Reliable Identification of Phospholipids for Untargeted Metabolomics with LC-ESI-QTOF-MS/MS." Journal of Proteome Research, 14, 8, 3204–3216, 2015. https://doi.org/10.1021/acs.jproteome.5b00169.

Goldberg, Stanley. "Mechanical/Physical Methods of Cell Disruption and Tissue Homogenization." In L'Ameto, 2261:563–85, 2021. https://doi.org/10.1007/978-1-0716-1186-9_36.

Gonzalez-Riano, Carolina, Ana Gradillas, and Coral Barbas. "Exploiting the Formation of Adducts in Mobile Phases with Ammonium Fluoride for the Enhancement of Annotation in Liquid Chromatography-High Resolution Mass Spectrometry Based Lipidomics." Journal of Chromatography Open, Volume 1, November 2021, 100018. https://doi.org/10.1016/j.jcoa.2021.100018.

Gorbenko, Galyna P. "Fluorescence Spectroscopy of Protein Oligomerization in Membranes." In Journal of Fluorescence, Volume 21, pages 945–951, 2011. https://doi.org/10.1007/s10895-010-0649-6.

Gottesman-Katz, Lena, Rocco Latorre, Stephen Vanner, Brian L. Schmidt, and Nigel W. Bunnett. "Targeting G Protein-Coupled Receptors for the Treatment of Chronic Pain in the Digestive System." Gut, Volume 70, Issue 5, 2021. https://doi.org/10.1136/gutjnl-2020-321193.

Goulding, Joelle, Lauren T. May, and Stephen J. Hill. "Characterisation of Endogenous A2A and A2B Receptor-Mediated Cyclic AMP Responses in HEK 293 Cells Using the GloSensorTM Biosensor: Evidence for an Allosteric Mechanism of Action for the A2B-Selective Antagonist PSB 603." Biochemical Pharmacology 147, 2018. 55–66. https://doi.org/10.1016/j.bcp.2017.10.013.

Griendling, Kathy K., and Garret A. FitzGerald. "Oxidative Stress and Cardiovascular Injury Part I: Basic Mechanisms and In Vivo Monitoring of ROS." Circulation, 108:1912–1916, 2003. https://doi.org/10.1161/01.CIR.0000093660.86242.BB.

Grillitsch, Karlheinz, Pablo Tarazona, Lisa Klug, Tamara Wriessnegger, Günther Zellnig, Erich Leitner, Ivo Feussner, and Günther Daum. "Isolation and Characterization of the Plasma Membrane from the Yeast Pichia Pastoris." Biochimica et Biophysica Acta - Biomembranes 1838, no. 7, 2014. 1889–97. https://doi.org/10.1016/j.bbamem.2014.03.012.

Grime, Rachael L., Joelle Goulding, Romez Uddin, Leigh A. Stoddart, Stephen J. Hill, David R. Poyner, Stephen J. Briddon, and Mark Wheatley. "Single Molecule Binding of a Ligand to a G-Protein-Coupled Receptor in Real Time Using Fluorescence Correlation Spectroscopy, Rendered Possible by Nano-Encapsulation in Styrene Maleic Acid Lipid Particles." Nanoscale 12, no. 21, 2020. 11518–25. https://doi.org/10.1039/d0nr01060j.

Grinberg, Asya V., Natalia M. Gevondyan, Natalia V. Grinberg, and Valerij Y. Grinberg. "The Thermal Unfolding and Domain Structure of Na+/K+-Exchanging ATPase: A Scanning Calorimetry Study." European Journal of Biochemistry, Volume 268, Issue 19, October 2001, Pages 5027-5036. https://doi.org/10.1046/j.0014-2956.2001.02436.x.

Grouleff, Julie, Sheeba Jem Irudayam, Katrine K. Skeby, and Birgit Schiøtt. "The Influence of Cholesterol on Membrane Protein Structure, Function, and Dynamics Studied by Molecular Dynamics Simulations." Biochimica et Biophysica Acta - Biomembranes, Volume 1848, Issue 9, September 2015, Pages 1783-1795. https://doi.org/10.1016/j.bbamem.2015.03.029.

Guan, Rongfa, Tianshu Kang, Fei Lu, Zhiguo Zhang, Haitao Shen, and Mingqi Liu. "Cytotoxicity, Oxidative Stress, and Genotoxicity in Human Hepatocyte and Embryonic Kidney Cells Exposed to ZnO Nanoparticles." Nanoscale Research Letters 7, 2012. 1–7. https://doi.org/10.1186/1556-276X-7-602.

Guieu, Régis, Jean-Claude Deharo, Baptiste Maille, Lia Crotti, Ermino Torresani, Michele Brignole, and Gianfranco Parati. "Adenosine and the Cardiovascular System: The Good and the Bad." Journal of Clinical Medicine 9, no. 5, 2020. 1366. https://doi.org/10.3390/jcm9051366.

Guixà-González, Ramon, José L. Albasanz, Ismael Rodriguez-Espigares, Manuel Pastor, Ferran Sanz, Maria Martí-Solano, Moutusi Manna, et al. "Membrane Cholesterol Access into a G-Protein-Coupled Receptor." Nature Communications, 8, Article number: 14505, 2017. https://doi.org/10.1038/ncomms14505.

Guixà-González, Ramon, Matti Javanainen, Maricel Gómez-Soler, Begoña Cordobilla, Joan Carles Domingo, Ferran Sanz, Manuel Pastor, Francisco Ciruela, Hector Martinez-Seara, and Jana Selent. "Membrane Omega-3 Fatty Acids Modulate

I. Company Marin, PhD Thesis, Aston University 2024

the Oligomerisation Kinetics of Adenosine A2A and Dopamine D2 Receptors." Scientific Reports, 6, Article number: 19839, 2016. https://doi.org/10.1038/srep19839.

Gulamhussein, Aiman A., Danyall Meah, Damian D. Soja, Stephen Fenner, Zakaria Saidani, Aneel Akram, Simran Lallie, et al. "Examining the Stability of Membrane Proteins within SMALPs." European Polymer Journal, Volume 112, March 2019, Pages 120-125. https://doi.org/10.1016/j.eurpolymj.2018.12.008.

Gulamhussein, Aiman A., Romez Uddin, Brian J. Tighe, David R. Poyner, and Alice J. Rothnie. "A Comparison of SMA, Styrene Maleic Acid. and DIBMA, Di-Isobutylene Maleic Acid. for Membrane Protein Purification." Biochimica et Biophysica Acta - Biomembranes 1862, no. 7, 2020. 183281. https://doi.org/10.1016/j.bbamem.2020.183281.

Gulati S, Jamshad M, Knowles TJ, et al. Detergent-free purification of ABC (ATP-binding-cassette) transporters. Biochem J. 2014;461(2):269-278. https://doi.org/10.1042/BJ20131477

Guo, Canyong, Lingyun Yang, Zhijun Liu, Dongsheng Liu, and Kurt Wüthrich. "Two-Dimensional NMR Spectroscopy of the G Protein-Coupled Receptor A2AAR in Lipid Nanodiscs." Molecules 28, no. 14, 2023. https://doi.org/10.3390/molecules28145419.

Guo, Dong, Albert C. Pan, Ron O. Dror, Tamara Mocking, Rongfang Liu, Laura H. Heitman, David E. Shaw, and Adriaan P. IJzerman. "Molecular Basis of Ligand Dissociation from the Adenosine A2A Receptor." Molecular Pharmacology 89, no. 5, 2016. 485–91. https://doi.org/10.1124/mol.115.102657.

Guo, Yuanke, Yang Liao, Jing Wang, Chen Ma, Jialun Qin, Jiao Feng, Yan Li, Xin Wang, and Kequan Chen. "Methylotrophy of Pichia Pastoris: Current Advances, Applications, and Future Perspectives for Methanol-Based Biomanufacturing." ACS Sustainable Chemistry and Engineering, 10, 5, 1741–1752, 2022. https://doi.org/10.1021/acssuschemeng.1c07755.

Gupta, Suneel, Sabeeh Kamil, Prashant R. Sinha, Jason T. Rodier, Shyam S. Chaurasia, and Rajiv R. Mohan. "Glutathione Is a Potential Therapeutic Target for Acrolein Toxicity in the Cornea." Toxicology Letters 340, 2021. 33–42. https://doi.org/10.1016/j.toxlet.2021.01.005.

Gutierrez, M. Gertrude, Jacob Deyell, Kate L. White, Lucia C. Dalle Ore, Vadim Cherezov, Raymond C. Stevens, and Noah Malmstadt. "The Lipid Phase Preference of the Adenosine A2A Receptor Depends on Its Ligand Binding State." Chemical Communications 55, no. 40, 2019. 5724–27. https://doi.org/10.1039/c8cc10130b.

Guzik, Tomasz J., and Rhian M. Touyz. "Oxidative Stress, Inflammation, and Vascular Aging in Hypertension." Hypertension, 70:660–667, 2017. https://doi.org/10.1161/hypertensionaha.117.07802.

Haffke, Matthias, Gabriele Rummel, Jacques Boivineau, Anna Münch, and Veli-pekka Jaakola. "Thermal Unfolding of GPCRs NanoDSF : Label-Free Thermal Unfolding Assay of G Protein- Coupled Receptors for Compound Screening and Buffer Composition Optimization." Application Note NT-PR-008, 2016. 1–8.

Hamann, Kristin, Genevieve Nehrt, Hui Ouyang, Brad Duerstock, and Riyi Shi. "Hydralazine Inhibits Compression and Acrolein-Mediated Injuries in Ex Vivo Spinal Cord." Journal of Neurochemistry, Volume 104, Issue 3, February 2008, Pages 708-718. https://doi.org/10.1111/j.1471-4159.2007.05002.x.

Hanson, Michael A., Vadim Cherezov, Mark T. Griffith, Christopher B. Roth, Veli Pekka Jaakola, Ellen Y.T. Chien, Jeffrey Velasquez, Peter Kuhn, and Raymond C. Stevens. "A Specific Cholesterol Binding Site Is Established by the 2.8 Å Structure of the Human B2-Adrenergic Receptor." Structure, Volume 16, Issue 6, 11 June 2008, Pages 897-905. https://doi.org/10.1016/j.str.2008.05.001.

Hardy, David, Roslyn M. Bill, Alice J. Rothnie, and Anass Jawhari. "Stabilization of Human Multidrug Resistance Protein 4, MRP4/ABCC4. Using Novel Solubilization Agents." SLAS Discovery, Volume 24, Issue 10, December 2019, Pages 1009-1017. https://doi.org/10.1177/2472555219867074.

Hardy, David, Elodie Desuzinges Mandon, Alice J. Rothnie, and Anass Jawhari. "The Yin and Yang of Solubilization and Stabilization for Wild-Type and Full-Length Membrane Protein." Methods, Volume 147, 1 September 2018, Pages 118-125. https://doi.org/10.1016/j.ymeth.2018.02.017.

Harvey, Faith Christine, Vanessa Collao, and Sanjoy K. Bhattacharya. "High-Resolution Liquid Chromatography-Mass Spectrometry for Lipidomics." Methods in Molecular Biology, Clifton, N.J., 2023, pp 57–63. https://doi.org/10.1007/978-1-0716-2966-6_4.

I. Company Marin, PhD Thesis, Aston University 2024

Hauser, Alexander S., Misty M. Attwood, Mathias Rask-Andersen, Helgi B. Schiöth, and David E. Gloriam. "Trends in GPCR Drug Discovery: New Agents, Targets and Indications." Nature Reviews Drug Discovery, 16, pages829–842, 2017. https://doi.org/10.1038/nrd.2017.178.

Hazell, Gavin, Thomas Arnold, Robert D. Barker, Luke A. Clifton, Nina Juliane Steinke, Cecilia Tognoloni, and Karen J. Edler. "Evidence of Lipid Exchange in Styrene Maleic Acid Lipid Particle, SMALP. Nanodisc Systems." Langmuir 32, no. 45, 2016. 11845–53. https://doi.org/10.1021/acs.langmuir.6b02927.

Hellmann, Nadja, and Dirk Schneider. "To Study Protein Structure" 1958, no. April, 2019. 379–401. https://doi.org/10.1007/978-1-4939-9161-7.

Hesketh, Sophie Janine. "Developing Our Understanding of the Transient Receptor Potential Melastatin By" 2, no. May, 2020.

Hino, Tomoya, Takatoshi Arakawa, Hiroko Iwanari, Takami Yurugi-Kobayashi, Chiyo Ikeda-Suno, Yoshiko Nakada-Nakura, Osamu Kusano-Arai, et al. "G-Protein-Coupled Receptor Inactivation by an Allosteric Inverse-Agonist Antibody." Nature 482, no. 7384, 2012. 237–40. https://doi.org/10.1038/nature10750.

Hinz, Sonja, Gemma Navarro, Dasiel Borroto-Escuela, Benjamin F Seibt, York-Christoph Ammon, Elisabetta de Filippo, Azeem Danish, et al. "Adenosine A2A Receptor Ligand Recognition and Signaling Is Blocked by A2B Receptors." Oncotarget 9, no. 17, March 2, 2018. 13593–611. https://doi.org/10.18632/oncotarget.24423.

Hishikawa, Daisuke, Tomomi Hashidate, Takao Shimizu, and Hideo Shindou. "Diversity and Function of Membrane Glycerophospholipids Generated by the Remodeling Pathway in Mammalian Cells." Journal of Lipid Research, Volume 55, Issue 5, May 2014, Pages 799-807. https://doi.org/10.1194/jlr.R046094.

Ho, C S, C W K Lam, M H M Chan, R C K Cheung, L K Law, L C W Lit, K F Ng, M W M Suen, and H L Tai. "Electrospray Ionisation Mass Spectrometry: Principles and Clinical Applications." The Clinical Biochemist. Reviews 24, no. 1, 2003. 3–12. https://doi.org/10.1002/9781118307816.ch34.

Hochuli, E., W. Bannwarth, H. Dobeli, R. Gentzi, and D. Stuber. "Genetic Approach to Facilitate Purification of Recombinant Proteins with a Novel Metal Chelate Adsorbent." Bio/Technology, 6, pages1321–1325, 1988. https://doi.org/10.1038/nbt1188-1321.

Horsey, Aaron J., Deborah A. Briggs, Nicholas D. Holliday, Stephen J. Briddon, and Ian D. Kerr. "Application of Fluorescence Correlation Spectroscopy to Study Substrate Binding in Styrene Maleic Acid Lipid Copolymer Encapsulated ABCG2." Biochimica et Biophysica Acta - Biomembranes, Volume 1862, Issue 6, 1 June 2020, 183218. https://doi.org/10.1016/j.bbamem.2020.183218.

Hossain, Mohammad, Umashankar Das, and Jonathan R. Dimmock. "Recent Advances in α,β-Unsaturated Carbonyl Compounds as Mitochondrial Toxins." European Journal of Medicinal Chemistry 183, 2019. https://doi.org/10.1016/j.ejmech.2019.111687.

Howie, Duncan, Herman Waldmann, and Stephen Paul Cobbold. "Nutrient Sensing via MTOR in T Cells Maintains a Tolerogenic Microenvironment." Frontiers in Immunology 5, no. AUG, 2014. https://doi.org/10.3389/fimmu.2014.00409.

Hu, Changfeng, Qiao Duan, and Xianlin Han. "Strategies to Improve/Eliminate the Limitations in Shotgun Lipidomics." Proteomics, Volume 20, Issue 11, Special Issue:Targeted Omics, June 2020, 1900070. https://doi.org/10.1002/pmic.201900070.

Hu, Changfeng, Wenqing Luo, Jie Xu, and Xianlin Han. "Recognition And Avoidance Of Ion Source-Generated Artifacts In Lipidomics Analysis." Mass Spectrometry Reviews, Volume 41, Issue 1, 2022, Pages 15-31. https://doi.org/10.1002/mas.21659.

Hu, Ting, and Jin Lan Zhang. "Mass-Spectrometry-Based Lipidomics." Journal of Separation Science 41, no. 1, 2018. 351–72. https://doi.org/10.1002/jssc.201700709.

Hu, Yin Ran, Hang Ma, Zong Yao Zou, Kai He, Yu Bo Xiao, Yue Wang, Min Feng, Xiao Li Ye, and Xue Gang Li. "Activation of Akt and JNK/Nrf2/NQO1 Pathway Contributes to the Protective Effect of Coptisine against AAPH-Induced Oxidative Stress." Biomedicine and Pharmacotherapy 85, 2017. 313–22. https://doi.org/10.1016/j.biopha.2016.11.031.

Huang, Ting, Jingjing Wang, Weichuan Yu, and Zengyou He. "Protein Inference: A Review." Briefings in Bioinformatics, Volume 13, Issue 5, September 2012, Pages 586–614. https://doi.org/10.1093/bib/bbs004.

I. Company Marin, PhD Thesis, Aston University 2024

Huang, Ying Juan, Ming Hua Jin, Rong Biao Pi, Jun Jie Zhang, Ying Ouyang, Xiao Juan Chao, Mei Hui Chen, et al. "Acrolein Induces Alzheimer's Disease-like Pathologies in Vitro and in Vivo." Toxicology Letters 217, no. 3, 2013. 184–91. https://doi.org/10.1016/j.toxlet.2012.12.023.

Hubbell, Wayne L., Christian Altenbach, Cheryl M. Hubbell, and H. Gobind Khorana. "Rhodopsin Structure, Dynamics, and Activation: A Perspective from Crystallography, Site-Directed Spin Labeling, Sulfhydryl Reactivity, and Disulfide Cross-Linking." Advances in Protein Chemistry, 2003. https://doi.org/10.1016/S0065-3233(03.63010-X.

Hübner, Christian A., Björn C. Schroeder, and Heimo Ehmke. "Regulation of Vascular Tone and Arterial Blood Pressure: Role of Chloride Transport in Vascular Smooth Muscle." Pflugers Archiv European Journal of Physiology 467, no. 3, 2015. 605–14. https://doi.org/10.1007/s00424-014-1684-y.

Hung, Wei Chin, Ming Tao Lee, Hsien Chung, Yi Ting Sun, Hsiung Chen, Nicholas E. Charron, and Huey W. Huang. "Comparative Study of the Condensing Effects of Ergosterol and Cholesterol." Biophysical Journal 110, no. 9, 2016. 2026–33. https://doi.org/10.1016/j.bpj.2016.04.003.

Hunter, Molly, Ping Yuan, Divya Vavilala, and Mark Fox. "Optimization of Protein Expression in Mammalian Cells." Current Protocols in Protein Science, 2019. https://doi.org/10.1002/cpps.77.

Hussain, Hirra, Rodrigo Maldonado-Agurto, and Alan J. Dickson. "The Endoplasmic Reticulum and Unfolded Protein Response in the Control of Mammalian Recombinant Protein Production." Biotechnology Letters, Volume 36, pages 1581–1593, 2014. https://doi.org/10.1007/s10529-014-1537-y.

Hussain, Tarique, Mahmoud Kandeel, Elsayed Metwally, Ghulam Murtaza, Dildar Hussain Kalhoro, Yulong Yin, Bie Tan, et al. "Unraveling the Harmful Effect of Oxidative Stress on Male Fertility: A Mechanistic Insight." Frontiers in Endocrinology 14, no. February, 2023. 1–13. https://doi.org/10.3389/fendo.2023.1070692.

Igonet, Sébastien, Claire Raingeval, Erika Cecon, Maja Pučić-Baković, Gordan Lauc, Olivier Cala, Maciej Baranowski, et al. "Enabling STD-NMR Fragment Screening Using Stabilized Native GPCR: A Case Study of Adenosine Receptor." Scientific Reports 8, no. 1, 2018. 1–14. https://doi.org/10.1038/s41598-018-26113-0.

Ikram, Muhammad, Tae Ju Park, Tahir Ali, and Myeong Ok Kim. "Antioxidant and Neuroprotective Effects of Caffeine against Alzheimer's and Parkinson's Disease: Insight into the Role of Nrf-2 and A2AR Signaling." Antioxidants 9, no. 9, September 22, 2020. 902. https://doi.org/10.3390/antiox9090902.

Isaac, Giorgis. "Electrospray Ionization Tandem Mass Spectrometry, ESI-MS/MS.-Based Shotgun Lipidomics." In Methods in Molecular Biology, 2011, pp 259–275. https://doi.org/10.1007/978-1-61737-985-7_16.

Islam, Mohammad Tawhidul, Abidali Mohamedali, Criselda Santan Fernandes, Mark S. Baker, and Shoba Ranganathan. "De Novo Peptide Sequencing: Deep Mining of High-Resolution Mass Spectrometry Data." In Methods in Molecular Biology, 2017, pp 119–134. https://doi.org/10.1007/978-1-4939-6740-7_10.

Itri, Rosangela, Helena C. Junqueira, Omar Mertins, and Maurício S. Baptista. "Membrane Changes under Oxidative Stress: The Impact of Oxidized Lipids." Biophysical Reviews, Volume 6, pages 47–61, 2014. https://doi.org/10.1007/s12551-013-0128-9.

Iuliano, Luigi. "Pathways of Cholesterol Oxidation via Non-Enzymatic Mechanisms." Chemistry and Physics of Lipids 164, no. 6, 2011. 457–68. https://doi.org/10.1016/j.chemphyslip.2011.06.006.

Ivashov, Vasyl A., Karlheinz Grillitsch, Harald Koefeler, Erich Leitner, Dominic Baeumlisberger, Michael Karas, and Günther Daum. "Lipidome and Proteome of Lipid Droplets from the Methylotrophic Yeast Pichia Pastoris." Biochimica et Biophysica Acta - Molecular and Cell Biology of Lipids, Volume 1831, Issue 2, February 2013, Pages 282-290. https://doi.org/10.1016/j.bbalip.2012.09.017.

Jaakola, V.-P., Mark T Griffith, Michael a Hanson, Vadim Cherezov, E. Y. T. Chien, J Robert Lane, A. P. IJzerman, and Raymond C Stevens. "The 2.6 Angstrom Crystal Structure of a Human A2A Adenosine Receptor Bound to an Antagonist." Science 322, no. 5905, November 21, 2008. 1211–17. https://doi.org/10.1126/science.1164772.

Jaakola, Veli Pekka, J. Robert Lane, Judy Y. Lin, Vsevolod Katritch, Adriaan P. IJzerman, and Raymond C. Stevens. "Ligand Binding and Subtype Selectivity of the Human A2A Adenosine Receptor: Identification and Characterization of Essential Amino Acid Residues." Journal of Biological Chemistry 285, no. 17, 2010. 13032–44. https://doi.org/10.1074/jbc.M109.096974.

I. Company Marin, PhD Thesis, Aston University 2024

Jafurulla, Md, Shrish Tiwari, and Amitabha Chattopadhyay. "Identification of Cholesterol Recognition Amino Acid Consensus, CRAC. Motif in G-Protein Coupled Receptors." Biochemical and Biophysical Research Communications, Volume 404, Issue 1, 7 January 2011, Pages 569-573. https://doi.org/10.1016/j.bbrc.2010.12.031.

Jaganjac, Morana, Tanja Matijevic, Marina Cindric, Ana Cipak, Lidija Mrakovcic, Wolfgang Gubisch, and Neven Zarkovic. "Induction of CMV-1 Promoter by 4-Hydroxy-2-Nonenal in Human Embryonic Kidney Cells." Acta Biochimica Polonica 57, no. 2, 2010. 179–83. https://doi.org/10.18388/abp.2010_2392.

Jager, T. L. de, A. E. Cockrell, and S. S. Du Plessis. "Ultraviolet Light Induced Generation of Reactive Oxygen Species." Advances in Experimental Medicine and Biology 996, 2017. 15–23. https://doi.org/10.1007/978-3-319-56017-5_2.

Jakubík, Jan, and Esam E. El-Fakahany. "Allosteric Modulation of GPCRs of Class a by Cholesterol." International Journal of Molecular Sciences, 22(4), 1953, 2021. https://doi.org/10.3390/ijms22041953.

Jamshad, Mohammed, Jack Charlton, Yu Pin Lin, Sarah J. Routledge, Zharain Bawa, Timothy J. Knowles, Michael Overduin, et al. "G-Protein Coupled Receptor Solubilization and Purification for Biophysical Analysis and Functional Studies, in the Total Absence of Detergent." Bioscience Reports 35, 2015. 1–10. https://doi.org/10.1042/BSR20140171.

Jamshad, Mohammed, Vinciane Grimard, Ilaria Idini, Tim J. Knowles, Miriam R. Dowle, Naomi Schofield, Pooja Sridhar, et al. "Structural Analysis of a Nanoparticle Containing a Lipid Bilayer Used for Detergent-Free Extraction of Membrane Proteins." Nano Research 8, no. 3, 2015. 774–89. https://doi.org/10.1007/s12274-014-0560-6.

Jamshad, Mohammed, Sundaresan Rajesh, Zania Stamataki, Jane A. McKeating, Timothy Dafforn, Michael Overduin, and Roslyn M. Bill. "Structural Characterization of Recombinant Human CD81 Produced in Pichia Pastoris." Protein Expression and Purification 57, no. 2, 2008. 206–16. https://doi.org/10.1016/j.pep.2007.10.013.

Jani, Niketa M., and John M. Lopes. "Regulated Transcription of the Saccharomyces Cerevisiae Phosphatidylinositol Biosynthetic Gene, PIS1, Yields Pleiotropic Effects on Phospholipid Synthesis." FEMS Yeast Research, Volume 9, Issue 4, June 2009, Pages 552–564. https://doi.org/10.1111/j.1567-1364.2009.00514.x.

Jin, Rui, Michael Grasso, Mingyang Zhou, Ronen Marmorstein, and Tobias Baumgart. "Unfolding Mechanisms and Conformational Stability of the Dimeric Endophilin N-BAR Domain." ACS Omega, 6, 32, 20790–20803, 2021. https://doi.org/10.1021/acsomega.1c01905.

Joardar, Ankita, Gourab Prasad Pattnaik, and Hirak Chakraborty. "Mechanism of Membrane Fusion: Interplay of Lipid and Peptide." Journal of Membrane Biology, Volume 255, pages 211–224, 2022. https://doi.org/10.1007/s00232-022-00233-1.

Jones, Andrew J.Y., Florian Gabriel, Aditi Tandale, and Daniel Nietlispach. "Structure and Dynamics of GPCRs in Lipid Membranes: Physical Principles and Experimental Approaches." Molecules, 25(20), 4729, 2020. https://doi.org/10.3390/molecules25204729.

Jones, Karlie R., and Elizabeth M. Kang. "Graft versus Host Disease: New Insights into A2A Receptor Agonist Therapy." Computational and Structural Biotechnology Journal 13, 2015. 101–5. https://doi.org/10.1016/j.csbj.2014.12.003.

Jong, Lutea A.A. De, Donald R.A. Uges, Jan Piet Franke, and Rainer Bischoff. "Receptor-Ligand Binding Assays: Technologies and Applications." Journal of Chromatography B: Analytical Technologies in the Biomedical and Life Sciences, Volume 829, Issues 1–2, 27 December 2005, Pages 1-25. https://doi.org/10.1016/j.jchromb.2005.10.002.

Jun Ma, BSc, Hons. "Mass Spectrometry Method Development to Identify Binding Ligands Against A 2A R Nanodisc Complex." Griffith University, 2017.

Jurneczko, Ewa, and Perdita E. Barran. "How Useful Is Ion Mobility Mass Spectrometry for Structural Biology? The Relationship between Protein Crystal Structures and Their Collision Cross Sections in the Gas Phase." Analyst, 2011. https://doi.org/10.1039/c0an00373e.

Jurowski, Kamil, Kamila Kochan, Justyna Walczak, Małgorzata Barańska, Wojciech Piekoszewski, and Bogusław Buszewski. "Analytical Techniques in Lipidomics: State of the Art." Critical Reviews in Analytical Chemistry, 2017, Pages 418-437. https://doi.org/10.1080/10408347.2017.1310613.

Juturu, Veeresh, and Jin Chuan Wu. "Heterologous Protein Expression in Pichia Pastoris: Latest Research Progress and Applications." ChemBioChem, Volume 19, Issue 1, January 2018, Pages 7-21. https://doi.org/10.1002/cbic.201700460.

I. Company Marin, PhD Thesis, Aston University 2024

Kalhan, A., B. Gharibi, M. Vazquez, B. Jasani, J. Neal, M. Kidd, I. M. Modlin, R. Pfragner, D. A. Rees, and J. Ham. "Adenosine A 2A and A 2B Receptor Expression in Neuroendocrine Tumours: Potential Targets for Therapy." Purinergic Signalling 8, no. 2, 2012. 265–74. https://doi.org/10.1007/s11302-011-9280-5.

Kang, Dong Soo, Xufan Tian, and Jeffrey L. Benovic. "Role of β-Arrestins and Arrestin Domain-Containing Proteins in G Protein-Coupled Receptor Trafficking." Current Opinion in Cell Biology, Volume 27, April 2014, Pages 63-71. https://doi.org/10.1016/j.ceb.2013.11.005.

Kano, Kuniyuki, Junken Aoki, and Timothy Hla. "Lysophospholipid Mediators in Health and Disease." Annual Review of Pathology: Mechanisms of Disease, Vol. 17:459-483, 2021. https://doi.org/10.1146/annurev-pathol-050420-025929.

Karbalaei, Mohsen, Seyed A. Rezaee, and Hadi Farsiani. "Pichia Pastoris: A Highly Successful Expression System for Optimal Synthesis of Heterologous Proteins." Journal of Cellular Physiology, Volume 235, Issue 9, September 2020, Pages 5867-5881. https://doi.org/10.1002/jcp.29583.

Katritch, Vsevolod, Vadim Cherezov, and Raymond C. Stevens. "Structure-Function of the G Protein–Coupled Receptor Superfamily." Annual Review of Pharmacology and Toxicology 53, no. 1, January 6, 2013. 531–56. https://doi.org/10.1146/annurev-pharmtox-032112-135923.

Katritch, Vsevolod, Gustavo Fenalti, Enrique E. Abola, Bryan L. Roth, Vadim Cherezov, and Raymond C. Stevens. "Allosteric Sodium in Class A GPCR Signaling." Trends in Biochemical Sciences 39, no. 5, 2014. 233–44. https://doi.org/10.1016/j.tibs.2014.03.002.

Kermani, Ali A. "A Guide to Membrane Protein X-Ray Crystallography." FEBS Journal, Volume 288, Issue 20, October 2021, Pages 5788-5804. https://doi.org/10.1111/febs.15676.

Kermanian, Fatemeh, Mansooreh Soleimani, Alireza Ebrahimzadeh, Hossein Haghir, and Mehdi Mehdizadeh. "Effects of Adenosine A2a Receptor Agonist and Antagonist on Hippocampal Nuclear Factor-KB Expression Preceded by MDMA Toxicity." Metabolic Brain Disease 28, no. 1, 2013. 45–52. https://doi.org/10.1007/s11011-012-9366-y.

Keuerleber, Simon, Ingrid Gsandtner, and Michael Freissmuth. "Biochimica et Biophysica Acta From Cradle to Twilight : The Carboxyl Terminus Directs the Fate of the A 2A -Adenosine Receptor." BBA - Biomembranes 1808, no. 5, 2011. 1350–57. https://doi.org/10.1016/j.bbamem.2010.05.009.

Khan, Kishwar Hayat. "Gene Expression in Mammalian Cells and Its Applications." Advanced Pharmaceutical Bulletin, 3(2), 257-263, 2013. https://doi.org/10.5681/apb.2013.042.

Kharche, Shalmali A., and Durba Sengupta. "Dynamic Protein Interfaces and Conformational Landscapes of Membrane Protein Complexes." Current Opinion in Structural Biology, Volume 61, April 2020, Pages 191-197. https://doi.org/10.1016/j.sbi.2020.01.001.

Khayat, Maan T, and Mohammed A Nayeem. "The Role of Adenosine A 2A Receptor, CYP450s , and PPARs in the Regulation of Vascular Tone", Volume 2017 | Article ID 1720920, 2017. https://doi.org/10.1155/2017/1720920.

Khelashvili, George, Xiaolu Cheng, Maria E. Falzone, Milka Doktorova, Alessio Accardi, and Harel Weinstein. "Membrane Lipids Are Both the Substrates and a Mechanistically Responsive Environment of TMEM16 Scramblase Proteins." Journal of Computational Chemistry, Volume 41, Issue 6, March 5, 2020, Pages 538-551. https://doi.org/10.1002/jcc.26105.

Khoury, George A., Richard C. Baliban, and Christodoulos A. Floudas. "Proteome-Wide Post-Translational Modification Statistics: Frequency Analysis and Curation of the Swiss-Prot Database." Scientific Reports, 1, Article number: 90, 2011. https://doi.org/10.1038/srep00090.

Kielkopf, Clara L., William Bauer, and Ina L. Urbatsch. "Preparation of Cell Extracts for Purification of Proteins Expressed in Pichia Pastoris." Cold Spring Harbor Protocols 2021, no. 1, 2021. 38–42. https://doi.org/10.1101/pdb.prot102186.

Killian, J. Antoinette. "Hydrophobic Mismatch between Proteins and Lipids in Membranes." Biochimica et Biophysica Acta - Reviews on Biomembranes, 1998. https://doi.org/10.1016/S0304-4157(98.00017-3.

Kim, Geon Ha, Jieun E. Kim, Sandy Jeong Rhie, and Sujung Yoon. "The Role of Oxidative Stress in Neurodegenerative Diseases." Experimental Neurobiology, 24(4): 325-340, 2015. https://doi.org/10.5607/en.2015.24.4.325.

Kim, Sun Il, Yuanzheng Wu, Ka Lyun Kim, Geun Joong Kim, and Hyun Jae Shin. "Improved Cell Disruption of Pichia Pastoris Utilizing Aminopropyl Magnesium Phyllosilicate (AMP) Clay." World Journal of Microbiology and Biotechnology, Volume 29, pages 1129–1132, 2013. https://doi.org/10.1007/s11274-013-1262-z.

I. Company Marin, PhD Thesis, Aston University 2024

Klinger, Markus, Mandy Kuhn, Herwig Just, Eduard Stefan, Timothy Palmer, and Michael Freissmuth. "Removal of the Carboxy Terminus of the A 2A -Adenosine Receptor Blunts Constitutive Activity: Differential Effect on CAMP Accumulation and MAP Kinase Stimulation," 2002, 287–98. https://doi.org/10.1007/s00210-002-0617-z.

Klose, Christian, Michal A. Surma, and Kai Simons. "Organellar Lipidomics-Background and Perspectives." Current Opinion in Cell Biology, Volume 25, Issue 4, August 2013, Pages 406-413. https://doi.org/10.1016/j.ceb.2013.03.005.

Klug, Lisa, Pablo Tarazona, Clemens Gruber, Karlheinz Grillitsch, Brigitte Gasser, Martin Trötzmüller, Harald Köfeler, et al. "The Lipidome and Proteome of Microsomes from the Methylotrophic Yeast Pichia Pastoris." Biochimica et Biophysica Acta - Molecular and Cell Biology of Lipids 1841, no. 2, 2014. 215–26. https://doi.org/10.1016/j.bbalip.2013.11.005.

Knowles, Timothy J, Rachael Finka, Corinne Smith, Yu-pin Lin, Tim Dafforn, and Michael Overduin. "Membrane Proteins Solubilized Intact in Lipid Containing Nanoparticles Bounded by Styrene Maleic Acid Copolymer" 7, 2009. 7484–85. https://doi.org/10.1021/ja810046q.

Kobilka, Brian K., and Xavier Deupi. "Conformational Complexity of G-Protein-Coupled Receptors." Trends in Pharmacological Sciences 28, no. 8, 2007. 397–406. https://doi.org/10.1016/j.tips.2007.06.003.

Koeppen, Michael, Tobias Eckle, and Holger K. Eltzschig. "Interplay of Hypoxia and A 2B Adenosine Receptors in Tissue Protection." In Advances in Pharmacology, Volume 61, 2011, Pages 145-186. https://doi.org/10.1016/B978-0-12-385526-8.00006-0.

Kostiainen, Risto, and Tiina J. Kauppila. "Effect of Eluent on the Ionization Process in Liquid Chromatography-Mass Spectrometry." Journal of Chromatography A, Volume 1216, Issue 4, 23 January 2009, Pages 685-699. https://doi.org/10.1016/j.chroma.2008.08.095.

Krainer, Florian W, Christian Dietzsch, Tanja Hajek, Christoph Herwig, Oliver Spadiut, and Anton Glieder. "Krainer 2012 Recombinant Protein." Microbial Cell Factories 22, no. 11, 2012. 1–14. https://doi.org/10.1186/1475-2859-11-22

Lanznaster, Débora, Caio M. Massari, Vendula Marková, Tereza Šimková, Romain Duroux, Kenneth A. Jacobson, Víctor Fernández-Dueñas, Carla I. Tasca, and Francisco Ciruela. "Adenosine A1-A2A Receptor-Receptor Interaction: Contribution to Guanosine-Mediated Effects." Cells 8, no. 12, 2019. https://doi.org/10.3390/cells8121630.

Laursen, Louise, Kasper Severinsen, Kristina Birch Kristensen, Xavier Periole, Malene Overby, Heidi Kaastrup Müller, Birgit Schiøtt, and Steffen Sinning. "Cholesterol Binding to a Conserved Site Modulates the Conformation, Pharmacology, and Transport Kinetics of the Human Serotonin Transporter." Journal of Biological Chemistry, Volume 293, Issue 10, 11 March 2018, Pages 3510-3523. https://doi.org/10.1074/jbc.M117.809046.

Lavington, Steven, and Anthony Watts. "Lipid Nanoparticle Technologies for the Study of G Protein-Coupled Receptors in Lipid Environments." Biophysical Reviews 12, no. 6, 2020. 1287–1302. https://doi.org/10.1007/s12551-020-00775-5.

Leaptrot, Katrina L., Jody C. May, James N. Dodds, and John A. McLean. "Ion Mobility Conformational Lipid Atlas for High Confidence Lipidomics." Nature Communications 10, no. 1, 2019. https://doi.org/10.1038/s41467-019-08897-5.

Lebon, Guillaume, Kirstie Bennett, Ali Jazayeri, and Christopher G. Tate. "Thermostabilisation of an Agonist-Bound Conformation of the Human Adenosine A2A Receptor." Journal of Molecular Biology 409, no. 3, 2011. 298–310. https://doi.org/10.1016/j.jmb.2011.03.075.

Lebon, Guillaume, Tony Warne, Patricia C. Edwards, Kirstie Bennett, Christopher J. Langmead, Andrew G.W. Leslie, and Christopher G. Tate. "Agonist-Bound Adenosine A2A Receptor Structures Reveal Common Features of GPCR Activation." Nature 474, no. 7352, 2011. 521–26. https://doi.org/10.1038/nature10136.

Lee, Anthony G. "A Database of Predicted Binding Sites for Cholesterol on Membrane Proteins, Deep in the Membrane." Biophysical Journal, Volume 115, Issue 3, 7 August 2018, Pages 522-532. https://doi.org/10.1016/j.bpj.2018.06.022.

Lee, Ming Yue, James Geiger, Andrii Ishchenko, Gye Won Han, Anton Barty, Thomas A. White, Cornelius Gati, et al. "Harnessing the Power of an X-Ray Laser for Serial Crystallography of Membrane Proteins Crystallized in Lipidic Cubic Phase." IUCrJ, Volume 7, Part 6, November 2020, Pages 976-984. https://doi.org/10.1107/S2052252520012701.

Lehman, Li Wei, Mohammed Saeed, George Moody, and Roger Mark. "Hypotension as a Risk Factor for Acute Kidney Injury in ICU Patients." Computing in Cardiology 37, no. 2010, 2010. 1095–98.

I. Company Marin, PhD Thesis, Aston University 2024

Leonard, Alison N., and Edward Lyman. "Activation of G-Protein-Coupled Receptors Is Thermodynamically Linked to Lipid Solvation." Biophysical Journal, Volume 120, Issue 9, 4 May 2021, Pages 1777-1787. https://doi.org/10.1016/j.bpj.2021.02.029.

Leone, Robert D., and Leisha A. Emens. "Targeting Adenosine for Cancer Immunotherapy." Journal for ImmunoTherapy of Cancer 6, no. 1, 2018. 1–9. https://doi.org/10.1186/s40425-018-0360-8.

Lera Ruiz, Manuel de, Yeon-hee Lim, and Junying Zheng. "Adenosine A 2A Receptor as a Drug Discovery Target." Journal of Medicinal Chemistry 57, no. 9, May 8, 2014. 3623–50. https://doi.org/10.1021/jm4011669.

Levental, Ilya, and Ed Lyman. "Regulation of Membrane Protein Structure and Function by Their Lipid Nano-Environment." Nature Reviews Molecular Cell Biology, 24, pages107–122, 2023. https://doi.org/10.1038/s41580-022-00524-4.

Leventis, Peter A., and Sergio Grinstein. "The Distribution and Function of Phosphatidylserine in Cellular Membranes." Annual Review of Biophysics, Vol. 39:407-427, 2010. https://doi.org/10.1146/annurev.biophys.093008.131234.

Li, Chang, Shiying Chu, Siyuan Tan, Xinchi Yin, You Jiang, Xinhua Dai, Xiaoyun Gong, Xiang Fang, and Di Tian. "Towards Higher Sensitivity of Mass Spectrometry: A Perspective From the Mass Analyzers." Frontiers in Chemistry, Volume 9, 2021. https://doi.org/10.3389/fchem.2021.813359.

Li, Yi Fang, Shu Hua Ouyang, Long Fang Tu, Xi Wang, Wei Lin Yuan, Guo En Wang, Yan Ping Wu, et al. "Caffeine Protects Skin from Oxidative Stress-Induced Senescence through the Activation of Autophagy." Theranostics 8, no. 20, 2018. 5713–30. https://doi.org/10.7150/thno.28778.

Liao, Chenyi, Mathilde P. de Molliens, Severin T. Schneebeli, Matthias Brewer, Gaojie Song, David Chatenet, Karen M. Braas, Victor May, and Jianing Li. "Targeting the PAC1 Receptor for Neurological and Metabolic Disorders." Current Topics in Medicinal Chemistry 19, no. 16, 2019. 1399–1417. https://doi.org/10.2174/1568026619666190709092647.

Liebisch, Gerhard, Eoin Fahy, Junken Aoki, Edward A. Dennis, Thierry Durand, Christer S. Ejsing, Maria Fedorova, et al. "Update on LIPID MAPS Classification, Nomenclature, and Shorthand Notation for MS-Derived Lipid Structures." Journal of Lipid Research 61, no. 12, 2020. 1539–55. https://doi.org/10.1194/jlr.S120001025.

Lim, Crystale Siew Ying, Chee Hong Tung, Rozita Rosli, and Pei Pei Chong. "An Alternative Candida Spp. Cell Wall Disruption Method Using a Basic Sorbitol Lysis Buffer and Glass Beads." Journal of Microbiological Methods 75, no. 3, 2008. 576–78. https://doi.org/10.1016/j.mimet.2008.07.026.

Liu, Wei, Eugene Chun, Aaron A. Thompson, Vadim Cherezov, and Raymond C. Stevens. "Structural Basis for Allosteric Regulation of GPCRs by Sodium Ions." Science 337, no. 6091, 2013. 232–36. https://doi.org/10.1126/science.1219218.Structural.

Liu, Ying Jiao, Jiao Chen, Xun Li, Xin Zhou, Yao Mei Hu, Shi Feng Chu, Ye Peng, and Nai Hong Chen. "Research Progress on Adenosine in Central Nervous System Diseases." CNS Neuroscience and Therapeutics 25, no. 9, 2019. 899–910. https://doi.org/10.1111/cns.13190.

Liu, Yonggang, Jianjie Xu, Li Han, Qiangqiang Liu, Yunfan Yang, Zeren Li, Zhongyuan Lu, Hang Zhang, Tengxiao Guo, and Qiao Liu. "Theoretical Research on Excited States: Ultraviolet and Fluorescence Spectra of Aromatic Amino Acids." Interdisciplinary Sciences – Computational Life Sciences, Volume 12, pages 530–536, 2020. https://doi.org/10.1007/s12539-020-00395-3.

Liu, Zhaoyang, and Kevin L. Schey. "Fragmentation of Multiply-Charged Intact Protein Ions Using MALDI TOF-TOF Mass Spectrometry." Journal of the American Society for Mass Spectrometry, 19, 2, 231–238, 2008. https://doi.org/10.1016/j.jasms.2007.06.006.

Logez, Christel, Marjorie Damian, Céline Legros, Clémence Dupré, Mélody Guéry, Sophie Mary, Renaud Wagner, et al. "Detergent-Free Isolation of Functional G Protein-Coupled Receptors into Nanometric Lipid Particles." Biochemistry, 55, 1, 38–48, 2016. https://doi.org/10.1021/acs.biochem.5b01040.

Lovell, Mark A., Chengsong Xie, and William R. Markesbery. "Acrolein Is Increased in Alzheimer's Disease Brain and Is Toxic to Primary Hippocampal Cultures." Neurobiology of Aging, 2001. https://doi.org/10.1016/S0197-4580(00.00235-9.

Luchini, Alessandra, Robin Delhom, Viviana Cristiglio, Wolfgang Knecht, Hanna Wacklin-Knecht, and Giovanna Fragneto. "Effect of Ergosterol on the Interlamellar Spacing of Deuterated Yeast Phospholipid Multilayers." Chemistry and Physics of Lipids, Volume 227, March 2020, 104873, 2020. https://doi.org/10.1016/j.chemphyslip.2020.104873.

I. Company Marin, PhD Thesis, Aston University 2024

Ludwig, Nils, Saigopalakrishna S. Yerneni, Juliana H. Azambuja, Delbert G. Gillespie, Elizabeth V. Menshikova, Edwin K. Jackson, and Theresa L. Whiteside. "Tumor-Derived Exosomes Promote Angiogenesis via Adenosine A2B Receptor Signaling." Angiogenesis 23, no. 4, 2020. 599–610. https://doi.org/10.1007/s10456-020-09728-8.

Lundstrom, K. "Structural Genomics and Drug Discovery: Molecular Pharmacology." Journal of Cellular and Molecular Medicine 11, no. 2, 2007. 224–38. https://doi.org/10.1111/j.1582-4934.2007.00028.x.

Luo, Jian, J. Paul Robinson, and Riyi Shi. "Acrolein-Induced Cell Death in PC12 Cells: Role of Mitochondria-Mediated Oxidative Stress." Neurochemistry International 47, no. 7, 2005. 449–57. https://doi.org/10.1016/j.neuint.2005.07.002.

Luo, Zhaoke, Xinyue Liao, Lili Luo, Qitong Fan, Xiaofen Zhang, Yuefeng Guo, Feng Wang, Zucheng Ye, and Daoshu Luo. "Extracellular ATP and CAMP Signaling Promote Piezo2-Dependent Mechanical Allodynia after Trigeminal Nerve Compression Injury." Journal of Neurochemistry, Volume 160, Issue 3, February 2022, Pages 376-391. https://doi.org/10.1111/jnc.15537.

Maciel, Elisabete, Bruno M. Neves, Deolinda Santinha, Ana Reis, Pedro Domingues, M. Teresa Cruz, Andrew R. Pitt, Corinne M. Spickett, and M. Rosário M. Domingues. "Detection of Phosphatidylserine with a Modified Polar Head Group in Human Keratinocytes Exposed to the Radical Generator AAPH." Archives of Biochemistry and Biophysics 548, 2014. 38–45. https://doi.org/10.1016/j.abb.2014.02.002.

Magnani, Francesca, Yoko Shibata, Maria J. Serrano-Vega, and Christopher G. Tate. "Co-Evolving Stability and Conformational Homogeneity of the Human Adenosine A2a Receptor." Proceedings of the National Academy of Sciences of the United States of America 105, no. 31, 2008. 10744–49. https://doi.org/10.1073/pnas.0804396105.

Maguire, Janet J., Rhoda E. Kuc, and Anthony P. Davenport. "Radioligand Binding Assays and Their Analysis." Methods in Molecular Biology, 2012, pp 31–77. https://doi.org/10.1007/978-1-61779-909-9_3.

Mahmood, Tahrin, and Ping Chang Yang. "Western Blot: Technique, Theory, and Trouble Shooting." North American Journal of Medical Sciences, 2012. https://doi.org/10.4103/1947-2714.100998.

Mairinger, Teresa, Tim J. Causon, and Stephan Hann. "The Potential of Ion Mobility–Mass Spectrometry for Non-Targeted Metabolomics." Current Opinion in Chemical Biology, Volume 42, February 2018, Pages 9-15. https://doi.org/10.1016/j.cbpa.2017.10.015.

Malinsky, Jan, Miroslava Opekarová, and Widmar Tanner. "The Lateral Compartmentation of the Yeast Plasma Membrane." Yeast, Volume 27, Issue 8, Special Issue of Yeast on Fungal Cell Walls, August 2010, Pages 473-478. https://doi.org/10.1002/yea.1772.

Manglik, Aashish, Tae Hun Kim, Matthieu Masureel, Christian Altenbach, Zhongyu Yang, Daniel Hilger, Michael T. Lerch, et al. "Structural Insights into the Dynamic Process of β 2 -Adrenergic Receptor Signaling." Cell 161, no. 5, May 2015. 1101–11. https://doi.org/10.1016/j.cell.2015.04.043.

Manglik, Aashish, and Andrew C. Kruse. "Structural Basis for G Protein-Coupled Receptor Activation." Biochemistry 56, no. 42, 2017. 5628–34. https://doi.org/10.1021/acs.biochem.7b00747.

Mao, Qingcheng, Gwenaëlle Conseil, Anshul Gupta, Susan P.C. Cole, and Jashvant D. Unadkat. "Functional Expression of the Human Breast Cancer Resistance Protein in Pichia Pastoris." Biochemical and Biophysical Research Communications, Volume 320, Issue 3, 30 July 2004, Pages 730-737. https://doi.org/10.1016/j.bbrc.2004.06.012.

Marino, Stefano M., Yehua Li, Dmitri E. Fomenko, Natalia Agisheva, Ronald L. Cerny, and Vadim N. Gladyshev. "Characterization of Surface-Exposed Reactive Cysteine Residues in Saccharomyces Cerevisiae." Biochemistry, 49, 35, 7709–7721, 2010. https://doi.org/10.1021/bi100677a.

Marsh, Derek, and Tibor Páli. "The Protein-Lipid Interface: Perspectives from Magnetic Resonance and Crystal Structures." Biochimica et Biophysica Acta - Biomembranes, Volume 1666, Issues 1–2, 3 November 2004, Pages 118-141. https://doi.org/10.1016/j.bbamem.2004.08.006.

Marzoog, Basheer Abdullah, and Tatyana Ivanovna Vlasova. "Membrane Lipids under Norm and Pathology." European Journal of Clinical and Experimental Medicine, T. 19, z. 1, 2021, s. 59–75. https://doi.org/10.15584/ejcem.2021.1.9.

Masih, Anup, Saumya Singh, Amol Kumar Agnihotri, Sabeena Giri, Jitendra Kumar Shrivastava, Nidhi Pandey, Hans Raj Bhat, and Udaya Pratap Singh. "Design and Development of 1,3,5-Triazine-Thiadiazole Hybrids as Potent Adenosine A2A

Receptor, A2AR. Antagonist for Benefit in Parkinson's Disease." Neuroscience Letters 735, no. June, 2020. 135222. https://doi.org/10.1016/j.neulet.2020.135222.

Massink, A., M. Holzheimer, A. Hölscher, J. Louvel, D. Guo, G. Spijksma, T. Hankemeier, and A. P. IJzerman. "Mass Spectrometry-Based Ligand Binding Assays on Adenosine A1 and A2A Receptors." Purinergic Signalling 11, no. 4, 2015. 581–94. https://doi.org/10.1007/s11302-015-9477-0.

Massink, Arnault, Hugo Gutiérrez-De-Terán, Eelke B. Lenselink, Natalia V.Ortiz Zacarías, Lizi Xia, Laura H. Heitman, Vsevolod Katritch, Raymond C. Stevens, and Adriaan P. IJzerman. "Sodium Ion Binding Pocket Mutations and Adenosine A2A Receptor Function." Molecular Pharmacology 87, no. 2, 2015. 305–13. https://doi.org/10.1124/mol.114.095737.

Matharu, Anne Lise, Stuart J. Mundell, Jeffrey L. Benovic, and Eamonn Kelly. "Rapid Agonist-Induced Desensitization and Internalization of the A 2B Adenosine Receptor Is Mediated by a Serine Residue Close to the COOH Terminus." Journal of Biological Chemistry 276, no. 32, 2001. 30199–207. https://doi.org/10.1074/jbc.M010650200.

Matyash, Vitali, Gerhard Liebisch, Teymuras V. Kurzchalia, Andrej Shevchenko, and Dominik Schwudke. "Lipid Extraction by Methyl-Terf-Butyl Ether for High-Throughput Lipidomics." In Journal of Lipid Research, 2008. https://doi.org/10.1194/jlr.D700041-JLR200.

May, Jody C., and John A. McLean. "Ion Mobility-Mass Spectrometry: Time-Dispersive Instrumentation." Analytical Chemistry, 2015. https://doi.org/10.1021/ac504720m.

McGraw, Claire, Lewen Yang, Ilya Leventhal, Edward Lyman, and Anne Skaja Robinson. "Membrane Cholesterol Depletion Reduces Downstream Signaling Activity of the Adenosine A2A Receptor." Biochimica et Biophysica Acta, BBA. - Biomembranes 1861, no. 4, April 2019. 760–67. https://doi.org/10.1016/j.bbamem.2019.01.001.

McKinney, Michael, and Rita Raddatz. "Practical Aspects of Radioligand Binding." Current Protocols in Pharmacology / Editorial Board, S.J. Enna, Editor-in-Chief. .. [et Al.], 2006. https://doi.org/10.1002/0471141755.ph0103s33.

McNeely, Patrick M., Andrea N. Naranjo, Kimberly Forsten-Williams, and Anne Skaja Robinson. "A2AR Binding Kinetics in the Ligand Depletion Regime." SLAS Discovery 22, no. 2, February 2017. 166–75. https://doi.org/10.1177/1087057116667256.

Mediavilla-Varela, Melanie, Julio Castro, Alberto Chiappori, David Noyes, Dalia C. Hernandez, Bertrand Allard, John Stagg, and Scott J. Antonia. "A Novel Antagonist of the Immune Checkpoint Protein Adenosine A2a Receptor Restores Tumor-Infiltrating Lymphocyte Activity in the Context of the Tumor Microenvironment." Neoplasia, United States. 19, no. 7, 2017. 530–36. https://doi.org/10.1016/j.neo.2017.02.004.

Meer, Gerrit Van, Dennis R. Voelker, and Gerald W. Feigenson. "Membrane Lipids: Where They Are and How They Behave." Nature Reviews Molecular Cell Biology 9, no. 2, 2008. 112–24. https://doi.org/10.1038/nrm2330.

Meo, Sergio Di, Tanea T. Reed, Paola Venditti, and Victor Manuel Victor. "Role of ROS and RNS Sources in Physiological and Pathological Conditions." Oxidative Medicine and Cellular Longevity, Volume 2016, 2016. https://doi.org/10.1155/2016/1245049.

Milne, Gillian R., and Timothy M. Palmer. "Anti-Inflammatory and Immunosuppressive Effects of the A2A Adenosine Receptor." TheScientificWorldJournal 11, 2011. 320–39. https://doi.org/10.1100/tsw.2011.22.

Min, Lie, Leila H. Choe, and Kelvin H. Lee. "Improved Protease Digestion Conditions for Membrane Protein Detection." Electrophoresis, Volume 36, Issue 15, Special Issue: Focus on AES Meeting 2014, August 2015, Pages 1690-1698. https://doi.org/10.1002/elps.201400579.

Mitchell, Drake C., Shui Lin Niu, and Burton J. Litman. "Enhancement of G Protein-Coupled Signaling by DHA Phospholipids." In Lipids, Volume 38, Issue 4, April 2003, Pages 437-443. https://doi.org/10.1007/s11745-003-1081-1.

Mittal, Rama Devi. "Tandem Mass Spectroscopy in Diagnosis and Clinical Research." Indian Journal of Clinical Biochemistry, Volume 30, pages 121–123, 2015. https://doi.org/10.1007/s12291-015-0498-9.

Mizumura, Takuya, Keita Kondo, Masatoshi Kurita, Yutaka Kofuku, Mei Natsume, Shunsuke Imai, Yutaro Shiraishi, Takumi Ueda, and Ichio Shimada. "Activation of Adenosine A2A Receptor by Lipids from Docosahexaenoic Acid Revealed by NMR." Science Advances 6, no. 12, 2020. 1–15. https://doi.org/10.1126/sciadv.aay8544.

I. Company Marin, PhD Thesis, Aston University 2024

Mohanty, Arun K., and Michael C. Wiener. "Membrane Protein Expression and Production: Effects of Polyhistidine Tag Length and Position." Protein Expression and Purification, Volume 33, Issue 2, February 2004, Pages 311-325. https://doi.org/10.1016/j.pep.2003.10.010.

Mol, Marco, Genny Degani, Crescenzo Coppa, Giovanna Baron, Laura Popolo, Marina Carini, Giancarlo Aldini, Giulio Vistoli, and Alessandra Altomare. "Advanced Lipoxidation End Products, ALEs. as RAGE Binders: Mass Spectrometric and Computational Studies to Explain the Reasons Why." Redox Biology 23, no. December 2018, 2019. 101083. https://doi.org/10.1016/j.redox.2018.101083.

Moldogazieva, Nurbubu T, Innokenty M Mokhosoev, Tatiana I Mel, Yuri B Porozov, and Alexander A Terentiev. "Review Article Oxidative Stress and Advanced Lipoxidation and Glycation End Products, ALEs and AGEs in Aging and Age-Related Diseases", Volume 2019, Article ID 3085756, 2019. https://doi.org/10.1155/2019/3085756.

Moldoveanu, Serban C., and Victor David. "Retention Mechanisms in Different HPLC Types." In Essentials in Modern HPLC Separations, 2013, Pages 145-190. https://doi.org/10.1016/b978-0-12-385013-3.00005-7.

Monici, Monica. "Cell and Tissue Autofluorescence Research and Diagnostic Applications." Biotechnology Annual Review, 2005. https://doi.org/10.1016/S1387-2656(05.11007-2.

Montuschi, Paolo, Peter J. Barnes, and L. Jackson Roberts. "Isoprostanes: Markers and Mediators of Oxidative Stress." The FASEB Journal 18, no. 15, 2004. 1791–1800. https://doi.org/10.1096/fj.04-2330rev.

Moon, C. Preston, and Karen G. Fleming. "Using Tryptophan Fluorescence to Measure the Stability of Membrane Proteins Folded in Liposomes." In Methods in Enzymology, Volume 492, 2011, Pages 189-211. https://doi.org/10.1016/B978-0-12-381268-1.00018-5.

Morello, Silvana, Rosalinda Sorrentino, and Aldo Pinto. "Adenosine A2a Receptor Agonists as Regulators of Inflammation: Pharmacology and Therapeutic Opportunities." Journal of Receptor, Ligand and Channel Research Volume 2, no. June 2014, 2009. 11–17. https://doi.org/10.2147/jrlcr.s4710.

Mosmann, Tim. "Rapid Colorimetric Assay for Cellular Growth and Survival: Application to Proliferation and Cytotoxicity Assays." Journal of Immunological Methods, 1983. https://doi.org/10.1016/0022-1759(83.90303-4.

Muller, C. E., and B. Stein. "Adenosine Receptor Antagonists: Structures and Potential Therapeutic Applications." Current Pharmaceutical Design, Volume 2, Issue 5, 2022, Pages: 501-530. https://doi.org/10.2174/1381612802666221004174507.

Muller, Melanie P., Tao Jiang, Chang Sun, Muyun Lihan, Shashank Pant, Paween Mahinthichaichan, Anda Trifan, and Emad Tajkhorshid. "Characterization of Lipid-Protein Interactions and Lipid-Mediated Modulation of Membrane Protein Function through Molecular Simulation." Chemical Reviews, 119, 9, 6086–6161, 2019. https://doi.org/10.1021/acs.chemrev.8b00608.

Mundell, S. J., A. L. Matharu, S. Nisar, T. M. Palmer, J. L. Benovic, and E. Kelly. "Deletion of the Distal COOH-Terminus of the A 2B Adenosine Receptor Switches Internalization to an Arrestin- and Clathrin-Independent Pathway and Inhibits Recycling." British Journal of Pharmacology, Volume 159, Issue 3, February 2010, Pages 518-533. https://doi.org/10.1111/j.1476-5381.2009.00598.x.

Mundell, Stuart, and Eamonn Kelly. "Adenosine Receptor Desensitization and Trafficking." Biochimica et Biophysica Acta - Biomembranes 1808, no. 5, 2011. 1319–28. https://doi.org/10.1016/j.bbamem.2010.06.007.

Murate, Motohide, and Toshihide Kobayashi. "Revisiting Transbilayer Distribution of Lipids in the Plasma Membrane." Chemistry and Physics of Lipids 194, 2016. 58–71. https://doi.org/10.1016/j.chemphyslip.2015.08.009.

Muro, Eleonora, G. Ekin Atilla-Gokcumen, and Ulrike S. Eggert. "Lipids in Cell Biology: How Can We Understand Them Better?" Molecular Biology of the Cell 25, no. 12, 2014. 1819–23. https://doi.org/10.1091/mbc.E13-09-0516.

Murphy, Katrina, Volodymyr Gerzanich, Hui Zhou, Svetlana Ivanova, Yafeng Dong, Gloria Hoffman, G. Alexander West, H. Richard Winn, and J. Marc Simard. "Adenosine-A2a Receptor down-Regulates Cerebral Smooth Muscle L-Type Ca 2+ Channel Activity via Protein Tyrosine Phosphatase, Not CAMP-Dependent Protein Kinase." Molecular Pharmacology 64, no. 3, 2003. 640–49. https://doi.org/10.1124/mol.64.3.640.

I. Company Marin, PhD Thesis, Aston University 2024

Naranjo, Andrea N, Patrick M. McNeely, John Katsaras, and Anne Skaja Robinson. "Impact of Purification Conditions and History on A2A Adenosine Receptor Activity: The Role of CHAPS and Lipids." Protein Expression and Purification 124, August 2016. 62–67. https://doi.org/10.1016/j.pep.2016.05.015.

Neale, Chris, Henry D. Herce, Régis Pomès, and Angel E. García. "Can Specific Protein-Lipid Interactions Stabilize an Active State of the Beta 2 Adrenergic Receptor?" Biophysical Journal, Volume 109, Issue 8, P1652-1662, October 2015. https://doi.org/10.1016/j.bpj.2015.08.028.

Nehmé, Rony, Byron Carpenter, Ankita Singhal, Annette Strege, Patricia C Edwards, Courtney F White, Haijuan Du, Reinhard Grisshammer, and Christopher G Tate. "Mini-G Proteins: Novel Tools for Studying GPCRs in Their Active Conformation The First Mini-G Protein Developed Was Mini-G s. Here We Extend the Family of Mini-G Proteins to Include Mini-G Olf, Mini-G I1 , Mini-G O1 and the Chimeras Mini-G s/q and Mini-G." Plos One, 2017, 1–26. https://doi.org/10.1371/journal.pone.0175642.g001.

Nesvizhskii, Alexey I. "Protein Identification by Tandem Mass Spectrometry and Sequence Database Searching." In Mass Spectrometry Data Analysis in Proteomics, 367:87–120. New Jersey: Humana Press, 2007. https://doi.org/10.1385/1-59745-275-0:87.

Ni, Zhixu, Laura Goracci, Gabriele Cruciani, and Maria Fedorova. "Computational Solutions in Redox Lipidomics – Current Strategies and Future Perspectives." Free Radical Biology and Medicine, Volume 144, 20 November 2019, Pages 110-123. https://doi.org/10.1016/j.freeradbiomed.2019.04.027.

Nicolson, Garth. "Update of the 1972 Singer-Nicolson Fluid-Mosaic Model of Membrane Structure." Discoveries, 2013. https://doi.org/10.15190/d.2013.3.

Nicolson, Garth L., and Michael E. Ash. "Lipid Replacement Therapy: A Natural Medicine Approach to Replacing Damaged Lipids in Cellular Membranes and Organelles and Restoring Function." Biochimica et Biophysica Acta - Biomembranes, Volume 1838, Issue 6, June 2014, Pages 1657-1679. https://doi.org/10.1016/j.bbamem.2013.11.010.

Nolting, Dirk, Robert Malek, and Alexander Makarov. "Ion Traps in Modern Mass Spectrometry." Mass Spectrometry Reviews, Volume 38, Issue 2, Special Issue on Mass Spectrometry in Germany Part 2, 2019, Pages 150-168. https://doi.org/10.1002/mas.21549.

Noor, Zainab, Seong Beom Ahn, Mark S. Baker, Shoba Ranganathan, and Abidali Mohamedali. "Mass Spectrometry-Based Protein Identification in Proteomics- A Review." Briefings in Bioinformatics 22, no. 2, 2021. 1620–38. https://doi.org/10.1093/bib/bbz163.

Numata, Mari, Pitchaimani Kandasamy, and Dennis R. Voelker. "The Anti-Inflammatory and Antiviral Properties of Anionic Pulmonary Surfactant Phospholipids." Immunological Reviews, Volume 317, Issue 1, Special Issue:Lipids as Modulators of Immunity, August 2023, Pages 166-186. https://doi.org/10.1111/imr.13207.

O'Malley, Michelle A., Andrea N. Naranjo, Tzvetana Lazarova, and Anne S. Robinson. "Analysis of Adenosine A2a Receptor Stability: Effects of Ligands and Disulfide Bonds." Biochemistry 49, no. 43, 2010. 9181–89. https://doi.org/10.1021/bi101155r.

Ohta, Akio, and Michail Sitkovsky. "Extracellular Adenosine-Mediated Modulation of Regulatory T Cells." Frontiers in Immunology 5, July 2014. 1–9. https://doi.org/10.3389/fimmu.2014.00304.

Oluwole, Abraham Olusegun, Bartholomäus Danielczak, Annette Meister, Jonathan Oyebamiji Babalola, Carolyn Vargas, and Sandro Keller. "Solubilization of Membrane Proteins into Functional Lipid-Bilayer Nanodiscs Using a Diisobutylene/Maleic Acid Copolymer." Angewandte Chemie - International Edition 56, no. 7, 2017. 1919–24. https://doi.org/10.1002/anie.201610778.

Oluwole, Abraham Olusegun, Johannes Klingler, Bartholomäus Danielczak, Jonathan Oyebamiji Babalola, Carolyn Vargas, Georg Pabst, and Sandro Keller. "Formation of Lipid-Bilayer Nanodiscs by Diisobutylene/Maleic Acid, DIBMA. Copolymer." Langmuir, 33, 50, 14378–14388, 2017. https://doi.org/10.1021/acs.langmuir.7b03742.

Orešič, Matej, Virve A. Hänninen, and Antonio Vidal-Puig. "Lipidomics: A New Window to Biomedical Frontiers." Trends in Biotechnology, Volume 26, Issue 12, P647-652, December 2008. https://doi.org/10.1016/j.tibtech.2008.09.001.

Öztürk, Sibel, İrem Demir, and Pınar Çalık. "Isolation of High-Quality RNA from Pichia Pastoris." Current Protocols in Protein Science, 2019. https://doi.org/10.1002/cpps.101.

I. Company Marin, PhD Thesis, Aston University 2024

Paila, Yamuna Devi, and Amitabha Chattopadhyay. "The Function of G-Protein Coupled Receptors and Membrane Cholesterol: Specific or General Interaction?" In Glycoconjugate Journal, Volume 26, pages 711–720, 2009. https://doi.org/10.1007/s10719-008-9218-5.

Pan, Xiao, and Richard W. Vachet. "Membrane Protein Structures And Interactions From Covalent Labeling Coupled With Mass Spectrometry." Mass Spectrometry Reviews, Volume 41, Issue 1, 2022, Pages 1-151. https://doi.org/10.1002/mas.21667.

Pandey, Shubhi, Debarati Roy, and Arun K. Shukla. Measuring Surface Expression and Endocytosis of GPCRs Using Whole-Cell ELISA. Methods in Cell Biology, Volume 149, 2019, Pages 131-140. https://doi.org/10.1016/bs.mcb.2018.09.014.

Parathodi Illam, Soorya, Ashif Hussain, Anu Elizabeth, Arunaksharan Narayanankutty, and Achuthan C. Raghavamenon. "Natural Combination of Phenolic Glycosides from Fruits Resists Pro-Oxidant Insults to Colon Cells and Enhances Intrinsic Antioxidant Status in Mice." Toxicology Reports 6, July, 2019. 703–11. https://doi.org/10.1016/j.toxrep.2019.07.005.

Park, Alderley, S Harborne, E Rejnowicz, and M Abbott. "Biophysical Methods for Studying Human GPCR Ligand Binding Properties" 44, no. 0, 2020. 238892.

Parton, Daniel L., Jochen W. Klingelhoefer, and Mark S.P. Sansom. "Aggregation of Model Membrane Proteins, Modulated by Hydrophobic Mismatch, Membrane Curvature, and Protein Class." Biophysical Journal, Volume 101, Issue 3, P691-699, August 03, 2011. https://doi.org/10.1016/j.bpj.2011.06.048.

Parvez, Saba, Marcus J C Long, Jesse R Poganik, and Yimon Aye. "Redox Signaling by Reactive Electrophiles and Oxidants." Review-article. Chemical Reviews 118, 2018. 8798–8888. https://doi.org/10.1021/acs.chemrev.7b00698.

Pasquini, Silvia, Chiara Contri, Pier Andrea Borea, Fabrizio Vincenzi, and Katia Varani. "Adenosine and Inflammation: Here, There and Everywhere." International Journal of Molecular Sciences 22, no. 14, 2021. 1–24. https://doi.org/10.3390/ijms22147685.

Patil, Avinash A., Szu Wei Chou, Pei Yu Chang, Chen Wei Lee, Chun Yen Cheng, Ming Lee Chu, and Wen Ping Peng. "High Mass Ion Detection with Charge Detector Coupled to Rectilinear Ion Trap Mass Spectrometer." Journal of the American Society for Mass Spectrometry, 28, 6, 1066–1078, 2017. https://doi.org/10.1007/s13361-016-1548-0.

Patwardhan, Anand, Norton Cheng, and Joann Trejo. "Post-Translational Modifications of g Protein–Coupled Receptors Control Cellular Signaling Dynamics in Space and Time." Pharmacological Reviews 73, no. 1, 2021. 120–51. https://doi.org/10.1124/pharmrev.120.000082.

Pavlos, Nathan J., and Peter A. Friedman. "GPCR Signaling and Trafficking: The Long and Short of It." Trends in Endocrinology and Metabolism, Volume 28, Issue 3, P213-226, March 2017. https://doi.org/10.1016/j.tem.2016.10.007.

Peruzzi, Justin A., Jan Steinkühler, Timothy Q. Vu, Taylor F. Gunnels, Peilong Lu, David Baker, and Neha P. Kamat. "Hydrophobic Mismatch Drives Self-Organization of Designer Proteins into Synthetic Membranes." BioRxiv, 2022. https://doi.org/10.1101/2022.06.01.494374

Peterson, Yuri K., and Louis M. Luttrell. "The Diverse Roles of Arrestin Scaffolds in g Protein–Coupled Receptor Signaling." Pharmacological Reviews, 69 (3) 256-297, 2017. https://doi.org/10.1124/pr.116.013367.

Piehowski, Paul D., Vladislav A. Petyuk, Daniel J. Orton, Fang Xie, Ronald J. Moore, Manuel Ramirez-Restrepo, Anzhelika Engel, et al. "Sources of Technical Variability in Quantitative LC-MS Proteomics: Human Brain Tissue Sample Analysis." Journal of Proteome Research, 12, 5, 2128–2137, 2013. https://doi.org/10.1021/pr301146m.

Pina, Ana Sofia, Christopher R. Lowe, and Ana Cecília A. Roque. "Challenges and Opportunities in the Purification of Recombinant Tagged Proteins." Biotechnology Advances, Volume 32, Issue 2, March–April 2014, Pages 366-381. https://doi.org/10.1016/j.biotechadv.2013.12.001.

Pohl, Elena E, and Olga Jovanovic. "The Role of Phosphatidylethanolamine Adducts in Modification of the Activity of Membrane Proteins under Oxidative Stress," no. Figure 1, 2019. 1–15. https://doi.org/10.3390/molecules24244545.

Pollock, Naomi L., Sarah C. Lee, Jaimin H. Patel, Aiman A. Gulamhussein, and Alice J. Rothnie. "Structure and Function of Membrane Proteins Encapsulated in a Polymer-Bound Lipid Bilayer." Biochimica et Biophysica Acta - Biomembranes 1860, no. 4, 2018. 809–17. https://doi.org/10.1016/j.bbamem.2017.08.012.

I. Company Marin, PhD Thesis, Aston University 2024

Ponnoth, Dovenia S., Mohammed A. Nayeem, Stephen L. Tilley, Catherine Ledent, and S. Jamal Mustafa. "CYP-Epoxygenases Contribute to A2A Receptor-Mediated Aortic Relaxation via Sarcolemmal KATP Channels." American Journal of Physiology - Regulatory Integrative and Comparative Physiology 303, no. 10, 2012. 1003–11. https://doi.org/10.1152/ajpregu.00335.2012.

Popot, J. L., and D. M. Engelman. "Membrane Protein Folding and Oligomerization: The Two-Stage Model." Biochemistry, 29, 17, 4031–4037, 1990. https://doi.org/10.1021/bi00469a001.

Porath, Jerker, Jan Carlsson, Ingmar Olsson, and Greta Belfrage. "Metal Chelate Affinity Chromatography, a New Approach to Protein Fractionation." Nature, 258, pages 598–599, 1975. https://doi.org/10.1038/258598a0.

Postle, Anthony D. "Lipidomics." Current Opinion in Clinical Nutrition and Metabolic Care, 15(2):127-133, 2012. https://doi.org/10.1097/MCO.0b013e32834fb003.

Prasanna, Xavier, Amitabha Chattopadhyay, and Durba Sengupta. "Cholesterol Modulates the Dimer Interface of the B2-Adrenergic Receptor via Cholesterol Occupancy Sites." Biophysical Journal, Volume 106, Issue 6, P1290-1300, March 18, 2014. https://doi.org/10.1016/j.bpj.2014.02.002.

Prosser, R. Scott, Libin Ye, Aditya Pandey, and Alexander Orazietti. "Activation Processes in Ligand-Activated G Protein-Coupled Receptors: A Case Study of the Adenosine A2A Receptor." BioEssays 39, no. 9, 2017. 1–10. https://doi.org/10.1002/bies.201700072.

Qu, Feng, Su Jun Zheng, Cai Sheng Wu, Zhi Xin Jia, Jin Lan Zhang, and Zhong Ping Duan. "Lipidomic Profiling of Plasma in Patients with Chronic Hepatitis C Infection." Analytical and Bioanalytical Chemistry, Volume 406, pages 555–564, 2014. https://doi.org/10.1007/s00216-013-7479-8.

Rader, A. J., Gülsüm Anderson, Basak Isin, H. Gobind Khorana, Ivet Bahar, and Judith Klein-Seetharaman. "Identification of Core Amino Acids Stabilizing Rhodopsin." Proceedings of the National Academy of Sciences of the United States of America, 101 (19) 7246-7251, 2004. https://doi.org/10.1073/pnas.0401429101.

Raffaelli, Andrea, and Alessandro Saba. "Ion Scanning or Ion Trapping: Why Not Both?" Mass Spectrometry Reviews, Volume 42, Issue 4, Special Issue for Pietro Traldi, 2023, Pages 1152-1173. https://doi.org/10.1002/mas.21746.

Ramadurai, Sivaramakrishnan, Ria Duurkens, Victor V. Krasnikov, and Bert Poolman. "Lateral Diffusion of Membrane Proteins: Consequences of Hydrophobic Mismatch and Lipid Composition." Biophysical Journal, Volume 99, Issue 5, P1482-1489, 2010. https://doi.org/10.1016/j.bpj.2010.06.036.

Ramaley, Louis, Lisandra Cubero Herrera, and Jeremy E. Melanson. "Determination of Regioisomers in Triacylglycerols." Rapid Communications in Mass Spectrometry, Volume 35, Issue 1, 2021, e8961. https://doi.org/10.1002/rcm.8961.

Ranjan, Ravi, Hemlata Dwivedi, Mithu Baidya, Mohit Kumar, and Arun K. Shukla. "Novel Structural Insights into GPCR–β-Arrestin Interaction and Signaling." Trends in Cell Biology, Volume 27, Issue 11, P851-862, 2017. https://doi.org/10.1016/j.tcb.2017.05.008.

Ray, Paul D., Bo Wen Huang, and Yoshiaki Tsuji. "Reactive Oxygen Species, ROS. Homeostasis and Redox Regulation in Cellular Signaling." Cellular Signalling 24, no. 5, 2012. 981–90. https://doi.org/10.1016/j.cellsig.2012.01.008.

Rehan, Shahid, Ville O. Paavilainen, and Veli Pekka Jaakola. "Functional Reconstitution of Human Equilibrative Nucleoside Transporter-1 into Styrene Maleic Acid Co-Polymer Lipid Particles." Biochimica et Biophysica Acta - Biomembranes, Volume 1859, Issue 5, May 2017, Pages 1059-1065. https://doi.org/10.1016/j.bbamem.2017.02.017.

Reis, Ana, Alisa Rudnitskaya, Pajaree Chariyavilaskul, Neeraj Dhaun, Vanessa Melville, Jane Goddard, David J. Webb, Andrew R. Pitt, and Corinne M. Spickett. "Top-down Lipidomics of Low Density Lipoprotein Reveal Altered Lipid Profi Les in Advanced Chronic Kidney Disease." Journal of Lipid Research, Volume 56, Issue 2, P413-422, February 2015. https://doi.org/10.1194/jlr.M055624.

Reis, Ana, and Corinne M Spickett. "Biochimica et Biophysica Acta Chemistry of Phospholipid Oxidation ☆." BBA - Biomembranes 1818, no. 10, 2012, 2374–87. https://doi.org/10.1016/j.bbamem.2012.02.002.

Risselada, Herre Jelger. "Cholesterol: The Plasma Membrane's Constituent That Chooses Sides." Biophysical Journal, Volume 116, Issue 12, P2235-2236, June 18, 2019. Https://doi.org/10.1016/j.bpj.2019.05.003.

I. Company Marin, PhD Thesis, Aston University 2024

Rivera, Ana Leonor, Denis Magaña-Ortíz, Miguel Gómez-Lim, Francisco Fernández, and Achim M. Loske. "Physical Methods for Genetic Transformation of Fungi and Yeast." Physics of Life Reviews 11, no. 2, 2014. 184–203. https://doi.org/10.1016/j.plrev.2014.01.007.

Roberts, Lee D., Amanda L. Souza, Robert E. Gerszten, and Clary B. Clish. "Targeted Metabolomics." Current Protocols in Molecular Biology, 2012. https://doi.org/10.1002/0471142727.mb3002s98.

Rothnie, Alice J. "Detergent-Free Membrane Protein Purification." In Methods in Molecular Biology, 2016, pp 261–267. https://doi.org/10.1007/978-1-4939-3637-3_16.

Routledge, Sarah J., Lina Mikaliunaite, Anjana Patel, Michelle Clare, Stephanie P. Cartwright, Zharain Bawa, Martin D.B. Wilks, et al. "The Synthesis of Recombinant Membrane Proteins in Yeast for Structural Studies." Methods 95, 2016. 26–37. https://doi.org/10.1016/j.ymeth.2015.09.027.

Routledge, Sarah J, Mohammed Jamshad, Haydn A Little, Yu-pin Lin, John Simms, Alpesh Thakker, Corinne M Spickett, et al. "BBA - Biomembranes Ligand-Induced Conformational Changes in a SMALP-Encapsulated GPCR ." Volume 1862, Issue 6, 1 June 2020, 183235. https://doi.org/10.1016/j.bbamem.2020.183235.

Royer, Catherine A. "Probing Protein Folding and Conformational Transitions with Fluorescence." Chemical Reviews, 106, 5, 1769–1784, 2006. https://doi.org/10.1021/cr0404390.

Różalska, Barbara, Beata Sadowska, Aleksandra Budzyńska, Przemysław Bernat, and Sylwia Różalska. "Biogenic Nanosilver Synthesized in Metarhizium Robertsii Waste Mycelium Extract – As a Modulator of Candida Albicans Morphogenesis, Membrane Lipidome and Biofilm." PLoS ONE 13, no. 3, 2018. 1–21. https://doi.org/10.1371/journal.pone.0194254.

Rudt, E., M. Feldhaus, C. G. Margraf, S. Schlehuber, A. Schubert, S. Heuckeroth, U. Karst, et al. "Comparison of Data-Dependent Acquisition, Data-Independent Acquisition, and Parallel Reaction Monitoring in Trapped Ion Mobility Spectrometry–Time-of-Flight Tandem Mass Spectrometry-Based Lipidomics." Analytical Chemistry, 95, 25, 9488–9496, 2023. https://doi.org/10.1021/acs.analchem.3c00440.

Rues, Ralf Bernhardt, Volker Dötsch, and Frank Bernhard. "Co-Translational Formation and Pharmacological Characterization of Beta1-Adrenergic Receptor/Nanodisc Complexes with Different Lipid Environments." Biochimica et Biophysica Acta - Biomembranes, Volume 1858, Issue 6, June 2016, Pages 1306-1316. https://doi.org/10.1016/j.bbamem.2016.02.031.

Rush, Michael D., and Richard B. van Breemen. "Role of Ammonium in the Ionization of Phosphatidylcholines during Electrospray Mass Spectrometry." Rapid Communications in Mass Spectrometry, Volume 31, Issue 3, 2017, Pages 264-268. https://doi.org/10.1002/rcm.7788.

Saleem, Meher A., Anna Mueller, and Sanjoy K. Bhattacharya. "Lipidomics Analysis with Triple Quadrupole Mass Spectrometry." Methods in Molecular Biology, Clifton, N.J., 2023, pp 103–106. https://doi.org/10.1007/978-1-0716-2966-6_9.

Salomon, Robert G. "Levuglandins and Isolevuglandins: Stealthy Toxins of Oxidative Injury." Antioxidants & Redox Signaling 7, no. 1–2, January 2005, 185–201. https://doi.org/10.1089/ars.2005.7.185.

Satoh, Kimihiko, Satoshi Yamada, Yukiko Koike, Yasuo Igarashi, Shinya Toyokuni, Takayuki Kumano, Takenori Takahata, Makoto Hayakari, Shigeki Tsuchida, and Koji Uchida. "A 1-Hour Enzyme-Linked Immunosorbent Assay for Quantitation of Acrolein- and Hydroxynonenal-Modified Proteins by Epitope-Bound Casein Matrix Method." Analytical Biochemistry, Volume 270, Issue 2, 1999, Pages 323-328. https://doi.org/10.1006/abio.1999.4073.

Savage, Emilia Elizabeth, Denise Wootten, Arthur Christopoulos, Patrick Michael Sexton, and Sebastian George Barton Furness. "A Simple Method to Generate Stable Cell Lines for the Analysis of Transient Protein-Protein Interactions." BioTechniques, 54, 42013. https://doi.org/10.2144/000114013.

Scassellati, Catia, Elisabetta Albi, Dusan Cmarko, Cinzia Tiberi, Jana Cmarkova, Cedric Bouchet-Marquis, Pernette J. Verschure, Roel Driel, Mariapia Viola Magni, and Stanislav Fakan. "Intranuclear Sphingomyelin Is Associated with Transcriptionally Active Chromatin and Plays a Role in Nuclear Integrity." Biology of the Cell, Volume102, Issue 6, June 2010, Pages 361-375. https://doi.org/10.1042/bc20090139.

Scherer, S., K. Altwegg, H. Balsiger, J. Fischer, A. Jäckel, A. Korth, M. Mildner, D. Piazza, H. Reme, and P. Wurz. "A Novel Principle for an Ion Mirror Design in Time-of-Flight Mass Spectrometry." International Journal of Mass Spectrometry, Volume 251, Issue 1, 15 March 2006, Pages 73-81. https://doi.org/10.1016/j.ijms.2006.01.025.

I. Company Marin, PhD Thesis, Aston University 2024

Schönfeld, Peter, and Lech Wojtczak. "Short- and Medium-Chain Fatty Acids in Energy Metabolism: The Cellular Perspective." Journal of Lipid Research, Volume 57, Issue 6, P943-954, June 2016. https://doi.org/10.1194/jlr.R067629.

Schuler, Mary A., Ilia G. Denisov, and Stephen G. Sligar. "Nanodiscs as a New Tool to Examine Lipid-Protein Interactions." Methods in Molecular Biology 974, 2013. 415–33. https://doi.org/10.1007/978-1-62703-275-9_18.

Schutter, Kristof De, Yao Cheng Lin, Petra Tiels, Annelies Van Hecke, Sascha Glinka, Jacqueline Weber-Lehmann, Pierre Rouzé, Yves Van De Peer, and Nico Callewaert. "Genome Sequence of the Recombinant Protein Production Host Pichia Pastoris." Nature Biotechnology 27, no. 6, 2009. 561–66. https://doi.org/10.1038/nbt.1544.

Schwartz, Thue W., Thomas M. Frimurer, Birgitte Holst, Mette M. Rosenkilde, and Christian E. Elling. "Molecular Mechanism of 7TM Receptor Activation - A Global Toggle Switch Model." Annual Review of Pharmacology and Toxicology, Vol. 46:481-519, 2006. https://doi.org/10.1146/annurev.pharmtox.46.120604.141218.

Schwarzhans, Jan Philipp, Tobias Luttermann, Martina Geier, Jörn Kalinowski, and Karl Friehs. "Towards Systems Metabolic Engineering in Pichia Pastoris." Biotechnology Advances, Volume 35, Issue 6, 1 November 2017, Pages 681-710. https://doi.org/10.1016/j.biotechadv.2017.07.009.

Schwudke, Dominik, Gerhard Liebisch, Ronny Herzog, Gerd Schmitz, and Andrej Shevchenko. "Shotgun Lipidomics by Tandem Mass Spectrometry under Data-Dependent Acquisition Control." Methods in Enzymology, 2007. https://doi.org/10.1016/S0076-6879(07.33010-3.

Seger, Christoph, and Linda Salzmann. "After Another Decade: LC–MS/MS Became Routine in Clinical Diagnostics." Clinical Biochemistry, Volume 82, August 2020, Pages 2-11. https://doi.org/10.1016/j.clinbiochem.2020.03.004.

Sengupta, Durba, and Amitabha Chattopadhyay. "Molecular Dynamics Simulations of GPCR-Cholesterol Interaction: An Emerging Paradigm." Biochimica et Biophysica Acta - Biomembranes, Volume 1848, Issue 9, September 2015, Pages 1775-1782. https://doi.org/10.1016/j.bbamem.2015.03.018.

Serebryany, Eugene, Gefei Alex Zhu, and Elsa C Y Yan. "Biochimica et Biophysica Acta Arti Fi Cial Membrane-like Environments for in Vitro Studies of Puri Fi Ed G-Protein Coupled Receptors" 1818, 2012, 225–33. https://doi.org/10.1016/j.bbamem.2011.07.047.

Sharma, Karan D., Frederick A. Heberle, and M. Neal Waxham. "Visualizing Lipid Membrane Structure with Cryo-EM: Past, Present, and Future." Emerging Topics in Life Sciences, 7 (1): 55–65, 2023. https://doi.org/10.1042/ETLS20220090.

Sheng, J., R. Vannela, and B. E. Rittmann. "Disruption of Synechocystis PCC 6803 for Lipid Extraction." Water Science and Technology 65, no. 3, 2012. 567–73. https://doi.org/10.2166/wst.2012.879.

Shim, Myoung Sup, Keun Young Kim, Jung Hyun Bu, Hye Seung Nam, Seung Won Jeong, Tae Lim Park, Mark H. Ellisman, Robert N. Weinreb, and Won Kyu Ju. "Elevated Intracellular CAMP Exacerbates Vulnerability to Oxidative Stress in Optic Nerve Head Astrocytes Article." Cell Death and Disease 9, no. 3, 2018. https://doi.org/10.1038/s41419-017-0171-8.

Shrivastava, Sandeep, Md Jafurulla, Shrish Tiwari, and Amitabha Chattopadhyay. "Identification of Sphingolipid-Binding Motif in G Protein-Coupled Receptors." In Advances in Experimental Medicine and Biology, pp 141–149, 2018. https://doi.org/10.1007/978-981-13-3065-0_10.

Simcock, Patrick W., Maike Bublitz, Flaviu Cipcigan, Maxim G. Ryadnov, Jason Crain, Phillip J. Stansfeld, and Mark S.P. Sansom. "Membrane Binding of Antimicrobial Peptides Is Modulated by Lipid Charge Modification." Journal of Chemical Theory and Computation, 17, 2, 1218–1228, 2021. https://doi.org/10.1021/acs.jctc.0c01025.

Sindrewicz, Paulina, Xiaoxin Li, Edwin A. Yates, Jeremy E. Turnbull, Lu Yun Lian, and Lu Gang Yu. "Intrinsic Tryptophan Fluorescence Spectroscopy Reliably Determines Galectin-Ligand Interactions." Scientific Reports, 9, Article number: 11851, 2019. https://doi.org/10.1038/s41598-019-47658-8.

Singer, S. J., and Garth L. Nicolson. "The Fluid Mosaic Model of the Structure of Cell Membranes." Science, Vol. 175, No. 4023, 1972. https://doi.org/10.1126/science.175.4023.720.

Singh, Shweta, Minghao Zhang, Nicolas Bertheleme, Elodie Kara, Philip G. Strange, and Bernadette Byrne. "Radioligand Binding Analysis as a Tool for Quality Control of GPCR Production for Structural Characterization: Adenosine A2aR as a Template for Study." Current Protocols in Protein Science 1, no. SUPPL.67, 2012. 1–22. https://doi.org/10.1002/0471140864.ps2903s67.

I. Company Marin, PhD Thesis, Aston University 2024

Singh, Shweta, Minghao Zhang, Nicolas Bertheleme, Elodie Kara, Philip G Strange, and Bernadette Byrne. "Radioligand Binding Analysis as a Tool for Quality Control of GPCR Production for Structural Characterization : Adenosine A 2a R as a Template for Study," no. February, 2012. 1–22. https://doi.org/10.1002/0471140864.ps2903s67.

Singh, Shweta, Minghao Zhang, Nicolas Bertheleme, Philip G Strange, and Bernadette Byrne. "Purification of the Human G Protein – Coupled Receptor Adenosine A 2a R in a Stable and Functional Form Expressed in Pichia Pastoris," no. February, 2012, 1–17. https://doi.org/10.1002/0471140864.ps2904s67.

Skopál, Adrienn, Gyula Ujlaki, Attila Tibor Gerencsér, Csaba Bankó, Zsolt Bacsó, Francisco Ciruela, László Virág, György Haskó, and Endre Kókai. "Adenosine A2A Receptor Activation Regulates Niemann–Pick C1 Expression and Localization in Macrophages." Current Issues in Molecular Biology 45, no. 6, 2023, 4948–69. https://doi.org/10.3390/cimb45060315.

Song, Wanling, Anna L. Duncan, and Mark S.P. Sansom. "Modulation of Adenosine A2a Receptor Oligomerization by Receptor Activation and PIP2 Interactions." Structure, 2021, 1–14. https://doi.org/10.1016/j.str.2021.06.015.

Song, Wanling, Hsin-yung Yen, Carol V Robinson, Mark S P Sansom, Wanling Song, Hsin-yung Yen, Carol V Robinson, and Mark S P Sansom. "State-Dependent Lipid Interactions with the A2a Receptor Revealed by MD Simulations Using In Vivo -Theory State-Dependent Lipid Interactions with the A2a Receptor Revealed by MD Simulations Using In Vivo -Mimetic Membranes." Structure/Folding and Design 27, no. 2, 2019. 392-403.e3. https://doi.org/10.1016/j.str.2018.10.024.

Sonntag, Yonathan, Maria Musgaard, Claus Olesen, Birgit Schiøtt, Jesper Vuust Møller, Poul Nissen, and Lea Thøgersen. "Mutual Adaptation of a Membrane Protein and Its Lipid Bilayer during Conformational Changes." Nature Communications, 2, Article number: 304, 2011. https://doi.org/10.1038/ncomms1307.

Sorrentino, Claudia, Fokhrul Hossain, Paulo C. Rodriguez, Rosa A. Sierra, Antonio Pannuti, Barbara A. Osborne, Lisa M. Minter, Lucio Miele, and Silvana Morello. "Adenosine A2A Receptor Stimulation Inhibits TCR-Induced Notch1 Activation in CD8+T-Cells." Frontiers in Immunology 10, 2019. 1–12. https://doi.org/10.3389/fimmu.2019.00162.

Sousa, Bebiana C., Tanzim Ahmed, William L. Dann, Jed Ashman, Alexandre Guy, Thierry Durand, Andrew R. Pitt, and Corinne M. Spickett. "Short-Chain Lipid Peroxidation Products Form Covalent Adducts with Pyruvate Kinase and Inhibit Its Activity in Vitro and in Breast Cancer Cells." Free Radical Biology and Medicine 144, no. March, 2019. 223–33. https://doi.org/10.1016/j.freeradbiomed.2019.05.028.

Sousa, Bebiana C, Andrew R Pitt, and Corinne M Spickett. "Free Radical Biology and Medicine Chemistry and Analysis of HNE and Other Prominent Carbonyl-Containing Lipid Oxidation Compounds." Free Radical Biology and Medicine 111, no. December 2016, 2017, 294–308. https://doi.org/10.1016/j.freeradbiomed.2017.02.003.

Spickett, Corinne M. "Oxidized Phospholipid Signaling: Distress to Eustress." Oxidative Stress, 2020, 263–85. https://doi.org/10.1016/b978-0-12-818606-0.00015-8.

Spriestersbach, Anne, Jan Kubicek, Frank Schäfer, Helena Block, and Barbara Maertens. "Purification of His-Tagged Proteins." Methods in Enzymology 559, 2015, 1–15. https://doi.org/10.1016/bs.mie.2014.11.003.

Stahelin, Robert V. "Lipid Binding Domains: More than Simple Lipid Effectors." Journal of Lipid Research, Volume 50, Supplement, S299-S304, 2009. https://doi.org/10.1194/jlr.R800078-JLR200.

Stepanenko, Aleksei A., and Henry H. Heng. "Transient and Stable Vector Transfection: Pitfalls, off-Target Effects, Artifacts." Mutation Research - Reviews in Mutation Research, Volume 773, July 2017, Pages 91-103. https://doi.org/10.1016/j.mrrev.2017.05.002.

Steyaert, Jan, and Brian K. Kobilka. "Nanobody Stabilization of G Protein-Coupled Receptor Conformational States." Current Opinion in Structural Biology 21, no. 4, 2011. 567–72. https://doi.org/10.1016/j.sbi.2011.06.011.

Steyaert, Jan, and Brian K Kobilka. "Nanobody Stabilization of G Protein-Coupled Receptor Conformational States." Current Opinion in Structural Biology 21, no. 4, August 2011. 567–72. https://doi.org/10.1016/j.sbi.2011.06.011.

Stowers, Chris C., and Erik M. Boczko. "Reliable Cell Disruption in Yeast." Yeast 24, no. 6, June 2007. 533–41. https://doi.org/10.1002/yea.1491.

Stroud, Zoe, Stephen C.L. Hall, and Tim R. Dafforn. "Purification of Membrane Proteins Free from Conventional Detergents: SMA, New Polymers, New Opportunities and New Insights." Methods 147, no. 2018, 106–17. https://doi.org/10.1016/j.ymeth.2018.03.011.

I. Company Marin, PhD Thesis, Aston University 2024

Subczynski, Witold K., Marta Pasenkiewicz-Gierula, Justyna Widomska, Laxman Mainali, and Marija Raguz. "High Cholesterol/Low Cholesterol: Effects in Biological Membranes: A Review." Cell Biochemistry and Biophysics, Volume 75, pages 369–385, 2017. https://doi.org/10.1007/s12013-017-0792-7.

Sud, Manish, Eoin Fahy, Dawn Cotter, Alex Brown, Edward A. Dennis, Christopher K. Glass, Alfred H. Merrill, et al. "LMSD: LIPID MAPS Structure Database." Nucleic Acids Research, Volume 35, Issue suppl_1, 1 January 2007, Pages D527–D532. https://doi.org/10.1093/nar/gkl838.

Sun, Changyan, Tong Jiao, Daphne Merkus, Dirk J. Duncker, S. Jamal Mustafa, and Zhichao Zhou. "Activation of Adenosine A2A but Not A2B Receptors Is Involved in Uridine Adenosine Tetraphosphate-Induced Porcine Coronary Smooth Muscle Relaxation." Journal of Pharmacological Sciences 141, no. 1, 2019. 64–69. https://doi.org/10.1016/j.jphs.2019.09.006.

Sushma, and Amal Chandra Mondal. "Role of GPCR Signaling and Calcium Dysregulation in Alzheimer's Disease." Molecular and Cellular Neuroscience 101, no. July, 2019. 103414. https://doi.org/10.1016/j.mcn.2019.103414.

Suvitaival, Tommi, Isabel Bondia-Pons, Laxman Yetukuri, Päivi Pöhö, John J. Nolan, Tuulia Hyötyläinen, Johanna Kuusisto, and Matej Orešič. "Lipidome as a Predictive Tool in Progression to Type 2 Diabetes in Finnish Men." Metabolism: Clinical and Experimental, 2018. https://doi.org/10.1016/j.metabol.2017.08.014.

Suzuki, Tokiko, Yutaro Obara, Takahiro Moriya, Hiroyasu Nakata, and Norimichi Nakahata. "Functional Interaction between Purinergic Receptors: Effect of Ligands for A 2A and P2Y 12 Receptors on P2Y 1 Receptor Function." FEBS Letters 585, no. 24, 2011. 3978–84. https://doi.org/10.1016/j.febslet.2011.10.050.

Swainsbury, David J.K., Stefan Scheidelaar, Rienk Van Grondelle, J. Antoinette Killian, and Michael R. Jones. "Bacterial Reaction Centers Purified with Styrene Maleic Acid Copolymer Retain Native Membrane Functional Properties and Display Enhanced Stability." Angewandte Chemie - International Edition, Volume 53, Issue 44, October 2014, Pages 11803-11807. https://doi.org/10.1002/anie.201406412.

Sych, Taras, Kandice R. Levental, and Erdinc Sezgin. "Lipid-Protein Interactions in Plasma Membrane Organization and Function." Annual Review of Biophysics 51, 2022, 135–56. https://doi.org/10.1146/annurev-biophys-090721-072718.

Tab, Mahzan Md, Noor Haza Fazlin Hashim, Nazalan Najimudin, Nor Muhammad Mahadi, Farah Diba Abu Bakar, and Abdul Munir Abdul Murad. "Large-Scale Production of Glaciozyma Antarctica Antifreeze Protein 1, Afp1. by Fed-Batch Fermentation of Pichia Pastoris." Arabian Journal for Science and Engineering, Volume 43, pages 133–141, 2018. https://doi.org/10.1007/s13369-017-2738-1.

Taghon, Geoffrey J., Jacob B. Rowe, Nicholas J. Kapolka, and Daniel G. Isom. "Predictable Cholesterol Binding Sites in GPCRs Lack Consensus Motifs." Structure, Volume 29, Issue 5, P499-506.E3, 2021. https://doi.org/10.1016/j.str.2021.01.004.

Takasugi, Hiraoka, Nakahara, Akiyama, Fujikawa, Nomura, Furuichi, and Uehara. "The Emerging Role of Electrophiles as a Key Regulator for Endoplasmic Reticulum, ER. Stress." International Journal of Molecular Sciences 20, no. 7, April 10, 2019, 1783. https://doi.org/10.3390/ijms20071783.

Talukder, Poulami, Shengxi Chen, C. Tony Liu, Edwin A. Baldwin, Stephen J. Benkovic, and Sidney M. Hecht. "Tryptophan-Based Fluorophores for Studying Protein Conformational Changes." Bioorganic and Medicinal Chemistry, Volume 22, Issue 21, 1 November 2014, Pages 5924-5934. https://doi.org/10.1016/j.bmc.2014.09.015.

Tamura, Pamela, Carl Fruehan, David K. Johnson, Paul Hinkes, Todd D. Williams, and Ruth Welti. "Fatty Acid Composition by Total Acyl Lipid Collision-Induced Dissociation Time-of-Flight, TAL-CID-TOF. Mass Spectrometry." In Methods in Molecular Biology, 2021, pp 117–133. https://doi.org/10.1007/978-1-0716-1362-7_8.

Tang, Xueqing, Jingwei Bian, and Zijian Li. "Posttranslational Modifications in GPCR Internalization." American Journal of Physiology - Cell Physiology 323, no. 1, 2022, C84–94. https://doi.org/10.1152/ajpcell.00015.2022.

Tanzarella, Paola, Anna Ferretta, Simona Nicol Barile, Mariella Ancona, Domenico De Rasmo, Anna Signorile, Sergio Papa, Nazzareno Capitanio, Consiglia Pacelli, and Tiziana Cocco. "Increased Levels of CAMP by the Calcium-Dependent Activation of Soluble Adenylyl Cyclase in Parkin-Mutant Fibroblasts." Cells, Volume 8, Issue 3, 2019, p250. https://doi.org/10.3390/cells8030250.

Tapaneeyakorn, Satita, Alan D Goddard, Joanne Oates, Christine L Willis, and Anthony Watts. "Biochimica et Biophysica Acta Solution- and Solid-State NMR Studies of GPCRs and Their Ligands." BBA - Biomembranes 1808, no. 6, 2011, 1462–75. https://doi.org/10.1016/j.bbamem.2010.10.003.

I. Company Marin, PhD Thesis, Aston University 2024

Tavares, Luciana P., Graziele L. Negreiros-Lima, Kátia M. Lima, Patrícia M.R. E Silva, Vanessa Pinho, Mauro M. Teixeira, and Lirlândia P. Sousa. "Blame the Signaling: Role of CAMP for the Resolution of Inflammation." Pharmacological Research, Volume 159, September 2020, 105030. https://doi.org/10.1016/j.phrs.2020.105030.

Teo, Alvin C.K., Sarah C. Lee, Naomi L. Pollock, Zoe Stroud, Stephen Hall, Alpesh Thakker, Andrew R. Pitt, Timothy R. Dafforn, Corinne M. Spickett, and David I. Roper. "Analysis of SMALP Co-Extracted Phospholipids Shows Distinct Membrane Environments for Three Classes of Bacterial Membrane Protein." Scientific Reports 9, no. 1, 2019. 1–10. https://doi.org/10.1038/s41598-018-37962-0.

Ternes, Philipp, Tobias Wobbe, Marnie Schwarz, Sandra Albrecht, Kirstin Feussner, Isabelle Riezman, James M. Cregg, et al. "Two Pathways of Sphingolipid Biosynthesis Are Separated in the Yeast Pichia Pastoris." Journal of Biological Chemistry, Volume 286, Issue 13, P11401-11414, 2011. https://doi.org/10.1074/jbc.M110.193094.

Thakur, Naveen, Arka P. Ray, Liam Sharp, Beining Jin, Alexander Duong, Niloofar Gopal Pour, Samuel Obeng, et al. "Anionic Phospholipids Control Mechanisms of GPCR-G Protein Recognition." Nature Communications 14, no. 1, 2023. 1–13. https://doi.org/10.1038/s41467-023-36425-z.

Tieleman, D. P., B. I. Sejdiu, E. A. Cino, P. Smith, E. Barreto-Ojeda, H. M. Khan, and V. Corradi. "Insights into Lipid-Protein Interactions from Computer Simulations." Biophysical Reviews, 2021. https://doi.org/10.1007/s12551-021-00876-9.

Tippett, David N., Brad Hoare, Tamara Miljus, David A. Sykes, and Dmitry B. Veprintsev. "ThermoFRET: A Novel Nanoscale G Protein Coupled Receptor Thermostability Assay Functional in Crude Solubilised Membrane Preparations." BioRxiv, 2020, 1–28. https://doi.org/10.1101/2020.07.07.191957

Tsikas, Dimitrios. "Assessment of Lipid Peroxidation by Measuring Malondialdehyde, MDA. and Relatives in Biological Samples: Analytical and Biological Challenges." Analytical Biochemistry 524, 2017, 13–30. https://doi.org/10.1016/j.ab.2016.10.021.

Tsugawa, Hiroshi, Kazutaka Ikeda, Mikiko Takahashi, Aya Satoh, Yoshifumi Mori, Haruki Uchino, Nobuyuki Okahashi, et al. "A Lipidome Atlas in MS-DIAL 4." Nature Biotechnology, 2020. https://doi.org/10.1038/s41587-020-0531-2.

Tycova, Anna, Jan Prikryl, Adela Kotzianova, Vladimira Datinska, Vladimir Velebny, and Frantisek Foret. "Electrospray: More than Just an Ionization Source." Electrophoresis, 2021. https://doi.org/10.1002/elps.202000191.

Tykocki, Nathan R., Erika M. Boerman, and William F. Jackson. "Smooth Muscle Ion Channels and Regulation of Vascular Tone in Resistance Arteries and Arterioles." Comprehensive Physiology 7, no. 2, 2017, 485–581. https://doi.org/10.1002/cphy.c160011.

Tzortzini, Efpraxia, and Antonios Kolocouris. "Molecular Biophysics of Class A G Protein Coupled Receptors–Lipids Interactome at a Glance—Highlights from the A2A Adenosine Receptor." Biomolecules 13, no. 6, 2023, 957. https://doi.org/10.3390/biom13060957.

Unger, Lucas, Alejandro Ronco-Campaña, Philip Kitchen, Roslyn M. Bill, and Alice J. Rothnie. "Biological Insights from SMA-Extracted Proteins." Biochemical Society Transactions, 49 (3): 1349–1359, 2021. https://doi.org/10.1042/bst20201067.

Vance, Jean E. "Historical Perspective: Phosphatidylserine and Phosphatidylethanolamine from the 1800s to the Present." Journal of Lipid Research, Volume 59, Issue 6, P923-944, 2018. https://doi.org/10.1194/jlr.R084004.

Vargas, Carolyn, Rodrigo Cuevas Arenas, Erik Frotscher, and Sandro Keller. "Nanoparticle Self-Assembly in Mixtures of Phospholipids with Styrene/Maleic Acid Copolymers or Fluorinated Surfactants." Nanoscale, Issue 48, 2015. https://doi.org/10.1039/c5nr06353a.

Vazdar, Katarina, Davor Margetic, and Mario Vazdar. "Revisited Mechanism of Reaction between a Model Lysine Amino Acid Side Chain and 4 - Hydroxynonenal in Different Solvent Environments," 84, 2, 526–535, 2019. https://doi.org/10.1021/acs.joc.8b02231.

Venkatakrishnan, A. J., Xavier Deupi, Guillaume Lebon, Franziska M. Heydenreich, Tilman Flock, Tamara Miljus, Santhanam Balaji, et al. "Diverse Activation Pathways in Class A GPCRs Converge near the G-Protein-Coupling Region." Nature 536, no. 7617, 2016. 484–87. https://doi.org/10.1038/nature19107.

I. Company Marin, PhD Thesis, Aston University 2024

Venkatakrishnan, A. J., Xavier Deupi, Guillaume Lebon, Christopher G. Tate, Gebhard F. Schertler, and M. Madan Babu. "Molecular Signatures of G-Protein-Coupled Receptors." Nature 494, no. 7436, 2013. 185–94. https://doi.org/10.1038/nature11896.

Verheggen, Kenneth, Lennart Martens, Frode S. Berven, Harald Barsnes, and Marc Vaudel. "Database Search Engines: Paradigms, Challenges and Solutions." In Advances in Experimental Medicine and Biology, 2016, pp 147–156. https://doi.org/10.1007/978-3-319-41448-5_6.

Viedma-Poyatos, Álvaro, Patricia González-Jiménez, Ophélie Langlois, Idoia Company-Marín, Corinne M. Spickett, and Dolores Pérez-Sala. "Protein Lipoxidation: Basic Concepts and Emerging Roles." Antioxidants 10, no. 2, February 16, 2021, 295. https://doi.org/10.3390/antiox10020295.

Vigor, Claire, Justine Bertrand-Michel, Edith Pinot, Camille Oger, Joseph Vercauteren, Pauline Le Faouder, Jean Marie Galano, Jetty Chung Yung Lee, and Thierry Durand. "Non-Enzymatic Lipid Oxidation Products in Biological Systems: ASSESSMENT of the Metabolites from Polyunsaturated Fatty Acids." Journal of Chromatography B: Analytical Technologies in the Biomedical and Life Sciences 964, 2014, 65–78. https://doi.org/10.1016/j.jchromb.2014.04.042.

Vinaixa, Maria, Emma L. Schymanski, Steffen Neumann, Miriam Navarro, Reza M. Salek, and Oscar Yanes. "Mass Spectral Databases for LC/MS- and GC/MS-Based Metabolomics: State of the Field and Future Prospects." TrAC - Trends in Analytical Chemistry, Volume 78, April 2016, Pages 23-35. https://doi.org/10.1016/j.trac.2015.09.005.

Vistoli, G, D De Maddis, A Cipak, N Zarkovic, M Carini, G Aldini, D De Maddis, et al. "Advanced Glycoxidation and Lipoxidation End Products, AGEs and ALEs . An Overview of Their Mechanisms of Formation" 5762, Volume 47, 2013 - Issue sup1. https://doi.org/10.3109/10715762.2013.815348.

Vivian, James T., and Patrik R. Callis. "Mechanisms of Tryptophan Fluorescence Shifts in Proteins." Biophysical Journal, 2001. https://doi.org/10.1016/S0006-3495(01.76183-8.

Vladislav Victorovich, Khrustalev, Khrustaleva Tatyana Aleksandrovna, Poboinev Victor Vitoldovich, Stojarov Aleksander Nicolaevich, Kordyukova Larisa Valentinovna, and Akunevich Anastasia Aleksandrovna. "Spectra of Tryptophan Fluorescence Are the Result of Co-Existence of Certain Most Abundant Stabilized Excited State and Certain Most Abundant Destabilized Excited State." Spectrochimica Acta - Part A: Molecular and Biomolecular Spectroscopy 257, 2021, 119784. https://doi.org/10.1016/j.saa.2021.119784.

Vogel, Reiner, and Friedrich Siebert. "Conformation and Stability of α-Helical Membrane Proteins. 2. Influence of PH and Salts on Stability and Unfolding of Rhodopsin." Biochemistry, 41, 11, 3536–3545, 2002. https://doi.org/10.1021/bi016024f.

Vogl, Thomas, and Anton Glieder. "Regulation of Pichia Pastoris Promoters and Its Consequences for Protein Production." New Biotechnology 30, no. 4, 2013, 385–404. https://doi.org/10.1016/j.nbt.2012.11.010.

Vögler, Oliver, Juana M. Barceló, Catalina Ribas, and Pablo V. Escribá. "Membrane Interactions of G Proteins and Other Related Proteins." Biochimica et Biophysica Acta - Biomembranes, Volume 1778, Issues 7–8, July–August 2008, Pages 1640-1652. https://doi.org/10.1016/j.bbamem.2008.03.008.

Volný, Michael. "Time-of-Flight Mass Analyzer." Chemicke Listy, 2020.

Vroling, Bas, Marijn Sanders, Coos Baakman, Annika Borrmann, Stefan Verhoeven, Jan Klomp, Laerte Oliveira, Jacob De Vlieg, and Gert Vriend. "GPCRDB: Information System for G Protein-Coupled Receptors." Nucleic Acids Research 39, no. SUPPL. 1, 2011. 309–19. https://doi.org/10.1093/nar/gkq1009.

Wagner, Elise K., Brittany N. Albaugh, and John M. Denu. "High-Throughput Strategy to Identify Inhibitors of Histone-Binding Domains." In Methods in Enzymology, Volume 512, 2012, Pages 161-185. https://doi.org/10.1016/B978-0-12-391940-3.00008-1.

Wagner, Renaud, Lucie Hartmann, and Estelle Metzger. "Chapter 3" Volume 1635, 2017. https://doi.org/10.1007/978-1-4939-7151-0.

Wang, Hsiang Tsui, Tzu Ying Chen, Ching Wen Weng, Chun Hsiang Yang, and Moonshong Tang. "Acrolein Preferentially Damages Nucleolus Eliciting Ribosomal Stress and Apoptosis in Human Cancer Cells." Oncotarget 7, no. 49, 2016. 80450–64. https://doi.org/10.18632/oncotarget.12608.

I. Company Marin, PhD Thesis, Aston University 2024

Wang, Miao, Chunyan Wang, Rowland H. Han, and Xianlin Han. "Novel Advances in Shotgun Lipidomics for Biology and Medicine." Progress in Lipid Research, Volume 61, January 2016, Pages 83-108. https://doi.org/10.1016/j.plipres.2015.12.002.

Wang, Qian, and F. M. Zhou. "CAMP-Producing Chemogenetic and Adenosine A2a Receptor Activation Inhibits the Inwardly Rectifying Potassium Current in Striatal Projection Neurons." Neuropharmacology, Volume 148, April 2019, Pages 229-243. https://doi.org/10.1016/j.neuropharm.2019.01.014.

Wang, Shu Yi, Yao Song, Ming Xu, Qi Hua He, Qi De Han, and You Yi Zhang. "Internalization and Distribution of Three A1-Adrenoceptor Subtypes in HEK293A Cells before and after Agonist Stimulation." Acta Pharmacologica Sinica, 28, pages 359–366, 2007. https://doi.org/10.1111/j.1745-7254.2007.00509.x.

Wang, Xianhuo, Tingting Zhang, Zheng Song, Linyu Li, Xuhan Zhang, Jing Liu, Xianming Liu, et al. "Tumor CD73/A2aR Adenosine Immunosuppressive Axis and Tumor-Infiltrating Lymphocytes in Diffuse Large B-Cell Lymphoma: Correlations with Clinicopathological Characteristics and Clinical Outcome." International Journal of Cancer 145, no. 5, 2019. 1414–22. https://doi.org/10.1002/ijc.32144.

Wang, Xijuan, Shuai Lv, Jianwei Sun, Meihui Zhang, Lei Zhang, Yan Sun, Ziyan Zhao, Dandan Wang, Xinjing Zhao, and Jiajie Zhang. "Caffeine Reduces Oxidative Stress to Protect against Hyperoxia-Induced Lung Injury via the Adenosine A2A Receptor/CAMP/PKA/Src/ERK1/2/P38MAPK Pathway." Redox Report 27, no. 1, 2022. 270–78. https://doi.org/10.1080/13510002.2022.2143114.

Warren, C. R. "A Liquid Chromatography–Mass Spectrometry Method for Analysis of Intact Fatty-Acid-Based Lipids Extracted from Soil." European Journal of Soil Science 69, no. 5, 2018. 791–803. https://doi.org/10.1111/ejss.12689.

Washburn, Michael P., Dirk Wolters, and John R. Yates. "Large-Scale Analysis of the Yeast Proteome by Multidimensional Protein Identification Technology." Nature Biotechnology, 19, pages 242–247, 2001. https://doi.org/10.1038/85686.

Waugh, David S. "Making the Most of Affinity Tags." Trends in Biotechnology, Volume 23, Issue 6, P316-320, June 2005. https://doi.org/10.1016/j.tibtech.2005.03.012.

Weis, William I, and Brian K Kobilka. "The Molecular Basis of G Protein-Coupled Receptor 1. Weis, W. I. & Kobilka, B. K. The Molecular Basis of G Protein-Coupled Receptor Activation. Annu. Rev. Biochem., 2018. Doi:10.1146/Annurev-Biochem-060614-033910Activation." Annual Review of Biochemistry, Vol. 87:897-919, 2018. http://doi.org/10.1146/annurev-biochem-060614-033910.

Welihinda, Ajith A., Manmeet Kaur, Kelly Greene, Yongjiao Zhai, and Edward P. Amento. "The Adenosine Metabolite Inosine Is a Functional Agonist of the Adenosine A2A Receptor with a Unique Signaling Bias." Cellular Signalling 28, no. 6, June 2016, 552–60. https://doi.org/10.1016/j.cellsig.2016.02.010.

Weller, Michael G. "Quality Issues of Research Antibodies." Analytical Chemistry Insights, 11, 2016. https://doi.org/10.4137/Aci.s31614.

Westerlund, Annie M., Oliver Fleetwood, Sergio Pérez-Conesa, and Lucie Delemotte. "Network Analysis Reveals How Lipids and Other Cofactors Influence Membrane Protein Allostery." Journal of Chemical Physics, 153, 141103, 2020. https://doi.org/10.1063/5.0020974.

Westhuizen, Emma T. Van Der, Celine Valant, Patrick M. Sexton, and Arthur Christopoulos. "Endogenous Allosteric Modulators of G Protein-Coupled Receptors." Journal of Pharmacology and Experimental Therapeutics, 353 (2) 246-260, 2015. https://doi.org/10.1124/jpet.114.221606.

Wheatley, Mark, D Wootten, M T Conner, J Simms, R Kendrick, R T Logan, and J Barwell. "Themed Section: Molecular Pharmacology of GPCRs Lifting the Lid on GPCRs : The Role of Extracellular Loops," Volume 165, Issue 6, Special Issue: Themed Section: Molecular Pharmacology of GPCRs. Guest Editor: Roger J Summers, March 2012, Pages 1688-1703. https://doi.org/10.1111/j.1476-5381.2011.01629.x.

Wheatley, Mark, Jack Charlton, Mohammed Jamshad, Sarah J. Routledge, Sian Bailey, Penelope J. La-Borde, Maria T. Azam, et al. "GPCR-Styrene Maleic Acid Lipid Particles, GPCR-SMALPs. Their Nature and Potential." Biochemical Society Transactions, 44 (2): 619–623, 2016. https://doi.org/10.1042/BST20150284.

Wilm, Matthias. "Principles of Electrospray Ionization." Molecular and Cellular Proteomics, Volume 10, Issue 7, M111.009407, July, 2011. https://doi.org/10.1074/mcp.M111.009407.

I. Company Marin, PhD Thesis, Aston University 2024

Wishart, David S., An Chi Guo, Eponine Oler, Fei Wang, Afia Anjum, Harrison Peters, Raynard Dizon, et al. "HMDB 5.0: The Human Metabolome Database for 2022." Nucleic Acids Research, Volume 50, Issue D1, 7 January 2022, Pages D622–D631. https://doi.org/10.1093/nar/gkab1062.

Wriessnegger, T., E. Leitner, M. R. Belegratis, E. Ingolic, and G. Daum. "Lipid Analysis of Mitochondrial Membranes from the Yeast Pichia Pastoris." Biochimica et Biophysica Acta - Molecular and Cell Biology of Lipids, Volume 1791, Issue 3, March 2009, Pages 166-172. https://doi.org/10.1016/j.bbalip.2008.12.017.

Wu, Tao, Xiao Yu, Antuo Hu, Li Zhang, Yuan Jin, and Muhammad Abid. "Ultrasonic Disruption of Yeast Cells : Underlying Mechanism and Effects of Processing Parameters." Innovative Food Science and Emerging Technologies 28, 2015. 59–65. https://doi.org/10.1016/j.ifset.2015.01.005.

Xu, Fei, Huixian Wu, Vsevolod Katritch, Gye Won Han, Kenneth A. Jacobson, Zhan Guo Gao, Vadim Cherezov, and Raymond C. Stevens. "Structure of an Agonist-Bound Human A2A Adenosine Receptor." Science 332, no. 6027, 2011. 322–27. https://doi.org/10.1126/science.1202793.

Yan, Luo, Joachim C. Burbiel, Astrid Maaß, and Christa E. Müller. "Adenosine Receptor Agonists: From Basic Medicinal Chemistry to Clinical Development." Expert Opinion on Emerging Drugs, 8(2), 537–576, 2003. https://doi.org/10.1517/14728214.8.2.537.

Yang, Lewen, and Edward Lyman. "Local Enrichment of Unsaturated Chains around the A2A Adenosine Receptor." Biochemistry, 58, 39, 4096–4105, 2019. https://doi.org/10.1021/acs.biochem.9b00607.

Yang, Xue, Guo Dong, Thomas J.M. Michiels, Eelke B. Lenselink, Laura Heitman, Julien Louvel, and Ad P. Ijzerman. "A Covalent Antagonist for the Human Adenosine A2A Receptor." Purinergic Signalling 13, no. 2, 2017, 191–201. https://doi.org/10.1007/s11302-016-9549-9.

Yang, Zhiliang, and Zisheng Zhang. "Engineering Strategies for Enhanced Production of Protein and Bio-Products in Pichia Pastoris: A Review." Biotechnology Advances 36, no. 1, 2018, 182–95. https://doi.org/10.1016/j.biotechadv.2017.11.002.

Yao, Xia, Xiao Fan, and Nieng Yan. "Cryo-EM Analysis of a Membrane Protein Embedded in the Liposome." Proceedings of the National Academy of Sciences of the United States of America, 117 (31) 18497-18503, 2020. https://doi.org/10.1073/pnas.2009385117.

Yao, Xiaojie, Charles Parnot, Xavier Deupi, Venkata R.P. Ratnala, Gayathri Swaminath, David Farrens, and Brian Kobilka. "Coupling Ligand Structure to Specific Conformational Switches in the B2-Adrenoceptor." Nature Chemical Biology, 2, pages 417–422, 2006. https://doi.org/10.1038/nchembio801.

Ye, Libin, Ned Van Eps, Marco Zimmer, Oliver P. Ernst, and R. Scott Prosser. "Activation of the A 2A Adenosine G-Protein-Coupled Receptor by Conformational Selection." Nature 533, no. 7602, 2016, 265–68. https://doi.org/10.1038/nature17668.

Yeagle, Philip L. "Non-Covalent Binding of Membrane Lipids to Membrane Proteins." Biochimica et Biophysica Acta - Biomembranes, Volume 1838, Issue 6, June 2014, Pages 1548-1559. https://doi.org/10.1016/j.bbamem.2013.11.009.

Yen, Hsin Yung, Kin Kuan Hoi, Idlir Liko, George Hedger, Michael R. Horrell, Wanling Song, Di Wu, et al. "PtdIns(4,5.P2 Stabilizes Active States of GPCRs and Enhances Selectivity of G-Protein Coupling." Nature, 2018. https://doi.org/10.1038/s41586-018-0325-6.

Yetukuri, Laxman, Kim Ekroos, Antonio Vidal-Puig, and Matej Orešič. "Informatics and Computational Strategies for the Study of Lipids." Molecular BioSystems, 559, pages 423–427, 2008. https://doi.org/10.1039/b715468b.

Yin, Zhao, Kaiyu Jiang, Lei Shi, Jia Fei, Jie Zheng, Shiyi Ou, and Juanying Ou. "Formation of Di-Cysteine Acrolein Adduct Decreases Cytotoxicity of Acrolein by ROS Alleviation and Apoptosis Intervention." Journal of Hazardous Materials 387, no. July 2019, 2020, 121686. https://doi.org/10.1016/j.jhazmat.2019.121686.

Yoshida, Kouhei, Satoru Nagatoishi, Daisuke Kuroda, Nanao Suzuki, Takeshi Murata, and Kouhei Tsumoto. "Phospholipid Membrane Fluidity Alters Ligand Binding Activity of a G Protein-Coupled Receptor by Shifting the Conformational Equilibrium." Biochemistry, 58, 6, 504–508, 2019. https://doi.org/10.1021/acs.biochem.8b01194.

Yu, Keyang, Zhaojun Liu, Shuyan Wu, Shuanghua Luo, Xing Weng, Zhou Wang, Maomao Zeng, Xiaoyuan Wang, and Xiaoqing Hu. "Comparative Lipidomics of Pichia Pastoris Using Constitutive Promoter Reveals Lipid Diversity and Variability at

I. Company Marin, PhD Thesis, Aston University 2024

Different Growth Phases." Canadian Journal of Microbiology, Volume 68, Number 12, December 2022, https://doi.org/10.1139/cjm-2021-0385.

Zezula, J., and M. Freissmuth. "The A 2A-Adenosine Receptor: A GPCR with Unique Features?" British Journal of Pharmacology 153, no. SUPPL. 1, 2008, 184–90. https://doi.org/10.1038/sj.bjp.0707674.

Zhang, Bingjie, Shanshan Li, and Wenqing Shui. "Post-Translational Modifications of G Protein–Coupled Receptors Revealed by Proteomics and Structural Biology." Frontiers in Chemistry, Volume 10, 2022. https://doi.org/10.3389/fchem.2022.843502.

Zhang, Qifeng, and Michael J.O. Wakelam. "Lipidomics in the Analysis of Malignancy." Advances in Biological Regulation, Volume 54, January 2014, Pages 93-98. https://doi.org/10.1016/j.jbior.2013.11.001.

Zhang, Xing Wei, Wei Fen Li, Wei Wei Li, Kan Han Ren, Chao Ming Fan, Ying Ying Chen, and Yue Liang Shen. "Protective Effects of the Aqueous Extract of Scutellaria Baicalensis against Acrolein-Induced Oxidative Stress in Cultured Human Umbilical Vein Endothelial Cells." Pharmaceutical Biology 49, no. 3, 2011, 256–61. https://doi.org/10.3109/13880209.2010.501803.

Zhao, Dongrui, Dongmei Shi, Jinyuan Sun, Hehe Li, Mouming Zhao, and Baoguo Sun. "Quantification and Cytoprotection by Vanillin, 4-Methylguaiacol and 4-Ethylguaiacol against AAPH-Induced Abnormal Oxidative Stress in HepG2 Cells." RSC Advances, 8, 35474-35484, 2018. https://doi.org/10.1039/C8RA06505E.

Zhao, Li, Yang Wuyue Liu, Ting Yang, Lin Gan, Nan Yang, Shuang Shuang Dai, and Fengtian He. "The Mutual Regulation between MiR-214 and A2AR Signaling Plays an Important Role in Inflammatory Response." Cellular Signalling 27, no. 10, 2015. 2026–34. https://doi.org/10.1016/j.cellsig.2015.07.007.

Zhao, Weiming, Li Ma, Cheng Cai, and Xiaohui Gong. "Caffeine Inhibits NLRP3 Inflammasome Activation by Suppressing MAPK/NF-KB and A2aR Signaling in LPS-Induced THP-1 Macrophages." International Journal of Biological Sciences 15, no. 8, 2019. 1571–81. https://doi.org/10.7150/ijbs.34211.

Zhong, Shanshan, Luxiao Li, Xia Shen, Qiujing Li, Wenxin Xu, Xiaoping Wang, Yongzhen Tao, and Huiyong Yin. "An Update on Lipid Oxidation and Inflammation in Cardiovascular Diseases." Free Radical Biology and Medicine 144, no. March, 2019. 266–78. https://doi.org/10.1016/j.freeradbiomed.2019.03.036.

Zhukovsky, Mikhail A., Angela Filograna, Alberto Luini, Daniela Corda, and Carmen Valente. "Phosphatidic Acid in Membrane Rearrangements." FEBS Letters 593, no. 17, 2019, 2428–51. https://doi.org/10.1002/1873-3468.13563.

Ziółkowska, Natasza E., Romain Christiano, and Tobias C. Walther. "Organized Living: Formation Mechanisms and Functions of Plasma Membrane Domains in Yeast." Trends in Cell Biology, Volume 22, Issue 3, P151-158, March 2012, https://doi.org/10.1016/j.tcb.2011.12.002.

Züllig, Thomas, and Harald C. Köfeler. "High Resolution Mass Spectrometry In Lipidomics." Mass Spectrometry Reviews, Volume 40, Issue 3, A Special Issue Dedicated To The Outstanding Scientific Career Of Prof. Michael L. Gross, May/June 2021, Pages 162-176. https://doi.org/10.1002/mas.21627.
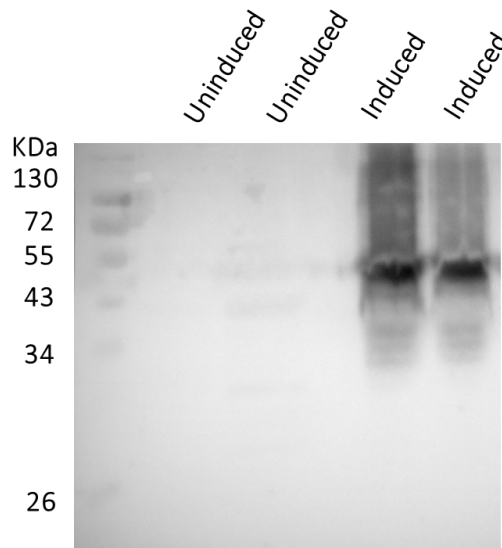
Figure 8.1. Expression of the A₂ₐR in Pichia pastoris. *The A₂ₐR was expressed in P. pastoris SMD1163 with the pPICZB-A₂ₐR plasmid. The expression was assessed by SDS-PAGE and Western blotting with a specific primary antibody against the A₂ₐR.*
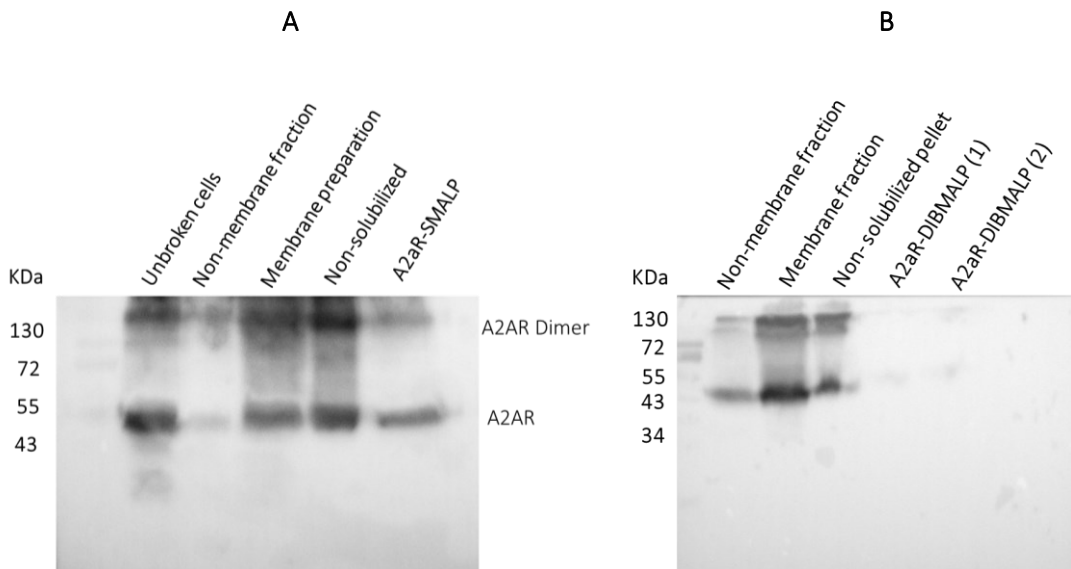
Figure 8.2. Solubilization of the A₂ₐR with SMA2000 and DIBMA free acid at 2.5% (w/v). *The A₂ₐR was solubilized from the membrane preparation using (**A**) SMA2000 at 2.5% (w/v) and (**B**) DIBMA free acid at 2.5% (w/v). Protein solubilization was monitored by SDS-PAGE and Western blotting using a specific primary antibody against the A₂ₐR.*
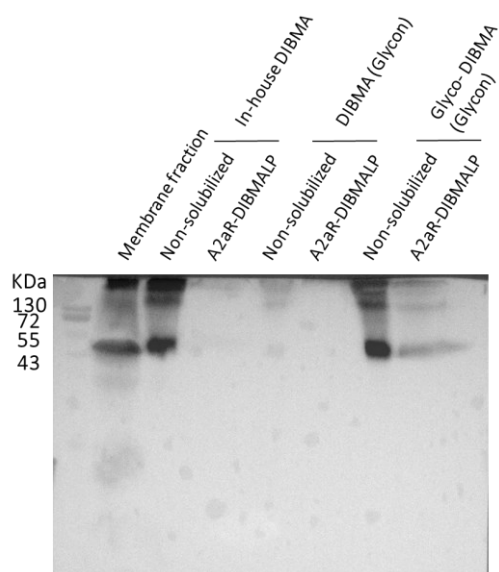
Figure 8.3. Solubilization of the A₂ₐR with DIBMA polymers at 5% (w/v). *The A₂ₐR was solubilized from the membrane preparation using DIBMA free acid, DIBMA monosodium salt, and Glyco-DIBMA at 5%. Protein solubilization was monitored by SDS-PAGE and Western blot using a specific primary antibody against the A₂ₐR.*
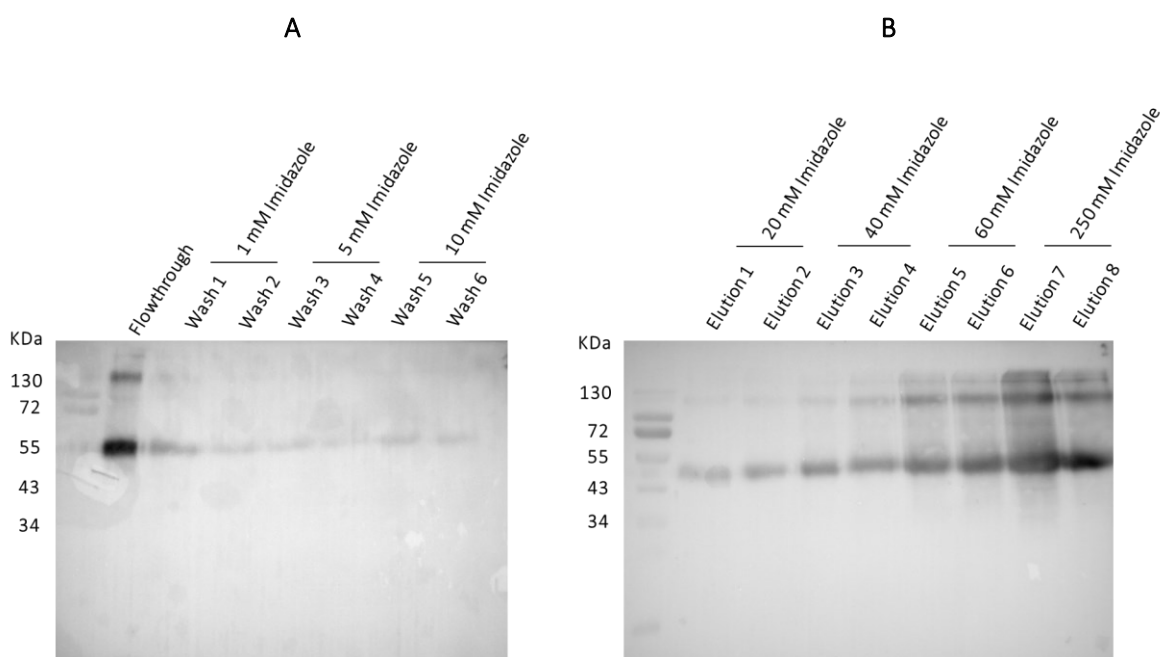
Figure 8.4. *Finding the optimal imidazole concentrations for the purification of the A₂ₐR-SMALP. Solubilized membranes were recirculated with His-select resin. (**A**) The resin was washed with 1, 5, and 10 mM imidazole. (**B**) The A₂ₐR-SMALP was eluted from the resin using 20, 40, 60, and 250 mM imidazole. Protein elution was analysed by Western blotting using an anti-A₂ₐR primary antibody.*

I. Company Marin, PhD Thesis, Aston University 2024
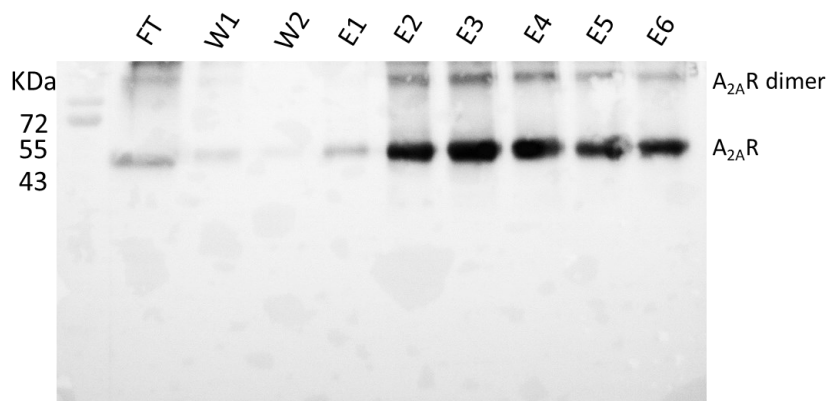
Figure 8.5. *Large-scale purification of the A₂ₐR-SMALP*. *P. pastoris cells expressing the A₂ₐR were broken using acid-washed glass beads to obtain the membrane preparation in Tris-HCl buffer. The A₂ₐR was solubilized using 2.5% SMA2000 and purified using His-pur Ni-NTA resin. The resin was washed with 20 mM imidazole, and A₂ₐR-SMALP eluted with 60 mM imidazole. A₂ₐR-SMALP elution was analysed by Western blotting analysis.*
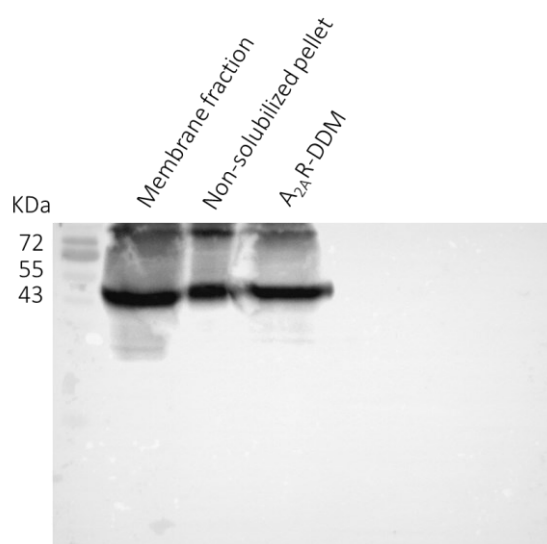
Figure 8.6. *Solubilization of the A₂ₐR with 2% (w/v) DDM*. *The A₂ₐR was solubilized from P. pastoris membranes with DDM. A₂ₐR solubilization was monitored by western Blotting with a specific primary antibody against the A₂ₐR.*

I. Company Marin, PhD Thesis, Aston University 2024
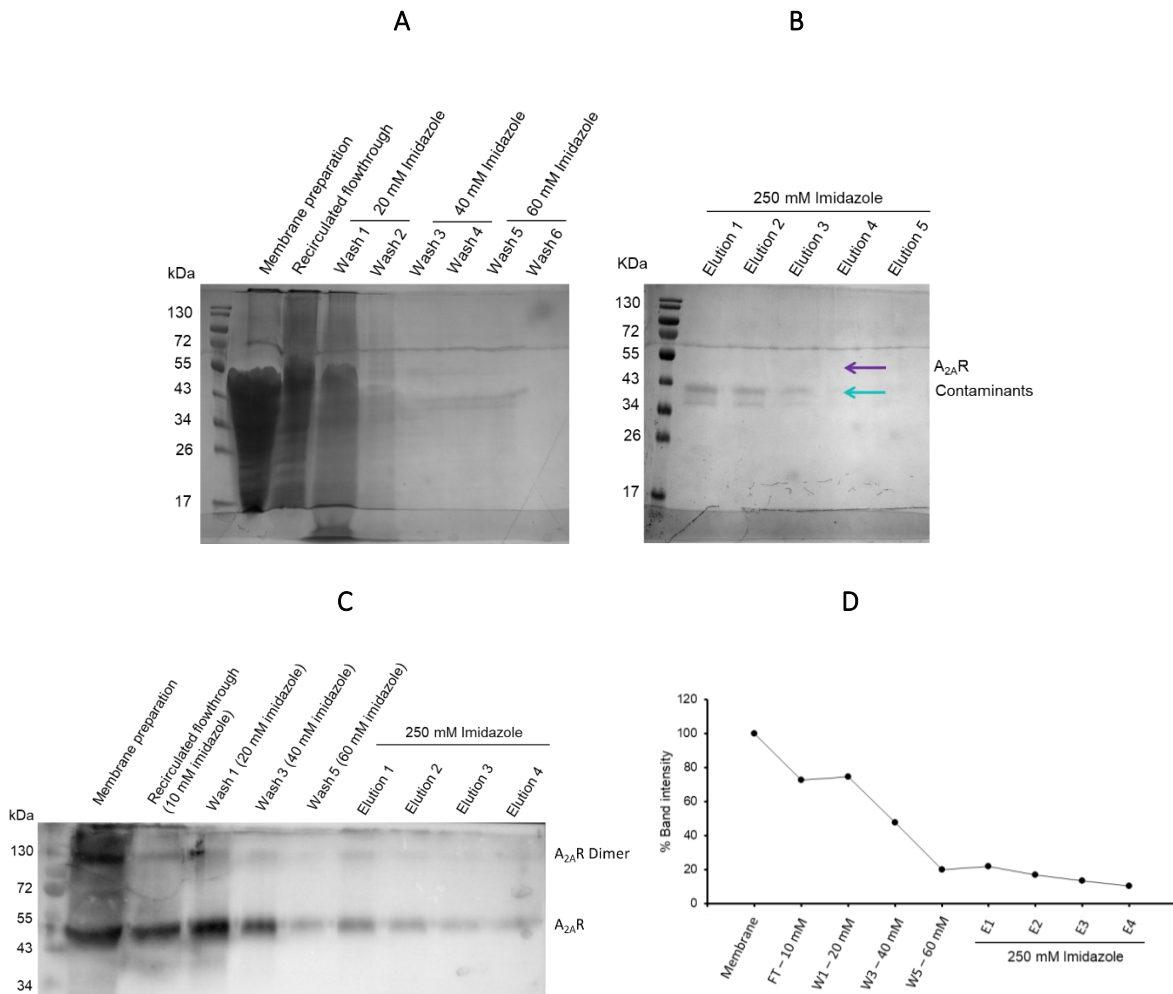
Figure 8.7. A₂ₐR-SMALP purification through affinity chromatography using Ni-NTA His-select affinity gel and high imidazole concentrations. The solubilized fraction containing the A₂ₐR-SMALP was recirculated with a previously equilibrated resin with 10 mM imidazole. The column was washed with 20, 40, and 60 mM imidazole and the A₂ₐR-SMALP was eluted from the resin with 250 mM imidazole. The results were analysed by SDS-PAGE, Coomassie staining, and Western blotting using an anti-A₂ₐR primary antibody. (A) SDS-PAGE and Coomassie staining of the membrane preparation, flow-through, and wash fractions. (B) SDS-PAGE and Coomassie staining of the elution fractions. (C) Western blot analysis of the membrane preparation, flow-through, wash, and elution fractions for the detection of the A₂ₐR. (D) Densitometric analysis of bands corresponding to the A₂ₐR detected by Western blotting in the different purification fractions (n=1).

227
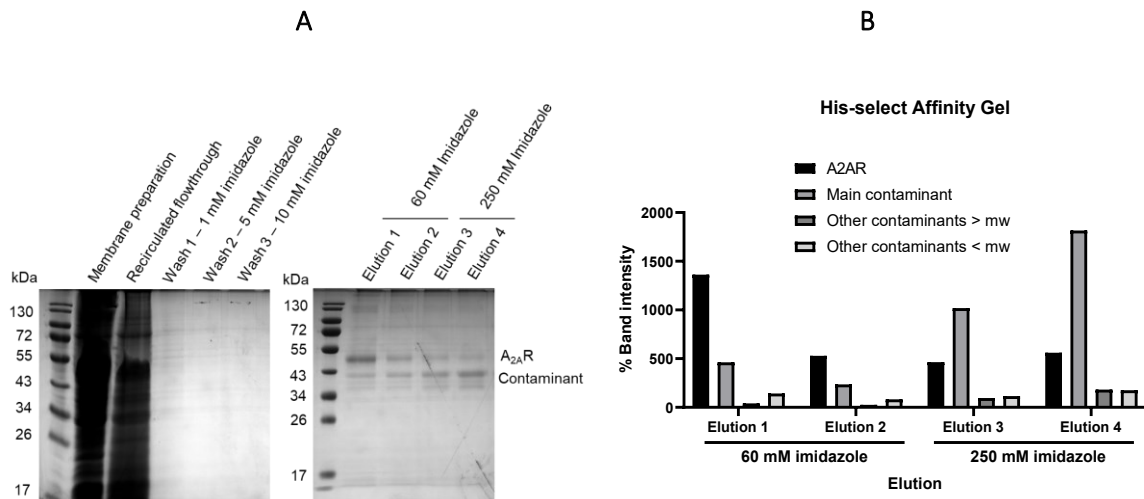
*Figure 8.8. A_{2A}R-SMALP purification by affinity chromatography using His-select affinity gel (Sigma) Ni^{+2}-NTA resin. The solubilized fraction containing the A_{2A}R-SMALP was recirculated with His-select affinity gel from Sigma, which was previously equilibrated without imidazole. The resin was washed with 1, 5, and 10 mM imidazole and the A_{2A}R-SMALP was eluted with 60 and 250 mM imidazole. (**A**) Flow-through, wash, and elution fractions were analysed by SDS-PAGE and Coomassie staining, and (**B**) bands corresponding to the A_{2A}R, P. pastoris main contaminant, and other contaminants were analysed by densitometry (n=1).*
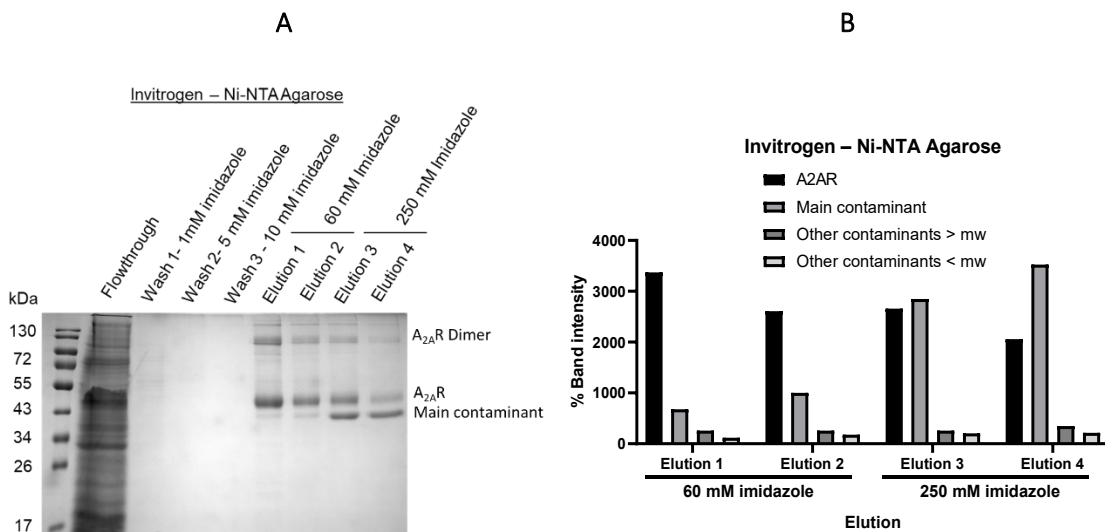
*Figure 8.9. A_{2A}R-SMALP purification by affinity chromatography using Ni-NTA agarose (Invitrogen) Ni^{+2}-NTA resin. The solubilized fraction containing the A_{2A}R-SMALP was recirculated with Ni-NTA agarose (Invitrogen) previously equilibrated without imidazole. The resin was washed with 1, 5, and 10 mM imidazole and the A_{2A}R-SMALP was eluted with 60 and 250 mM imidazole. (**A**) Flow-through, wash, and elution fractions were analysed by SDS-PAGE and Coomassie staining, and (**B**) bands corresponding to the A_{2A}R, P. pastoris main contaminant, and other contaminants were analysed by densitometry (n=1).*
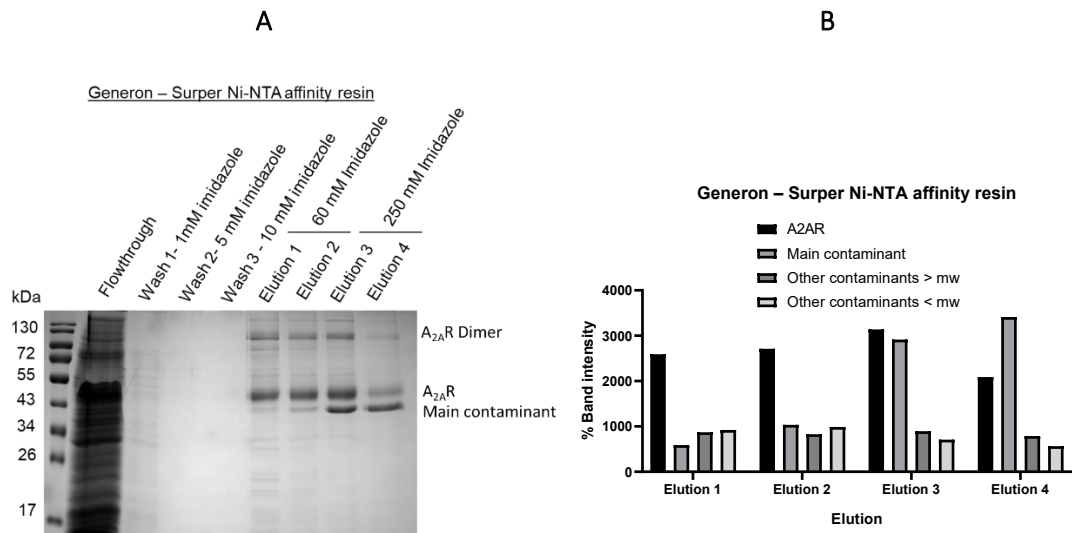
Figure 8.10. A₂ₐR-SMALP purification by affinity chromatography using Super Ni-NTA affinity resin (Generon) Ni⁺²-NTA resin. The solubilized fraction containing the A₂ₐR-SMALP was recirculated with Super Ni-NTA affinity resin (Generon) previously equilibrated without imidazole. The resin was washed with 1, 5, and 10 mM imidazole and the A₂ₐR-SMALP was eluted with 60 and 250 mM imidazole. (**A**) Flow-through, wash, and elution fractions were analysed by SDS-PAGE and Coomassie staining, and (**B**) bands corresponding to the A₂ₐR, P. pastoris main contaminant, and other contaminants were analysed by densitometry (n=1).
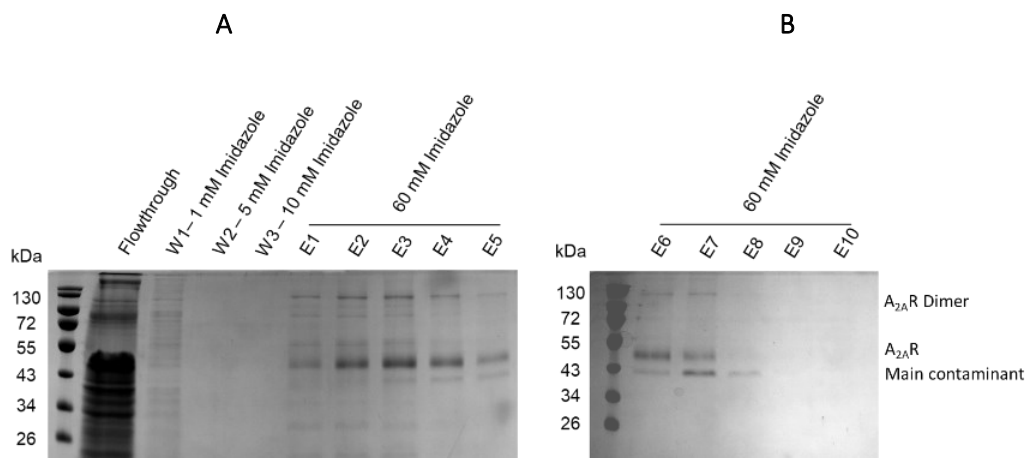
Figure 8.11. A₂ₐR-SMALP and P. pastoris main contaminant elution from His-pur Ni-NTA resin with 60 mM imidazole. The solubilized fraction containing the A₂ₐR-SMALP was recirculated with previously equilibrated His-pur Ni-NTA resin without imidazole. The resin was washed with 1, 5, and 10 mM imidazole and the A₂ₐR-SMALP eluted with 60 mM and 1 CV at a time for a total of 10 elution steps. Results were analysed by SDS-PAGE and Coomassie staining for (A) Flouthrough, wash fractions and 1-5 elution fractions, and (B) 6-10 elution fractions.

I. Company Marin, PhD Thesis, Aston University 2024
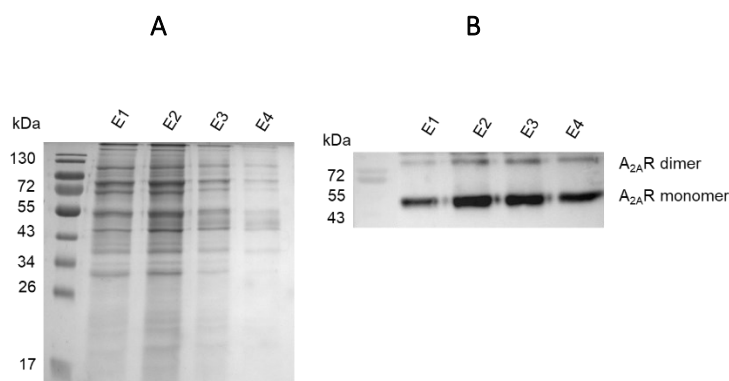
Figure 8.12. Large-scale purification of the A$_{2A}$R-SMALP prepared with the C3 cell disrupter in HEPES buffer. *P. pastoris cells expressing the A$_{2A}$R were broken using the C3 cell disrupter to obtain the membrane preparation in HEPES buffer, from which the A$_{2A}$R was solubilized using SMA2000 at 2.5%. The solubilized fraction containing the A$_{2A}$R-SMALP was recirculated with a previously equilibrated His-pur Ni-NTA resin without imidazole. The resin was washed with 10 mM imidazole, and A$_{2A}$R-SMALP was eluted with 60 mM imidazole. The elution fractions were analysed by (**A**) SDS-PAGE and Coomassie staining and (**B**) Western blotting using an anti-A$_{2A}$R primary antibody.*
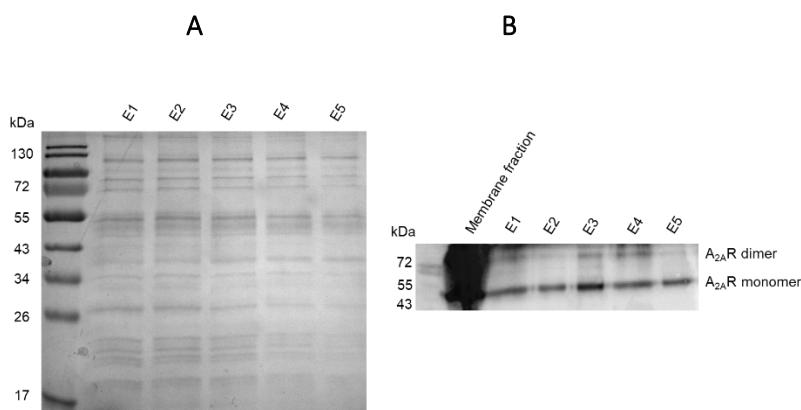
Figure 8.13. Large-scale purification of the A$_{2A}$R-SMALP prepared with the C3 cell disrupter in HEPES buffer increasing imidazole concentrations to wash the resin. *P. pastoris cells expressing the A$_{2A}$R were broken using the C3 cell disrupter to obtain the membrane preparation in HEPES buffer, from which the A$_{2A}$R was solubilized using SMA2000 at 2.5%. The solubilized fraction containing the A$_{2A}$R-SMALP was recirculated with a previously equilibrated His-pur Ni-NTA resin without imidazole. The resin was washed with 20 mM imidazole, and A$_{2A}$R-SMALP eluted with 60 mM imidazole. The elution fractions were analysed by (**A**) SDS-PAGE and Coomassie staining and (**B**) Western blotting using an anti-A$_{2A}$R primary antibody.*
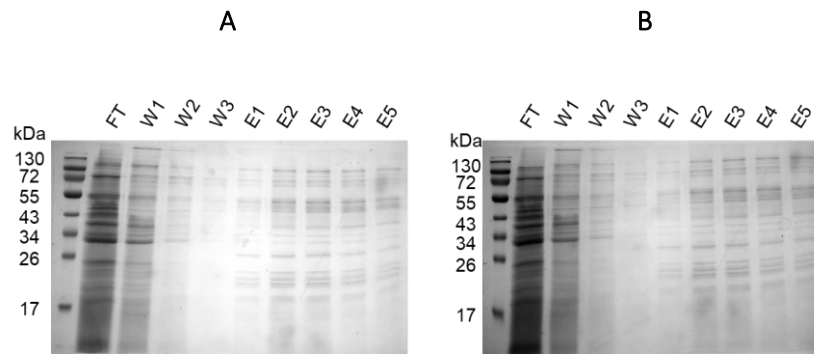
Figure 8.14. Large-scale purification of the A2AR-SMALP prepared with the C3 cell disrupter in HEPES buffer using different SMA2000 and resin stocks. P. pastoris cells expressing the $A_{2A}R$ were broken using the C3 cell disrupter to obtain the membrane preparation in HEPES buffer, from which the $A_{2A}R$ was solubilized and purified using (A) SMA2000 at 2.5% from the same stock used for previous experiments and reused resin and (B) SMA2000 at 2.5% from a new stock and resin. The solubilized fraction containing the $A_{2A}R$ -SMALP was recirculated with a previously equilibrated His-pur Ni-NTA resin without imidazole. Resins were washed with 20 mM imidazole and $A_{2A}R$-SMALP was eluted with 60 mM imidazole. Flow-through, wash, and elution fractions were analysed by SDS-PAGE and Coomassie staining.
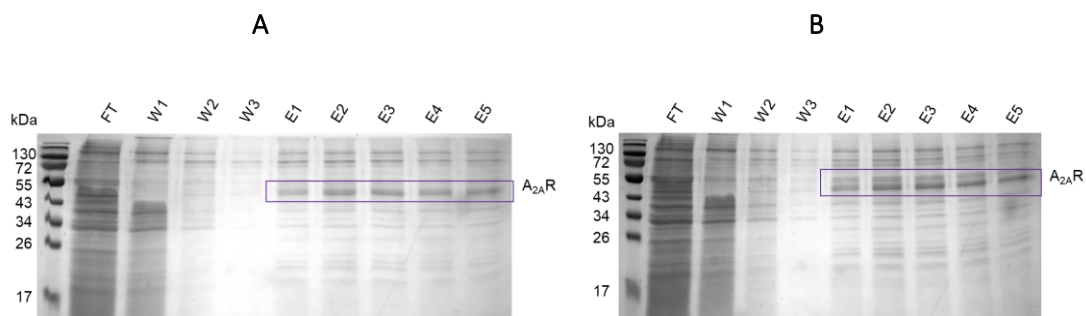
Figure 8.15. Large-scale purification of the $A_{2A}R$-SMALP prepared with the Glass beads or the French press in HEPES buffer. P. pastoris cells expressing the $A_{2A}R$ were broken using (A) acid-washed Glass beads or (B) the French press, to obtain the membrane preparation in HEPES buffer, from which the $A_{2A}R$ was solubilized using SMA2000 at 2.5%. The solubilized fractions containing the $A_{2A}R$-SMALP were recirculated with a previously equilibrated His-pur Ni-NTA resin without imidazole. The resins were washed with 20 mM imidazole, and $A_{2A}R$-SMALP eluted with 60 mM imidazole. The flow-trhough, wash, and elution fractions were analysed by SDS-PAGE and Coomassie staining.
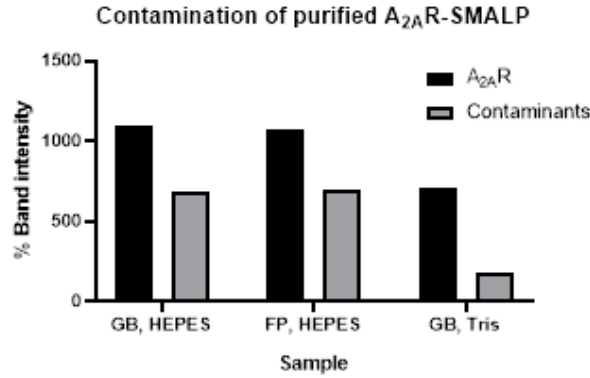
Figure 8.16. Densitometric analysis of the bands corresponding to the A₂ₐR-SMALP and other contaminants detected by SDS-PAGE and Coomassie staining in the different elution fractions. *A₂ₐR-SMALP was prepared using different cell-breaking methods: glass beads (GB) or French press (FP), and different buffers: Tris-HCl and HEPES. A₂ₐR-SMALP elution was compared to the elution of other contaminants in different purification tests (n=1).*
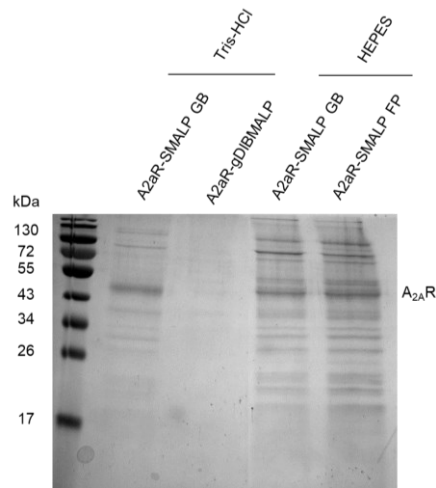
Figure 8.17. Analysis of the 5X concentrated A₂ₐR-SMALP and A₂ₐR-Glyco-DIBMALP in different buffers. *Purified A₂ₐR-SMALP GB and A₂ₐR-Glyco-DIBMALP GB prepared in Tris-HCl buffer and A₂ₐR-SMALP GB and A₂ₐR-SMALP FP prepared in HEPES buffer were concentrated five times and the results were analysed by SDS-PAGE and Coomassie staining.*
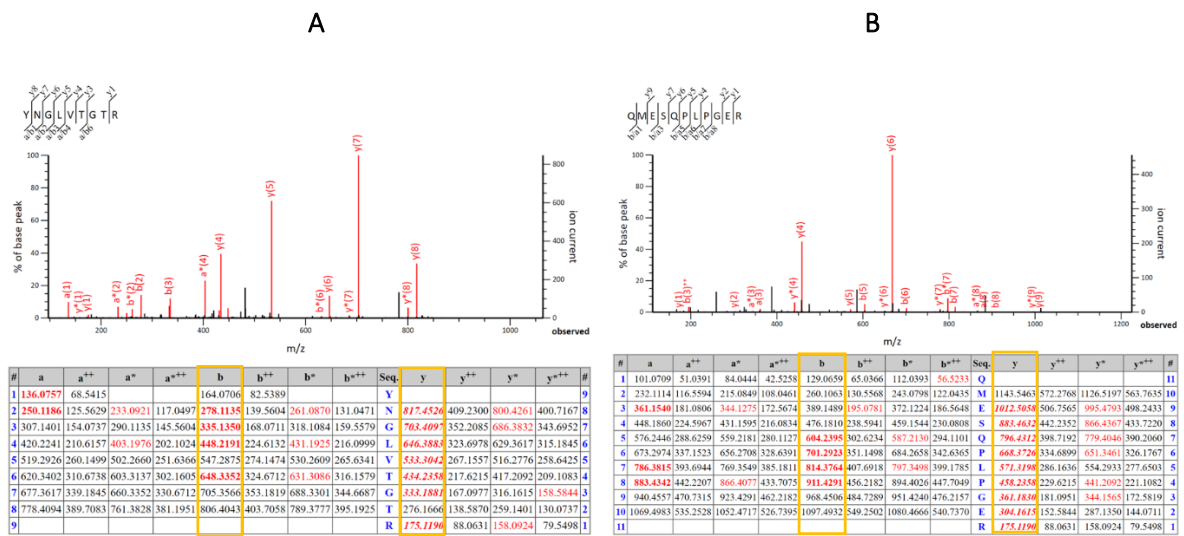
Figure 8.18. A₂AR monomer identification by LC-MS/MS after trypsin in-gel digestion. Bands corresponding to the A₂AR monomer were in-gel digested with trypsin and analysed by LC-MS/MS. (A) Fragmentation spectrum of the YNGLVTGTR peptide and Y and B ion coverage. (B) Fragmentation spectrum of the QMESQPLPGER peptide and Y and B ion coverage. Covered ions are highlighted in red, whereas non-covered ions are presented in black.

I. Company Marin, PhD Thesis, Aston University 2024

A

B

C
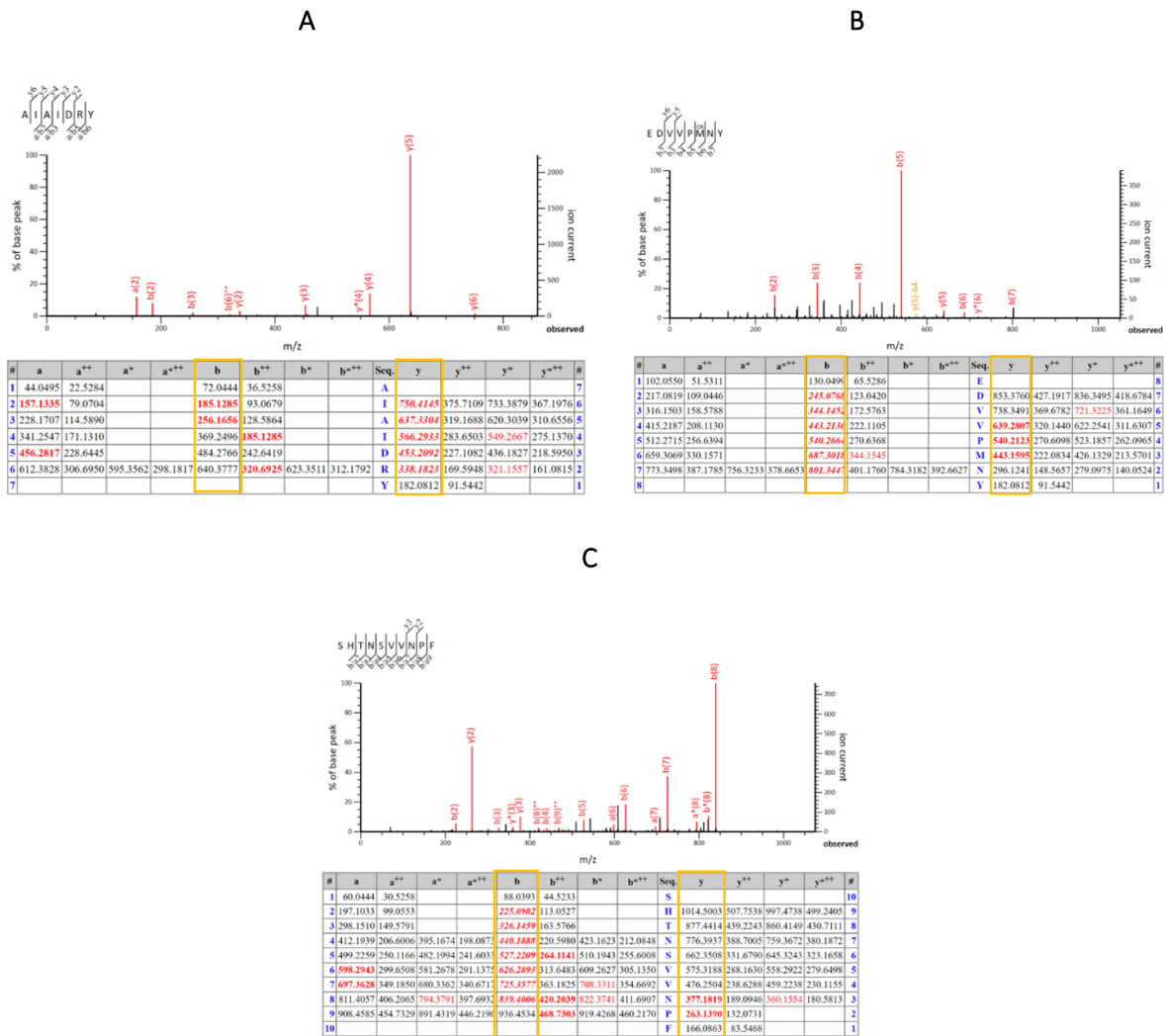
Figure 8.19. A$_{2A}$R dimer identification by LC-MS/MS after chymotrypsin in-gel digestion. Bands corresponding to the A$_{2A}$R dimer were in-gel digested with chymotrypsin and analysed by LC-MS/MS. (A) Fragmentation spectrum of the AIAIDRY peptide and Y and B ion coverage. (B) Fragmentation spectrum of the EDVVPMNY peptide and Y and B ion coverage. (C) Fragmentation spectrum of the SHTNSVVNPF peptide and Y and B ion coverage. Covered ions are highlighted in red whereas non-covered ions are presented in black.

A

Peptide: L N S N L Q N V T N Y

#	a	a++	a*	a*++	b	b++	b*	b*++	Seq.	y	y++	y*	y*++	#
1	86.0964	43.5519			114.0913	57.5493			L					11
2	200.1394	100.5733	183.1128	92.0600	228.1343	114.5708	211.1077	106.0575	N	1166.5436	583.7755	1149.5171	575.2622	10
3	287.1714	144.0893	270.1448	135.5761	315.1663	158.0868	298.1397	149.5735	S	1052.5007	526.7540	1035.4742	518.2407	9
4	401.2143	201.1108	384.1878	192.5975	429.2092	215.1082	412.1827	206.5950	N	965.4687	483.2380	948.4421	474.7247	8
5	514.2984	257.6528	497.2718	249.1395	542.2933	271.6503	525.2667	263.1370	L	851.4258	426.2165	834.3992	417.7032	7
6	642.3569	321.6821	625.3304	313.1688	670.3519	335.6796	653.3253	327.1663	Q	738.3417	369.6745	721.3151	361.1612	6
7	756.3999	378.7036	739.3733	370.1903	784.3948	392.7010	767.3682	384.1878	N	610.2831	305.6452	593.2566	297.1319	5
8	855.4683	428.2378	838.4417	419.7245	883.4632	442.2352	866.4367	433.7220	V	496.2402	248.6237	479.2136	240.1105	4
9	956.5160	478.7616	939.4894	470.2483	984.5109	492.7591	967.4843	484.2458	T	397.1718	199.0895	380.1452	190.5763	3
10	1070.5589	535.7831	1053.5323	527.2698	1098.5538	549.7805	1081.5273	541.2673	N	296.1241	148.5657	279.0975	140.0524	2
11									Y	182.0812	91.5442			1

B

Peptide: A A A D I A V G V L

#	a	a++	b	b++	Seq.	y	y++	#
1	44.0495	22.5284	72.0444	36.5258	A			10
2	115.0866	58.0469	143.0815	72.0444	A	828.4825	414.7449	9
3	186.1237	93.5655	214.1186	107.5629	A	757.4454	379.2264	8
4	301.1506	151.0790	329.1456	165.0764	D	686.4083	343.7078	7
5	414.2347	207.6210	442.2296	221.6185	I	571.3814	286.1943	6
6	485.2718	243.1396	513.2667	257.1370	A	458.2973	229.6523	5
7	584.3402	292.6738	612.3352	306.6712	V	387.2602	194.1337	4
8	641.3617	321.1845	669.3566	335.1819	G	288.1918	144.5995	3
9	740.4301	370.7187	768.4256	384.7162	V	231.1703	116.0888	2
10					L	132.1019	66.5546	1

C

Peptide: A I T I S T G F

#	a	a++	b	b++	Seq.	y	y++	#
1	44.0495	22.5284	72.0444	36.5258	A			8
2	157.1335	79.0704	185.1285	93.0679	I	738.4032	369.7053	7
3	258.1812	129.5942	286.1761	143.5917	T	625.3192	313.1632	6
4	371.2653	186.1363	399.2602	200.1337	I	524.2715	262.6394	5
5	458.2973	229.6523	486.2922	243.6498	S	411.1874	206.0974	4
6	559.3450	280.1761	587.3399	294.1736	T	324.1554	162.5813	3
7	616.3665	308.6869	644.3614	322.6843	G	223.1077	112.0575	2
8					F	166.0863	83.5468	1

D

Peptide: S L L A I A I D R Y

#	a	a++	a*	a*++	b	b++	b*	b*++	Seq.	y	y++	y*	y*++	#
1	60.0444	30.5258			88.0393	44.5233			S					10
2	173.1285	87.0679			201.1234	101.0653			L	1047.6197	524.3135	1030.5932	515.8002	9
3	286.2125	143.6099			314.2074	157.6074			L	934.5356	467.7715	917.5091	459.2582	8
4	357.2496	179.1285			385.2445	193.1259			A	821.4516	411.2294	804.4250	402.7162	7
5	470.3337	235.6705			498.3286	249.6679			I	750.4145	375.7109	733.3879	367.1976	6
6	541.3708	271.1890			569.3657	285.1865			A	637.3304	319.1688	620.3039	310.6556	5
7	654.4549	327.7311			682.4498	341.7285			I	566.2933	283.6503	549.2667	275.1370	4
8	769.4818	385.2445			797.4767	399.2420			D	453.2092	227.1082	436.1827	218.5950	3
9	925.5829	463.2951	908.5564	454.7818	953.5778	477.2926	936.5513	468.7793	R	338.1823	169.5948	321.1557	161.0815	2
10									Y	182.0812	91.5442			1

E

Peptide: A I G L T P M L G W

#	a	a++	b	b++	Seq.	y	y++	#
1	44.0495	22.5284	72.0444	36.5258	A			10
2	157.1335	79.0704	185.1285	93.0679	I	1003.5281	502.2677	9
3	214.1550	107.5811	242.1499	121.5786	G	890.4441	445.7257	8
4	327.2391	164.1232	355.2340	178.1206	L	833.4226	417.2149	7
5	428.2867	214.6470	456.2817	228.6445	T	720.3385	360.6729	6
6	525.3395	263.1734	553.3344	277.1709	P	619.2908	310.1491	5
7	672.3749	336.6911	700.3698	350.6886	M	522.2381	261.6227	4
8	785.4590	393.2331	813.4539	407.2306	L	375.2027	188.1050	3
9	842.4804	421.7439	870.4754	435.7413	G	262.1186	131.5629	2
10					W	205.0972	103.0522	1

F

Peptide: F E D V V P M N Y

#	a	a++	a*	a*++	b	b++	b*	b*++	Seq.	y	y++	y*	y*++	#
1	120.0808	60.5440			148.0757	74.5415			F					9
2	249.1234	125.0653			277.1183	139.0628			E	982.4186	491.7130	965.3921	483.1997	8
3	364.1503	182.5788			392.1452	196.5763			D	853.3760	427.1917	836.3495	418.6784	7
4	463.2187	232.1130			491.2136	246.1105			V	738.3491	369.6782	721.3225	361.1649	6
5	562.2871	281.6472			590.2821	295.6447			V	639.2807	320.1440	622.2541	311.6307	5
6	659.3399	330.1736			687.3348	344.1710			P	540.2123	270.6098	523.1857	262.0965	4
7	806.3753	403.6913			834.3702	417.6887			M	443.1595	222.0834	426.1329	213.5701	3
8	920.4182	460.7128	903.3917	452.1995	948.4131	474.7102	931.3866	466.1969	N	296.1241	148.5657	279.0975	140.0524	2
9									Y	182.0812	91.5442			1

G

#	a	a++	a*	a*++	b	b++	b*	b*++	Seq.	y	y++	y*	y*++	#
1	60.0444	30.5258			88.0393	44.5233			S					12
2	197.1033	99.0553			225.0982	113.0527			H	1290.6477	645.8275	1273.6212	637.3142	11
3	298.1510	149.5791			326.1459	163.5766			T	1153.5888	577.2980	1136.5623	568.7848	10
4	412.1939	206.6006	395.1674	198.0873	440.1888	220.5980	423.1623	212.0848	N	1052.5411	526.7742	1035.5146	518.2609	9
5	499.2259	250.1166	482.1994	241.6033	527.2209	264.1141	510.1943	255.6008	S	938.4982	469.7527	921.4716	461.2395	8
6	598.2943	299.6508	581.2678	291.1375	626.2893	313.6483	609.2627	305.1350	V	851.4662	426.2367	834.4396	417.7234	7
7	697.3628	349.1850	680.3362	340.6717	725.3577	363.1825	708.3311	354.6692	V	752.3978	376.7025	735.3712	368.1892	6
8	811.4057	406.2065	794.3791	397.6932	839.4006	420.2039	822.3741	411.6907	N	653.3293	327.1683	636.3028	318.6550	5
9	908.4585	454.7329	891.4319	446.2196	936.4534	468.7303	919.4268	460.2170	P	539.2864	270.1468			4
10	1055.5269	528.2671	1038.5003	519.7538	1083.5218	542.2645	1066.4952	533.7513	F	442.2336	221.6205			3
11	1168.6109	584.8091	1151.5844	576.2958	1196.6058	598.8066	1179.5793	590.2933	I	295.1652	148.0863			2
12									Y	182.0812	91.5442			1

Figure 8.20. A₂ₐR monomer identification by LC-MS/MS after chymotrypsin in-gel digestion. Bands corresponding to the A$_{2A}$R were in-gel digested with chymotrypsin and analysed by LC-MS/MS. (A) Fragmentation spectrum of the LNSNLQNVTNY peptide and Y and B ion coverage. (B) Fragmentation spectrum of the AAADIAVGVL peptide and Y and B ion coverage. (C) Fragmentation spectrum of the AITISTGF peptide and Y and B ion coverage (D) Fragmentation spectrum of the SLLAIAIDRY peptide and Y and B ion coverage (E) Fragmentation spectrum of the AIGLTPMLGW peptide and Y and B ion coverage (F) Fragmentation spectrum of the FEDVVPMNY peptide and Y and B ion coverage (G) Fragmentation spectrum of the SHTNSVVNPFIY and Y and B ion coverage. Covered ions are highlighted in red whereas non-covered ions are presented in black.
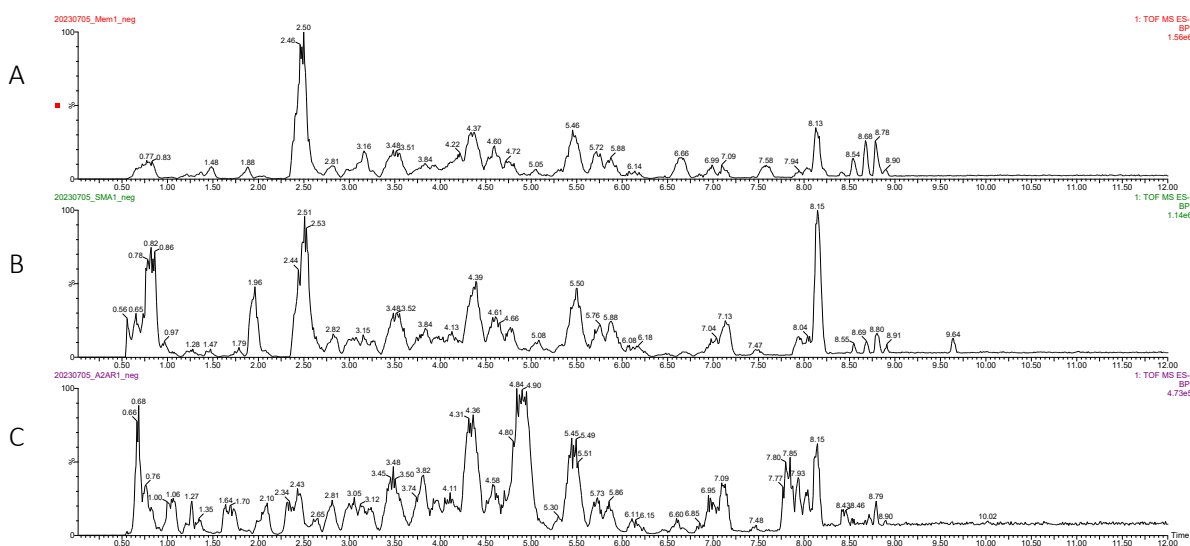
Figure 8.21. Low-energy base peak intensity (BPI) chromatograms for comparative lipid profiling of P. pastoris bulk membranes, SMA-solubilized fraction, and purified A₂ₐR-SMALP. Lipids were extracted following the MTBE method from (A) P. pastoris bulk membranes, (B) SMA-solubilized fraction, and (C) purified A₂ₐR-SMALP. Lipids were resuspended in IPA and analysed by LC-MS/MS in ESI negative ion mode. An ACQUITY Premier CSH C18 Column (1.7 µm, 2.1 x 100 mm) was coupled to the SELECT SERIES Cyclic ion mobility separation (IMS) mass spectrometry system (Waters) in single pass Q-cIM-TOF mode.
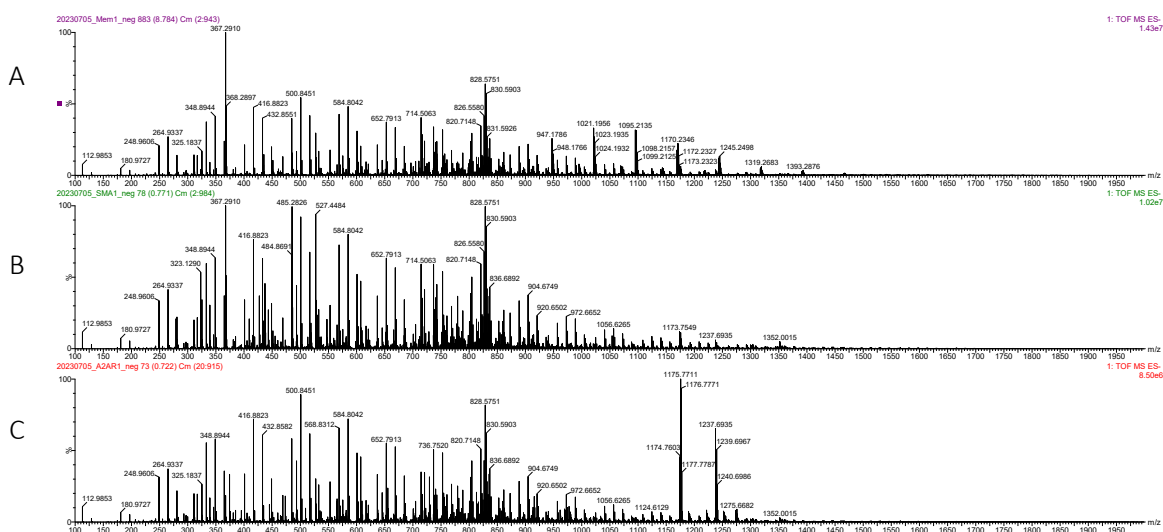
Figure 8.22. Low-energy (MS) combined spectra in the 100-2000 m/z range for comparative lipid profiling of P. pastoris bulk membranes, SMA-solubilized fraction, and purified A₂ₐR-SMALP. Lipids were extracted following the MTBE method from (A) P. pastoris bulk membranes, (B) SMA-solubilized fraction, and (C) purified A₂ₐR-SMALP. Lipids were resuspended in IPA and analysed by LC-MS/MS in ESI negative ion mode. An ACQUITY Premier CSH C18 Column (1.7 µm, 2.1 x 100 mm) was coupled to the SELECT SERIES Cyclic ion mobility separation (IMS) mass spectrometry system (Waters) in single pass Q-cIM-TOF mode.

Table 8.1 Phosphatidylcholine (PC) species detected by LC-MS/MS in ESI positive mode.

Adducts	Description	Formula	m/z	Mass Error (ppm)	RT (min)	CCS (angstrom^2)	Score	Fragment Score
M+H, M+Na, M+K	PC(32:1)	C40H78NO8P	732.5545	0.97	3.98	185.67	43.5	25.3
M+H, M+Na, M+K	PC(32:2)	C40H76NO8P	730.5388	0.92	3.06	183.61	43.7	26
M+H	PC(34:1)	C42H82NO8P	760.5825	-3.42	3.52	185.54	52.3	66
M+H, M+Na	PC(34:2)	C42H80NO8P	758.5724	3.96	4.12	187.60	40.3	10.7
M+H, M+Na, M+K	PC(34:3)	C42H78NO8P	756.5565	0.25	3.26	185.56	52.8	67.3
M+H, M+Na, M+K	PC(34:4)	C42H76NO8P	754.5397	2.09	2.66	183.50	53.8	76.8
M+H, M+Na, M+K	PC(36:1)	C44H86NO8P	788.6177	0.68	6.71	197.37	49.5	50.7
M+H, M+Na, M+K	PC(36:2)	C44H84NO8P	786.6044	4.64	5.49	193.48	46.4	40.3
M+H, M+Na, M+K	PC(36:3)	C44H82NO8P	784.5892	5.20	4.39	189.51	49.9	57.8
M+H	PC(36:4)	C44H80NO8P	782.5734	5.04	5.37	187.50	39.2	4.93
M+H, M+Na, M+K	PC(36:6)	C44H76NO8P	778.5387	0.74	2.32	185.47	53.9	79.5

Table 8.2. Phosphatidylethanolamine (PE) species detected by LC-MS/MS in ESI positive mode.

Adducts	Description	Formula	m/z	Mass Error (ppm)	RT (min)	CCS (angstrom^2)	Score	Fragment Score
M+H, M+K	PE(34:1)	C39H76NO8P	718.5391	0.21	5.77	181.57	49.1	48.8
M+H, M+Na, M+K	PE(34:2)	C39H74NO8P	716.5238	1.78	4.64	179.46	51.1	62.9
M+H, M+Na, M+K	PE(36:1)	C41H80NO8P	746.57	0.72	4.64	189.68	45.8	34.2
M+H, M+K	PE(36:2)	C41H78NO8P	744.5554	0.89	5.90	183.54	46.5	41.2
M+H	PE(36:3)	C41H76NO8P	742.5397	2.10	4.79	181.46	46.9	41.6
M+H, M+Na	PE(36:4)	C41H74NO8P	740.5236	1.57	3.78	179.35	53.2	78.5
M+H, M+Na, M+K	PE(38:2)	C43H82NO8P	772.5873	2.92	4.78	191.56	46.7	39.4
M+H, M+Na, M+K	PE(38:3)	C43H80NO8P	770.5716	0.13	3.77	189.57	47	37.7
M+H, M+Na, M+K	PE(38:4)	C43H78NO8P	768.5552	1.79	3.07	187.55	45.4	32
M+H, M+Na, M+K	PE(40:2)	C45H86NO8P	800.6166	0.32	6.15	199.24	50.5	60.6

Table 8.3. Phosphatidylserine (PS) species detected by LC-MS/MS in ESI positive mode.

Adducts	Description	Formula	m/z	Mass Error (ppm)	RT (min)	CCS (angstrom^2)	Score	Fragment Score
M+H	PS(32:1)	C38H72NO10P	734.4961	-0.73	3.00	181.50	58.5	99.3
M+H, M+Na	PS(33:1)	C39H74NO10P	748.5092	-4.21	3.46	181.43	45.5	40.7
M+H, M+Na, M+K	PS(34:1)	C40H76NO10P	762.5287	0.95	3.99	185.54	47.2	44.8
M+H, M+Na, M+K	PS(34:2)	C40H74NO10P	760.5119	-0.51	3.18	183.48	45.9	38.1
M+H, M+Na	PS(34:3)	C40H72NO10P	758.4965	-0.25	2.63	181.39	55	82.3
M+H, M+Na, M+K	PS(36:2)	C42H78NO10P	826.5003	-5.87	4.12	195.28	41.7	19.4
M+H, M+Na, M+K	PS(36:3)	C42H76NO10P	786.5287	0.99	3.31	185.43	44.2	31.7
M+H, M+Na	PS(36:4)	C42H74NO10P	784.5126	0.33	2.67	183.38	41	12.5
M+H	PS(38:2)	C44H82NO10P	816.5709	-4.95	5.51	148.77	36.8	0
M+H, M+Na, M+K	PS(38:7)	C44H72NO10P	844.4481	-5.12	4.02	191.27	35.4	0.59

Table 8.4. Phosphatidylglycerol (PG) species detected by LC-MS/MS in ESI positive mode.

Adducts	Description	Formula	m/z	Mass Error (ppm)	RT (min)	CCS (angstrom^2)	Score	Fragment Score
M+NH4	PG(24:0)	C30H59O10P	628.4197	2.08	1.47	141.53	37.4	0
M+NH4	PG(34:2)	C40H75O10P	764.5428	-1.15	3.32	189.59	38.9	0.889
M+NH4	PG(36:3)	C42H77O10P	790.5598	0.66	5.38	189.48	38.5	7.15
M+NH4	PG(36:4)	C42H75O10P	788.5446	1.33	4.13	187.47	39	6.63
M+NH4	PG(38:5)	C44H77O10P	814.5551	-5.16	4.39	148.77	51.1	71.1
M+NH4	PG(38:6)	C44H75O10P	812.539	-5.82	3.49	146.19	50	66.9

Table 8.5. Phosphatidylinositol (PI) species detected by LC-MS/MS in ESI positive mode.

Adducts	Description	Formula	m/z	Mass Error (ppm)	RT (min)	CCS (angstrom^2)	Score	Fragment Score
M+NH4	PI(30:0)	C39H75O13P	800.5316	4.21	4.15	191.44	34.5	1.21
M+NH4	PI(32:0)	C41H79O13P	828.5642	5.64	5.53	197.20	33.6	0.802
M+NH4, M+Na, M+K	PI(33:0)	C42H79O13P	840.5601	0.45	3.32	199.08	42.9	41.9
M+NH4, M+Na, M+K	PI(34:0)	C43H81O13P	875.5057	1.04	3.83	198.95	46.1	42.9
M+NH4, M+Na, M+K	PI(34:1)	C43H79O13P	873.4899	0.93	3.04	197.04	40.7	18.1
M+NH4, M+Na, M+K	PI(36:0)	C45H83O13P	901.5211	0.76	3.94	202.63	46	39.4
M+NH4, M+Na, M+K	PI(36:1)	C45H79O13P	876.5603	0.32	2.52	198.94	53.3	71.1
M+NH4, M+Na, M+K	PI(36:2)	C45H75O13P	872.5282	0.10	1.75	195.11	44.5	34.7
M+NH4, M+K	PI(40:0)	C49H87O13P	953.5544	1.92	2.06	218.62	36.8	0
·NH4, M+Na, M+K	PI(40:3)	C49H89O13P	955.5717	3.66	2.09	207.99	43.5	30.5

Table 8.6. Lysophosphatidylcholine (LPC) species detected by LC-MS/MS in ESI positive mode.

Adducts	Description	Formula	m/z	Mass Error (ppm)	RT (min)	CCS (angstrom^2)	Score	Fragment Score
M+H	LPC(12:0)	C20H42NO7P	440.2764	-1.64	0.72	118.67	39.7	14.4
M+H, M+K	LPC(14:0)	C22H46NO7P	468.3071	-2.96	1.13	128.04	38.5	0
M+H, M+K	LPC(16:0)	C24H50NO7P	496.3397	-0.10	0.98	139.56	42.4	13
M+H	LPC(16:1)	C24H48NO7P	494.324	-0.21	0.82	133.84	38.9	11.5
M+H, M+Na	LPC(17:1)	C25H50NO7P	508.3395	-0.55	0.90	136.64	41.1	22.6
M+H, M+K	LPC(18:0)	C26H54NO7P	524.3712	0.22	1.23	147.52	39.2	0.726
M+H, M+Na, M+K	LPC(18:1)	C26H52NO7P	522.3558	0.74	1.00	142.15	52.7	69.1
M+H, M+Na, M+K	LPC(18:2)	C26H50NO7P	520.3395	-0.44	0.87	136.56	42.5	18.7
M+H, M+Na, M+K	LPC(18:3)	C26H48NO7P	518.3254	2.40	0.78	133.68	35.8	11.9
M+H, M+Na, M+K	LPC(20:1)	C28H56NO7P	550.3865	-0.91	1.24	147.34	37.4	0
M+H	LPC(22:2)	C30H58NO7P	576.4043	3.31	2.73	157.36	35.9	0

Table 8.7. Lysophosphatidylethanolamine (LPE) species detected by LC-MS/MS in ESI positive mode.

Adducts	Description	Formula	m/z	Mass Error (ppm)	RT (min)	CCS (angstrom^2)	Score	Fragment Score
M+H, M+Na	LPE(16:0)	C21H44NO7P	454.2927	-0.30	1.02	121.84	42.5	16.4
M+H	LPE(16:1)	C21H42NO7P	452.277	-0.44	0.86	115.20	36.7	0
M+H, M+Na, M+K	LPE(18:0)	C23H48NO7P	482.3242	0.15	1.29	130.97	39.6	2.77
M+H, M+Na, M+K	LPE(18:1)	C23H46NO7P	480.3088	0.69	1.04	124.84	46.9	37
M+H, M+Na	LPE(18:2)	C23H44NO7P	478.2931	0.58	0.89	118.39	46.3	49.3
M+H, M+K	LPE(18:3)	C23H42NO7P	476.2773	0.31	0.80	115.03	34.9	5.72
M+H	LPE(18:4)	C23H40NO7P	474.2615	-0.04	0.76	131.03	31.4	0
M+H	LPE(20:0)	C25H52NO7P	510.3532	-4.30	1.09	142.23	37.6	0
M+H, M+K	LPE(22:0)	C27H56NO7P	538.3863	-0.72	1.39	150.04	38.6	0
M+H, M+K	LPE(22:1)	C27H54NO7P	536.3711	0.05	1.11	144.77	39.7	9.35
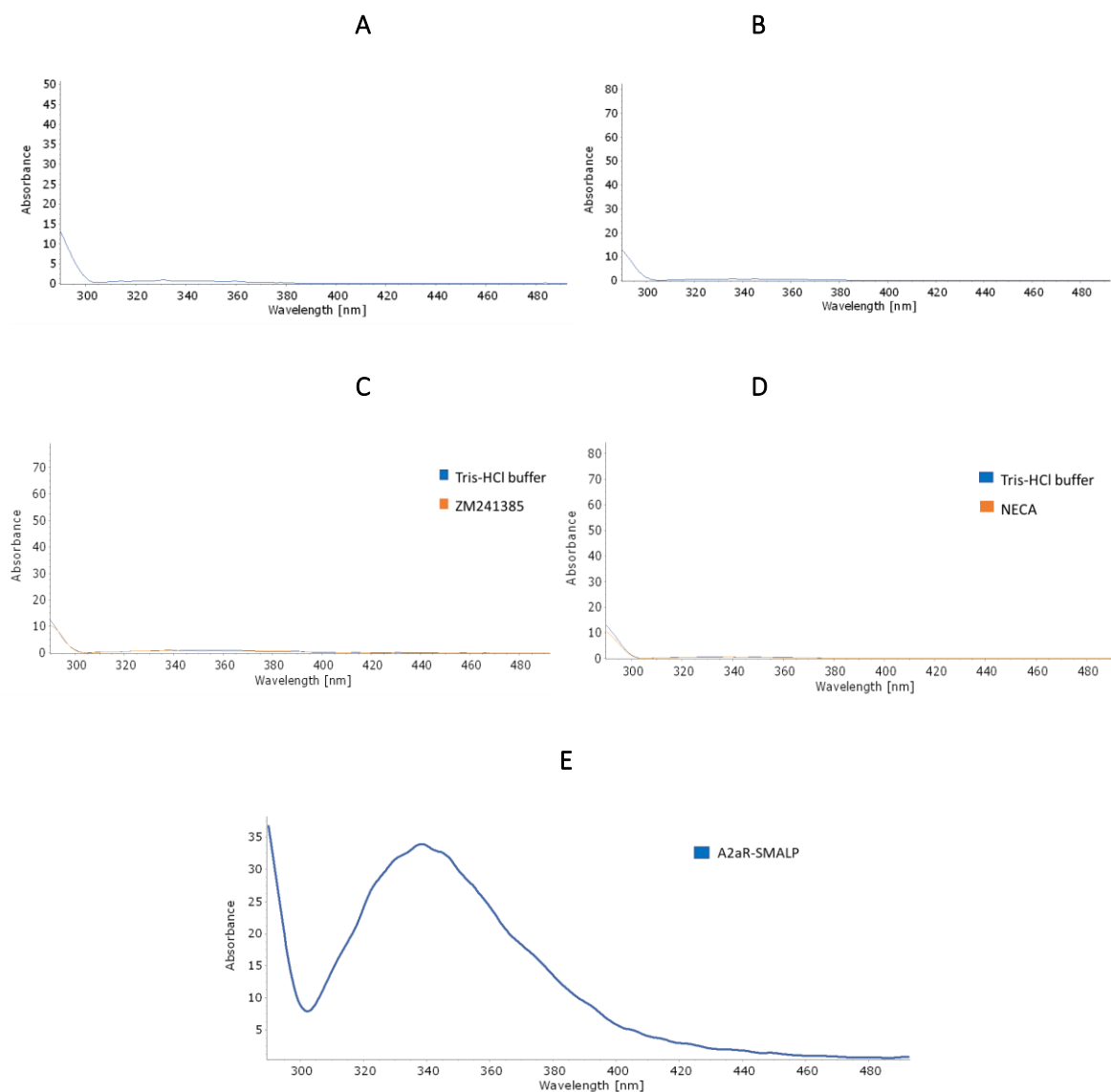
Figure 8.23. Intrinsic fluorescence of the buffers, ligands, and A$_{2A}$R-SMALP. *The fluorescence emissions of (**A**) Tris-HCl buffer, (**B**) HEPES buffer, (**C**) ZM241385 in Tris-HCl buffer, (**D**) NECA in Tris-HCl buffer, and (**E**) A$_{2A}$R-SMALP in Tris-HCl buffer were measured between 290 and 500 nm after excitation at 280 nm.*
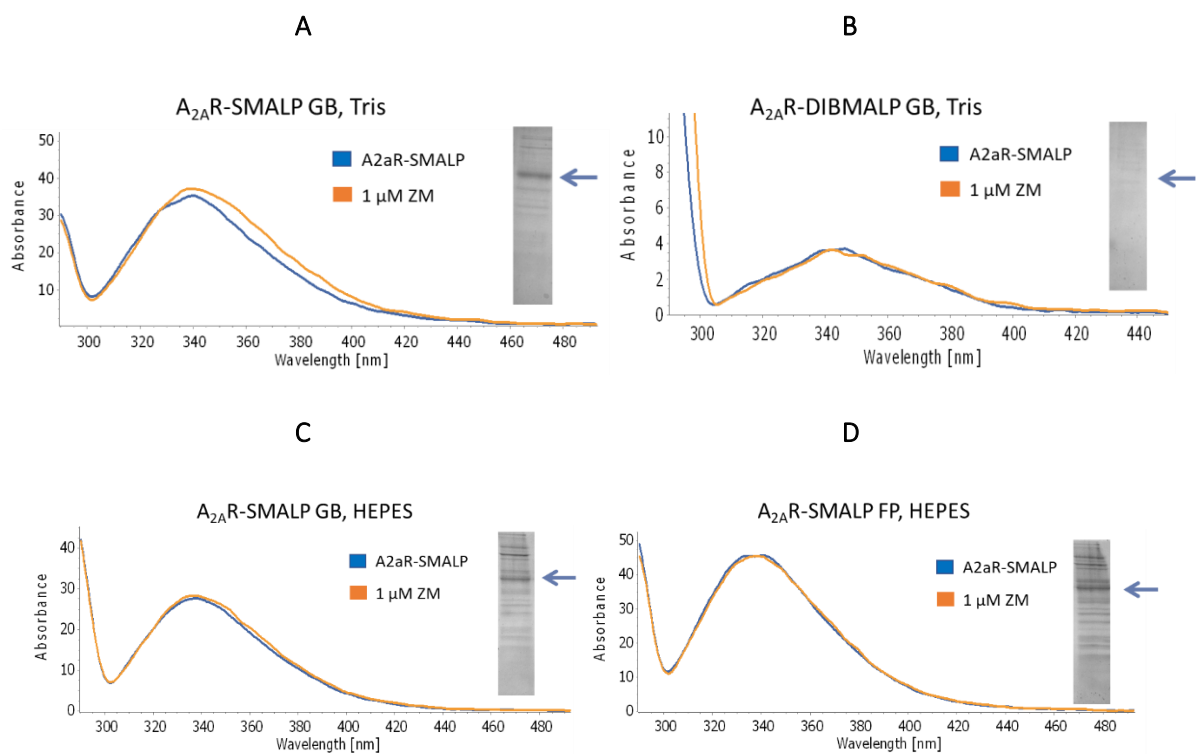
Figure 8.24. Fluorescence of the A₂ₐR-SMALP in the absence and presence of the antagonist ZM241385. The fluorescence emission of (A) A₂ₐR-SMALP prepared with Glass Beads (GB) and Tris-HCl buffer, (B) A₂ₐR-SMALP prepared with GB and HEPES buffer, (C) A₂ₐR-DIBMALP prepared with GB and in Tris-HCl buffer, and (D) A₂ₐR-SMALP prepared with French press (FP) in HEPES buffer were measured between 290 and 500 nm after excitation at 280 nm before (apo A₂ₐR-SMALP or apo A₂ₐR-DIBMALP; blue) and after the addition of 1 μM ZM241385 (orange). The results are presented as raw data together with each SDS-PAGE gel lane corresponding to the purified, concentrated, and encapsulated A₂ₐR.

A

B
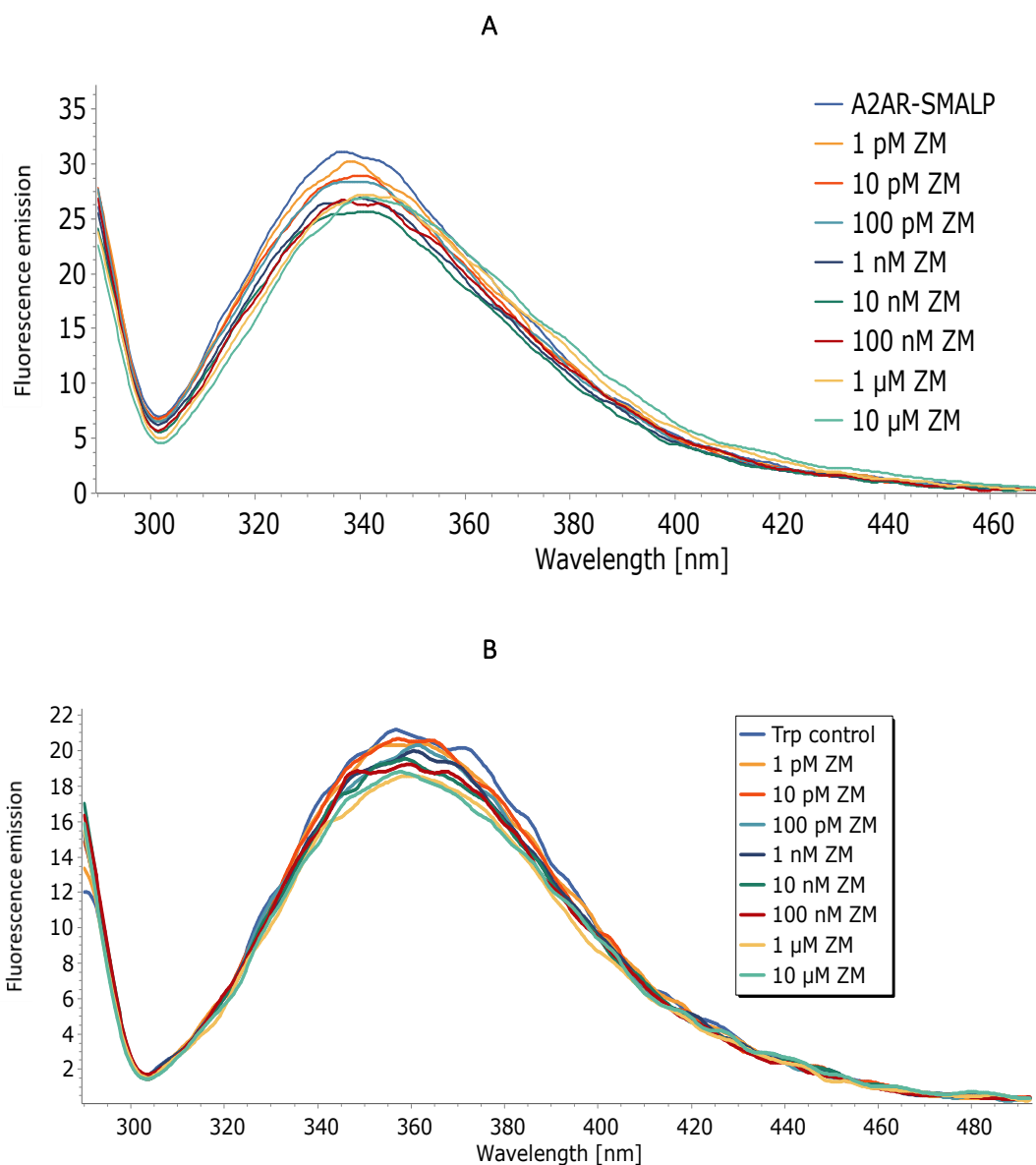
***Figure 8.25. ZM241385-induced changes in overall A₂ₐR-SMALP fluorescence.** The fluorescence emission of apo A₂ₐR-SMALP and Trp control after the addition of increasing concentrations of the antagonist ZM241385 by titration were measured between 290 and 500 nm after excitation at 280 nm. Results are presented as (**A**) Raw data for the A₂ₐR-SMALP, (**B**) Raw data for the Trp control and (**C**) Percentage Trp signal of dose-dependent effect of ZM241385 binding on the overall fluorescence, considering apo A₂ₐR-SMALP and apo Trp control to be 100% and normalized by the dilution effect. Data are presented as the mean of all replicates (n=3) ± SD.*
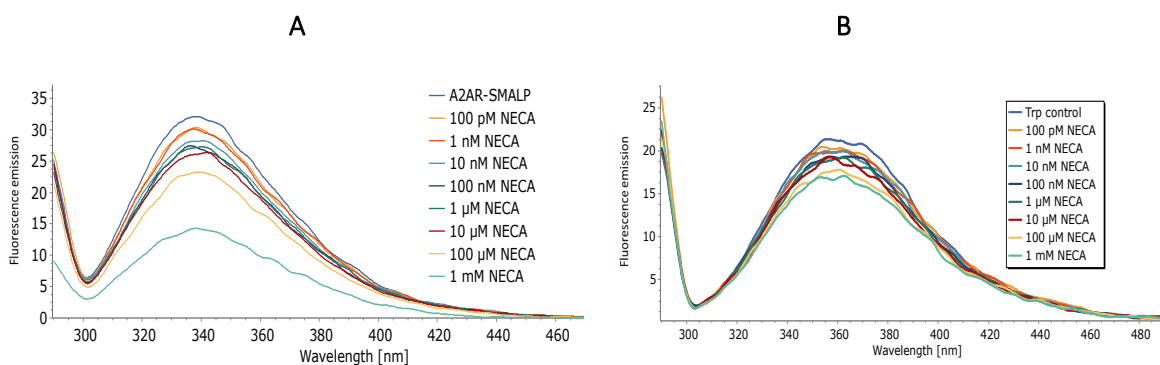
Figure 8.26. NECA-induced changes in overall A₂AR-SMALP fluorescence. *The fluorescence emission of apo A$_{2A}$R-SMALP and Trp control and after titration with increasing concentrations of the agonist NECA were measured between 290 and 500 nm after excitation at 280 nm. The results are presented as (A) Raw data for the A$_{2A}$R-SMALP, (B) Raw data for the Trp control.*
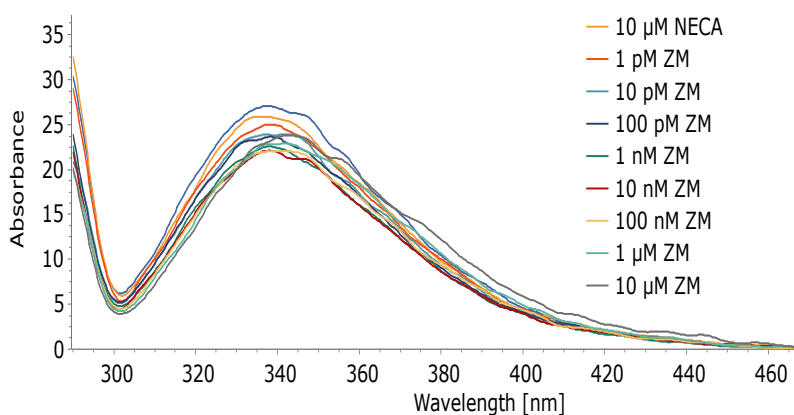
Figure 8.27. ZM241385-induced changes in the overall fluorescence of A₂AR-SMALP after the addition of saturating concentrations of NECA. *The fluorescence emission of apo A$_{2A}$R-SMALP after the addition of the agonist at 10 µM and increasing concentrations of the antagonist ZM241385 by titration were measured between 290 and 500 nm after excitation at 280 nm. The results are presented as (A) raw data and (B) percentage of Trp signal of dose-dependent effect of NECA and ZM241385 binding on overall fluorescence. The apo A$_{2A}$R-SMALP was considered to be 100%, and the data were normalized to the dilution effect. Data are presented as the mean of all replicates (n=3) ± SD.*
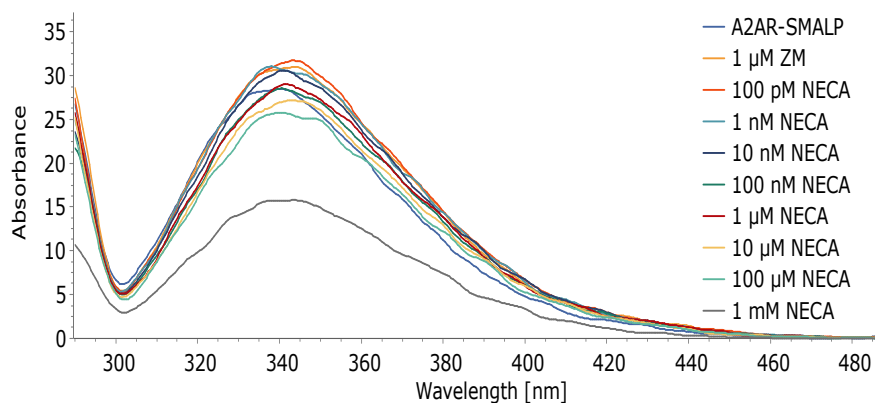
Figure 8.28. NECA-induced changes in the overall fluorescence of A₂ₐR-SMALP after the addition of saturating concentrations of the antagonist ZM241385. *The fluorescence emission of apo A₂ₐR-SMALP after the addition of the antagonist at 1 μM and increasing concentrations of the agonist NECA by titration was measured between 290 and 500 nm after excitation at 280 nm. The results are presented as (**A**) raw data and (**B**) percentage of Trp signal of the dose-dependent effect of ZM241385 and NECA binding on the overall fluorescence, considering apo A₂ₐR-SMALP to be 100%. The data were normalized to the dilution effect and presented as the mean of all replicates (n=3) ± SD.*
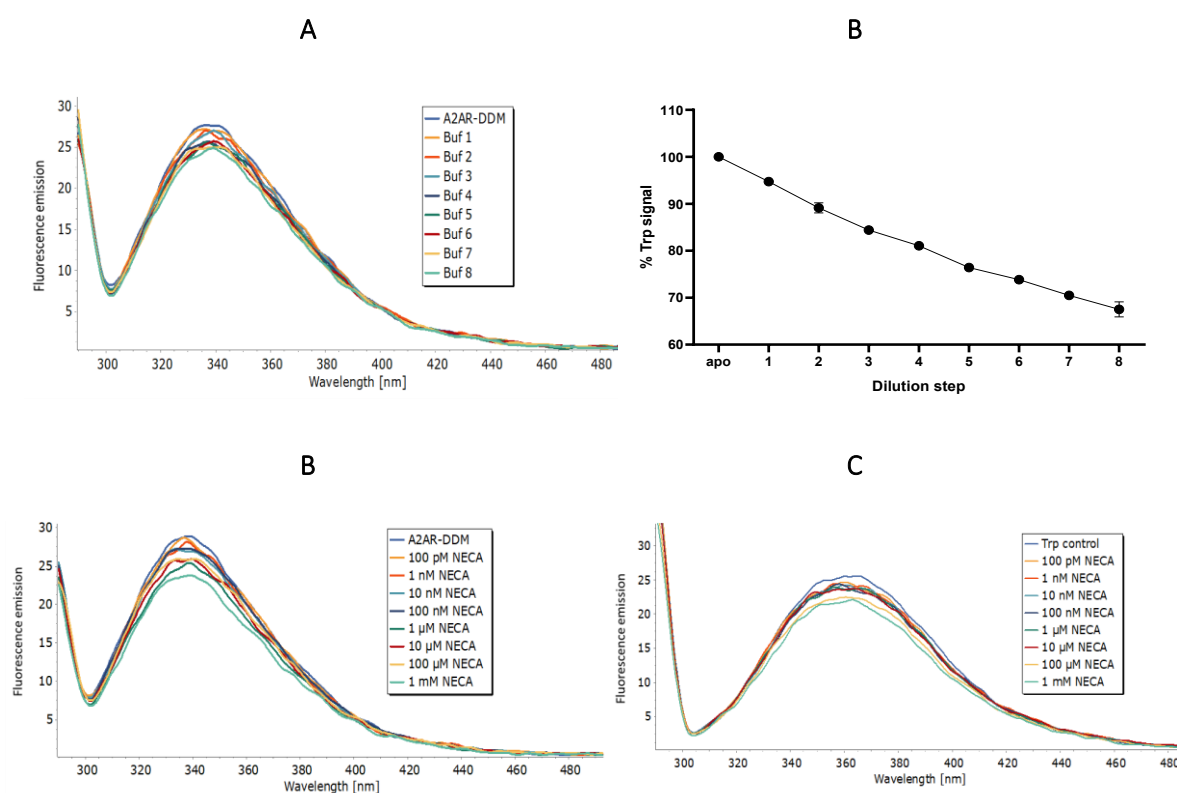
Figure 8.29. NECA-induced changes in the overall fluorescence of A₂ₐR-SMALP. *The fluorescence emission of apo A₂ₐR-DDM and Trp control after the addition of increasing concentrations of the agonist NECA by titration was measured between 290 and 500 nm after excitation at 280 nm. The results are presented as (**A**) raw data for the A₂ₐR-DDM, (**B**) percentage of Trp signal of the dilution effect on the overall fluorescence considering apo A₂ₐR-DDM as 100%, (**C**) raw data for the Trp control in DDM buffer, and (**C**) percentage Trp signal of the dose-dependent effect of NECA binding on the overall fluorescence. Apo A₂ₐR-DDM and apo Trp control were considered to be 100%.*
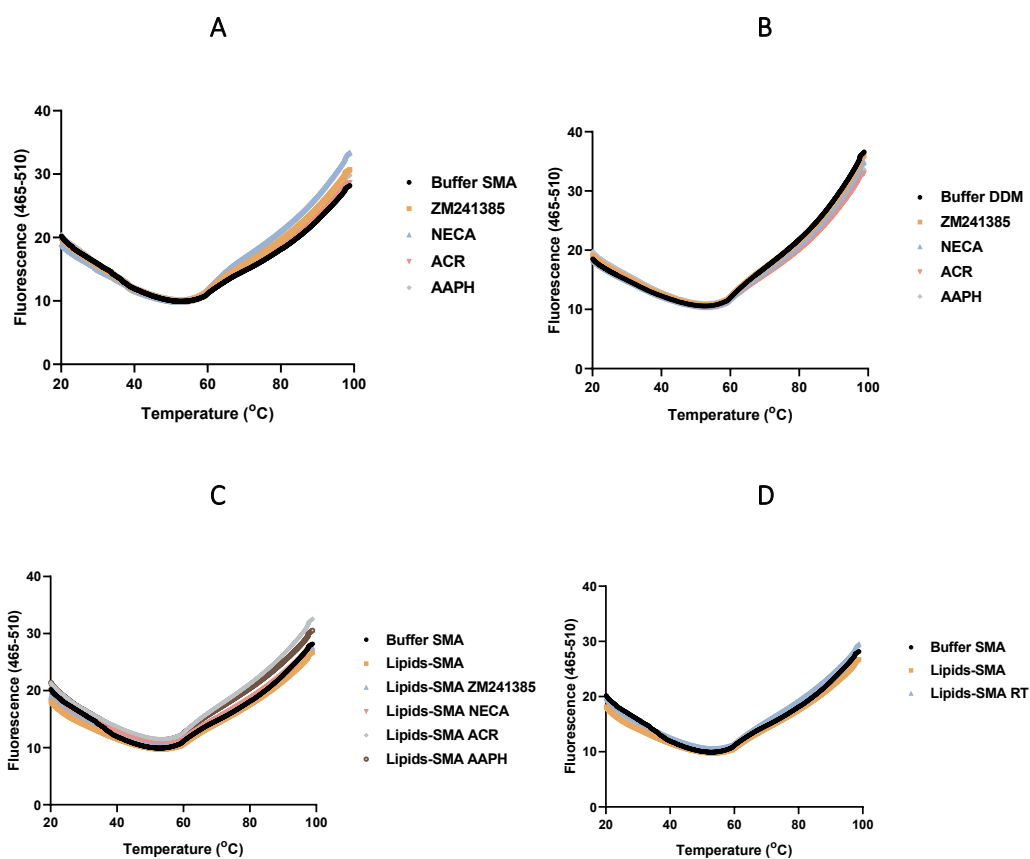
Figure 8.30.Non-specific CPM fluorescence in SMA buffer, DDM buffer, and SMA-encapsulated lipid in the presence of $A_{2A}R$ agonist and antagonist, or oxidative treatments acrolein (ACR) and AAPH. (A) Non-specific CPM fluorescence in SMA buffer and in the presence of $A_{2A}R$ antagonist ZM241383, $A_{2A}R$ agonist NECA, and oxidative treatments ACR and AAPH. (B) Non-specific CPM fluorescence in DDM buffer and in the presence of ZM241383, NECA, ACR, and AAPH. (C) non-specific CPM fluorescence in SMA buffer and SMA-encapsulated lipids in the absence or presence of ZM241383, NECA, ACR, and AAPH. (D) non-specific CPM fluorescence in SMA buffer and non-incubated or incubated SMA-encapsulated lipids at room temperature (RT).
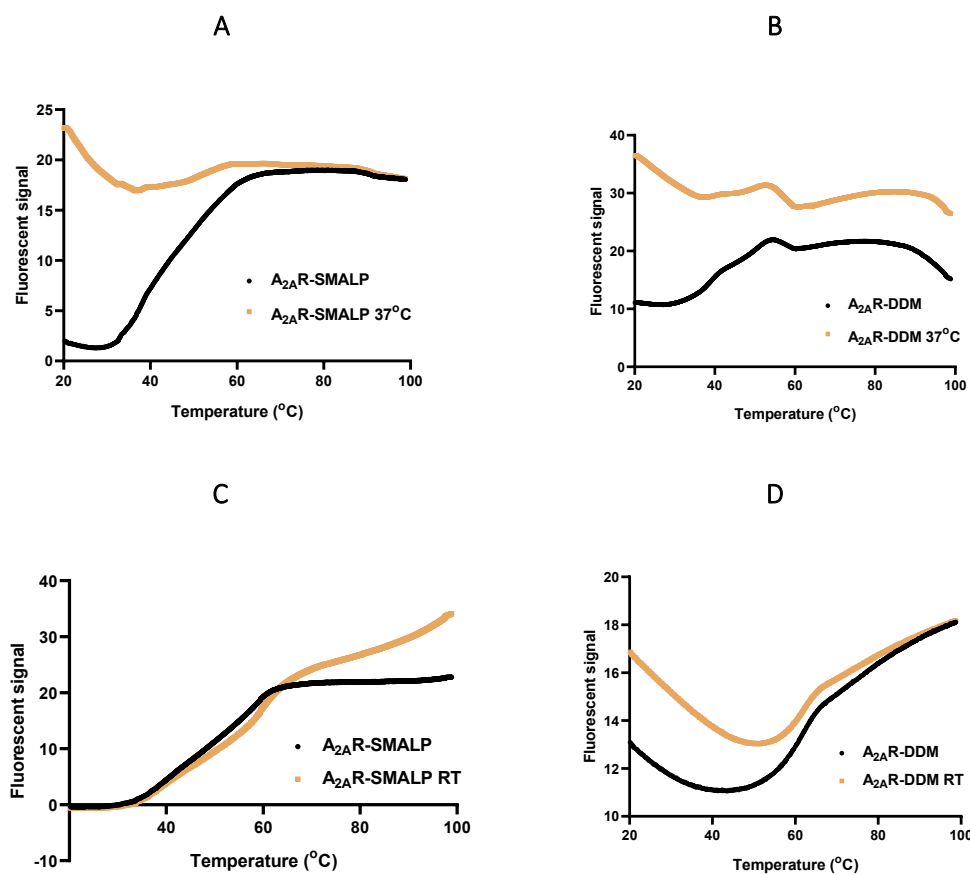
Figure 8.31. Effect of incubating A$_{2A}$R-SMALP and A$_{2A}$R-DDM at 37ºC or RT for 1 hour on protein thermal unfolding monitored by CPM fluorescence. (A) A$_{2A}$R-SMALP and (B) A$_{2A}$R-DDM were incubated at 37ºC for 1 hour and their thermal unfolding profiles were compared to those of the non-incubated A$_{2A}$R-SMALP and A$_{2A}$R-DDM controls, respectively, by measuring CPM fluorescence. Alternatively, (C) A$_{2A}$R-SMALP and (D) A$_{2A}$R-DDM were incubated at room temperature (RT) for 1 hour, and their thermal unfolding profiles were compared to those of the non-incubated A$_{2A}$R-SMALP and A$_{2A}$R-DDM controls, respectively.

Table 8.8. Structural studies publications of the human Adenosine A2a receptor and Protein Data bank (PDB) references that had been considered for the design of the sequence of interest for this project and can be found in "Membrane proteins of Known 3D structure" (mpstruc) database.

Protein	PDB Code	Links	Reference (links are to PubMed)
A$_{2A}$ adenosine receptor: *Homo sapiens* E (expressed in *S. frugiperda*), 2.6 Å **In complex with a high-affinity subtype-selective antagonist ZM241385. Engineered protein: T4 lysozyme inserted between TM helices V and VI.**	**3EML**	PDB MemProt MD	Jaakola *et al.* (2008).
A$_{2A}$ adenosine receptor with bound agonist (UK-432097): *Homo sapiens* E (expressed in *S. frugiperda*), 2.71 Å **Reveals structural changes in helices III, V, & VI relative to inactive, antagonist-bound form. Engineered protein: T4 lysozyme inserted between TM helices V and VI.**	**3QAK**	PDB MemProt MD	Xu *et al.* (2011).
A$_{2A}$ adenosine receptor (engineered) with bound adenosine: *Homo sapiens* E (expressed in *Trichoplusia ni*), 3.00 Å **With synthetic agonist NECA, 2.6 Å:2YDV**	**2YDO**	PDB MemProt MD	Lebon *et al.* (2011).
A$_{2A}$ adenosine receptor in complex with caffeine: *Homo sapiens* E (expressed in *S. frugiperda*), 3.60 Å **Engineered protein, designated A$_{2A}$-StaR2: A54L, T88A, R107A, K122A, L202A, L235A, V239A, S277A In complex with ZM241385, 3.30 Å: 3PWH In complex with XAC, 3.31 Å: 3REY**	**3RFM**	PDB MemProt MD	Doré *et al.* (2011).
A$_{2A}$ adenosine receptor in complex inverse-agonist antibody: *Homo sapiens* E (expressed in *Pichia pastoris*), 2.70 Å **The structure was determined with bound mouse Fab2838 in the presence of the antagonist ZM241385. High-occupancy ZM241385 structure, 3.10 Å: 3VGA**	**3VG9**	PDB MemProt MD	Hino *et al.* (2012).
A$_{2A}$ adenosine receptor in complex with ZM241385: *Homo sapiens* E (expressed in *S. frugiperda*), 1.80 Å **Engineered protein: Apocytochrome b$_{562}$ replaces loop 3 of wild-type protein. Structure reveals stabilizing cholesterol molecules, 23 ordered lipids, and 57 ordered waters.**	**4EIY**	PDB MemProt MD	Liu *et al.* (2012).
A$_{2A}$ adenosine receptor (engineered) with bound CGS21680 (P2$_1$): *Homo sapiens* E (expressed in *Trichoplusia ni*), 2.60 Å **P212121 space group, 2.60 Å: 4UG2**	**4UHR**	PDB MemProt MD	Lebon *et al.* (2015).
A$_{2A}$ adenosine receptor with bound engineered G protein: *Homo sapiens* E (expressed in *Trichoplusia ni*), 3.4 Å	**5G53**	PDB MemProt MD	Carpenter *et al.* (2016).
A2A adenosine receptor by by serial millisecond crystallography (SMC): *Homo sapiens* E (expressed in *Trichoplusia ni*), 2.14 Å **by serial femtosecond crystallography (SFX), 1.70 Å: 5NM4 by cryo-EM, 1.95 Å: 5NM2**	**5NLX**	PDB MemProt MD	Weinert *et al.* (2017).
A$_{2A}$ adenosine receptor with bound miniGs heterotrimer: *Homo sapiens* E (expressed in *Trichoplusia ni*), 4.11 Å **cryo-EM structure**	**6GDG**	PDB MemProt MD	García-Nafría *et al.* (2018).
A$_{2A}$ adenosine receptor with bound ZM241385: *Homo sapiens* E (expressed in *S. frugiperda*), 1.85 Å **XFEL structure using transient ligand exchange starting with LUF5843. See also 6PRZ**	**6PS7**	PDB MemProt MD	Ishchenko *et al.* (2019).
A$_{2A}$ adenosine receptor in complex with ZM241385: *Homo sapiens* E (expressed in *S. frugiperda*), 2.25 Å **Structure obtained from SFX experiments under atmospheric pressure.**	**6JZH**	PDB MemProt MD	Shimazu *et al.* (2019).
A$_{2A}$ adenosine receptor with SRP2070_Fab complex: *Homo sapiens* E (expressed in *Spodoptera frugiperda*), 3.40 Å **Engineered protein: Apocytochrome b$_{562}$ (BRIL) replaces loop 3 of wild-type protein**	**7C6A**	PDB MemProt MD	Miyagi *et al.* (2020).

A$_{2A}$ adenosine receptor with bound UK432097, D52N mutant: *Homo sapiens* E (expressed in *P. pastoris*), 2.60 Å **S91A mutant, 2.90 Å: 5WF6** **Engineered protein: T4 lysozyme inserted between TM helices V and VI**	**5WF5** PDB MemProt MD	White *et al.* (2018).
A$_{2A}$ adenosine receptor in complex with theophylline: *Homo sapiens* E (expressed in *Trichoplusia ni*), 2.0 Å **Engineered protein: Apocytochrome b$_{562}$ replaces loop 3 of wild-type protein** **in complex with caffeine, 2.1 Å: 5MZP** **in complex with PSB36, 2.8 Å: 5N2R**	**5MZJ** PDB MemProt MD	Cheng *et al.* (2017).
A$_{2A}$ adenosine receptor in complex with Chromone 4d: *Homo sapiens* E (expressed in *Trichoplusia ni*), 1.92 Å **engineered protein: Apocytochrome bRIL$_{562}$ in intracellular loop 3.** **in complex with Chromone 5d, 2.13 Å: 6ZDV**	**6ZDR** PDB MemProt MD	Jespers *et al.* (2020).
A$_{2A}$ adenosine receptor, structure using XFEL-SFX diffraction: *Homo sapiens* E (expressed in *Spodoptera frugiperda*), 2.0 Å	**6WQA** PDB MemProt MD	Lee *et al.* (2020).
A$_{2A}$ adenosine receptor in EROCOC17+4, LCP-SFX at 293 K: *Homo sapiens* E (expressed in *Spodoptera frugiperda*), 1.80 Å **at 277 K, 1.80 Å: 6LPJ** **at 100 K, 2.00 Å: 6LPL**	**6LPK** PDB MemProt MD	Ihara *et al.* (2020).
A$_{2A}$ adenosine receptor with bound nonriboside partial agonist: *Homo sapiens* E (expressed in *Spodoptera frugiperda*), 3.12 Å **Engineered protein. Nine thermo-stabilizing mutations. Apocytochrome b$_{562}$ inserted in 3rd intracellular loop.**	**7ARO** PDB MemProt MD	Amelia *et al.* (2021).
A$_{2A}$ adenosine receptor: *Homo sapiens* E (expressed in *S. frugiperda*), 2.6 Å **In complex with a high-affinity subtype-selective antagonist ZM241385. Engineered protein: T4 lysozyme inserted between TM helices V and VI.**	**3EML** PDB MemProt MD	Jaakola *et al.* (2008).
A$_{2A}$ adenosine receptor with bound agonist (UK-432097): *Homo sapiens* E (expressed in *S. frugiperda*), 2.71 Å **Reveals structural changes in helices III, V, & VI relative to inactive, antagonist-bound form. Engineered protein: T4 lysozyme inserted between TM helices V and VI.**	**3QAK** PDB MemProt MD	Xu *et al.* (2011).
A$_{2A}$ adenosine receptor (engineered) with bound adenosine: *Homo sapiens* E (expressed in *Trichoplusia ni*), 3.00 Å **With synthetic agonist NECA, 2.6 Å:2YDV**	**2YDO** PDB MemProt MD	Lebon *et al.* (2011).
A$_{2A}$ adenosine receptor in complex with caffeine: *Homo sapiens* E (expressed in *S. frugiperda*), 3.60 Å **Engineered protein, designated A$_{2A}$-StaR2: A54L, T88A, R107A, K122A, L202A, L235A, V239A, S277A** **In complex with ZM241385, 3.30 Å: 3PWH** **In complex with XAC, 3.31 Å: 3REY**	**3RFM** PDB MemProt MD	Doré *et al.* (2011).
A$_{2A}$ adenosine receptor in complex inverse-agonist antibody: *Homo sapiens* E (expressed in *Pichia pastoris*), 2.70 Å **The structure was determined with bound mouse Fab2838 in the presence of the antagonist ZM241385.** **High-occupancy ZM241385 structure, 3.10 Å: 3VGA**	**3VG9** PDB MemProt MD	Hino *et al.* (2012).

I. Company Marin, PhD Thesis, Aston University 2024

CLUSTAL O(1.2.4) multiple sequence alignment

```
6JZH_1|ChainA|AdenosinereceptorA2a,Solublecytochromeb562,AdenosinereceptorA2a|Homosapiens(9606)   MKTIIALSYIFCLVFADYKDDDD------GAPPIMGSSVYITVELAIAVLAILGNVLVCW   54
4EIY_1|ChainA|AdenosinereceptorA2a/Solublecytochromeb562chimera|Homosapiens(9606)                 MKTIIALSYIFCLVFADYKDDDD------GAPPIMGSSVYITVELAIAVLAILGNVLVCW   54
6PS7_1|ChainA|AdenosinereceptorA2a,Solublecytochromeb562,AdenosinereceptorA2a|Homosapiens(9606)   -----ALSYIFCLVFADYKDDDD------GAPPIMGSSVYITVELAIAVLAILGNVLVCW   49
6WQA_1|ChainA|AdenosinereceptorA2a/Solublecytochromeb562chimera|Homosapiens(9606)                 MKTIIALSYIFCLVFADYKDDDD------GAPPIMGSSVYITVELAIAVLAILGNVLVCW   54
6LPK_1|ChainA|AdenosinereceptorA2a,Solublecytochromeb562,AdenosinereceptorA2a|Homosapiens(9606)   MKTIIALSYIFCLVFADYKDDDD------GAPPIMGSSVYITVELAIAVLAILGNVLVCW   54
5MZJ_1|ChainA|AdenosinereceptorA2a,Solublecytochromeb562,AdenosinereceptorA2a|Homosapiens(9606)   --------------ADYKDDDD------GAPPIMGSSVYITVELAIAVLAILGNVLVCW   39
6ZDR_1|ChainA|AdenosinereceptorA2a,Solublecytochromeb562,AdenosinereceptorA2a|Homosapiens(9606)   ----------------DYKDDDD------GAPPIMGSSVYITVELAIAVLAILGNVLVCW   38
7ARO_1|ChainA|AdenosinereceptorA2a,Solublecytochromeb562,AdenosinereceptorA2a|Homosapiens(9606)   ----------------DYKDDDD------GAPPIMGSSVYITVELAIAVLAILGNVLVCW   38
3EML_1|ChainA|HumanAdenosineA2Areceptor/T4lysozymechimera|Homosapiens(9606)                       ---------------DYKDDDDAMGQPVGAPPIMGSSVYITVELAIAVLAILGNVLVCW   44
3QAK_1|ChainA|AdenosinereceptorA2a,lysozymechimera|HomoSapien(9606)                               ---------------DYKDDDDAMGQPVGAPPIMGSSVYITVELAIAVLAILGNVLVCW   44
5WF5_1|ChainA|HumanA2aadenosinereceptorT4Lchimera|Homosapiens(9606)                               MKTIIALSYIFCLVFADYKDDDDAMGQPVGAPPIMGSSVYITVELAIAVLAILGNVLVCW   60
3RFM_1|ChainA|AdenosinereceptorA2a|Homosapiens(9606)                                              --------------------------------MPIMGSSVYITVELAIAVLAILGNVLVCW   29
2YDO_1|ChainA|ADENOSINERECEPTORA2A|HOMOSAPIENS(9606)                                              --------------------------------MPIMGSSVYITVELAIAVLAILGNVLVCW   29
4UHR_1|ChainA|THERMOSTABILISEDHUMANA2ARECEPTOR|HOMOSAPIENS(9606)                                  --------------------------------MPIMGSSVYITVELAIAVLAILGNVLVCW   29
3VG9_1|ChainA|AdenosinereceptorA2a|Homosapiens(9606)                                              --------------------------------MPIMGSSVYITVELAIAVLAILGNVLVCW   29
sp|P29274|AA2AR_HUMANAdenosinereceptorA2aOS=HomosapiensOX=9606GN=ADORA2APE=1SV=2                  --------------------------------MPIMGSSVYITVELAIAVLAILGNVLVCW   29
5G53_1|ChainsA,B|ADENOSINERECEPTORA2A|HOMOSAPIENS(9606)                                           --------------------------------MPIMGSSVYITVELAIAVLAILGNVLVCW   29
                                                                                                                                  *************************


6JZH_1|ChainA|AdenosinereceptorA2a,Solublecytochromeb562,AdenosinereceptorA2a|Homosapiens(9606)   AVWLNSNLQNVTNYFVVSLAAADIAVGVLAIPFAITISTGFCAACHGCLFIACFVLVLTQ   114
4EIY_1|ChainA|AdenosinereceptorA2a/Solublecytochromeb562chimera|Homosapiens(9606)                 AVWLNSNLQNVTNYFVVSLAAADIAVGVLAIPFAITISTGFCAACHGCLFIACFVLVLTQ   114
6PS7_1|ChainA|AdenosinereceptorA2a,Solublecytochromeb562,AdenosinereceptorA2a|Homosapiens(9606)   AVWLNSNLQNVTNYFVVSLAAADIAVGVLAIPFAITISTGFCAACHGCLFIACFVLVLTQ   109
6WQA_1|ChainA|AdenosinereceptorA2a/Solublecytochromeb562chimera|Homosapiens(9606)                 AVWLNSNLQNVTNYFVVSLAAADIAVGVLAIPFAITISTGFCAACHGCLFIACFVLVLTQ   114
6LPK_1|ChainA|AdenosinereceptorA2a,Solublecytochromeb562,AdenosinereceptorA2a|Homosapiens(9606)   AVWLNSNLQNVTNYFVVSLAAADIAVGVLAIPFAITISTGFCAACHGCLFIACFVLVLTQ   114
5MZJ_1|ChainA|AdenosinereceptorA2a,Solublecytochromeb562,AdenosinereceptorA2a|Homosapiens(9606)   AVWLNSNLQNVTNYFVVSLAAADILVGVLAIPFAITISTGFCAACHGCLFIACFVLVLAQ   99
6ZDR_1|ChainA|AdenosinereceptorA2a,Solublecytochromeb562,AdenosinereceptorA2a|Homosapiens(9606)   AVWLNSNLQNVTNYFVVSLAAADILVGVLAIPFAITISTGFCAACHGCLFIACFVLVLAQ   98
7ARO_1|ChainA|AdenosinereceptorA2a,Solublecytochromeb562,AdenosinereceptorA2a|Homosapiens(9606)   AVWLNSNLQNVTNYFVVSLAAADILVGVLAIPFAITISTGFCAACHGCLFIACFVLVLAQ   98
3EML_1|ChainA|HumanAdenosineA2Areceptor/T4lysozymechimera|Homosapiens(9606)                       AVWLNSNLQNVTNYFVVSLAAADIAVGVLAIPFAITISTGFCAACHGCLFIACFVLVLTQ   104
3QAK_1|ChainA|AdenosinereceptorA2a,lysozymechimera|HomoSapien(9606)                               AVWLNSNLQNVTNYFVVSLAAADIAVGVLAIPFAITISTGFCAACHGCLFIACFVLVLTQ   104
5WF5_1|ChainA|HumanA2aadenosinereceptorT4Lchimera|Homosapiens(9606)                               AVWLNSNLQNVTNYFVVSLAAANIAVGVLAIPFAITISTGFCAACHGCLFIACFVLVLTQ   120
3RFM_1|ChainA|AdenosinereceptorA2a|Homosapiens(9606)                                              AVWLNSNLQNVTNYFVVSAAAADILVGVLAIPFAITISTGFCAACHGCLFIACFVLVLAQ   89
2YDO_1|ChainA|ADENOSINERECEPTORA2A|HOMOSAPIENS(9606)                                              AVWLNSNLQNVTNYFVVSAAAADILVGVLAIPFAIAISTGFCAACHGCLFIACFVLVLTA   89
4UHR_1|ChainA|THERMOSTABILISEDHUMANA2ARECEPTOR|HOMOSAPIENS(9606)                                  AVWLNSNLQNVTNYFVVSAAAADILVGVLAIPFAIAISTGFCAACHGCLFIACFVLVLTA   89
3VG9_1|ChainA|AdenosinereceptorA2a|Homosapiens(9606)                                              AVWLNSNLQNVTNYFVVSAAAADIAVGVLAIPFAITISTGFCAACHGCLFIACFVLVLTQ   89
sp|P29274|AA2AR_HUMANAdenosinereceptorA2aOS=HomosapiensOX=9606GN=ADORA2APE=1SV=2                  AVWLNSNLQNVTNYFVVSLAAADIAVGVLAIPFAITISTGFCAACHGCLFIACFVLVLTQ   89
5G53_1|ChainsA,B|ADENOSINERECEPTORA2A|HOMOSAPIENS(9606)                                           AVWLNSNLQNVTNYFVVSLAAADIAVGVLAIPFAITISTGFCAACHGCLFIACFVLVLTQ   89
                                                                                                 ***************** ***.* **********:***********************:


6JZH_1|ChainA|AdenosinereceptorA2a,Solublecytochromeb562,AdenosinereceptorA2a|Homosapiens(9606)   SSIFSLLAIAIDRYIAIRIPLRYNGLVTGTRAKGIIAICWVLSFAIGLTPMLGWNNCGQP   174
4EIY_1|ChainA|AdenosinereceptorA2a/Solublecytochromeb562chimera|Homosapiens(9606)                 SSIFSLLAIAIDRYIAIRIPLRYNGLVTGTRAKGIIAICWVLSFAIGLTPMLGWNNCGQP   174
6PS7_1|ChainA|AdenosinereceptorA2a,Solublecytochromeb562,AdenosinereceptorA2a|Homosapiens(9606)   SSIFSLLAIAIDRYIAIRIPLRYNGLVTGTRAKGIIAICWVLSFAIGLTPMLGWNNCGQP   169
6WQA_1|ChainA|AdenosinereceptorA2a/Solublecytochromeb562chimera|Homosapiens(9606)                 SSIFSLLAIAIDRYIAIRIPLRYNGLVTGTRAKGIIAICWVLSFAIGLTPMLGWNNCGQP   174
6LPK_1|ChainA|AdenosinereceptorA2a,Solublecytochromeb562,AdenosinereceptorA2a|Homosapiens(9606)   SSIFSLLAIAIDRYIAIRIPLRYNGLVTGTRAKGIIAICWVLSFAIGLTPMLGWNNCGQP   174
5MZJ_1|ChainA|AdenosinereceptorA2a,Solublecytochromeb562,AdenosinereceptorA2a|Homosapiens(9606)   SSIFSLLAIAIDRYIAIRIPLRYNGLVTGTRAAGIIAICWVLSFAIGLTPMLGWNNCGQP   159
6ZDR_1|ChainA|AdenosinereceptorA2a,Solublecytochromeb562,AdenosinereceptorA2a|Homosapiens(9606)   SSIFSLLAIAIDRYIAIRIPLRYNGLVTGTRAAGIIAICWVLSFAIGLTPMLGWNNCGQP   158
7ARO_1|ChainA|AdenosinereceptorA2a,Solublecytochromeb562,AdenosinereceptorA2a|Homosapiens(9606)   SSIFSLLAIAIDRYIAIRIPLRYNGLVTGTRAAGIIAICWVLSFAIGLTPMLGWNNCGQP   158
3EML_1|ChainA|HumanAdenosineA2Areceptor/T4lysozymechimera|Homosapiens(9606)                       SSIFSLLAIAIDRYIAIRIPLRYNGLVTGTRAKGIIAICWVLSFAIGLTPMLGWNNCGQP   164
3QAK_1|ChainA|AdenosinereceptorA2a,lysozymechimera|HomoSapien(9606)                               SSIFSLLAIAIDRYIAIRIPLRYNGLVTGTRAKGIIAICWVLSFAIGLTPMLGWNNCGQP   164
5WF5_1|ChainA|HumanA2aadenosinereceptorT4Lchimera|Homosapiens(9606)                               SSIFSLLAIAIDRYIAIRIPLRYNGLVTGTRAAGIIAICWVLSFAIGLTPMLGWNNCGQP   180
3RFM_1|ChainA|AdenosinereceptorA2a|Homosapiens(9606)                                              SSIFSLLAIAIDRYIAIRIPLRYNGLVTGTRAAGIIAICWVLSFAIGLTPMLGWNNCGQP   149
2YDO_1|ChainA|ADENOSINERECEPTORA2A|HOMOSAPIENS(9606)                                              SSIFSLLAIAIDRYIAIRIPLRYNGLVTGTRAKGIIAICWVLSFAIGLTPMLGWNNCGQP   149
4UHR_1|ChainA|THERMOSTABILISEDHUMANA2ARECEPTOR|HOMOSAPIENS(9606)                                  SSIFSLLAIAIDRYIAIRIPLRYNGLVTGTRAKGIIAICWVLSFAIGLTPMLGWNNCGQP   149
3VG9_1|ChainA|AdenosinereceptorA2a|Homosapiens(9606)                                              SSIFSLLAIAIDRYIAIRIPLRYNGLVTGTRAKGIIAICWVLSFAIGLTPMLGWNNCGQP   149
sp|P29274|AA2AR_HUMANAdenosinereceptorA2aOS=HomosapiensOX=9606GN=ADORA2APE=1SV=2                  SSIFSLLAIAIDRYIAIRIPLRYNGLVTGTRAKGIIAICWVLSFAIGLTPMLGWNNCGQP   149
5G53_1|ChainsA,B|ADENOSINERECEPTORA2A|HOMOSAPIENS(9606)                                           SSIFSLLAIAIDRYIAIRIPLRYNGLVTGTRAKGIIAICWVLSFAIGLTPMLGWNNCGQP   149
                                                                                                 ***************** ************* ****************************


6JZH_1|ChainA|AdenosinereceptorA2a,Solublecytochromeb562,AdenosinereceptorA2a|Homosapiens(9606)   KEGKQHSQGCGEGQVACLFEDVVPMNYMVYFNFFACVLVPLLLMLGVYLRIFLAARRQLA   234
4EIY_1|ChainA|AdenosinereceptorA2a/Solublecytochromeb562chimera|Homosapiens(9606)                 KEGKNHSQGCGEGQVACLFEDVVPMNYMVYFNFFACVLVPLLLMLGVYLRIFLAARRQLA   234
6PS7_1|ChainA|AdenosinereceptorA2a,Solublecytochromeb562,AdenosinereceptorA2a|Homosapiens(9606)   KEGKNHSQGCGEGQVACLFEDVVPMNYMVYFNFFACVLVPLLLMLGVYLRIFLAARRQLA   229
6WQA_1|ChainA|AdenosinereceptorA2a/Solublecytochromeb562chimera|Homosapiens(9606)                 KEGKNHSQGCGEGQVACLFEDVVPMNYMVYFNFFACVLVPLLLMLGVYLRIFLAARRQLA   234
6LPK_1|ChainA|AdenosinereceptorA2a,Solublecytochromeb562,AdenosinereceptorA2a|Homosapiens(9606)   KEGKNHSQGCGEGQVACLFEDVVPMNYMVYFNFFACVLVPLLLMLGVYLRIFLAARRQLA   234
5MZJ_1|ChainA|AdenosinereceptorA2a,Solublecytochromeb562,AdenosinereceptorA2a|Homosapiens(9606)   KEGKAHSQGCGEGQVACLFEDVVPMNYMVYFNFFACVLVPLLLMLGVYLRIFAAARRQLA   219
6ZDR_1|ChainA|AdenosinereceptorA2a,Solublecytochromeb562,AdenosinereceptorA2a|Homosapiens(9606)   KEGKAHSQGCGEGQVACLFEDVVPMNYMVYFNFFACVLVPLLLMLGVYLRIFAAARRQLA   218
7ARO_1|ChainA|AdenosinereceptorA2a,Solublecytochromeb562,AdenosinereceptorA2a|Homosapiens(9606)   KEGKAHSQGCGEGQVACLFEDVVPMNYMVYFNFFACVLVPLLLMLGVYLRIFAAARRQLA   218
3EML_1|ChainA|HumanAdenosineA2Areceptor/T4lysozymechimera|Homosapiens(9606)                       KEGKNHSQGCGEGQVACLFEDVVPMNYMVYFNFFACVLVPLLLMLGVYLRIFLAARRQLN   224
3QAK_1|ChainA|AdenosinereceptorA2a,lysozymechimera|HomoSapien(9606)                               KEGKNHSQGCGEGQVACLFEDVVPMNYMVYFNFFACVLVPLLLMLGVYLRIFLAARRQLN   224
5WF5_1|ChainA|HumanA2aadenosinereceptorT4Lchimera|Homosapiens(9606)                               KEGKNHSQGCGEGQVACLFEDVVPMNYMVYFNFFACVLVPLLLMLGVYLRIFLAARRQLN   240
3RFM_1|ChainA|AdenosinereceptorA2a|Homosapiens(9606)                                              KEGKNHSQGCGEGQVACLFEDVVPMNYMVYFNFFACVLVPLLLMLGVYLRIFAAARRQLK   209
2YDO_1|ChainA|ADENOSINERECEPTORA2A|HOMOSAPIENS(9606)                                              KEGKAHSQGCGEGQVACLFEDVVPMNYMVYFNFFACVLVPLLLMLGVYLRIFLAARRQLK   209
4UHR_1|ChainA|THERMOSTABILISEDHUMANA2ARECEPTOR|HOMOSAPIENS(9606)                                  KEGKAHSQGCGEGQVACLFEDVVPMNYMVYFNFFACVLVPLLLMLGVYLRIFLAARRQLK   209
3VG9_1|ChainA|AdenosinereceptorA2a|Homosapiens(9606)                                              KEGKQHSQGCGEGQVACLFEDVVPMNYMVYFNFFACVLVPLLLMLGVYLRIFLAARRQLK   209
sp|P29274|AA2AR_HUMANAdenosinereceptorA2aOS=HomosapiensOX=9606GN=ADORA2APE=1SV=2                  KEGKNHSQGCGEGQVACLFEDVVPMNYMVYFNFFACVLVPLLLMLGVYLRIFLAARRQLK   209
5G53_1|ChainsA,B|ADENOSINERECEPTORA2A|HOMOSAPIENS(9606)                                           KEGKAHSQGCGEGQVACLFEDVVPMNYMVYFNFFACVLVPLLLMLGVYLRIFLAARRQLK   209
                                                                                                 **** ************************************************* ******


6JZH_1|ChainA|AdenosinereceptorA2a,Solublecytochromeb562,AdenosinereceptorA2a|Homosapiens(9606)   DLEDNWETLNDNLKVIEKADNAAQVKDALTKMRAAALDAQKATPPKLEDKSP-----DSP   289
4EIY_1|ChainA|AdenosinereceptorA2a/Solublecytochromeb562chimera|Homosapiens(9606)                 DLEDNWETLNDNLKVIEKADNAAQVKDALTKMRAAALDAQKATPPKLEDKSP-----DSP   289
6PS7_1|ChainA|AdenosinereceptorA2a,Solublecytochromeb562,AdenosinereceptorA2a|Homosapiens(9606)   DLEDNWETLNDNLKVIEKADNAAQVKDALTKMRAAALDAQKATPPKLEDKSP-----DSP   284
6WQA_1|ChainA|AdenosinereceptorA2a/Solublecytochromeb562chimera|Homosapiens(9606)                 DLEDNWETLNDNLKVIEKADNAAQVKDALTKMRAAALDAQKATPPKLEDKSP-----DSP   289
6LPK_1|ChainA|AdenosinereceptorA2a,Solublecytochromeb562,AdenosinereceptorA2a|Homosapiens(9606)   DLEDNWETLNDNLKVIEKADNAAQVKDALTKMRAAALDAQKATPPKLEDKSP-----DSP   289
5MZJ_1|ChainA|AdenosinereceptorA2a,Solublecytochromeb562,AdenosinereceptorA2a|Homosapiens(9606)   DLEDNWETLNDNLKVIEKADNAAQVKDALTKMRAAALDAQKATPPKLEDKSP-----DSP   274
6ZDR_1|ChainA|AdenosinereceptorA2a,Solublecytochromeb562,AdenosinereceptorA2a|Homosapiens(9606)   DLEDNWETLNDNLKVIEKADNAAQVKDALTKMRAAALDAQKATPPKLEDKSP-----DSP   273
7ARO_1|ChainA|AdenosinereceptorA2a,Solublecytochromeb562,AdenosinereceptorA2a|Homosapiens(9606)   DLEDNWETLNDNLKVIEKADNAAQVKDALTKMRAAALDAQKATPPKLEDKSP-----DSP   273
3EML_1|ChainA|HumanAdenosineA2Areceptor/T4lysozymechimera|Homosapiens(9606)                       IFEMLRIDEGLRLKIYKDTEGYYTIGIGHLLTKSPSLNAAKSELDKAIGRNTNGVITKDE   284
3QAK_1|ChainA|AdenosinereceptorA2a,lysozymechimera|HomoSapien(9606)                               IFEMLRIDEGLRLKIYKDTEGYYTIGIGHLLTKSPSLNAAKSELDKAIGRNTNGVITKDE   284
5WF5_1|ChainA|HumanA2aadenosinereceptorT4Lchimera|Homosapiens(9606)                               IFEMLRIDEGLRLKIYKDTEGYYTIGIGHLLTKSPSLNAAKSELDKAIGRNTNGVITKDE   300
3RFM_1|ChainA|AdenosinereceptorA2a|Homosapiens(9606)                                              QMESQPL-----------------------------------------------------   216
2YDO_1|ChainA|ADENOSINERECEPTORA2A|HOMOSAPIENS(9606)                                              QMESQPL-----------------------------------------------------   216
4UHR_1|ChainA|THERMOSTABILISEDHUMANA2ARECEPTOR|HOMOSAPIENS(9606)                                  QMESQPL-----------------------------------------------------   216
3VG9_1|ChainA|AdenosinereceptorA2a|Homosapiens(9606)                                              QMESQPL-----------------------------------------------------   216
sp|P29274|AA2AR_HUMANAdenosinereceptorA2aOS=HomosapiensOX=9606GN=ADORA2APE=1SV=2                  QMESQPL-----------------------------------------------------   216
5G53_1|ChainsA,B|ADENOSINERECEPTORA2A|HOMOSAPIENS(9606)                                           QMESQPL-----------------------------------------------------   216
                                                                                                  :*


6JZH_1|ChainA|AdenosinereceptorA2a,Solublecytochromeb562,AdenosinereceptorA2a|Homosapiens(9606)   EGKVKEA----------QAAAEQLKTTRNAYIQKYLERARSTLQKEVHAAKSLAIIVGLF   363
4EIY_1|ChainA|AdenosinereceptorA2a/Solublecytochromeb562chimera|Homosapiens(9606)                 EGKVKEA----------QAAAEQLKTTRNAYIQKYLERARSTLQKEVHAAKSLAIIVGLF   363
6PS7_1|ChainA|AdenosinereceptorA2a,Solublecytochromeb562,AdenosinereceptorA2a|Homosapiens(9606)   EGKVKEA----------QAAAEQLKTTRNAYIQKYLERARSTLQKEVHAAKSLAIIVGLF   358
6WQA_1|ChainA|AdenosinereceptorA2a/Solublecytochromeb562chimera|Homosapiens(9606)                 EGKVKEA----------QAAAEQLKTTRNAYIQKYLERARSTLQKEVHAAKSLAIIVGLF   363
6LPK_1|ChainA|AdenosinereceptorA2a,Solublecytochromeb562,AdenosinereceptorA2a|Homosapiens(9606)   EGKVKEA----------QAAAEQLKTTRNAYIQKYLERARSTLQKEVHAAKSLAIIVGLF   363
5MZJ_1|ChainA|AdenosinereceptorA2a,Solublecytochromeb562,AdenosinereceptorA2a|Homosapiens(9606)   EGKVKEA----------QAAAEQLKTTRNAYIQKYLERARSTLQKEVHAAKSAAIIAGLF   348
6ZDR_1|ChainA|AdenosinereceptorA2a,Solublecytochromeb562,AdenosinereceptorA2a|Homosapiens(9606)   EGKVKEA----------QAAAEQLKTTRNAYIQKYLERARSTLQKEVHAAKSAAIIAGLF   347
7ARO_1|ChainA|AdenosinereceptorA2a,Solublecytochromeb562,AdenosinereceptorA2a|Homosapiens(9606)   EGKVKEA----------QAAAEQLKTTRNAYIQKYLERARSTLQKEVHAAKSAAIIAGLF   347
3EML_1|ChainA|HumanAdenosineA2Areceptor/T4lysozymechimera|Homosapiens(9606)                       QKRWDEAAVNLAKSRWYNQTPNRAKRVITTFRTGTWDAYRSTLQKEVHAAKSLAIIVGLF   404
3QAK_1|ChainA|AdenosinereceptorA2a,lysozymechimera|HomoSapien(9606)                               QKRWDEAAVNLAKSRWYNQTPNRAKRVITTFRTGTWDAYRSTLQKEVHAAKSLAIIVGLF   404
5WF5_1|ChainA|HumanA2aadenosinereceptorT4Lchimera|Homosapiens(9606)                               QKRWDEAAVNLAKSRWYNQTPNRAKRVITTFRTGTWDAYRSTLQKEVHAAKSLAIIVGLF   420
3RFM_1|ChainA|AdenosinereceptorA2a|Homosapiens(9606)                                              ----------------------------------PGERARSTLQKEVHAAKSAAIIAGLF   242
2YDO_1|ChainA|ADENOSINERECEPTORA2A|HOMOSAPIENS(9606)                                              ----------------------------------PGERARSTLQKEVHAAKSLAIIVGLF   242
4UHR_1|ChainA|THERMOSTABILISEDHUMANA2ARECEPTOR|HOMOSAPIENS(9606)                                  ----------------------------------PGERARSTLQKEVHAAKSLAIIVGLF   242
3VG9_1|ChainA|AdenosinereceptorA2a|Homosapiens(9606)                                              ----------------------------------PGERARSTLQKEVHAAKSLAIIVGLF   242
sp|P29274|AA2AR_HUMANAdenosinereceptorA2aOS=HomosapiensOX=9606GN=ADORA2APE=1SV=2                  ----------------------------------PGERARSTLQKEVHAAKSLAIIVGLF   242
5G53_1|ChainsA,B|ADENOSINERECEPTORA2A|HOMOSAPIENS(9606)                                           ----------------------------------PGERARSTLQKEVHAAKSLAIIVGLF   242
                                                                                                  :      ************* ***.***
```

I. Company Marin, PhD Thesis, Aston University 2024

```
6JZH_1|ChainA|AdenosinereceptorA2a,Solublecytochromeb562,AdenosinereceptorA2a|Homosapiens(9606)   ALCWLPLHIINCFTFFCPDCSHAPLWLMYLAIVLSHTNSVVNPFIYAYRIREFRQTFRKI   423
4EIY_1|ChainA|AdenosinereceptorA2a/Solublecytochromeb562chimera|Homosapiens(9606)                 ALCWLPLHIINCFTFFCPDCSHAPLWLMYLAIVLSHTNSVVNPFIYAYRIREFRQTFRKI   423
6PS7_1|ChainA|AdenosinereceptorA2a/Solublecytochromeb562chimera|Homosapiens(9606)                 ALCWLPLHIINCFTFFCPDCSHAPLWLMYLAIVLSHTNSVVNPFIYAYRIREFRQTFRKI   418
6WQA_1|ChainA|AdenosinereceptorA2a/Solublecytochromeb562chimera|Homosapiens(9606)                 ALCWLPLHIINCFTFFCPDCSHAPLWLMYLAIVLSHTNSVVNPFIYAYRIREFRQTFRKI   423
6LPK_1|ChainA|AdenosinereceptorA2a,Solublecytochromeb562,AdenosinereceptorA2a|Homosapiens(9606)   ALCWLPLHIINCFTFFCPDCSHAPLWLMYLAIVLSHTNSVVNPFIYAYRIREFRQTFRKI   423
5MZJ_1|ChainA|AdenosinereceptorA2a,Solublecytochromeb562,AdenosinereceptorA2a|Homosapiens(9606)   ALCWLPLHIINCFTFFCPDCSHAPLWLMYLAIVLAHTNSVVNPFIYAYRIREFRQTFRKI   408
6ZDR_1|ChainA|AdenosinereceptorA2a,Solublecytochromeb562,AdenosinereceptorA2a|Homosapiens(9606)   ALCWLPLHIINCFTFFCPDCSHAPLWLMYLAIVLAHTNSVVNPFIYAYRIREFRQTFRKI   407
7ARO_1|ChainA|AdenosinereceptorA2a,Solublecytochromeb562,AdenosinereceptorA2a|Homosapiens(9606)   ALCWLPLHIINCFTFFCPDCSHAPLWLMYLAIVLAHTNSVVNPFIYAYRIREFRQTFRKI   407
3EML_1|ChainA|HumanAdenosineA2Areceptor/T4lysozymechimera|Homosapiens(9606)                        ALCWLPLHIINCFTFFCPDCSHAPLWLMYLAIVLSHTNSVVNPFIYAYRIREFRQTFRKI   464
3QAK_1|ChainA|AdenosinereceptorA2a,lysozymechimera|HomoSapien(9606)                                ALCWLPLHIINCFTFFCPDCSHAPLWLMYLAIVLSHTNSVVNPFIYAYRIREFRQTFRKI   464
5WF5_1|ChainA|HumanA2aadenosinereceptorT4Lchimera|Homosapiens(9606)                                ALCWLPLHIINCFTFFCPDCSHAPLWLMYLAIVLSHTNSVVNPFIYAYRIREFRQTFRKI   480
3RFM_1|ChainA|AdenosinereceptorA2a|Homosapiens(9606)                                               ALCWLPLHIINCFTFFCPDCSHAPLWLMYLAIVLSHTNSVVNPFIYAYRIREFRQTFRKI   302
2YDO_1|ChainA|ADENOSINERECEPTORA2A|HOMOSAPIENS(9606)                                               ALCWLPLHIINCFTFFCPDCSHAPLWLMYLAIVLSHTNSVVNPFIYAYRIREFRQTFRKI   302
4UHR_1|ChainA|THERMOSTABILISEDHUMANA2ARECEPTOR|HOMOSAPIENS(9606)                                   ALCWLPLHIINCFTFFCPDCSHAPLWLMYLAIVLSHTNSVVNPFIYAYRIREFRQTFRKI   302
3VG9_1|ChainA|AdenosinereceptorA2a|Homosapiens(9606)                                               ALCWLPLHIINCFTFFCPDCSHAPLWLMYLAIVLSHTNSVVNPFIYAYRIREFRQTFRKI   302
sp|P29274|AA2AR_HUMANAdenosinereceptorA2aOS=HomosapiensOX=9606GN=ADORA2APE=1SV=2                    ALCWLPLHIINCFTFFCPDCSHAPLWLMYLAIVLSHTNSVVNPFIYAYRIREFRQTFRKI   302
5G53_1|ChainsA,B|ADENOSINERECEPTORA2A|HOMOSAPIENS(9606)                                            ALCWLPLHIINCFTFFCPDCSHAPLWLMYLAIVLSHTNSVVNPFIYAYRIREFRQTFRKI   302
                                                                                                  ********************************.:**************************


6JZH_1|ChainA|AdenosinereceptorA2a,Solublecytochromeb562,AdenosinereceptorA2a|Homosapiens(9606)   IRSHVLRQQEPFKAHHHHHHHHHH---------------------------------   447
4EIY_1|ChainA|AdenosinereceptorA2a/Solublecytochromeb562chimera|Homosapiens(9606)                 IRSHVLRQQEPFKAHHHHHHHHHH---------------------------------   447
6PS7_1|ChainA|AdenosinereceptorA2a/Solublecytochromeb562,AdenosinereceptorA2a|Homosapiens(9606)   IRSHVLRQQEPFKAHHHHHHHHHH---------------------------------   442
6WQA_1|ChainA|AdenosinereceptorA2a/Solublecytochromeb562chimera|Homosapiens(9606)                 IRSHVLRQQEPFKAHHHHHHHHHH---------------------------------   447
6LPK_1|ChainA|AdenosinereceptorA2a,Solublecytochromeb562,AdenosinereceptorA2a|Homosapiens(9606)   IRSHVLRQQEPFKAHHHHHHHHHH---------------------------------   447
5MZJ_1|ChainA|AdenosinereceptorA2a,Solublecytochromeb562,AdenosinereceptorA2a|Homosapiens(9606)   IRSHVLRQQEPFKAAAHHHHHHHHH--------------------------------   434
6ZDR_1|ChainA|AdenosinereceptorA2a,Solublecytochromeb562,AdenosinereceptorA2a|Homosapiens(9606)   IRSHVLRQQEPFKAAAHHHHHHHHH--------------------------------   433
7ARO_1|ChainA|AdenosinereceptorA2a,Solublecytochromeb562,AdenosinereceptorA2a|Homosapiens(9606)   IRSHVLRQQEPFKAAAHHHHHHHHH--------------------------------   433
3EML_1|ChainA|HumanAdenosineA2Areceptor/T4lysozymechimera|Homosapiens(9606)                        IRSHVLRQQEPFKAHHHHHHHHHH---H-----------------------------   488
3QAK_1|ChainA|AdenosinereceptorA2a,lysozymechimera|HomoSapien(9606)                                IRSHVLRQQEPFKAHHHHHHHHHH---H-----------------------------   488
5WF5_1|ChainA|HumanA2aadenosinereceptorT4Lchimera|Homosapiens(9606)                                IRSHVLRQQEPFKAHHHHHHHHHH---H-----------------------------   504
3RFM_1|ChainA|AdenosinereceptorA2a|Homosapiens(9606)                                               IRSHVLRQQEPFKAAAAHHHHHHHHH-------------------------------   329
2YDO_1|ChainA|ADENOSINERECEPTORA2A|HOMOSAPIENS(9606)                                               IRSHVLRQQEPFKAAAAENLYFQ---------------------------------   325
4UHR_1|ChainA|THERMOSTABILISEDHUMANA2ARECEPTOR|HOMOSAPIENS(9606)                                   IRSHVLRQQEPFKAAAAENLYFQ---------------------------------   325
3VG9_1|ChainA|AdenosinereceptorA2a|Homosapiens(9606)                                               IRSHVLRQQEPFKAHHHHHHHHHH-H-------------------------------   326
sp|P29274|AA2AR_HUMANAdenosinereceptorA2aOS=HomosapiensOX=9606GN=ADORA2APE=1SV=2                    IRSHVLRQQEPFKAAGTSARVLAAHGSDGEQVSLRLNGHPPGVWANGSAPHPERRPNGYA   362
5G53_1|ChainsA,B|ADENOSINERECEPTORA2A|HOMOSAPIENS(9606)                                            IRSHVLENLYFQ--------------------------------------------   314
                                                                                                  ******.:


6JZH_1|ChainA|AdenosinereceptorA2a,Solublecytochromeb562,AdenosinereceptorA2a|Homosapiens(9606)   --------------------------------------------------   447
4EIY_1|ChainA|AdenosinereceptorA2a/Solublecytochromeb562chimera|Homosapiens(9606)                 --------------------------------------------------   447
6PS7_1|ChainA|AdenosinereceptorA2a/Solublecytochromeb562,AdenosinereceptorA2a|Homosapiens(9606)   --------------------------------------------------   442
6WQA_1|ChainA|AdenosinereceptorA2a/Solublecytochromeb562chimera|Homosapiens(9606)                 --------------------------------------------------   447
6LPK_1|ChainA|AdenosinereceptorA2a,Solublecytochromeb562,AdenosinereceptorA2a|Homosapiens(9606)   --------------------------------------------------   447
5MZJ_1|ChainA|AdenosinereceptorA2a,Solublecytochromeb562,AdenosinereceptorA2a|Homosapiens(9606)   --------------------------------------------------   434
6ZDR_1|ChainA|AdenosinereceptorA2a,Solublecytochromeb562,AdenosinereceptorA2a|Homosapiens(9606)   --------------------------------------------------   433
7ARO_1|ChainA|AdenosinereceptorA2a,Solublecytochromeb562,AdenosinereceptorA2a|Homosapiens(9606)   --------------------------------------------------   433
3EML_1|ChainA|HumanAdenosineA2Areceptor/T4lysozymechimera|Homosapiens(9606)                        --------------------------------------------------   488
3QAK_1|ChainA|AdenosinereceptorA2a,lysozymechimera|HomoSapien(9606)                                --------------------------------------------------   488
5WF5_1|ChainA|HumanA2aadenosinereceptorT4Lchimera|Homosapiens(9606)                                --------------------------------------------------   504
3RFM_1|ChainA|AdenosinereceptorA2a|Homosapiens(9606)                                               --------------------------------------------------   329
2YDO_1|ChainA|ADENOSINERECEPTORA2A|HOMOSAPIENS(9606)                                               --------------------------------------------------   325
4UHR_1|ChainA|THERMOSTABILISEDHUMANA2ARECEPTOR|HOMOSAPIENS(9606)                                   --------------------------------------------------   325
3VG9_1|ChainA|AdenosinereceptorA2a|Homosapiens(9606)                                               --------------------------------------------------   326
sp|P29274|AA2AR_HUMANAdenosinereceptorA2aOS=HomosapiensOX=9606GN=ADORA2APE=1SV=2                    LGLVSGGSAQESQGNTGLPDVELLSHELKGVCPEPPGLDDPLAQDGAGVS   412
5G53_1|ChainsA,B|ADENOSINERECEPTORA2A|HOMOSAPIENS(9606)                                            --------------------------------------------------   314
```

Figure 8.32. Multiple alignment results of all considered sequences of the hA2aR (see Figure, Appendix) through using Clustal Omega tool.

Table 8.9. Amino acid and nucleotide sequence encoding for both FLAG and His$_{10}$ tags, and its respective protein terminus location, chosen to be incorporated to the human adenosine A2a receptor sequence.

	FLAG tag	Deca-Histidine tag
Amino acid sequence	DYKDDDDAMGQPVGAPPI	HHHHHHHHHH
Nucleic acid sequence	GACTACAAGGACGATGACGATGCCATGGGTCAGCCAGTTGGCGCACCACCGATC	CATCACCATCATCATCACCACCACCATCAC
Protein terminus	Amino terminus	Carboxy terminus

Table 8.10. Amino acid and nucleotide sequence encoding for both Kozak consensus sequence and unstructured flexible linker, and its respective protein terminus location, chosen to be incorporated to the human adenosine A2a receptor sequence.

	Kozak consensus sequence	Unstructured flexible linker
Amino acid sequence	AT	GGSGSG
Nucleic acid sequence	GCCACC	GGAGGGTCTGGCTCTGGG
Protein terminus	Amino terminus	Carboxy terminus

*5'GAATTCGCCACCATGGACTACAAGGACGATGACGATGCCATGGGTCAGCCAGTTGGCGCACCACCGATCATGGGCTCAAGCGTGTACA
TAACCGTCGAACTGGCCATTGCAGTGCTGGCAATTCTGGGGAATGTTCTGGTATGCTGGGCCGTGTGGCTGAATAGCAATCTGCAGAATG
TGACGAACTACTTTGTCGTCAGTCTGGCTGCAGCCGATATAGCAGTTGGGGGTCTTGGCCATTCCCTTTGCTATCACCATCTCCACAGGGTTC
TGCGCTGCTTGCCATGGATGCCTGTTCATAGCCTGCTTCGTGCTTGTGCTCACTCAGAGTTCCATCTTTTCACTCCTCGCCATTGCGATCGAC
CGTTATATTGCGATTCGAATACCACTGAGGTACAATGGCTTGGTCACCGGAACAAGAGCCAAAGGCATCATCGCTATCTGTTGGGTGCTCT
CATTCGCCATAGGGCTGACACCCATGCTTGGATGGAACAATTGCGGCCAACCCAAGGAAGGCAAGAACCACAGCCAGGGTTGTGGTGAA
GGACAAGTGGCCTGTTTGTTCGAGGATGTAGTGCCCATGAACTACATGGTGTACTTCAACTTCTTCGCATGTGTGCTGGTTCCCCTGTTGC
TGATGCTGGGCGTCTATCTGCGGATATTTCTCGCGGCACGCAGACAGCTGAAACAGATGGAGTCTCAGCCTCTTCCTGGTGAAAGAGCTC
GCAGTACTCTGCAGAAGGAGGTTCATGCCGCTAAAAGCCTCGCCATCATTGTGGGACTGTTTGCGCTTTGTTGGCTCCCTCTGCACATTAT
CAACTGCTTCACCTTCTTTTGCCCTGACTGTAGCCACGCTCCTCTGTGGCTCATGTATCTGGCAATCGTCCTTTCCCACACTAATAGCGTAGT
GAACCCGTTCATCTATGCCTATCGGATCAGGGAGTTTCGCCAGACATTTCGGAAGATTATCAGGTCCCACGTGTTGCGACAACAGGAGCCA
TTTAAAGCCGCTGGAGGGTCTGGCTCTGGGCATCACCATCATCATCACCACCACCATCACGCGGCCGC3'*

*N-t ATMDYKDDDDAMGQPVGAPPIMGSSVYITVELAIAVLAILGNVLVCWAVWLNSNLQNVTNYFVVSLAAADIAVGVLAIPFAITISTGFCAAC
HGCLFIACFVLVLTQSSIFSLLAIAIDRYIAIRIPLRYNGLVTGTRAKGIIAICWVLSFAIGLTPMLGWNNCGQPKEGKNHSQGCGEGQVACLFEDVV
PMNYMVYFNFFACVLVPLLLMLGVYLRIFLAARRQLKQMESQPLPGERARSTLQKEVHAAKSLAIIVGLFALCWLPLHIINCFTFFCPDCSHAPLW
LMYLAIVLSHTNSVVNPFIYAYRIREFRQTFRKIIRSHVLRQQEPFKAAGGSGSGCHHHHHHHHHHH C-t*

Figure 8.33. Design of the de-glycosylated A$_{2A}$R construct. *(A) Nucleotide sequence of the A$_{2A}$R construct.
(B) Amino acid sequence of the A$_{2A}$R construct.*

Table 8.11. Clone TubeSeq Sanger sequencing by Eurofins Genomics. *The clones were subjected to
TubeSeq Sanger sequencing to Eurofins Genomics using the Primer Synthesis T7
(TAATACGACTCACTATAGGG).*

	Score	Identities	Gaps
Clone 1	1989 bits (1077)	1082/1084 (99%)	1/1084 (0%)
Clone 2	1969 bits (1066)	1088/1097 (99%)	8/1097 (0%)
Clone 3	1995 bits (1080)	1082/1083(99%)	0/1083 0%)

**Figure 8.34. Analysis of A$_{2A}$R expression in transiently transfected HEK293T cells with PEI or
Lipofectamine**. *HEK293T cells seeded onto 6-well plates were transiently transfected with 2 µg of the
pcDNA3-hA$_{2A}$R plasmid using 8 µL of polyethylenimine (PEI). Alternatively, cells were transfected with 3
µg of the plasmid using 12 µL of Lipofectamine. The plasmids used for transfection were obtained from
E. coli DH5α clones generated by cell transformation with the cloning ligation product. A non-transfected
control was included in this experiment. For the analysis of protein expression, cells were lysed and*
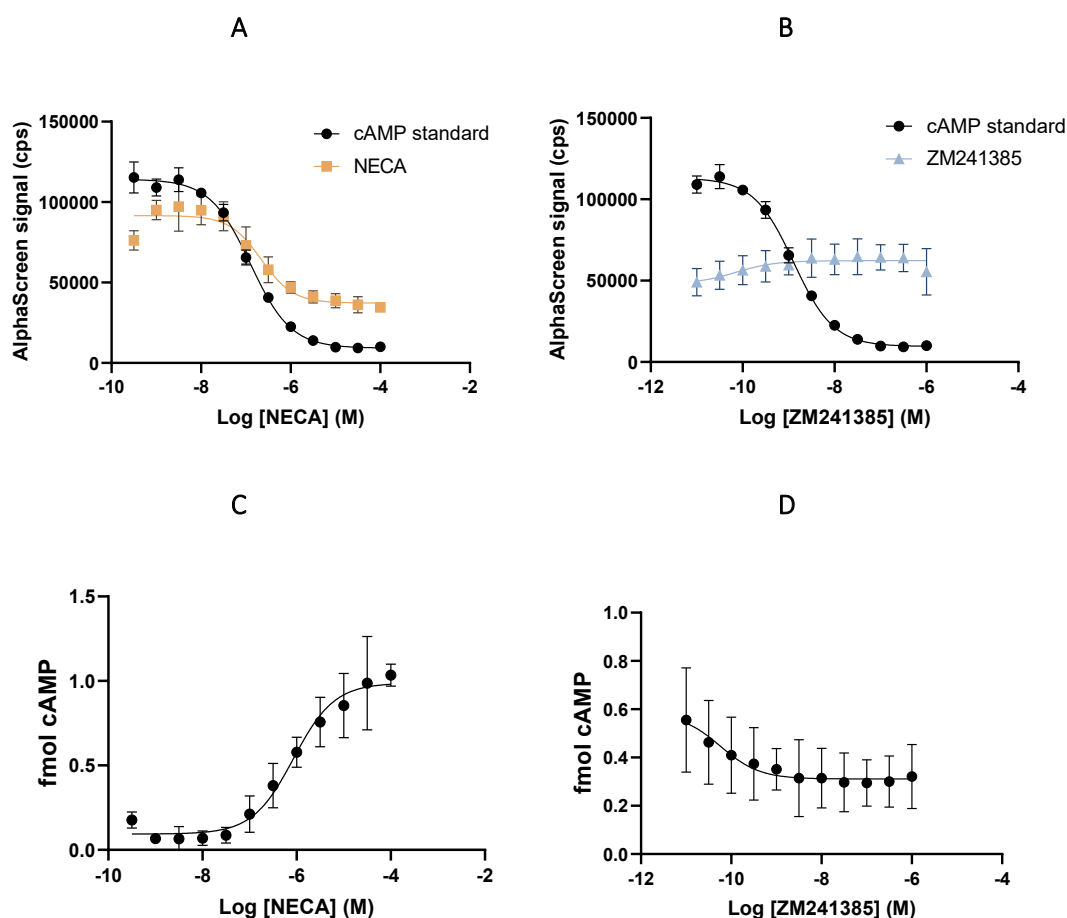
Figure 8.35. cAMP production measured as AlphaScreen signal and fmoles of cAMP in HEK293T cells stimulated by NECA and blocked by ZM241385. *The production of cAMP in transiently transfected HEK293T cells expressing the $A_{2A}R$ was (**A**) stimulated by NECA or (**B**) blocked by ZM241385 in the presence of 316 nM NECA (calculated NECA EC_{75}) and measured as AlphaScreen signal plotted against the logarithm of the ligand concentration. cAMP production was quantified by interpolation with the cAMP standard curve (**C**) after cell stimulation with NECA or (**D**) after inhibition by ZM241385, and plotted against the logarithm of the agonist concentration. Data are presented as the mean of all replicates (n=3) ± SD.*